

Figure 2.4-103 {Distribution of Fracture Dip Directions in Monitoring Well MW310C}

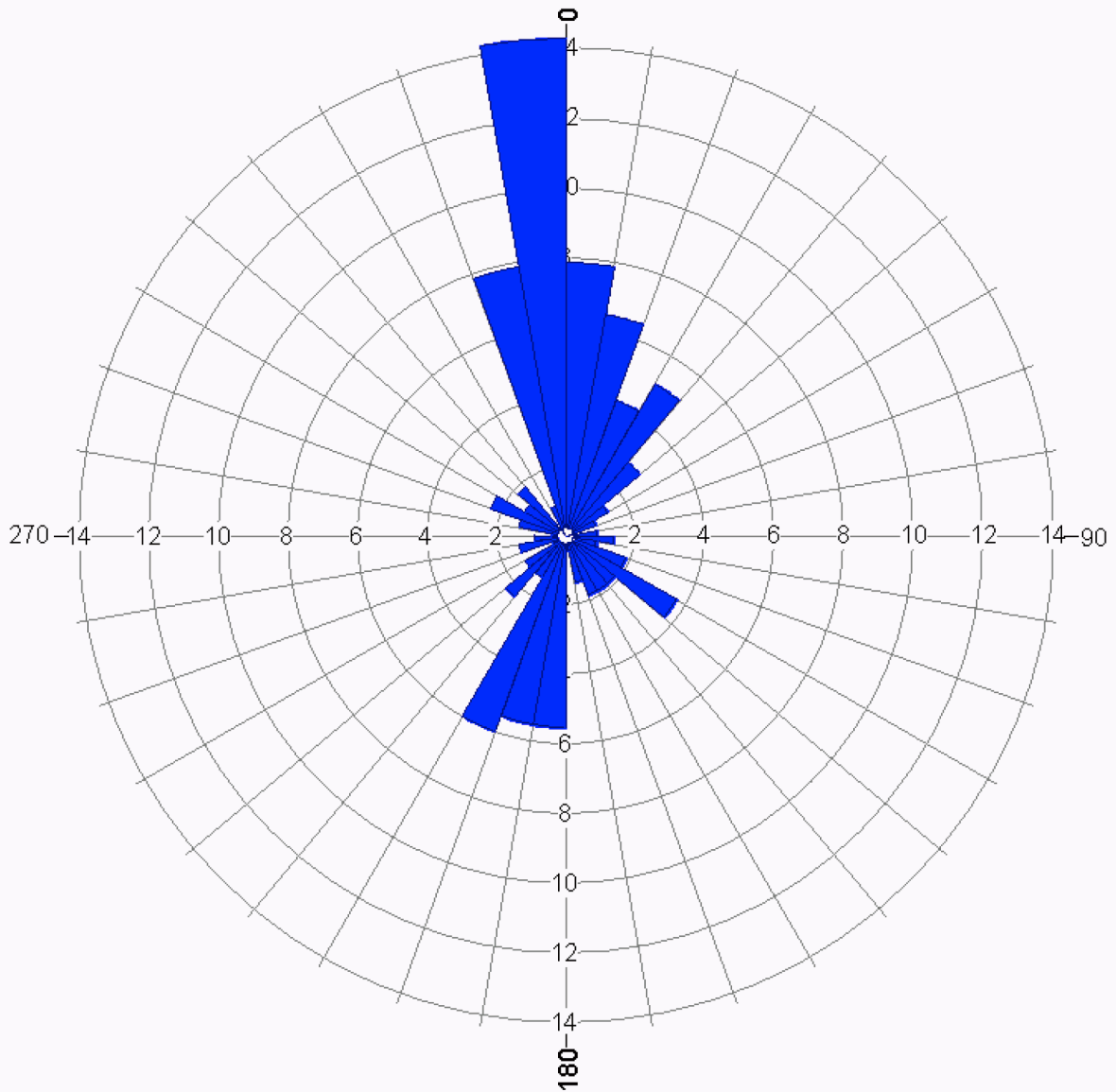
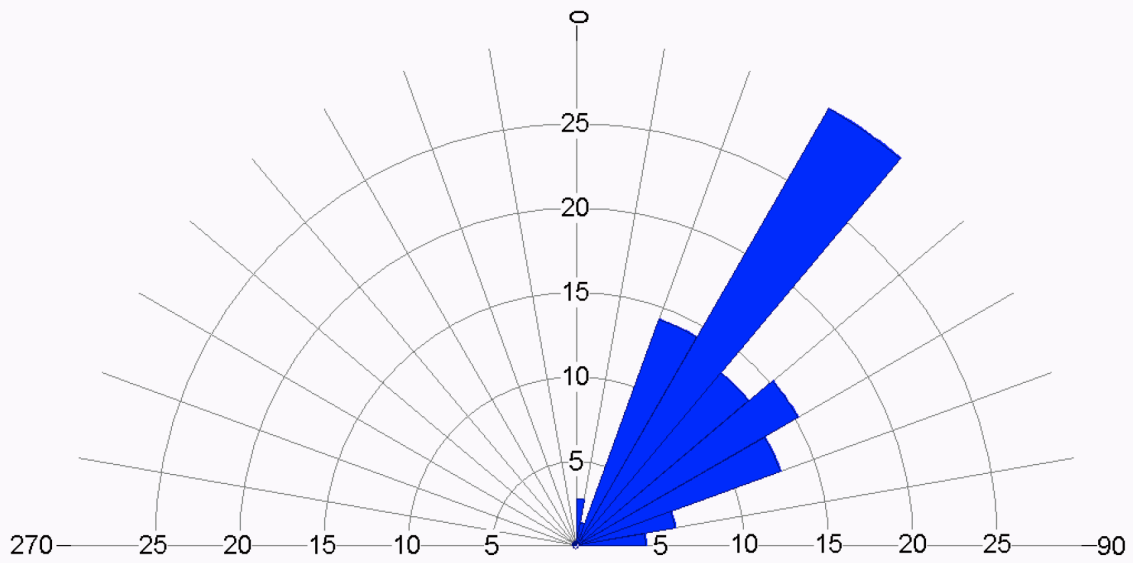


Figure 2.4-104 {Distribution of Fracture Dip Angles in Monitoring Well MW310C}



2.5 GEOLOGY, SEISMOLOGY, AND GEOTECHNICAL ENGINEERING

This section of the U.S. EPR FSAR is incorporated by reference with the following departure(s) and/or supplement(s).

This section presents information on the geological, seismological, and geotechnical engineering properties of the {Bell Bend Nuclear Power Plant (BBNPP)} site. Section 2.5.1 describes basic geological and seismologic data, {focusing on those data developed since the publication of the Final Safety Analysis Report (FSAR) for licensing Susquehanna Steam Electric Station Units 1 and 2.} Section 2.5.2 describes the vibratory ground motion at the site, including an updated seismicity catalog, description of seismic sources, and development of the Safe Shutdown Earthquake and Operating Basis Earthquake ground motions. Section 2.5.3 describes the potential for surface faulting in the site area, and Section 2.5.4 and Section 2.5.5 describe the stability of surface materials at the site.

Appendix D of Regulatory Guide 1.165, {Identification and Characterization of Seismic Sources and Determination of Safe Shutdown Earthquake Ground Motion,} (NRC, 1997) provides guidance for the recommended level of investigation at different distances from a proposed site for a nuclear facility.

- The site region is that area within 200 mi (322 km) of the site location (Figure 2.5-1).
- The site vicinity is that area within 25 mi (40 km) of the site location (Figure 2.5-2).
- The site area is that area within 5 mi (8 km) of the site location (Figure 2.5-3).
- The site is that area within 0.6 mi (1 km) of the site location (Figure 2.5-4).

These terms, site region, site vicinity, site area, and site, are used in Section 2.5.1 through 2.5.4 to describe these specific areas of investigation. These terms are not applicable to other sections of the FSAR.

The geological and seismological information presented in this section was developed from a review of previous reports prepared for the existing units, published geologic literature, interpretation of aerial photography, and a subsurface investigation and field and aerial reconnaissance conducted for preparation of this application. {Previous site-specific reports reviewed include the Susquehanna Steam Electric Station Units 1 and 2 (SSES) Final Safety Analysis Report (FSAR) (SSES FSAR, 2003).} A review of published geologic literature was used to supplement and update the existing geological and seismological information. In addition, relevant unpublished geologic literature, studies, and projects were identified by contacting the U.S. Geological Survey (USGS), State geological surveys and universities. The list of references used to compile the geological and seismological information is presented in the applicable section.

{Field reconnaissance of the site vicinity was conducted by geologists in teams of two or more. Two field reconnaissance visits in late fall and winter 2007 focused on exposed portions of Salem Township and Berwick, other rock exposures along the Susquehanna River, and roads traversing the site within a 5 mi (8 km) radius of the BBNPP site. Key observations and discussion items were documented in field notebooks and photographs. Field locations were logged by hand on detailed topographic base maps and with hand-held Global Positioning System (GPS) receivers.

The aerial reconnaissance investigated the geomorphology of the Berwick, PA area and targeted numerous previously mapped geologic features and potential seismic sources within a 200 mi (322 km) radius of the BBNPP site (e.g., Berwick Anticlinorium and Light Street Fault). Key observations and discussion items were documented in field notebooks and photographs. Photograph locations, and locations of key observations were logged with hand-held GPS receivers.

The investigations of regional and site physiographic provinces, geomorphic process, geologic history, stratigraphy, regional and site tectonics, and structural geology were conducted by Paul C. Rizzo Associates Inc. (Rizzo).}

This section is intended to demonstrate compliance with the requirements of paragraph c of 10 CFR 100.23, "Geologic and Seismic Siting Criteria" (CFR, 2007).

2.5.1 BASIC GEOLOGIC AND SEISMIC INFORMATION

The U.S. EPR FSAR includes the following COL Item in Section 2.5.1:

A COL applicant that references the U.S. EPR design certification will use site-specific information to investigate and provide data concerning geological, seismic, geophysical, and geotechnical information.

The COL Item is addressed as follows:

This section presents information on the geological and seismological characteristics of the site region (200 mi (322 km) radius), site vicinity (25 mi (40 km) radius), site area (5 mi (8 km) radius) and site (0.6 mi (1 km) radius). Section 2.5.1.1 describes the geologic and tectonic characteristics of the site region. Section 2.5.1.2 describes the geologic and tectonic characteristics of the site vicinity and location. The geological and seismological information was developed in accordance with the following NRC guidance documents:

- Regulatory Guide 1.70, Section 2.5.1, "Basic Geologic and Seismic Information," (NRC, 1978)
- Regulatory Guide 1.206, Section 2.5.1, "Basic Geologic and Seismic Information," (NRC, 2007) and
- Regulatory Guide 1.165, "Identification and Characterization of Seismic Sources and Determination of Safe Shutdown Earthquake Ground Motion," (NRC, 1997).

2.5.1.1 Regional Geology (200 mi (322 km) radius)

The U.S. EPR FSAR includes the following COL Item in Section 2.5.1.1:

Regional geology is site specific and will be addressed by the COL applicant.

This COL Item is addressed as follows:

This section discusses the physiography, geologic history, stratigraphy, and tectonic setting within a 200 mi (322 km) radius of the site. The regional geologic map and explanation as shown in Figure 2.5-5 and Figure 2.5-7 contain information on the geology, stratigraphy, and tectonic

setting of the region surrounding the {BBNPP site (King, 1974)}. Summaries of these aspects of regional geology are presented to provide the framework for evaluation of the geologic and seismologic hazards presented in the succeeding sections.

{Section 2.5.1.1.1 through Section 2.5.1.1.4.4.13 are added as a supplement to the U.S. EPR FSAR.

2.5.1.1.1 Regional Physiography and Geomorphology

The BBNPP site lies within the Ridge and Valley Physiographic Province as shown in Figure 2.5-6. The area within a 200 mi (322 km) radius of the site encompasses parts of seven other physiographic provinces. These are the Appalachian Plateaus Province, the Piedmont Province, the New England Province, the Atlantic Coastal Plain Province, the Blue Ridge Province, the Central Lowlands Province, and the Adirondack Province (Barnes, 2002).

Each of these physiographic provinces is briefly described in the following sections. The physiographic provinces in the site region are shown on Figure 2.5-6 (USGS, 2002). A map showing the different sections within the physiographic provinces of Pennsylvania, as depicted by the Pennsylvania Geological Survey (PGS), is shown on Figure 2.5-8.

2.5.1.1.1.1 Ridge and Valley Physiographic Province

The Ridge and Valley Physiographic Province occupies most of central Pennsylvania, extending from West Virginia and Maryland to northeastern Pennsylvania within the site region. The Ridge and Valley Province is bordered to the west and north by the Appalachian Plateaus Province and to the southeast by the Piedmont Province as shown in Figure 2.5-6. The Ridge and Valley Province is subdivided into two main sections, the Appalachian Mountain Section and the Great Valley Section. The Appalachian Mountain Section of the Ridge and Valley Province consists of long, narrow ridges and broad to narrow valleys exhibiting moderate to very high relief. These ridges typically are the remnant flanks of breached anticlines, typically capped by Cambrian sandstone and quartzite, and synclines underlain by resistant cherty limestones and sandstones of the Upper Silurian and Lower Devonian Keyser and Oriskany formations (DCNR, 2008a). The Great Valley Section of the Ridge and Valley Province consists of a very broad lowland that lies south of the Blue Mountain in southeastern Pennsylvania. The lowland has gently undulating hills eroded into shales and siltstones on the north side of the valley and a lower elevation, flatter landscape developed on limestones and dolomites on the south side (DCNR, 2008b). The full Cambrian section in central Pennsylvania is approximately 3,500-4,000 ft (1,067-1,219 m) thick with varying intervals of shale and limestone strata while the carbonates comprise more than 4,500-5,500 feet (1,372-1,676 m) of Lower, Middle, and Upper Ordovician strata in this area (DCNR, 2008a). Elevations in the Appalachian Mountain Section range from 440-2,775 ft (134-846 m) above sea level while elevations in the Great Valley Section range from 140-1,100 feet (43-335 m) above sea level (DCNR, 2008b).

Four main periods of continental glaciation occurred in Pennsylvania with three glacial periods directly impacting the site region and the Ridge and Valley Physiographic Province. These glacial events occurred in the following order from oldest to youngest; early Pleistocene, early middle Pleistocene, middle middle Pleistocene, and late Pleistocene (Braun, 2004). The oldest glaciation extended the farthest south, with each subsequent glacial event never advancing past the previous one, as shown in Figure 2.5-9. These older glacial advances are more difficult to identify due to the eroding attributes of more recent glaciers. The area south of the late Pleistocene glacial limit is characterized by extensive colluvial deposits and other features of

periglacial origin (Braun, 2004) including frost riving and congelifluction (Sevon, 1999). The limit of the late Pleistocene glacial event, also known as the Late Wisconsinan (17,000-22,000 yrs), is marked by heads-of-outwash in the valleys with an 'indistinct' moraine on adjacent hillsides (Braun, 2004) and is labeled as Olean Till as shown in Figure 2.5-9. The overall trend of the late Wisconsinan margin across northeastern Pennsylvania is N60°W and hilltop striae on the Appalachian and Pocono plateaus within 30 mi (48 km) of the margin indicate a regional ice flow direction of North-South to S20°W (Braun, 1988). The Late Illinoian (132,000-198,000 yrs) glacial event advanced only a few miles from the more recent Late Wisconsinan event, as shown in Figure 2.5-9, and is identified by heads-of-outwash in the valleys and discontinuous patches of till or colluvium derived from till (Braun, 1988). Pre-Illinoian glaciations advanced approximately 20-40 mi (32-64 km) beyond the Late Illinoian limit, as shown in Figure 2.5-9. Glacial lake sediments and two belts of "markedly thicker glacial deposits" suggest that Pre-Illinoian era northeastern Pennsylvania was subjected to two glacial events (Braun, 2004). The first of which extended to the maximum glacial limit as shown in Figure 2.5-9, and the second extended only several miles northeast of the maximum glacial limit (Braun, 2004). During glacial retreats, large volumes of glacial melt-waters formed broad, high energy streams including the Susquehanna, and other neighboring rivers such as the Delaware and Potomac Rivers that incised deep canyons into the continental shelf.

2.5.1.1.1.2 Appalachian Plateaus Physiographic Province

Located west of the Ridge and Valley Province, the Appalachian Plateaus Physiographic Province includes the western part of the Appalachian Mountains, stretching from New York to Alabama. The mountains within the Appalachian Plateaus Province are generally long, narrow, and even crested and valleys are highly variable in width and elevation (Way, 1999). Much of the current day landscape developed during multiple periods of glaciation within the Pleistocene period (Way, 1999), and a trellis drainage pattern is well-developed throughout. The Allegheny Front is the topographic and structural boundary between the Appalachian Plateaus and the Ridge and Valley Province (Clark, 1992). It is a bold, high escarpment, underlain primarily by clastic sedimentary rocks capped by sandstone. In eastern West Virginia, elevations along this escarpment reach 4,790 ft (1,460 m) above sea level (Hack, 1989) while in Pennsylvania, its highest point is 3,210 ft (978 m) above sea level. West of the Allegheny Front, the Appalachian Plateaus topographic surface slopes gently to the northwest and merges imperceptibly into the Interior Low Plateaus. A large portion of the Appalachian Plateaus Province lies within 200 mi (322 km) of the BBNPP site as shown in Figure 2.5-6.

2.5.1.1.1.3 Piedmont Physiographic Province

The Piedmont Physiographic Province extends southwest from New York, through southeast Pennsylvania, to Alabama and lies southeast of, and adjacent to, the Ridge and Valley Physiographic Province as shown in Figure 2.5-6. The Piedmont Province is about 60 mi (97 km) wide in southeastern Pennsylvania and narrows northward to about 10 mi (16 km) wide in southeastern New York.

In Pennsylvania, the Piedmont Province is divided into the Piedmont Lowland Section, the Gettysburg-Newark Lowland Section, and the Piedmont Upland Section. With the exception of the Piedmont Lowland Section, the majority of the Piedmont Province consists mainly of rolling low hills and valleys developed on red sedimentary rock (DCNR, 2007a). Almost all of the underlying sedimentary rock dips to the north or northwest with relatively low relief. The piedmont Lowland Section consists of broad, moderately dissected valleys separated by broad low hills and is developed primarily on limestone and dolomite rock highly susceptible to karst

topography (DCNR, 2007b). The Gettysburg-Newark Lowland Section runs adjacent to the Great Valley Section of the Ridge and Valley Province as shown in Figure 2.5-8. The Gettysburg-Newark Section consists mainly of rolling low hills and valleys developed on red sedimentary fluvial and lacustrine clastic rock deposits that represent a series of exposed rift basins (Root, 1999). The Piedmont Upland section is underlied primarily of metamorphosed and complexly deformed sedimentary, volcanic, and plutonic rocks (Crawford, 1999). Overlying this basement to the west are the metacarbonate rocks of Cambrian and Ordovician age and Mesozoic clastic sedimentary rocks to the east (Crawford, 1999). Elevation in the Piedmont Province ranges from 20-1,355 feet (6-413 m) mean sea level (msl) (DCNR, 2007b; DCNR, 2007c; and DCNR, 2007d).

2.5.1.1.1.4 New England Physiographic Province

The New England Physiographic Province is bounded on the north by the Ridge and Valley Province and on the south by the Piedmont Province as shown in Figure 2.5-6. The New England Province, aligned in a northeast-southwest direction, extends from the eastern border of Pennsylvania to mid-southeastern Pennsylvania occupying only a small amount of area as compared to the surrounding provinces. The province has an average width of about 5 mi (8 km) within Pennsylvania, and consists of circular to linear, rounded low hills or ridges that project upward in significant contrast to surrounding lowlands (DCNR, 2007e). The hills and ridges are made up of granitic gneiss, granodiorite, and quartzite thus making them very resistant to erosion (DCNR, 2007e). This province has a local relief ranging from 300-600 ft (91-183 m) with elevations ranging from 140-1,364 ft (43-416 m) (DCNR, 2007e).

2.5.1.1.1.5 Atlantic Coastal Plain Physiographic Province

The Atlantic Coastal Plain Physiographic Province lies east of, and adjacent to, the Piedmont Province and occupies much of the eastern seaboard, as shown in Figure 2.5-6. In Pennsylvania, this area is designated as the Lowland and Intermediate Upland Section of the Atlantic Coastal Plain Province as shown in Figure 2.5-8. This section consists of a flat upper terrace surface that is cut by numerous short streams, which are typically narrow and steep sided (DCNR, 2008c). The province is aligned in a northeast-southwest direction and is, on average, 6 mi (10 km) wide in Pennsylvania but attains a width of up to 156 mi (251 km) in New Jersey. The unconsolidated to poorly consolidated sand and gravel deposits of the Coastal Plain, dip gently to the southeast (NJGS, 2003). These sediments rest on various metamorphic rocks (DCNR, 2008c). Local relief is very low in the Lowland and Intermediate Upland Section of Pennsylvania, and elevations range from sea level to 200 ft (61 m) msl (DCNR, 2008c). The highest elevation of the Atlantic Coastal Plain Province in New Jersey is 391ft (119 m) msl (NJGS, 2003).

2.5.1.1.1.6 Blue Ridge Physiographic Province

The Blue Ridge Physiographic Province is bounded on the east by the Piedmont Province and on the west by the Valley and Ridge Province as shown in Figure 2.5-6. The Blue Ridge Province extends from Pennsylvania to Georgia in a northeast-southwest direction and is underlain primarily by metamorphosed Precambrian and Early Paleozoic igneous and sedimentary rock (VADOT, 2008). Soils of the Blue Ridge are predominantly colluvium with small amounts of alluvium along the rivers and streams (VADOT, 2008). The Blue Ridge is a long, linear province which ranges in width from about 5 mi (8 km) in Maryland to over 50 mi (80 km) in southern Kentucky.

2.5.1.1.1.7 Central Lowlands Physiographic Province

The Central Lowlands Physiographic Province, also known as the Ontario Lowlands, has relatively low relief (Komor, 1998) and is located between the Appalachian Plateaus Province to the south and Lake Ontario to the north as seen on Figure 2.5-6. The Central Lowlands were subjected to glaciation and as a result, consist mainly of unconsolidated surficial materials including mostly sands and gravels (DCNR, 2008d). Elevation within the province ranges from 570 ft (174 m) to approximately 1,000 ft (305 m) as erosion processes along the shores of Lake Erie have created a steep lake-land interface along much of the shoreline (DCNR, 2008d).

2.5.1.1.1.8 Adirondack Physiographic Province

The Adirondack Physiographic Province is located in northern New York and is surrounded by the Ridge and Valley to the southeast, the Appalachian Plateaus to the south, the Central Lowlands to the west, and the St. Lawrence Valley to the north as seen in Figure 2.5-6. The bedrocks of the Adirondacks are primarily Precambrian to early Paleozoic, metamorphic rocks and are part of the great Canadian Shield that has been uplifted to its present day geography (McDonnell, 2008). The bedrock generally supplements long, straight valleys, gently curved ridges, and a radial drainage pattern (Komor, 1998) throughout the province. The Adirondack has moderate to high relief throughout and its circular shape attains a diameter of over 150 mi (241 km) wide.

2.5.1.1.2 Regional Geologic History

The geologic and tectonic setting of the BBNPP site region is the product of a long, complex history of continental and island arc collisions and rifting, which spanned a period of over one billion years and formed the Appalachian Mountains (Appalachian Orogen) extended continental crust as shown in Figure 2.5-10 (Barnes, 2002). This history of deformation is started from pre-existing structures in the crust that has created post-seismotectonic setting of the region. Episodes of continental collisions have produced a series of terranes separated, in part, by low angle detachment faults (Pohn, 2000). Sources of seismicity may occur in the stratigraphy along structures within the North American basement, along the terranes, and over thrust plates. Seismic episodes of continental rifting have produced high angle normal and boundary faults that extend to the detachment faults and/or through the upper crust.

Major tectonic events in the site region include four compressional orogenies and one extensional episode (Faill, 1997). Direct evidence of these deformational events is visible in the Ridge and Valley province, as described in Section 2.5.1.1.4.3, and borehole data as described in Section 2.5.1.1.3. The site region is located currently on the passive, divergent trailing margin of the North American plate following the last episode of continental extension and rifting. Each of these tectonic events is described in the following paragraphs.

2.5.1.1.2.1 Greenville Orogeny

The Greenville Orogeny occurred over one billion years ago during the Middle Precambrian (Precambrian Y) time in the eastern part of Canada. The orogeny produced mountain ranges from the collision of continents to develop a supercontinent, Rodinia (Milot, 2001). Over the next four hundred million years, compressional orogenies and extensional episodes were maintained to a minimum, causing extensive erosion of the mountain range and decreased the size to flat land. During the time of the orogeny, the Iapetus Ocean bordered the eastern side of North America, upon which a new continental margin was formed at this time, creating the development of the Appalachian Mountains. In these areas, crystalline limestone and other

metamorphic sediments are present. In the Adirondack Mountains of upper New York, Greenville gneiss and sedimentary rocks are present from the Greenville orogeny (Millot, 2001).

2.5.1.1.2.2 Late Precambrian Rifting

Following the Greenville orogeny, late Precambrian sediments accumulated in rift-related basins at either end of the Appalachian foreland. In the Grenvillian basement, sedimentary sequence dominantly consists of well cemented red sandstones containing less than 75% quartz, unstable rock fragments, and feldspars. The material was deposited in semi-arid and arid terrestrial deposits (Shrake, 1991). The rift is related to the breakup of the North American continent to form the Iapetus Ocean. Thin basal alluvial arkoses and conglomerates, and one narrow right-bounded sedimentary unit are overlain by a bimodal volcanic suite including basalt pillow lavas and rhyolitic pyroclastics. Clastic stratigraphic sequence consists of pelites, siltstones, sandstones and basal pyroclastic pelites capping carbonate over the sedimentary unit. According to Crangle (Crangle, 2002), the sedimentary sequence shows continental-margin sequences after rifting of early seafloor. The Paleozoic marine transgression across the foreland from the southeast of Pennsylvania as shown in Figure 2.5-11 created the beginning of the Appalachian sedimentary wedge that decreases in thickness to the northwest into Ohio (the location for the cross section in 2.5-11 is in Figure 2.5-12; the correlation chart for 2.5-11 is in Figure 2.5-13). The depositions of a wedge of terrigenous sediments along the continental margin developed during much of the latest Precambrian into Early Cambrian time. These sediments are lithified sediments and volcanic, and their deposition was followed by several thousand feet of shelf carbonates. Two uplifts, South Mountain and Reading Prong, occur along the margin between the internal metamorphic zone and foreland of the Appalachian orogen and are termed external basement massifs.

2.5.1.1.2.3 Taconic Orogeny

From the middle Ordovician, a convergent plate boundary developed along the eastern edge of a small island chain. Crustal material beneath the Iapetus Ocean sank into the mantle along a subduction zone with an eastward dipping orientation. During closure of the oceanic basin, the carbonate platform beneath an east-dipping subduction complex along the eastern margin created the Taconic Orogeny (Harper, 1999). The distribution of facies shown in Figure 2.5-11 reflects the general westward migration of limestone and siliciclastic association depositions throughout the Ordovician period as the Appalachian basin evolved from passive margin to the foreland basin from the uplift of the Orogeny. The subduction of the tectonic highland above the thrusts developed on the foreland basin overlaying the former carbonate platform. The Martinsburg, Bald Eagle and Juniata Formations were derived from the erosion of the tectonic highland and eventually developed the eastern margin of the basin. The erosion was concentrated in the eastern portion of Pennsylvania and decreased westerly toward Ohio. Taconic structures began to appear near the collision zone and on the shelf to the west. The earliest event was the development of the Hamburg nappe (Pohn, 2000). The Hamburg nappe developed from early Paleozoic terrigenous sediments overlying the shelf east of the Lebanon Valley nappe. During the subduction zone, the nappes contained Precambrian Greenville gneiss, which were migrated northwestward on low angle thrusts into the Martinsburg shales and siltstones, being deposited toward the craton on the continental shelf. These nappes were stacked and partially overlapped, along the Appalachian trend. These nappes such as Lebanon Valley, Irish Mountain, Applebutter, Musconetcong and Lon Station-Paulins Kill formed the Musconetcong nappe megasystem. As tectonic rising highlands continued to elevate to the east, the sediments increased in volume and coarseness towards western Pennsylvania and western

New York. By the end of the Late Ordovician, the Appalachian basin was covered with a sequence of sandstone, shale and conglomerates (Harper, 1999).

2.5.1.1.2.4 Acadian Orogeny

During the late Devonian, large thrust sheets of the Avalon continent collided with the Laurentia continent. The Avalon collided into the North America Plate from the southeast. The collision created mountain development in the north, which later migrated south. In the north, the province of Canada started, primarily, by the deformed igneous and metamorphic rocks of Nova Scotia with sediments spreading southward. Deposition in New Jersey, southeastern New York, and eastern Pennsylvania developed the Catskill foreland basin. The Catskill clastic wedge, in east-central Pennsylvania, is several thousands feet thick and diminishes to the west and southwestward through western Virginia and eastern West Virginia, toward Tennessee. During the Mississippian Period, the Acadian Mountains were completely eroded, and the basement rocks of the Avalon terrane were exposed (Fichter, 2000).

2.5.1.1.2.5 Alleghanian Orogeny

From the Carboniferous period to the Permian, European and African (West Gondwana) plates collided with North American (Laurasia) plates to form the supercontinent of Pangaea. The collision caused the eastern seaboard of North America to uplift the entire region. Near the plate collision, metamorphism occurred on igneous and sedimentary rocks. Thrust faults, strike-slip faults, and structural folding occurred throughout the continental collision. The Allegheny tectonics occurred in three phases: compression of bedding planes, structural deformation, and migration along low-angle thrusting (Faill, 1999).

The form of southeast-dipping, low angle thrust faults through the older crustal rocks such as the Greenville orogeny and earlier Taconic fault surfaces, migrated to the west where the Precambrian Greenville blocks were thrust into the Cambrian-Ordovician rocks. The tectonic faults were also created in the basement and into the Paleozoic rocks beneath the Piedmont terrane. The faults were concentrated in the shale layers, between the basal siliciclastics and the overlying carbonates trending northwestward. Decollement folds followed along faults through crystalline basement westward in the hanging wall. As the Precambrian rocks advanced into the layered Paleozoic rocks, the foreland advanced, creating fractures. The folds developed joints, bedding-plane wedges, distorted fossils, mud cracks, and cleavage. The Ridge and Valley Providence was bounded to the northwest by the Allegheny structural front that separates the Appalachian Plateaus structural provinces. The other boundary, the Blue Mountain structural front, separates the Appalachian Mountain section of the Ridge and Valley province from the Great Valley section.

During the Late Alleghanian Orogeny, complexes of low angle thrusts advanced the Piedmont and Reading Prong crystalline terrace to the north-northwest direction, creating overturned beds of the Taconic nappes. The regional nappe was thrust over the Blue Mountain and into the Anthracite region. The presence of the Allegheny nappe generated the anthracite beds during the lower greenschist facies metamorphism. In the Piedmont, the Oregon and Chickies thrusts carried the eastern continuation of the Blue Ridge over the Taconic nappe rocks. The late thrusting created the Appalachian highland, consisting of long parallel mountains in the foreland and irregular topography to the southeast, on the stacked and overthrust nappes (Faill, 1999).

2.5.1.1.2.6 Early Mesozoic Extensional Episode (Triassic Rifting)

During the Late Triassic, the eastern North American plate and African plate began to separate at the rift zone (currently the Mid-Atlantic Ridge) to create the Atlantic Ocean. A series of rift basins, such as the Gettysburg-Newark basin and Baltimore trough, developed in southeastern Pennsylvania and along the North American coastline, respectively. The rift basins are arranged in northeast-southwest asymmetric trend. Subsequently, the basins were filled with sediments such as conglomerates, sandstones and shales. During the early Jurassic period, the process of seafloor spreading caused deep-seated magma to approach the surface and tectonic normal faulting within the basins. The magma created basalt diabase located in the Gettysburg-Newark basin of the Piedmont province (Schlische, 2003).

2.5.1.1.2.7 Cenozoic History

During the Cenozoic Era, the North American Plate continued to move northward, where the plate currently is sitting relative to the equator. The Atlantic Ocean continued to widen at the Mid-Atlantic ridge. At the center, the active ridge forces magma to the ocean floor while creating a divergent continental margin. From the Cretaceous Period to early Cenozoic Era, the climatic conditions changed to a warm and moist climate, causing chemical weathering. During the Miocene Epoch, the climate began to change to cooler climate conditions. The conditions were dominated by physical weathering, otherwise known as erosion, of clastic sediments while chemical weathering decreased.

From Pre-Illinoian to late Wisconsinian, three major glacial advancements occurred from ice accumulation in Canada advancing into Pennsylvania, and into the BBNPP site area. The glaciers were located at the northern portion of Pennsylvania and covered most of the Appalachian Plateaus province. The earlier glaciers migrated south approximately 800,000 years ago while the most recent occurred about 24,000 years ago (Barnes, 2002).

The advancements scoured valleys and deposited till, sand and gravel outwash material throughout BBNPP site area while the nearby Susquehanna River deposited sand and gravel outwash, filling the bottoms of valleys. During the period of elevated physical weathering, freezing and thawing at the surface caused the breakup of large quantities of rock at the crests of ridges in the Ridge and Valley province. As a result, the crests of these ridges were lowered by several feet. In addition, loose talus rock accumulated on the slopes of many ridges within central Pennsylvania.

2.5.1.1.3 Regional Stratigraphy

This section contains information on the regional stratigraphy within the major physiographic provinces in the Commonwealth of Pennsylvania. The regional geology and generalized stratigraphy within a 200 mi (322 km) radius of the BBNPP site is shown on Figure 2.5-5.

2.5.1.1.3.1 Ridge and Valley Physiographic Province

2.5.1.1.3.1.1 Pre-Cretaceous Basement Rock

The crystalline basement rock underlying Pennsylvania is of Precambrian age (Saylor, 1999) and rarely exposed throughout the state. Due to this lack of exposure, and younger, overlying Paleozoic strata (Gold, 2008), the limited information and research of Precambrian basement rock is based on several exploratory wells in western Pennsylvania (Gold, 2008) (Saylor, 1999). It is inferred from these deep wells that the Precambrian basement is approximately 1 Ga old

(Gold, 2008) and that is composed of metamorphosed greenschist or amphibolite. It is also inferred that this Precambrian basement is a regular, gently sloping surface, dipping eastward and forming the western margin of the Appalachian miogeosyncline (Saylor, 1999). Due to the heavily metamorphosed state of this Precambrian basement, little is known as to its depositional environment. Estimated depth of this basement rock at the BBNPP site is at approximately 33,000 ft (10,058 m) as shown in Figure 2.5-14. Earliest deformation of this basement rock appears to have been during the Greenville Orogeny (Saylor, 1999), resulting in multiple folding events and faulting.

The closest borehole to the BBNPP site that penetrates the basement rock, as seen on Figure 2.5-14, is located in Erie County, Pennsylvania (labeled -1829 (-1817)) about 200 mi (322 km) northwest of the site. It has been indicated (Saylor, 1999) that the few borings that penetrate the underlying Precambrian basement in northwestern Pennsylvania, eastern Ohio, and northern West Virginia, have encountered metamorphic or igneous rocks. For example a well, labeled Temple No. 1 in Mercer County PA, located approximately 208 mi (335 km) west of the BBNPP site, was drilled into a biotite granite/quartz-biotite gneissic basement rock at 9,810 ft (2,990 m) in depth (Saylor, 1999). Another well, labeled Fleck in Mercer County PA, located 205 mi (330 km) west of the BBNPP site, was drilled into basement rock at a depth of 9,136 ft (2,785 m) with rock composition including weathered chloritic schist and granite grading into gneiss (Saylor, 1999). The basement rock was only sampled in the drill cuttings and suggests a gneiss/schist from the mineralogy present, (i.e., biotite, chlorite, and clear quartz).

Overlying the Precambrian metamorphic and igneous basement of the Ridge and Valley Province, are the sedimentary deposits of the Early Cambrian with a transition to the carbonate rich sediments of the Early Ordovician. These early Cambrian deposits created a wedge of terrigenous sediments, best described today as the Chilhowee Group, which were the result of marine waters of the Iapetus (Proto-Atlantic Ocean) slowly transgressing across the continent shortly after the Greenville Orogeny (Kauffman, 1999). Overlying these sediments is a carbonate platform (Bradley, 1989) (Kauffman, 1999) showing signs of uplift and erosion during the Taconic Orogeny during the Ordovician (Bradley, 1989). Above the clastic sediments of the Chilhowee Group is the brown sandstone interbedded with red and green shale beds of the Waynesboro Group (Kauffman, 1999). The Waynesboro Group, according to Kauffman (Kauffman, 1999) is the oldest exposed outcrop in Central Pennsylvania with an Early to Middle Cambrian age. Overlying the Waynesboro Group is a limestone formation identified as the Warrior Formation (Ryder, 1992) of Middle to Late Cambrian age. The lithology of the Warrior Formation is further defined by Kauffman (Kauffman, 1999) as a dark, fossiliferous, fine grained limestone interbedded with silty dolomite and has a thickness of up to 1,340 ft (408 m) in the Ridge and Valley Province. Bordering the Cambrian-Ordovician contact, and overlying the Warrior Formation is the Gatesburg Formation. The Gatesburg Formation consists of a series of sequential sandstone and dolomite units and can be labeled as Late Cambrian age through the identification of gastropod fossils in the uppermost member (Ryder, 1992).

The Ordovician Period followed the Cambrian with significant geologic occurrences, most of which are evident throughout the Ridge and Valley Province of Pennsylvania. The Ridge and Valley rocks of Ordovician age are primarily sedimentary in nature, with evidence of uplifting during the Taconic Orogeny. According to Thompson (Thompson, 1999), the Ordovician sedimentation can be broken down into three major phases with early Ordovician being a depositional environment of a stable carbonate-platform. During Middle Ordovician, there was a submergence of the carbonate-platform, due to the Taconic Orogeny, with marine limestone and siliciclastic sedimentation during the submergence (Thompson, 1999). This submergence

resulted in the creation of a basin which was in filled with further marine limestone and siliciclastic sediments (Thompson, 1999). Stratigraphically, Early Ordovician rocks are generally referred to as part of the Beekmantown Group (Harper, 2003), are composed primarily of dolomite-limestone, and reach a thickness of up to 4,200 ft (1280 m) (Thompson, 1999). The Middle Ordovician shows a transition zone from the dolomite-limestone to rocks of primarily limestone composition deposited in both shallow and deep-water environments (Thompson, 1999). In central-Pennsylvania, the Loysburg Formation best represents this transition from a tidal-zone to a shallow marine zone with a dolomitic and stromatalite rich limestone underlying a coarse grained, fossiliferous limestone (Thompson, 1999). It is also during the Middle Ordovician that the lapetus stopped widening and began to close meaning this formerly passive area of sedimentation became tectonically active, thus giving birth to the Taconic Orogeny (Cotter, 2008). This active margin setting became the depositional environment of the sandstone and greywacke-shales that comprise almost 3,500 ft (1,067 m) of Late Ordovician formations including the Juniata, Bald Eagle, and Reedsville Formations of central Pennsylvania.

During the early Silurian, shallow marine conditions returned to central Pennsylvania (Cotter, 2008) as it became a depositional environment for sediments being eroded and transported from the Taconic highlands in the eastern part of the state. The Silurian basement rocks throughout Pennsylvania have a thickness ranging from 3,000 ft (914 m) in central Pennsylvania to 4,000 ft (1,219 m) in North-Eastern Pennsylvania (Laughrey, 1999). The Silurian represents a transition from a coastal plain in the east to a delta in the west, through the alluvial clastic deposits of the Shawangunk and Tuscarora formations (eastern and central Pennsylvania respectively) to the offshore facies of the Medina Formation of western Pennsylvania (Laughrey, 1999). The Tuscarora Formation, prevalent throughout the Ridge and Valley Province in central Pennsylvania, is composed primarily of quartzose, sublithic, and argillaceous sandstones and shales (Laughrey, 1999) and ranges in thickness from 492 ft (150 m) to 656 ft (200 m). The Rose Hill, Keefer, and Mifflintown formations (in ascending order) best describe the stratigraphic members of the Middle Ordovician. Rose Hill Formation, which overlies the Tuscarora Formation, is defined as predominantly an olive shale with interbedded layers of hematitic sandstone, purplish shale, and fossiliferous limestone (Laughry, 1999). The Keefer Formation is described mainly as a quartzose and hematitic sandstone with some mudstone and the overlying Mifflintown Formation is composed of shallow marine mudrocks and limestones (Laughry, 1999). The Upper Silurian is identified by the Bloomsburg Formation, a grayish-red clay-siltstone with some interbedded sandstone, transitioning to the limestone and thin shale beds of the Tonoloway Formation (Laughrey, 1999).

In Pennsylvania, the Devonian Age rocks represent a "westward-thinning wedge of sediments" that range in thickness from 2,400 ft (732 m) in the western portion of the state, to over 12,000 ft (3,658 m) in the east (Harper, 1999). These Devonian sediments are generally broken down into two basic groups: the Pre-Acadian Orogeny comprised of stable shelf sedimentary deposits and Post-Acadian Orogeny strata that emphasize the presence of "tectonism, subsidence, and filling of a foreland basin" (Milici, 2006). The base for the Devonian age rocks of the Ridge and Valley Province in Pennsylvania is the Keyser Formation, a primarily gray, fossiliferous limestone (Laughrey, 1999). Above the Keyser Formation lie other stages of the Lower Devonian including (in ascending order) the cherty limestone of the Helderberg Stage, the quartz rich sandstones, shales and siltstones of the Deerpark Stage, and the detrital sediments of the Onesquethawan Stage (Harper, 1999). The Onesquethawan Stage carries into and becomes the basement for the Middle Devonian timeframe which consists of basinal marine shales to nonmarine sandstone. Other stages within the Middle Devonian Ridge and Valley Province include the fossiliferous shale of the Needmore Formation, the argillaceous and silty Selinsgrove Limestone, the volcanic

Tioga ash and shales, and the Mahantango Formation (Harper, 1999). The Mahantango Formation, which comprises the bedrock of the BBNPP site, is described by Harper (Harper, 1999) as "a complex series of interbedded shales, siltstones, and sandstones ranging from 1,200 ft (366 m) to 2,200 ft (671 m) thick." Milici (Milici, 2006) also refers to the Mahantango Formation as silty shale. Overlying the Mahantango Formation, and bordering the Upper Devonian, is the fossiliferous shaley limestone of the Tully Limestone Formation (Harper, 1999). The marine and non-marine rocks of the Upper Devonian only add to the complexity of the Devonian as a whole, as it represents sediment deposition during the progradation of the Catskill deltaic system (Harper, 1999). This system, as it relates to the Ridge and Valley Province in central Pennsylvania, can be "broadly defined" by four main depositional episodes including (in ascending order) the rarely fossiliferous basal shales of the Harrell Formation, the interbedded shales, siltstones, and sandstones of the Brallier Formation, the shales, thin siltstone, sandstones, and conglomerates of the Scherr and Lock Haven Formations, and the nonmarine sandstones and mudrock that overlap the Devonian-Mississippian boundary (Harper, 1999).

The Carboniferous Period of the Ridge and Valley Province is a topic of on-going research but the most commonly accepted 'boundary' between the Mississippian and Upper Devonian is the Spechty Kopf Formation (Berg, 1999). The Spechty Kopf Formation, which ranges in thickness up to 1,280 ft (390 m), is typically labeled as an unconformity lying between the previously discussed Catskill Formation and the fluvial sandstones of the Pocono Formation (Berg, 1999). The Spechty Kopf Formation is predominantly sandstone with some shale and siltstone interbedded. Above it lies the Pocono Formation which, in north-eastern Pennsylvania, consists mainly of non-red medium to coarse-grained sandstones and conglomerates (Brezinski, 1999). In central Pennsylvania, the Pocono Formation is better represented by the Huntley Mountain and Rockwell Formations which are characterized by greenish-gray to tan sandy siltstone and silty shale with some sandstone (Brezinski, 1999). The red shales, sandstones, and conglomerates of the Mauch Chunk Formation (Van Diver, 1993) mark the original uplifting of the Alleghenian Orogeny as well as the uppermost boundary of the Mississippian in the Ridge and Valley Province. The Mauch Chunk Formation ranges in thickness throughout the state but is generally believed to be between 3,000 ft (914 m) and 4,000 ft (1,219 m) (Brezinski, 1999). Above the Mauch Chunk Formation in northeastern and central Pennsylvania lies the Pottsville Formation, which ranges in thickness from 100 ft (30 m) to 1,600 ft (488 m) and is comprised mainly of conglomerate and conglomeratic sandstone with some sandstone and coal (Edmunds, 1999). Overlying the Pottsville Formation and marking the northern boundary between the Pennsylvanian and Permian Periods is the Llewellyn Formation. The Llewellyn Formation has a thickness of up to 3,500 ft (1,067 m) and consists mainly of conglomerates and sandstones with numerous coal beds and some clayey shale (Edmunds, 1999).

As shown in Figure 2.5-6, there are no post-Carboniferous outcrops in the Ridge and Valley Province of Central and Northeastern Pennsylvania.

2.5.1.1.3.1.2 Plio-Pleistocene and Quaternary Deposits

No Plio-Pleistocene or Quaternary Deposits are mapped within the bedrock of the Ridge and Valley Province of Pennsylvania. Though Quaternary Deposits exist throughout the site region, these deposits differ in composition and thickness dependent upon the geographic and geologic setting. Site and site area specific Quaternary Deposits are discussed in further detail in Section 2.5.1.2.2 and Section 2.5.1.2.3.4.

2.5.1.1.3.2 Piedmont Physiographic Province

There are three distinct sections that comprise the Piedmont Physiographic Province. The first is the Gettysburg-Newark Lowland, the second is the Piedmont Lowland, and the third is the Piedmont Upland (as shown in Figure 2.5-8).

2.5.1.1.3.2.1 Gettysburg-Newark Lowland Section

The Gettysburg-Newark Lowland Section forms a 140-mile arc across Southeastern Pennsylvania with a series of exposed rift basins of Late Triassic to Early Jurassic age that are filled with fluvial and clastic deposits. These basins are underlain by nonmetamorphic Cambrian and Ordovician basement rocks and are bordered "by a continuous, complex system of normal faults" (Root, 1999).

2.5.1.1.3.2.2 Piedmont Lowland Section

Mesozoic sedimentary rocks of the Piedmont Province occur primarily within the highly folded and faulted region of the Piedmont Lowland section (Figure 2.5-8). The sediments were deposited in a series of northeast-trending basins. Sediments filling the basins include conglomerates, shales, siltstones and sandstones, and basic igneous intrusive dikes, diabase, and lava flows (VADOT, 2008). The Lower Mesozoic sediments deposited in these basins usually are referred to as Triassic basin deposits, although the basins are now known to also contain Lower Jurassic rocks. The folding and faulting of this section, as well as lithologies, are very similar to that of the Lebanon Valley Section of the Great Valley, where Cambrian quartzite and Precambrian gneiss are brought into contact with rocks as young as the lower Ordovician (Gray, 1999).

2.5.1.1.3.2.3 Piedmont Upland Section

Crystalline rocks of the Piedmont Province primarily occur within the Piedmont Upland section. The crystalline rocks consist of deformed and metamorphosed meta-sedimentary and meta-igneous rocks, with overlying saprolite (VDEQ, 2008). The rocks belong to a number of northeast-trending belts that are defined on the basis of rock type, structure and metamorphic grade and are interpreted to have formed along and offshore of ancestral North America (Pavrides, 1994).

Surficial sediments in the Piedmont Province consist of residual and transported material. The residual soils have developed in place from weathering of the underlying rocks, while the transported material - alluvium and colluvium - has been moved by water or gravity and deposited as unconsolidated deposits of clay, silt, sand, and gravel. Surficial sediments in the Piedmont Upland section are interpreted to be the product of Cenozoic weathering, Quaternary periglacial erosion and deposition, and recent anthropogenic activity (Sevon, 2000).

Residual soil in the Piedmont Province consists of completely decomposed rock and saprolite. Residual soils occur almost everywhere, except where erosion has exposed the bedrock on ridges and in valley bottoms. Saprolite comprises the bulk of residual soil in the Piedmont Province and is defined as an earthy material in which the major rock-forming minerals (other than quartz) have been altered to clay but the material retains most of the textural and structural characteristics of the parent rock. The saprolite forms by chemical weathering, its thickness and mineralogy being dependent on topography, parent rock lithology, and the presence of surface and/or groundwater (Cleaves, 1992).

Relief affects the formation of soils by causing differences in internal drainage, runoff, soil temperatures, and geologic erosion. In steep areas where there is rapid runoff, little percolation of water through the soil and little movement of clay, erosion is severe and removes soil as rapidly as it forms. Gently sloping areas, on the other hand, are well drained and geologic erosion in these areas is generally slight. The characteristics of the underlying rock strongly influence the kind of changes that take place during weathering. Because of differences in these characteristics, the rate of weathering varies for different rock types. The igneous, metamorphic, and sedimentary rocks of the Piedmont Province are all sources of parent material for the soils.

Colluvium in the Piedmont Province occurs discontinuously on hilltops and side slopes, while thicker colluvium occurs in small valleys lacking perennial streams. Alluvium is present in all valleys with perennial streams (Sevon, 2000).

2.5.1.1.3.3 New England Physiographic Province

The basement rocks of the Reading Prong Section of the New England Physiographic Province are believed to have formed during the Greenville Orogeny and are comprised of metamorphosed sedimentary rocks. These rocks were then subjected to the intense thrust faulting and continual folding associated with the Taconic Orogeny, thus creating a complex nappe megasystem (Drake, 1999). Continued folding and faulting during the Alleghanian Orogeny has led to "extremely complicated geologic relations" (Drake, 1999) within the Reading Prong. The Middle Proterozoic carbonate and crystalline rocks that were transported overtop of the basement rocks (Drake, 1999), were also subjected to folding and faulting and range in sequence depending upon the area of the Reading Prong being studied. Seismic-reflection studies have suggested that the basement of the Reading Prong ranges in thickness from 15,000 ft (4,572 m) in the easternmost part of the Pennsylvania, to 45,000 ft (13,716 m) in Lebanon and Lancaster Counties (Drake, 1999).

2.5.1.1.3.4 Atlantic Coastal Plain Physiographic Province

The Atlantic Coastal Plain Physiographic Province is one of the flattest of the many physiographic provinces. The province covers more than 3,200 mi (5,150 km) from Cape Cod to the Yucatan Peninsula, and forms the continental shelf along the Atlantic Ocean (Komor, 1998). The province represents repeated cycles of transgression and regression of the ocean resulting in over 100 million years of sediment accumulation (Komor, 1998). Underlying most of the province are sediments of Cretaceous and Tertiary age with Pleistocene fluvial sediments overlying areas in and around current day state of New Jersey. These Cretaceous sediments, in addition to moraine outwash from the Pleistocene continental glaciers, comprise the underlying geology of Long Island and the eastern shores of Staten Island (Komor, 1998). The total sediment accumulation comprising the Atlantic Coastal Plain Province account for nearly 30,000 ft (9,194 m) in thickness and consist of many disconformities and several unconformities representing great cyclical depressions in sea level occurring several times (Komor, 1998).

2.5.1.1.3.5 Appalachian Plateau Physiographic Province

The Appalachian Plateau Physiographic Province is underlain by rocks that are continuous with those of the Ridge and Valley Province but, in the Appalachian Plateau, the layered rocks are nearly flat-lying or gently tilted and warped, rather than being intensely folded and faulted. Rocks of the Allegheny Front along the eastern margin of the province consist of thick sequences of sandstone and conglomerate, interbedded with shale, ranging in age from Devonian to

Pennsylvanian. Rocks of the Appalachian Plateau west of the Allegheny Front are less resistant and consist of Permian age sandstone, shale and coal (Hack, 1989).

2.5.1.1.4 Regional Tectonic Setting

In 1986, the Electric Power Research Institute (EPRI) developed a seismic source model for the Central and Eastern United States (CEUS). The BBNPP site region is a stable continental region (SCR) characterized by low rates of crustal deformation and no active plate boundary conditions (EPRI, 1986). The EPRI source model included the independent interpretations of six Earth Science Teams. The seismic source models developed by each of the six teams were based on the tectonic setting and the occurrence, rates, and distribution of historical seismicity. The original seismic sources identified by EPRI (EPRI, 1986) are thoroughly described in the EPRI study reports (EPRI, 1986).

Earthquakes in the surrounding area that occurred in the time period of Mesozoic and Cenozoic extended crust are positively correlated with large SCR earthquakes. Nearly 70% of SCR earthquakes with magnitude 6 occurred in areas of Mesozoic and Cenozoic extended crust. Additional evidence shows an association between Late Proterozoic rifts and modern seismicity in eastern North America. There is no evidence for late Cenozoic seismogenic activity of any tectonic feature or structure in the site region (Crone, 2000) (Wheeler, 2005). No new structures or features have been identified in the site region since 1986 as described in the EPRI study (EPRI, 1986) seismic source model.

The following sections describe the tectonic setting of the site region by discussing the: (1) plate tectonic evolution of eastern North America at the latitude of the site, (2) origin and orientation of tectonic stress, (3) gravity and magnetic data and anomalies, (4) principal tectonic features, and (5) seismic sources defined by regional seismicity.

2.5.1.1.4.1 Plate Tectonic Evolution of the Atlantic Margin

The Late Precambrian to Recent plate tectonic evolution of the site region is summarized in Section 2.5.1.1.2 and in Figure 2.5-10. The plate tectonic theory formalized and accepted during the 1970s helps to describe the evolution of the Appalachian orogenic belt (Rodgers, 1970). Several studies from the 1980s to the present have concentrated on the relationship of stratigraphy and structure of the Paleozoic era as it relates to orogenies and plate tectonics (Hibbard, 2006). The following subsections divide the regional plate tectonic history into: (1) Late Proterozoic and Paleozoic tectonics and assembly of North American continental crust, (2) Mesozoic rifting and passive margin formation, and (3) Cenozoic vertical tectonics.

2.5.1.1.4.1.1 Late Proterozoic and Paleozoic Plate Tectonic History

The plate boundary deformation has occurred repeatedly in the site region since late Precambrian time. The development of continents and rift zones were created by breakup of supercontinents during this time interval. Foreland strata, deformation structures, and metamorphism associated with the Greenville (Middle Proterozoic) and Allegheny (Late Paleozoic) orogenies shows the closing of ocean basins and connection of continents to form the supercontinents Rodinia and Pangaea, respectively (Figure 2.5-10). Synrift basins, normal faults, and postrift strata associated with the opening of the Iapetus (Late Proterozoic to Early Cambrian) and Atlantic (Early Mesozoic) Ocean basins record the break-up of the supercontinents (Hibbard, 2006).

2.5.1.1.4.1.1.1 Paleozoic Plate Tectonic Overview

The Appalachian Mountains represent a series of Paleozoic orogenies along the eastern margin of North America. The Appalachians extend from Alabama through Maine in the United States, and continue across the southeastern provinces of Canada to Newfoundland (Berg, 1980). The Appalachian Mountains are divided, classically, into four main provinces (Aber, 2001):

Piedmont Province extends from Alabama to New York; the Piedmont is a plateau of moderate elevation 492 to 984 ft (150 to 300 m) in the eastern portion of the mountain system. Bedrock consists of crystalline metamorphic and igneous rocks of Paleozoic age and with depositional environment of marine sediments and volcanic deposits on the oceanic crust. The bedrock was deformed and metamorphosed to the green schist facies of chlorite, biotite schists, and slate. Granite intrusions form domes within the Piedmont.

Blue Ridge Province is a narrow ridge separating the Piedmont and the Ridge and Valley provinces. The ridge is located on the up thrust Proterozoic basement rocks. In the south Appalachian, the Brevard Fault zone separates the boundary between the Piedmont and Blue Ridge and reveals sedimentary bedrock from the deep décollements beneath the Piedmont Province.

Ridge and Valley Province consists of Paleozoic sedimentary rocks that were faulted and folded into large anticlines and synclines. The tectonic structures were created by shallow décollements within the sedimentary sequence. Due to the irregular erosional patterns, Ridge and Valley structures have distinctive weathering and decrease in erosion to the west in a transition into the Appalachian Plateau.

Appalachian Plateau Province is underlain by gently folded Paleozoic sedimentary strata with elongated folded structures. Heavy physical erosion has developed high relief topography in the plateau.

The Appalachian Mountains were divided into three main orogenic phases during the Paleozoic. Each phase begins with accumulation of marine sediments and volcanic deposits, deformation of structural folding and faulting, tectonic uplift of mountains, and erosion of uplift land. A particular consequence of orogeny is the production of sediment as uplifted mountains erode. Thus, each phase creates a delta, filling shallow seas on the continental side of the orogeny. Clastic fans deposited in terrestrial, coastal, near-shore, and off-shore settings (Aber, 2001).

Taconic Orogeny occurred during the Ordovician. Structural deformation progressed in the northern portion of United States creating uplifted mountains which eroded west to create the Queenstown delta near Albany, New York.

Acadian Orogeny occurred during the Devonian and was centered in New England and southern New York. The orogeny showed structural features such as folding and thrust faults along with metamorphism and granite intrusions. Across southern New York and northern Pennsylvania, the Catskill delta was created and developed a massive thickness of sediments.

Alleghanian Orogeny occurred in the southern Appalachians during the Pennsylvanian Period. Thrust faulting and structural folding developed with limited metamorphism and

intrusion from Pennsylvania southward to Alabama, resulting in a clastic delta spread over western Pennsylvania, West Virginia, Kentucky and Tennessee.

All three orogenies are interpreted in terms of collisions during the closing of the Iapetus Ocean between North America, Europe and Africa (Gondwana). Both continental and oceanic terrains were involved with collisions at different times and places. The Taconic Orogeny represented terrane collisions with North America. The Acadian Orogeny took place between North America and Europe, and is contemporaneous with the Caledonian Orogeny of the British Isles, Greenland, and Scandinavia. Finally, the Alleghanian Orogeny involved the collision between Africa (a portion of Gondwana) and the North American-European continent to create Pangaea by the end of the Paleozoic (Aber, 2001).

Tectonic structures developed during the interval between the Late Proterozoic and Triassic Periods. Late Proterozoic and early Cambrian rifting associated with the breakup of Rodinia and development of the Iapetus Ocean formed east-dipping normal faults through Laurentian (proto-North American) crust (Figure 2.5-10). Late Proterozoic extended crust of the Iapetan margin probably underlies the Appalachian fold belt southeastward to beneath much of the Piedmont Province (Wheeler, 1996). Paleozoic compressional events associated with the Taconic, Acadian, and Allegheny orogenies formed predominantly west-vergent structures that include (1) Ridge and Valley Province shallow folding and thrusting within predominantly passive margin strata, (2) Blue Ridge Province nappes of Laurentian crust overlain by Iapetan continental margin deposits, (3) Piedmont Province thrust-bounded exotic and suspect terrains including island arc and accretionary complexes interpreted to originate in the Iapetan Ocean, and (4) Piedmont Province and sub-Coastal Plain Province east-dipping thrust, oblique, and reverse fault zones that collectively are interpreted to penetrate much of the crust and represent major sutures that juxtapose crustal elements (Hatcher, 1987) (Horton, 1991) (Glover, 1995) (Hibbard, 2006).

2.5.1.1.4.1.2 Mesozoic and Cenozoic Passive Margin Evolution

During the break up of the Pangaea in the Middle Triassic, rift basins developed in eastern North America. The rift basins were typically asymmetrical and trended northwest to southeast as the current Atlantic passive continental margin has evolved since rifting initiated in the Early Triassic. The progression from active continental rifting to sea-floor spreading and a passive continental margin included: (1) initial rifting and hot-spot plume development, (2) thinning of warm, buoyant crust with northwest-southeast extension, normal faulting and deposition of synrift sedimentary and volcanic rocks, and (3) cooling and subsidence of thinned crust and deposition of postrift sediments on the coastal plain and continental shelf, slope, and rise (Klitgord, 1988) (Klitgord, 1995). The transition between the second (rifting) and third (drifting) phases during the Early Jurassic marked the initiation of a passive margin setting in the site region, in which active spreading migrated east, away from the margin.

The Mid Atlantic ridge system has an active axis creating the combination of intrusion, extrusion and extensional faulting. The initial rifting with the effusion of Triassic basalts and the associated formation of basins caused the opening of the North Atlantic during the Triassic (MacLachlan, 1999). The dispersion of continents during the end of the Jurassic created additional generation of new oceanic crust by sea floor spreading on opposing limbs of the North Atlantic-Caribbean rift and widening of the North American basin. This rift grew northward blocking out the Labrador coastline and splitting off the western margin of Greenland from Canada. With this rift extension, the European continent was cast as far as Scotland and was also blocked out at, or within, the late Cretaceous. North America continued its drift to the northwest, further widening the Atlantic

Ocean and increasing the gap to both Africa and South America. The eastern seaboard of the United States at this time had an almost east-west strike.

The continental margin moves away from the spreading center of the mid-Atlantic and horizontal northwest-southeast tension changed to horizontal compression as gravitational potential energy from the spreading ridge exerted a lateral "ridge push" force on the oceanic crust. Northwest-southeast-directed post rift activities in the Mesozoic basin caused inversion to many structures present during this time (Withjack, 1998).

The rift system is located within the Appalachian orogen. The majority of the rift basins in eastern North America are asymmetrical fault-bounded half-grabens (Schlische, 2002). In the site area, the rift basins such as the Culpeper, Gettysburg, and Newark are parallel to the existing continental shelf (Klitgord, 1995) (Figure 2.5-15 and Figure 2.5-22). Normal faults in the continental rifts transect the sedimentary rocks and igneous rocks forming horsts and grabens. The normal faults strike roughly parallel to the rift trend and are steeply dipping.

The intrusion of diabase dikes and sills and the extrusion of basalt flows occurred throughout eastern North America during the early Jurassic. However, the duration of the magmatic activity in the northeastern United States and southeastern Canada was limited to 600,000 yrs (Withjack, 1998). A massive wedge, presumably composed of volcanic or volcanoclastic rocks, is present along the edge of the passive margin of the eastern United States. The wedge lies near the continent-ocean boundary and formed during the transition from rifting to drifting (Withjack, 1998).

Rifting continued until the Middle Jurassic. After rifting, the deformational regime and stress state changed in the northeastern United States. By the late Triassic, most of the rugged topography had been reduced by erosion. The rocks in the hanging wall and footwall of Mesozoic rift graben show the same degree of burial and unroofing. The opening of the Atlantic Ocean in the late Triassic and early Jurassic was accompanied by a thermally-uplifted rift shoulder, basic volcanism and intrusions, and rift basin sedimentation. An Atlantic slope drainage formed on the newly rifted margin and the continental divide began marching westward unsteadily into the foreland, reversing a drainage that had been to the west for most of the Paleozoic and early Mesozoic. The transition from a rift to a drift margin through the remainder of the Mesozoic and into the Cenozoic along with the westward push of the continental divide, would dominate the tectonic and geomorphic development of the eastern United States up to the modern time period (Schlische, 2003). Post rift deformation is recorded in synrift basins and within post rift strata as normal faults seaward of the basement hinge zone and as contractional features landward of the basement hinge zone. Extensive normal faulting penetrates the post rift strata (and upper strata of the volcanic wedge) of the marginal basin overlying the volcanic wedge (Figure 2.5-10).

Contractional postrift deformation is interpreted to record the change in stress regime from horizontal maximum extension during rifting to horizontal maximum compression during passive margin drifting. The hypothesis that the change in stress regime following rifting was recorded in reverse and strike slip faulting and folding was known prior to the 1986 EPRI study (e.g., (Sanders, 1963) (Swanson, 1982) (Wentworth, 1983)), but significant advances in the documentation and characterization of the rift to drift transition and postrift deformation has occurred since the mid-1980s (Withjack, 1998) (Schlische, 2003).

2.5.1.1.4.1.3 Cenozoic Passive Margin Flexural Tectonics

Tectonic processes along the Atlantic passive continental margin in the Cenozoic Era include vertical tectonics associated with lithospheric flexure (Pazzaglia, 1993). Vertical tectonics are dominated by: (1) cooling of the extended continental, transitional, and oceanic crust as the spreading center migrates eastward, and (2) the erosion of the Appalachian Mountains to the Coastal Plain and extension of the Continental Shelf and Slope. Erosion and exhumation of the Allegheny crustal root of the Piedmont, Blue Ridge, Ridge and Valley, and Appalachian Plateau Provinces has been balanced by deposition on and loading of the Coastal Plain and offshore provinces by fluvial, fluvial-deltaic, and marine sediment transport (Pazzaglia, 1993). Based on models of the Cenozoic flexural deformation, surface material from the Appalachian Mountains erodes and is deposited on the Coastal Plain and Continental Shelf. The sediment is mainly deposited in the Salisbury Embayment and Baltimore Canyon Trough. The Fall Line is the axis for the depositional downward pressure and the uplift from the erosional environment. The elastic model has been reported to be as much as 33 ft (10 m) per million years of uplift in the Piedmont province (Pazzaglia, 1994). According to EPRI (EPRI, 1986), the Fall Line hinge zone is not considered as a tectonic feature.

2.5.1.1.4.1.4 Tectonic Stress in the Mid-Continent Region

The 1986 EPRI evaluation of plate tectonic stress in the BBNPP region is characterized by northeast-southwest-directed horizontal compression. As indicated in the subsequent studies, the tectonic stress created by the Mid Atlantic ridge forced stress orientation, shows uniform compression in northeast to southwest on the North America plate (Gough, 1983). Other potential forces acting on the North American plate are considered minor stress levels of magnitude and orientation. Regional tectonic stress in the CEUS since the EPRI study (EPRI, 1986) has not significantly altered the characterization of the northeast-southwest orientation of the maximum compressive principal stress. There has been no significant change in the understanding of the static stress in the CEUS since the publication of the EPRI source models in 1986, and there are no significant implications for existing characterizations of potential activity of tectonic structures.

2.5.1.1.4.2 Gravity and Magnetic Data and Features of the Site Region and Site Vicinity

Gravity and magnetic anomaly datasets of the site region have been published following the 1986 EPRI study. Regional maps of the gravity and magnetic fields are presented for North America by the Geological Society of America (GSA), as part of the Society's Decade of North America Geology (DNAG) project (Tanner, 1987) (Hinze, 1987) as shown in Figure 2.5-17 (Kucks, 1999) and Figure 2.5-18 (Bankey, 2002).

These maps present the potential field data at 1:5,000,000-scale, and show gravity and magnetic anomalies with wavelengths. Regional gravity anomaly maps are based on Bouguer gravity anomalies onshore and free-air gravity anomalies offshore. The primary sources of magnetic data reviewed for this BBNPP study are from aeromagnetic surveys onshore and offshore (Kucks, 1999). Large-scale compilations (1:2,500,000-scale) of the free-air anomalies offshore and Bouguer anomalies onshore were published in 1982 by the Society of Exploration Geophysicists (Lyons, 1982) (Sheridan, 1988). The DNAG magnetic anomaly maps were based on a prior analog map of magnetic anomalies of the U.S. published in the early 1980's (Zietz, 1982) (Behrendt, 1983) (Sheridan, 1988).

In addition, the DNAG Continent-Ocean transect program published a synthesis of gravity and magnetic data with seismic and geologic data (Klitgord, 1995). No gravity and magnetic data

published since 1986 reveal new anomalies related to geologic structures. The following sections discuss the gravity and magnetic anomalies.

2.5.1.1.4.2.1 Gravity Data and Features

Gravity data compiled at 1:5,000,000-scale for the DNAG project provide documentation of previous observations that the gravity field in the site region is characterized by a long-wavelength, east-to-west gradient in the Bouguer gravity anomaly over the continental margin (Kucks, 1999) (Figure 2.5-17). Bouguer gravity values increase eastward from about -80 milligals (mgal) in the Ridge and Valley Province of western Virginia to about +10 mgal in the Coastal Plain Province (Figure 2.5-17). Gravity highs, or positive anomalies, are created by abundant thickness while gravity lows are from mass deficiencies. The folded and faulted structures, basins, igneous intrusions, lithologic variations, and basement uplifts create variations in mass. Gravity anomalies occur from density contrast in size, depth, and structural depth. Long wavelengths show shallow structures or highly concentrated deep structures. Shorter wavelengths are created by shallower structures (Lavin, 1999). As shown on (Figure 2.5-17), gradient gravity extends from Canada to Alabama and parallels the Appalachian Mountains. The Mesozoic rift basins show gravity lows and northeast-trending border faults.

The gravity map also shows northeast-trending, long wavelengths of gravity highs and lows. The alignments are variations of thickness of the sedimentary rocks and crustal structures (Lavin, 1999). Low gravity dominates the western part of Pennsylvania and eastern Ohio, including areas such as Beaver Falls gravity lows and Somerset gravity high. The Chambersburg anomaly is another low, broad, northeast-trending gravity low which extends the length of the Appalachian Mountain system. In the northeast, the Scranton gravity high is surrounded by the Williamsport and Reading lows. The lows are deep Paleozoic sedimentary basin and/or increased crustal thickness. The Scranton gravity high is related to mafic material during late Precambrian rifting (Lavin, 1999). All anomalies were known at the time of the 1986 EPRI study.

2.5.1.1.4.2.2 Magnetic Data and Features

Magnetic data compiled for the 2002 Magnetic Anomaly Map of North America reveal numerous northeast-southwest-trending magnetic anomalies, generally parallel to the structural features of the Appalachian orogenic belt (Bankey, 2002) (Figure 2.5-18). The magnetic map allows a visualization of the geological structure of the upper crust in the subsurface showing the spatial geometry of bodies of rock and the presence of faults and folds. Prominent north- to northeast-trending magnetic anomalies in the BBNPP site region include the interior New York-Alabama, New Bloomfield high, subsurface nappes near Scranton and Allentown, anomalies over largely subsurface Proterozoic rocks at Reading Prong, Philadelphia and Lancaster, and an inferred basement fault located south of Pittsburgh (King, 1999). The 1,000 mi (1,609 km) long lineament in aeromagnetic maps of the eastern U.S. is referred to as the "New York-Alabama Lineament" (NY-AL) (Figure 2.5-18). The NY-AL primarily is defined by a series of northeast-southwest-trending linear magnetic anomalies in the Ridge and Valley province of the Appalachian fold belt. The NY-AL is located about 50 mi (80 km) northwest of the BBNPP site. Based on studies, the NY-AL is related to the Precambrian Greenville Front. The source of the lineament has interpreted the NY-AL to be a major strike-slip fault in the Precambrian basement beneath the thin-skinned, fold-and-thrust structures of the Ridge and Valley province and created a base model for the Appalachian fold belt (King, 1999).

The Clingman-Ocoee lineament is an approximately 750 mi (1,207 km) long, northeast-trending aeromagnetic lineament that passes through parts of the Blue Ridge and eastern Ridge and

Valley provinces from Alabama to Pennsylvania (King, 1999). The Clingman-Ocoee lineaments are sub-parallel to and located about 30 to 60 mi (48 to 97 km) east of the NY-AL. These lineaments are located about 50 mi southeast of the BBNPP site. The Clingman-Ocoee lineament also is interpreted to arise from a source or sources in the Precambrian basement beneath the accreted and transported Appalachian terrains (Nelson, 1983). The Clingman - Ocoee block is a Precambrian basement block bounded by the NY-AL and Clingman-Ocoee lineaments (Johnston, 1985b).

The Newark and Gettysburg rift basins consist of clastic rocks. The basins present magnetic anomalies consisting of elongated shaped bodies of diabase. The Mesozoic rocks have been downfaulted against Proterozoic and Paleozoic rocks. The Buckingham Mountain anomaly is produced by a fault-bound structure creating a northeast trending ridge, and dividing the Newark basin. The faults cut the Mesozoic rocks and bound small diabase sheets on the north, just as the larger sheets are bounded along the northern boundary fault. The Buckingham Magnetic high indicates a large subsurface ridge of magnetic Proterozoic rocks extending 15 mi (24 km) southwest (King, 1999).

Magnetic rocks occur in the Reading Prong and Blue Ridge. The Magnetic anomalies over the Reading Prong are produced by a complex of magnetite-rich, gneissic Proterozoic rocks at the surface. These rocks are related to the center of a nappe system that is over thrust from the southeast. Small anomalies occur east of Lancaster and are related to gneisses exposed in the Minde Ridge anticline and related structures. The magnetic data indicate similar rocks at shallow depths to the west toward Lancaster and to the east of the Honey Brook Upland, under the Triassic Basin (King, 1999). In summary, magnetic data published since the mid-1980's confirm and provide additional documentation of previous observations (i.e., pre-EPRI) across this region of eastern North America, and do not reveal any new anomalies related to geologic structures previously unknown to EPRI (EPRI, 1986).

2.5.1.1.4.3 Principal Tectonic Structures

Since the EPRI study (EPRI, 1986) was completed, new Late Precambrian through the Cenozoic tectonic features have been proposed and described in the site region, and previously described features have since been characterized in more detail. New features identified since the EPRI study (EPRI, 1986) in the BBNPP site region includes folds and faults of the BBNPP site (Pohn 2000) (Wheeler 2006).

In the sections below, specific tectonic features and their evidence for activity published since the EPRI (1986) study are discussed. No new information has been published since 1986 on any tectonic feature within the BBNPP site region that would cause a significant change in the EPRI seismic source model.

As reviewed, principal tectonic structures within the 200 mi (322 km) BBNPP site region are broken down into five categories based on their age of formation or most recent reactivation. These categories include Late Proterozoic, Paleozoic, Mesozoic, Tertiary, and Quaternary. Late Proterozoic, Paleozoic, and Mesozoic structures are related to major plate tectonic events and are mapped regionally on the basis of geological and/or geophysical data. Late Proterozoic structures include normal faults active during post-Greenville orogeny rifting and formation of the Iapetan passive margin. Paleozoic structures include thrust and reverse faults active during Taconic, Acadian, and Alleghenian orogenies. Mesozoic structures include normal faults active during break-up of Pangaea and formation of the Atlantic passive margin.

Tertiary and Quaternary structures within the BBNPP site region are related to the tectonic environment of the Atlantic passive margin. This passive margin environment is characterized by southwest- to northeast-oriented, horizontal principal compressive stress, and vertical crustal motions. In addition, tectonic feature zones not related to seismicity are also discussed in below sections.

2.5.1.1.4.3.1 Late Proterozoic Tectonic Structures

Plate tectonic activity has generated the structures of the BBNPP site region. The main orogeny episodes, Greenville orogeny, Late Ordovician Taconic orogeny, and the Alleghanian Orogeny at the end of the Paleozoic Era caused structural deformation (Section 2.5.1.1.4.1.1.1). Rifting occurred in the late Precambrian and into the Late Triassic to Early Jurassic. Within the 200 mi (322 km) site region, discrete Late Proterozoic features include the New York-Alabama Lineament (King, 1978) and The Rome Trough (Ervin, 1975).

Extended crust of the lapetan passive margin extends eastward beneath the Appalachian thrust front to the approximate eastern edge of Mesozoic extended crust within the eastern Piedmont physiographic province (Wheeler, 1996) (Figure 2.5-10). This marks the western boundary of major Paleozoic sutures that juxtapose Laurentian crust against exotic crust amalgamated during the Paleozoic orogenies (Wheeler, 1996). At its closest approach, the area of extended lapetan crust is located about 70 mi (113 km) northwest of the BBNPP site.

The earthquake potential of lapetan normal faults was recognized by the EPRI team members due to the association between the Reelfoot rift and the 1811 to 1812 New Madrid earthquake sequence (EPRI, 1986). According to Wheeler (Wheeler, 2005) and Crone (Crone, 2000), seismic zones in eastern North America include the Lancaster seismic zone of Reading, PA and Newberry, MA seismic zone, which are located inside and outside, respectively, of the BBNPP site region (Figure 2.5-15). No new information has been published since 1986 on any Late Proterozoic feature within the BBNPP site region that would cause a significant change in the EPRI study (EPRI, 1986) seismic source model.

2.5.1.1.4.3.2 Paleozoic Tectonic Structures

Structures within all seven of provinces are associated with high angle reverse faults, thrust sheets, and normal faults sutures that formed during transpressional Appalachian orogenic events of the Paleozoic Era. Paleozoic structures shown on Figure 2.5-15 are thrust faults, wrench faults, and strike-slip faults. The structures have shown deformation of large folds along subordinated structures resulting from buckling and flexural-slip folding of horizontal strata responding to a unidirectional horizontal compression (Faill, 1999). The strike of structures was oriented in a northeast-southwest direction along with an easterly dip in the Appalachian Mountain section (Figure 2.5-15). The thrust faults from basal décollement are predominantly located in the core of the anticlines and tend to be steeper and parallel to the overlying bedding in the southeast limbs of the anticlines which are low angles in the northwest limbs and cross the bedding. These thrust faults are located in the North American basement complex (Faill, 1999).

2.5.1.1.4.3.2.1 Appalachian Structures

Paleozoic faults within 200 mi (322 km) of the BBNPP site and catalog seismicity are shown on Figure 2.5-15 and Figure 2.5-16, respectively. Paleozoic faults with tectonostratigraphic units are also shown on Figure 2.5-15 and Figure 2.5-19. The stratigraphic description for the regional cross section in Figure 2.5-19 is shown in Figure 2.5-20. Faults mapped within the Appalachian provinces (Blue Ridge, Ridge and Valley) are discussed in this section. Paleozoic faults are

discussed below from west to east, across the BBNPP site region. Major Paleozoic tectonic structures of the Appalachian Mountains within 200 mi (322 km) of the site include the Yellow Breeches Fault Zone, Rome Trough, Pleasant Valley-Huntingdon Valley Fault, Plummers Island and Pleasant Valley Shear Zone, Light Street Thrust Fault, Ramapo Fault, Anthracite Region and Transylvania Fault Zone, Plummers Island and Pleasant Grove Shear Zone, and Light Street Thrust Fault (Figure 2.5-15). These structures are bound lithotectonic units as defined in recent literature (Inners, 1978) (Pohn, 2000) (Crawford, 1999) (Wheeler, 2005) (Wheeler, 2006).

2.5.1.1.4.3.2.1.1 Yellow Breeches Fault Zone

The northeast-striking Yellow Breeches Fault Zone is located within the northeastern portion of the Ridge and Valley Physiographic Province in southwestern Pennsylvania and extends to Virginia (Figure 2.5-15). The Martinsburg/Hamburg foreland segment is divided by the Yellow Breeches fault. The thrust rocks of Cocalico terrane are oriented northward and are part of the overturned limb of the Lebanon Valley nappe which occurred during the Alleghanian Orogeny (Pohn, 2000). The east-dipping Yellow Breeches Fault, part of the Reading Prong nappe megasystem, is shown as several miles in length (Figure 2.5-15). This décollement represents an upper-level detachment above a deeper décollement about 5 mi (8 km) deep (Fail, 1999). The Yellow Breeches fault is exposed in outcrops of the Ordovician St. Paul Group located within the Ridge and Valley Province. The Yellow Breeches fault zone is not considered a capable tectonic source. Based on published literature, no seismicity is attributed to the Yellow Breeches fault zone and published literature does not indicate that it offsets late Cenozoic deposits or exhibits geomorphic expression indicative of Quaternary deformation. Therefore, this Paleozoic fault is not considered to be a capable tectonic source (Wheeler, 2006).

2.5.1.1.4.3.2.1.2 Rome Trough

The Rome Trough is a Cambrian extensional graben system that extends from northern Tennessee, northeastward through Kentucky, West Virginia, and into western Pennsylvania. This northeast-trending graben, which underlies the Appalachian Plateau Province, is mainly characterized by normal faults of early Paleozoic age. On the other hand complex folds and thrust faults of late Paleozoic age characterize the eastern Appalachian Plateau (Kulander, 2005). Kulander and Ryder (Kulander, 2005) studied data from seismic lines across the Rome trough in West Virginia, western Maryland, and southwestern Pennsylvania. Basement-involved thrust faults have been reported in some parts of the Rome trough and attributed to regional compression dating 0.8-1.0 Billion years ago. Major normal movements along the Rome trough boundary faults occurred in the Early to Middle Ordovician, and no other movement seems to have occurred since then (Kulander, 2005). The details of basement structure in western Pennsylvania and interpretations of the faults accompanying the Rome trough are based on limited data (Ryder, 2002). However, as Kulander and Ryder (Kulander, 2005) indicate, the latest movements seem to have occurred in the Middle Ordovician. The association of this feature with seismicity is also limited. It is therefore concluded that Rome trough is not a capable tectonic source.

2.5.1.1.4.3.2.1.3 Pleasant Valley Huntingdon Valley Fault

Pleasant Valley-Huntingdon Valley Fault is the eastward continuation of the Cream Valley fault. The fault separates the Baltimore Gneiss, overlain by the Chickies and Ledger Formation on the north, from Wissahickonn Formation schist on the south. The fault was active during the post Ordovician period and located 120 mi (193 km) south of the site (Crawford, 1999). Major

subvertical northeast striking faults including the Brandywine Manor fault, Cream Valley fault, the Pleasant Valley-Huntingdon Valley Fault, and Rosemont fault, intersect through the blocks containing Greenville-age gneisses and juxtaposed them against younger rocks. The Pleasant Valley-Huntingdon Valley Fault borders the Piedmont Upland Section, Piedmont Lowland Section, and Gettysburg-Newark Lowland Section. Based on review of published literature and historical seismicity, there is no reported geomorphic expression, historical seismicity, or Quaternary deformation along the Huntingdon Valley Fault, thus this feature is not considered to be a capable tectonic source.

2.5.1.1.4.3.2.1.4 Anthracite Region

The Anthracite region, located within a northeast plunging syncline, is the most faulted area of the Appalachian Ridge and Valley province. The asymmetric basin is evident in the contrast between the northwestern and southeastern sides, in terms of the intensity and manner of production of folds and tectonic structures (Hornberger, 2004). The dominant faults consist of thrust faults, as part of the base décollement. The thrust faults are dominantly located in the cores of the anticlines. These faults tend to be low angle dipping and transect the bedding planes along the northwest limbs of the folds (Faill 1999). Other faults associated with these structures are steeply dipping and are parallel to the stratigraphic beds located in the southeast limbs of the anticlines. The fault system was active during the post Carboniferous period and located 20 mi (32 km) north of the site (Berg, 1980). Based on review of published literature and historical seismicity, there is no reported geomorphic expression, historical seismicity, or Quaternary deformation along the Anthracite region, thus this feature is not considered to be a capable tectonic source.

2.5.1.1.4.3.2.1.5 Transylvania Fault Zone

Transylvania Fault Zone, near the latitude 40° N extends from the Early Mesozoic Gettysburg Basin (Figure 2.5-15) in Pennsylvania, westward into Ohio and striking at roughly 270 degrees (Dodson, 2008). The fault system is located approximately 170 mi (274 km) west of the BBNPP site (Berg, 1980). The fault zone is mapped as large subvertical east-west trending faults extending through the Blue Ridge, Great Valley and Ridge and Valley provinces. Through the Appalachian Plateau, the fault zones are detected through subsurface records and geophysical studies. Root and Hoskins (Root, 1977) proposed a zone of east-west trending faults which extend from the eastern margin of the Blue Ridge to the Allegheny front near latitude 40° N, for about 75 mi (121 km). The fault zone transects strata nearly across the entire length of Pennsylvania. In the eastern part of the region two faults, 9 mi (14 km) apart, have been previously mapped for about 23 mi (37 km). These are Shippensburg and Carbaugh-Marsh Creek faults which extend east-west in parallel. Root and Hoskins (Root, 1977) describe the following faults in the zone: Sideling Hill, Breezewood, Everret gap, and Wills Mountain faults. Root and Hoskins (Root, 1977) do not consider the fault zone as a major transcurrent fault because the apparent strike-slip movement associated with the fault is no more than 2.5 mi (4 km). Root and Hoskins (Root, 1977) conclude that the Transylvania fault zone is a fundamental fracture, which possibly extends through the continental plate. The fault system originated in the Precambrian, and was reactivated during the Taconic Orogeny in the middle Ordovician and again in the Carboniferous Period during the Alleghanian Orogeny. The Transylvania fault also reactivated in the Early Jurassic (Root, 1977). This fault zone has been included by EPRI (EPRI, 1986) study teams as a tectonic feature but has not been associated with seismicity. Based on review of published literature and historical seismicity, there is no reported geomorphic

expression, historical seismicity, or Quaternary deformation along the Transylvania fault zone. Thus, this feature is not considered to be a capable tectonic source.

2.5.1.1.4.3.2.1.6 Plummers Island and Pleasant Grove Shear Zones

Plummers Island Shear Zone and Pleasant Grove Shear Zone are a series of thrust faults (Plummers Island fault, Pleasant Grove fault, Hyattstown fault and Martic fault) (Kunk, 2004). The faults strike in a northeast-southwest trend with a high angle westerly dipping orientation and are located in the south central Appalachians. The fault zones are located 175 mi (282 km) south of the BBNPP site (Kunk, 2004). The faults were active during the Acadian Orogeny in the Early Devonian period and reactivated in the Carboniferous period during the Alleghanian Orogeny, and are part of the south central Appalachians. Based on review of published literature and historical seismicity, there is no reported geomorphic expression, historical seismicity, or Quaternary deformation along the Plummers Island shear zone and Pleasant Grove shear zone. Thus, this feature is not considered to be a capable tectonic source (Wheeler, 2006).

2.5.1.1.4.3.2.1.7 Light Street Thrust Fault

Light Street Thrust Fault is the wedge fault located approximately 2 mi (3.2 km) west of the BBNPP site (Inners, 1978). The fault was active during the lower Devonian period. Based on studies, the fault dips to the south, at a small angle of 10 to 30 degrees to stratigraphic bedding. The strike of the fault has a northeast-southwest orientation. The fault is located in the north side of the Berwick anticlinorium and extends for about 20 mi (32 km) west of Berwick. The fault overlaps the Old Port and Keyser formations. Seismic reflection profiles indicate that the fault originated during the Triassic (Inners, 1978). Based on review of published literature and historical seismicity, there is no reported geomorphic expression, historical seismicity, or Quaternary deformation along the Light Street Thrust Fault. Thus, this feature is not considered to be a capable tectonic source.

2.5.1.1.4.3.3 Mesozoic Tectonic Structures

Based on the EPRI Study (EPRI, 1986), the rift basins occurring in the late Triassic to early Jurassic has created several earthquakes along eastern North America. The rift zone, developed within the breakup of Pangaea, created a series of exposed and buried rift. The basins are originated from previous structures from pre-existing orogenies (Withjack, 2005). The rift basins, developed during the breakup of Pangaea supercontinent as Africa and North America, rifted apart to form the modern Atlantic Ocean. The regions created multiple block-faulted uplifts adjacent to sediment-filled half graben-type valleys. The basins consisted of sedimentary rocks such as conglomerates, sandstones, and shale. The rocks were deposited during the movement of border faults which created the half graben relief and in turn released sediments into the adjoining basin area. Along the border fault large alluvial fans developed consisting of coarse material (sand, gravel and boulders) while toward the center of the basins, fine grained deposits of mudstone and shale were deposited. Within the 200 mi (322 km) BBNPP site region, rift basins with rift-bounding faults on the western margin include the exposed Culpeper, Gettysburg, and Newark basins (Figure 2.5-15).

Since the EPRI (EPRI, 1986) study, the location and dimension of the buried rift basins have expanded along the eastern North America based on field, seismic and drill-hole data (Whithjack, 2006) (Figure 2.5-15). Reactivation of faults occurs on the margin of the Mesozoic basins throughout Delaware, New Jersey and southern New York, and southeastern Pennsylvania.

Based on historical data, faults occurring with a north-northeast to northwest trend occur more frequently due to the release of stress along the mid plate shear stress (Dewey, 1999). No new data have been developed to demonstrate the Mesozoic basins are currently active (Crone, 2000) (Wheeler, 2005).

2.5.1.1.4.3.3.1 Newark-Gettysburg Basin

The Newark-Gettysburg (NG) Basin extends from southeast New York through New Jersey to southern Pennsylvania, and is located south approximately 60 mi (97 km) of the BBNPP site (Faill, 1973). NG Basin, one of the several Triassic basins in eastern North America, has been developed either by downthrown block and subsequent sediment deposition from the northwest and southeast direction or as fault-troughs or grabens faulting and sedimentation occurring at the same time. Newark and Gettysburg basins are two separate basins that formed the NG Basin. These two basins along with Culpeper Basin and Barbourville Basin (both in Virginia) are the remnants of a larger Triassic feature called Birdsboro Basin (Faill, 2004). Faults and folds have tilted and deformed the Birdsboro Basin in Early Jurassic (Faill, 2004). The Newark Basin is bounded to the northwest by Ramapo Fault system in northern New Jersey and connects (southward) to the Gettysburg Basin in Pennsylvania. Fault structures within the basin strike in the northeast direction. Border faults, normal faulting and wrench faulting are associated with the NG basin. Furlong Fault, Hopewell Fault and Chalfont Fault were generated by wrenching faulting in the NG basin (Root, 1999).

The Woodward-Clyde Group (EPRI, 1986) concludes that the Newark Basin is seismically limited but the basin may be responsible for the localization of events in the region. Seismicity occurs near the edges of the basin with two notable concentrations of earthquakes, one near the transition from the Newark Basin into the Gettysburg Basin, that corresponds to the Lancaster Seismic Zone (LSZ) south of the narrowest of the NG Basin (Armbruster, 1987); the other occurs near the Maryland-West Virginia border, outside the southern edge of the basin. Most well-located epicenters in the LSZ are located just outside the NG Basin (Scharnberger (2006) (EPRI (1986). Detailed description for the LSZ is provided in section 2.5.1.1.4.4.3.

2.5.1.1.4.3.3.2 Hartford Basin

The Hartford Basin of Massachusetts and Connecticut, is the largest Mesozoic-age graben in New England with two bound faults. East Border Fault extends about 130 mi (208 km) from Knee, New Hampshire to New Haven, Connecticut and further to Long Island Sound. The fault is located approximately 180 mi (290 km) east of the site. The fault strikes generally north and dips west, and changes in strike to north-northeast from central Connecticut toward southern direction (Wheeler, 2005). Stratigraphy at Farm River marsh, nearly 1 mi (1.6 km) inland from the Sound, showed the downthrown block of southeastern portion of the marsh with respect to northwestern portion coincided spatially with the buried trace of the fault, and has been active since 2000 years ago and reactivated in the present day compressional field (Wheeler, 2005).

Wheeler (Wheeler, 2005) argues that no fault surface has been reported within the overlying marsh deposits. In addition, the downthrown block shows the displacement across a wide slope as opposed to a sharp offset on a fault plane. The area also lacks evidence for sudden movements that would imply tectonic faulting. Wheeler (Wheeler, 2005) concludes that evidence of faulting has not been reported in Quaternary sediments of the Farm River marsh and accordingly classifies the East Border fault as Class "C". Seismicity has not been associated with the Eastern Border fault. Therefore, it is concluded that the Hartford Basin is not a capable tectonic source.

2.5.1.1.4.3.3.3 Connecticut Basin

The Connecticut Basin is the largest onshore Mesozoic-age graben in New England (Wheeler, 2005). From Long Island Sound in the south, the basin crosses through central Connecticut and Massachusetts and extends to southern New Hampshire in the north. The basin is located approximately 175 mi (282 km) northeast of the site. The series is called Newark Super Group. Sedimentation continued until the early Jurassic period during which, the basin also experienced intrusive volcanic activity (Bennington, 2006). The Connecticut Basin has been evaluated by Rondout Associates Inc. (RAI) tectonic team (EPRI, 1986) which considered the basin as seismically active. The Connecticut Basin feature defined by RAI contains the Moodus Seismic Zone. Even though seismicity has been associated with the Connecticut Basin, Quaternary activity has not been demonstrated for the structures within the basin or for its boundary faults. Therefore it is concluded that the Connecticut basin is not a capable tectonic source.

2.5.1.1.4.3.3.4 Everona Fault-Mountain Run Fault Zone

The Mountain Run Fault Zone is a regional geologic and tectonic feature of central Virginia, which extends from the eastern margin of the Mesozoic Culpeper basin near the Rappahannock River southwestward, to near Charlottesville, VA (Pavlides, 1986) (Pavlides, 1994). The fault zone that is located about 180 mi (290 km) southwest of the site, trends northeast and extends for 63 mi to 94 mi (100 km to 150 km) (Wheeler, 2006). The Fault zone forms part of the southeast boundary of Early Mesozoic Culpeper Basin. The Everona Fault occurs in close proximity to the Mountain Run Fault Zone (about 0.6 mi (1.0 km)) and has an estimated age of late Cenozoic (Crone, 2000) (Bobyarchick, 2007). The fault zone is a reverse fault that dips about 20° NW and truncates layers of rocks in the footwall of the Mountain Run fault zone (Bobyarchick, 2007). This small fault displaces the base of late Tertiary or Pleistocene gravel located about 0.6 mi (1.0 km) west of the Mountain Run Fault Zone (Wheeler, 2006).

Thrust faulting along the Mountain Run Fault Zone started at the end of Ordovician. Subsequent strike-slip movement in the fault zone occurred prior to middle Mesozoic, since undeformed basaltic dikes of Jurassic age cut the Mountain Run Fault Zone rocks (Pavlides, 1994). To the northeast, two scarps occur along the fault zone: (1) Mountain Run scarp, located on the southeast side of the Mountain Run extends for 8 mi (13 km), and (2) Kellys Ford scarp, located on the northeast part of Mountain Run Fault Zone, bounds the Culpeper Basin. Kelly Ford scarp is 1 mi (1.6 km) long and is related to the southeastern border fault of Mesozoic Culpeper Basin. Pavlides (Pavlides, 1994) argued that rugged topography of both scarps implies Cenozoic or possibly Pleistocene age. Based on the displaced saprolites in the area, Everona Fault is a structure of tectonic origin involving the basement, and is not confined to the overlying surficial deposits. (Bobyarchick, 2007).

Crone (Crone, 2000) and Wheeler (Wheeler, 2006) conclude that while the faulting at Everona is likely to be of Quaternary age, no Quaternary activity has been demonstrated for the feature. They classify the feature as Class "C", but mention that this feature did not have a detailed paleoseismological study to determine whether it has been a site of Quaternary earthquake. Additional investigation has been done for the North Anna Early Site Permit which shows that Mountain Run Fault Zone has not been active during the Quaternary. It is therefore concluded that Everona Fault-Mountain Run fault zone is not a capable tectonic source.

2.5.1.1.4.3.4 Tertiary Tectonic Structures

Some faults were active during the Tertiary Period within the 200 mi (322 km) BBNPP site region (Figure 2.5-15). These faults include the relatively well characterized Stafford Fault System and Brandywine Fault System.

2.5.1.1.4.3.4.1 Stafford Fault System

The Stafford fault system approaches within 180 mi (290 km) south of the site (Figure 2.5-15). The 42 mi (68 km) long fault system strikes approximately N35°E for a distance of 45 mi (72 km) along the west bank of the Potomac River in northeastern Virginia (Mixon, 1977). The Stafford Fault System consists of five northwest dipping, high-angle reverse faults and follows the inner margin of the Coastal Plain province. Four faults are Dumfries Fault Zone, Fall Hill Fault, Hazel Run Fault, and unnamed fault, and strike northeast. The fifth fault is the Brooke Fault Zone, northeast of the unnamed fault and toward the northernmost end; Brooke Fault Zone is named the Tank Creek Fault (Wheeler, 2005). The Stafford Fault System was originally activated in the Early Cretaceous time. The fault was reactivated at the Fall Hill Fault showing displacement in the Pliocene-Pleistocene sandy gravel, and Cretaceous strata (Mixon, 2000).

Recurrent movement has been demonstrated on the Stafford Fault System by displacements that decrease upward in the Coastal Plain (Mixon, 1977). None of the reports and maps used by Wheeler (Wheeler, 2005) documented Quaternary activity on any faults of the Stafford Fault System. The youngest movement, demonstrating late Tertiary activity, has been documented on the Fall Hill Fault, of the Stafford Fault System, which offsets Pliocene-Pleistocene sandy gravel (Wheeler, 2005). The Stafford Fault System was assigned to Class "C" based on lack of evidence of Quaternary slip.

Marple (Marple, 2004) suggested a significantly longer Stafford Fault System which extends from Fredericksburg, Virginia to New York City (Marple, 2004). It was proposed as part of a northeastern extension of the East Coast Fault System, previously postulated by Marple and Talwani (Marple, 2000). Existing data do not support the extended Stafford Fault System beyond its previous extent and, despite the suggested correlation of some historical earthquakes with the northern extension of the fault system by Marple and Talwani (Marple, 2000), seismicity data show a poor association between earthquake epicenters and extended segment of the Stafford Fault System.

Based on the foregoing discussion the Stafford Fault System may not be a capable tectonic source. However it was included as a source zone in the EPRI study (EPRI, 1986). The fault system has a probability of activity of 0.08 in both the Dames and Moore, and the LAW Engineering groups tectonic feature assessments. The numbers mainly reflect the low probabilities assigned by groups because of (1) poor association with seismicity and (2) lack of demonstrated Quaternary slip along the fault.

2.5.1.1.4.3.4.2 Brandywine Fault System

The Brandywine Fault System is located approximately 180 mi (290 km) south of the site and north of the Potomac River (Figure 2.5-15). The 12 to 30 mi (19 to 48 km) long Brandywine fault system consists of a series of en echelon high angle reverse fault segments with associated flexing of the overlying Coastal Plain sedimentary strata. The fault system trend north-northeast with displacement ranging from a few feet to 250 ft (76 m). The Brandywine Fault System consists of the Cheltenham Fault and Danville Fault (Cumbest, 2000). The Brandywine Fault System was active in the Cretaceous and middle Eocene and middle Miocene (Mixon, 1977).

The Brandywine Fault System is located 6 mi to 12 mi (10 km to 19 km) east of the Stafford Fault Zone and strikes roughly parallel to the fault system. Wheeler (Wheeler, 2005) considers Skinkers Neck and Brandywine as a single fault zone, southeast of Stafford Fault System. Compared to Stafford Fault System, the Skinkers Neck-Brandywine Fault Zone is less known and its boundary is shown by dashed line (inferred) in the map of Mixon, 2000 in (Wheeler, 2005). The last activity of the fault was during the Miocene. There is no seismicity associated and no evidence of Quaternary activity with the fault has been demonstrated. Therefore, the Brandywine Fault System is not considered as a capable tectonic source (Wheeler 2005).

2.5.1.1.4.3.5 Quaternary Tectonic Features

Quaternary tectonic features were recently studied by several authors and they compiled geological information on Quaternary faults, liquefaction features, and possible tectonic features in the CEUS. Crone (Crone, 2000) and Wheeler (Wheeler, 2005) (Wheeler, 2006) evaluated and classified these features into one of the following four categories.

Class A: Geologic evidence demonstrates the existence of a Quaternary fault of tectonic origin, whether the fault is exposed by mapping or inferred from liquefaction or other deformational features.

Class B: Geologic evidence demonstrates the existence of Quaternary deformation, but either (1) the fault might not extend deeply enough to be a potential source of significant earthquakes, or (2) the currently available geologic evidence is too strong to confidently assign the feature to Class C but not strong enough to assign it to Class A.

Class C: Geologic evidence is insufficient to demonstrate (1) the existence of tectonic faulting, or (2) Quaternary slip or deformation associated with the feature.

Class D: Geologic evidence demonstrates that the feature is not a tectonic fault or feature. This category includes features such as joints, landslides, erosional or fluvial scarps, or other landforms resembling fault scarps but of demonstrable nontectonic origin.

Within a 200 mi (322 km) radius of the BBNPP site, Crone (Crone, 2000) and Wheeler (Wheeler, 2005) (Wheeler, 2006) identified 8 potential Quaternary features (Figure 2.5-15). Work performed as part of the BBNPP investigation, including literature review, interviews with experts, and geologic reconnaissance, did not identify any additional potential Quaternary tectonic features within the BBNPP site region. The following sections provide descriptions of 8 potential Quaternary features identified by Crone (Crone, 2000) and Wheeler (Wheeler, 2005) (Wheeler, 2006). The 8 features evaluated for this BBNPP study are classified as Class C features.

The features are labeled with the reference numbers utilized in Figure 2.5-15:

- (15) Ramapo Fault System (Class C)
- (6) Kingston Fault (Class C)
- (5) New York Bight Fault (Class C)
- (9) New Castle County Fault (Class C)

- (3) Dobbs Ferry Fault (Class C)
- (4) Mosholu Fault (Class C)
- (25) Upper Marlboro Faults (Class C)
- (24) Furlong-Flemington Fault System (Class C)

2.5.1.1.4.3.5.1 Ramapo Fault System

The Ramapo Fault System is located in northern New Jersey and southern New York State, approximately 124 mi (200 km) north-northeast from the BBNPP site (Figure 2.5-15). This fault system consists of northeast-striking, southeast-dipping, normal faults and classified as border faults for the Mesozoic Newark Basin (Jacob, 2004) (Figure 2.5-15). Ramapo Fault System has a northeast strike and dips (approximately 70°) to the southeast. Although earlier tectonic episodes characterize parts of the Fault System evolution, it is best characterized as a normal, Mesozoic basin boundary fault (EPRI, 1986). Evidence of the repeated slip since Preterozoic time (including Mesozoic extensional reactivation) are contained in different faults of the system (Ratcliffe, 1971). Earthquakes have occurred in the general vicinity of the Ramapo Fault System. Many of the earthquakes have not been well located mainly because of poor seismic station distribution prior to 1970's. Therefore, while the association of earthquakes with the Ramapo Fault System is possible, the uncertainty in the locations allows the association with other structures in the area as well. Additional seismographs have been installed in the area of the Ramapo Fault since 1970's and a large amount of micro earthquake data has been recorded. Based on earthquake hypocenters and single event focal mechanisms, Aggarwal and Sykes (Aggarwal, 1978) inferred a reverse slip on a surface dipping 60°-65° southeast from the trace of the Ramapo Fault. The history of repeated slip during the Preterozoic and correlation of fault trend with epicenters, led Aggarwal and Sykes (Aggarwal, 1978) to conclude that the Ramapo Fault System is active. Based on the scattered epicenters, they also concluded that the seismicity was concentrated along a group of northeast-trending faults of which the Ramapo Fault appeared to be the most active. Yang (Yang, 1981) determined locations for 364 local earthquakes and derived focal mechanisms for 22 events in northeastern United States and adjacent Canada. He concluded that the Ramapo Fault System is probably the most active fault system in the greater New York City area.

Examination of small earthquakes and re-evaluation of some focal mechanisms in 1980's did not favor the association of the epicenters with the Ramapo Fault. Seborowski (Seborowski, 1982) studied a sequence of micro earthquakes near Annsville, New York, recorded during January, 1980, and derived a composite focal mechanism solution. Their solution indicated east-northeast compression resulting in thrust motion on a north-northwest striking fault plane. This direction is transverse to the northeast trend of the major structures in the epicentral region including the Ramapo Fault (Aggarwal, 1978). The dominant reverse mechanisms (Aggarwal, 1978) imply east-southeast maximum (horizontal) compressive stress. However, the maximum horizontal compressive stress trend throughout most of the eastern United States including the area of the Ramapo Fault System is east-northeast (Crone, 2000).

An improved 3-D velocity model (Thurber, 1985) which shows 10-15 percent velocity difference across the Ramapo Fault has changed some of the epicenters and depths of the earthquakes studied by Aggarwal and Sykes (Aggarwal, 1978). Kafka (Kafka, 1985) used earthquake data of the greater New York City area and refined the catalog to eliminate station and detection bias

from the network seismicity. They only considered the events recorded between 1974 and 1983, during which the configuration of stations remained stationary and type of recording devices did not change. This allowed for uniform measurement of magnitudes and earthquake locations. The results showed half of the earthquakes occurred about 6 mi (10 km) from the Ramapo Fault and, about half were located about 31 mi (50 km) from this fault, around the northern part of Newark Basin. Kafka (Kafka, 1985) concludes that "while the Ramapo Fault can by no means be ruled out as a possible source zone for earthquakes in the greater New York City area, the cause of earthquakes in this region is, in the final analysis, still unknown."

In general, even though the epicenters align along the Ramapo Fault, the association is less significant than the one suggested by Aggarwal and Sykes (Aggarwal, 1978). Therefore, the Ramapo Fault system seems to dominate the seismicity (Crone, 2000). Many earthquakes in the area have been attributed to the reactivation of the Ramapo Fault by the present-day compressional stress field. The results of core analyses (in the area of Ramapo Fault in New York and New Jersey) by Ratcliffe and Burton (Ratcliffe, 1984) are not consistent with the reactivation of Ramapo Fault and related faults in the present-day stress field.

Crone (Crone, 2000) also summarize a few reports that indicate some forms of Quaternary deformation near the Ramapo Fault but argue that none of the reports provide convincing evidence for Quaternary faulting or sudden offset which can be used to distinguish prehistoric seismic slip from a seismic creep. The Ramapo Fault or Fault System is probably capable of generating small or rare large earthquakes but it has been assigned to Class "C" feature since evidence for quaternary faulting has not been presented yet (Crone, 2000).

2.5.1.1.4.3.5.2 Kingston Fault

The Kingston Fault is located in central New Jersey, approximately 87 mi (140 km) east-southeast of the BBNPP (Figure 2.5-15). The Kingston Fault is 8 mi (13 km) long, north to northeast strike with a nearly vertical dip (Owens, 1995). The fault is located in the Mesozoic formation of the Newark Basin (Crone, 2000). Parker (Parker, 1990) showed the northern part of the fault trace on the map and reported a dip of 85° SE with extensional slip during the formation of the Basin in Mesozoic (Stanford, 1995). Results of well, boring, and geophysical data showed movement of southeast side of the fault based on the thickened Pliocene gravel across the fault. The Pliocene gravel that thickens across the fault is overlain by late Pleistocene gravel, which is not offset by the fault, indicating the fault probably moved during Pliocene or early to middle Pleistocene (Stanford, 1995). Quaternary activity for the fault can not be demonstrated and the fault slip rate is unknown. Additionally, no paleoseismological study has been performed on the thickness of the Pliocene gravel to determine seismic creep, or different episodes of seismic faulting (Crone, 2000). According to Wheeler (Wheeler, 2005), Kingston Fault was assigned to a Class "C" feature. No seismicity has been associated with the fault. Accordingly, it is concluded that the Kingston fault is not a capable tectonic feature.

2.5.1.1.4.3.5.3 New York Bight Fault

On the basis of seismic surveys, the New York Bight Fault is characterized as an approximately 31 mile (50 km) long, north-northeast-striking fault, located offshore of Long Island, New York (Schwab, 1997) (Hutchinson, 1985) (Figure 2.5-15), and parallel to the New Jersey coast (Hutchinson, 1985). Seismic reflection data of the fault showed at least 19 mi (30 km) and extended southward. Based on the results, the fault had offset Upper Cretaceous rocks and lower Tertiary and Quaternary deposits, therefore it may be as young as the Quaternary (Hutchinson, 1985).

The fault was mapped (Crone, 2000) along 24 mi (39 km) of its northern extension and dips almost vertically and was traced to within 6 mi (10 km) of the Long Island Coast (Lotto, 1997). Cretaceous to Eocene strata have been offset by the fault, but an unconformity which separates the Eocene and Miocene strata (and Miocene strata overlying it) are not offset sufficiently within the resolution of the available seismic profiles (Hutchinson, 1985). Ongoing seismic reflection work indicated that middle to late Quaternary sediments overlay Cretaceous and Tertiary strata at the fault (Lotto, 1997). These Quaternary sediments are not offset more than 3 ft (0.9 m) which is the resolution of the measurement (Crone, 2000).

The seismicity near the fault show small magnitudes (less than 3.00) have been located within 13 mi (21 km) from the fault. The location error for the offshore earthquakes exceeds 6 mi (10 km) for the offshore events (Yang, 1981) because of the seismic station distribution, therefore the location of these events is not reliable. Crone and Wheeler (Crone, 2000) and Wheeler (Wheeler, 2006) classify the New York Bight Fault Zone as a Class "C" feature, based on the lack of Quaternary activity evidence. Based on the information above, the New York Bight Fault is not a capable tectonic source.

2.5.1.1.4.3.5.4 New Castle County Faults

The New Castle faults are characterized as 146 mi (235 km) long buried north and northeast-striking faults that displace an unconformable contact between Precambrian to Paleozoic bedrock and overlying Cretaceous deposits. The faults are located in northern Delaware, near New Castle, about 150 mi (242 km) southeast of the BBNPP site (Figure 2.5-15). Based on research (Spoljaric, 1973), a graben is present in New Castle County with a northeastern strike near Delaware City. The graben is bounded by faults that are part of the basement fault that underlies the Coastal Plain of Northern Delaware. The bounded faults have shown displacements ranging from 32 to 98 ft (10 to 30 m) across the basement-Cretaceous boundary (Spoljaric, 1972). Along this fault zone, earthquakes have occurred and have showed magnitudes as high as 3.8. According to studies completed by the Delaware Geological Survey (DGS) (McLaughlin, 2002), a subsurface investigation utilizing seismic reflection and seismic refraction, subsurface drilling, geophysical logging and trench excavation was performed to potentially locate displacement from faults near New Castle, Delaware. No shallow faults were detected during the subsurface drilling program and trench excavation. Seismic section identified extensive faulting in the investigation site where the New Castle fault is projected. DGS concluded that minimal, if any, modern fault activities occurred in the area of New Castle County. Wheeler (Wheeler, 2005) characterizes the New Castle County faults as a Class C features. Based on McLaughlin (McLaughlin, 2002) there is strong evidence to suggest that the New Castle County Faults are not a capable tectonic source.

2.5.1.1.4.3.5.5 Dobbs Ferry Fault

The Dobbs Ferry Fault is located in Westchester County, New York about 6 mi (10 km) north-northeast of New York City (Wheeler, 2006). The fault is approximately 155 mi (249 km) east of the BBNPP (Figure 2.5-15). Dobbs Ferry fault zone is a zone of abundant fractures and joints that extends southeastward from the east bank of the Hudson River and crosses the Bronx River. The fault had dextral slip during the Mesozoic as part of the Pangaea separation (Crone, 2000). Different orientations of superimposed slickenside show more than one episode of slip on the fault. Sinistral slip can be inferred from the majority of slip sense indicators which is consistent with the present day, east-northeast, regional orientation of the maximum horizontal compressive stress. Some indicators are dextral and older, and perhaps date from Mesozoic extension (Seeber, 1998). The October 19, 1985, Ardsley earthquake occurred with a magnitude of 4.1

along with six aftershocks ranging from 4 to 4.5 in magnitude. The location of the first six aftershocks (within a week of the main shock) defined a vertical northwest trending rupture zone with an approximate diameter of 2300 ft (700 m) and a depth ranging from 2.8 to 3.4 mi (4.5 to 5.5 km). The rupture zone corresponds directly to a 0.6 mi (1 km) segment of the Dobbs Ferry fault (Hough, 1991). First motion data of the main shock and this group of aftershocks yielded well constrained focal mechanism solutions indicating sinistral slip on a northwest striking plane (Hough, 1991) (Crone, 2000). Later aftershocks defined a northeast striking plane. These results led Seeber (Seeber, 1998) to conclude that the earthquakes probably occurred on the fault zone. However, the earthquake did not rupture the surface along its trace. Crone (Crone, 2000) assigns the Dobbs Ferry fault zone to a class "C" feature because no paleoseismological evidence for Quaternary seismic activity has been reported for the fault. Therefore, the Dobbs Ferry Fault is not considered as a capable tectonic force.

2.5.1.1.4.3.5.6 Mosholu Fault

The Mosholu Fault is located in Bronx County, New York City, New York (Wheeler, 2006). The fault is approximately 135 mi (217 km) east of the BBNPP (Figure 2.5-15). The Mosholu Fault is 5.6 mi (9 km) long northwest trending right-lateral oblique-slip fault with a steep dip that crosses the Bronx River channel. Merguerian (Merguerian, 1996) suggested that the fault showed postglacial age uplift forming the buried ridge. The ridge caused the creation of a lake where clay settled in the Bronx River and overlay the glacial deposits detected north of the bedrock barrier. The fault has also been mapped and renamed by Baskerville (in Crone, 2000). The fault has been located by geological mapping and using subsurface data (Crone, 2000). Localized surface deformation of post glacial times may have occurred in the area where the Bronx River crosses the Mosholu Fault (Merguerian, 1997). The blockage of the Webster Avenue lowland, which has caused the diversion of Bronx River, resulted from neotectonic uplift of a block of bedrock along NE side of Mosholu fault. Crone (Crone, 2000) argues that while attributing the uplift to post glacial slip on the Mosholu fault, is not demonstrated. Merguerian (Merguerian, 1997) could not prove that the uplift occurred seismically. Additionally they mentioned that none of the previous New York City's magnitude ~ 5.0 earthquakes of 1737, 1783, and 1884 has been connected with surface blockage of crustal rocks. Merguerian (Merguerian, 1997) was not able to associate historic earthquakes with the faults in New York City area. However, based on the circumstantial evidence from the Bronx River, Merguerian and Sanders suggest that NW-trending faults in New York City area, such as Mosholu Fault and Dobbs Ferry Fault, are seismically capable. Earthquakes have not been associated with the Mosholu Fault and the fault has not been studied in detail for paleoseismological evidence of possible Quaternary activity. The Mosholu Fault has been assigned to class "C" by Crone (Crone, 2000) and it is not considered as a capable tectonic force.

2.5.1.1.4.3.5.7 Upper Marlboro Faults

The Upper Marlboro Faults are located in Prince Georges County, Maryland approximately 150 mi (241 km) southeast of the BBNPP site. The faults are a series of features, which cut the Coastal Plain sediments (Crone, 2000). The faults have a low angle dip, which is more consistent with a surficial origin, and extend to hypocentral depths (Crone, 2000). Wheeler (Wheeler, 2006) related the faults to surficial land slides based on low angle dips. The faults are assigned to Class "C" feature by Crone and Wheeler (Crone, 2000) and Wheeler (Wheeler, 2006) because no evidence of Quaternary activity has been presented for the faults. Seismicity has not been associated with the fault. Accordingly, the Upper Marlboro Faults are not considered as a capable tectonic feature.

2.5.1.1.4.3.5.8 Furlong-Flemington Fault System

Furlong Fault is located in the west portion of the Newark Basin, near New Hope in eastern Pennsylvania. This major intrabasinal Mesozoic fault connects to the north, with the Flemington fault in the New Jersey (Ratcliffe, 1988). It is located about 75 mi (121 km) southeast of the BBNPP. Furlong and Flemington faults have been considered as a fault system (Root, 1999). Ratcliffe and Burton (Ratcliffe, 1988) determined the Furlong fault zone using data from coring and surface observations and consists of two closely parallel faults that dip at 47° to 50° to the southeast. Structural analysis also indicated a normal fault with some component of strike slip for the Furlong fault. Many of the Mesozoic border faults, such as the Ramapo and Flemington faults, coincide with thrust Paleozoic faults. It seems that the reactivation of the Paleozoic thrusts by Mesozoic border faults controlled the overall structure of the basin (Ratcliffe, 1985). However, there is no indication or evidence of later activities for the fault system. Seismicity has not been associated with either Flemington or Furlong faults or with larger Chalfont Fault, which is intersected by Furlong Fault. Based on the lack of evidence of recent or Quaternary activity, Furlong-Flemington Fault System is not a capable tectonic source.

2.5.1.1.4.4 Seismic Sources Defined by Regional Seismicity

Within 200 mi (322 km) of the BBNPP site, several potential seismic sources are defined by a concentration of small to moderate earthquakes. Several authors, such as Crone and Wheeler (Crone, 2000), and Wheeler (Wheeler, 2005) (Wheeler, 2006), compiled geological information on Quaternary faults, liquefaction features, and possible tectonic features in the CEUS. Crone and Wheeler (Crone, 2000) and Wheeler (Wheeler, 2005) evaluated and classified these features into one of four categories. Within a 200 mi (322 km) radius of the BBNPP site, Crone and Wheeler (Crone, 2000), and Wheeler (Wheeler, 2005) (Wheeler, 2006) identified 13 potential Seismic Sources (Figure 2.5-15). The following sections provide descriptions of 13 potential Seismic Source features that were evaluated for this BBNPP study.

The features are labeled below with the reference numbers or figure location utilized in Figure 2.5-15 in paranthesis:

1. Saint Lawrence Valley (Not shown on drawing due to scale)
2. New York-Alabama Lineament (28)
3. Lancaster Seismic Zone (8)
4. Cacoosing Valley Earthquake Sequence (7)
5. Moodus Seismic Zone (1)
6. Clarendon-Linden Fault Zone (20)
7. Clinton-Newbury Fault Zone (21)
8. Hudson River Valley Trend (27)
9. Scranton Gravity High (Figure 2.5-17)
10. Fall Lines of Weems (26)
11. Offset Glaciated Surfaces (23)
12. Pittsburgh-Washington and Tyrone-Mt. Union Lineaments (30)

13. Bristol Block Geopotential Trends (31)

2.5.1.1.4.4.1 Saint Lawrence Valley

The Saint Lawrence Valley or St. Lawrence rift system is a seismically active zone parallel to the Saint Lawrence River which extends approximately 621.3 mi (1000 km) from Quebec to Newfoundland. The Charlevoix Seismic Zone, one of the most active seismic regions in eastern Canada is situated in the Saint Lawrence Valley. The Saint Lawrence Rift System, incorporating the Charlevoix Seismic Zone, has the potential for producing moderate to large earthquakes. The March 1, 1925 earthquake with an estimated magnitude between 6.0 to 6.5 M_b is the largest instrumentally recorded earthquake of the Charlevoix Seismic Zone. However, several other large earthquakes have been reported in the region since the first settlements (Bent, 1992). The extent of the Charlevoix Seismic Zone has been defined using instrumentally recorded data (Anglin, 1981). Hypocentral data with additional time has shown no migration of seismicity (Anglin, 1984) that is indicative of confinement of high activity to the same area. The EPRI study (EPRI, 1986) excludes the Charlevoix Seismic Zone from the Saint Lawrence Rift System and considers it as a separate seismic zone.

2.5.1.1.4.4.2 New York-Alabama Lineament

The New York-Alabama Lineament (NY-AL) is a northeast trending lineament characterized by aeromagnetic mapping and regional gravity data which extends more than 1,000 mi (1,609 km) from Alabama to New York (King, 1978). The NY-AL is approximately 30 mi (48 km) west of the BBNPP site. The NY-AL in Pennsylvania has been disrupted or offset between two major features called Tyrone-Mt. Union (TMU) lineament and Pittsburgh-Washington (PW) lineament (Lavin, 1982). TMU and PW crustal features define the boundaries of a northwest trending feature called Lake Erie-Maryland crustal block. A right-lateral offset of 38 mi (61 km) along TMU is indicated by disruption of NY-AL in southwestern Pennsylvania (Muller et al. in Lavin, 1982). Earthquakes have occurred at different locations along the feature and association with the feature cannot be established (EPRI, 1986). Johnston et al. (Johnston, 1985a) concluded that between 80% and 90% of southern Appalachian earthquakes (recorded from 1981 to 1983) lie between the NY-AL and a parallel structure to the southeast called Clingman lineament. Johnston et al. (Johnston, 1985a) further conclude that the NY-AL and the Clingman lineament do not appear to be seismogenic but rather bound by crustal block that generate the earthquakes. Appalachian seismicity occurs beneath the decollement which separates thrust and folded Paleozoic rocks from Precambrian basement rocks, indicating that Appalachian seismicity is not related to tectonic and geological features at the surface (Johnston, 1985b).

Kaufman and Long (Kaufmann, 1999) inverted travel time residuals from relocated earthquakes in southeastern Tennessee to obtain the velocity structure of upper crust. They stated that the results do not agree with the NY-AL as a linear feature extending through southeastern Tennessee parallel to contours in gravity anomalies. The southeastern Tennessee seismicity is not constrained by major crustal features but is rather associated with low velocity regions in midcrustal depths. Joint hypocenter-velocity inverted on the eastern Tennessee seismic zone suggest a strong low-velocity zone parallel to the seismicity with a northeast trend. The southern margin of this trend coincides with the NY-AL. According to Vlahoic (Vlahoic, 1998) research utilizing 3-D velocity earthquake, most earthquakes were located in regions of average velocity or small velocity anomalies and reject the association of eastern Tennessee seismicity with low velocity regions in the crust (Vlahoic, 1998).

2.5.1.1.4.4.3 Lancaster Seismic Zone

According to Armbruster (Armbruster, 1987), the Lancaster Seismic Zone (LSZ) is located in southeast Pennsylvania. The seismic zone is of circular shape with a diameter of about 31 mi to 38 mi (50 km to 61 km) and is 55 mi (88 km) south of the BBNPP site (Figure 2.5-15). The Lancaster seismic zones consist of short discontinuous north striking faults. The faults transect Triassic and Paleozoic rocks. The age of the faulting occurred during the early Mesozoic extension relating to the Atlantic margin. It also crosses the Newark-Gettysburg Triassic rift basin which consists of extensional faults associated with Mesozoic rifting. Most well-located epicenters in the Lancaster seismic zone lie directly outside the Gettysburg-Newark Basin (Scharnberger, 2006). The epicenters of 11 events with magnitudes 3.04 to 4.61 from 1889 to 1994 from the western part of Lancaster seismic zone define a north-south trend that intersects the juncture between the Gettysburg and Newark sub-basins (Armbruster, 1987). The highest earthquakes near the seismic zone were at Marticville in 1984 at a magnitude of 3.7 and Cacoosing in 1994 at a magnitude of 4.6. The earthquakes occurred 31 mi (50 km) apart and were related to tectonic fault lines. The Marticville earthquake occurred at a depth ranging from 3 mi to 9 mi (5 km to 14 km).

Prior to the January 16, 1994 Cacoosing Valley earthquake of magnitude 4.6, Modified Mercalli Intensity (MMI) VI-VII, the 1984 Martic earthquake was the largest recorded event of the zone. Ambruster and Seeber (Armbruster, 1987) suggested a seismogenic shallow fault (centered at 4.0 km depth) based on the hypocentral distribution and first motion data from several recorded earthquakes of the 1984 sequence. The 1984 rupture geometry (while not in correlation with the trend of Paleozoic structures in the epicenter area) conforms to the strike of the Jurassic dikes and their associated faults. Earthquakes in the zone may have been related with the Rockhill dike in particular (which bisects LSZ and is close to the 1984 rupture area), and its related faults (Armbruster, 1987). The January 16, 1994 Cacoosing Valley earthquake which struck the northeastern edge of the zone, is known to be the largest earthquake of the LSZ (Seeber, 1998). This earthquake has been discussed in detail in the historical seismicity section. As in the case of 1984 Martic earthquake, the 1994 Cacoosing Valley earthquake, and its aftershocks, provided seismological evidence for an active fault in the LSZ. The zone of the rupture, obtained from the aftershock locations, matched a nodal plane with reverse and left-lateral slip (strike 135°, dip 54° SW) of a focal mechanism obtained from aftershock first motions and main shock waveforms, but the rupture did not correlate with any of the mapped faults in the area (Seeber, 1998). The suggested faults, for both 1984 and 1994 earthquakes, were based merely on seismological evidence. In either case no geological evidence such as surface rupture or liquefaction has been found (Crone, 2000).

Some of the previous works summarized by Crone and Wheeler (Crone, 2000) indicate a seismically active fault, or fault zone, in the LSZ. Many studies provide evidence for high density north-striking, near surface structures and fracture zone in the LSZ. Spatial association of the epicenters in the LSZ with the area of these fractures (including the Fruitville Fault) has been shown by Armbruster and Seeber (Armbruster, 1987) and other researchers (e.g. Alexanders et al. in Crone, 2000), but they have not suggested that the association is causal. Many earthquakes nucleate at depths 5-15 km east of Rocky Mountains and faults of short length do not penetrate deep enough to reach the depth of 1984 earthquake or typical depth of earthquakes in central and eastern United States. The length of the Fruitville Fault is unknown and it has been interpreted with different lengths in different geological maps. It probably consists of one or a few short faults, which do not extend deep enough to reach the typical depths of the earthquakes in the region.

Some of these features of this seismic zone were explained in relation to the Newark Gettysburg Basin. The seismic zone, as defined by Armbruster and Seeber (Armbruster, 1987), is located about 55 mi (88 km) south of the site and has been a source of seismicity for more than 2 centuries. The zone approximately coincides with Lancaster County, Pennsylvania. It marks the southwestern edge of the Newark Basin Seismic Zone (NBSZ). Thrust faults and folds (formed during the Paleozoic Appalachian orogeny) and extensional faults (associated with Mesozoic rifting) are among the main structures along the NBSZ and LSZ. Regional Jurassic dikes, striking north-northeast, traverse the LSZ. Coinciding with brittle faults, many of these dikes are perhaps among the youngest structures in the region which persist as large planar zones of weakness and cut through the crust (Seeber, 1998).

No other evidence of Quaternary faulting (e.g., paleoliquefaction) in the LSZ has been reported and it has been assigned to Class "C" (Crone, 2000). Crone and Wheeler (Crone, 2000) note that even short and shallow faults can host earthquakes as demonstrated by unusually shallow seismicity of the LSZ. There might be other deeper geologic controls on seismicity which are reflected by the shallow faults of the LSZ (Wise, 1998). None of the EPRI study (EPRI, 1986) groups has considered the LSZ as a separate seismic source zone. However, the maximum magnitudes (ranges from 5.2 to 7.2) that have been assigned by the groups are larger than any reported earthquakes in the LSZ. Therefore, the maximum magnitude for the region in which the LSZ is situated adequately characterizes the seismic zone in terms of the upper bound magnitude.

As described above, Cacoosing Valley Earthquake sequence occurred along the eastern margin of the LSZ. Additional information relative to the earthquake is in section 2.5.1.1.4.4.3.1. Besides the LSZ, an additional seismic zone is described in section 2.5.1.1.4.4.3.2 and is known as the Moodus Seismic Zone which is located in Middlesex and New London County, Connecticut.

2.5.1.1.4.4.4 Cacoosing Valley Earthquake Sequence

The 1993 to 1997 Cacoosing Valley earthquake sequence occurred along the eastern margin of the Lancaster Seismic Zone with the main shock occurring on January 16, 1994, near Reading, Pennsylvania about 52 mi (84 km) south of the BBNPP site (Crone, 2000) (Figure 2.5-15). The maximum magnitude earthquake associated with this sequence is an event of magnitude 4.6 (Crone, 2000). Forty one (41) aftershock hypocenters occurred around the rim within 1 mi (1.6 km) diameter and a depth ranging from 0 to 2 mi (0 to 3.2 km) and orientation of N43° W and 54° SW. The main shock occurred at a depth of 1 mi (1.6 km) and aftershocks occurring from depth to surface (Seeber, 1998). The main shock occurred under an abandoned quarry. In December 1992, the quarry was allowed to flood with water rapidly. The unloading during the quarry process and increased pore pressure caused by subsequent flooding created the release of energy. However, the earthquake did not rupture the ground surface. Wheeler (Wheeler, 2006) defines the seismic event as a feature having insufficient evidence to demonstrate that no other faulting occurred in the Quaternary and assigns the Cacoosing Valley earthquake sequence as a Class "C" feature. Based on the findings of Seeber (Seeber, 1998), Wheeler (Wheeler 2005) interpreted this earthquake sequence to be unrelated to a capable tectonic source.

2.5.1.1.4.4.5 Moodus Seismic Zone

The Moodus Seismic Zone is located in Middlesex and New London County, Connecticut (Wheeler, 2005). The seismic zone is approximately 190 mi (306 km) northeast of the BBNPP (Figure 2.5-15). The town of Moodus is located about 20 mi (32 km) southeast of Hartford,

Connecticut. The area around the towns of Moodus and Haddam has been the most seismically active region in the Connecticut, and the earliest records of earthquake activity in the area dates back to the second half of the 16th century (Ebel, 1982). The largest historical earthquake occurred in 1791 and had estimated MMI in the range of VI-VIII (Ebel, 1982) (Crone, 2000). Four shallow microearthquakes occurred in the Moodus Seismic Zone in 1980's (Ebel, 1982) (Ebel, 1989). The seismic sources of the earthquakes were reviewed and utilized geological and geophysical methods (Koch, 1978) (Crone, 2000) but no causative fault has been identified (Crone, 2000). No evidence of liquefaction or paleoliquefaction has been found in the reconnaissance efforts in the Moodus area (Gelinas, 1993). Accordingly Crone and Wheeler (Crone, 2000) assign the seismic zone as a Class "C" feature. There is no new information about the seismic zone in Wheeler (Wheeler, 2005) compilation of possible Quaternary features of CEUS. Therefore, it is concluded that Moodus seismic zone is not a capable tectonic source.

2.5.1.1.4.4.6 Clarendon-Linden Fault Zone

A major north-south trending system of thrust faults forms the Clarendon-Linden fault zone. The fault zone is approximately 150 mi (241 km) from the BBNPP site (Figure 2.5-15) where it extends over 62 mi (100 km) from western New York State to northern Allegheny County (Fletcher, 1977) and, according to recent works into central Allegheny County, near the Pennsylvania border (Crone, 2000). The presence of a north-south striking fault was inferred from the surface geology of the area (Herrmann, 1978). Since then, the fault zone has been mapped geologically at the surface and characterized by geophysical methods such as seismic reflection at subsurface (Crone, 2000). The August 12, 1929 Attica earthquake, with an estimated magnitude of 5.2 (Street, 1977) and epicentral density of VIII, was located near the Clarendon-Linden Fault Zone. Herrmann (Herrmann, 1978) studied two other events (both with epicentral intensities VI) that occurred on January 1, 1966 and June 12, 1967 in the Attica region, and found shallow depth 1 mi to 2 mi (1.6 km to 3.2 km) for both events. The historical seismicity also shows a diffuse east-west trend that does not correlate with the north-south trend of the structure around Attica. Fault plane solutions for 1966 and 1967 events showed similar nodal planes for both events striking about 120° and 20°. The fault plane on the NNE nodal plane is parallel to the Clarendon-Linden structure (Herrmann, 1978).

There is no paleoseismological evidence of Quaternary slip on the fault zone so the zone has been assigned to Class "C" feature by Crone and Wheeler (Crone, 2000). Tuttle et al. (Tuttle, 2002) concluded that the Clarendon-Linden Fault Zone has not generated large events (moment magnitude, magnitude > 6) during the past 12,000 years. Based on the lack of earthquake-induced liquefaction features along the fault zone, including the area of the 1929 Attica earthquake, the fault zone is probably the source of the 1929 shock. Tuttle concluded that the Clarendon-Linden Fault Zone, is capable of producing future events of approximately magnitude 5 events.

2.5.1.1.4.4.7 Clinton-Newbury Fault Zone

The Clinton-Newbury Fault Zone are northeast trending faults that extend from Connecticut to New Brunswick. The fault zones are approximately 262 mi (422 km) northeast of the BBNPP site (Figure 2.5-15). Strike slip movements have been documented along the fault zone. The trend along this fault system has been the location of several moderate to large earthquakes (EPRI, 1986). Based on research, the fault zone has been assigned an activity probability of 0.2, since location uncertainties prevented association of the apparent trend of earthquakes with the trend of the tectonic feature. The stress information in the area of this tectonic feature was inconclusive (EPRI, 1986).

The Newbury area passes northeastern Massachusetts and has been the subject of some recent research. Crone and Wheeler (Crone, 2000) in their compilation of faults and tectonic features of central and eastern United States selected the name "Newbury Liquefaction Features" for the part of the structure located near Newbury (Essex County, MA) and assigned it to a Class "A" feature. They assign a feature to Class "A" when "Geologic evidence demonstrates the existence of a Quaternary fault of tectonic origin, whether the fault is exposed for mapping or inferred from liquefaction or other deformational features." Their reason for assignment to Class "A" was eyewitness reports of liquefaction during an earthquake in 1727 (MMI VII, Magnitude = 4.8) and sand dikes that were attributed to the 1727 earthquake. Tuttle and Seeber (Tuttle, 1991) concluded that the liquefaction was caused by strong ground motion but the causative fault responsible for the ground motion and liquefaction remains unidentified.

2.5.1.1.4.4.8 Hudson River Valley Trend

Also known as Hudson River Line (HRL), this feature trends north-south for about 156 mi (251 km) along the Hudson River Valley Trend. The feature is weakly associated with the western part of the isostatic gravity low at the New Jersey, border to the southeastern edge of Adirondack gravity high. Due to large uncertainty in subsurface geometry, the actual structure of the feature is not determined (EPRI, 1986). Based on early instrumentally recorded seismicity (Yang, 1981), the feature was seismically limited. Subsequent observations of seismicity indicate that few earthquakes are located along some parts of the trend. The moderate-sized earthquakes occur only near the edges of the feature. Therefore the overall seismicity does not indicate the localization of activity along the trend. Recent earthquakes west of the Hudson River range in estimated depth from 9 to 12 mi (14 to 19 km), indicating the possibility of a deep structure, but this is not supported by the isostatic gravity data (Yang, 1981). No evidence of the recent tectonic activity has been demonstrated and based on the forgoing discussion, the seismicity is only poorly associated with the feature. Therefore, it is concluded that HRL is not a capable tectonic source.

2.5.1.1.4.4.9 Scranton Gravity High

The Scranton Gravity High (SGH) is located underneath the BBNPP site. The SGH extends about 250 mi (402 km) from Albany, New York, to Harrisburg, Pennsylvania. The large gravity anomaly covers portions of the Appalachian Plateaus and Ridge and Valley Provinces (Hawman, 1992). There is no apparent spatial relationship to the seismicity and the seismicity in the area of the SGH is sparse. Earthquakes occur southeast of SGH in southeastern Pennsylvania and Western New Jersey but there is no localization of events along the feature (EPRI, 1986).

2.5.1.1.4.4.10 Fall Lines of Weems

Weems (Weems, 1998) identified numerous short stream segments or fall zones with steep gradients while examining longitudinal profiles of major rivers that flow southeastward or northwestward across the Piedmont and Blue Ridge provinces of North Carolina and Virginia. The northeastern tip of the Blue Ridge fall line is located about 140 mi (225 km) southwest of the BBNPP site. He noticed the alignment of fall zones of different streams and used the term "fall lines" for the curvilinear trend of the alignments. He defined seven fall lines that trend northeastward, paralleling the regional tectonic fabric and gravitational gradient of the Appalachian Orogeny. The fall lines tend to merge northeastward. Weems (Weems, 1998) states that "limited available evidence favors a neotectonic origin" for the fall lines and rules out climate control. Wheeler (Wheeler, 2005) argues that the identification of fall zones is subjective; therefore Weems (Weems, 1998) arguments and conclusions depend on the choice of the fall zones. Wheeler (Wheeler, 2005) concludes that tectonic faulting is not yet demonstrated for the

fall lines and assigns the fall lines to Class "C." The fall lines of Weems have not been associated with seismicity and they are not considered as capable tectonic features.

2.5.1.1.4.4.11 Offset Glaciated Surfaces

Small steeply dipping faults offset glacially smoothed rock surfaces at different locations in the northeastern U.S. including Maine, Massachusetts, New Hampshire, New York, and Vermont (Crone, 2000). The offset glaciated surfaces are located 75 mi (121 km) northeast of the BBNPP site. The offsets are small in the range of millimeter to decimeter with some exceptions of larger displacements. Crone and Wheeler (Crone, 2000) summarizes a few studies of localities in which such surfaces are located, but indicates that no systematic and comprehensive field or literature search has been done for such localities in the Northeast. Although some studies favor a tectonic origin over other frosting processes, frost heaving was likely origin for the offset glaciated surfaces (Crone, 2000). In Hudson River Valley of eastern New York, Quebec, and New Brunswick, the small faults show offsets that are uniform in size over distance and are parallel to the strike of cleavage in the heaved irregular size blocks. According to (Crone, 2000), tectonic origin of the small faults in the present-day stress field is unlikely because these small faults have been found in all directions (Crone, 2000). Ratcliffe (Ratcliffe, 1982) studied Paleozoic slates, which had been summarized, favoring frost heaving over recent tectonic activity as the origin of the examined small faults.

Crone and Wheeler (Crone, 2000) conclude that evidence supports frost-wedging more than any other process as the likely origin of small faults. Even by assuming a tectonic origin, these small faults do not penetrate deep downward and therefore do not have a significant effect on seismic hazard. Crone and Wheeler (Crone, 2000) mention that offset glaciated surfaces are Quaternary in age but classify them as Class "C" features based on the conclusion that the small faults with limited length and depth extent do not affect seismic hazard significantly. These small faults have been observed over a large area in 5 states and there has been no seismicity associated with them. Based on the available information and evidence, it is concluded that these small faults are not capable tectonic forces

2.5.1.1.4.4.12 Pittsburgh-Washington and Tyrone-Mt. Union Lineaments

These two major lineaments have been identified from analysis of regional gravity and magnetic patterns, LANDSAT images and geological data (Lavin, 1982). Trending NW-SE, they cross Appalachian orogen to the vicinity of Lake Erie (EPRI, 1986). Pittsburgh-Washington (PW) and Tyrone-Mt. Union (TMU) lineaments are expressions of deep crustal fracture zones which extend over a distance of 375 mi (604 km) across western Pennsylvania and parts of surrounding states. The PW-TMU lineaments are located approximately 115 mi (185 km) southwest of BBNPP site. Striking parallel to each lineament, TMU and PW lineaments are parallel and form NE and SW boundaries of the Lake Erie-Maryland crustal block respectively (Lavin, 1982). Major crustal displacements have occurred along the TMU lineament during late Cambrian to early Ordovician time. There is no concentration of seismicity along the TMU lineament. Evidence for displacement along PW lineament is not as strong as TMU. Concentration of seismicity has been observed near the northern end of PW lineament in northeastern Ohio but earthquake activity is not localized along the feature in general (EPRI, 1986). The PW and TMU features have been evaluated and the probability of activity for both features is very low (EPRI, 1986). Therefore, it is concluded that PW-TMU lineament system is not a capable tectonic source.

2.5.1.1.4.4.13 Bristol Block Geopotential Trends

The Bristol Block is an area of magnetic and gravity lows and extends from Tennessee to Pennsylvania. It is bordered by the New York-Alabama lineament on the west, and by the Clingman lineament on the east. The northern portion of the Block is located about 80 mi (129 km) southwest of the site (EPRI, 1986). It includes a series of low gravity and magnetic anomalies associated with some earthquakes, since these anomalies extend over a large area. Small earthquakes occur within this block but not all the tectonic features within the block are associated with earthquakes. Giles County, Virginia seismic zone, which is located within the Bristol block, has been considered separately as seismic source zone (EPRI, 1986).

2.5.1.2 Site Geology

The U.S. EPR FSAR includes the following COL Item in Section 2.5.1.2:

Site-specific geology information will be addressed by the COL applicant.

This COL Item is addressed as follows:

{Sections 2.5.1.2.1 through 2.5.1.2.6 are added as a supplement to the U.S. EPR FSAR.

2.5.1.2.1 Site Area Physiography and Geomorphology

The BBNPP site area is located within the Susquehanna Lowland Section of the Ridge and Valley Physiographic Province and is bordered by the Appalachian Plateaus Province to the west and north, and the New England Province to the east (Figure 2.5-7 and Figure 2.5-8).

The site area bedrock geologic map (Figure 2.5-23), compiled by Inners (1978), indicates that most of the site area surrounding, and including, the BBNPP site are underlain by Late Silurian, Devonian, and Lower Mississippian bedrock. Remnants of kame terrace and outwash (labeled as stratified drift deposits of sand and gravel outwash in Figure 2.5-9) are mapped as overlying site bedrock as shown in Figure 2.5-25. A geologic cross section of the site area, shown as Figure 2.5-24, indicates that the site bedrock is underlain by rocks of Lower Devonian and Upper Silurian age.

The topography within 5 mi (8 km) of the site consists of low to moderately high, linear ridges and valleys with elevations ranging from about 260 ft (79 m) to nearly 2,368 ft (722 m) msl (Figure 2.5-3). The site is well-drained principally by two streams, the first being Walker Run, which flows from North to South along the west border of the site. There is also a third unnamed, unmapped tributary that flows from east to west through the middle of the site, feeds the mapped wetlands area to the southwest of the site (as shown in Figure 2.5-4), and ultimately drains into Walker Run. As shown on the site area cross section, the ground surface above approximately 660 ft (21 m) msl is capped by outwash terrace deposits which are underlain by the Lower Devonian Mahantango Formation (Figure 2.5-24). The longest stream near the site is Walker Run which is approximately 2 mi (3.2 km) long and ultimately drains into the Susquehanna River. The ephemeral stream channels in the vicinity of the BBNPP site flow directly into the Susquehanna River. These stream channels maintain their dendritic pattern as they cut down into the underlying Trimmers Rock and Mahantango formations.

Confers Lane and PPL SSES form the eastern boundary of the BBNPP site. The SSES is located approximately 200 ft (61 m) above the Susquehanna River with a long, gradual slope

leading from the SSES to the banks of the river. To the north of the site, elevation increases significantly, to as high as 1,500 ft (457 m) at the peak of Lee Mountain. With the increase in elevation, the steepness in the slope, from the top of the mountain to the banks of the Susquehanna River, also increases to near vertical northeast of the site. Private property borders the BBNPP site to the immediate south and west. Approximately 7,000 ft (2,134 m) south of the site lays the Susquehanna River and approximately 10,000 ft (3,048 m) south of the site lays a steep embankment creating the base of Nescopeck Mountain, which reaches an elevation of approximately 2,368 ft (722 m) msl. The BBNPP will be constructed at a final grade elevation of 674 ft (205 m) msl and will be set back approximately 7,500 ft (2,286 m) from the Susquehanna River bank.

As described in Section 2.5.1.1.1, the area within a 5 mile radius of the site was formed toward the end of the Wisconsin glacial stage, which marked the end of the Pleistocene epoch. As glaciers retreated, huge volumes of melting ice fed the ancestral Susquehanna and Potomac Rivers, which eroded older deposits from the Susquehanna River Valley.

2.5.1.2.2 Site Area Geologic History

The site area geologic history prior to the early Ordovician is inferred from scattered borehole data, geophysical surveys and a synthesis of published information. Limited geophysical and borehole data indicate that the basement rock beneath the site most likely consists of a crystalline metamorphosed greenschist or amphibolite (Gold, 2008). Although the basement has not been penetrated directly beneath the site with drill holes, regional geologic cross sections developed from geophysical, gravity and aeromagnetic, as well as limited deep borehole stratigraphic data beyond the site area, suggest Precambrian (approximately +542 million years ago) rocks are most likely present at a depth of about 33,000 ft (10,058 m) beneath the site (as described in Section 2.5.1.1.3.1.1). Tectonic models discussed in Section 2.5.1.1.2 and Section 2.5.1.1.4 hypothesize that the crystalline basement was accreted to the pre-Taconic North American margin during the Greenville Orogeny.

As discussed in Section 2.5.1.1.3.1.1, the site area during the Cambrian era represents a time of carbonate rich sediment deposition. These sediments, deposited over a period of nearly 50 million years (approximately 542-488 million years ago), comprise the shales and limestones overlying the Cambrian basement. The depositional environment for the Cambrian bedrocks underlying the site is primarily a marine setting that was uplifted and later exposed to the erosional mechanisms associated with the Taconic Orogeny as described in Section 2.5.1.1.2.3 (Kauffman, 1999).

The site area during the Ordovician (approximately 488-444 million years ago) represented a chaotic timeframe in which the passive margin of the present day Atlantic Ocean became active, thrusting the ocean floor upon the North American plate. As discussed in Section 2.5.1.1.2.3, this timeframe is better known as the Taconic Orogeny. This mountain building event forced the site area back into a marine environment in which more siliciclastic sediment was deposited, creating the shale and sandstone units that outcrop in places throughout central Pennsylvania but underlie the site area by over thousands of feet (Thompson, 1999).

The continued erosion of the Taconic Mountains during the early part of the Silurian Period (444-416 million years ago) added to the sedimentation throughout the site area. This early period of sedimentation differed from that of the Ordovician, in that the sand and gravels deposited during the early Silurian were extremely quartz-rich in mineral composition (Barnes, 2002), thus creating

a very erosion-resistant sandstone. After the Taconic Mountains were almost completely eroded away during the Late Ordovician, carbonate sedimentation continued through the site area creating shale and limestone intervals (Laughrey, 1999).

The Devonian Period (approximately 416-359 million years ago) primarily marks the Acadian Orogeny (as discussed in Section 2.5.1.1.2.4), the result of the North American landmass colliding with current day Europe (Harper, 1999). The site area remained a basin area while the Acadian mountain range, to the east of the site area, was subjected to erosional processes. These eroded sediments were deposited in the site area and are represented by the modern day black and gray shales underlying the site (Barnes, 2002). As sedimentation from the Acadian Mountain range continued, what now constitutes the site area became an alluvial plain, which is displayed by the upward coarsening of sediment west of the site area (Barnes, 2002).

The Carboniferous Period (approximately 359-299 million years ago) is best described in two distinct categories including the older Mississippian and younger Pennsylvanian eras. The Mississippian (approximately 359-318 million years ago) was a time of continued sedimentation from the Acadian mountains but a change of meteorological climate is represented in the lack of oxidation of rocks from this time frame (Barnes, 2002). Near the end of the Mississippian the site and surrounding area likely became well drained and was an area of thick forests and swamps. During the early Pennsylvanian these forests deposited great amounts of organics which did not rot or oxidize due to the water rich environment of the swamps (Edmunds, 1999). These organics were then overlain by sediment deposits and compacted into the coal fields that occupy the Anthracite Valley Section to the north and the Anthracite Upland Section to the south of the site (Edmunds, 1999) (Figure 2.5-8).

During the Permian Period (approximately 299-251 million years ago) North America collided with Africa in what is known as the Alleghenian Orogeny (discussed in detail in Section 2.5.1.1.2.5). In addition to the Alleghenian Mountains, the orogeny formed numerous thrust faults, fractures, anticlines and synclines throughout Pennsylvania, including the site area (Barnes, 2002). By the end of the Permian Period, the Alleghenian Mountains were greatly eroded and the depositional sediments, from this erosion, settled into the alluvial plain that the site area had likely reverted to (Edmunds, 1999).

The Triassic (approximately 251-199 million years ago), Jurassic (approximately 199-145 million years ago), and the Cretaceous (approximately 145-65 million years ago) Periods were all time zones of slow erosional processes for many areas of Pennsylvania, including the site area (Barnes, 2002). During these periods of erosion, new drainage patterns and streams were formed. By the end of the Cretaceous Period, chemical erosion became the dominant erosional source of rocks that likely comprised the site area, changing them into clays and saprolite (MacLachlan, 1999).

Though there is little record as to what happened at or around the site area during the Cenozoic Period (approximately 65 million years to present), much can be inferred from the glacial deposits of the Quaternary Period (approximately 1.8 million years ago to present). It is believed that during the Tertiary Period (approximately 65-1.8 million years ago) erosion at the site area continued with chemical erosion primarily during the early Tertiary, but transitioning to intense physical erosion during the Late Tertiary (Barnes, 2002). This physical erosion was the result of cooler and drier conditions. It is also believed that during this time many of the modern day rivers and streams, such as the Susquehanna, established themselves (Sevon, 1999). During the Quaternary, continental glaciers covered Canada and advanced into a small portion of

Pennsylvania, including the site area as shown in Figure 2.5-9. The site area was subjected to three different periods of glaciation with the earliest occurring approximately 800,000 yrs ago and the most recent occurring approximately 24,000 yrs ago. These periods of glacial advance and retreat had both erosional and depositional effects on the site area, the degree of which is truly immeasurable. The main effect of glaciation on the site area was enhancing drainage changes that were already in progress (Sevon, 1999). During and after glacial retreat, the site has been an area of deposit for stratified drift which includes sand and gravel, kame terraces, and outwash (Figure 2.5-25 and Figure 2.5-26).

2.5.1.2.3 Site Area Stratigraphy

Site specific information on the stratigraphy underlying the BBNPP site is limited by the total depths of the various borings advanced by site investigators and by investigations of neighboring outcrops over the years (SSES FSAR, 2003). A total of 250 exploratory borings were made in soil and rock in late 1970, Spring 1971, and in 1983 at or near the SSES site. Additionally, test pits were excavated at selected locations at or near the SSES site. The deepest boring known to have been advanced at the BBNPP site is boring B-301 which was drilled to a total depth of 400 ft (122 m) and completed as a geotechnical boring during the site investigation on October 11, 2007. This boring is further discussed in Section 2.5.4.2.2.2 and penetrates the full Quaternary overburden stratigraphic section and intersects the contact between the overburden and the Middle Devonian Mahantango Formation. The basement rock in Pennsylvania is limited to the exposed metamorphic rock in the Piedmont Physiographic Province and several exploratory wells in western Pennsylvania (Saylor, 1999). As discussed in Section 2.5.1.1.3.1.1, there are no known borings that have reached the basement rock in the site area but based on available data (Saylor, 1999), it is assumed that the basement rock beneath the site is likely to be similar to the schists and gneisses found in the Piedmont Physiographic Province approximately 50 mi (80 km) to the southeast of the BBNPP site (Figure 2.5-7). Many of the borings completed during the BBNPP site investigation were drilled to 100 ft (30 m) in total depth, four were advanced to a total depth of 200 ft (61 m), and eleven were drilled to 70 ft (21 m) as discussed in Section 2.5.4.2.2.2.

The BBNPP site is located on stratified drift sediments, mainly Holocene in age, which were deposited capping the Middle Devonian bedrock. The cross section of the site area, Figure 2.5-24, is based on field mapping conducted by the U.S. Geological Survey (Inners, 1978).

Rocks of the Ridge and Valley Province are representative of formations deposited in a foreland basin that have undergone numerous cycles of marine regression/transgression. The Province extends from eastern New Jersey to Alabama and has been subjected to multiple orogenies as stated in Section 2.5.1.1.2. Due to a general lack of deep drill borings in and around the site area (subsurface exploration is discussed in Section 2.5.4.2.2.2 in greater detail and explains the basis for the required depth of borings), stratigraphy of the site area is inferred based on numerous publications. Stratigraphic formations, and their depositional environments, are also discussed in Section 2.5.1.1.3 and 2.5.1.1.2. A site specific stratigraphic column was created for this report and shown in Figure 2.5-21.

2.5.1.2.3.1 Cambrian Formations

The oldest inferred Cambrian Formation underlying the site area is the Waynesboro Formation. The Waynesboro Formation consists of sandstone with interbedded red and green shales and has a thickness of approximately 1,000 ft (305 m) or more (Kauffman, 1999). Overlying the Waynesboro Formation is the Pleasant Hill Formation, which is primarily a limestone formation with interbedded sandy and silty layers throughout (Kauffman, 1999). Overlying the Pleasant Hill

Formation is the Warrior Formation. Defined by Kauffman (1999) it is a dark, fossiliferous, fine grained limestone interbedded with silty dolomite with a thickness up to 1,340 ft (408 m). Overlying the Warrior Formation, and marking the Cambrian-Ordovician boundary, is the Gatesburg Formation. The Gatesburg Formation consists of a series of sequential sandstone and dolomite units that are also fossiliferous (Ryder, 1992) that are in excess of 1211 ft (369 m) (Gold, 2003). Both the Warrior and Gatesburg formations likely represent a shallow-water carbonate bank or shelf that was subjected to periodic episodes of near-drying conditions (Kauffman, 1999).

2.5.1.2.3.2 Ordovician Formations

Overlying the Gatesburg Formation are formations that comprise the Beekmantown Group. These Early Ordovician formations, from oldest to most recent, include the Stonehenge Formation, Nittany Dolomite, Axemann Limestone, and Bellefonte Dolomite. They are composed primarily of dolomite-limestone (Harper, 2003) and reach a combined thickness of up 4,200 ft (1,280 m) (Thompson, 1999). The Middle Devonian time period of the site area is best described as the Loysburg Formation. The Loysburg Formation is typically a dolomitic and stromatalite rich limestone underlying a coarse grained, fossiliferous limestone (Thompson, 1999) with an average thickness of 263 -475 ft (80-145 m). Overlying the Loysburg Formation, and representing the first unit (in ascending unit) of the Upper Ordovician, is the Black River Group that mainly consists of Snyder and Linden Hall formations (Thompson, 1999) and attains a thickness of about 632 ft (193 m). These formations are composed primarily of siliciclastic clay and shale and underlay the fine-grained, black, graded limestone-shale of the Solona and Coburn formations of the Trenton Group (Thompson, 1999). Rocks of the Beekmantown Group, Loysburg Formation, Black River Group, Solona Formation, and Coburn Formation were deposited in marine to marginal-marine environments. Where a platform existed and the seas over top of this platform shallowed progressively, depositional environments became more intertidal (Thompson, 1999). The upper most units within the Trenton Group is the Antes Formation, a fossiliferous, generally black, shale (Thompson, 1999) that was likely deposited in shallow water, above the wave base. The Antes, Coburn, and Salona formations collectively attain a thickness of approximately 842 ft (257 m).

Above the Trenton Group lies the Reedsville Shale. Overlying the Reedsville Shale are the Bald Eagle and Juniata Formations (in ascending order). The Reedsville, Bald Eagle, and Juniata formations represent the uppermost units of the Upper Ordovician period. The Reedsville Formation, with a thickness of approximately 600-1800 ft (183-549 m) (Thompson, 1999)(Gold, 2003), is comprised mainly of interbedded shale and sandstone beds with some limestone (Thompson, 1999) and, like the Antes Formation underlying it, was likely deposited in shallow water. The Bald Eagle Formation and the Juniata Formation, which are 700-1313 ft (213-400 m) and 600-1,125 ft (183-343 m) thick respectively (Gold, 2003)(Thompson, 1999), are both represented by nonfossiliferous sandstones, conglomerates, and mudstones but differ in color with the Bald Eagle being gray and the Juniata red (Thompson, 1999). Unlike the Reedsville Shale, the Bald Eagle and Juniata Formations are non-fossiliferous and non-marine, leading their depositional environment to likely be that of low sinuosity streams on alluvial fans (Thompson, 1999).

2.5.1.2.3.3 Silurian Formations

The Tuscarora Formation typically marks the boundary between Upper Ordovician and Silurian Formations. The Lower Silurian Tuscarora Formation is quartzose, sublithic, and argillaceous sandstone with few shale beds throughout (Laughrey, 1999). The thickness of the Tuscarora

Formation ranges between 400 ft (122 m) and 700 ft (213 m), is extremely resistant to erosional processes, and generally represents a fluvial depositional environment (Laughrey, 1999 and Gold, 2003). Overlying the Tuscarora Formation (in ascending order) are the Rose Hill, Keefer, Mifflintown, Bloomsburg, Wills Creek, Tonoloway, and Keyser formations.

The Rose Hill Formation is olive shale with interbedded layers of hematitic sandstone, purplish shale, and fossiliferous limestone (Laughrey, 1999). Above the Rose Hill Formation lies the Keefer Formation, a quartzose and hematitic sandstone with some mudstone. The Rose Hill and Keefer formations combine for a thickness that ranges between 600 ft (183 m) and 670-1070 ft (204-326 m) (Gold, 2003). The Mifflintown Formation reaches a thickness of about 336 ft (102 m) (Gold, 2003) and is composed of mudrocks and limestone of a shallow marine setting (Laughrey, 1999). The likely depositional environment for the Rose Hill, Keefer, and Mifflintown formations is that of a submarine ramp that deepened from the proximal basin margin (Laughrey, 1999) during the Taconic Orogeny as discussed in Section 2.5.1.2.3 and Section 2.5.1.1.2.3.

Conformably overlying the Mifflintown Formation is the Bloomsburg Formation (the oldest identified formation in Figure 2.5-24), a grayish-red clay-siltstone with some interbedded fine to coarse grained sandstone that ranges in thickness from 85 ft (26 m) to 464 ft (141 m). The Bloomsburg Formation is very slightly fossiliferous and probably represents sediments deposited in deltaic waters with a high enough salinity to allow some fauna to exist (Laughrey, 1999). The Wills Creek Formation, conformably overlying the Bloomsburg Formation, is mostly a claystone to silty claystone with some argillaceous limestone and has an approximate thickness of 750 ft (229 m) (Inners, 1978). The Tonoloway Formation is primarily a thinly-bedded limestone with a few thin beds of calcareous shale (Laughrey, 1999) with a thickness of about 100 ft (30 m) (Inners, 1978). Both the Wills Creek and Tonoloway formations represent numerous shallowing-upward cycles that have been interpreted as repeated progradational events on very large tidal flats (Laughrey, 1999).

The Keyser Formation conformably overlies the Tonoloway Formation and is mainly a gray, fossiliferous limestone with some dark gray cherty nodules present toward the upper part of the formation. The Keyser Formation straddles the boundary between the Late Silurian and Early Devonian as the formation represents continuous carbonate sedimentation from both periods and has a thickness of about 125 ft (38 m) (Inners, 1978).

2.5.1.2.3.4 Devonian Formations

The Devonian system of rocks is described by Harper (Harper, 1999) as a westward-thinning wedge of sediments with a thickness of almost 11,000 ft (3,353 m) throughout much of Pennsylvania. As stated in Section 2.5.1.2.3.3, the Upper Keyser Formation, makes up the basal unit for the Devonian period formations. Overlying the Keyser Formation is the Old Port Formation, which consists of (in ascending order) the Corriganville Limestone, the Mandata Shale, Shriver Chert, and Ridgeley Sandstone (Harper, 1999). The Corriganville Limestone, which consists of finely crystalline, thick to thinly bedded limestone, ranges from 10 ft (3 m) to 30 ft (10 m) thick (Harper, 1999). The Mandata Shale is dark gray to black, thinly bedded, siliceous shale, and ranges in thickness from 20 ft (6 m) to 100 ft (30 m) (Harper, 1999). Light colored cherty, mudstones and calcareous siltstones characterize the Shriver Chert (Harper, 1999), which ranges in thickness from 80 ft (24 m) to 170 ft (52 m). The Ridgeley Sandstone ranges in thickness from 8 ft (2 m) to 170 ft (52 m) and is generally white to light-gray, medium grained, quartzose sandstone (Harper, 1999). These units of the Old Port Formation represent the gradual deepening of the Appalachian basin as discussed in Section 2.5.1.1.2 and range in

overall thickness within the site from 100 ft (30 m) to 150 ft (46 m) (Inners, 1978). Overlying the Old Port Formation disconformably is the Onondaga Formation which reaches a thickness of about 175 ft (53 m) (Inners, 1978). The Onondaga Formation consists of silty, shaley, and cherty limestones, in ascending order, and likely represents a shelf margin depositional environment (Harper, 1999).

The middle unit of the Middle Devonian rock system is the Marcellus Formation. The Marcellus Formation, part of the Hamilton Group, consists of approximately 350 ft (107 m) (Inners, 1978) of dark-gray to black shales that are carbonaceous, containing pyrite and few fossils (Harper, 1999). The Marcellus Formation, likely deposited in a variety of shallow-water anoxic environments (Harper, 1999), underlies the Mahantango Formation, which is the immediate bedrock of the BBNPP site, as seen in Figure 2.5-21. Harper (1999) describes the Mahantango Formation as "a complex series of interbedded shales, siltstones, and sandstones ranging from 1,200 ft (366 m) to 2,200 ft (671 m)" although Inners (1978) reports a site specific thickness of approximately 1,500 ft (457 m). The shales and siltstones encountered during the BBNPP site investigation were typically dark gray, ranged in hardness from soft to moderately hard, increased progressively in the level of calcareous content with depth, and were slightly pyritic and fossiliferous throughout. Harper (1999) suggests that the Mahantango Formation deposited as a prograding marine shoreline during the early stages of the Catskill Delta. While the Mahantango Formation is the immediate bedrock of the site, other formations that were deposited after the Mahantango Formation exist within the site area. These formations comprise many of the outcrops and bedrocks of Lee Mountain, to the north of the site, and Nescopeck Mountain, to the south of the site.

Conformably overlying the Mahantango Formation and marking the initial unit of the Upper Devonian within the site area is the Harrell Formation. The Harrell Formation is typically represented by dark colored, organic-rich shales (Harper, 1999) which reach about 120 ft (37 m) in thickness (Inners, 1978). The Trimmers Rock Formation, referred to as the Brallier Formation by Harper (Harper, 1999), is primarily medium to dark gray, thinly bedded siltstones with some fine grained sandstones and few layers of subfissile shale (Inners, 1978; Harper, 1999). The Trimmers Rock Formation has a calculated thickness of approximately 3,000 ft (914 m) (Inners, 1978) and likely represents a delta fed submarine slope of the Appalachian Basin. Above the Trimmers Rock Formation, within the site area, lie the members of the Catskill Formation including (in ascending order) the Irish Valley, Sherman Creek, and Duncannon Members. Each member of the Catskill ranges in thickness from 150 ft (46 m) to 3,700 ft (1,128 m) and generally consists of gray to red mudstones, claystones, siltstones, and conglomerates that were deposited in mixed continental, fluvial-deltaic, and marginal-marine environments (Harper, 1999). The uppermost unit of Devonian age rocks in the site area is the Spechty Kopf Formation, which also spans into, and identifies the beginning of the Carboniferous Period. The Spechty Kopf Formation has a thickness of about 575 ft (175 m) (Inners, 1978) and is comprised mainly of medium gray to olive sandstone with other components including siltstone, shale, and conglomerates (Berg, 1999). The likely depositional environment of the Spechty Kopf Formation was that of ephemeral lakes formed on the surface of the Catskill alluvial plain (Berg, 1999).

2.5.1.2.3.5 Carboniferous Formations

Carboniferous formations are commonly broken down into the Mississippian Epoch and the Pennsylvanian Epoch. While Mississippian rocks of the site area represent a transition from the prograding deltas of the Late Devonian (Brezinski, 1999), Pennsylvanian rocks primarily

represent the sedimentation within an elongate basin aligned in a northeast to southwest direction (Edmunds, 1999).

The Mississippian is marked by the presence of the Spechty Kopf Formation, which is described in further detail in Section 2.5.1.2.3.4. Unconformably overlying the Spechty Kopf Formation is the Pocono Formation, which was likely deposited on a high-gradient alluvial plain or alluvial fan, is represented by the non-red beds of medium to coarse grained sandstone, siltstone, and conglomerates (Brezinski, 1999) with a thickness of about 600-650 ft (183-198 m) (Inners, 1978). Overlying the Pocono Formation within the 5 mile site area radius, is the Mauch Chunk Formation, easily recognizable by its red to reddish-brown mudstone and siltstone with reddish-brown and greenish-gray sandstones and conglomerates (Brezinski, 1999). The Mauch Chunk ranges in thickness throughout the site area but has been estimated to be between 3,000 ft (914 m) to 4,000 ft (1,219 m) thick (Brezinski, 1999). The depositional environment of the Mauch Chunk Formation was likely that of a broad alluvial plain in which deposits came from two distinct sources. The first source was red clastics, likely derived from the taconic highlands, and the second was the non-red, quartz sand from the erosion of the previously deposited sandstones (Brezinski, 1999).

The Mississippian-Pennsylvanian boundary in the site area is generally the top of the Mauch Chunk Formation and bottom of the Pottsville Formation. The Pennsylvanian Pottsville Formation overlies the Mauch Chunk Formation conformably and ranges in thickness from 100 ft (30 m) to 1,600 ft (488 m) (Edmunds, 1999). The Pottsville Formation consists mainly of a cobble and pebble conglomerate with some sandstones and finer clastics and coal (Edmunds, 1999). The youngest rock formation within a 5 mile radius of the site area, and overlying the Pottsville Formation, is the Llewellyn Formation. The Llewellyn Formation reaches a thickness of approximately 3,500 ft (1,067 m) through other portions of Pennsylvania and generally consists of subgraywacke clastics, ranging from conglomerates to clay shale and containing numerous coal beds (Edmunds, 1999). The Llewellyn Formation forms the uppermost geologic unit within the 5 mile radius of the site, appearing at the Peak of Lee Mountain near the town of the Shickshinny, as seen in Figure 2.5-27.

2.5.1.2.3.6 Quaternary Formations

Quaternary deposits of the site area are primarily the result of glacial deposits from at least three known glacial events that are believed to have impacted the site area. Of these three events, Quaternary deposits from two of them comprise the soil overburdens present within the site area. The earliest deposit is of Late Illinoian age and can be stratigraphically correlated to that of the Titusville Till in Northwestern Pennsylvania, as seen in Figure 2.5-9. The Titusville Till is described as a thin, gray to brown and grayish-red clay and sand (Sevon, 2000). This was almost entirely eroded away during the next period of glaciation through the site, the Wisconsinan (Crowl, 1999). The resulting glacial deposits from the Wisconsinan event is known as Olean Till, which is described as moderately thick, gray to grayish-red sandy till (Sevon, 2000). In addition to glacial till, the site area has also been impacted by stratified drift, as seen in Figure 2.5-9. Stratified drift, as defined by Sevon (2000) is sand and gravel in eskers, kame terraces, and outwash. Stratified drift has been impacting the site area since the Late Illinoian (Sevon, 2000), during glacial melts/retreats, and continues to deposit along the banks of the Susquehanna River from upstream (Inners, 1978).

2.5.1.2.4 Site Area Structural Geology

The local structural geology of the BBNPP site described in this section is based primarily on a summary of published geologic mapping, aeromagnetic and gravity surveys, detailed lithostratigraphic profiles along the Berwick Anticlinorium, results of earlier investigations performed at the SSES site, as well as BBNPP site reconnaissance and subsurface exploration performed for this BBNPP study. Sparse geophysical and borehole data indicate that the basement likely consists of exotic crystalline magmatic arc material (Hansen, 1986) (Glover, 1995). Although the basement beneath the site has not been penetrated with drill holes, regional geologic cross sections developed from geophysical, gravity and aeromagnetic, as well as limited deep borehole data from outside of the BBNPP site area, suggest that complexly deformed, metamorphosed crystalline igneous rocks (Crawford, 1999) of Precambrian and Paleozoic age are likely present at about 33,000 ft (10,058 m) msl (Section 2.5.1.1.3.1.1 and Section 2.5.1.2.2).

Tectonic models hypothesize that the crystalline basement underlying the site was accreted to a pre-Taconic North American margin in the Precambrian (Section 2.5.1.1.2). The major structure of the site area is the Berwick Anticlinorium, defined by Inners (1978) as "a moderately complex, first order fold which trends in a northeast-southwest direction". Further investigations by Inners (Inners, 1978) found that the apparent structural relief of the anticlinorium within the site region was 12,000 ft (3,658 m) and wavelength was approximately 8.2 mi (13 km). The northwest section of the site area is the likely axis of the Lackawanna Synclinorium, and the southeast section of the site area is likely the main axis of the Catawissa-McCauley Mountain Synclinorium, continuing the en echelon order of synclines in the vicinity (Inners, 1978). These synclines are delineated from numerous outcrop searches (Inners, 1978), geophysical data and a limited number of deep boreholes that penetrate the crust (Pohn, 2001). On the basis of a review of existing published geologic literature, site-specific data, and field reconnaissance suggests there is no known syncline-related fault or geologic evidence of syncline-related faulting in the basement directly beneath the BBNPP site area.

1:24,000-scale mapping (Inners, 1978) for the Berwick Quadrangle shows the stratigraphy at the BBNPP site area consisting of folded Silurian, Devonian, and Carboniferous rocks that have accumulated within the north-eastern part of the Ridge and Valley Province. The Ridge and Valley Province is defined as "alternating ridges and valleys developed on folded and faulted non-metamorphosed rocks" (Way, 1999) that ranges in length from New York to northern Alabama. In the site area, the Ridge and Valley Province is underlain by a Paleozoic sedimentary sequence that reaches an estimated thickness of 33,000 ft (10,058 m) msl. Overlying this Paleozoic basement are few post-Paleozoic rock formations with primarily glacial till and colluvium overburden, the result of multiple Quaternary glacial events, as discussed in Section 2.5.1.1.1.1. These Paleozoic strata are best displayed in the Berwick Anticlinorium, a cross-section of which is presented in Figure 2.5-24.

The local geologic cross section of the site area (Figure 2.5-24) depicts an anticlinal, Paleozoic Ridge and Valley formations in an unconformable contact with overlying Quaternary glacial deposits (Inners, 1978). One inferred fault and one mapped fault are depicted on this geologic cross section, labeled Light Street Fault and Berwick Fault. The Light Street Fault, also referenced in the SSES FSAR (SSES FSAR, 2003), identifies a disconformable contact separating the Marcellus Formation from the Onondaga and Old Port formations while the Berwick Fault identifies a disconformity between the Old Port and Keyser formations. Findings from the SSES FSAR concluded that no concrete evidence exists to support or argue the

existence of the Light Street Fault within the site area, and that the alleged fault "is perhaps better explained by an unconformity than by faulting" (SSES FSAR, 2003). The SSES FSAR also states that, even if a fault exists, it "pre-dates the formation of the Berwick Anticlinorium." This supports the findings of the BBNPP site area reconnaissance, that no surface faulting was identified and can also explain the mapping of the Berwick Fault as seen in Figure 2.5-24 and Figure 2.5-27. It is also worth noting that a paleoseismological study of geologic features thought to result from Quaternary tectonic faulting in the Eastern United States by Wheeler (Wheeler, 2006), did not identify either of these faults. Based on these findings it can be inferred that neither of these mapped faults within the site area pose a safety concern to the site.

On the basis of literature review, and aerial and field reconnaissance, the main structural features within the BBNPP site area consist of the two aforementioned east-trending faults (Inners, 1978), the Berwick Anticlinorium (Inners, 1978)(Wood, 1970), and two synclinoriums including the Catawissa-McCauley Mountain Synclinorium to the south of the site area, and the Lackawanna Synclinorium to the north of the site area (Inners, 1978)(Wood, 1970). The Berwick and Light Street Faults enter the 5 mile radius of the site vicinity to the west and are discussed in more detail below. The Berwick Anticlinorium, also referred to as the Montour Anticline (Pohn, 2001), traverses the site area from the southwest to the northeast and is also discussed below.

2.5.1.2.4.1 Site Area Structures

Some faults and folds occurred within the 25 mi (40 km) BBNPP site vicinity (Figure 2.5-23). These faults include the Light Street Fault and Berwick Fault, and the Lackawanna Synclinorium.

Light Street Fault: The 20 mile (32 km) long Light Street Fault approaches to within 2 mi (3.2 km) of the BBNPP site (Figure 2.5-27) and has been described in Section 2.5.1.1.4.3.2.1.7. Based on limited published data (Inners, 1978) and historical seismicity (EPRI, 1986), the nature of this fault is only inferred and is likely (1) a reverse fault that dips in a southerly direction and eliminates a section of the stratigraphy between the Wills Creek and Marcellus formations; (2) the detachment of a major décollement that dips to the north or; (3) a combination of (1) and (2) (Inners, 1978). The style and location of faulting are based on field investigations of local outcroppings by Inners (Inners, 1978). According to Inners (Inners, 1978), the simplest explanation for the unconformity in the area is a south-dipping reverse fault as mapped in Figure 2.5-22. Inners (Inners, 1978) also correlates this apparent loss of section in the log of Parvin Good No. 1, located approximately 7 mi northeast of the mapped area. Information on this well could not be retrieved for review to confirm this finding. Inners (Inners, 1978) also states that stratigraphic thinning of the Old Port-Onondaga section may also explain the unconformity within these formations. Inners (1978) attributes the presence of the Light Street Fault to the folding and faulting actions that occurred at the site area during the Alleghanian Orogeny, approximately 250 million years ago. There is no pre-EPRI and post-EPRI study (EPRI, 1986) seismicity spatially associated with this feature nor is there any geomorphic evidence of Quaternary deformation. The Light Street Fault is not considered a capable tectonic source.

Berwick Fault: In conjunction with the Light Street Fault as discussed above, the Berwick Fault is mapped as inferred and is based on limited surface data and a water well log drilled at the Berwick Lumber and Supply Company at 329 West Second Street in Berwick, PA (Inners, 1978). The Rizzo investigators were unable to locate this well and it was possibly abandoned prior to the site investigation. The inferred Berwick Fault lies within the site area and comes to within approximately 3.5 mi (5.6 km) of the BBNPP site. The exact length of the Berwick Fault is not completely mapped and is believed to be a south-dipping reverse fault on the south flank of the

Berwick Anticlinorium (Inners, 1978). Inners (Inners, 1978) also states that the Berwick fault extends east-northeastward into an exposed third order anticline in the Marcellus-Mahantango interval, and represents an unconformity in the Old Port and Keyser Formations. Inners (Inners, 1978) attributes the presence of the Berwick Fault to the folding and faulting actions that occurred at the site area during the Alleghanian Orogeny, approximately 250 million years ago. There is no pre-EPRI or post-EPRI study (EPRI, 1986) seismicity spatially associated with this feature nor is there any geomorphic evidence of Quaternary deformation. The Berwick fault is not considered a capable tectonic source.

Lackawanna Synclinorium: A first order fold syncline is mapped within the 5 mi (8 km) radius of the BBNPP site area. The Lackawanna Synclinorium (Inners, 1978) is shown in the northwest corner of Figure 2.5-23 as it trends southwest-northeast. Although just outside the 5 mi (8 km) radius of the site, the Catawissa-McCauley Mountain synclinorium is likely represented by the synclinal axis in the extreme lower right corner of Figure 2.5-23, opposite Nescopeck Mountain from the site. An alternative explanation for this synclinorium is that this axis may be one of several en echelon, second-order synclines that form the synclinorium of the area (Inners, 1978). In addition to the flexural-slip mechanisms responsible for many of the folds in the mapped area of Figure 2.5-23, flexural-flow folding was likely another strong component to their formation (Inners, 1978). Inners (Inners, 1978) identifies several features of flexural-slip folds evident in the Berwick Quadrangle including the common occurrence of slickenlines on bedding surfaces and maintenance of approximately the same bedding thickness across the folds. Flexural-flow folding characteristics, within any structure, include prominent cleavage in argillaceous rocks and thickening of beds within the hinges.

Inners (Inners, 1978) prepared a lithostratigraphic column along an almost 9 mi (14.5 km) long stretch of the Berwick Quadrangle that intersects much of the BBNPP site area. When these stratigraphic columns are compiled into a cross section (Table 2.5-24), they collectively provide an almost 9 mi (14 km) long, nearly continuous exposure of Silurian, Devonian, and Mississippian formations. Inners' (Inners, 1978) stratigraphic analysis indicates that these Paleozoic formations dip to the north on the north side of the Susquehanna River and dip to the south on the south side. Erosional processes of the Berwick Anticlinorium have produced two mountain ridges, Lee Mountain to the north of the site and Nescopeck Mountain to the south, and have produced similar topography on each mountain (Inners, 1978). The Light Street and Berwick faults are also mapped on this cross section, as seen in Table 2.5-24, and discussed above. The apparent structural relief of the Berwick Anticlinorium is approximately 12,000 ft (3,658 m) with a wavelength of about 8.2 mi (13.2 km) (Inners, 1978). Quaternary deposits overlying the site show little or no signs of faulting or folding, due mostly to their relatively young age in comparison to the underlying Paleozoic bedrock.

There is no pre-EPRI or post-EPRI study (EPRI, 1986) seismicity spatially associated with the Inners (Inners, 1978) features, the hypothetical features are not aligned or associated with gravity and magnetic anomalies, nor is there data to indicate that the features proposed by Inners (Inners, 1978) are capable tectonic sources.

The most detailed subsurface exploration of the site was performed as part of the SSES FSAR (SSES FSAR, 2003) for the existing SSES foundation and supporting structures. The SSES FSAR study included drilling as many as 250 geotechnical boreholes, collecting downhole geophysical data, and acquiring seismic refraction data across the site. Findings from the SSES FSAR were referred throughout the site investigation for the BBNPP site.

Geologic sections developed from geotechnical borehole data collected as part of the BBNPP study also provide additional detailed sedimentological and structural relations for the upper approximately 400 ft (122 m) of strata directly beneath the footprint of the site as discussed in Section 2.5.4.2.2.2. Similar to the previous cross sections prepared for the site, new geologic borehole data support the interpretation of flat-lying, unfaulted Quaternary and steeply dipping Devonian stratigraphy at the BBNPP site (as shown in Figure 2.5-28, Figure 2.5-29, Figure 2.5-30, Figure 2.5-31, Figure 2.5-32, and Figure 2.5-33). Cross sections prepared oblique to previously mapped northeast-trending structures (i.e., Light Street and Berwick faults) and inferred folds (Inners, 1978) (Gwinn, 1970) show similar stratigraphy directly below the BBNPP site. Multiple key stratigraphic markers, or lack thereof, provide evidence for the absence of quaternary faulting and folding beneath the site.

Numerous investigations of the Ridge and Valley Province and Susquehanna Valley over many decades by government researchers, stratigraphers, and by consultants for Pennsylvania Power and Light (the predecessor of PPL), as well as investigations for the BBNPP, have reported few visible signs of tectonic deformation within the exposed Devonian bedrock near the site, including the Light Street and Berwick faults (Inners, 1978), which were the result of tectonic deformation over 250 million years ago (Inners, 1978). Collectively, the majority of published and unpublished geologic cross sections compiled for much of the site area and site, coupled with regional sections (Inners, 1978) (King, 1974) and site and aerial reconnaissance, indicate the absence of Pleistocene and younger faulting and folding. A review and interpretation of aerial photography and digital elevation models of the BBNPP site area identified few discontinuous north to northeast-striking lineaments. None of these lineaments were interpreted as fault-related, nor coincident with the Light Street Fault, Berwick Fault, or the other previously inferred Paleozoic structures mapped by Inners (Inners, 1978) and the Berg (Berg, 1980). A review of regional geologic sections suggest that the features postulated by Inners (Inners, 1978), if present, are not moderate or prominent structures, and do not deform Quaternary strata. In summary, on the basis of regional and site geologic and geomorphic data, there are no known faults within the site area that pose a structural hazard to the site, including the poorly constrained Light Street and Berwick faults that lie within the southwestern section of the 5 mi (8 km) radius of the site.

2.5.1.2.4.2 Site Faulting

No faulting has been revealed within 5 mi (8 km) of the site either by drilling, by reconnaissance field mapping, by detailed excavation geologic mapping, or by the study of aerial photographs and Earth Resources Technology Satellite (ERTS) imagery obtained from both the SSES FSAR and from the current study as discussed in Section 2.5.3. The nearest fault is contained within the Middle Devonian stratigraphic units (over 350 million years) and is named the Light Street Fault. Based on (Inners, 1978) and SSES FSAR (SSES FSAR, 2003), the fault dips to the south at a small angle of 10 to 30 degrees to stratigraphy bedding. The strike of the fault is of northeast-southwest orientation. The fault is located on the north side of the Berwick anticlinorium and extends for about 20 mi (32 km) west of Berwick. The fault overlaps the Old Port and Keyser Formations. Seismic reflection profiles indicate that the fault originated during the early Triassic. Based on review of published literature and historical seismicity, there is no reported geomorphic expression, historical seismicity, or Quaternary deformation along the Light Street Fault, thus this feature is not considered to be a capable tectonic source.

2.5.1.2.4.3 Paleo-liquefaction

No liquefaction feature has been revealed within 25 mi (40 km) of the site either by drilling, by reconnaissance field mapping, by detailed excavation geologic mapping, or by the study of aerial photographs and ERTS imagery in either the SESS Units 1 and 2 FSAR and the current study.

There are six kinds of evidence suggesting or demonstrating Quaternary tectonic faulting in the Eastern United States (EUS) (Wheeler, 2006):

1. Some faults demonstrably offset strata or erosional surfaces that might be as young as Quaternary or even post-glacial in age;
2. Known paleoliquefaction features demonstrate the occurrence of Quaternary tectonic faulting even if the causal fault cannot be identified;
3. Rarely, moderate historical earthquakes can be attributed to known faults by analyses of highly precise earthquake epicenters and depths, single-earthquake focal mechanisms, or tabular distributions of aftershocks;
4. The youthfulness, lack of weathering, and other aspects of escarpments and similar geomorphic features can suggest a recent tectonic origin;
5. Named seismic zones have had noticeably more abundant historical earthquakes than surrounding regions. Most of the more numerous earthquakes are small, but their greater abundance within the seismic zone suggests that the zone might be more prone to larger earthquakes than the surrounding regions; and
6. Some known EUS faults formed or were significantly reactivated in tectonic settings that are known to produce large earthquakes worldwide.

A remote imagery interpretation, followed by a detailed ground truthing investigation, yielded no evidence of paleo-liquefaction in the area of the site. Most of the surrounding site area has been impacted by agricultural activities or is wooded, which could mask such features on remote imagery. However, no such features were found in non-developed areas along water bodies either -- areas where paleo-liquefaction features would tend to be more prevalent if they exist at all in the site area.

No paleo-liquefaction features were found in the area of the site, thus eliminating such features as a geologic hazard which could impact the safety-related facilities of the proposed plant.

The closest reported Quaternary liquefaction feature to the BBNPP Site is the Class A Central Virginia seismic zone (Crone, 2000). Here evidence for Quaternary faulting is described in Central Virginia (Amelia, Buckingham, Caroline, Chesterfield, Cumberland, Fluvanna, Goochland, Hanover, Henrico, Louisa, Orange, Powhatan, Richmond, and Spotsylvania Counties), approximately 200-250 miles (330-400 km) south-southwest of the BBNPP site. It is a roughly circular area with a diameter of 120-150 km (75 - 93 miles), with a low level of diffuse seismicity, three-quarters of which is in the upper 11 km of the crust. The Quaternary tectonic feature classification by Crone (Crone, 2000) is described in Section 2.5.1.1.4.3.5.

The geologic evidence for Quaternary faulting in the Central Virginia seismic zone consists of one site with a few small, latest Holocene sand dikes, and a second site several tens of kilometers away with a few small, possible dikes of early Holocene or younger (Obermeier, 1998) (Crone, 2000). The causative faults remain unidentified.

No surface rupture or liquefaction is reported. Similarly, no prehistoric surface rupture is known in the seismic zone, and the only reported paleoliquefaction features are those few described in Obermeier (Obermeier, 1998) and in Crone (Crone, 2000). Authors examined cutbanks along more than 186 mi (300 km) of streams throughout the seismic zone, in search of geologic evidence for paleoliquefaction. This geologic record extends back 2,000-3,000 years throughout the seismic zone, and at least 5,000 years in the eastern part of the zone. One site has a few small clastic dikes that formed within the last few centuries. A second site tens of kilometers away has a few small, severely weathered, probable dikes that might have formed as long ago as early Holocene. From detailed reconnaissance and the scarcity of observed dikes, authors (Obermeier (Obermeier, 1998) and Crone (Crone, 2000) concluded that the seismic zone has not experienced an earthquake of magnitude larger than approximately 7 for the last 2,000-5,000 years. However the geologic records of more earthquakes of magnitudes 6-7 may be concealed between streams or between cutbanks. Regardless, such earthquakes could not have been abundant in the seismic zone.

Radiocarbon data and the lack of severe weathering indicate that the dikes present in one stream exposure are a few centuries old. Severity of weathering indicates that the dikes in the other exposure could be as old as early Holocene. However, the two exposures are several tens of kilometers apart, across the regional structural grain, so they are unlikely to record earthquakes on the same fault. Accordingly, no recurrence interval for an individual Quaternary fault can be calculated.

The next Quaternary liquefaction report is for the Class A Newbury liquefaction features (Crone, 2000). Here, evidence for Quaternary faulting is observed in northeastern Massachusetts, approximately 290 miles (467 km) east-northeast of the BBNPP site. This report is based on: (1) eyewitness report of liquefaction during an earthquake of MMI VII (moment magnitude M 4.8) in 1727; (2) sand dikes found in trenches and attributed to the 1727 earthquake, and (3) Mid to Late Holocene sand dikes and a sand sill that are cut by the 1727 dikes.

The area is underlain by Paleozoic and Precambrian metamorphic and igneous rocks that were folded and juxtaposed by slip on numerous mapped faults during the assembly of the northern Appalachians (Zen, 1983) (Crone, 2000). However, the locations of both earthquakes and faults at depth have large uncertainties. To date no New England earthquakes have been convincingly associated with known faults and the causative fault remains unidentified (Crone, 2000).

The only paleo-seismological study for this area is that of Tuttle (Tuttle, 1991) (Crone, 2000). During their reconnaissance of sand and gravel pits and other excavations in Late Pleistocene glacial deposits in northeastern Massachusetts and southeastern New Hampshire, field workers observed abundant soft-sediment deformation features. None of the features could be attributed solely to earthquakes. However, accounts of the 1727 earthquake described several areas of ground failure typical of earthquake-induced liquefaction. In one or more trenches at a single site, they observed that dikes of white, very fine grained sand crosscut Late Pleistocene, glaciomarine clay and a sandy B horizon soil. At a second site 5 km away, the sandy B horizon contains a basal layer of gray, silty, virtually unweathered sand, which Tuttle (Tuttle, 1991) (Crone, 2000) interpreted as a sill emplaced beneath possibly frozen ground. Some dikes appear to feed the

sill, whereas other dikes cut across it. A separate reconnaissance of riverbank and marsh outcrops in northeastern Massachusetts and nearby New Hampshire found no evidence of liquefaction in salt marsh deposits that are 1500-3000 years old and underlain by highly liquefiable sands (Gelinias, 1993).

The closest Class B features to the BBNPP site are described in Section 2.5.1.1.4.4.3 for the Lancaster Seismic Zone (55 mi (88 km) south of the BBNPP site), and Section 2.5.1.1.4.4.4 for the Cacoosing Valley Earthquake Sequence (52 mi (84 km) south of the BBNPP site). In both Seismic zones no geological evidence such as surface rupture or liquefaction has been found (Crone, 2000). In addition, no evidence of liquefaction or paleoliquefaction has been observed in the reconnaissance efforts (Gelinias, 1993) in the Moodus Seismic Zone (190 mi (306 km) northeast of the BBNPP), described in Section 2.5.1.1.4.4.5.

2.5.1.2.5 Site Area Geologic Hazard Evaluation

No geologic hazards have been identified within the BBNPP site area. No geologic units at the site are subject to dissolution. No deformation zones were encountered in the exploration or excavation for SSES Units 1 and 2 and none have been encountered in the site investigation for BBNPP site. Because the BBNPP site is located at an elevation of 674 ft (205 m) msl and approximately 174 ft (53 m) above the banks of the Susquehanna River, it is unlikely that shoreline erosion or flooding will impact the BBNPP site.}

2.5.1.2.6 Site Engineering Geology Evaluation

2.5.1.2.6.1 Engineering Soil Properties and Behavior of Foundation Materials

Engineering soil properties, including index properties, static and dynamic strength, and compressibility are discussed in Section 2.5.4. Variability and distribution of properties for the foundation bearing soils will be evaluated and mapped as the excavation is completed.

Settlement monitoring will be based on analyses performed for the final design.

2.5.1.2.6.2 Zones of Alteration, Weathering, and Structural Weakness

No unusual weathering profiles have been encountered during the site investigation. No dissolution is expected to affect foundations. Any noted desiccation, weathering zones, joints or fractures will be mapped during excavation and evaluated.

2.5.1.2.6.3 Deformational Zones

No deformation zones were encountered in the exploration or excavation for SSES Units 1 and 2 and none have been encountered in the site investigation for BBNPP. Excavation mapping is required during construction and any noted deformational zones will be evaluated. No capable tectonic sources as defined by Regulatory Guide 1.165 (NRC, 1997) exist within the BBNPP site area.

2.5.1.2.6.4 Prior Earthquake Effects

Outcrops are common within the BBNPP site area. Studies of the SSES Unit 1 and 2 excavation, available outcrops, and extensive exposures along the road cuts of Nescopeck and Lee Mountain, have not indicated any evidence for earthquake activity that affected the Paleozoic bedrock or Quaternary surficial deposits within the site area.

2.5.1.2.6.5 Effects of Human Activities

The nearest coal mining operations have occurred 11 mi (18 km) east of the BBNPP site near the town of Shickshinny, PA for deep anthracite coal mining. The nearest oil and gas reserves occurs nearly 25 mi (40 km) north of the BBNPP site near the town of Harveys Lake. Based on the Inners (Inners, 1978) and SSES FSAR (SSES FSAR, 2003) and (Hornberger, 2004), no mining operations have occurred at the site nor has excessive extraction or injection of groundwater or impoundment of water occurred within the site area that can affect geologic conditions.

2.5.1.2.6.6 Site Groundwater Conditions

A detailed discussion of groundwater conditions is provided in Section 2.4.12.}

2.5.1.3 References

{This section is added as a supplement to the U.S. EPR FSAR.

Aber, 2001. Appalachian Mountains, J. S. Aber, Website: http://academic.emporia.edu/aberjame/struc_geo/appalach/appalach.htm, Date accessed: January 23, 2008.

Aggarwal, 1978. Earthquakes, Faults, and Nuclear Power Plants in Southern New York and New Jersey, Science, Volume 200, p 425-429, Y. Aggarwal and L. Sykes, 1978.

Anglin, 1981. Microseismicity in the mid-St. Lawrence Valley Charlevoix zone, Bulletin of the Seismological Society of America, Volume 71, p 1553-1560, F. Anglin and G. Buchbinder, 1981.

Anglin, 1984. Seismicity and Faulting in the Charlevoix Zone of the St. Lawrence Valley, Bulletin of the Seismological Society of America, Volume 74, Number 2, p 595-603, F.M. Anglin, April, 1984.

Armbruster, 1987. The 23 April 1984 Martic Earthquake and The Lancaster Seismic Zone In Eastern Pennsylvania, Bulletin of the Seismological Society of America, Volume 77, Number 2, p 877-890, J. Armbruster and L. Seeber, 1987.

Bankey, 2002. Magnetic Anomaly Map of North America, U.S. Geological Survey, scale 1:10,000,000, 1 sheet, V. Bankey, A. Cuevas, D. Daniels, C. Finn, I. Hernandez, P. Hill, R. Kucks, W. Miles, M. Pilkington, C. Roberts, W. Roest, V. Rystrom, S. Shearer, S. Snyder, R. Sweeney and J. Velez, 2002.

Barnes, 2002. The Geological Story of Pennsylvania (3rd ed.), Pennsylvania Geological Survey, 4th ser., Educational Series 4, p 1-44, J.H. Barnes and W.D. Sevon, 2002.

Behrendt, 1983. Structural elements of the U.S. Atlantic margin delineated by the second vertical derivative of the aeromagnetic data, U.S. Geological Survey Geophysical Investigation Map GP-956, scale 1-2,500,000, J. Behrendt and M. Grim, 1983.

Bennington, 2006. Geology of New York and New Jersey, Hofstra University, 21 p, J. B. Bennington and C. Merguerian, 2006.

Bent, 1992. A re-examination of the 1925 Charlevoix, Quebec, earthquake, Bulletin of the Seismological Society of America, Volume 82, p 2097-2113, A. Bent, 1992.

Berg, 1980. Geologic map of Pennsylvania, Pennsylvania Geological Survey, 4th ser., Map1, scale 1:250,000, 3 sheets, T.M. Berg, 1980.

Berg, 1999. Part II, Stratigraphy and Sedimentary Tectonics, Chapter 8: Devonian-Mississippian Transition, in C.H. Shultz ed., The Geology of Pennsylvania: Pennsylvania Bureau of Topographic and Geologic Survey Special Publication 1, p 128-137, T.M. Berg, 1999.

Bobyarchick, 2007. Kinematics of the Everona fault, central Virginia, Geological Society of America Abstracts with Programs, Volume 39, Number 2, p 89, A. Bobyarchik, 2007.

Bradley, 1989. Taconic Plate Kinematics as Revealed by Foredeep Stratigraphy, Appalachian Orogen, Tectonics, Volume 8, No. 5, p 1037-1049, D.C. Bradley, 1989.

Braun, 1988. Glacial Geology of the Anthracite and North Branch Susquehanna Lowland Regions, p 1-25, D. Braun, 1988.

Braun, 2004. Late Wisconsin Deglaciation of the Great Bend- Tunkhannock Region of Northeastern Pennsylvania, Guidebook for the 67th Annual Reunion of the Friends of the Pleistocene, p 1-26, D. Braun, 2004.

Brezinski, 1999. Part II, Stratigraphy and Sedimentary Tectonics, Chapter 9: Mississippian, in C.H. Shultz ed., The Geology of Pennsylvania: Pennsylvania Bureau of Topographic and Geologic Survey Special Publication 1, p 138-147, D.K. Brezinski, 1999.

CFR, 2007. Geologic and Seismic Siting Criteria, Title 10, Part 100.23, Code of Federal Regulations, CFR, 2007.

Clark, 1992. Central Appalachian Periglacial Geomorphology, A Field Excursion Guidebook under the auspices of the 27th International Geographical Congress, Commission on Frost Action Environments, Agronomy Series Number 120, G. Clark, R. Behling, D. Braun, E. Ciolkosz, J. Kite and B. Marsh, August 1992.

Cleaves, 1992. Regoliths of the Middle-Atlantic Piedmont and Evolution of the Polymorphic Landscape, Southeastern Geology, Volume 39, Number 3 and 4, p 122-199, E. Cleaves, October, 1992.

Cotter, 2008. The Geologic History of Central Pennsylvania, Introduction, p 1-3, Plate Tectonics, p 1-4, Episode Two, p 1-7, End of Episode Two, p 1-2, Episode Three, p 1-2, Episode Four, p 1-4, E. Cotter, 2008.

Crangle, 2002. Stratigraphic Framework of Cambrian and Ordovician Rocks in the Central Appalachian Basin from Medina County, Ohio, through Southwestern and South-Central Pennsylvania to Hampshire County, West Virginia, Revised and Digitized from Ryder, Stratigraphic Framework of Cambrian and Ordovician Rocks in the Central Appalachian Basin from Medina County, Ohio, through Southwestern and South-Central Pennsylvania to Hampshire County, West Virginia, R.D. Crangle Jr., 2002.

Crawford, 1999. Part III, Structural Geology and Tectonics, Chapter 16: Piedmont Upland, in C.H. Shultz ed., The Geology of Pennsylvania: Pennsylvania Bureau of Topographic and Geologic Survey Special Publication 1, p 234-241, M.L. Crawford, W.A. Crawford, A.L. Hoersch, and M.E. Wagner, 1999.

Crone, 2000. Data for Quaternary Faults, Liquefaction Features, and Possible Tectonic Features in the Central and Eastern United States, East of the Rocky Mountain Front, U.S. Geological Survey, Open-File Report 00-260, p 1-332, A.J. Crone and R.L. Wheeler, 2000.

Crowl, 1999. Part II, Quaternary, Chapter 15, in C.H. Shultz ed., The Geology of Pennsylvania: Pennsylvania Bureau of Topographic and Geologic Survey Special Publication 1, p 224-232, G.H. Crowl and W.D. Sevon, 1999.

Cumbest, 2000. Comparison of Cenozoic Faulting at the Savannah River Site to Fault Characteristics of the Atlantic Coast Fault Province: Implications for Fault Capability, U.S. Dept. of Energy Contract No. DE-AC09-96SR18500, 51 p, R. Cumbest, D. Wyatt, D. Stephenson, and M. Maryak, 2000.

DCNR, 2007a. Geologic Map of Pennsylvania, Pennsylvania Department of Conservation and Natural Resources, Website: <http://www.dcnr.state.pa.us/topogeo/maps/map7.pdf>, Date accessed: December 14, 2007.

DCNR, 2007b. Piedmont Lowland Section Piedmont Province, Pennsylvania Department of Conservation and Natural Resources, Website: <http://www.dcnr.state.pa.us/topogeo/map13/13pls.aspx>, Date accessed: December 14, 2007.

DCNR, 2007c. Gettysburg-Newark Lowland Section Piedmont Province, Pennsylvania Department of Conservation and Natural Resources, Website: <http://www.dcnr.state.pa.us/topogeo/map13/13gnls.aspx>, Date accessed: December 14, 2007.

DCNR, 2007d. Piedmont Upland Section Piedmont Province, Pennsylvania Department of Conservation and Natural Resources, Website: <http://www.dcnr.state.pa.us/topogeo/map13/13pus.aspx>, Date accessed: December 14, 2007.

DCNR, 2007e. Reading Prong Section, Pennsylvania Department of Conservation and Natural Resources, Website: <http://www.dcnr.state.pa.us/topogeo/map13/13rps.aspx>, Date accessed: December 14, 2007.

DCNR, 2008a. Trenton Black River Carbonates: Introduction, Pennsylvania Geological Survey, Pennsylvania Department of Conservation and Natural Resources, Website: <http://www.dcnr.state.pa.us/topogeo/tbr/tbrintro.aspx>, Date accessed: July 5, 2008.

DCNR, 2008b. Great Valley Section Ridge and Valley Province, Pennsylvania Department of Conservation and Natural Resources, Website: <http://www.dcnr.state.pa.us/topogeo/map13/13gvs.aspx>, Date accessed: January 22, 2008.

DCNR, 2008c. Lowland and Intermediate Upland Section Atlantic Coastal Plain Province, Pennsylvania Department of Conservation and Natural Resources, Website: <http://www.dcnr.state.pa.us/topogeo/map13/13lius.aspx>, Date accessed: January 22, 2008.

DCNR, 2008d. Eastern Lake Section Central and Lowland Provinces, Pennsylvania Department of Conservation and Natural Resources, Website: <http://www.dcnr.state.pa.us/topogeo/map13/13els.aspx>, Date accessed: April 10, 2008.

Dewey, 1999. Part IV. Regional Geophysics, Chapter 27 Seismotectonic Framework, in C.H. Shultz ed., The Geology of Pennsylvania, Pennsylvania Bureau of Topographic and Geologic Survey Special Publication 1, p 339-341, J. Dewey and D. Gordon, 1999.

Dodson, 2008. Structural Geology of the Transylvania Fault Zone in the Appalachian Thrust Belt, Bedford County, Pennsylvania, Northeastern Section - 43rd Annual Meeting, E. Dodson, March, 2008.

Drake, 1999. Part III, Structural Geology and Tectonics, Chapter 17: South Mountain and Reading Prong, in C.H. Shultz ed., The Geology of Pennsylvania: Pennsylvania Bureau of Topographic and Geologic Survey Special Publication 1, p 242-255, A.A. Drake, Jr., 1999.

Ebel, 1982. The 1981 microearthquake swarm near Moodus, Connecticut, Geophysical Research Letters, Volume 9, Number 4. p 397-400, J. E. Ebel, V. Vudler, and M. Celata, 1982.

Ebel, 1989. A comparison of the 1981, 1982, and 1987-1988 microearthquake swarms at Moodus, Connecticut, Seismological Research Letters, Volume 60, p 177-188, J. E. Ebel, 1989.

Edmunds, 1999. Part II, Stratigraphy and Sedimentary Tectonics, Chapter 10: Pennsylvanian, in C.H. Shultz ed., The Geology of Pennsylvania: Pennsylvania Bureau of Topographic and Geologic Survey Special Publication 1, p 148-169, W.E. Edmunds, V.W. Skema, and N.K. Flint, 1999.

EPRI, 1986. Seismic Hazard Methodology for the Central and Eastern United States, EPRI Report NP-4726, Electric Power Research Institute, July 1986.

Ervin, 1975. Reelfoot Rift: reactivated precursor to the Mississippi Embayment, Geological Society of America Bulletin, Volume 86, Number 9, p 1287-1295, C. Ervin and L. McGinnis, 1975.

ESRI, 2007. Street Map Pro [CD-ROM], 2007 State Boundaries, Roads, Streams, County Boundaries, ESRI, 2007.

Fail, 1973. Tectonic development of the Triassic Newark-Gettysburg Basin in Pennsylvania, Geological Society of America Bulletin, Volume 84, p 725-740, R. T. Fail, 1973.

Fail, 1997. A Geologic History of the North-Central Appalachians, Part 1, Orogenesis from the Mesoproterozoic through the Taconic Orogeny, Journal of Science, Volume 297, p 551-619, R. Fail, 1997.

Fail, 1999. Part III. Structural Geology and Tectonics, Chapter 19 Appalachian Mountain Section of the Ridge and Valley Province, in C.H. Shultz ed., The Geology of Pennsylvania: Pennsylvania Bureau of Topographic and Geologic Survey Special Publication 1, p 268-285, R. Fail and R. Nickelsen, 1999.

Fail, 2004. The Birdsboro Basin, Pennsylvania Geology, Volume 34, Number 4, p 2-11, R. T. Fail, 2004.

Fichter, 2000. Cross Section J: The Devonian Acadian Orogeny and Catskill Clastic Wedge, in The Geological Evolution of Virginia and the Mid-Atlantic Region, p 1-6, L.S. Fichter, 2000.

Fletcher, 1977. Earthquakes related to hydraulic mining and natural seismic activity in western New York State, Journal of Geophysical Research, Volume 82, p 3767-3780, J. B. Fletcher and L .R. Sykes, 1977.

Gelinas, 1993. Evaluation of liquefaction-susceptible materials near moderate magnitude historical earthquakes in New England, [abs], Seismological Research Letters, Volume 64, p 259-260, R. L. Gelinas, H. M. A. Kempinen, and D. C. Amick, 1993.

Glover, 1995. E-3 Southwestern Pennsylvania to Baltimore Canyon Trough, Geological Society of America Centennial Continent/Ocean Transect #19, L. Glover III and K. Klitgord, 1995.

Gold, 2003. Geological Report on the Skytop Road Cuts, Pennsylvania State University, Department of Geosciences, p 1-27, D.P. Gold and A.G. Doden, 2003.

Gold, 2005. Precambrian Basement Map of the Appalachian Basin and Piedmont Province of Pennsylvania, D.P. Gold, S.S. Alexander, R. Cakir, and others, 2005.

Gold, 2008. Basement Depth and Related Geospatial Database for Pennsylvania, Pennsylvania Geological Survey, Open-File General Geology (OFGG) Report OFGG 05-01.0, p 1-6, D.P. Gold, 2008.

Gough, 1983. A Stress Province Boundary and Traction on the North American Plate, Nature, Volume 305, Issue 5935, p 619-621, D. Gough and C. Fordjor, 1983.

Gray, 1999. Chapter 18 Great Valley and Piedmont Lowland, Part III. Structural Geology and Tectonics, p 256-267, C. Gray and S.I. Root, 1999.

Gwinn, 1970. Kinematic Pattern and Estimates of Lateral Shortening, Valley and Ridge and Great Valley Provinces, Central Appalachians, South-Central Pennsylvania, Studies of Appalachian Tectonics: Central and Southern, Chapter 8, p 127-146, Gwinn, 1970.

Hack, 1989. Geomorphology of the Appalachian Highlands, R. Hatcher Jr., W. Thomas and G. Viele, eds., The Geology of North America, Volume F-2, The Appalachian-Ouachita Orogen in the United States, Geological Society of America, J. Hack, 1989.

Hansen, 1986. The Lithology and Distribution of Pre-Cretaceous basement rocks beneath the Maryland Coastal Plain, Department of Natural Resources Maryland Geological Survey Report of Investigations No. 44, 27 p, H. Hansen and J. Edwards Jr., 1986.

Harper, 1999. Part II. Stratigraphy and Sedimentary Tectonics, Chapter 7: Devonian, in C.H. Shultz ed., The Geology of Pennsylvania: Pennsylvania Bureau of Topographic and Geologic Survey Special Publication 1, p 108-127, J.A. Harper, 1999.

Harper, 2003. Ordovician Carbonates in Central Pennsylvania, Trenton and Black River Carbonates in the Union Furnace Area of Blair and Huntingdon Counties, Pennsylvania, A Field Trip Guidebook for the Eastern Section AAPG Meeting, J. Harper Ed., J. Harper, May 2003.

Hatcher, 1987. Tectonics of the southern and central Appalachian internides, Annual Reviews of Earth and Planetary Science, Volume 15, p 337-362, R. Hatcher Jr., 1987.

Hawman, 1992. Structure of the crust and upper mantle beneath the great Valley and Allegheny Plateau of eastern Pennsylvania, II, Gravity modeling and migration of wide-angle reflection data, Journal of Geophysical Research, Volume 97, p 393-415, R. B. Howmann and R. A. Phinney, 1992.

Herrmann, 1978. A seismological study of two Attica, New York earthquakes, Bulletin of the Seismological Society of America, Volume 68, p 641-651, R. B. Herrmann, 1978.

Hibbard, 2006. Lithotectonic map of the Appalachian Orogen, Canada-United States of America, Geological Survey of Canada Map 02096A, 2 sheets, Scale 1: 1,500,000, J. Hibbard, C. Van Staal, D. Rankin and H. Williams, 2006.

Hinze, 1987. Magnetic Anomaly Map of North America, Decade of North American Geology (DNAG), Geological Society of America, W. Hinze and P. Hood, 1987.

Hornberger, 2004. Chapter 2. Geology of the Pennsylvania Coal Regions, Website: http://www.dep.state.pa.us/dep/deputate/minres/bmr/beneficial_use/10%20CHAPT%202/Chapter%202%20final.pdf, Date accessed: January 22, 2008.

Horton, 1991. Preliminary Tectonostratigraphic Terrain Map of the Central and Southern Appalachians, U.S. Geological Survey Miscellaneous Investigations Series Map I-2163, J. Horton, A. Drake and D. Rankin, 1991.

Hough, 1991. Seismological constraints on source properties of the $m_b=4.0$ 1985 Ardsley, New York Earthquake: A characteristic rupture?, Journal of Geophysical Research, Volume 96, Number B11, p 18,183-18,195, S. E. Hough and L. Seeber, 1991

Hutchinson, 1985. New York Bight fault, Geological Society of America Bulletin, Volume 96, p 975-989, D. R. Hutchinson and J. A. Crow, 1985.

Inners, 1978. Geology and Mineral Resources of the Berwick Quadrangle, Luzerne and Columbia Counties, Pennsylvania, Pennsylvania Geological Survey, Fourth Series, p 1-34, J.D. Inners, 1978.

Jacob, 2004. Earthquakes and the Ramapo fault system in southeastern New York State, Lamont-Doherty Earth Observatory, K. Jacob, W. Kim, A. Lerner-Lam, L. Seeber, Web Site: http://www.ldeo.columbia.edu/news/2004/04_30_04.htm, Date accessed: April 29, 2008.

Johnston, 1985a. Seismotectonics of the Southern Appalachians, Bulletin of the Seismological Society of America, Volume 75, Number 1, p 291-312, A.C. Johnston, D.J. Reinbold, and S.I. Brewer, February 1985.

Johnston, 1985b. A basement block model for Southern Appalachian Seismicity, Geological Society of America-Abstracts with Programs, Volume 17, Number 2, p 97, A. Johnston and D Reinbold, 1985.

Kafka, 1985. Earthquake Activity in the Greater New York City Area: Magnitudes, Seismicity and Geologic Structures, Bulletin of the Seismological Society of America, Volume 75, Number 5, p 1285-1300, A. Kafka, E. Schlesinger-Miller and N. Barstow, 1985.

Kauffman, 1999. Part II, Stratigraphy and Sedimentary Tectonics, Chapter 4: Eocambrian, Cambrian, and Transition to Ordovician, in C.H. Shultz ed., The Geology of Pennsylvania: Pennsylvania Bureau of Topographic and Geologic Survey Special Publication 1, p 59-73, M.E. Kauffman, 1999.

King, 1974. A digital representation of the 1974 P.B. King and H.M. Beikman Map: U.S. Geological Survey Digital Data Series DDS-11, downloaded from <http://pubs.usgs.gov/dds/dds11/kb.html>.

King, 1978. The New York-Alabama lineament: Geophysical Evidence for a Major Crustal Break in the Basement Beneath the Appalachian Basin, Geology, Volume 6, p 312-318, E. King and I. Zietz, 1978.

King, 1999. Part IV. Regional Geophysics, Chapter 24 Aeromagnetism, in C.H. Shultz ed., The Geology of Pennsylvania: Pennsylvania Bureau of Topographic and Geologic Survey Special Publication 1, p 323-327, E. King, 1999.

Klitgord, 1988. U. S. Atlantic Continental Margin: Structural and Tectonic Framework, R. Sheridan and J. Grow, eds., The Atlantic Continental Margin, U.S., Geological Society of America, The Geology of North America, Volume 1-2, p 19-55, K. Klitgord, D. Hutchinson and H. Schouten, 1988.

Klitgord, 1995. Mid-Atlantic Continental Margin: The Mesozoic-Cenozoic Continent-Ocean Boundary, in L. Glover III and K. Klitgord, Chief Compilers, E-3 Southwestern Pennsylvania to Baltimore Canyon Trough, Geological Society of America Continent/Ocean Transect #19, Explanatory Pamphlet, K. Klitgord, C. Poag, L. Glover, R. Sheridan, D. Hutchinson, R. Mixon and R. Benson, 1995.

Koch, 1978. Geology and geophysics of the Moodus seismic area, Connecticut, Geological Society of America Abstracts with Programs, Volume 10, Number 2, p 71, B. F. Koch, R. J. Fahey, S. S. Quarrier, and J. F. Kick, 1978.

Komor, 1998. Sources of Geospatial Data for Central and Western New York - 1998, U.S. Geological Survey, Open-File Report 99-191, 42 p, S.C. Komor, 1998

Kucks, 1999. Bouguer Gravity Anomaly Data Grid for the Conterminous US, Kucks, 1999.

Kulander, 2005. Regional Seismic Lines Across the Rome Trough and Allegheny Plateau of Northern West Virginia, Western Maryland, and Southwestern Pennsylvania, US Geological Survey, pamphlet to accompany Map I-2791, C.S. Kulander, and R. Ryder, 2005.

Kunk, 2004. Multiple Paleozoic Metamorphic Histories, Fabrics, and Faulting in the Westminster and Potomac Terranes, Central Appalachian Piedmont, Northern Virginia and Southern Maryland, U.S. Geological Survey, 9 p, M. Kunk, R. Wintsch, C. Southworth, B. Mulvey, C. Naeser and N. Naeser, 2004.

Laughrey, 1999. Part II, Stratigraphy and Sedimentary Tectonics, Chapter 6: Silurian and Transition to Devonian, in C.H. Shultz ed., The Geology of Pennsylvania: Pennsylvania Bureau of Topographic and Geologic Survey Special Publication 1, p 91-107, C.D. Laughrey, 1999.

Lavin, 1982. Major lineaments and the Lake Erie-Maryland crustal block, Tectonics, Volume 1, p 431-440, P. M. Lavin, D. L. Chaffin, and W. F. Davis, 1982.

Lavin, 1999. Gravity, The Geology of Pennsylvania, Part IV. Regional Geophysics, Chapter 23, p 317-321, P. Lavin, 1999.

Lotto, 1997. Seismic stratigraphy of the New York bight, NY/NJ continental shelf, Geological Society of America Abstracts with Programs, Volume 29, Number 1, p 62, L. Lotto, M. A. Allison, W. C. Schwab, B. Butman, D. Foster, J. Denny, and W. Corso, 1997.

Lyons, 1982. Gravity Anomaly Map of the United States, Society of Exploration Geophysicists, Scale 1: 2,500,000, P. Lyons and N. O'hare, 1982.

MacLachlan, 1999. Part VI, Geologic History, Chapter 34: Mesozoic, in C.H. Shultz ed., The Geology of Pennsylvania: Pennsylvania Bureau of Topographic and Geologic Survey Special Publication 1, p 435-449, D.B. MacLachlan, 1999.

Marple, 2000. Evidence for a Buried Fault System in the Coastal Plain of the Carolinas and Virginia-Implications for Neotectonics in the Southeastern United States, Geological Society of America Bulletin, Volume 112, Number 2, p 200-220, R. Marple and P. Talwani, February 2000.

Marple, 2004. Relationship of the Stafford Fault Zone to the Right-Stepping Bends of the Potomac, Susquehanna and Delaware Rivers and Related Upstream Along the U.S. Mid-Atlantic Fall Line: In Southeastern Geology, Volume 42, Number 3, p 123-144, R. Marple, 2004.

McDonnell, 2008. Physical Geography of New York, T. McDonnell, Website: http://www.nygeo.org/ny_geo.html, Date accessed: April 9, 2008.

McElroy, 2007. Bedrock Geologic Map of the Allensville Quadrangle, Huntingdon and Mifflin Counties, Pennsylvania, Pennsylvania Geological Survey, 4th ser., OpenFile Report OFBM 07-02.0, T.A. McElroy and D.M. Hoskins, 2007.

McLaughlin, 2002. Results of Trenching Investigations Along the New Castle Railroad Survey-1 Seismic Line, New Castle, Delaware, Delaware Geological Survey, Open-File Report 43, 19 p, P. McLaughlin, S. Baxter, K. Ramsey, T. McKenna and S. Strohmeier, 2002.

Merguerian, 1996. Stratigraphy, Structural Geology, and Ductile- and Brittle Faults of New York City, Website: <http://www.dukelabs.com/Abstracts%20and%20Papers/CM1996c.htm>, 26 p, Date accessed: March 25, 2008.

Merguerian, 1997. Bronx River diversion- Neotectonic implications, International Journal of Rock Mechanics and Mining Sciences, Volume 34, Number 3-4, Paper Number 298, C. Merguerian and J. E. Sanders, 1997.

Milici, 2006. Assessment of Appalachian Basin Oil and Gas Resources: Devonian Shale-Middle and Upper Paleozoic Total Petroleum System, US Geological Survey, Open-File Report Series 2006-1237, p 1-70, R.C. Milici and C.S. Swezey, 2006.

Millot, 2001. Proterozoic Eon: Mesoproterozoic Era- Greenville Orogeny, L. Sniatkowski ed., J. Millot, 2001.

Mixon, 1977. Stafford Fault System: Structure Documenting Cretaceous and Tertiary Deformation Along the Fall Line in Northeastern Virginia, *Geology*, Vol. 5, p. 437-440, R. Mixon and W. Newell, 1977.

Mixon, 2000. Geologic Map of the Fredricksburg 30' x 60' Quadrangle, Virginia and Maryland, Report 2607, IMAP, R. Mixon, L. Pavlides, D. Powars, A. Froelich, R. Weems, J. Schindler, W. Newell, L. Edwards, and L. Ward, 2000.

National Atlas, 2008. Shaded Relief (200 Meter) 2008. downloaded from www.nationalatlas.gov/mld/srld48i.html, U.S. National Atlas, 2008.

Nelson, 1983. The Clingman Lineament: Aeromagnetic Evidence for a Major Discontinuity in the North American Basement, *Geological Society of America, Southeastern Section, Abstracts with Programs*, Volume 13, Number 1, p 31, A. Nelson and I. Zietz, January 1983.

NJGS, 2003. Generalized Glacial Sediments of New Jersey, New Jersey Geological Survey, Website: <http://www.state.nj.us/dep/njgs/geodata/dgs96-1.gif>, Date accessed: December 14, 2007.

NRC, 1978. Regulatory Guide 1.70, Standard Format and Content of Safety Analysis Reports for Nuclear Power Plants, LWR Edition, Revision 3, Nuclear Regulatory Commission, 1978.

NRC, 1997. Regulatory Guide 1.165, Identification and Characterization of Seismic Sources and Determination of Safe Shutdown Earthquake Ground Motion, Nuclear Regulatory Commission, March 1997.

NRC, 2007. Basis Geologic and Seismic Information, Regulatory Guide 1.206, Section 2.5.1, Nuclear Regulatory Commission, June, 2007.

Obermeier, 1998. Paleoliquefaction Evidence for Seismic Quiescence in Central Virginia During Late and Middle Holocene Time [abs.]: *Eos, Transactions of the American Geophysical Union*, v. 79, no. 17, p. S342, Obermeier, S.F., and McNulty, W.E., 1998

Owens, 1995. Geologic map of New Jersey: Central Sheet, U.S. geological Survey Open-File Report 95-0253, 60 p, 3 pls., scale 1:100,000, J. P. Owens, P. J. Sugarman, N. F. Sohl, R. A. Parker, H. F. Houghton, R. A. Volkert, A. A. Drake, R. C. Orndroff, 1995.

Parker, 1990. Bedrock geologic map of Monmouth junction quadrangle, New Jersey, U.S. Geological Survey Open-File Report 90-219, 1 pl., scale 1:24000, R. A. parker and H. F. Houghton, 1990.

Pavrides, 1986. Mountain Run fault zone of Virginia, in M. L. Jacobsen and T. R. Rodriguez, comp., National Earthquake Hazard reduction Program, Summaries of Technical Reports, Volume XXIII, U.S. Geological Survey Open-File Report 87-63, p 93-93, L. Pavrides, 1986.

Pavrides, 1994. Early Paleozoic Alkalic and Calc-Alkalic Plutonism and Associated Contact Metamorphism, Central Virginia Piedmont, U.S. Geological Survey Professional Paper 1529, L. Pavrides, J. Arth, J. Sutter, T. Stern and H. Cortesini Jr., 1994.

Pazzaglia, 1993. Stratigraphy, Petrography, and Correlation of Late Cenozoic Middle Atlantic Coastal Plain Deposits: Implications for Late-Stage Passive-Margin Geologic Evolution, Geological Society of American Bulletin, Volume 105, p 1617-1634, F.J. Pazzaglia, 1993.

Pazzaglia, 1994. Late Cenozoic Flexural Deformation of the Middle U.S. Atlantic Passive Margin, Journal of Geophysical Research, Volume 99, Number B6, p 12143-12157, F. J. Pazzaglia and T.W. Gardner, 1994.

Pohn, 2000. Lateral Ramps in the Folded Appalachians and in Overthrust Belts Worldwide- a Fundamental Element of Thrust-Belt Architecture, U.S. Geological Survey Bulletin 2163, p 1-63, H.A. Pohn, 2000.

Pohn, 2001. Lateral Ramps in the Folded Appalachians and in Overthrust Belts Worldwide- A Fundamental Element of Thrust-Belt Architecture, U.S. Geological Survey Bulletin 2163, p 1-21, H.A. Pohn, 2001.

Ratcliffe, 1971. The Ramapo Fault System in New York and Adjacent Northern New Jersey-A Case of Tectonic Heredity, Geological Society of America Bulletin, Volume 82, p 125-142, N. Ratcliffe, 1971.

Ratcliffe, 1982. Results of Core Drilling of the Ramapo Fault at Sky Meadow Road, Rockland County, New York, and Assessment of Evidence for Reactivation to Produce Current Seismicity, U.S. Geological Survey Miscellaneous Investigations, Map I-1401, 1 sheet, N. Ratcliffe, 1982.

Ratcliffe, 1984. Brittle fault fabrics, mineralogy, and geometry of border faults of the Newark basin, NY-NJ, from drill-core information, Geological Society of America Abstracts with Programs, Volume 16, Number 1, p 57, N. M. Ratcliffe and W. C. Burton, 1984.

Ratcliffe, 1985. Proceedings of the Second U.S. Geological Survey Workshop on the Early Mesozoic Basins of the Eastern United States, U.S. Geological Circular 946, G.R. Robinson, Jr., and A.J. Froelich eds., U.S. Geological Survey, Ratcliffe, 1985.

Ratcliffe, 1988. Structural analysis of Furlong fault and the relation of mineralization to faulting and diabase intrusion, Newark basin, Pennsylvania, in A. J. Frolich and G. R. Robinson Jr., eds., Studies of early Mesozoic basins of the eastern United States, U.S. Geological Survey Bulletin 1776, p 176-193, N. M. Ratcliffe and W. C. Burton, 1988.

Rodgers, 1970. The Tectonics of the Appalachians, Wiley-Interscience: New York, NY, p 271, J. Rodgers, 1970.

Root, 1977. North 40° latitude fault zone, Pennsylvania; a new interpretation, Geology, Volume 5, p 719-723, S. I. Root and D. M. Hoskins, 1977.

Root, 1999. Part III, Structural Geology and Tectonics, Chapter 21: Gettysburg-Newark Lowland, in C.H. Shultz ed., The Geology of Pennsylvania: Pennsylvania Bureau of Topographic and Geologic Survey Special Publication 1, p 298-305, S.I. Root and D.B. MacLachlan, 1999.

Ryder, 1992. Stratigraphic Framework of Cambrian and Ordovician Rocks in the Central Appalachian Basin from Medina County, Ohio, through Southwestern and South-Central Pennsylvania to Hampshire County, West Virginia, US Geological Survey Bulletin 1839, p 1-40, R.T. Ryder, A.G. Harris, and J.E. Repetski, 1992.

Ryder, 2002. Stratigraphic framework of Cambrian and Ordovician Rocks in the central Appalachian basin from Medina County, Ohio, through southwestern and south-central Pennsylvania to Hampshire County, West Virginia, U.S. Geological Survey Bulletin 1839-K, R.T. Ryder, A. G. Harris and J. E. Repeteski, 2002.

Sanders, 1963. Late Triassic Tectonic History of the Northeastern United States, American Journal of Science, Vol. 261, p 501-524, J. Sanders, 1963. in Olsen, Transtensional Arm of the Early Mesozoic Fundy Rift Basin: Penecontemporaneous Faulting and Sedimentation, Geology, Volume 18, p 695-698, R. Schlische.

Saylor, 1999. Part II, Stratigraphy and Sedimentary Tectonics, Chapter 3C: Precambrian and Lower Paleozoic Metamorphic and Igneous Rocks- in the Subsurface, in C.H. Shultz ed., The Geology of Pennsylvania: Pennsylvania Bureau of Topographic and Geologic Survey Special Publication 1, p 51-57, T.E. Saylor, 1999.

Scharnberger, 2006. The Lancaster Seismic Zone of the Southeast Pennsylvania in relation to the Gettysburg-Newark Basin, Geological Society of America, Abstracts with Programs, Volume 38, Number 2, p 83, C. Scharnberger, 2006.

Schlische, 2002. Progress in Understanding the Structural Geology, Basin Evolution, and Tectonic History of the Eastern North American Rift System, Structural Geology of the Eastern North American Rift System, p 23-64, Schlische, 2002.

Schlische, 2003. Progress in Understanding the Structural Geology, Basin Evolution, and Tectonic History of the Eastern North American Rift System, P. Letourneau and P. Olsen, eds., The Great Rift Valleys of Pangaea in Eastern North America, Volume 1, p 21-64, R. Schlische, 2003.

Schwab, 1997. Seafloor Characterization Offshore of the New York-New Jersey Metropolitan Area Using Sidescan-Sonar, U.S. Geological Survey, Open-File Report 00-295, 16 p, Schwab, 1997.

Seborowski, 1982. Tectonic implications of recent earthquakes near Ansville, New York, Bulletin of the Seismological Society of America, Volume 72, p 1601-1609, D. D. Seborowski, G. Williams, J. A. Kelleher, and C. T. Statton, 1982.

Seeber, 1998. The 1994 Cacoosing Valley Earthquakes Near Reading, Pennsylvania: A Shallow Rupture Triggered By Quarry Unloading, Journal of Geophysical Research, Volume 103, Number B10, p 24,505-24,521, L. Seeber, J. Armbruster, W. Kim, N. Barstow and C. Scharnberger, 1998.

Sevon, 1999. Part VI, Geologic History, Chapter 35: Cenozoic, in C.H. Shultz ed., The Geology of Pennsylvania: Pennsylvania Bureau of Topographic and Geologic Survey Special Publication 1, p 451-455, W.D. Sevon and G.M. Fleeger, 1999.

Sevon, 2000. Regolith in the Piedmont Upland Section, Piedmont Province, York, Lancaster and Chester Counties, Southeastern Pennsylvania, Southeastern Geology, Volume 39, Number 3 and 4, p 223-241, W. Sevon, October 2000.

Sheridan, 1988. The Atlantic Continental Margin, U.S. Geological Society of America, The Geology of North America, Volume 1-2, p 610, R. Sheridan and J. Grow, 1988.

Shrake, 1991. Pre-Mount Simon basin under the Cincinnati Arch: Geology, Volume 19, p.139-142, 1991.

Spoljaric, 1972. Geology of the Fall Zone in Delaware, Delaware Geological Survey, p 30, N. Spoljaric, March 1972.

Spoljaric, 1973. Normal Faults in Basement Rocks of the Northern Coastal Plain, Delaware, Geological Society of America Bulletin, Volume 84, p 2781-2783, N. Spoljaric, 1973.

SSES FSAR, 2003. Susquehanna Steam Electric Station Units 1 and 2 Final Safety Analysis Report, Section 2.5, Geology, Seismology, and Geotechnical Engineering, Rev. 58, Pennsylvania Power and Light, 2003.

Stanford, 1995. Possible Pliocene-Pleistocene Movement on a Reactivated Mesozoic Fault In Central New Jersey, Geological Society of America Abstracts with Programs, Volume 27, Number 1, p 83, S. Stanford, D. Jagel, and D. Hall, 1995.

Street, 1977. A study of northeastern North American spectral moments, magnitudes, and intensities, Bulletin of the Seismological Society of America, Volume 67, p 599-614, R. L. Street and F. T. Turcotte, 1977.

Swanson, 1982. Preliminary model for early transform history in central Atlantic rifting, Geology, 10:317-320, M. Swanson, 1982.

Tanner, 1987. Gravity Anomaly Map of North America, Decade of North American Geology (DNAG), Geological Society of America, J. Tanner, 1987.

Thompson, 1999. Part II, Stratigraphy and Sedimentary Tectonics, Chapter 5: Ordovician, in C.H. Shultz ed., The Geology of Pennsylvania: Pennsylvania Bureau of Topographic and Geologic Survey Special Publication 1, p 74-89, A.M. Thompson, 1999.

Thurber, 1985. Crustal structure along the Ramapo fault zone, New York State, Earthquake Notes, Volume 56, p 145-152, C. Thurber and T. Caruso, 1985.

Tuttle, 1991. Historic and prehistoric earthquake-induced liquefaction in Newbury, Massachusetts, Geology, Volume 19, p 594-597, M. Tuttle and L. Seeber, 1991.

- Tuttle, 2002.** Paleoliquefaction study of the Clarendon-Linden fault system, western New York State, Tectonophysics, Volume 353, p 263-286, M. Tuttle, K. Dyer-Williams and N. L. Barstow, 2002.
- USGS, 1969.** 1:250,000 Topographic Maps: Newark, New Jersey, and Harrisburg, Pennsylvania, USGS, 1969.
- USGS, 1974.** 1:250,000 Topographic Maps: Williamsport, Pennsylvania, USGS, 1974.
- USGS, 1976.** 1:250,000 Topographic Maps: Scranton, Pennsylvania, USGS, 1976.
- USGS, 1984.** 1:100,000 Topographic Maps: Williamsport East and Sunbury, Pennsylvania, USGS, 1984.
- USGS, 1989.** 1:24,000 Topographic Maps: Berwick, Pennsylvania, USGS, 1989.
- USGS, 2001.** Documentation for the 2002 Update of the National Seismic Hazard Maps, USGS Open-File Report 02-420, 33 p, USGS, 2001.
- USGS, 2002.** Physiographic Divisions of the US, Polygon coverage of Physiographic Divisions in the conterminous United States automated from Fenneman and Johnson 1946, 1:7,000,000-scale map "Physical Divisions of the United States". <http://water.usgs.gov/GIS/metadata/usgswrd/XML/physio.xml>, USGS, 2002.
- USNRC, 2007.** Exelon Generation Company, LLC, ESP Site, DOKET NO. 52-007, Early Site Permit, Early Site Permit No. ESP-001. U.S. Nuclear Regulatory Commission, March 2007.
- VADOT, 2008.** Aggregate Plant Certification Study Guide, The Virginia Dept. of Transportation, 32nd Ed., Appendix F, P. F-1~F-26, VADOT, 2008
- Van Diver, 1993.** Plate Tectonics, Roadside Geology of Pennsylvania, Roadside Geology Series, 352 p, Van Diver, 1993.
- VDEQ, 2008.** Virginia's Mineral and Energy Resources, Virginia Resource-Use Education Council, Virginia's Natural Resources Education Guide, 17 p., VDEQ, 2008.
- Vlahoic, 1998.** Joint hypocenter-velocity inversion for the eastern Tennessee seismic zone, Journal of Geophysical Research, Volume 103, p 4,879-4,896, G. Vlahoic, C. A. Powell, M. C. Chapman, and S. Sibol, 1998.
- Way, 1999.** Part IV. Physiography, Chapter 29: Appalachian Mountain Section of the Ridge and Valley Province, in C.H. Shultz ed., The Geology of Pennsylvania: Pennsylvania Bureau of Topographic and Geologic Survey Special Publication 1, p 353-361, J.H. Way, 1999.
- Weems, 1998.** New recognized en echelon fall lines in the Piedmont and Blue Ridge provinces of North Carolina and Virginia, with a discussion of their possible ages and origins, U.S. Geological Survey Open-File Report 98-374, 52 p, R. E. Weems, 1998.

Wentworth, 1983. Regenerate Faults of Small Cenozoic Offset - Probable Earthquake Sources in the Southeastern United States, U.S. Geological Survey, Professional Paper 1313-S, C. Wentworth and M. Mergner-Keefer, 1983.

Wheeler, 1996. Earthquakes and the Southeastern Boundary of the Intact Iapetan margin in Eastern North America, Seismological Research letters, Volume 67, Number 5, p 77-83, R. Wheeler, 1996.

Wheeler, 2005. Known or suggested Quaternary tectonic faulting, central and eastern United States-New and updated assessments for 2005, U.S. Geological Survey Open-File Report 2005-1336, p 37, R. L. Wheeler, 2005.

Wheeler, 2006. Quaternary tectonic faulting in the Eastern United States, Engineering Geology, Volume 82 (2006), p 165-186, R.L. Wheeler, 2006.

Wise, 1998. Lancaster County seismic zone (Penna)- Reactivation of a tectonic structural feature. Geological Society of America Abstracts with Programs, Volume 30, Number 7, p A-320, D. U. Wise and T. R. Faill, 1998.

Withjack, 1998. Diachronous Rifting, Drifting, and Inversion on the Passive Margin of Central Eastern North America: An Analog for Other Passive Margins, AAPG Bulletin, Volume 82, Number 5A, p 817-835, M.O. Withjack, R.W. Schlische, and P.E. Olsen, 1998.

Withjack, 2005. The Early Mesozoic Birdsboro Central Atlantic Margin Basin in the Mid-Atlantic Region, Eastern United States: Discussion, GSA Bulletin, Volume 117, Number 5/6, p 823-832, R.W. Schlische and M.O. Withjack, 2005.

Wood, 1970. Structural Controls of the Anthracite Region, Pennsylvania, Studies of Appalachian Tectonics: Central and Southern, Chapter 9, p 147-160, G. Wood and M. Bergin, 1970.

Yang, 1981. Seismotectonics of Northern United States and Adjacent Canada, Journal of Geophysical Research, Volume 86, p 4,981-4,998, J. P. Yang and Y. P. Aggarwal, 1981.

Zen, 1983. Bedrock Geologic Map of Massachusetts, U.S. Geologic Survey in cooperation with The Commonwealth of Massachusetts Department of Public Works, 3 sheets, scale 1:250,000, Zen, E.-A., ed., Goldsmith, R., Ratcliffe, N.M., Robinson, P., Stanley, R.S., compilers, Hatch, N.L., Jr., Shride, A.F., Weed, E.G.A., and Wones, D.R., 1983.

Zietz, 1982. Composite magnetic anomaly map of the United States, Part A: Conterminous United States, U.S. Geological Survey Map GP-54923, Scale 1:2,500,000, I. Zietz, 1982.}

2.5.2 VIBRATORY GROUND MOTION

The U.S. EPR FSAR includes the following COL Items for Section 2.5.2:

A COL applicant that references the U.S. EPR design certification will review and investigate site-specific details of the seismic, geophysical, geological, and geotechnical information to determine the safe shutdown earthquake (SSE) ground motion for the site and compare site-specific ground motion to the Certified Seismic Design Response Spectra (CSDRS) for the U.S. EPR.

This COL Item is addressed as follows:

This section provides a detailed description of the vibratory ground motion assessment that was carried out for the {BBNPP} site, resulting in the development of the {BBNPP} site Safe Shutdown Earthquake (SSE) ground motion response spectra. {Starting points for this site assessment are the United States Geological Service (USGS) documentation of the studies for the 2002 and 2008 National Seismic Hazard maps (USGS, 2002)(USGS, 2008), the EPRI-SOG probabilistic seismic hazard analysis (PSHA) methodology outlined in EPRI NP-4726-A 1988 (EPRI, 1988), and the Early Site Permit (ESP) Application for the Clinton Nuclear Power Plant site (EGC, 2006) submitted to the NRC on April 16, 2006 by Exelon Generation Company (EGC).

Nuclear Regulatory Commission (NRC) Regulatory Guide 1.208, "A Performance-Based Approach to Define Site-Specific Earthquake Ground Motion," March, 2007, (NRC, 2007a) states in Section B, Discussion:

"The CEUS is considered to be that part of the United States east of the Rocky Mountain front or east of Longitude 105 West (Refs. 13, 14). A PSHA in the CEUS must account for credible alternative seismic sources through the use of a decision tree with appropriate weighting factors that are based on the most up-to-date information and relative confidence in alternative characterizations for each seismic source. Seismic sources identified and characterized by Lawrence Livermore National Laboratory (LLNL) (Refs. 13-15) and the Electric Power Research Institute (EPRI) (Ref. 16, 17) were used for CEUS studies in the past. In addition to the LLNL and EPRI resources, the United States Geological Survey maintains a large database of seismic sources for both the CEUS and the WUS. The characterization of specific seismic sources found in these databases may still represent the latest information available at the time that a PSHA is to be undertaken. However, if more up-to-date information is available, it should be incorporated."

Regulatory Guide 1.165 (NRC, 1997a) provides the framework for assessing the appropriate SSE ground motion levels for new power generating nuclear plants. Regulatory Guide 1.165 also notes that an acceptable starting point for the SSE assessment at sites in the Central and Eastern United States (CEUS) is the PSHA conducted by the Electric Power Research Institute (EPRI) for the Seismicity Owners' Group (SOG) in the 1980's. Regulatory Guide 1.165 further specifies that the adequacy of the EPRI-SOG hazard results must be evaluated in light of more recent data and evolving knowledge pertaining to seismic hazard evaluation in the CEUS.

Reference 16 of the NRC Regulatory Guide 1.208 is Electric Power Research Institute, "Probabilistic Seismic Hazard Evaluations at Nuclear Power Plant Sites in the Central and Eastern United States," NP-4726, All Volumes, 1989-1991. The title and number of the referenced document are not in agreement. The title of EPRI-4726 is "Seismic Hazard Methodology for the Central and Eastern United States." No document could be found that had the title provided by the NRC. In lieu of the reference 16, Section 2.5.2 of this document has used concepts from and interpretations presented in EPRI NP-4726, "Seismic Hazard Methodology for the Central and Eastern United States," 1986; EPRI-4726-A, "Seismic Hazard Methodology for the Central and Eastern United States," 1988; and EPRI NP-6395-D-1989 (EPRI, 1989a).

As stated in Regulatory Guide 1.208, the PSHA should incorporate the detailed guideline from NUREG-6372 "Recommendations for Probabilistic Seismic Hazard Analysis: Guidance on Uncertainty and Use of Experts" Vol. 1 and 2. However, RG-1.208 does not limit the procedure to

conduct the PSHA to the approach described in “Seismic Hazard Methodology for the Central and Eastern United States” (EPRI NP-4726). The USGS information is also included in Regulatory Guide 1.208 as a potential starting point. USGS information can be used not only to define seismic sources but also to implement the PSHA procedure. In addition, the PSHA results developed by the USGS (Frankel, 1995) are prescribed in several building codes such as Minimum Design Loads for Buildings and Other Structures (ASCE/SEI 7-05)(ASCE, 2005a), and International Building Code. These building codes are widely accepted by the engineering community.

Frankel’s smoothed seismicity approach was developed to be applied in the calculation of annual probabilities of exceedance as low as $10E-05$. In his original paper, Frankel (Frankel, 1995) shows that his smoothed seismicity methodology reproduces the hazards obtained at 30 nuclear power plants sites following the EPRI methodology. He also shows that at four sites, the PSHA results obtained by his and the EPRI methodologies are very similar down to hazards of $10E-04$ to $10E-05$.

The USGS and the EPRI PSHA methodologies are essentially the same. Their most noticeable difference is in their approach to calculate the seismicity parameters. Even in this step, both methodologies rely mainly on the historical seismicity, including estimates of incompleteness, and using a Gaussian smoothing procedure. The USGS, as the consultant of the NRC to review the EPRI NP-4726 report expressed several concerns about the EPRI PSHA methodology in calculating the seismicity parameters. However, after discussions among EPRI, USGS, and NRC staffs, they concluded that both the USGS and the EPRI approaches for calculating the seismicity parameters of the source zones provided satisfactorily hazard results. Neither approach is superior to the other in performing PSHA especially in the CEUS.

Accordingly, the evaluation of vibratory ground motions made for the BBNPP site addresses seismic hazard update requirements in Regulatory Guide 1.165 (NRC, 1997a) and meets the SSE requirements given in paragraph (d) of 10 CFR 100.23 (CFR, 2007). Following the recommendation of Regulatory Guide 1.165 (NRC, 1997a), the 1989 EPRI study, EPRI NP-6395-D (EPRI, 1989a) provides a basis to start seismic hazard calculations. A Probabilistic Seismic Hazard Analysis (PSHA) determines the annual frequency of exceedance as a function of minimum ground motion. This annual frequency results from the integration of hazard contributions of seismic sources characterized by spatial extent and location, magnitude, frequency recurrence, and propagating the ground motion from the sources to the site. These calculations incorporate parametric variability, including alternative models and parametric distributions, as well as consideration of statistical uncertainties.

The following subsections summarize the procedure followed and results from the vibratory ground motion studies that were carried out for the BBNPP Site.

1. As a starting step, the EPRI-SOG tectonic interpretations in EPRI NP-4726 1986 (EPRI, 1986) were examined in light of more recent geological, seismological, and geophysical data under the guidance of NRC Regulatory Guide 1.208, (NRC, 2007a). Sections 2.5.2.1 through 2.5.2.3 document this review and update of the EPRI-SOG seismicity, seismic source, and ground motion models.
2. Section 2.5.2.4 develops PSHA parameters at the site assuming the very hard rock foundation conditions implied by currently accepted ground motion attenuation models.

3. Section 2.5.2.5 summarizes information about the seismic wave transmission characteristics of the BBNPP site with reference to more detailed discussion of all engineering aspects of the subsurface in Section 2.5.4.
4. Section 2.5.2.6 describes the development of the horizontal SSE ground motion for the BBNPP site.

The selected SSE ground motion is based on the risk-consistent/performance-based approach of Regulatory Guide 1.208 (NRC, 2007a), with reference to NUREG/CR-6728 (NRC, 2001), NUREG/CR-6769 (NRC, 2002), and ASCE/SEI 43-05 (ASCE, 2005b). Horizontal ground motion amplification factors are developed using site-specific data and estimates of near-surface soil and rock properties. These amplification factors are then used to scale the hard rock spectra to develop Uniform Hazard Spectra accounting for site-specific conditions using Approach 2B of NUREG/CR-6728 (NRC, 2001) and NUREG/CR-6769 (NRC, 2002). Horizontal SSE spectra are developed from these soil Uniform Hazard Response Spectra using the performance-based approach of ASCE/SEI 43-05 (ASCE, 2005b), as implemented in Regulatory Guide 1.208 (NRC, 2007a). The SSE motion is defined at the free ground surface of a hypothetical outcrop at the base of the nuclear island foundation. See Sections 2.5.4 and 2.5.2.5 for further discussion of the subsurface conditions. Section 2.5.2.6 also describes vertical SSE spectra developed by scaling the horizontal SSE by a frequency-dependent vertical-to-horizontal (V/H) factor.

The SSE spectra described herein are considered performance goal-based (risk-informed) site specific safe shutdown earthquake response spectra. As discussed below, the SSE spectra for the BBNPP Site have been developed following the graded performance-based, risk-consistent method described in ASCE/SEI Standard 43-05 (ASCE, 2005b). The method specifies the level of conservatism and rigor in the seismic design process such that the performance of structures, systems, and components (SSC) of the plant achieve a uniform seismic safety performance consistent with the NRC's safety goal policy statement.

The SSE spectra, and its specific location at a free ground surface, reflect the seismic hazard in terms of a PSHA and geologic characteristics of the site and represent the site-specific ground motion response spectrum (GMRS) of Regulatory Guide 1.208 (NRC, 2007a). These spectra are expected to be modified as appropriate to develop ground motion for design considerations.

The SSE developed in this section meets the requirements of paragraph (d) of 10 CFR 100.23 (CFR, 2007).}}

2.5.2.1 Seismicity

The U.S. EPR FSAR includes the following COL Item in Section 2.5.2.1:

Seismicity is site specific and will be addressed by the COL applicant.

This COL Item is addressed as follows:

{Current probabilistic hazard methodologies consider that the activity in area seismic sources can be adequately represented by the Gutenberg-Richter (G-R) recurrence equation in terms of body wave magnitude, m_b . A quantitative derivation of the G-R parameters is based on historical seismicity, i.e., on catalogs of seismic events. The seismic hazard analysis conducted by EPRI as delineated in NP-6395-D 1989 (EPRI, 1989a) relied, in part, on an analysis of historical seismicity in the Central and Eastern United States (CEUS) to estimate seismicity parameters

(rates of activity, a , and slope b -values of the Guttenberg Richter equation) for individual seismic sources. The historical earthquake catalog used in the EPRI analysis was complete through 1984.

As recognized in NRC Regulatory Guide 1.208 (NRC, 2007a), the United States Geological Survey (USGS) maintains a large database of seismic sources for both the Central and Eastern United States, as part of their efforts to develop National Seismic-Hazard Maps (USGS, 1996)(USGS, 2002)(USGS, 2008) , In Open-File Report 96-532, entitled "National Seismic-Hazard Maps: Documentation June 1996 (USGS, 1996) the USGS states that their CEUS catalog was primarily based on a catalog by Seeber (Seeber, 1991), who conducted a refinement of the EPRI 1986 catalog (EPRI, 1986).

Thus, the catalog compiled by the USGS up to the end of 2001, has been used in the determination of G-R parameters for the area seismic sources that affect the BBNPP. This catalog constitutes the most recently updated list in terms of body-wave magnitude, m_b , units.

Section 2.5.2.1.1 and Section 2.5.2.1.2 are added as a supplement to the U.S. EPR FSAR.}

2.5.2.1.1 Regional Seismicity Catalog Used for 1989 Seismic Hazard Analysis Study

{Many seismic networks record earthquakes in the CEUS. A large effort is continuously made by the USGS to examine and combine available data on historical earthquakes and to develop a homogeneous earthquake catalog that contains all recorded earthquakes for the region. "Homogeneous" means that estimates of m_b for all earthquakes are consistent, duplicate earthquakes have been eliminated, non-earthquakes (e.g., mine blasts and sonic booms) have been eliminated, and significant events in the historical record have not been missed. Thus, the USGS catalog forms a strong basis on which to estimate seismicity parameters. The USGS catalog updated up to 2001 has been used because this is the latest year for which the m_b units were reported. The use of m_b is required in view that the Guttenberg-Richter equation that describes the seismicity in area sources is considered to be valid in m_b units.

2.5.2.1.2 Updated Seismicity Data

Regulatory Guide 1.165 (NRC, 1997a) specifies that earthquakes of a Modified Mercalli Intensity (MMI) greater than or equal to IV or of a magnitude greater than or equal to 3.0 should be listed for seismic sources, "any part of which is within a radius of 200 mi (320 km) of the site (the site region)." The USGS catalog and methodology for determining seismicity parameters consider precisely the minimum magnitude of m_b equal to 3.0

Figure 2.5-40 shows the BBNPP and its associated "site region," i.e., a window that incorporates the 200 mi (320 km) radius around the site. Figure 2.5-34 through Figure 2.5-40 also show such a site region and display the epicenters of historical seismic events.

The USGS updated catalogs are compiled by examining and combining events listed in several CEUS source catalogs (Mueller, 1997). In this effort, the USGS intent is to develop a catalog dominated by entries from the best-researched sources and they use this priority to choose the best location and magnitude from among multiple source catalogs for each earthquake. In addition, the secondary events have been filtered as explained in a recent USGS publication (USGS, 2008). Traditionally, most CEUS earthquake magnitudes are reported as a short-period surface-wave magnitude (m_{bLg}) and the ground-motions used in the hazard analysis are

predicted based on m_{bLg} . In most cases a preferred magnitude from a catalog was assumed by the USGS to be equivalent to m_{bLg} , calling it m_b .

The catalog of use is the USGS catalog updated to the year 2007. Recent applications, such as the Clinton ESP, conclude that the update in the seismicity from the 1984 EPRI-SOG study do not significantly affect the seismicity parameters, i.e. the slope of the G-R (Gutenberg-Richter) equation (b parameter) and seismic rate (recurrent rate) in their respective regions of study. The same conclusion is reached in relation to the geometry of the seismic sources. The only relevant updates that were identified are the maximum magnitude of the Wabash Valley area source and the introduction of the New Madrid characteristic cluster events. A cluster model is required to represent the events that occurred in the three-series cluster with large magnitude ($>7.5M$). The seismic parameters related to the New Madrid events are not in agreement with the general G-R equation utilized in the area source hazard computation, and therefore need to be treated separately. The New Madrid events occurred in a cluster of three events. The event shown in the catalog is considered to be the main New Madrid event for the 1811-1812 cluster set. The other two events are considered as the foreshock/aftershock events and are filtered out from the catalog by USGS. This New Madrid event is treated as the New Madrid Characteristic Cluster events in the PSHA since it does not follow the G-R (Gutenberg-Richter) relationship for seismicity rate. Therefore, this 1811-1812 main event (shown in the catalog) is ignored when calculating the seismicity rate for the New Madrid area source.

The catalog update methodology adopted the approach described in the USGS open file report 2008-1128 "The 2008 Update of the United States National Seismic Hazard Maps" that USGS uses to update the USGS 2001 catalog to the year 2006 to reduce the additional epistemic uncertainty related to the magnitude conversion between different units to the m_{bLg} unit used in the USGS 2001 catalog. It is considered that the magnitude may be adopted from the reported values, since the difference from the conversion between different units is considerably small for small magnitude earthquakes. Only two events of low magnitude are incorporated in the period between 2002 and 2007.

The update to the catalog does not have a significant effect on the b-parameter, seismic occurrence rate, and/or the entire PSHA study at the BBNPP site. The use of the updated earthquake catalog results in a marginal reduction of the seismic occurrence rates, when compared to the USGS 2001 catalog. The resulting ground motion levels are marginally lower.

The USGS 2001 G-R parameters are selected for the BBNPP PSHA since: (1) though small, there is additional epistemic uncertainty in the unit use of the 2002-2007 seismicity; and (2) the effect on the seismic hazard of the 2002-2007 update is a marginal reduction in the ground motion levels, which is deemed as un-conservative.

The update in the introduction of the New Madrid characteristic cluster events is performed. These updates are adapted to the BBNPP site from the Clinton ESP Application.

A PSHA results showed that the New Madrid Seismic Zone (NMSZ) is a significant contributor to the hazard at the BBNPP site at low frequencies. As such, characterizaion of this seismic source was added to the PSHA input for BBNPP. After a literature review of the existing NMSZ models, the characteristic earthquake model as described in the Clinton ESP (EGC, 2006) was selected as the input.

The Clinton ESP (EGC, 2006) also conducted paleoliquefaction evaluations where evidence of soil liquefaction that occurred in prehistoric times is inferred from features such as sand boils or blows, dikes, and sills. By estimating the date and geographical distribution of these features, it is possible to infer the magnitude of the earthquake that originated the features. Earlier investigations of paleoliquefaction features in the southern Illinois basin and in parts of Indiana, Illinois, and Missouri have identified paleoliquefaction occurrences that could have been caused by Holocene and latest Pleistocene earthquakes with estimated moment magnitudes (**M**) of 6 to 7.8. Details about the paleoliquefaction reconnaissance carried out for the Clinton ESP Site seismic hazard evaluation are given in Section 2.1.4 and Attachment 1 of Appendix B of the Clinton ESP document (EGC, 2006). These details include a discussion of each of the identified features, pictures of the features, results of radiocarbon dating, and criteria for differentiating seismic versus non-seismic liquefaction features. The Clinton ESP was issued by the NRC in March 2007 (NRC, 2007c).

These paleoliquefaction studies have been utilized for developing improved representations of characteristic earthquakes in the New Madrid Fault System. It was also concluded, from these paleoliquefaction evaluations, that the range of maximum magnitude earthquakes assigned to a random background earthquake in the PSHA for the Clinton ESP Site must include events comparable to that estimated for the Springfield, IL earthquake which occurred approximately 22 mi (35 km) northeast of Springfield, IL and 30 mi (48 km) southwest of EGC ESP site, that is, **M** 6.2 to 6.8.5. The Springfield earthquake is located approximately 22 mi (35 km) northeast of Springfield, Illinois, and 30 mi (48 km) southwest of the Clinton ESP site.

Another significant source of severe seismic events in the East Coast of the United States is the Charleston seismic source that is about 620 mi (1000 km) from the BBNPP site. Despite this long distance, it was considered that this source could still have some significant contribution to the hazard at the BBNPP site, particularly at low frequency ground motion. Thus, the Charleston seismic source has been included in the present PSHA. Since publication of the EPRI seismic hazard analyses, paleoliquefaction investigations and other studies have impacted the characterization of the geometry, M_{max} , and recurrence in the Charleston seismic source. Paleoliquefaction studies in the area of the 1886 Charleston earthquake date back to Cox and Talwani (Cox, 1983) who discovered evidence for earthquake induced liquefaction features preserved in the South Carolina Coastal Plain sediments. Following this discovery, USGS conducted intensive studies to identify the spatial extent of paleoliquefaction features. USGS studies led to the discovery of sand blows that predated 1886, hence providing a basis for estimating the recurrence interval of large earthquakes in the Charleston area (Obermeier, 1987). More recent studies and interpretations have led to the refinement of the Charleston source zone parameters (Johnston, 1996; Bakun, 2004; Marple, 2000; Talwani, 2000; USGS, 2002; USGS, 2008). For example, radiocarbon dating techniques in new studies account for the fluctuation of atmospheric C-14 over time while previous studies assumed that the amount of C-14 has remained constant (Talwani, 2000). Based on the new interpretations, alternative geometries have been used for this zone. Marple (Marple, 2000) proposed a postulated East Coast Fault System (ECFS) in the Coastal Plain of Eastern US and argued that the southern segment of this fault system is probably the source of 1886 Charleston earthquake. In their 2008 version of National Seismic Hazard Maps, USGS (USGS, 2008) extended the Charleston area source offshore to include the Helena Banks fault zone as a possible source. USGS (USGS, 2008) also define another (elongated) area source which encloses Woodstock lineament. This area source envelops half of the southern segment of ECFS. These two area sources have equal weights. Bechtel has examined these new data and developed an Updated Charleston Seismic Source (UCSS) model. The UCSS model has been used in development of the FSAR

for the Vogtle ESP (SNOC, 2008). The UCSS model as described in Vogtle ESP (SNOC, 2008) has been adopted here after review and comparison with other models of Charleston seismic source.

The mean of M_{\max} distribution used in UCSS model (M_w 7.1) is very close to that of USGS (M_w 7.2). The source geometry used by UCSS considers four source zones with different weights. Beside the area of strong shaking during 1886 Charleston earthquake, this source zone combination accounts for the liquefaction features that are distributed far from the epicentral area. It also includes the southern segment of ECFS (Marple, 2000) as a possible source of the 1886 Charleston earthquake with a low weight of 0.1.

Recurrence interval of Charleston characteristic earthquake in the UCSS model is based on the work of Talwani (Talwani, 2000). While Talwani (Talwani, 2000) argue that only the 2000 year record of paleoliquefaction data is complete, UCSS model uses a combination of 2000 year and 5000 year record, therefore considering the possibility that the paleoliquefaction features may have been preserved in the 5000 year data. The 5000 year record, however, has a lower weight (0.2) than the 2000 year data (0.8). Based on comparisons between the UCSS model and other Charleston characteristic earthquake models including the USGS (USGS, 2008) model, it is concluded that the UCSS model better addresses the epistemic uncertainty in source zone parameters (including recurrence times) and therefore is used here to characterize the Charleston seismic source. This model is discussed in section 2.5.2.2.4. The description of the UCSS model is based on the Vogtle ESP FSAR (SNOC, 2008).

As a result of the investigations performed, relevant updates in maximum magnitude and geometry have been performed for the New Madrid cluster events and the UCSS. These events are distant from the BBNPP site but they still contribute to the hazard at the low frequencies.}

2.5.2.2 Geologic and Tectonic Characteristics of Site and Region

The U.S. EPR FSAR includes the following COL Item in Section 2.5.2.2:

Geologic and tectonic characteristics are site specific and will be addressed by the COL applicant.

This COL Item is addressed as follows:

{As described in Section 2.5.1, a comprehensive review of available geological, seismological, and geophysical data has been performed for the BBNPP Site region and adjoining areas. As discussed in Section 2.5.1.2, excavation mapping is required during construction and any noted deformational zones will be evaluated and NRC notified when excavations are open for inspection. The seismotectonic characteristics of the region constitute the basis for defining the seismic source zones that affect the BBNPP Site.

This section summarizes the geologic structure and activity that could potentially result in seismic-induced vibratory ground motions at the BBNPP Site. The summary addresses Regulatory Positions 1 and 2 within Regulatory Guide 1.165 (NRC, 1997a), which requires that investigation of seismic sources to be performed within a 200 mi (320 km) radius of the site. The following sections summarize the seismic source interpretations (EPRI, 1986) that lie at least partially within this radius, relevant post-EPRI seismic source characterization studies and

updated interpretations based on new data. The evaluation identified no new information which involved a change to the catalog that could impact the outcome of the PSHA.

Major sources of potential seismic activity such as the New Madrid Seismic Zone (NMSZ) and the Charleston Seismic Zone (CSZ) are located beyond 200 mi (320 km) from the site. However, based on new paleo-seismology data, updated characteristic earthquake models have been recently formulated for the NMSZ and the CSZ. A sensitivity analysis for the BBNPP Site using these updated models showed that characteristic earthquake events from both sources are significant contributors to low frequency ground motion at the site. The sensitivity analysis also showed that Charlevoix seismic zone (in Canada) is a significant contributor to the hazard at low frequencies. Therefore these three sources have been included in the PSHA study for the site.

Three major updates on seismic sources and characteristic earthquake models include:

The East Coast Fault System (ECFS) represents a new postulated seismic source along the Atlantic Seaboard (Section 2.5.1.1.4.3.4.1). The southern segment of the ECFS has been proposed by Marple (Marple, 2000) as being the source of the 1886 Charleston earthquake;

The average recurrence interval for large magnitude earthquakes in the Charleston characteristic model has been updated to 550 years based on paleoliquefaction data. The Charleston seismic source geometry also has been updated to include the southern segment of the ECFS as a possible source of the 1886 earthquake;

Assessments of magnitude, location, and return periods of large characteristic earthquakes of the New Madrid Seismic Zone (NMSZ) have been updated.

Detailed discussions of the updated source models are presented in the following sections.

Section 2.5.2.2.1 and Section 2.5.2.2.2 are added as a supplement to the U.S. EPR FSAR.

2.5.2.2.1 Summary of EPRI Seismic Sources

The evaluations of new information examined in previous ESPs (EGC, 2006)(NRC, 2005) concluded that the EPRI-SOG seismic sources remain appropriate for assessing seismic hazards in CEUS. Therefore, the seismic sources defined in the 1989 EPRI/SOG study (EPRI, 1989a) have been adopted for updating the BBNPP site PSHA. However, it is noted that updates and adjustments are required for the maximum magnitude distribution for the area sources and that characteristic earthquake models must be used to properly account for more recent information on the seismic activity in the New Madrid and Charleston seismic zones.

In the 1986 EPRI study (EPRI, 1986), six independent Earth Science Teams (ESTs) evaluated geological, geophysical, and seismological data to develop seismic sources in the CEUS. These sources were used to model the occurrence of future earthquakes and evaluate earthquake hazards at nuclear power plant sites across the CEUS. The six ESTs involved in the EPRI project were: Bechtel Group, Dames & Moore, Law Engineering, Rondout Associates, Weston Geophysical Corporation, and Woodward-Clyde Consultants. Each team produced a report, included in EPRI NP-4726, (EPRI, 1986), that provides detailed descriptions of how they identified and defined seismic sources.

The EPRI/SOG ESTs also determined recurrence parameters and maximum magnitudes for each source in m_b or magnitude units, including their corresponding weights. These models were implemented into a probabilistic seismic hazard analysis (PSHA) reported in EPRI NP-6395-D (EPRI, 1989a). EPRI NP-6452-D (EPRI, 1989b) summarized the parameters used in the final PSHA calculations, and this reference is the primary source for defining the geometry of area seismic sources for the BBNPP PSHA presented herein. For the computation of hazard, some of the 1989 EPRI seismic source parameters were updated, as discussed below.

The following sections list the seismic source interpretations in the 1989 EPRI PSHA study (EPRI, 1989a), relevant post-EPRI seismic source characterization studies, and updated interpretations provided by the more recent data. The summary of seismic sources and parameters was developed from the 1989 EPRI project EPRI NP-6452-D (EPRI, 1989b). The listed area seismic sources are those that at least partially lie within the "site region," i.e. within the circle with a 200-mi (320-km) radius centered at the BBNPP Site. The list includes the code used by each team to designate each source, the name of the source, the assigned recurrence parameter b and the assigned maximum magnitude, and weights assigned to each value of the parameter b and of the maximum magnitude.

Figure 2.5-34 through Figure 2.5-39 present the geometry of the seismic sources selected to estimate the hazard at the BBNPP Site, including plots of earthquakes with m_b equal to or higher than 3.0 in the updated earthquake catalog, to illustrate the spatial relationships between seismicity and seismic sources. Earthquake epicenters in the updated earthquake catalog include events from the period between 1627 and 2007, as listed in Table 2.5-1. Following the 1989 EPRI study (EPRI, 1989a) and the 1996, 2002 and 2008 USGS studies (USGS, 1996; USGS, 2002; USGS, 2008), the recurrence parameters for area seismic sources were computed for each one-degree latitude and longitude cell that intersects any portion of a seismic source.

The PSHA conducted in the EPRI-SOG study employed three strong ground motion attenuation relationships developed by Boore and Atkinson (Boore, 1987) and McGuire and others (McGuire, 1988) combined with the response spectral shapes by Newmark and Hall (Newmark, 1982) which are based on Western North America earthquake records. More recently-developed ground motion attenuation models (EPRI, 2004) are supported by a better understanding of earthquake generation and indicate that significant differences in the crustal properties between western and eastern North America lead to significant differences in the frequency content of ground motions between the two regions. In addition, the more recent ground motion models include an improved assessment of variability about median estimates, and thus have been used for this evaluation.

2.5.2.2.1.1 Sources Used for EPRI PSHA – Bechtel Group

The seismic sources and recurrence parameters identified by the Bechtel EPRI/SOG EST (EPRI, 1989a) that are within 200 mi (320 km) of the BBNPP Site are listed in Table 2.5-3.

Figure 2.5-34 illustrates the locations and geometries of the Bechtel Group seismic sources contributing to 99% of the seismic hazard along with plots of earthquakes with m_b equal to or higher than 3.0 between 1627 and 2007.

2.5.2.2.1.2 Sources Used for EPRI PSHA – Dames & Moore

The seismic sources and recurrence parameters identified by the Dames & Moore EPRI/SOG EST (EPRI, 1989a) that are within 200 mi (320 km) of the BBNPP Site are listed in Table 2.5-4.

Figure 2.5-26 illustrates the locations and geometries of the Dames and Moore seismic sources contributing to 99% of the seismic hazard along with plots of earthquakes with m_b equal to or higher than 3.0 between 1627 and 2007.

2.5.2.2.1.3 Sources Used for EPRI PSHA – Law Engineering

The seismic sources and recurrence parameters identified by the Law Engineering EPRI/SOG EST (EPRI, 1989a) that are within 200 mi (320 km) of the BBNPP Site are listed in Table 2.5-5.

Figure 2.5-36 illustrates the locations and geometries of Law Engineering seismic sources contributing to 99% of the seismic hazard along with plots of earthquakes with m_b equal to or higher than 3.0 between 1627 and 2007.

2.5.2.2.1.4 Sources Used for EPRI PSHA – Rondout Associates

The seismic sources and recurrence parameters identified by the Rondout Associates EPRI/SOG EST (EPRI, 1989a) that are within 200 mi (320 km) of the BBNPP Site are listed in Table 2.5-6.

Figure 2.5-37 illustrates the locations and geometries of Rondout seismic sources contributing to 99% of the hazard along with plots of earthquakes with m_b equal to or higher than 3.0 between 1627 and 2007.

2.5.2.2.1.5 Sources Used for EPRI PSHA – Weston Geophysics Consultants

The seismic sources and recurrence parameters identified by the Weston Geophysical EPRI/SOG EST (EPRI, 1989a) that are within 200 mi (320 km) of the BBNPP Site are listed in Table 2.5-7.

Figure 2.5-38 illustrates the locations and geometries of Weston seismic sources contributing to 99% of the hazard along with plots of earthquakes with m_b equal to or higher than 3.0 between 1627 and 2007.

2.5.2.2.1.6 Sources Used for EPRI PSHA – Woodward-Clyde Consultants

The seismic sources and recurrence parameters identified by the Woodward-Clyde Consultants EPRI/SOG EST (EPRI, 1989a) that are within 200 mi (320 km) of the BBNPP Site are listed in Table 2.5-8.

Figure 2.5-39 illustrates the locations and geometries of Woodward-Clyde seismic sources contributing to 99% of the hazard along with plots of earthquakes with m_b equal to or higher than 3.0 between 1627 and 2007.

2.5.2.2.1.7 Characterization of the New Madrid Fault System

As reported by the USGS and illustrated on Figure 2.5-21, very significant seismic activity occurs in the area of the New Madrid Fault System (NMFS). In 1811 through 1812 three large magnitude

earthquakes occurred in the New Madrid region (Hough, 2001). These severe earthquakes are thought to have ruptured the Reelfoot Fault and fault segments to the south and the north. The precise locations of these three large events are not entirely known. The only evidence of surface rupture appears along the Reelfoot Fault and earthquake locations are generally constrained only by intensity and paleoseismic data. However, the available information indicates that the seismic activity at the NMFS can be attributed to the following three sources (Bakun, 2004):

New Madrid South (NS) Fault;

New Madrid North (NN) Fault; and

Reelfoot Fault (RF).

The USGS studies for updating the 1996 U.S. national seismic map (USGS, 1996) considered this seismic activity as a "characteristic" rupture model. The USGS 1996 study (USGS, 1996) included a moment magnitude **M** of 8.0 and a recurrence time of 1000 years for such an event. Later, in the USGS work for the 2002 update of the national seismic hazard map (USGS, 2002), significant changes were introduced in mean recurrence time, characteristic magnitude, and spatial concentration of New Madrid sources of large earthquakes. It was recognized that the locations of these three large events are generally constrained only by intensity (felt) and paleoseismic data and a logic-tree approach was introduced to represent optional interpretations of fault locations and magnitudes of the New Madrid characteristic events. This logic tree was meant to characterize the range of expert opinions on the magnitude of the largest events of the 1811-12 sequence by 2000. The 2002 USGS study (USGS, 2002) represented the NMFS as three hypothetical sources: one fault with trace matching the observed microearthquake activity and two adjacent sources situated near the borders of the Reelfoot Rift. Also, a shorter mean return time of 500 years for characteristic earthquakes was considered by the USGS in the development of the 2002 maps (USGS, 2002). The end result was that the probabilistic ground motions for the 10% probability of exceedance level increased markedly around the New Madrid area, compared to the 1996 maps.

It is important to note that in the 1996 and 2002 models, the USGS (USGS, 1996; USGS, 2002) employed a single large earthquake that affects all three of the hypothetical faults, since these source models assumed that all earthquakes were independent.

Very recently, for the 2008 update of the hazard maps (USGS, 2008), the USGS takes into account the uncertainty in the locations of previous earthquakes by using five fictitious parallel fault-traces, similar to those used in the 2002 model (USGS, 2002). The central trace is weighted 0.7, the traces just outside of the central traces are weighted 0.1 each, and the outer traces are weighted 0.05 each. The USGS summarized expert opinions on the magnitudes of the 1811-1812 events, which shows that the estimated magnitudes range from **M** 7.0 up to **M** 8.1. Of the three largest New Madrid earthquakes, the one in January 1812 is the most likely to have ruptured the northern arm of the seismic zone (Figure 2.5-40). The three leading sets of magnitude estimates for the New Madrid sequence suggest that the January earthquake was 0.2 ± 0.1 magnitude units smaller than the December shock (Johnston, 1996)(Hough, 2000)(Bakun, 2004).

Based on the updated information, for developing the 2008 maps, the USGS has assigned magnitudes for the northern section of the NMFS that are 0.2 units lower than those assigned for

the central and southern sections (USGS, 2008). For the northern arm model the USGS applies the following weighting: **M** 7.1 (wt 0.15), **M** 7.3 (wt 0.2), **M** 7.5 (wt 0.5), **M** 7.8 (wt 0.15). The central and southern segments remain characterized as in 2002, i.e., **M** 7.3 (wt 0.15), **M** 7.5 (wt 0.2), **M** 7.7 (wt 0.5), **M** 8.0 (wt 0.15).

Regarding large earthquake recurrence for the NMFS, the USGS 2008 study (USGS, 2008) has used paleoliquefaction data indicating a 500 year recurrence. Three large earthquake sequences are recognized from cross-cutting relationships and radiometric dating of sandblows (liquefaction effects). The USGS refers to Tuttle and others (Tuttle, 2002) who have recognized that events about 900 A.D., 1450 A.D., and 1811-1812 A.D. have occurred. These dates agree with a 500-year mean recurrence. However, citing lack of certainty on whether or not the northern portion of the fault system ruptured in the 1450 A.D. sequence, the USGS consider the possibility of 750-year and 500-year recurrences, equally weighted, for the northern arm of New Madrid. The 500 year recurrence for the southern and central sections remained unchanged in view that Tuttle and others (Tuttle, 2002) published evidence that all three of the sequences affected those arms.

Another relevant modification made by the USGS in their 2008 New Madrid source modeling (USGS, 2008) is that in addition to an unclustered model, as used in the 1996 and 2002 studies, a clustered large earthquake model was included. A clustered model postulates that the 1811-1812 earthquakes involved a sequence of three large earthquakes. This hypothesis is supported by geologic data of Tuttle and others (Tuttle, 2002) showing evidence that pre-historical earthquakes on the NMFS typically occur in sequences of three large earthquakes similar to those observed in 1811-1812. The relevance of this consideration is that a particular site will have a larger probability of exceeding a ground motion level if it is affected by three dependent events rather than one independent event.

The USGS 2008 study assigns equal weight to a clustered model for the NMFS characteristic earthquake and to a 2002-type unclustered source model. In addition, a more extensive logic tree was used to represent the rates and location of seismic activity at the NMFS.

The recent ESP submitted by Exelon for the Clinton Site (EGC, 2006) also recognizes that seismologic, geologic, and geophysical studies have associated faults within the New Madrid region with the large-magnitude historical earthquakes that occurred during 1811 and 1812. The Clinton Site was included in the 1989 EPRI/SOG study; however, the Clinton ESP notes that paleoliquefaction studies indicate that large-magnitude events have occurred on the NMFS more frequently than the seismicity rates specified in the EPRI/SOG source characterizations. Thus, Exelon decided to update the seismic source evaluations for the Clinton Site focusing on the characteristic large-magnitude events along New Madrid. To this end, Exelon supported a vast paleoseismicity investigation to develop an improved model for the characteristic events at the NMFS. This investigation provides the most complete available representation of New Madrid characteristic events, particularly regarding the development of logic trees for representing various rupture scenarios and optional recurrence models. Details of the Clinton ESP characterization of the NMFS are presented in subsequent sections of this document. Due to its proximity to the Clinton Site, Exelon conducted comprehensive studies for characterizing the seismic activity in the NMSZ as presented in the 2006 Clinton ESP application (EGC, 2006). The Exelon efforts included a thorough review of the technical literature as well as paleoliquefaction studies to identify the fault source geometry and to estimate recurrence parameters in the NMSZ. It was recognized that paleoliquefaction studies indicate that clustered large-magnitude earthquakes have occurred in this zone which can be properly modeled as characteristic events. Recent work for characterizing seismic activity at the NMSZ has also been conducted by the

USGS for the 2008 update of the National Seismic Hazard Maps (USGS, 2008). The USGS also considers a temporal clustering model for the large NMSZ earthquakes and has developed a logic tree for representing these events. Rizzo has conducted a detailed review of the Exelon and the 2008 USGS characteristic earthquake models for the NMSZ. Estimates of the locations, potential magnitudes, and recurrence of the characteristic events are similar in both models, even though the Exelon model is appreciably more detailed. The main difference is that the USGS also considers an un-clustered model giving only 50% weight to their clustered model while the Exelon model incorporates only the clustered model with a 100% weight. Thus the Exelon approach is appreciably more conservative and it is considered that this level of conservatism is adequate for assessing seismic hazard for critical facilities such as nuclear power plants. The Exelon model for the NMSZ has also been adopted by EPRI in the 2004 update of the seismic hazard for nuclear power plant sites in the CEUS.

2.5.2.2.2 Post-EPRI Seismic Source Characterization Studies

Seismic hazard evaluations more recent than the EPRI/SOG study have identified new information that could affect the assessment of seismic hazard at the BBNPP Site. Specifically, updated data and information can have an impact on:

- Characterization of the rate of earthquake occurrences;
- Estimates of the maximum magnitude for seismic sources;
- Updated earthquake ground motions for the CEUS.

Studies that have used new data and information are described with emphasis on the items relevant for the evaluation of seismic hazard at the BBNPP Site. These descriptions are provided in Section 2.5.2.2.2.1 through Section 2.5.2.2.2.5.

2.5.2.2.2.1 USGS Studies for the United States National Maps

Between 1996 and 2008, the USGS produced updated seismic hazard maps for the United States based on updated seismological, geophysical, and geological information (USGS, 1996)(USGS, 2002)(USGS, 2008). Each map reflects changes to the source models used to construct the previous version of the national seismic hazard maps. Among the most significant modifications to the CEUS portion of the source models are changes in the recurrence, maximum magnitude (M_{max}), and geometry of the Charleston and New Madrid sources. Unlike the EPRI models that incorporate many local sources, the USGS source model in the BBNPP site region (200-mi (320-km) radius) includes only three sources that are important to the site hazard: the Extended Margin background, Stable Craton background, and New Madrid. Except for the New Madrid zone, where earthquake recurrence is modeled as characteristic earthquakes, the hazard for the large background or "maximum magnitude" zones is largely based on historical seismicity and the variation of that seismicity.

Since 1996, the USGS considered the occurrence of large events in the New Madrid as a characteristic rupture model with a characteristic moment magnitude **M** of 8.0, similar to the estimated magnitudes of the largest events in 1811-12 (USGS, 1996). The geometry of the New Madrid source was modeled as three S-shaped parallel faults encompassing the area of highest historic seismicity. The USGS study used an average recurrence time of 1000 years for the New Madrid characteristic earthquakes.

The 1996 USGS study (USGS, 1996) also recognized that several paleoearthquakes have been identified in the areas of Wabash Valley area. This seismic activity modeled as an area zone with a maximum magnitude of **M** 7.5. For background zones, values of the Guttenberg-Richter (G-R) parameter "a" were determined in the 1996 USGS study (USGS, 1996) by counting the number of $m_b=3$ and larger events within the zone since 1927 and adjusting the rate to equal that since 1976. The area-normalized a-value was then disaggregated into a set of grid cells to calculate the hazard considering the smoothed historic seismicity. The G-R parameter "b" was assigned a value of 0.95, based on calculations for the entire CEUS (USGS, 1996).

Some changes in the 2002 USGS study (USGS, 2002) that most affected the hazard estimates in BBNPP Site vicinity were the use of an updated mean recurrence time, characteristic magnitude, and spatial concentration to characterize the New Madrid sources of large earthquakes. A shorter mean recurrence time of 500 years was adopted and logic trees were developed for the characteristic magnitude related to the same configuration of three fictitious fault sources as in the 1996 maps, giving to the central fictitious source twice the weight of each of the faults to the sides. These changes increased markedly the probabilistic ground motions for the 10% probability of exceedance around the New Madrid area, compared to the 1996 results.

The documentation reported by the USGS for 2008 (USGS, 2008) update of the national seismic hazard maps points out the following changes related to the Central and Eastern U.S.:

- Revise catalog and account for magnitude uncertainty

- Develop a logic tree for New Madrid (lower recurrence on northern arm and reduced magnitude)

- Implement a cluster model for New Madrid earthquakes

- Modify hypothetical fault geometry for New Madrid

- Develop a logic tree for M_{max} area sources

The USGS basic methodology for hazard estimates in the -CEUS for the 2008 hazard maps is similar to that implemented in the 1996 and 2002 maps. Such methodology includes background-seismicity and fault source models (USGS, 1996)(USGS, 2002)(USGS, 2008). Background sources account for random earthquakes that occur off known faults and moderate size earthquakes that occur on modeled faults. The USGS-2008 background source model (USGS, 2008) is composed of three smoothed gridded seismicity models, a large regional zone model, and local special seismicity-based zones. The gridded seismicity models are based on recorded historical earthquakes and account for the observation that larger earthquakes occur in regions that have experienced previous smaller earthquakes. Large regional zones account for low potential of random seismicity in areas without historical seismicity and establish a floor to the seismic hazard calculations. The special local zones allow for local variability in the G-R seismicity parameters. Fault models account for earthquakes on mapped active faults that have paleoseismic or historical evidence of repeated large earthquakes. One of the four CEUS fault model considered in 2008 by the USGS is the New Madrid Fault System (NMFS).

The USGS gridded seismicity, large regional zone and the local seismicity models require a declustered earthquake catalog for calculation of earthquake rates. The USGS develops this

gridded seismicity rates from their seismic catalog for the Central and Eastern United States. The truncated Gutenberg-Richter (Gutenberg, 1944) magnitude-frequency distribution is used to model rates for different sizes of earthquakes in each grid cell or source zone. The USGS estimates completeness levels from the earthquake catalog, and calculates Gutenberg-Richter (G-R) parameters of the magnitude-rate relationship (intercept a and slope b) using a maximum-likelihood method (Weichert, 1980) that accounts for variable completeness. The rates in the gridded cells are spatially smoothed using a two-dimensional Gaussian smoothing operator.

In 2008, the USGS (USGS, 2008) has used five fictitious parallel fault traces, each one having three arms. This is meant to represent the aleatory uncertainty in the locations of future large magnitude earthquakes in New Madrid, in a way similar to the three traces used in their 2002 model. The center of the five traces most closely follows the seismicity pattern and is assigned a weight of 0.7; the traces just outside of the central traces are weighted 0.1 each, and the outer traces are weighted 0.05.

USGS studies have also continuously incorporated developments in ground motion model (attenuations equations). In 1996, the USGS adopted attenuation relationships derived for "hard rock conditions" recognizing that most attenuation relations for the CEUS published at that time were based on those site conditions. The USGS noted that it was less problematic to convert these to a firm-rock condition instead of converting them to soil conditions, since there would be less concern over possible non-linearity for the firm-rock site compared to the soil site.

The USGS 2008 study (USGS, 2008) includes several new simulation-based attenuation relations that were not available in 2002. While in 1996 and 2002 the USGS used ground motion models based on a single corner model (USGS, 1996; USGS, 2002), a double corner and hybrid models additionally incorporated in the 2008 study (USGS, 2008). The following is a list of the eight attenuation relationships used by the USGS in 2008, along with their assigned weights.

Single corner - finite fault

Toro and others (Toro, 1997), weight 0.2

Silva and others (Silva, 2002), constant stress drop with saturation, weight 0.1

Single corner - point source with Moho bounce

USGS (USGS, 1996), weight 0.1

Dynamic corner frequency

Atkinson and Boore (Atkinson, 2006), 140 bar stress drop, weight 0.1

Atkinson and Boore (Atkinson, 2006), 200 bar stress drop, weight 0.1

Full waveform simulation

Somerville and others (Somerville, 2001), for large earthquakes, weight 0.2

Hybrid empirical

Campbell (Campbell, 2003), weight 0.1

Tavakoli and Pezeshk (Tavakoli, 2005), weight 0.1

The 2002 and 2008 USGS efforts (USGS, 2002; USGS, 2008) have produced ground motion maps for a return period of 2475 years for building code applications.

2.5.2.2.2 Clinton ESP Application

A seismic source characterization study was performed as part of an Early Site Permit application for the Clinton Site, located in Illinois, by Exelon (EGC, 2006). In particular, Exelon performed additional paleoliquefaction studies to better characterize the occurrence of large-magnitude earthquakes in the New Madrid and the Wabash Valley. Rizzo has conducted a detailed review of the Exelon and the 2008 USGS characteristic earthquake models for the NMSZ. These models have been judged based on the most acceptable models of magnitude and recurrence intervals obtained using paleoliquefaction studies (Cramer, 2001; Tuttle, 2000).

From the data obtained post the EPRI-SOG study, the Clinton ESP concluded that:

There are no additional specific seismic sources that can be identified in the site region.

The EPRI-SOG recurrence parameters (a and b values in the G-R relationship) still provide a good estimate of the current rate of seismicity;

The maximum magnitude distributions for the central Illinois and Wabash Valley/Southern Illinois source zones are likely bigger than those assigned by the EPRI-SOG expert teams;

The significant recent research on ground motion modeling in the CEUS has produced appreciably better relationships than those used in the EPRI-SOG study.

On this basis, the PSHA presented in the Clinton ESP incorporated the following changes:

Large characteristic earthquakes on the central faults of the NMSZ were characterized with improved logic trees to account for updated assessments of magnitude, location, and return periods.

The maximum magnitude for the Wabash Valley Seismic Zone was appreciably increased

EPRI CEUS 2004 attenuation models were used.

Several sensitivity tests are reported in the Clinton ESP. These sensitivity tests indicated that the post-EPRI-SOG information results in significant changes in site hazard at the Clinton ESP Site. Thus an updated PSHA was performed to determine the SSE.

Additional information from the Clinton ESP is referred to in the following sections.

2.5.2.2.3 Updated New Madrid Model

As previously noted, seismologic, geologic, and geophysical studies have associated faults within the New Madrid region with the large-magnitude historical earthquakes that occurred during 1811 and 1812. In particular, paleoliquefaction studies indicate that large-magnitude

events have occurred on these faults more frequently than the seismicity rates specified in the EPRI/SOG source characterizations. Thus, the updated seismic source evaluations focus on the characteristic large-magnitude events along the New Madrid Fault System.

Fault Geometry

As reported by the USGS and illustrated on Figure 2.5-41, very significant seismic activity occurs in the area of the New Madrid Fault System (NMFS). The severe 1811 through 1812 earthquakes are thought to have ruptured the Reelfoot Fault and fault segments to the south and the north. The precise locations of these three large events are not entirely known. The only evidence of surface rupture appears along the Reelfoot Fault and earthquake locations are generally constrained only by intensity and paleoseismic data. However, the available information indicates that the seismic activity at the NMFS can be attributed to the following three sources:

- New Madrid South (NS) Fault;
- New Madrid North (NN) Fault; and
- Reelfoot Fault (RF).

Based on the Clinton ESP (EGC, 2006), the logic tree used to represent the uncertainty in the model for the NMFS characteristic events is shown on Figure 2.5-42. The first two levels of the logic tree take into account the uncertainty in the location and extent of the faults that can rupture in an earthquake sequence, by considering alternative geometries for the NS, RF and NN Faults. The considered fault locations are displayed on Figure 2.5-74. Distances to the BBNPP Site for the various options are listed in Table 2.5-9.

For the New Madrid South fault arm, two alternatives are considered:

1. Blytheville arch/Bootheel lineament (BA/BL); weight 0.6, length 82 mi (132 km), and
2. Blytheville arch/Blytheville fault (BA/BFZ); weight 0.4, length 71 mi (115 km).

Two alternative total lengths are considered for the New Madrid North fault arm:

1. With a weight of 0.7, rupture of the NN 37-mi (60-km) segment, and
2. The 60 mi (97 km) length including the NN and NNE is given a 0.3 weight.

Two possible alternatives are considered for the Reelfoot arm:

1. A full length segment including the northwest part, with weight 0.7, and
2. A central segment, excluding the northwest part, with 0.3 weight.

New Madrid Characteristic Earthquake Magnitude

Table 2.5-10 contains expected moment magnitudes for characteristic earthquake ruptures for each fault within the New Madrid Fault System along with their corresponding weights. As

considered in the Clinton ESP, the size of the next characteristic earthquake is assumed to vary randomly about the expected value following a uniform distribution over a range of ± 0.25 moment magnitude units, to represent the aleatory variability in the size of individual characteristic earthquakes.

For the Clinton ESP, constraints on recurrence of characteristic NMFS events were derived from paleoliquefaction and paleoseismic investigations of the Reelfoot fault scarp and associated fold. It was concluded that the NMFS has generated temporally clustered large earthquakes in AD 900 ± 100 , AD 1450 ± 150 years and in 1811 to 1812; the time between clustered events may be from 200 to 800 years, with an estimated average of 500 years. Thus, a quantitative assessment of the uncertainty in the dates for prehistoric New Madrid earthquakes was developed, using a Monte Carlo simulation of constraints on the possible dates for the prehistoric earthquakes. The time intervals between these simulated dates were then fit with poissonian and renewal recurrence models. Table 2.5-10 lists the discrete distribution for equivalent annual frequency for characteristic New Madrid earthquakes. In this table, for Model A, all ruptures are similar in size to the 1811 and 1812 earthquakes. In Model B, 1/3 of the sequences consider a smaller (lower magnitude) rupture of the New Madrid North fault and 1/3 of the sequences assume a smaller rupture of the New Madrid South fault. The difference in magnitude from the 1811 and 1812 ruptures was set to be no more than 1/2 magnitude unit, and no magnitude ruptures are considered to be less than **M** 7. Model A and Model B were assigned weights of 2/3 and 1/3, respectively.

New Madrid Characteristic Earthquake Recurrence

The recurrence estimates, based on the poissonian and renewal models, used to represent the occurrence of characteristic New Madrid earthquakes in the Clinton ESP have been used herein, as well as their corresponding weights, as summarized in Table 2.5-10. Since the site is affected by three dependent events, the frequency of exceedance, $v(z)$, of a spectral value z from a characteristic earthquake sequence is:

$$v(z)_{characteristic} = \lambda_{rate\ of\ cluster} (1 - (1 - P_1)(1 - P_2)(1 - P_3))$$

where:

$v(z)_{characteristic}$ is the probability of exceeding ground motion z ,

rate of cluster is the equivalent mean annual rate of occurrence of the event cluster, and

P_1 , P_2 , and P_3 are the probabilities of exceeding the ground motion level z , when an earthquake of specified magnitude and distance occurs.

The values and weights for the rate of cluster are included in Table 2.5-10.

New Madrid Characteristic Earthquake Ground Motion Assessment

Consistent with the hazard calculation for area sources, the contribution of the New Madrid characteristic events was conducted using the CEUS ground motions developed by EPRI (EPRI,

2004). Figure 2.5-75 shows the logic tree structure defined by EPRI to represent the uncertainty in the median ground motion equation and in the aleatory variability about the median. As noted in the previous sections for area sources, the EPRI 2004 Report defines four clusters of median ground motion models to represent the alternative modeling approaches. All four clusters have been used for assessing the hazard from the New Madrid characteristic earthquakes, as illustrated on Figure 2.5-75. The rift option was selected for the fourth cluster, instead of the non-rift option that is used for area sources.

The three branches of the second level of the logic tree on Figure 2.5-75 represent the epistemic uncertainty in the median attenuation relationship for each cluster. The branches incorporate a three-point discrete distribution with weights of 0.63, 0.185 and 0.185 for the median, the 5th and the 95th percentiles, respectively. The third branching level addresses the uncertainty in the model for the aleatory variability in ground motions about the median attenuation relationship. Models 1A and 1B, as well as their weights, are those proposed by Abrahamson (EPRI, 2006a)(EPRI, 2006b) to account for inter-event and intra-event variability for events with distances longer than 12.4 mi (20 km) (termed s_1 by Abrahamson). The additional standard deviation, s_2 , developed by Abrahamson to incorporate additional variability at short distances, is not applicable for the distances between the BBNPP Site and any of the arms of the New Madrid faults.

The EPRI 2004 ground motion attenuation relationships use either the closest distance to the rupture plane or closest distance to the surface projection of the rupture plane (Joyner-Boore distance). Thus, the EPRI 2004 document also presents adjustments for use when the hazard integration is conducted based on point-source distances. These adjustments were unnecessary in the hazard calculations due to the New Madrid characteristic events, since the specific closest or Joyner-Boore distance was calculated for each fault arm, for input to the EPRI ground motion models.

2.5.2.2.2.4 Updated Charleston Seismic Source (UCSS) Model

Results of several post-EPRI studies have demonstrated that the parameters of the Charleston seismic source need to be updated. These parameters include the geometry, the maximum magnitude and the recurrence of characteristic events. Recent models of Charleston characteristic earthquake are significantly different from the 1986 EPRI characterizations. The most recent and detailed study over the Charleston characteristic events has been conducted by for the Vogtle ESP (SNOC, 2008) producing the so-called Updated Charleston Seismic Source (UCSS) Model. The present PSHA for the BBNPP has adopted the UCSS model that was also used in the seismic hazard studies that support the recent FSAR for the CCNPP Unit 3 (UniStar Nuclear, 2007). The following description of the UCSS model is based on section 2.5.2 of the CCNPP Unit 3 FSAR. The information with the largest relevance for the BBNPP Site is the assessment of characteristic magnitude. The exact location is less important in view of the large distance, more than 500 mi (800 km), to the BBNPP Site. The UCSS model (as described in Vogtle ESP (SNOC, 2008)) has been adopted here to use for BBNPP PSHA. The selection of UCSS model has been based on the review of current literature related to the geometry (Marple, 2000; USGS 2002; USGS 2008;), maximum magnitude (Johnston, 1996; Bakun 2004; USGS 2008), and recurrence intervals (Obermeier, 1987; Talwani, 2000). Based on this literature review (including UCSS model), it was concluded that UCSS model better captures the epistemic uncertainty in recurrence intervals and source zone geometries. The mean of maximum magnitude distribution is very similar to other models. For this reason, the UCSS model was

selected as the preferred model to characterize characteristic earthquake for the Charleston seismic source.

UCSS Geometry

The UCSS model includes four mutually exclusive source zone geometries (A, B, B', and C; Figure 2.5-82). These geometries have been defined based on the current understanding of geologic and tectonic features and shaking intensity in the region affected by the 1886 Charleston earthquake; on the distribution of seismicity; and on the geographic distribution, age, and density of liquefaction features associated with both the 1886 and prehistoric earthquakes. These features indicate that most of the evidence related to the Charleston source is concentrated in the Charleston area and is not widely distributed throughout South Carolina.

Geometry A

Geometry A is a northeast-oriented area centered at the 1886 Charleston meizoseismal area (Figure 2.5-82). This geometry encompasses the 1886 earthquake MMI X isoseismal (Bollinger, 1977), most identified Charleston area tectonic features and inferred fault structures and the majority of reported 1886 liquefaction features. Geometry A excludes outlying liquefaction features, because liquefaction occurs as a result of strong ground shaking that may extend well beyond the aerial extent of the tectonic source.

Existing evidence indicates that the seismic source for the 1886 Charleston earthquake was located in a relatively restricted zone defined by Geometry A. This zone envelopes the local tectonic features, the area of ongoing concentrated seismicity, the area of high density liquefaction features, and meizoseismal area of the 1886 earthquake. These observations suggest that future earthquakes with magnitudes comparable to the 1886 Charleston earthquake will likely occur within the area of Geometry A. Thus, a weight of 0.7 has been assigned to Geometry A (Figure 2.5-83).

Geometries B, B', C

Geometries B, B', and C are defined to capture the possibility that future earthquakes may not be restricted to Geometry A. The distribution of liquefaction features along the entire coast of South Carolina suggests that the Charleston source could extend beyond Geometry A. Therefore, Geometries B and B' represent larger source zones, while Geometry C represents the southern segment of the hypothesized East Coast Fault System source zone. Geometry B' is a subset of B and defines the onshore coastal area as a source thus restricting the earthquakes in such onshore regions.

Geometry B - Coastal and Offshore Zone

Geometry B is a coast-parallel source including entirely Geometry A and elongated to the northeast and southwest to capture more distant liquefaction features in coastal South Carolina. The source also extends to the southeast region to include the offshore Helena Banks fault zone. This geometry is assigned a weight of 0.1.

Geometry B' - Coastal Zone

Geometry B' is a coast-parallel source that also incorporates all of Geometry A, as well as the majority of reported paleoliquefaction features. However, it does not include the Helena Banks Fault Zone. A weight of 0.1 has been assigned to this geometry.

Geometry C - East Coast Fault System (ECFS South Segment)

Geometry C envelopes the southern segment of the proposed East Coast Fault System (Marple, 2000) as a possible source for the 1886 Charleston earthquake. A weight of 0.1 has been assigned to geometry C.

UCSS Maximum Magnitude Return Period

Based on currently available data and interpretations regarding modern M_{\max} estimates (Table 2.5-18), the UCSS model modifies the USGS magnitude distribution (USGS, 2002) to include a total of five discrete magnitude values each separated by 0.2 M units (Figure 2.5-83). The UCSS M_{\max} distribution includes a discrete value of M 6.9 to represent the Bakun best estimate of the 1886 Charleston earthquake magnitude, as well as a lower value of M 6.7 to capture a low probability that the 1886 earthquake was smaller than the Bakun mean estimate of M 6.9 (Bakun, 2004).

The UCSS magnitudes and weights are as follows:

M	Weight
6.7	0.10
6.9	0.25
7.1	0.30
7.3	0.25
7.5	0.10

This, results in a weighted mean Maximum magnitude of M 7.1 for the UCSS. This is slightly lower than the mean magnitude of M 7.2 in the USGS model (USGS, 2002).

The UCSS model incorporates geologic data to characterize the return period of M_{\max} earthquakes. Identifying and dating paleoliquefaction data provides a basis for estimating the recurrence of large earthquakes. Recent estimates of M_{\max} recurrence intervals are significantly shorter than estimates in the EPRI models. Details regarding the processing, aging, and completeness of Charleston paleoliquefaction data can be found in Talwani (Talwani, 2001) and the CCNPP Unit 3 FSAR (UniStar Nuclear, 2007).

Records along two different time intervals (2000 yr and 5000 yr) are used in UCSS model. Return periods derived from recorded paleoliquefaction features assume that these features were produced by large M_{\max} events and that both the 2000-year and 5000-yr records are complete.

The UCSS model calculates two average recurrence intervals covering two different time intervals, which are used as two recurrence branches on the logic tree (Figure 2.5-83). The first average recurrence interval is based on four events that occurred in the past 2000 years. The second average recurrence interval is based on events that occurred within the last 5000 years. The 2000 and 5000 records have been assigned weights of 0.8 and 0.2, respectively.

2.5.2.2.2.5 Characterization of Lancaster Seismic Zone

The Lancaster seismic zone (LSZ) is located in southeastern Pennsylvania and is known as a post-EPRI study seismic zone located about 55 mi (88 km) south of the BBNPP Site (Section 2.5.1.1.4.4.3). The largest known earthquake of the LSZ is the January 16, 1994 Cacoosing Valley earthquake of $m_{bLg} = 4.6$ near Reading Pennsylvania (Seeber, 1998). This event was located about 52 mi (84 km) south of the BBNPP Site. The Cacoosing Valley event has been attributed to unloading during a quarry process (Seeber, 1998) but it has not been removed from the standard earthquake catalogs used in PSHA studies. The LSZ is not included in the original EPRI source zone model (EPRI, 1986) as a separate source zone. However, the range of M_{max} values assigned to other EPRI source zones, adequately characterizes the LSZ in terms of the upper bound magnitude (Section 2.5.1.1.4.4.3). Therefore no update is required for the EPRI (EPRI, 1986) seismic source zone model within the region of BBNPP Site.}

2.5.2.3 Correlation of Earthquake Activity with Seismic Sources

The U.S. EPR FSAR includes the following COL Item in Section 2.5.2.3:

Correlation of earthquake activity with seismic sources is site specific and will be addressed by the COL applicant, consistent with the guidance of RG 1.208 and RG 1.165, as appropriate.

This COL Item is addressed as follows:

{Following Regulatory Guide 1.165 (NRC, 1997a) and 10 CFR 100.23 (CFR, 2007), a PSHA was conducted to determine the SSE and to account for uncertainties in the seismological and geological evaluations for the BBNPP site. The probabilistic approach was based on the PSHA conducted by the EPRI for CEUS in the mid to late 1980s (EPRI, 1989a) with changes to incorporate updated data. Expert opinion was incorporated following a Senior Seismic Hazard Analysis Committee (SSHAC) approach (NRC, 1997b).

The location of earthquakes was accounted for by an updated USGS catalog (USGS, 2002), covering events between 1627 and 2007. The updated catalog has been adopted for assessing the BBNPP site seismic hazard. This update is a refinement of the EPRI SOG catalog that listed earthquakes between 1627 and 1984 (EPRI, 1988). Figure 2.5-34 through Figure 2.5-39 show the distribution of earthquake epicenters from both the EPRI (EPRI, 1986) and updated 2001 USGS (USGS, 2002) earthquake catalogs in comparison to the seismic sources identified by each of the EPRI ESTs. The comparison of earthquake distributions from both earthquake catalogs supports the following conclusions:

- The updated catalog does not show any earthquakes within the site region that can be associated with a known geologic or tectonic structure.
- The updated catalog does not show a unique cluster of seismicity that would suggest a new seismic source outside of the EPRI seismic source model (EPRI, 1986).

- The updated catalog does not show a pattern of seismicity that would require significant revision to the EPRI seismic source geometry.
- Two events were added to the 2001 USGS catalog in the period of 2002-2007. This update does not impact the result of the PSHA.}

2.5.2.4 Probabilistic Seismic Hazard Analysis and Controlling Earthquake

The U.S. EPR FSAR includes the following COL Item in Section 2.5.2.4:

The probabilistic seismic hazard analysis is site specific and will be addressed by the COL applicant, consistent with the guidance of NUREG/CR-6372, RG 1.165 and RG 1.208, as appropriate.

This COL Item is addressed as follows:

{Sections 2.5.2.4.1 through 2.5.2.4.6 are added as a supplement to the U.S. EPR FSAR.

2.5.2.4.1 1989 EPRI Probabilistic Seismic Hazard Analysis

The seismic hazard for the BBNPP was calculated using the original EPRI EST teams area sources, plus the New Madrid and Charleston characteristic earthquakes, and with the updated ground motion model and aleatory uncertainty model. This calculation was first made for hard rock conditions, and these results were then modified to account for local site conditions.

The analysis of seismic hazard consists of calculating annual frequencies of exceeding different amplitudes of ground motion, for all combinations of seismic sources, seismicity parameters, maximum magnitudes, ground motion equations, and ground motion aleatory uncertainties. This calculation is made separately for the New Madrid zone, for the Charleston zone and for the seismic sources defined by each of the six EPRI EST teams and results in a family of seismic hazard curves. The alternative assumptions on seismic sources, seismicity parameters, maximum magnitudes, ground motion equations, and ground motion aleatory uncertainties are weighted, resulting in a combined weight associated with each hazard curve. From the family of hazard curves and their weights, the mean hazard (and the distribution of hazard) can be calculated.

The quantification of the Probabilistic Seismic Hazard at hard rock utilizes Rizzo's in-house software, ProHazard. This code uses the definition of site area seismic sources, the seismic potential of these sources in terms of generating future earthquakes, and the ground motion models, to estimate the annual exceedence probabilities for various levels of spectral accelerations at different spectral frequencies.

The technical methodology utilized in ProHazard follows the approach implemented in the 1989 Electric Power Research Institute study for Nuclear Power Plant Sites in the Central and Eastern United States (EPRI, 1989). This methodology is generally based on the early work of Cornell (Cornell, 1968) (Cornell, 1971) and integrates the product of the conditional probability that a ground motion measure will be exceeded given the earthquake magnitude and distance, and the probability distribution of magnitude and distance over all sources that can significantly contribute to the site seismic ground motion. This is expressed as:

$$v(z) = \sum \alpha_n(m_0) \int f(m) \left[\int f(r | m) P(Z > z | m, r) dr \right] dm$$

where:

Z is the peak ground acceleration or the spectral pseudo-acceleration at prescribed natural frequencies,

$P(Z > z | m, r)$ is the conditional probability that Z will exceed a value z , given the earthquake magnitude, m , and distance, r ,

$f(m)$ and $f(r)$ are the probability density functions for magnitude and distance, and

$\alpha_n(m_0)$ is the number of earthquakes per year above a prescribed minimum magnitude m_0 , in the n -th seismic source.

The integration over magnitude is performed from m_0 to and upper bound magnitude m_u , and the integration over distance is performed usually over a prescribed radius from the site, typically larger than 186 mi (300 km). The probability density function for distance assumes that earthquakes can occur randomly over the source areas or faults. The functions $f(m)$ and $\alpha(m_0)$ define the recurrence relationships for the respective source zones.

The conditional probability in the above equation represents the random uncertainties in the natural phenomenon (aleatory). ProHazard, additionally, addresses epistemic uncertainties in sources and recurrence parameters and the ground motion attenuation resulting from limitations in the available data and alternative interpretations of this data. Alternative assumptions on seismic sources, seismicity parameters, maximum magnitudes, ground motion equations, and ground motion aleatory uncertainties are weighted, resulting in a combined weight associated with each hazard curve. The mean hazard and the distribution of hazard (i.e., median and fractiles) are obtained from the resulting family of hazard curves and the associated weights.

The attenuation relationships developed in 2004 by EPRI (EPRI, 2004) for the CEUS have been implemented in ProHazard. This model was the outcome of several workshops that convened a panel of six ground motion experts who developed a consensus-based ground motion model consisting of weighting of several attenuation relationships. The ground motion model relates spectral accelerations at frequencies of 100 Hz (equivalent to peak ground acceleration (PGA)), 25 Hz, 10 Hz, 5 Hz, 2.5 Hz, 1 Hz, and 0.5 Hz for generic hard rock conditions to moment magnitude at and distance to a given source. Epistemic uncertainty is represented using multiple ground motion equations and multiple estimates of aleatory uncertainty (sigma), all with associated weights. Further, EPRI (EPRI, 2006) corrects the excessive aleatory uncertainties in the 2004 study, particularly for low frequencies.

The above uncertainties are implemented in ProHazard the analysis utilizing the logic tree formalism. The logic trees represent discrete alternatives of models and model parameters and assign relative weights to the alternatives. These weights develop from statistical analysis of the data and represent the best judgment of experts. Thus, several analyses reflecting various scenarios quantitatively assess the modeling uncertainties.

ProHazard has been subjected to the verification and validation procedures stipulated in Rizzo's Quality Assurance Manual. Computer software control for ProHazard has been done according to Rizzo's Quality Assurance Manual. The Quality Assurance Manual addresses software activities including software acquisition and development, tracking installation of design and

analysis software on individual computers, program verification and validation, in-use testing, software usage, change control, configuration control, error notice documentation and distribution, software maintenance, virus protection, software retirement, records and monitoring.

The method used to verify and validate the capabilities of ProHazard are in accordance with methods accepted by the NRC and as described in EPRI NP-4726 (EPRI, 1986). Validation test problems are selected for testing specific combination of analysis capabilities of the ProHazard. The problems are modeled and analyzed using ProHazard. The analysis results obtained from ProHazard are then compared with the benchmark solutions from published technical literatures.

2.5.2.4.2 Effects of New Regional Earthquake Catalog

A sensitivity study was done in order to determine if the activity rates have changed. Seismicity rates in the EPRI study (EPRI, 1986) were based on an earthquake catalog that extended through 1984. The USGS 2001 catalog (USGS, 2002) has 17 more years of data and it was updated to include seismicity data up through the year 2007. Using the USGS 2001 catalog and completeness periods the b values for some of the EPRI source zones were computed and compared to the b values obtained by EPRI teams. The differences between the two sets of b values are small and can be attributed to using different catalogs and different completeness periods. For example the EPRI b value for Rondout source zone 31 is 0.96 while the estimated b value using USGS 2001 catalog is 1.02. For many of the source zones the differences are less than 0.05. Therefore, the EPRI b values do not need any update with exception of the Charlevoix seismic zone. Except the Dames and Moore and Woodward-Clyde teams, other EPRI EST teams have derived a b value between 0.70 and 0.79 for the Charlevoix seismic zone. The USGS used a b value of 0.76 (USGS, 1996) (USGS, 2002) (USGS, 2008) for this source zone based on the work of Adams and others in the Geological Survey of Canada. b values for the Charlevoix seismic zone were computed using the USGS 2001 (USGS, 2002) catalog and source zone geometries of Dames and Moore and Woodward-Clyde and a value of 0.7 was obtained in both cases. This is consistent with the b value obtained by other EPRI EST teams. Therefore, b value for the Charlevoix seismic zone for those two teams was changed to 0.7. A b value of 0.7 is slightly more conservative than 0.79. However, considering the long distance of the Charlevoix seismic zone from the BBNPP site, the new b value equal to 0.7 does not have a significant impact on the PSHA results. No other changes in EPRI seismicity parameters are required.

2.5.2.4.3 New Maximum Magnitude Information

The upper magnitude, M_{\max} , utilized in the magnitude recurrence equation could significantly affect the low probability seismic hazard, in particular from the near field events. In the 1989 EPRI/SOG (EPRI, 1989a) study, each EST developed alternative values of M_{\max} for each seismic source in a body wave (m_b) unit. More recent studies (USGS, 2008; Bakun, 2004), however, have revised M_{\max} for the Charleston, New Madrid, and local sources. In addition, it has been recognized that large historical events have occurred at the New Madrid and the Charleston fault systems that cannot be adequately modeled by the G-R equation. Instead, the concept of characteristic earthquakes (Schwartz, 1984; Youngs, 1985) has been introduced to more appropriately represent the seismic activity at New Madrid and Charleston. Thus, characteristic events have been adopted in the calculation of the hazard at the BBNPP Site. Moment magnitudes M between 7 and 8.1 were considered for the New Madrid source and between 6.5 and 6.7 for the Charleston source. Table 2.5-3 through Table 2.5-8 list revised maximum magnitudes and their corresponding weights for the seismic sources selected for the BBNPP Site PSHA.

The EPRI/SOG ESTs defined the maximum magnitude for each of their seismic sources using either body wave magnitude, m_b , or seismic moment magnitude, M . Furthermore, the G-R parameters a and b are derived in terms of m_b , while the equations for ground motion models are functions of M . Therefore, conversions from body wave magnitude into moment magnitude are required. The three magnitude-conversion relationships shown in Table 2.5-2 were used in the BBNPP PSHA and the three of them were assigned equal weight.

2.5.2.4.4 New Seismic Source Characterizations

New characteristic earthquake New Madrid and Charleston source models have been adopted to reflect updated estimates of the possible geometries and maximum magnitude at both fault zones. The Gutenberg-Richter (G-R) equation (Gutenberg, 1944) has been used to describe recurrence in area seismic sources. This equation was truncated at the maximum magnitude, M_{max} . The a and b parameters characterizing the potential of area seismic sources have been updated as well as their maximum earthquake magnitude. As noted before, each EPRI EST (EPRI, 1989a) developed G-R parameters a and b for each of their seismic sources, identifying their selected smoothing options and their corresponding weights. Smoothing allows incorporation of the variation of the G-R parameters a and b within the seismic source. For the BBNPP PSHA, the smoothing approach developed by USGS (USGS, 2002)(USGS, 2008) has been used. This approach considers only the variation of the intercept parameter a for prescribed constant values of the slope parameter b . The constant values of b have been taken as the averages of the b -values adopted for each seismic source by each EPRI EST (EPRI, 1989a), along with the corresponding weights for each smoothing option. Table 2.5-3 through Table 2.5-8 present the values of the average seismic parameter b used as input to the BBNPP PSHA.

Four smoothing options are considered for characterizing the recurrence parameter a in the USGS 2008 approach. Each of the first three smoothing options is based on an incompleteness period, a minimum incompleteness magnitude, and a smoothing correlation distance. The fourth option is considered only for the background seismic source since it has negligible effect on main sources such as New Madrid or Charleston that have a much smaller area than the background source. The information for each model is listed in Table 2.5-16.

2.5.2.4.5 New Ground Motion Models

Once the earthquake sources are defined, attenuation relations relate the source characteristics of the earthquake and propagation path of the seismic waves to the ground motion at a site. Predicted ground motions are typically quantified in terms of a median value (a function of magnitude, distance, site condition, and other factors) and a probability density function of peak horizontal ground acceleration or spectral accelerations.

The estimation of strong ground motion for specified magnitude, distance, and site conditions in the CEUS is difficult due to the paucity of physical data. Most of the available data correspond to $M < 5.8$ and distances exceeding about 31 mi (50 km). Considerable effort has been directed to developing appropriate attenuation relations for the CEUS conditions. In general, the attenuation relationships utilize standard forms to regress on recorded data in the region, augmented by data from other similar tectonic regimes and stochastic time histories tied to source types and styles of faulting.

Since publication of the 1989 EPRI study (EPRI, 1989a), much work has been done to evaluate strong earthquake ground motion in the CEUS. In 2004, the EPRI completed a study on strong ground motion prediction in the CEUS following the SSHAC (NRC, 1997b) guidelines for a Level III Analysis. A panel of six ground motion Experts was reconvened during several workshops to provide advice to a Technical Integrator (TI) on the adequacy of available CEUS ground motion relationships. On this basis, the TI developed a representation of the current scientific understanding on the subject, consisting of "clusters" of ground motion relationships with associated weights to represent the uncertainty in predicting the median ground motion, in terms of moment magnitude. Each cluster corresponds to relationships based on a similar approach for ground motion modeling. The uncertainty in the median model for each ground motion cluster is defined by two additional models: one representing the 5th percentile of the median uncertainty distribution and the other corresponding to the 95th percentile.

Epistemic uncertainty is modeled using multiple ground motion equations and multiple estimates of aleatory uncertainty (sigma), all with associated weights. Different sets of equations are recommended for sources that represent rifted versus non-rifted parts of the earth's crust. Equations are available for spectral frequencies of 100 Hz (equivalent to PGA), 25 Hz, 10 Hz, 5 Hz, 2.5 Hz, 1 Hz, and 0.5 Hz, and these equations apply to hard rock conditions, i.e., rock with a shear wave velocity of 9200 ft/sec (2800 m/sec).

EPRI has published updated estimates of aleatory uncertainty (EPRI, 2006a). This update reflected the observation that sources of the aleatory uncertainties in the original EPRI attenuation study (EPRI, 2004) were probably too large, resulting in over-estimates of seismic hazard. The 2006 EPRI study (EPRI, 2006a) recommends a revised set of aleatory uncertainties (sigmas) with weights that can be used to replace the original aleatory uncertainties published in the 2004 EPRI study (EPRI, 2004).

In accordance with Regulatory Guide 1.208 (NRC, 2007a), the hazard curves from the PSHA have to be defined for generic hard rock conditions as defined in the development of the attenuation equations. The 2004 EPRI ground motion models correspond to a shear wave velocity (V_s) of 9200 ft/sec (2800 m/sec). These EPRI 2004 equations have been adopted for median ground motion estimates, and the Abrahamson log-sigma model (EPRI, 2006a) is used to incorporate aleatory variability. Within this context, Figure 2.5-76 shows the logic tree for general area sources such as background or local source, and Figure 2.5-75 shows the logic tree for non-general sources such as New Madrid and Charleston. Adopting the EPRI 2004 ground motion model implies that the seismic hazard is calculated at the location where the rock reaches a V_s of 9200 ft/sec (2800 m/sec).

EPRI TR-1014381 (EPRI, 2006a) was used in lieu of the Regulatory Guide 1.208 cited document, i.e. EPRI Report 1013105 (EPRI, 2006b). EPRI Report 1013105 (EPRI, 2006b) was an Update Report while EPRI TR-1014381 (EPRI, 2006a) is the final report. For the purposes of revised estimates of aleatory uncertainty in the CEUS, there is no technical difference between the documents. The "Recommended CEUS Sigma" values and "Conclusions" of both reports are identical.

Earthquakes occurring within the area seismic sources were treated as point sources. Thus, the adjustments to the ground motion equations developed in EPRI (EPRI, 2004) to account for this point-source representation were incorporated in the hazard calculations.

2.5.2.4.6 Updated EPRI Probabilistic Seismic Hazard Analysis Deaggregation, and 1 Hz, 2.5 Hz, and 10 Hz Spectral Accelerations Incorporating Significant Increases Based on the Above Sensitivity Studies

Figure 2.5-67 through Figure 2.5-73 and Tables 2.5-19 through 2.5-25 present the resulting updated probabilistic seismic hazard hard rock curves for the seven spectral ordinates (100 Hz (equivalent to PGA), 25 Hz, 10 Hz, 5.0 Hz, 2.5 Hz, 1.0 Hz, and 0.5 Hz). The mean and fractile (5%, 16%, 50% (median), 84% and 95%) hazard curves are indicated.

Figure 2.5-43 shows mean and median uniform hazard spectra for 10^{-4} , 10^{-5} , and 10^{-6} annual frequencies of exceedance from these calculations at seven structural frequencies. Numerical values of these spectra are documented in Table 2.5-14.

The mean rock hazard has been de-aggregated for the 10^{-4} and 10^{-5} levels of probability of exceedance. The magnitude and distance bins for the de-aggregation table were taken from Regulatory Guide 1.208 (NRC, 2007a). The results have been plotted in Figure 2.5-44 through Figure 2.5-47 and Figure 2.5-67 through Figure 2.5-73, for the required low frequency (1 and 2.5 Hz), the high frequency (5 and 10 Hz) ranges, and for the 10^{-4} and 10^{-5} levels of probability of exceedance, respectively. These figures depict the percent contribution of each magnitude-distance bin to the total hazard.

Approach 2B of NUREG/CR-6728 (NRC, 2001) was used to derive the controlling events at the BBNPP Site. First, the controlling events were identified using the de-aggregation results. Table 2.5-11 lists the de-aggregated controlling events. Each de-aggregated earthquake (DE) is prescribed as a pair of distance and its associated contribution to a high frequency (HF) or low frequency (LF) response. DEL indicates the low end of the distance range, while DEM and DEH refer to the middle and high ends, respectively. Using the magnitude-distance pairs for each sub-controlling event, DEL, DEM, and DEH, the CEUS single corner spectral shapes from NUREG/CR-6728 (NRC, 2001) were adopted to develop the corresponding spectral shapes. Then, the response spectra of each sub-controlling event were scaled to match the rock UHRS at 1.75 or 7.5 Hz for low frequency and high frequency events, respectively. The resulting scaled response spectra are presented on Figure 2.5-77 and Figure 2.5-78 for hazard levels of 10^{-4} and 10^{-5} , respectively.

The de-aggregation of the total hazard clearly reveals that the nearby area sources largely govern the hazard at the BBNPP Site. The influence of local earthquakes is more appreciable in the HF motion. Each of the controlling earthquakes (DEL, DEM, and DEH) of both LF and HF was taken as input for the seismic site amplification analyses as described in the following section. For each sub-controlling event, all selected time histories have been scaled and modified to match their calculated response spectra with the target scaled response spectrum. Figure 2.5-79 compares the target response spectrum with the response spectra of selected time histories, after performing the spectral matching for the 10^{-4} hazard low frequency controlling event of the sub-controlling DEL and DEH.}

2.5.2.5 Seismic Wave Transmission Characteristics of the Site

The U.S. EPR FSAR includes the following COL Item in Section 2.5.2.5.

Seismic wave transmission characteristics are site specific and will be addressed by the COL applicant.

This COL Item is addressed as follows:

{The uniform hazard spectra developed through Section 2.5.2.4 and displayed on Figure 2.5-43 are defined on hard rock (shear-wave velocity of 9200 ft/sec (2800 m/sec)). Rock layers with shear-wave velocities of such value are located at depths between 190 ft (57.9 m) below the foundation level at the BBNPP Site. To determine the SSE at the ground surface, it is necessary to adjust the uniform hazard spectra for amplification or de-amplification as the vibratory ground motion propagates through the soil media. As mentioned above, the adjustment was made by conducting Site Response Analyses following Approach 2B described in NUREG/CR-6728 (NRC, 2001). These analyses consist in defining the shear wave velocity and material damping characteristics in the soil and rock profile between the ground surface and the depth of hard rock. Then uni-dimensional site analyses are conducted using equivalent linear procedure (Schnabel, 1972). The results are used to derive site amplification factors for modifying the response spectra at rock on account of the seismic wave transmission characteristics of the soil layers. This section describes the various steps involved in the calculation and application of the site amplification factors. The seismic wave transmission characteristics and effects of this thick soil column on hard rock ground motions are described in this section.

Section 2.5.2.5.1 is added as a supplement to the U.S. EPR FSAR.

2.5.2.5.1 Development of Site Amplification Functions

2.5.2.5.1.1 Methodology

The calculation of site amplification factors is performed in the following 4 steps:

1. Develop a best estimate soil and rock column in which mean low-strain shear wave velocities and material damping values, and strain-dependencies of these properties, are estimated for relevant layers from the surface to the hard rock horizon. At the BBNPP site, hard rock ($V_s = 9200$ ft/sec (2800 m/sec)) is at sloping depths between 190 ft (57.9 m) and 237 ft (72.2 m);
2. Develop a probabilistic model that describes the uncertainties in the above properties, locations of layer boundaries, and correlation between the velocities in adjacent layers, and generate a set of 60 artificial "randomized" profiles;
3. For each of the sub-controlling earthquakes (DEL, DEM, and DEH) of 10^{-4} and 10^{-5} annual frequencies of exceedance for both LF and HF earthquakes, use the corresponding controlling time histories for input into dynamic response analysis as the outcrop motion at the hard rock elevation;
4. Use an equivalent-linear time-history site-response formulation to calculate the dynamic response of the site for each of the 60 artificial profiles, and calculate the mean of site response. This step is repeated for each de-aggregated earthquake of the four input motions (10^{-4} and 10^{-5} annual frequencies, HF and LF events).

These steps are described in the following subsections. The calculation of site effects was performed with an in-house version of the computer program SHAKE (Schnabel,

1972). This program computes the response in a system of viscous-elastic, horizontally layered, soil units, overlying a uniform half-space, subjected to transient, vertical travelling shear waves.

The analytical method implemented in SHAKE is based on the solution of the wave equation and the Fast Fourier Transform algorithm. The nonlinearity of the shear modulus and damping is accounted for by the use of equivalent linear soil properties within an iterative procedure to obtain values for modulus and damping compatible with the effective strains in each layer. Therefore, for any set of layer properties, SHAKE performs a linear analysis.

The motion used as basis for the analysis (i.e., the motion that is considered to be known) can be applied to any layer in the system. An iterative procedure is used to account for the nonlinear behavior of the soils. The object motion can be specified at the top of any sub-layer within the soil profile or at the corresponding outcrop.

It is noted that the solution of a particular problem requires use of realistic ground motions (loading), modeling site dynamics (response), and the interpretation and prediction of soil behavior subject to dynamic loading (analysis). To facilitate conducting and verifying these tasks, modifications incorporated in Rizzo's in-house version include the following:

- The number of sub-layers was increased to up to 500 to allow a more accurate representation of deeper and/or softer soil deposits;
- Modulus reduction and damping relationships can be specified by the user, up to 13 different curves;
- User specified periods are allowed for calculating spectral ordinates;
- The code can accept input data to generate random soil/rock columns by utilizing best estimates of the mean and the standard deviation along with prescribed probabilistic distributions for material properties (stiffness, mass and damping) and for layer thickness.

Computer software control for SHAKE has been done according to Rizzo's Quality Assurance Manual. The Quality Assurance Manual addresses software activities including software acquisition and development, tracking installation of design and analysis software on individual computers, program verification and validation, in-use testing, software usage, change control, configuration control, error notice documentation and distribution, software maintenance, virus protection, software retirement, records and monitoring.

To verify and validate the reliability and functionality of the Rizzo's in-house version of SHAKE, six validation problems are chosen. Each function in the program is verified at least once by the sample problems. One of the sample problem intents to verify the capability of the number of soil layers of 500 in the in-house version. The results calculated by the program are compared to analytical solutions from public sources. The validation and verification presents a good agreement between SHAKE computational solution and analytical solution for each sample problem.

2.5.2.5.1.2 Base Case Soil/Rock BBNPP and Uncertainties

Development of a best estimate soil/rock column is described in detail in Section 2.5.4. Summaries of the low strain shear wave velocity, material damping, and strain-dependent properties of the base case materials are provided below in this section. These parameters are used in the site response analyses.

The total depth of approximately 386 ft (117.7 m) of the BBNPP Site was investigated using test borings and geophysical methods. The geotechnical investigation is described in detail in Section 2.5.4.

The layers in the 386 ft (117.7 m) of the site consist of the following stratigraphic units:

- Overburden Soils:
 - Glacial Overburdens
- Rock Formations:
 - Mahantango Shale

A layer of concrete with an average thickness of 10 ft (3 m) below the center line of the planned nuclear reactor facility will be built on top of the Mahantango Shale. This concrete layer is placed between the power block basemat and the bedrock. Section 2.5.4 provides detailed contour information related to the position of the bedrock below the power block's footprint.

The compressional and shear-wave velocities are taken from geophysical field tests using two different techniques:

1. Four sets of downhole tests,
2. Four sets of suspension logging tests

Of the eight geophysical measurements, two borings, G301 and B301, provide the deeper site-specific geophysical information collected during the geotechnical investigation. P-S Suspension and Downhole tests were performed down to a depth of approximately 400 ft (120 m) (GeoVision, 2008; NGA, 2008). These two locations are at the center line of the projected containment footprint.

The downhole profiles consist of average compressional and shear-wave velocities for thicknesses varying from 13 ft (4 m) to 120 ft (36.6 m). The suspension logging profiles provide detailed discrete compressional and shear-wave velocities for thickness of approximate 1.5 ft (0.5 m).

Resonant Column and Torsional Shear Laboratory Tests were performed on soil and backfill samples. The complete set of results from these tests is reported in Section 2.5.4.2.3. Generic cohesionless soil curves (EPRI, 1993) were adopted to describe the strain dependencies of shear modulus and damping for the backfill based on available results from the site investigation. As required by Regulatory Guide 1.208 (NRC, 2007a) the damping curves for soils were truncated at 15 percent for the site response analysis.

In these areas, there are numerous records of deep gamma ray surveys and geologic columns with lithologic descriptions. The analysis of shear wave velocities at depths beyond the reach of the boring exploration program became irrelevant since the 9200 ft/sec (2800 m/sec) horizon was clearly encountered by the geophysical exploration program.

The Mahantango Formation reached such shear wave velocity above a depth of 350 ft (107m). Past reports place the total thickness of the Mahantango Formation at approximately 1,500 ft (457 m) (Inners, 1978).

The geologic column at the site is an extension of the Mahantango Shale, which is a dark gray to black formation, with few to no fractures. Some distinctive features are the presence of calcareous zones, the presence of thin pyrite lenses that increase in abundance with depth, and the presence of calcite veins perpendicular to the bedding plane that are micro-faulted. The upper surface of the Mahantango Formation shows the effects of solution and weathering in a few areas, but it is predominantly very competent and indurated.

For the Site Response Analyses, the concrete and Mahantango Shale is assumed to behave linearly during earthquake shaking. "Free-Free" Direct arrival tests were performed on undisturbed rock samples by the University of Texas. The "Free-Free" Direct arrival test results are provided in Table 2.5-42. The tests provided material velocity and damping values associated with shear-waves as well as those associated with compressional waves.

The average of the laboratory test results for damping for the Mahantango Shale is 0.86 percent. Lower values, 0.8 and 0.7 percent, are conservatively used for the analysis. The Mahantango Shale has a very high Rock Quality Designation (RQD) and as a rock mass it capable of transmitting shear waves very efficiently with small amounts of damping. Therefore, the lower reported laboratory values are selected for the analysis. The RQD of the Mahantango Shale is reported in the field boring logs.

2.5.2.5.1.3 Site Properties Representing Uncertainties and Correlations

To account for variations in shear-wave velocity across the site, 60 artificial profiles were generated using the stochastic model developed by Toro (Toro, 1996), with the approximation of the standard deviation of $\ln V_s$ as the coefficient of variation of V_s (Ang and Tang, 1975). These artificial profiles represent the soil column from the top of the ground surface to the top of bedrock with a shear-wave velocity of 9,200 ft/s (2800 m/sec). The model uses as inputs the following quantities:

- The best estimate of the shear-wave velocity profile and other soil properties described above;
- The coefficient of variation of the shear wave velocity as a function of depth, developed using available site data (refer to Section 2.5.4);
- Correlation coefficients between V_s in adjacent layers, determined using correlation results for the USGS site characterization category (Toro, 1996);
- The probabilistic characterization of layer thickness as a function of depth, computed assuming a normal distribution;

The depth to bedrock, which is randomized assuming a normal distribution to account for epistemic uncertainty in the bedrock-depth data described in Section 2.5.4.

Figure 2.5-50 shows the mean V_s value and corresponding coefficient as a function of depth of the downhole tests and suspension logging tests at different boreholes.

The coefficient of variation of shear wave velocities calculated from the best estimate soil/rock column is used as the standard deviation of $\ln(V_s)$ as a function of depth. Figure 2.5-51 shows the coefficient of variation of shear-wave velocity, which were used to generate multiple profiles. The correlation coefficients between shear wave velocities in adjacent layers were determined using USGS empirical relationships.

The randomly generated thicknesses of layer were computed assuming a normal distribution using the coefficient of variation of 0.10 to 0.15 for thickness of each layer. For consistency with the site-specific data, the generated \ln -velocities and the generated thicknesses were truncated at $\pm 2s$ according to the recommendations of Toro (Toro, 1996).

Figure 2.5-52 illustrates the V_s profiles generated for profiles 1 through 60, using the median, logarithmic standard deviation, and correlation models described. These profiles include uncertainty in depth to bedrock. In total, 60 profiles were generated. Figure 2.5-53 compares the mean of these 60 V_s profiles to the mean V_s profile described in the previous section, indicating very good agreement. This figure also shows the ± 1 standard deviation values of the 60 profiles, reflecting the coefficient of variations indicated on Figure 2.5-51.

Mean values of shear stiffness (G/G_{MAX}) and damping for each geologic unit are described in Section 2.5.4. Uncertainties in the properties for each soil unit are characterized using the values obtained by Costantino (Costantino, 1996). Figure 2.5-54 and Figure 2.5-56 illustrate the shear stiffness and damping curves generated for backfill, although that is not present in the Best Estimate soil column model. Stiffness and damping of soils depend on the strain level during ground shaking. However, for significantly stiff materials such as concrete and the Mahantango Shale, these properties are independent of the strain level during earthquake ground motion. Both properties retain their "low-strain" values. These values are also subject to the random variation procedure.

This set of 60 profiles, consisting of V_s versus depth, depth to bedrock, stiffness, and damping, are used to calculate and quantify site response and its uncertainty, as described in the following sections.

2.5.2.5.1.4 Development of Smooth Uniform Hazard, Controlling, and Reference Response Spectra

In order to derive smooth spectra corresponding to the 10^{-4} and 10^{-5} amplitudes, the magnitude and distance pairs of both controlling and reference earthquakes summarized in Table 2.5-12 were used as described below.

The magnitudes and distances were applied to spectral shape equations from NUREG/CR-6728 (NRC, 2001) to determine realistic spectral shapes for the four representative earthquakes (at spectral frequency 0.5, 1.75, 7.5, and 25 Hz) of 10^{-4} and 10^{-5} events.

For smooth Uniform Hazard Response Spectra (UHRS), the 25 Hz smooth shapes were utilized and scaled to the Uniform Hazard Spectra mean values for 10^{-4} or 10^{-5} between 25 Hz and 100 Hz. The 7.5 Hz smooth shapes were utilized and scaled to the Uniform Hazard Spectra mean values for 10^{-4} or 10^{-5} between 5 Hz and 10 Hz. The 1.75 Hz smooth shapes were utilized and scaled to the Uniform Hazard Spectra mean values for 10^{-4} or 10^{-5} between 0.5 Hz and 2.5 Hz. Below 0.5 Hz, the 0.5 Hz smooth shapes were scaled and utilized without any modification. The smooth UHRS are presented in Table 2.5-15, in Figure 2.5-48 and Figure 2.5-49.

For the reference response spectra, the HF reference spectra shapes for 10^{-4} or 10^{-5} at the spectral frequency above 5 Hz were the same as the smooth UHRS. The spectral shape at 7.5 Hz was extrapolated from 5 Hz without regard to Uniform Hazard Spectra amplitudes at lower frequencies. The LF reference spectra shapes were scaled to the smooth UHRS values for 10^{-4} or 10^{-5} for frequency less than 2.5 Hz. Above 2.5 Hz, the spectral shape was extrapolated from 2.5 Hz, without regard to Uniform Hazard Spectra amplitudes at higher frequencies by using the smooth spectral shape at frequency of 1.75 Hz.

Creation of smooth 10^{-4} and 10^{-5} reference spectra in this way ensures that the HF spectra match the 10^{-4} and 10^{-5} Uniform Hazard Spectra values at high frequencies (5 Hz and above), and ensures that the LF spectra match the 10^{-4} and 10^{-5} Uniform Hazard Spectra values at low frequencies (2.5 Hz and below). In between calculated values, the spectra have smooth and realistic shapes that reflect the magnitudes and distances dominating the seismic hazard, as reflected in Table 2.5-12. The smooth reference spectra are presented in Figure 2.5-80 and Figure 2.5-81. For controlling response spectra, the smooth spectra shapes for 10^{-4} and 10^{-5} events, LH and HF, and sub-event, DEL, DEM, and DEH were developed directly from the NUREG/CR-6728 using the magnitudes and distances in Table 2.5-12 without any modification. These smooth spectra then scaled to match the smooth UHRS at 1.75 Hz for LF events and at 7.5 Hz for HF events. The smooth controlling response spectra are presented on Figure 2.5-77 and Figure 2.5-78.

2.5.2.5.1.5 Controlling Time Histories

Four initial time histories were selected from the rock time histories database from NUREG/CR-6728 (NRC, 2001) for sub-controlling earthquakes (DEL, DEM, and DEH) for the 10^{-4} and 10^{-5} levels and for both LF and HF events according to their deaggregated magnitudes and distances. These time histories were then modified according to the spectral matching criteria set for time histories in Appendix F of Regulatory Guide 1.208 (NRC, 2007a) to match their target smooth controlling response spectra. The selected time histories are listed in Table 2.5-18.

2.5.2.5.1.6 Site Response Analysis

The site response analysis performed for the BBNPP Site used a time history-based procedure in conjunction with the following assumptions:

- Vertically-propagating shear waves are the dominant contributor to site response.
- An equivalent-linear formulation of soil nonlinearity is appropriate for the characterization of site response.

Sixty response analyses were performed using the program SHAKE (Schnabel, 1972) to calculate the site amplification function for each de-aggregation earthquake. The 60 randomized velocity profiles were paired with the 60 sets of randomized modulus reduction and damping curves (one profile with one set of modulus reduction and damping curves) to define 60 soil columns, each characterized by a set of shear wave velocities, modulus reduction curves, and material damping curves. Each of the four scaled time histories corresponding to a de-aggregated earthquake was used to compute the response of fifteen profile-soil property curve sets.

For each analysis, the response spectrum for the computed motion at the top of the concrete was divided, frequency by frequency, by the response spectrum for the input motion at the hard rock to obtain a site amplification function. The arithmetic mean of these 60 individual response spectral ratios was taken as the mean site amplification function for each de-aggregated earthquake.

The following figures describe the site amplification factors for the high and low frequencies and 10^{-4} and 10^{-5} input motions:

- Figure 2.5-56: mean site amplification factor and coefficient of variation at the top of concrete for 10^{-4} HF DEM input motion;
- Figure 2.5-57: maximum strains vs. depth for 10^{-4} HF DEM input motion;
- Figure 2.5-58: mean site amplification factor and coefficient of variation at the top of concrete for 10^{-4} LF DEM input motion;
- Figure 2.5-59: maximum strains vs. depth for 10^{-4} LF DEM input motion;
- Figure 2.5-60: mean site amplification factor and coefficient of variation at the top of concrete for 10^{-5} HF DEM input motion;
- Figure 2.5-61: maximum strains vs. depth for 10^{-5} HF DEM input motion
- Figure 2.5-62: mean site amplification factor and coefficient of variation at the top of concrete for 10^{-5} LF DEM input motion; and
- Figure 2.5-63: maximum strains vs. depth for 10^{-5} LF DEM input motion.}

2.5.2.6 Ground Motion Response Spectra

The U.S. EPR FSAR includes the following COL Item in Section 2.5.2.6:

A COL applicant that references the U.S. EPR design certification will verify that the site-specific seismic parameters are enveloped by the CSDRS (anchored at 0.3 g PGA) and the

10 generic soil profiles discussed in Section 2.5.2 and Section 3.7.1 and summarized in Table 3.7.1-6.

This COL Item is addressed as follows:

This section and Section 3.7.1 describe the reconciliation of the site-specific parameters for the BBNPP and demonstrates that these parameters are enveloped by the Certified Seismic Design Response Spectra (CSDRS), anchored at 0.3 g PGA, and the 10 generic soil profiles used in the design of the U.S. EPR.

Table 5.0-1 of the U.S. EPR FSAR identifies shear wave velocity as a required parameter to be enveloped, defined as “Minimum shear wave velocity of 1000 feet per second (Low strain best estimate average value at bottom of basemat).”

Figure 2.5-75 compares the 10 generic soil profile cases used for the U.S. EPR and the average shear wave velocity profile that was adopted for the BBNPP site (shown in Figure 2.5-42).

Reconciliation of the BBNPP site-specific seismic parameters with the U.S. EPR certified seismic design response spectra (CSDRS) and the 10 generic soil profiles used for the U.S. EPR is addressed in Section 3.7.1. The evaluation guidelines in U.S. EPR FSAR Section 2.5.2.6 are used to perform the reconciliation.

The steps and conclusions of the seismic parameter reconciliation are summarized below. Summaries of select U.S. EPR structures, systems, and components evaluations which confirm they are adequate for the BBNPP site are also provided as required by seismic reconciliation Step 9.

The seismic reconciliation steps and conclusions:

1. Step 1 of the U.S. EPR FSAR Section 2.5.2.6 seismic reconciliation guidelines is confirmation that the peak ground acceleration for the ground motion response spectrum (GMRS) is less than 0.3g. The BBNPP site-specific GMRS are described in Section 3.7.1. The peak ground acceleration for the BBNPP site-specific GMRS is confirmed to be less than 0.3g.
2. Step 2 of the U.S. EPR FSAR Section 2.5.2.6 seismic reconciliation guidelines is confirmation that the low strain, best estimate value of the shear wave velocity at the bottom of the foundation basemat of the NI Common Basemat Structures is 1000 fps, or greater. The low strain, best estimate value of the BBNPP site-specific shear wave velocity at the bottom of the foundation basemat of the NI Common Basemat Structures is confirmed to be greater than 1000 fps.
3. Step 3 of the U.S. EPR FSAR Section 2.5.2.6 seismic reconciliation guidelines is confirmation that the foundation input response spectra (FIRS) are enveloped by the certified seismic design response spectra (CSDRS). Comparison of the BBNPP site-specific GMRS/ FIRS with the U.S. EPR CSDRS is described in Section 3.7.1. The site-specific horizontal and vertical GMRS/FIRS exceed the envelope of the U.S. EPR CSDRS ground motions, primarily in the high frequency region. The BBNPP design ground motion response spectra are as described in Section 3.7.1, instead of the CSDRS, because the GMRS/FIRS exceed the CSDRS. This represents a departure from the U.S. EPR FSAR, as described in Section 3.7.1.

4. Step 4 of the U.S. EPR FSAR Section 2.5.2.6 seismic reconciliation guidelines is confirmation that the site-specific soil profile is laterally uniform. Horizontal soil layering is confirmed for the BBNPP site-specific soil profile.
5. Step 5 of the U.S. EPR FSAR Section 2.5.2.6 seismic reconciliation guidelines is confirmation that the idealized site soil profile is similar to or bounded by the 10 generic soil profiles used for the U.S. EPR. The BBNPP idealized site soil profile is described in Section 3.7.1. The BBNPP idealized site soil profile is not considered bounded by the U.S. EPR 10 generic soil profiles. This represents a departure from the U.S. EPR FSAR, as described in Section 3.7.1.
6. Step 6 of the U.S. EPR FSAR Section 2.5.2.6 seismic reconciliation guidelines is confirmation that the conditions of Steps 1 through 5 are met. The conditions of Steps 3 and 5 are not met for the BBNPP site because the BBNPP site-specific GMRS/FIRS exceed the envelope of the U.S. EPR CSDRS and the BBNPP site-specific idealized site soil profile is not bounded by the 10 generic soil profiles used for the U.S. EPR. Because the conditions of Steps 3 and 5 are not met for the BBNPP site, seismic reconciliation guideline Step 7 is performed.
7. Step 7 of the U.S. EPR FSAR Section 2.5.2.6 seismic reconciliation guidelines is performance of intermediate-level studies, such as evaluation of the site-specific motion at the top the of the basemat, to demonstrate that the site is bounded by the design of the U.S. EPR. BBNPP site-specific response spectra are developed for the NI Common Basemat Structures basemat and the footprints of the EPGB and ESWB and are compared to the corresponding U.S. EPR design certification spectra. The BBNPP site-specific spectra exceed the envelope of the U.S. EPR certified design spectra; therefore, seismic reconciliation guideline Step 8 is performed.
8. Step 8 of the U.S. EPR FSAR Section 2.5.2.6 seismic reconciliation guidelines is performance of site-specific soil-structure interaction (SSI) analyses, development of in-structure response spectra (ISRS), and confirmation that the BBNPP site-specific ISRS do not exceed the ISRS for the U.S. EPR design certification by more than 10% at the key building locations. BBNPP site-specific SSI analyses are performed and site-specific ISRS are developed for comparison to the U.S. EPR design certification ISRS. The U.S. EPR design certification SSI analysis methodology is used to perform the site-specific SSI analyses, except as noted in Sections 3.7.1 and 3.7.2. Performance of the SSI analyses and comparison of the BBNPP site-specific ISRS with the U.S. EPR design certification ISRS is described in Section 3.7.1. The BBNPP site-specific ISRS exceed the envelope of the U.S. EPR certified design ISRS by more than 10% at some of the specified key building locations. This represents a departure from the U.S. EPR FSAR, as described in Section 3.7.1. Therefore, seismic reconciliation guideline Step 9 is performed.
9. Step 9 of the U.S. EPR FSAR Section 2.5.2.6 seismic reconciliation guidelines is performance of additional evaluations to confirm that safety-related structures, systems, and components of the U.S. EPR at the building locations where BBNPP site-specific ISRS exceed the ISRS for the U.S. EPR design certification by more than 10% are not affected. These evaluations, summarized below, confirm that the safety-related structures, systems and components of the U.S. EPR are not affected.

The BBNPP average shearwave velocity profile shown in the above figure is for soils below elevation +638 ft (195 m) (bottom of the basemat). Soils such as Glacial Overburdens will not be used for support of foundations of the BBNPP Nuclear Island. Therefore, shear wave velocity

measurements in the BBNPP site soils above elevation +638 ft (195 m) regardless of value, are excluded from this evaluation as they lie above the basemat. Results from the above figure indicate that:

1. The BBNPP average shearwave velocity profile is bounded by the 10 generic profiles used for the U.S.EPR.
2. The BBNPP average shearwave velocity Profile offers a shear wave velocity at the bottom of the basemat (approximate elevation +638 ft (195 m)(or depth = 0 in the above figure)) of 7,240 ft/sec (2,207 m/sec).
3. The minimum shear wave velocity from the BBNPP average shearwave velocity profile is 6,800 ft/sec (2,073 m/sec).

On the above basis, it is concluded that the BBNPP site shear wave velocity profile is bounded by the 10 generic soil profiles used for the U.S. EPR and meets the minimum 1,000 ft/sec (305 m/sec) criterion identified in the U.S. EPR FSAR.

As described in Section 2.5.2.4, the end results of the site response analysis are weighted average site amplification factors. In this section, these factors are used to develop the ground motion response spectra (GMRS) by modifying the spectra at rock. The GMRS was developed in accordance with the performance-based approach described in Regulatory Position 5 of Regulatory Guide 1.208 (NRC, 2007a).

The Safe Shutdown Earthquake (SSE) ground motion was developed starting from the 10^{-4} and 10^{-5} rock Uniform Hazard Spectra. At high frequencies, the appropriate (10^{-4} or 10^{-5}) HF mean amplification factor was applied to the 10^{-4} or 10^{-5} HF smooth rock spectrum, to calculate site spectral amplitudes for 10^{-4} and 10^{-5} annual frequencies of exceedance. At low frequencies, a similar technique was used with the LF mean amplification factors. At intermediate frequencies, the larger of the HF and LF site spectral amplitudes was used.

Figure 2.5-64 illustrates the resulting site spectra. At high frequencies, the HF spectral amplitudes are always greater, and at low frequencies, the LF spectral amplitudes are always greater.

This procedure implements Approach 2B in NUREG/CR-6728 (NRC, 2001) and NUREG/CR-6769 (NRC, 2002), where in the rock Uniform Hazard Spectra (for example, at 10^{-4}) is multiplied by a mean amplification factor at each frequency to estimate the 10^{-4} site Uniform Hazard Spectra. Note that the amplification factors plotted on Figure 2.5-56, Figure 2.5-58, Figure 2.5-60, and Figure 2.5-62 are logarithmic mean amplification factors, which correspond approximately to the median. The amplification factors used to prepare Figure 2.5-64 are arithmetic mean amplification factors, which are slightly higher than the median.

The low-frequency character of the spectra on Figure 2.5-64 reflects the low-frequency amplification of the site, as shown in the amplification factors of Figure 2.5-56, Figure 2.5-58, Figure 2.5-60, and Figure 2.5-62. That is, there is a fundamental site resonance at about 0.22 Hz, with a dip in site response at about 0.4 Hz, and this dip occurs for all 60 of the site profiles

that were used to characterize the site profile. As a result, there is a dip in the site spectra for 10^{-4} and 10^{-5} at 0.4 Hz that reflects the site characteristics.

The ASCE (ASCE, 2005b) performance-based approach was used to derive an SSE from the 10^{-4} and 10^{-5} site spectra. The SSE spectrum is derived at each structural frequency as follows:

$$A_R = SA(10^{-5})/SA(10^{-4})$$

$$DF = 0.6 A_R^{0.8}$$

$$SSE = \max(SA(10^{-4}) \times \max(1.0, DF), 0.45 \times SA(10^{-5}))$$

The last term in the above equation was not published in this form in ASCE (ASCE, 2005) but is a supplemental modified form, as presented in NRC Regulatory Guide 1.208 (NRC, 2007a). The resulting horizontal SSE spectrum is plotted in Figure 2.5-65.

A vertical SSE spectrum was constructed from the horizontal SSE spectrum following the approach described in NUREG/CR-6728 (NRC, 2001) by deriving vertical-to-horizontal (V/H) ratios and applying them to the horizontal SSE. As background and for comparison purposes, V/H ratios were obtained by the following methods:

The vertical SSE spectrum was constructed from the horizontal Design Response Spectrum (DRS) using vertical to horizontal (V/H) response spectral ratios appropriate for the BBNPP Site. The V/H ratios are developed following the approach described in NUREG/CR-6728 (NRC, 2001). Figure 2.5-66 shows the V/H ratios recommended for CEUS rock sites as a function of spectral frequency and the level of peak ground acceleration (PGA) for the horizontal component. Figure 2.5-66 shows the weighted average of these V/H ratios based on the PGA for the de-aggregated earthquakes (DE's) that make up the high-frequency (HF) and low-frequency (LF) mean 10^{-4} reference earthquakes (RE's). The weights assigned to the DE are listed in Table 2.5-12. The weighted V/H ratios are essentially the same for the HF and LF mean 10^{-4} DE.

The EPRI 2004 ground motion model for CEUS is defined at the hard rock or at the elevation that the shear wave velocity in the material is approximately 9200 ft/sec (2800 m/sec). Only the horizontal component of the ground motion is defined in this ground motion model, not the vertical component. Consequently, the PSHA is done at the hard rock level for the horizontal ground motion component. The site response analysis is performed to bring the ground motion from the hard rock elevation to the ground surface or top of competent material to define the GMRS according to Regulatory Guide 1.208 (NRC, 2007a). The end result of the site response analysis is the horizontal ground motion at free field or top of competent material. In order to define the vertical ground motion component, Regulatory Guide 1.208 (NRC, 2007a) Section C5.2 permits using the procedure described in NUREG/CR-6728 (NRC, 2001) for the CEUS soil site. The procedure begins by calculating the V/H ratio of the rock site in the CEUS via the set of equations provided in NUREG/CR-6728 (NRC, 2001). The transfer function calculated from the ratio of V/H ratio of the soil site with respect to the V/H ratio of the rock site in the WUS soil site is applied the V/H ratio of the rock site in the CEUS to obtain V/H ratio for the soil site in the CEUS. The Clinton ESP (EGC, 2006) also performed the GMRS calculation according to this procedure. The Clinton ESP application has been accepted by the NRC (NRC, 2007c).

The vertical DRS is obtained by scaling the horizontal DRS by the soil V/H ratios shown on Figure 2.5-66. A smooth spectrum enveloping the vertical DRS was then constructed. The resulting vertical SSE is shown on Figure 2.5-65 and is tabulated in Table 2.5-13 along with the horizontal SSE spectrum.

Refer to Sections 3.7.1 and 3.7.2 for a description of the soil-structure interaction analyses performed for the U.S. EPR design certification.

CAV Filtering In Surface Ground Motions

The use of a lower bound magnitude in the calculation of the probabilistic seismic hazard could result into some excessive conservatism as a consequence of including the effects of non-damaging earthquakes. The reason is that, according to probabilistic methodologies and current attenuation equations, small magnitude near site events could occur very frequently having a significant contribution to the integrated hazard. However, it has been found that facilities designed and built with sound engineering practices do not suffer damage from this type of events (EPRI, 1988a). Examining this issue, the Cumulative Absolute Velocity (CAV) was proposed as a parameter for quantifying the damage potential associated to an earthquake record (EPRI, 1988). For a given accelerogram, $a(t)$, the CAV is calculated with the following equation:

$$CAV = \sum_i H(pga_i - 0.025g) \int_i |a(t)| dt$$

where pga is peak ground acceleration, g is gravity and $H(x)$ is the Heaviside function (unity for $x > 0$ and 0 otherwise).

It should be noted that the surface ground motion $a(t)$ is used to calculate the CAV. It has been observed that no damage occurs on well designed and built structures when the CAV is equal to or lower than 0.16g-sec (EPRI, 2006).

Recently, EPRI (EPRI, 2006) has published methodologies for incorporating the CAV filter into seismic hazard calculations. The most direct method consists in including the probability of exceeding the 0.16g-sec threshold into the integral to calculate the hazard. This, however, would require that site effects be included in the hazard integration, for instance, in the attenuation equations. In addition, the computation time would be significantly increased. Thus, EPRI (EPRI, 2006) has also developed a more efficient method for applying the minimum as a post-processing procedure to the hazard calculation. EPRI TR-1014099 (EPRI, 2006) was used in lieu of the Regulatory Guide 1.208 (NRC, 2007a) cited document (EPRI Report 1012965). EPRI Report 1012965 was an update report for CAV research while EPRI TR-1014099 (EPRI, 2006) is the final report. For the purposes of revised calculation of the CAV in the CEUS, there is no technical difference between the documents. The methodologies of calculation of the CAV of both reports are identical. This approach uses the hazard curve and the de-aggregation obtained in the PHSA at rock to calculate the rate of occurrence, $v(z_k, i, j)$, of the spectral acceleration around a small acceleration range close to z_k , due to a magnitude-distance pair (M_i, R_j). Equations developed by EPRI to estimate the CAV in terms of M and peak ground acceleration (PGA) can then be used to calculate the probability that $P(CAV \geq 0.16)$ for the corresponding M_i, R_j pair, and the filtered hazard $v'(S)$ is calculated as follows:

$$v'(S > z) = \sum_i \sum_j \sum_k v(z_k, i, j) P(CAV \geq 0.16)$$

The CAV filtering is implemented by first breaking the hazard curve at rock into rates of occurrence of scenario earthquakes (M, R, PGA). We can then compute the probability that this scenario will lead to a CAV value greater than 0.16g-sec. This probability is then multiplied by the rate of the scenario, and the sum of the filtered rates furnishes the CAV filtered hazard. The spectral value can be related to a corresponding PGA using the uniform hazard spectrum shape at the corresponding exceedance rate.

Following details presented in EPRI (EPRI, 2006), the CAV filtering was incorporated as a post-processing application into the hazard calculation at the BBNPP Site. Very modest reductions in spectral values were obtained, particularly for the 10-5 hazard. The explanation is that after applying the site amplification factors, the PGA values corresponding to this hazard level are relatively high (about 0.4g) and, consequently, almost certainly damaging. In fact, CAV reductions on the GMRS were negligible.

2.5.2.7 Conclusions

{This section is added as a supplement to the U.S. EPR FSAR.

An updated evaluation of the vibratory ground motion has been conducted for the BBNPP Site. A Probabilistic Seismic Hazard Analysis (PSHA) was selected as the appropriate basis for evaluating the vibratory ground motion accounting for all credible alternative seismic sources. The alternative seismic sources identified by the Electric Power Research Institute (EPRI) for the Central and Eastern United States (CEUS), Seismic Hazard Methodology for the Central and Eastern United States (EPRI, 1986) issued in 1986 are still considered to constitute an adequate definition of seismic area sources. However, updated information available from databases maintained by the United States Geological Survey has been used to determine recurrence parameters. Since the New Madrid Fault System (NMFS) and the Charleston Seismic Source (CSS) have some contribution to the seismic hazard at the BBNPP Site, updated logic-tree representations of the clustered characteristic earthquakes at the NMFS and the un-clustered CSS have been incorporated into the PSHA. The NMFS characterization is provided by Exelon in the Clinton ESP application (EGC, 2006) and the CSS characterization is the one presented in the CCNPP Unit 3 FSAR (UniStar Nuclear, 2007). Both characterizations have been verified with USGS modeling of the New Madrid and Charleston Faults. The PSHA for the BBNPP Site makes use of a decision tree approach with appropriate weighting factors that are based on the most up-to-date information and relative confidence in alternative characterizations for each area and characteristic seismic source.

The guidance of Regulatory Guide 1.208, "A performance -Based Approach to define the Site-Specific Earthquake Ground Motion," (NRC, 2007a) was used to develop the Ground Motion Response Spectrum (GMRS) at the BBNPP Site. This GMRS adequately represents the regional and local seismic hazards and accurately includes the effects of the local soils at the BBNPP Site.

It is concluded that the performance-based approach outlined in Regulatory Guide 1.208 (NRC, 2007a) constitutes an advancement over the solely hazard-based reference probability approach recommended in Regulatory Guide 1.165 (NRC, 1997a) and used it where appropriate in the determination of the GMRS. The performance-based approach uses not only the seismic hazard characterization of the site from the PSHA but also basic seismic fragility SSC modeling in order to define a ground motion that directly targets a structural performance frequency value. It is concluded that the application for the BBNPP Site is acceptable from a geologic and seismologic

standpoint and meets the requirements of 10 CFR 100.23(d) (CFR, 2007). Deviations from the NRC guidance in Regulatory Guide 1.165 (NRC, 1997a), Regulatory Guide 1.208 (NRC, 2007a), or review criteria in Standard Review Plan 2.5.2 (NRC, 2007b) have been identified and acceptable alternatives, including technical justification, have been provided.}

2.5.2.8 References

{This section is added as a supplement to the U.S. EPR FSAR.

Abrahamson, 1997. Empirical Response Spectral Attenuation Relations for Shallow Crustal Earthquakes. N. A. Abrahamson and W. J. Silva. *Seismological Research Letters*, Volume 68, Number 1, 1997.

Ang and Tang, 1975. Probabilistic Concepts in Engineering Planning and Design, Volume 1, A.H. Ang and W.H. Tang, John Wiley and Sons, New York, 1975.

Atkinson, 2006. Earthquake Ground-Motion Prediction Equations for Eastern North America," G. M. Atkinson and D. M. Boore, *Seismological Society of America, Bulletin*, Volume 96, Number 6, pp. 2181-2205, 2006.

ASCE, 2005a. Minimum Design Loads for Buildings and Other Structures, ASCE/SEI 7-05, American Society for Civil Engineers/Structural Engineering Institute, 2005.

ASCE, 2005b. Seismic Design Criteria for Structures, Systems, and Components in Nuclear Facilities, ASCE/SEI 43-05, American Society for Civil Engineers/Structural Engineering Institute, 2005.

Bakun, 2004. Magnitudes and Locations of the 1811-1812 New Madrid, Missouri, and the 1886 Charleston, South Carolina, Earthquakes, W. H. Bakun and M. G. Hopper, *Seismological Society of America, Bulletin*, Volume 94, Number 1, pp. 64-75, 2004.

Bollinger, 1977. Reinterpretation of the Intensity Data for the 1886 Charleston, South Carolina, Earthquake in Studies Related to the Charleston, South Carolina, Earthquake of 1886 -A Preliminary Report, in D. W. Rankin, Editor, G. A. Bollinger, U. S. Geological Survey Professional Paper 1028, pp. 17-32, 1977.

Boore, 1987. Stochastic Prediction of Ground Motion Response Parameters at Hard-Rock Sites in Eastern North America, D.M. Boore and G.M. Atkinson, *Bulletin Seismological Society of America*, Volume 77, Number 2, pp. 440-467, 1987.

Campbell, 2003. Updated Near-Source Ground-Motion (Attenuation) Relations for the Horizontal and Vertical Components of Peak Ground Acceleration and Acceleration Response Spectra. K. W. Campbell, and Y. Bozorgnia. *Bulletin of the Seismological Society of America*. Volume 93, No. 1. pp. 314-331. 2003.

CFR, 2007. Title 10, Code of Federal Regulations, Part 100.23(d), Geologic and Seismic Siting Factors, 2007.

Cornell, 1968. Engineering Seismic Risk Analysis, C.A. Cornell, *Bulletin of Seismological Society of America*, Volume 58, pp. 1583-1606, 1968.

Cornell, 1971. Probabilistic Analysis of Damage to Structure Under Seismic Loads, C.A. Cornell, Dynamic Waves in Civil Engineering, Chapter 27, edited by D.A. Howells, I.P Haigh, and C. Taylor, 1971.

Costantino, 1996. Recommendations for Uncertainty Estimates in Shear Modulus Reduction and Hysteretic Damping Relationships, C. J. Costantino, 1996, Published as an appendix in "Description and validation of the stochastic ground motion model," W.J. Silva, N. Abrahamson, G. Toro and C. Costantino, 1997, Report Submitted to Brookhaven National Laboratory, Associated Universities, Inc. Upton, New York 11973, Contract No. 770573.

Cox, 1983. Paleoseismic Studies in the 1886 Charleston Earthquake Meizoseismal Area, Geological Society of America Abstracts with Programs, J. Cox and P. Talwani, 1983.

Cramer, 2000. A Seismic Hazard Uncertainty Analysis for the New Madrid Seismic Zone, Engineering Geology, C. H. Cramer, Volume 62, pp 251-266, 2000.

EGC, 2006. Submittal of Revision 4 to Exelon Generation Company's Early Site Permit Application for Clinton, Including Administrative Information, Emergency Plan, Site Redress Plan, Environmental Report and Site Safety Analysis Report, April 14, 2006.

EPRI, 1986. Seismic Hazard Methodology for the Central and Eastern United States, NP-4726, Volumes 1-10, Electric Power Research Institute, July 1986.

EPRI, 1988. Seismic Hazard Methodology for the Central and Eastern United States, NP-4726-A, Revision 1, Volume 1, Part 2, Electric Power Research Institute, 1988.

EPRI, 1988a. A Criterion for Determining Exceedance of the Operating Basis Earthquake, NP-5930, Electric Power Research Institute, 1988.

EPRI, 1989a. Probabilistic Seismic Hazard Evaluations at Nuclear Power Plant Sites in the Central and Eastern United States: Resolution of the Charleston Earthquake Issue, NP-6395-D, Electric Power Research Institute, 1989.

EPRI, 1989b. EQHAZARD Primer, NP-6452-D, Electric Power Research Institute, June 1989.

EPRI, 1993. Guidelines for Determining Design Basic Ground Motions, TR-102293, Volume 1, Electric Power Research Institute, 1993.

EPRI, 2004. CEUS Ground Motion Project Final Report, TR-1009684 2004, Electric Power Research Institute, December 2004.

EPRI, 2006. Program on Technology Innovation: Use of Cumulative Absolute Velocity (CAV) in Determining Effects of Small Magnitude Earthquakes on Seismic Hazard Analyses, Report 1014099, Electric Power Research Institute, Palo Alto, CA, and U.S. Department of Energy, Germantown, MD, 2006.

EPRI, 2006a. Program on Technology Innovation: Truncation of the Lognormal Distribution and Value of the Standard Deviation for Ground Motion Models in the Central and Eastern United States, TR-1014381, Electric Power Research Institute, August 2006.

EPRI, 2006b. Program on Technology Innovation: Truncation of the Lognormal Distribution and Value of the Standard Deviation for Ground Motion Models in the Central and Eastern United States, Technical Update 1013105, Electric Power Research Institute, February 2006.

Frankel, 1995. Mapping Seismic Hazard in the Central and Eastern United States, A.D. Frankel, Seismological Research Letters, Volume 66, Number 4, pp. 8-21, 1995.

GEOvision, 2008. Report Revision B, Boring Geophysical Logging, Borings B301, G-301, G302, and G-303, Berwick Unit 1 COL Project, GEOvision Geophysical Services, 2008.

Gutenberg, 1944. Frequency of earthquakes in California. B. Gutenberg, and C. F. Richter, Bulletin of the Seismological Society of America, Volume 34, p. 185-188, 1944.

Hough, 2000. On the Modified Mercalli intensities and magnitudes of the 1811-1812 New Madrid earthquakes. S. E. Hough, Armbruster, J.G., Seeber, L., and Hough, J.F Journal of Geophysical Research, Volume 105, Number B10, pp. 23,839-23,864, 2000.

Hough, 2001. Triggered Earthquakes and the 1811-1812 New Madrid, Central United States, Earthquake Sequence, Bulletin of the Seismological Society of America, S. Hough, Volume 91, pp 1574-1581, 2001.

Inners, 1978. Geology and Mineral Resources of the Berwick Quadrangle, Luzerne and Columbia Counties, Pennsylvania, Pennsylvania Geological Survey, Fourth Series, pp. 1-34, J.D. Inners, 1978.

Johnston, 1996. Seismic Moment Assessment of Earthquake in Stable Continental Regions - III. New Madrid 1811-1812, Charleston 1886 and Lisbon 1755, A. C. Johnston, Geophysical Journal International, Volume 126, pp. 314-344, 1996.

Marple, 2000. Evidence of a buried fault system in the Coastal Plain of the Carolinas and Virginia- Implications for neotectonics in the southeastern United States, R. Marple and P. Talwani, Geological Society of America Bulletin, Volume 112, Number 2., pp. 200-220, 2000.

McGuire, 1988. Engineering Model of Earthquake Ground Motion for Eastern North America, Electric Power Research Institute Technical Report NP-6074, R. K. McGuire, G.R. Toro and W.J. Silva, 1988.

Mueller, 1997. Preparation of Earthquake Catalogs for the National Seismic-Hazard Maps: Contiguous 48 States, C. M. Mueller, C., M. Hopper, and A. Frankel, U.S. Geological Survey Open-File Report 97-464, 1997.

Newmark, 1982. Earthquake Spectra and Design, N. M. Newmark and W.J. Hall, Earthquake Engineering Research Institute, Berkeley, California, 1982.

NGA, 2008. Final Report Revision 0, Susquehanna Unit 3 Nuclear Power Plant Downhole Seismic Velocity Survey, Berwick, Pennsylvania, Northwest Geophysical Associates, Inc., 2008.

NRC, 1997a. Identification and Characterization of Seismic Sources and Determination of Safe Shutdown Earthquake Ground Motion, Regulatory Guide 1.165, U. S. Nuclear Regulatory Commission, March 1997.

NRC, 1997b. Recommendations for Probabilistic Seismic Hazard Analysis: Guidance on Uncertainty and Use of Experts, Prepared by Senior Seismic Hazard Analysis Committee (SSHAC), NUREG/CR-6372, U. S. Nuclear Regulatory Commission, 1997.

NRC, 2001. Technical Basis for Revision of Regulatory Guidance on Design Ground Motions, Hazard- and Risk-Consistent Ground Motion Spectra Guidelines, NUREG/CR-6728, U. S. Nuclear Regulatory Commission, 2001.

NRC, 2002. Technical Basis for Revision of Regulatory Guidance on Design Ground Motions: Development of Hazard- & Risk-Consistent Seismic Spectra for Two Sites, NUREG/CR-6769, U. S. Nuclear Regulatory Commission, 2002.

NRC, 2005. Safety Evaluation Report for an Early Site Permit (ESP) at the North Anna ESP Site, NUREG-1835, U. S. Nuclear Regulatory Commission, September 2005.

NRC, 2007a. A Performance-Based Approach to Define the Site-Specific Earthquake Ground Motion, Regulatory Guide 1.208, U. S. Nuclear Regulatory Commission, March 2007.

NRC, 2007b. Vibratory Ground Motion, Standard Review Plan, NUREG-0800, Section 2.5.2, Revision 4, U.S. Nuclear Regulatory Commission, March 2007.

NRC, 2007c. Issuance of Early Site Permit for Exelon Generation Company, LLC (ESP-001), Letter from D.B. Matthews (NRC) to M.C. Kray (Exelon Nuclear), March 15, 2007.

Obermeier, 1987. Earthquake Induced Liquefaction Features in the Coastal South Carolina Region, U.S. Geological Survey Open File Report 87-504, S.F. Obermeier, R.E. Weems, R.B. Jacobson, 1987.

Schnabel, 1972. SHAKE - A Computer Program for Earthquake Response Analysis of Horizontally Layered Sites, P.B. Schnabel, J. Lysmer and H.B. Seed, Report No. EERC 72-12, University of California, Berkeley, 1972.

Schwartz, 1984. Fault Behavior and Characteristic Earthquakes: Examples from the Wasatch and San Andreas Fault Zones, Journal of Geophysical Research, D.P. Schwartz and K.J. Coppersmith, Volume 89, Number B7, pp 5681-5698, 1984.

Seeber, 1991. The NCEER-91 earthquake catalog: improved intensity-based magnitudes and recurrence relations for U.S. earthquakes east of New Madrid, L. Seeber and J. G. Armbruster National Center for Earthquake Engineering Research, NCEER-91-0021, 1991.

Seeber, 1998. The 1994 Cacoosing Valley earthquakes near Reading, Pennsylvania: A shallow rupture triggered by quarry unloading, L. Seeber, J. G. Armbruster, W.Y. Kim, N. Barstow, and C. Scharnberger, Journal of Geophysical Research, Volume 103, Number B10, pp. 24,505-24,521, 1998.

Silva, 2002. Development of regional hard rock attenuation relations for central and eastern North America, W. Silva, N. Gregor and R. Darragh, Pacific Engineering Analysis, El Cerrito, CA, 2002.

SNOC, 2008. Early Site Permits - Southern Nuclear Operating Company Application for the Vogtle ESP Site, Revision 4, Southern Nuclear Operating Company, 2008.

Somerville, 2001. Ground-Motion Attenuation Relations for the Central and Eastern United States, P. G. Somerville, N. Collins, N. A. Abrahamson, R. Graves and C. K. Saikia, Report to the USGS, NEHRP External Research Program, Award No. 99-HQ-GR-0098, 2001.

Southern Nuclear Operating Company (2008). Early Site Permits - Southern Nuclear Operating Company Application for the Vogtle ESP Site (revision 4), USNRC 2008.

Talwani, 2001. Recurrence rates of Large Earthquakes in the South Carolina Coastal Plain Based on Paleoliquefaction Data, P. Talwani and W. T. Schaeffer, Journal of Geophysical Research, Volume 106, Number B4, pp. 6621-6642, 2001.

Tavakoli, 2005. Empirical-stochastic ground-motion prediction for eastern North America, B. Tavakoli, B. and S. Pezeshk, Bulletin of the Seismological Society of America, Volume 95, pp. 2283-2296, 2005.

Toro, 1996. Probabilistic Models of Site Velocity Profiles for Generic and Site-Specific Ground Motion Amplification Studies, G. R. Toro, Published as an appendix in W. J. Silva, N. Abrahamson, G. Toro and C. Costantino, 1997, Description and validation of the stochastic ground motion model, Report Submitted to Brookhaven National Laboratory, Associated Universities, Inc. Upton, New York 11973, Contract No. 770573, 1996.

Toro, 1997. Model of Strong Ground Motions from Earthquakes in Central and Eastern North America: Best Estimates and Uncertainties, G. R. Toro, N. A. Abrahamson, and J. F. Schneider, Seismological Research Letters, Volume 68, Number 1, pp. 41-57, 1997.

Tuttle, 2000. Late Holocene earthquakes and earthquake potential of the New Madrid seismic zone, Central United States, M. Tuttle, E.S. Schweig, R.H. Lafferty, M. Haynes, Seismological research Letters, v. 71, p 119-120, 2000.

Tuttle, 2002. The Earthquake Potential of the New Madrid Seismic Zone, M. P. Tuttle, E.S. Schweig, J.D. Sims, R.H. Lafferty, L.W. Wolf, and M.C. Haynes, Bulletin of the Seismological Society of America, Volume 92, Number 6, pp. 2080-2089, 2002.

Tuttle, 2002. The Earthquake Potential of the New Madrid Seismic Zone, M. P. Tuttle, E.S. Schweig, J.D. Sims, R.H. Lafferty, L.W. Wolf, and M.C. Haynes, Bulletin of the Seismological Society of America, Vol. 92, No. 6, pp. 2080-2089, 2002.

UniStar Nuclear, 2007. Calvert Cliffs Nuclear Power Plant Unit 3, Combined License Application, Revision 0, Part 2 Final Safety Analysis Report, Section 2.5.2, Vibratory Ground Motion, UniStar Nuclear, 2007.

USGS, 1996. National seismic-hazard maps: documentation, U. S Geological Survey, Open-File Report 96-532, A. Frankel, T. Barnhard, D. Perkins, E. V. Leyendecker, N. Dickman, S. Hanson, and M. Hopper, 1996.

USGS, 2002. Documentation for the 2002 Update of the National Seismic Hazard Maps, U.S. Geological Survey Open-File Report 02-420, A. D. Frankel, M. D. Petersen, C. S. Mueller, K. M

Haller, R. L. Wheeler, E. V. Leyendecker, R. L. Wesson, S. C. Harmsen, C. H. Cramer, D. M. Perkins, and K. S. Rukstales, 2002.

USGS, 2008. Documentation for the 2008 update of the United States National Seismic Hazard Maps: U.S. Geological Survey Open-File Report 2008-1128, M. D. Peterson, A. D. Frankel, S. C. Harmsen, C. S. Muller, K. M. Haller, R. L. Wheeler, R. L. Wesson, Y. Zeng, O.S. Boyd, D. M. Perkins, N. Luco, E. H. Field, C. J. Wills, and K. S. Rukstales, 2008.

Weichert, 1980. Estimation of the earthquake recurrence parameters for unequal observation periods for different magnitudes, D. H. Weichert, Bulletin of the Seismological Society of America, Volume 70, pp. 1337-1356, 1980.

Youngs, 1985. Implications of Fault Slip Rates and Earthquake Recurrence Models to Probabilistic Seismic Hazard Estimates, Bulletin of the Seismological Society of America, R.R. Youngs and K.J. Coppersmith, Volume 75, Number 4, pp 939-964, 1985.}

2.5.3 SURFACE FAULTING

The U.S. EPR FSAR includes the following COL Item in Section 2.5.3:

A COL applicant that references the U.S. EPR design certification will investigate site-specific surface and subsurface geologic, seismic, geophysical, and geotechnical aspects within 25 miles around the site and evaluate any impact to the design. The COL applicant will demonstrate that no capable faults exist at the site in accordance with the requirements of 10 CFR 100.23 and 10 CFR 50, Appendix S. If non-capable surface faulting is present under foundations for safety-related structures, the COL applicant will demonstrate that the faults have no significant impact on the structural integrity of safety-related structures, systems or components.

This COL Item is addressed as follows:

{There is no potential for tectonic fault rupture and there are no capable tectonic sources within a 25 mi (40 km) radius of the BBNPP site.} A capable tectonic source is a tectonic structure that can generate both vibratory ground motion and tectonic surface deformation, such as faulting or folding at or near the earth's surface in the present seismotectonic regime (NRC, 1997). The following sections provide the data, observations, and references to support this conclusion. Information contained in these sections was developed in accordance with RG 1.165 (NRC, 1997), and is intended to satisfy 10 CFR 100.23, "Geologic and Seismic Siting Criteria" (CFR, 2007a) and 10 CFR 50, Appendix S, "Earthquake Engineering Criteria for Nuclear Power Plants" (CFR 2007b).

Section 2.5.3.1 through Section 2.5.3.9 are added as a supplement to the U.S. EPR FSAR.

2.5.3.1 Geological, Seismological, and Geophysical Investigations

The following investigations were performed to assess the potential for surface fault rupture at and within a 5 mi (8 km) radius of the BBNPP site:

- Compile and review existing geologic and seismologic data
- Interpret aerial photography

- Field reconnaissance
- Seismic refraction tests performed at the site
- Review of pre-EPRI and post-EPRI (1989) seismicity (e.g. earthquake catalog used in EPRI (1989) ended in 1983. Pre-EPRI catalog is 1500's through 1983; post-EPRI is 1983 through 2006)
- Discuss site area geology with researchers at the U.S. Geological Survey (USGS), Pennsylvania Geological Survey (PGS), and academic institutions.

The geologic and geotechnical data available for the existing Susquehanna Steam Electric Station (SSES) Units 1 and 2 site, as well as the proposed BBNPP site, is contained in three principal sources:

1. Work performed for the existing SSES Units 1 and 2 and complementary structures (SSES FSAR, 2003).
2. Published Geologic mapping performed primarily by the USGS and Pennsylvania Department of Conservation and Natural Resources (PA DCNR).
3. Seismicity data compiled and analyzed in published journal articles and, more recently, as part of Section 2.5.2.

Existing information was supplemented by field reconnaissance within a 5 mi (8 km) radius of the site, and interpretation of aerial photography along all known faults within the 25 mi (40 km) radius of the site. Satellite imagery (raster imagery) of the BBNPP site region also was acquired for review and interpretation. These field and office-based studies were performed to verify, where possible, the existence of mapped bedrock faults in the BBNPP site area and to assess the presence or absence of geomorphic features suggestive of potential Quaternary fault activity along the mapped faults, or previously undetected faults. Features reviewed during the field reconnaissance and office-based analysis of aerial photography and satellite imagery were based on a compilation of existing regional geologic information, as well as discussions with experts at the USGS and professors at local Universities who have worked at and/or performed studies in the vicinity of the BBNPP site.

Field reconnaissance within a 5 mi (8 km) radius of the site was conducted by geologists in teams of two or more. Two field reconnaissance visits in late autumn and winter, 2007 focused on exposed portions of the Mahantango Formation, other formation exposures along the faces of Lee and Nescopeck Mountains, and roads traversing the site. Key observations and discussion items were documented in field notebooks and photographs. Field locations were logged by hand on detailed topographic base maps and with hand-held Global Positioning System (GPS) receivers.

Aerial reconnaissance within a 25 mi (40 km) radius of the site was conducted by various personnel using aerial photographs from numerous publications. The aerial reconnaissance investigated geomorphology of northeastern Pennsylvania and targeted numerous previously mapped geologic features and potential seismic sources within a 200 mi (320 km) radius of the site (e.g., New York Bight fault, Oak Bay fault, Ramapo fault, Dobbs Ferry fault zone, Kingston fault, Berwick fault, Light Street fault, and Berwick anticlinorium). Key observations and discussion items are documented in depth throughout Section 2.5.1.

The investigations of regional and site physiographic provinces and geomorphic processes, geologic history, and stratigraphy were conducted by Paul C. Rizzo Associates Inc. The investigations of regional and site tectonics and structural geology were also conducted by Paul C. Rizzo Associates Inc.

2.5.3.1.1 Previous Site Investigations

Previous site investigations performed for the existing units are summarized in the SSES Final Safety Analysis Report (FSAR) (SSES FSAR, 2003). As cited in the SSES FSAR, these previous investigations provide the following results documenting the absence of Quaternary faults at and within the area of the BBNPP site:

Interpretation of satellite photos and topographic maps. This interpretation revealed no evidence of surface rupture, surface warping, or offset of geomorphic features indicative of active faulting.

Interviews with personnel from government agencies and private organizations. These interviews concluded that no known faults are present beneath the existing SSES Units 1 and 2 or BBNPP site areas.

Seismicity Analysis -This analysis showed that no microseismic activity has occurred in the site area; the site is located in a region that has experienced only infrequent minor earthquake activity approximately 35 mi (56 km) northeast of the BBNPP site, between Lackawanna and Wyoming Counties; the closest fault (Anthracite Zone) related epicentral location is greater than 25 mi (40 km) away. No earthquake within 50 mi (80 km) of the BBNPP site has been large enough to cause significant damage in the time the region has been populated, approximately 270 years. Section 2.5.2 provides a full discussion on the seismicity analysis for the BBNPP site.

Approximately 250 exploratory boreholes were drilled at the SSES Units 1 and 2 site area. Borehole data have provided evidence for the lateral continuity of strata across the existing SSES site area and BBNPP site area (SSES FSAR, 2003). The inspection of soil samples has revealed no adverse effects indicative of geologically recent or active faulting.

Field reconnaissance of many surface outcrops at the site and within the 5 mi (8 km) radius of the site, coupled with geophysical surveys, provided evidence for no faulting at the BBNPP site.

At the time of the original studies for the SSES FSAR (SSES FSAR, 2003), published maps showing bedrock faults within a 5 mi (8 km) radius of the BBNPP site identified only the Light Street fault, which is approximately 1.8 mi (2.9 km) southeast of the BBNPP site. The closest significant bedrock faults mapped prior to 1975 were faults located about 80 mi (128 km) southwest of the BBNPP site near Lewistown, PA (SSES FSAR, 2003). Figure 2.5-87 (USGS, 2001) shows two earthquakes within the 25 mi (40 km) radius of the BBNPP site. Further analysis of these mapped earthquakes revealed that the sources for these earthquakes were quarry blasts or mine collapse (Faill, 2004). Neither of these seismic events were fault related or associated with bedrock/basement rock deformation. No publications reported vibratory ground motions being felt as a result of either of these seismic events, at or near the BBNPP site area. Based on this information, there are no significant hazard potential faults within a 25 mi (40 km) radius of the BBNPP site as seen in Figure 2.5-87.

2.5.3.1.2 Regional and Local Geological Studies

Since the late 1960's, extensive mapping of the BBNPP site region within the Ridge and Valley Province has been performed by the PGS and other governmental agencies (Inners, 1978) (USGS, 2001) (Wheeler, 2006) to improve the industry's knowledge of the Ridge and Valley stratigraphy and other geologic structures within the region. Ridge and Valley mapping includes geologic mapping across the BBNPP site area (Inners, 1978) (as seen in Figure 2.5-88), a developed geologic cross section of the central Appalachian Basin based on mapping and borehole data (Ryder, 1992) (as seen in Figure 2.5-89, Figure 2.5-90, and Figure 2.5-91), and a Precambrian Basement Map (Gold, 2005) based on borehole and seismic reflection data (as seen in Figure 2.5-92). This compilation of previous mapping and exploration studies, coupled with site-specific reconnaissance for BBNPP, provides the principal basis for the few bedrock faults recognized within the site area.

In addition, the USGS recently completed a compilation of all Quaternary faults, liquefaction features, and possible tectonic features in the eastern U.S. (Crone, 2000) (Wheeler, 2005) (Wheeler, 2006). These compilations do not show any Quaternary faults or features within a 25 mi (40 km) radius of the site as shown in Figure 2.5-94. The nearest potential Quaternary feature (Crone, 2000) is the Cacoosing Valley earthquake, part of the Lancaster seismic zone, approximately 52 mi (84 km) south of the BBNPP site. The closest documented paleo-liquefaction site (Crone, 2000), in northeastern Massachusetts, is known as the Newbury liquefaction features and is located over 260 mi (418 km) from the BBNPP site.

A local geologic cross-section oriented north-south within the site area (5 mi (8 km) radius) depicts slightly faulted anticlinal Silurian-Mississippian bedrock that is unconformably overlain by Pliocene-Holocene deposits (DCNR, 2007) (Inners, 1978) as shown in Figure 2.5-94. A review of the SSES FSAR reported the presence of the Light Street Fault but failed to uncover evidence, through either published reports or field investigations, to support the existence of the inferred Berwick fault (SSES FSAR, 2003). Folds, as reported by Inners (Inners, 1978), are prevalent structures throughout the bedrock of the BBNPP site, mainly in second- and third-order. The major structure of the area is the Berwick Anticlinorium, a moderately complex, first order fold that passes through the center of Figure 2.5-88 (Inners, 1978).

The most detailed previous subsurface exploration of the BBNPP site was performed as part of the original SSES FSAR (SSES FSAR, 2003) for the SSES Units 1 and 2 foundation and supporting structures. This FSAR study included drilling 250 geotechnical boreholes, collecting down-hole geophysical data, and acquiring seismic refraction data across the site. However, the most detailed cross-section of the site area was created by Inners (Inners, 1978) as part of a study conducted on behalf of the Commonwealth of Pennsylvania Department of Environmental Resources-Bureau of Topographic and Geologic Survey. This geologic cross-section, Figure 2.5-95, was developed extending from just north of Lee Mountain, northwest of the BBNPP site, to near Black Creek, just south of Nescopeck Mountain, south of the BBNPP site. It provides valuable subsurface information on the lateral continuity of the Silurian-Mississippian Ridge and Valley sediments and overlying Quaternary sediments. This cross-section depicts moderately dipping, undeformed geologic contacts between the Middle Devonian Mahantango Formation, the overlying Middle Devonian Harrell Formation, and underlying Marcellus Formation as shown in Figure 2.5-95.

Geologic cross-sections developed from geotechnical data collected from 45 boreholes as part of the BBNPP study (as discussed in Section 2.5.4) also provide additional detailed information for

the upper approximately 400 ft (122 m) of strata on the presence, or absence, of structures directly beneath the footprint of the site. Similar to the previous cross sections prepared for the site, the new geologic borehole data support an apparent interpretation of steeply-dipping (south-southeast), unfaulted Middle Devonian stratigraphy at the BBNPP site as shown in Figure 2.5-96, Figure 2.5-97, Figure 2.5-98, Figure 2.5-99, and Figure 2.5-100. Northeast-trending structures (i.e., Light Street fault; inferred Berwick fault (DCNR, 2007) (Inners, 1978) and Berwick Anticlinorium (Inners, 1978)) show moderately dipping Devonian stratigraphy directly underlying the BBNPP site as shown in Figure 2.5-95. Multiple key sedimentary markers provide evidence for the absence of Pleistocene faulting and folding beneath the BBNPP site. Although the bedrock formations underlying the BBNPP site are moderately dipping and have experienced evident folding (Williams, 1987) during the Alleghanian Orogeny (Faill, 1999), surficial sediments of the site display no signs of faulting or folding during the Pleistocene to Holocene time period.

Geotechnical data collected to the southern portion of the BBNPP site was compiled along cross section D-D' shown in Figure 2.5-99. Although these geotechnical boreholes are limited in depth (from 99.5 ft to 200 ft (30.3 m to 60.9 m)), they provide additional evidence of the lateral continuity between the Pleistocene glacial outwash deposits and Devonian Mahantango Formation. Figure 2.5-98, Figure 2.5-96, and Figure 2.5-99 display a general thickening of surficial sediments across the site (from north to south), support detailed published reports of the site area local geology, and comply with the above statement that surficial faulting and folding are absent in the interpreted cross sections within the BBNPP site.

In addition, seismic refraction tests were performed, as part of the BBNPP site investigation, in the immediate area of the proposed reactor core of the BBNPP. These findings are discussed in further detail in Section 2.5.3.2.3 of this report.

2.5.3.2 Geological Evidence, or Absence of Evidence, for Surface Deformation

As shown on Figure 2.5-88 and Figure 2.5-94, the Light Street fault (DCNR, 2007) and the Berwick Anticlinorium (Inners, 1978) have been mapped at or within the 5 mi (8 km) radius of the BBNPP site. In addition, two other structures have been proposed within the 5 mi (8 km) radius of the site, the Lackawanna Synclinorium (Inners, 1978), approximately 4 mi (6.4 km) northwest of the BBNPP site, and the inferred Berwick fault (Inners, 1978) (DCNR, 2007), approximately 3 mi (4.8 km) southwest of the BBNPP site. All of the previously mentioned structural features are consistent with published evidence (Faill, 1999) (Harper, 1999) (Way, 1999) of the intense folding and faulting that occurred to the bedrock formations during the Alleghanian Orogeny as discussed in Section 2.5.1. The Light Street fault, inferred Berwick fault (Inners, 1978) (DCNR, 2007) and inferred folds (Inners, 1978) are described previously in Section 2.5.1 and below. None of these features are considered capable tectonic sources, as defined in Appendix A of Regulatory Guide 1.165 (NRC, 1997).

Considering the evidence provided above as well as the previous site investigations (SSES FSAR, 2003) discussed in Section 2.5.3.1.1, no deformation or geomorphic evidence indicative of potential Quaternary activity has been reported in the literature for the Light Street and/or Berwick faults. No evidence of Quaternary deformation along these inferred structures was identified during aerial and field reconnaissance interpretation undertaken for the BBNPP study. The Light Street fault has three interpretations and is discussed in depth below.

2.5.3.2.1 Light Street Fault and Berwick Fault

The Light Street fault is approximately 20 mi (32 km) long and approaches to within 2 mi (3.2 km) of the BBNPP site. Due to insufficient research, the nature of this fault is only inferred and, according to Inners (Inners, 1978), is likely (1) a reverse fault that dips in a southerly direction and eliminates a section of the stratigraphy between the Wills Creek and Marcellus Formations; (2) the detachment of a major decollement that dips to the north or; (3) a combination of (1) and (2). The style and location of faulting are based on field investigations of local outcroppings by Inners (1978). According to Inners (Inners, 1978), the simplest explanation for the unconformity in the area is a south-dipping reverse fault as mapped in Figure 2.5-94. Inners (Inners, 1978) also correlates this apparent loss of section in the log of the Parvin Good No. 1 well, located approximately 7 mi (11 km) northeast of the mapped area. Information on this well could not be retrieved for review to confirm this finding. Inners (Inners, 1978) also states that stratigraphic thinning of the Old Port-Onondaga section may also explain the thinning of this formation. Inners (Inners, 1978) attributes the presence of the Light Street fault to the folding and faulting actions that occurred at the site area during the Alleghanian Orogeny, approximately 250 million years ago. There is no pre-EPRI and post-EPRI study (EPRI, 1986) seismicity spatially associated with this feature nor is there any geomorphic evidence of Quaternary deformation.

In conjunction with the Light Street Fault (Inners, 1978), the Berwick fault is also mapped as inferred by Inners (Inners, 1978) and DCNR (DCNR, 2007) and is based on limited surface data and a water well log drilled at the Berwick Lumber and Supply Company at 329 West Second Street in Berwick, PA. This well could not be identified by Rizzo investigators and was possibly abandoned prior to the site investigation. The inferred Berwick Fault lies within the site area and comes to within approximately 3 mi (4.8 km) southwest of the BBNPP site as seen in Figure 2.5-88. The exact length of the Berwick fault is not completely mapped and is believed to be a south-dipping reverse fault on the south flank of the Berwick Anticlinorium (Inners, 1978). Inners (Inners, 1978) also states that the Berwick fault extends east-northeastward into an exposed third order anticline in the Marcellus-Mahantango interval and represents an unconformity in the Old Port and Keyser Formations. Inners (Inners, 1978) attributes the presence of the Berwick fault to the folding and faulting actions that occurred at the site area during the Alleghanian Orogeny, approximately 250 million years ago. There is no pre-EPRI and post-EPRI study (EPRI, 1986) seismicity spatially associated with this feature nor is there any geomorphic evidence of Quaternary deformation.

Field reconnaissance, coupled with interpretation of aerial photography (review and inspection of features preserved in aerial photos) shows that there are no geomorphic features indicative of potential Quaternary activity along the surface-projection of the Light Street fault as discussed in Section 2.5.3.1.1. In addition, an analysis of Figure 2.5-101 and Figure 2.5-104 revealed no evidence of faulting within the Pleistocene surficial sediments. Based on the absence of geomorphic expression, seismicity, and offset of Quaternary surficial deposits, it is concluded that the Light Street and Berwick faults are not surface-fault rupture hazards at the BBNPP site.

2.5.3.2.2 Stratigraphic Undulations

Multiple folds and faults have been mapped (Inners, 1978) (Williams, 1987) (DCNR, 2007) in bedrock outcrops to the southwest of the BBNPP site. Lithostratigraphic columns were compiled by Inners (Inners, 1978) to create a cross section approximately 9 mi (14.5 km) long which transects the mapped folds (Berwick Anticlinorium and Lackawanna Synclinorium), faults (Light Street fault and Berwick fault, as discussed above), and nearly continuous exposure of Silurian, Devonian and Mississippian bedrock of the site area (Figure 2.5-95). A stratigraphic analysis

indicates the major structure of the site area is the Berwick Anticlinorium, defined by Inners (Inners, 1978) as "a moderately complex, first order fold which trends in a northeast-southwest direction". The proposed axis of this fold lies approximately 1 mi (1.6 km) south of the BBNPP site and plunges approximately N76E at 2 to 4 degrees (Inners, 1978). Further investigations by Inners (1978) found that the apparent structural relief of the anticlinorium within the site region was 12,000 ft (3,700 m) and wavelength was approximately 8.2 mi (13.2 km). The northwest section of the site area is the likely axis of the Lackawanna Synclinorium and to the southeast of the site area is the likely main axis of the Catawissa-McCauley Mountain Synclinorium, continuing the en echelon order of synclines in the vicinity (Inners, 1978). These synclines are delineated from numerous outcrop searches (Inners, 1978), geophysical data and a limited number of deep boreholes that penetrate the crust (Pohn, 2001).

In addition to the first order folds that comprise the anticlines and synclines in the site area/ vicinity, exposed second and third order folds are developed but identified only in the Marcellus-Mahantango interval and the Mauch Chunk formation (Inners, 1978) with apparent wavelengths of 100 to 3,000 feet (30 to 914 m) and very low structural relief of about 50 feet (15 m) or less. Inners (Inners, 1978) attributes many of these folds to a flexural-slip mechanism and flexural-flow folding during past orogenies. Characteristic features associated with flexural-slip folds identified throughout the Berwick Quadrangle include the occurrence of slickenlines on bedding planes, consistent bedding thickness across smaller fourth order folds, and occurrence(s) of wedge fault(s) such as the mapped Light Street fault and inferred Berwick fault shown in Figure 2.5-88, Figure 2.5-94, and Figure 2.5-95.

Field reconnaissance coupled with interpretation of aerial photography (review and inspection of features preserved in aerial photos) conducted for this investigation shows that there are no geomorphic features indicative of potential Quaternary activity along trend with the postulated folds and faults interpreted by Inners (Inners, 1978) and Williams (Williams, 1987). No features suggestive of tectonic deformation were interpreted in the Quaternary glaciofluvial deposits. There is no pre-EPRI or post-EPRI study (EPRI, 1986) seismicity spatially associated with the Light Street fault or inferred Berwick fault (Inners, 1978) (Williams, 1987). The Berwick Anticlinorium (Inners, 1978) (Williams, 1987) is not aligned with any magnetic or gravity anomaly previously interpreted by others, suggesting that the apparent elevation change across the site area cross section (Figure 2.5-95) is related to deformation occurring during the Alleghanian Orogeny about 250 million years ago (Inners, 1978).

In summary, numerous investigations of the BBNPP site vicinity by government researchers, stratigraphers, by consultants for Pennsylvania Power and Light (the predecessor of PPL), and by this study, as discussed above, have reported there is no known syncline-related fault or geologic evidence of syncline-related faulting in the basement directly beneath the BBNPP site area, and no visibly distinct signs of tectonic deformation within the exposed Quaternary deposits near the BBNPP site. Collectively, the published and unpublished geologic information for the BBNPP site area, coupled with regional geologic sections (Inners, 1978) (Williams, 1987) and site and aerial reconnaissance, indicate the absence of Pleistocene and younger faulting and folding. A review of regional geologic sections (Figure 2.5-92 and Figure 2.5-96) suggest that the features, if present, are not prominent structures and do not appear to be developed within the Quaternary landscape. In summary, on the basis of regional and site data, there are no known tectonically active faults within the site area. The Light Street fault and Berwick fault (if present) have been documented as being last active in the Late Permian (Inners, 1978).

2.5.3.2.3 Seismic Refraction Surveys

Seismic refraction tests were performed to support site characterization studies for the BBNPP. Seismic refraction surveys were operated along 6 profile lines totaling 4,000 linear feet (1219 linear meters) of coverage, as seen in Figure 2.5-103, Figure 2.5-104, and Figure 2.5-105. Seismic refraction field data were collected during the period from January 7th, 2008 through January 10th, 2008 (Weston, 2008).

The following is a summary of observations and foundation material descriptions derived from the geophysical investigations. These observations are reported for a specific location at an elevation of approximately 638 ft (194 m) msl in the area of the containment structure at the intersections of refraction Line 2 and Line B. At this location, this elevation datum corresponds to the bottom elevation of the common basemat and is approximately 38 ft (11.5 m) below the proposed plant grade ground surface elevation (674 ft (205 m) msl).

Interpretations of seismic refraction data across the site support the following observations.

P-wave velocity at top of bedrock across the site was measured in range of 11,000 to 16,000 ft/sec (3353 to 4877 m/sec) and increased to greater than 16,000 ft/sec (4877 m/sec) 10 ft (3 m) below top of bedrock.

The predominant top of bedrock velocity is approximately 14,000 ft/sec (4267 m/sec).

The general trend of the top of bedrock is shallower on the northern portion of the site and shallower in the western half of the area of investigation, as seen in Figure 2.5-105.

These seismic refraction test results support the field findings of the BBNPP geotechnical investigation discussed in detail in section 2.5.1. The complete Seismic Refraction Surveys Report is included in Part 11.

2.5.3.3 Correlation of Earthquakes with Capable Tectonic Sources

As discussed in Section 2.5.3.1.1, Figure 2.5-87, Earthquake Epicenters in and Near Pennsylvania, (USGS, 2001) shows two earthquakes within the 25 mi (40 km) radius of the BBNPP site. Further analysis of these mapped earthquakes revealed that the sources for these earthquakes were quarry blasts or mine collapse (Faill, 2004). Neither of these seismic events were fault related or associated with bedrock/basement rock deformation. No publications reported vibratory ground motions being felt as a result of either of these seismic events, at or near the BBNPP site area. No reported historical earthquake epicenters have been associated with bedrock faults within the 25 mi (40 km) radius of the BBNPP site vicinity as shown in Figure 2.5-87.

2.5.3.4 Ages of Most Recent Deformations

As presented in Section 2.5.3.2.2, the Light Street fault, and postulated folds and faults within 5 mi (8 km) of the BBNPP site do not exhibit evidence of Quaternary activity. It is interpreted (Inners, 1978) that the Light Street fault and inferred Berwick fault formed during the Paleozoic Era as part of the regional Alleghanian Orogeny. Based on a review of available published geologic literature, field reconnaissance, and interpretation of aerial photography (review and inspection of features preserved in aerial photos), activities associated with the postulated

structures (Inners, 1978) (Williams, 1987) (DCNR, 2007), if they exist, are constrained to the Late Permian and do not appear to affect Quaternary deposits.

2.5.3.5 Relationship of Tectonic Structures in the Site Area to Regional Tectonic Structures

Of the four features evaluated within the 5 mi (8 km) radius of the BBNPP site (Light Street fault, Berwick fault, Berwick Anticlinorium, and Lackawanna Synclinorium), all have been linked with regional tectonic events, mainly the Alleghanian Orogeny. Tectonic models hypothesize that the crystalline basement underlying the BBNPP site was accreted to a pre-Taconic North American margin in the Precambrian. Episodes of continental collisions have produced a series of accreted terrains separated, in part, by low angle detachment faults, as discussed in detail in Section 2.5.1.1.2. In association with these continental collisions, the Paleozoic bedrocks of eastern North America, including the Ridge and Valley Province, consist of generally northeast striking thrust faults (Schlische, 2003) such as the Light Street fault and inferred Berwick fault. The Berwick Anticlinorium and Lackawanna Synclinorium are both results of regional extension and compression, commonly found throughout the Appalachian Mountain section of the Ridge and Valley Province, due to the orogenic events discussed in detail in Section 2.5.1.1.2.

2.5.3.6 Characterization of Capable Tectonic Sources

Based on previous discussions in Section 2.5.3.2, Section 2.5.3.3 and Section 2.5.3.4, there are no capable tectonic sources within 5 mi (8 km) of the BBNPP site.

2.5.3.7 Designation of Zones of Quaternary Deformation Requiring Detailed Fault Investigation

There are no zones of Quaternary deformation requiring detailed investigation within the BBNPP site area. A review and interpretation of digital elevation models coupled with aerial reconnaissance identified few, if any discontinuous north to northeast-striking lineaments. None of these lineaments are interpreted as fault-related, or coincident with the Light Street fault or the other previously inferred Miocene-Pliocene structures.

2.5.3.8 Potential for Tectonic or Non-Tectonic Deformation at the Site

Based on previous discussions in Section 2.5.3.2, 2.5.3.3, 2.5.3.4, and 2.5.3.5, the potential for tectonic deformation at the site is negligible. This is based on:

1. The steeply dipping Devonian stratigraphy beneath the site interpreted from both existing and new borehole data,
2. The absence of faulting or evidence of liquefaction found at the site or surrounding outcrops within the site area.
3. The interpretation of aerial photography and extensive mapping of the site area, vicinity, and region by various government officials, private parties, and independent companies over the past several decades as discussed in previous sections in Section 2.5.3.

Collectively, these data support the interpretation for the absence of any Quaternary surface faults or capable tectonic sources within the BBNPP site area. In addition, there is no evidence of non-tectonic deformation at the site, such as glacially induced faulting, collapse structures, growth faults, salt migration, or volcanic intrusion.

2.5.3.9 References

- Berg, 1980.** Geologic map of Pennsylvania, Pennsylvania Geological Survey, 4th ser., Map1, scale 1:250,000, 3 sheets, T.M. Berg, 1980.
- CFR, 2007a.** Title 10, Code of Federal Regulations, Part 100, Reactor Site Criteria, 2007.
- CFR, 2007b.** Title 10, Code of Federal Regulations, Part 50, Appendix S, Earthquake Engineering Criteria for Nuclear Power Plants, 2007.
- Crangle, 2002.** Stratigraphic Framework of Cambrian and Ordovician Rocks in the Central Appalachian Basin from Lake County, Ohio, to Juniata County, Pennsylvania, Revised and Digitized from Ryder, Stratigraphic Framework of Cambrian and Ordovician Rocks in the Central Appalachian Basin from Lake County, Ohio, to Juniata County, Pennsylvania, R.D. Crangle Jr., 2002.
- Crone, 2000.** Data for Quaternary Faults, Liquefaction Features, and Possible Tectonic Features in the Central and Eastern United States, East of the Rocky Mountain Front, U.S. Geological Survey, Open-File Report 00-260, p 1-332, A.J. Crone and R.L. Wheeler, 2000.
- DCNR, 2007.** Geologic Map of Pennsylvania, Pennsylvania Department of Conservation and Natural Resources, Website: <http://www.dcnr.state.pa.us/topogeo/maps/map7.pdf>, Date accessed: December 14, 2007.
- EPRI, 1986.** Seismic Hazard Methodology for the Central and Eastern United States, NP-4726, Electric Power Research Institute, July 1986.
- ESRI, 2007.** ESRI StreetMap Pro (CD-ROM), State Boundry, County Boundry, Road, and Stream/River, ESRI, 2007.
- FailI, 1999.** Appalachian Mountain Section of the Ridge and Valley Province, The Geology of Pennsylvania, Part III. Structural Geology and Tectonics, Chap. 19, p. 268-285, R. FailI and R. Nickelsen, 1999.
- FailI, 2004.** The Birdsboro Basin, Pennsylvania Geology, Volume 34, Number 4, p 2-11, R. T. FailI, 2004.
- Gold, 2005.** Basement depth and related geospatial database for Pennsylvania, Pennsylvania Geological Survey, 4th ser., Open-File General Geology Report 05-01.0, Pennsylvania Department of Conservation and Natural Resources, downloaded from www.dcnr.state.pa.us/topogeo/openfile/basementmap.aspx, D. Gold, 2005.
- Harper, 1999.** Part II, Stratigraphy and Sedimentary Tectonics, Chapter 7: Devonian, in C.H. Shultz ed., The Geology of Pennsylvania: Pennsylvania Bureau of Topographic and Geologic Survey Special Publication 1, p 108-127, J.A. Harper, 1999.
- Hibbard, 2006.** Lithotectonic map of the Appalachian Orogen, Canada-United States of America, Geological Survey of Canada Map 02096A, 2 sheets, Scale 1: 1,500,000, J. Hibbard, C. Van Staal, D. Rankin and H. Williams, 2006.

Inners, 1978. Geology and Mineral Resources of the Berwick Quadrangle, Luzerne and Columbia Counties, Pennsylvania, Pennsylvania Geological Survey, Fourth Series, p 1-34, J.D. Inners, 1978.

King, 1974. Glacial Limits Modified after King & Beikman, as digitized by Schruben (1994), downloaded from <http://pubs.usgs.gov/dds/dds11/kb.html>, P. B. King and H.M. Beikman, 1974.

King, 1978. The New York-Alabama lineament: Geophysical Evidence for a Major Crustal Break in the Basement Beneath the Appalachian Basin, *Geology*, Volume 6, p 312-318, E. King and I. Zietz, 1978.

National Atlas, 2008. Shaded Relief (200 Meter) 2008, downloaded from www.nationalatlas.gov/mld/srld48i.html, U.S. National Atlas, 2008.

NRC, 1997. Identification and Characterization of Seismic Sources and Determination of Safe Shutdown Earthquake Ground Motion, Regulatory Guide 1.165, U.S. Nuclear Regulatory Commission, March 1997.

Pohn, 2001. Lateral Ramps in the Folded Appalachians and in Overthrust Belts Worldwide- A Fundamental Element of Thrust-Belt Architecture, U.S. Geological Survey Bulletin 2163, p 1-21, H.A. Pohn, 2001.

Ryder, 1992. Stratigraphic Framework of Cambrian and Ordovician Rocks in the Central Appalachian Basin from Medina County, Ohio, through Southwestern and South-Central Pennsylvania to Hampshire County, West Virginia, US Geological Survey Bulletin 1839, p 1-40, R.T. Ryder, A.G. Harris, and J.E. Repetski, 1992.

Schlische, 2003. Progress in Understanding the Structural Geology, Basin Evolution, and Tectonic History of the Eastern North American Rift System, P. leTourneau and P. Olsen, eds., *The Great Rift Valleys of Pangea in Eastern North America*, Vol. 1, p 21-64, R. Schlische, 2003.

SSES FSAR, 2003. Susquehanna Steam Electric Station Final Safety Analysis Report, Section 2.5, Geology, Seismology, and Geotechnical Engineering, Rev. 58, Pennsylvania Power and Light, 2003.

USGS, 2001. Earthquake Epicenters In and Near Pennsylvania, USGS, 2001.

Way, 1999. Part IV, Physiography, Chapter 29: Appalachian Mountain Section of the Ridge and Valley Province, in C.H. Shultz ed., *The Geology of Pennsylvania: Pennsylvania Bureau of Topographic and Geologic Survey Special Publication 1*, p 353-361, J.H. Way, 1999.

Weems, 1998. New recognized en echelon fall lines in the Piedmont and Blue Ridge provinces of North Carolina and Virginia, with a discussion of their possible ages and origins, U.S. Geological Survey Open-File Report 98-374, R. E. Weems, 1998.

Weston, 2008. Seismic Refraction Surveys for the Bell Bend Site Characterization, March 24, 2008, Weston Geophysical Engineers, Inc., 2008.

Wheeler, 2005. Known or Suggested Quaternary Tectonic Faulting, Central and Eastern United States-New and Updated Assessments for 2005, U.S. Geological Survey, Open-File Report 2005-1336, R.L. Wheeler, 2005.

Wheeler, 2006. Quaternary tectonic faulting in the Eastern United States, Engineering Geology, Volume 82 (2006), p 165-186, R.L. Wheeler, 2006.

Williams, 1987. Groundwater Resources of the Berwick-Bloomsburg-Danville Area, East-Central Pennsylvania, Pennsylvania Dept of Environmental Resources, Topographic and Geologic Survey, Water Resource Report 61, 76 p., J. Williams and D. Eckhardt, 1987.}

2.5.4 STABILITY OF SUBSURFACE MATERIALS AND FOUNDATIONS

The U.S. EPR FSAR includes the following COL Item for Section 2.5.4:

A COL Applicant that references the U.S. EPR design certification will present site-specific information about the properties and stability of soils and rocks that may affect the nuclear power plant facilities, under both static and dynamic conditions including the vibratory ground motions associated with the CSDRS and the site-specific SSE.

This COL Item is addressed as follows:

This section addresses site-specific subsurface materials and foundation conditions. It was prepared based on the guidance in relevant sections of NRC Regulatory Guide 1.206, Combined License Applications for Nuclear Power Plants (LWR Edition) (NRC, 2007a).

{The information presented in this section is based on results of a subsurface investigation program implemented at the Bell Bend Nuclear Power Plant (BBNPP) site, and evaluation of the collected data, unless otherwise indicated. The Susquehanna Steam Electric Station (SSES) Units 1 and 2 Final Safety Analysis Report (FSAR) (PPL, 2004) contains a summary of the geotechnical information collected previously for the construction of SSES Units 1 and 2. The planned Bell Bend NPP is to be located approximately 0.5 mi (0.8 km) west of SSES Units 1 and 2. The geologic and geotechnical work performed for the BBNPP is a "stand-alone" investigation. The outcome and conclusions do not rely on the existing SSES Units 1 and 2 FSAR. This document provides the complete investigation data set, including both geotechnical boring logs, and results from the laboratory testing program. The body, tables, and figures in the text organize the data, providing an engineering recommendation for the use of geotechnical parameters. The topographic reference to elevation values in this subsection are based, for the initial ground control and establishment, on the state Plane Coordinates North American Datum of 1983 (NAD83) PA NORTH datum, and for the establishment of the vertical datum, North American Vertical Datum, 1988 (NAVD 88), unless stated otherwise.}

2.5.4.1 Geologic Features

The U.S. EPR FSAR includes the following COL Item in Section 2.5.4.1:

Geologic features are site-specific and will be addressed by the COL applicant.

This COL Item is addressed as follows.

Section 2.5.1.1 addresses the regional geologic settings, including regional physiography and geomorphology, regional geologic history, regional stratigraphy, regional tectonic and non-tectonic conditions, and geologic hazards, as well as maps, cross-sections, and references. Section 2.5.1.2 addresses the geologic conditions specific to the site, including site structural geology, site physiography and geomorphology, site geologic history, site stratigraphy and lithology, site structural geology, seismic conditions, and site geologic hazard evaluation, accompanied by figures, maps, and references. Pre-loading influences on soil deposits, including estimates of consolidation, pre-consolidation pressures, and methods used for their estimation are addressed in Section 2.5.4.2. Related maps and stratigraphic profiles are also addressed in Section 2.5.4.2.

{The site lies within the Ridge and Valley Physiographic Province (Inners, 1978). The soils at the site are characterized by glacio-fluvial deposits, and were subjected to both glacial and periglacial events during the Quaternary period. Underneath this glacio-fluvial overburden (glacial overburden) lies the middle Devonian bedrock denominated the Mahantango Formation, part of the Hamilton Group. This formation is characterized by dark gray, slightly fossiliferous, hard shale and was found to be at least 400 ft (122 m) thick based upon the BBNPP site geotechnical investigation. A past report places the total thickness of the Mahantango Formation at approximately 1,500 ft (457 m) (Inners, 1978). Harper (Harper, 1999) describes the Mahantango Formation as "a complex series of interbedded shales, siltstones, and sandstones ranging from 1,200 ft (366 m) to 2,200 ft (671 m)" although Inners (Inners, 1978) reports a site specific thickness of approximately 1,500 ft (457 m). The shales and siltstones encountered during the BBNPP site investigation were typically dark gray, ranged in hardness from soft to moderately hard, increased progressively in the level of calcareous content with depth, and were slightly pyritic and fossiliferous throughout. Harper (Harper, 1999) suggests that the Mahantango Formation was deposited as a prograding marine shoreline during the early stages of the Catskill delta.

The glacial overburden soils and the Mahantango formation were the subject of a detailed subsurface exploration for the COL investigation, as described below.}

2.5.4.2 Properties of Subsurface Materials

The U.S. EPR FSAR includes the following COL Item in Section 2.5.4.2:

A COL applicant that references the U.S. EPR design certification will reconcile the site-specific soil properties with those used for design of U.S. EPR Seismic Category I structures and foundations described in Section 3.8.

This COL Item is addressed as follows:

{This section presents the properties of underlying materials encountered at the BBNPP Site. It is divided into five subsections, as follows.

- Section 2.5.4.2.1 provides an introduction to the soil profile and subsurface conditions,
- Section 2.5.4.2.2 provides a description of the field investigation program, including borings, sampling, and in-situ tests,
- Section 2.5.4.2.3 provides a description of the laboratory testing program,

- Section 2.5.4.2.4 provides a narrative on the origin and characteristics of the engineered fill soils, and
- Section 2.5.4.2.5 provides the BBNPP recommended soil properties.

2.5.4.2.1 BBNPP Soil Profile

The natural topography at the BBNPP site, at the time of the subsurface exploration, was a gently sloping open field cut across by a highly eroded east-west trending bedrock anticline with a dip of approximately 70°. The maximum variation in relief was about 144.5 ft (44 m) across the site. Ground surface elevations at the time of exploration ranged from approximately 800 ft to 656 ft (244 to 200 m) mean sea level (msl), with an average elevation of about 680 ft (207 m). The ground surface elevations in the Powerblock area ranged from about 656 ft to 675 ft (200 to 206 m), with the centerline of the BBNPP through the Reactor Building at an elevation of 666.6 ft (203.2 m). The Powerblock includes the Reactor Building, Fuel Pool Building, Reactor Auxiliary Building, Safeguard Buildings, Radioactive Waste Processing Building, Emergency Power Generating Buildings, Essential Service Water System (ESWS) Cooling Towers, and Turbine Building.

The BBNPP subsurface investigation focused on the upper 400 ft (122 m) of the subsurface structure. The site geology is comprised of glacial soil deposits underlain by bedrock, which is, on average, 38.9 ft (11.9 m) below the ground surface. The subsurface structure is divided into the following stratigraphic units:

- Overburden Soil: - Glacial Till
- Bedrock: - Mahantango Formation

Identification of soil and rock layers was based on their physical and engineering characteristics. The characterization of the soils and rocks was based on a suite of tests performed on these soils and rocks, consisting of standard penetration tests (SPT) in soil borings including auto-hammer energy measurements, geophysical testing, pressuremeter tests (PMTs) and laboratory testing.

Table 2.5-106 provides a general soil column profile. Overall, the subsurface conditions encountered throughout the site are uniform, in both depth and area extension.

The thickness of the glacial till varies from 12.5 (3.8 m) to 62.0 ft (18.9 m). With the exception of some loose sand pockets, the till consists of over-consolidated brown silty sand or sand containing gravel and large rounded cobbles and boulders. The presence of boulders increases with depth.

The overburden soil is not an adequate foundation strata for safety related structures or facilities that will impose high contact pressures. Even though these soils have shear wave velocities in the excess of 1000 ft/sec (305 m/sec), several zones of loose sands were encountered during the investigation. These zones originated from wind deposited processes during the glaciation periods. Low blow counts were recorded in areas at the south side of the power block. Such areas are susceptible to liquefaction.

The Mahantango Shale is very dark gray to black, thin bedded to massive bedded, with few to no fractures. There are also calcareous zones, thin pyrite lenses that increase in abundance with

depth, and calcite veins perpendicular to the bedding plane that are micro-faulted. The upper surface of the Mahantango Formation shows the effects of solution and weathering in a few areas, but it is predominantly very competent and indurated. For SSES Units 1 and 2, this layer supports large and safety-related structures (PPL, 2004).

The thicknesses and termination elevations of rock are summarized in Table 2.5-26. The table provides the minimums, maximums, and averages from forty eight geotechnical boring logs. The positions of the soil and rock strata are best visualized by cross section drawings and contour elevation plots. These are developed at locations where the main power block and other safety related facilities will be placed. The following plots are presented for visualization purposes:

- Figure 2.5-106, Boring Location Plan
- Figure 2.5-107, Location of Cross Sections
- Figure 2.5-108, Geotechnical Subsurface Section A-A'
- Figure 2.5-109, Geotechnical Subsurface Section B-B'
- Figure 2.5-110, Geotechnical Subsurface Section C-C'
- Figure 2.5-111, Geotechnical Subsurface Section D-D'
- Figure 2.5-112, Surface Elevation Contours
- Figure 2.5-113, Overburden Thickness
- Figure 2.5-114, Thickness of Weathered Rock
- Figure 2.5-115, Elevation of Competent Rock
- Figure 2.5-116, Overburden Thickness and Elevation of Rock (Area near Essential Service Water Emergency Makeup System - ESWEMS)

2.5.4.2.2 Field Investigation Program

A thorough field investigation program was designed and implemented at the BBNPP site. The program included:

- Boring Program,
- Wash Rotary Drilling/ CasiRock Coring (NQ Wireline),
- In-Situ Pressuremeter Testing,
- Geophysical Exploration,
- Downhole Tests,
- PS Suspension Logging Tests,
- Deviation Surveys,
- Refraction Surveys.

The field investigation was performed under the guidance provided in NRC Regulatory Guide 1.132, "Site Investigations for Foundations of Nuclear Power Plant" (NRC, 2003a). The work was performed in accordance with work procedures developed specifically for the BBNPP

subsurface exploration, including a subsurface exploration plan developed under the Rizzo Quality Assurance Program. Subsection 2.5.4.2.2.1 provides a brief summary of the field investigation conducted for SSES Units 1 and 2, and subsection 2.5.4.2.2.2 details the field investigation program for the BBNPP site.

2.5.4.2.2.1 Previous Subsurface Investigations

Based on information available from the SSES FSAR (PPL, 2004), it was determined that approximately 250 exploratory borings were made in the soil and rock at the site. The subsurface investigations for SSES Units 1 and 2 began in late 1970 (100 and 200 series borings) to establish general geologic relationships over the site area and to determine the general soil and rock conditions at the site. A more intensive program (300 series borings) was conducted in the Spring of 1971 to define foundation conditions in the principal plant structures area. Two 45-degree angle holes were drilled in the reactor area. Additional exploration drilling was necessary to locate the site for the Susquehanna River intake and discharge structures (700-800 series borings), to define soil and rock conditions at the spray pond and ESSW pumphouse (1100 series and some 400 series borings), and to investigate foundation conditions for the cooling towers (borings B1 to B10) and the railroad spur and bridge over State Highway 11 (borings 417 to 455 and 929 to 940). An investigation program (borings 1 through 7) was conducted in 1983 to determine soil and rock conditions in the area of the diesel generator 'E' building. Because of the safety-related (Category 1) function of the spray pond and ESSW pumphouse, the exploration program for these facilities was comprehensive and included split spoon and undisturbed samples, laboratory testing, hydrologic surveys, permeability tests, and seismic cross-hole and up-hole surveys. Split spoon sample laboratory testing, hydrologic surveys, and permeability tests were also performed in the area of the diesel generator 'E' fuel tank. After completion of geologic borings, static water levels were measured in some of the borings drilled on the site.

Geological descriptions in the SSES FSAR (PPL, 2004) indicate that two primary layers existed at the site, the glacial overburden soils and the bedrock. The site is blanketed by till and glacial outwash which grades upward from a gravelly boulder zone to a surface layer of silty fine sands and sandy silt. The surface layer is believed to be reworked loess. The maximum thickness of overburden is around 40 ft (12 m) in the southern half of the site, with bedrock occasionally cropping out at the surface. North of the east-west bedrock ridge situated just north of the reactors, the glacial deposits fill a valley eroded into bedrock to a depth exceeding 100 ft (30.5 m). The upper bedrock at the site area includes the Middle Devonian Mahantango Formation. The upper part of the Mahantango is a dark gray siltstone, with bedding generally delineated by thin, consistent, light gray, fine-grained sandstone stringers. Beneath the upper member, the Mahantango is comprised of 120 to 150 ft (37 to 46 m) of dark gray, hard calcareous siltstone, typically having bedding obscure to absent and displaying cleavage. This member, which supports the SSES power block structures, is harder, more massive, and more resistant to erosion than the upper member. Minor faulting in the form of small bedding-plane slips and intraformational shear zones occur, but they are of no significance to the site. They apparently developed during the Paleozoic (more than 200 million years ago) during the Appalachian Orogeny. The zones are typically healed with calcite and quartz.

Comparable observations were made on these soil and rock layers from the BBNPP investigation borings. Given the reasonably parallel geologic conditions between SSES Units 1 and 2, and BBNPP, exploration and testing at BBNPP resulted in enhanced characterization of

the subsurface conditions. Findings from previous investigations are not discussed further, unless a differing condition is reported from the previous investigation.

2.5.4.2.2.2 BBNPP Subsurface Exploration

The subsurface exploration was performed in accordance with the guidance outlined in Regulatory Guide 1.132 (NRC, 2003a). Deviations are identified at point of use and alternatives and/or basis for deviations are provided.

Regulatory Guide 1.132 (NRC, 2003a) provides guidance on spacing and depth of borings, sampling procedures, in-situ testing, geophysical investigations, etc. This guidance was used in preparing a technical specification, addressing the basis for the BBNPP subsurface exploration. Per Regulatory Guide 1.132 (NRC, 2003a), "the minimum required depth of borings in competent bedrock should extend to the greatest depth where discontinuities or zones of weakness or alteration can affect foundations or at least 20 ft (6 m) into sound rock. For safety-related structures, one boring per 10,000 ft² (929 m²) and at least one-fourth of those borings should penetrate into sound rock." In accordance with this guideline, a subsurface exploration program was developed.

In total 45 boreholes were completed for sampling and standard penetration test (STP) purposes. These boreholes are designated as the B-Series boreholes. In addition, 3 boreholes were performed for geophysical testing purposes. These boreholes are designated as the G-Series boreholes.

B-Series boreholes were completed for the BBNPP site, of which 27 boreholes were located in the vicinity of the proposed Category I structures and the remainder were located in other plant locations. It was determined that 1 boring (B-301) should be extended to depth of 400 ft (122 m) for detailed core logging and geophysical testing at the location of the proposed Nuclear Island structure. In addition, 2 borings from the Nuclear Island buildings were extended to about 350 ft (107 m) at a 30° angle to determine the existence of vertical discontinuities. Such discontinuities were not encountered. Three G-Series destructive drilling boreholes were extended for geophysical testing purposes in the proposed location of the Reactor Building and in two of the ESWS Cooling Towers.

A team consisting of a geologist, a geotechnical engineer, and a member of the project management performed a site reconnaissance prior to start of the field investigation. The focus of this task was to observe the site and assess conditions, locations of borings and wells, and identify potential test relocation areas.

According to Regulatory Guide 1.132 (NRC, 2003a), boreholes with depths greater than 100 ft (30.5 m) should be surveyed for deviation. At the BBNPP site, rock was penetrated at an average depth of 41.1 ft (12.5 m) and deviation surveys were limited to boreholes with geophysical testing. The deviation was taken because bedrock was encountered at an average depth of 41.1 ft (12.5 m).

Regulatory Guide 1.132 (NRC, 2003a) provides guidance for color photographs of all cores to be taken immediately upon removal from the borehole to document the condition of the soils and rocks at the time of drilling. Undisturbed samples were sealed in steel tubes, and could not be photographed. Sample photography was taken of SPT and rock core samples.

The BBNPP subsurface geotechnical field exploration was conducted from August 2007 through November 2007. This work consisted of an extensive investigation to define the subsurface conditions at the BBNPP site. Locations of the geotechnical field investigation field tests are shown in Figure 2.5-106 (Boring Location Plan), and the extent of the field tests are summarized in Table 2.5-27. Surveying was conducted in order to establish the horizontal and vertical locations of exploration points as shown in Table 2.5-28. Each boring location was investigated for the presence of underground utilities prior to drilling boreholes.

Subsurface explorations were performed using geotechnical drill rigs mounted on trucks or tracked vehicles. Field borings logs and other field records were maintained by a rig geologist (geologist or geotechnical engineer). A rig geologist was assigned to each rig and was responsible for maintaining the field records associated with activities conducted at a specific exploration point.

Forty-five (45) B-Series borings were advanced with SPT sampling, and 12 undisturbed samples (using Shelby push tubes) collected from the overburden soils. Soils were sampled using the SPT sampler in accordance with ASTM D1586 (ASTM, 1999). Disturbed soil samples were obtained using 1.5-in (3.8-cm) inside diameter split-spoon samplers in conjunction with the SPT, as described by ASTM D1586 (ASTM, 1999). The split spoon sampler was driven a minimum of 18 in (46 cm) or to refusal. The sampling interval was continuous or 2.5 ft (0.7 m) for borings in the vicinity of Category I structures, and 5 ft (1.5 m) in the vicinity of the proposed non-safety-related structures. At least one boring below each proposed safety-related structure was performed with continuous sampling. The recovered soil samples were visually described and classified by the rig geologist in accordance with ASTM D2488 (ASTM, 2006c). Two representative samples of the soil recovered from each SPT were placed in glass jars with moisture-preserving lids. The sample jars were labeled, placed in boxes, and transported to the on-site storage facility.

Undisturbed samples were obtained in accordance with ASTM D1587 (ASTM, 2000b) using the push Shelby tubes. Immediately upon sample retrieval, the disturbed portions at both ends of the tube were removed, both ends were trimmed square to establish an effective seal, and pocket penetrometer (PP) tests were performed on the trimmed lower end of the samples. Both ends of the sample were then sealed with hot wax, filled with sand to the top, covered with plastic caps, and sealed once again using electrician tape and wax to preserve their natural moisture content and prevent soil movement. The tubes were labeled and transported in a vertical orientation to the on-site storage area. Undisturbed samples were stored in an upright position with the top side of the sample up. The locations from which the undisturbed samples were obtained are shown in Figure 2.5-117.

Due to the extremely rocky nature of the overburden, the majority of the borings were advanced using a three inch casing advancer system. The advancer system attached to the three inch casing. The system consisted of a diamond shoe (similar to a diamond drill bit), and a roller bit attached to a carrier that locks and unlocks into the system (similar to a wire line core barrel). The center bit is adjusted to ride just forward of the shoe. The center bit was removed to allow a sampler to be lowered down the casing for SPT sampling. When the boulders were too large for roller bit to penetrate through, a core barrel was placed through the system in-lieu of the roller bit mechanism, allowing the driller to core through the boulder. After coring, the driller switched back to mud rotary to allow sampling of the overburden to the top of bed rock. Once the presence of rock was confirmed, that is, 50 blows/6" or 10 hammer refusals, rock coring was initiated, as summarized below.

All boreholes advanced during the field investigation program, penetrated the rock layer. The top of the rock layer was identified by the refusal of the split-spoon sampler and/or by the presence of shale rock fragments in the sampler. Rock coring was performed using wire line core barrels and NQWL dual tube (1.875 in (47.6 mm) core diameter), diamond-tipped rock core tools. Dual tube core barrels, 5 ft or 10 ft (1.5 m or 3 m) in length were used to collect continuous rock samples in accordance with ASTM D2113 (ASTM, 2006e). The recovered rock samples were visually described and classified by the geologist or engineer in accordance with ASTM D5878 (ASTM, 2005d). "Routine care" and "special care" rock core samples were collected during this exploration. Routine care samples were placed directly into wooden rock core boxes with a locking lid and photographed. Wood spacers were placed in the core box when needed to stabilize the core laterally. Special care samples were wrapped tightly in a plastic film and aluminum foil, coated with wax, wrapped in a bubble wrap and stored in a polyvinyl chloride (PVC) tube to preserve the in-situ characteristics. The locations from which special care rock samples were obtained are shown in Figure 2.5-118.

The rig geologist visually described the core and noted the presence of joints and fractures, distinguishing mechanical breaks from natural breaks where possible. The rig geologist also calculated percent recovery and Rock Quality Designation (RQD) prior to moving the core from the drill site. Field boring logs and photographs were used to document the drilling operations and recovered materials. In borings to be geophysically logged, PVC casing was grouted in place in lieu of the temporary casing.

An on-site storage facility for soil and rock samples was established prior to initiating the boring exploration program. The site facility had to provide adequate temperature control conditions in accordance with Regulatory Guide 1.132 (NRC, 2003a). The soil and rock samples obtained were logged into an inventory system. Samples removed from the facility were noted in the logbook. A chain-of-custody form was completed for all samples removed from the facility. Material storage and handling was in accordance with ASTM D4220 (ASTM, 2000a) and ASTM D5079 (ASTM, 2006f) for soil and rock samples, respectively.

2.5.4.2.2.1 Hammer Calibration and SPT Measurements

The depth of soil and rock penetrated by each borehole is shown in Table 2.5-28. Soil and rock samples retrieved are identified on the boring logs included with the COLA.

Energy measurements were made on the hammer-rod system on 2 of the 4 drilling rigs used in the subsurface investigation. One of the rigs was retired from the investigation due to mechanical failure. This rig was not calibrated, but SPT measurements associated with this rig were only performed at two locations underneath the turbine building. Data from the damaged, non-calibrated rig was not used. Overall, SPT data was only used to establish the potential of the overburden soils. These soils are potentially liquefiable and will be removed from the site. In-situ soils at the BBNPP site will not be used for foundation or lateral support purposes.

A Pile Driving Analyzer (PDA) was used to acquire and process hammer energy data. A summary of measured energies is provided in Table 2.5-29. The total number of measurements made at each boring was ten (10) for borehole B-336, and 9 at borehole B-327A. Energy transfer to the gage locations was estimated using the Case Method, in accordance with ASTM D4633 (ASTM, 2005a). The average energy transfer efficiency measurements ranged from 60 to 87 percent, with an average of 80 percent. As shown in Figure 2.5-108, Figure 2.5-109, Figure 2.5-110, and Figure 2.5-111, the soil on site is relatively consistent, and the blow counts

recorded with the CME 75 Track and CME 55 drill rigs are consistent with those taken by other rigs used on-site.

Soil samples were collected from the borings by means of Standard Penetration Test (SPT) and tube samples. Samples were collected more frequently in the borings located in the vicinity of the proposed Category I (safety-related) structures for BBNPP. SPT N-values were measured during the sampling and recorded on the boring logs included with the COLA. SPT N-values ranged from 0 blows/ft to 131 blows/ft (0 blows/m to 437 blows/m), with an average measured N-value of 36 blows/ft (120 blows/m). Most of the recordings were done in the overburden soils. It was possible to take a limited amount of readings in the weathered part of the Mahantango Shale. These were typically above 50 counts. SPT information on the overburden soil layer is presented in Table 2.5-30. The variability of measured SPT N-values is presented in Figure 2.5-119. The figure indicates that there is not a consistent relationship between the SPT values and depth. Some readings are extremely low and they correspond to the presence of loose sand pockets. As the percentage of glacial boulders increased, the SPT process was interrupted at 50 counts when hammer rejection was observed. There were some instances for which the behavior of the hammer allowed for the continuation of the test beyond 50 blow counts. The selected subsurface profiles, Figure 2.5-108, Figure 2.5-109, Figure 2.5-110, and Figure 2.5-111 show the samples collected with their corresponding SPT N-values and classification symbols. The figures indicate if the sample was disturbed or undisturbed, and the number recorded field SPT blows/feet. Additional discussion pertaining to the presence of loose sand pockets is provided in Section 2.5.4.8

SPT hammer energies were measured for 2 of the 4 drilling rigs used for the subsurface exploration. Energy measurements were made in 2 borings (B-336 and B-327A). Because the SPT N-value used in correlations with engineering properties is the value corresponding to 60 percent hammer efficiency, the measured SPT N-values were adjusted based on the energy measurements, in accordance with American Society for Testing and Materials (ASTM) D6066 (ASTM, 2004b). The average energy transfer ratio (ETR) obtained from hammer energy measurements for each drilling rig was applied to the measured SPT N-values. A summary of the measured ETR values for each drill rig is shown in Table 2.5-29. The measured SPT N-values from each boring were adjusted using the ETR value shown in Table 2.5-29 for the drill rig utilized. The adjusted average field-measured N-values are shown in Table 2.5-31.

Figure 2.5-119 indicates the scatter of the SPT blow counts versus the depth. There is no clear pattern and the plot is a reflection of the natural composition of the glacial till. Higher blow counts are attributed to the presence of boulders and consolidated mixtures of sands and gravels. As previously discussed, there are zones with extremely low number of blow counts that originate from wind deposition during the coldest spells of the glaciation process.

2.5.4.2.2.2 Pressuremeter Tests

Pressuremeter tests were conducted in four boreholes on the BBNPP site, B-301, B-322, B-325 and B-327 in accordance with ASTM D4917 (ASTM, 2000c) at two depth intervals to measure the volumetric change of a pressurized cell surrounded by in-situ rock, specifically by the weathered Mahantango Formation. The Pressuremeter test is an in situ stress-strain test performed on the wall of a borehole using a cylindrical probe that is expanded in the radial stress direction. The Pressuremeter was field-calibrated using a steel pipe as the surrounding media of the pressure cell. The pressure and displacement gages were properly calibrated and the field geologists matched the serial numbers with the calibration records documentation. Table 2.5-32

presents the results of the borehole pressuremeter tests. These results are later discussed in Section 2.5.4.2.4 within the context of soil and rock properties.

2.5.4.2.2.3 Geophysical Tests

Geophysical tests were conducted in the three G-Series boreholes, and one B-Series borehole. Geophysical logging consisted of surface seismic refraction surveys, P-S suspension logging surveys, and downhole velocity measurements.

This section provides a summary of the geophysical surveys undertaken for the BBNPP site. Information obtained from these surveys was utilized in the analysis of and discussions pertaining to the site geology and characterization of geologic features as presented in Subsection 2.5.1.2, and surface faulting potential presented in Subsection 2.5.3.

The location, and depth or extent of each test is shown by Figure 2.5-106. Figure 2.5-121, Figure 2.5-122, Figure 2.5-123, and Figure 2.5-124 present the plots for compressional and shear wave velocities. The plots provide the results from the two different surveys performed: downhole test, and P-S Suspension Logging.

A surface seismic refraction survey was performed for the 6 profile lines indicated by Figure 2.5-106. The results of the survey are provided by Figure 2.5-125 through Figure 2.5-131. The findings of the refraction survey are consistent with the boring program in the sense that the rock horizon was defined at the position indicated by the boreholes. The measured compressional shear wave velocities are consistent with those obtained from downhole and PS-suspension logging.

Downhole Seismic Velocity Surveys

Downhole seismic velocity surveys were conducted in borings G-301, G-302, G-303, and B-301. Installation of PVC casing was critical for acquiring good downhole data. The space between the outside of the casing had to be backfilled with low-strength grout to ensure that the casing follows the motions of the adjacent soil exactly. The boreholes were purged of water to a depth of 50 ft (15 m) to reduce the effect of tube waves, traveling down the borehole. B-301 was an uncased borehole. Measurements in an uncased borehole provides more accurate information because the equipment is in direct contact with the rock formation; the casing is installed mainly to protect the instrument from damage. If there is structural integrity of the borehole, it is possible to perform the survey without casing. This was the case at the B-301 location.

Downhole seismic velocity surveys are conducted by measuring the time for seismic waves (generated by an impulsive source at the surface) to travel to a sensor located at a sequence of depths in the borehole. A typical sensor consists of three orthogonal geophones. The two horizontal geophones are used to detect shear-wave (S-wave) arrivals and a vertical geophone is used to detect compression-wave (P-wave) arrivals. Various methods are used to align one of the horizontal geophones with the source polarization. At each measurement level, the sensor assembly is locked to the borehole wall using a clamping mechanism so that the geophones will couple with the seismic signals propagating in the earth.

Seismic waveforms for each depth interval are analyzed and the travel time picked from those waveforms. Interval velocities are calculated and reported as seismic velocity versus depth. This procedure is typically repeated every 2.5 ft (0.76 m) through overburden soil, and every 5 ft

(1.5 m) through bedrock. The shear wave source was a wooden plank approximately 6 in x 6 in x 8 ft (15 cm x 15 cm x 2.4 m) with steel end caps and cleats attached to the bottom to better couple with the ground. The compressional wave (P-wave) source was sledge hammer blows on a steel or aluminum plate adjacent to the borehole.

P-S Suspension Logging

P-S suspension logging was performed in four (4) boreholes. P-S suspension velocity logging was performed in borings B-301, G-301, G-302, and G-303 shown in Figure 2.5-106. The objective of the suspension and downhole logging tests was to obtain shear wave (V_s) and compressional wave (V_p) velocity measurements as a function of depth within each borehole.

In the absence of an accepted ASTM standard, the following procedure was used to perform P-S suspension velocity logging. P-S suspension velocity logging uses a 23 ft (7 m) probe containing a source near the bottom, and two geophone receivers spaced 3.3 ft (1 m) apart, suspended by a cable. The probe is lowered into the borehole to a specified depth where the source generates a pressure wave in the borehole fluid. The pressure wave is converted to seismic waves (P-wave and S-wave) at the borehole wall. At each receiver location, P- and S-waves are converted to pressure waves in the fluid and received by the geophones mounted in the probe, which in turn send the data to a recorder on the surface. At each measurement depth, two opposite horizontal records and one vertical record are obtained. This procedure is typically repeated every 1.6 ft (0.5 m) or 3.3 ft (1 m) as the probe is moved from the bottom of the borehole toward the ground surface. The elapsed time between arrivals of the waves at the geophone receivers is used to determine the average velocity of a 1.6 ft (0.5 m) high column of soil around the borehole.

Surface Seismic Refraction Surveys

Surface seismic refraction surveys are used to generate a cross sectional acoustic image of the subsurface strata. This method identifies mapping depth to bedrock, identifying voids, determining strength and quality of bedrock, and locating faults or steeply dipping contacts. The geophysical refraction seismic survey was performed in 6 selected lines as shown by Figure 2.5-106. The survey is conducted by laying out a series of geophones (typically every 10 ft (3 m)) in intersecting grid lines spaced approximately every 250 ft (76 m), which is then connected to a 24-channel data acquisition system. An individual refraction spread covered 250 linear feet (76 linear meters) and seven "shot points" were operated for each spread. Seismic energy at the shot points was delivered by a sledge hammer striking a metal plate. Depths to which seismic refraction data are acquired are functions of magnitude of the seismic energy source and overall refraction spread lengths. Seismic velocities measured by this technique are used to calculate the mechanical properties of subsurface materials (moduli values), as well as for material identification and for assisting in stratigraphic correlations. Interpretations are made from travel times representing the time required for a compressional seismic wave to travel from an energy source location to each of an array of vibration sensitive geophones. Geophones are located at pre-determined intervals along the ground surface with spacing between individual geophones selected to be appropriate for the intended depth of the investigation (Weston, 2008).

The elastic wave measured in the seismic refraction method, the "P-wave" or compressional wave, is the first arrival of energy from the seismic source at each receiver, or geophone. This elastic wave travels from the energy source in a path causing adjacent solid particles to oscillate in the direction of wave propagation. At shorter distances between source and geophone the first arriving waves will be direct waves that travel near the ground surface through the lower velocity

material. At greater distance, the first arrival at the geophone will be a refracted wave that has taken an indirect path through the two layers. The refracted wave will arrive before the direct wave at a greater distance along the spread because the time gained in travel through the higher-speed material compensates for the longer path. For all configurations of seismic sources and receivers, P-wave energy will arrive at a given geophone location in the shortest possible time as required by Fermat's Principal (Dobrin, 1976). This principal was utilized to develop several analytical methods for calculating seismic velocity structure versus depth using only first arrival times of seismic P-wave energy measured along arrays of geophones deployed at ground surface (Weston, 2008).

The results of the survey are provided by Figure 2.5-125 through Figure 2.5-131. The interpretation of the results was performed with borehole data in the form of contour profiles. Figure 2.5-113 through Figure 2.5-115 provide these contours and do not show any evidence of faulting or discontinuity. The thickness of the overburden to top of bedrock constructed from over 45 borings that penetrated the glacial material shows that there has been no thinning or thickening of the glacial material to suggest that this material has been faulted. Further, the surface of the bedrock (i.e., contact between the glacial material and bedrock) is irregular, but is due to glacial scour indicating that post-Devonian faulting has not occurred.

The somewhat irregular surface of the bedrock noted in the Refraction Survey is not interpreted as significant offsets within the Mahantango event that could be attributed to faulting. The irregular surface is mimicked in the overlying glacial till layer suggesting a glacially eroded surface, followed by a folding event associated with the Appalachian Orogeny. Most likely, the apparent irregular surface is the result of glacial scour, an erosional feature, within the upper part of the Mahantango Shale. Other apparent offsets may be a result of low fold (low statistical redundancy) that occurs at the line ends of seismic reflection data and thus reducing the confidence of the interpreted apparent offsets.

The results and interpretation of the geophysical tests are further discussed in the following Sections:

- Section 2.5.3, in the context of surface faulting
- Section 2.5.4.2.5, in the context of recommended soil properties for engineering design purposes,
- Section 2.5.4.4, in the context of the approach to select the best estimate soil column profile for dynamic analysis at the BBNPP site.

2.5.4.2.2.4 Hydrogeologic Investigation

The hydrogeologic field investigation included a site specific data collection to support a comprehensive hydrogeological evaluation of the BBNPP site and surrounding areas as required for Section 2.4.

The objective of the hydrogeological field investigation was to collect the necessary data and information to characterize the existing surface water and groundwater flow conditions at the site, including subsurface borings for geological stratigraphy, monitoring of groundwater potential and quality, slug and pumping tests for analysis of aquifer parameters, and gauging of surface water flow in creeks.

The data collected in the field and from other sources (i.e., SSES FSAR, USACE, USGS) were utilized to support the surface hydrology analysis, hydrogeological characterization, and the development of a groundwater flow model. The model has the capability to evaluate the impact of successive rain events on groundwater elevations across the facility as well as the hypothetical discharge of water from facility operations and storage structures to the ground and the resulting impact to groundwater flow and transport of radionuclides from the facility, including the release of radionuclides and other potential contaminants into these flow systems.

Section 2.4 presents the detailed information related to the hydrogeological field investigation.

2.5.4.2.3 LABORATORY TESTING PROGRAM

The laboratory investigation of soils and rocks was performed in accordance with the guidance of the NRC Regulatory Guide 1.138, "Laboratory Investigations of Soils and Rocks for Engineering Analysis and Design of Nuclear Power Plants" (NRC, 2003b). Soil and rock samples were shipped under chain-of-custody from the on-site storage to the testing laboratories. ASTM Standards ASTM D4220 (ASTM, 2000a) and ASTM D5079 (ASTM, 2006f) provide guidance on standard practices for preserving and transporting soil and rock core samples, respectively. These guidelines were referenced in preparing technical specifications for the BBNPP subsurface investigation, addressing sample storage and transportation, as well as other subsurface investigation and geotechnical requirements.

Laboratory testing consisted of testing soils and rocks samples obtained from the subsurface investigation program. Laboratory testing of soil samples consisted of index and engineering properties on selected SPT disturbed samples, strength, consolidation, permeability, and chemical tests on undisturbed samples, rock cores recovered from borings, and samples gathered from potential borrow areas of fill and backfill. Laboratory tests included the following: engineering classification, moisture (water) content, unit weight, specific gravity, Atterberg limits, grain size (sieve and hydrometer), percent passing #200 sieve, permeability, consolidated-undrained triaxial compression (C \bar{U}), unconfined compression (UC), consolidation, resonant column torsional shear (RCTS), free-free resonant column (FF), resistivity, chloride ion content, and sulphate ion content.

The number and types of tests selected were consistent with the field investigation findings, and the uniform conditions encountered at the site. Overall, the SPT blow counts were very consistent both in depth and spatial distribution. The soil strata at the site were distinguishable and there was a good correlation between the in-situ soil classification and the SPT results. At the BBNPP, the comprehensive index testing program along with refined testing at strategically selected locations has provided the required information to adequately characterize the soil properties.

A summary of laboratory tests and specifications used for the laboratory testing program is shown in Table 2.5-27. The soil and rock laboratory tests listed in Regulatory Guide 1.138 (NRC, 2003b) are common tests performed in most well-equipped soil and rock testing laboratories. Additional tests that are not covered in regulatory guides were also performed for the BBNPP field exploration (i.e. RCTS, FF, and chemical tests).

Resonant Column Torsional Shear (RCTS) tests were performed at Fugro Laboratories. These tests were performed under the Fugro Laboratories Quality Assurance Program. Free-Free

Resonant Column (FF) tests were performed at the University of Texas under the RIZZO Quality Assurance Program.

The following sections provide a summary of each test, showing the most important and relevant results.

2.5.4.2.3.1 LABORATORY INDEX TESTS

Soil samples were classified in the laboratory using the Unified Soil Classification System (USCS) in accordance with ASTM D2487 (ASTM, 2006a). Rock samples were classified in the laboratory using the Unified Rock Classification System (URCS) in accordance with ASTM D5878 (ASTM, 2005d).

2.5.4.2.3.1.1 GRAIN SIZE ANALYSES

Grain size analyses were performed on selected SPT samples of overburden soils. The grain size tests were done in accordance with ASTM D422-63 (ASTM, 2002a). The results of these tests were used for classification and correlation purposes.

2.5.4.2.3.1.2 MOISTURE CONTENT

Moisture content was determined from samples in accordance with ASTM D2216 (ASTM, 2005c). Moisture content was also obtained during hydraulic conductivity tests on undisturbed samples and during unconfined compressive strength tests of rock core samples. Consistently throughout the site, and down through the depth of the borings, the laboratory results showed natural moisture content in the overburden soils ranging between 5 and 20 percent and an average of 10.7 percent. Moisture content laboratory results are provided by Table 2.5-34. The moisture content of rock samples is extremely low, sometimes not even recorded. This condition is due to the extremely high density of the shales at the site.

2.5.4.2.3.1.3 UNIT WEIGHT DETERMINATIONS

Unit weight determinations were made based on a weight-volume relationship on undisturbed glacial overburden samples and Mahantango Formation rock core samples. Table 2.5-35 lists the samples with the corresponding dry and wet unit weights. On soils, unit weight measurements were performed during resonant column, and hydraulic conductivity tests. Unit weight measurements on rock samples were performed during "Free-Free" tests and during unconfined compressive strength tests.

2.5.4.2.3.1.4 SPECIFIC GRAVITY

Specific gravity tests were performed on Glacial overburden soil samples and Mahantango Formation in accordance with ASTM D854 (ASTM, 2006b). Typical values of specific gravity of most soils lie within the narrow range of 2.7 ± 0.1 . For hard rocks samples, ASTM D6473 (ASTM, 2005b) was used to determine the specific gravity. Specific Gravity results are listed in Table 2.5-36.

2.5.4.2.3.1.5 CHEMICAL CLASSIFICATION TESTS

Chemical tests were conducted on SPT samples selected from the glacial overburden soils and the Mahantango Formation in accordance with ASME D4972 (ASTM, 2001), AASHTO T290 (AASHTO, 2007), and AASHTO T291 (AASHTO, 2004). These tests provide quantitative information related to the aggressiveness of the soil conditions, and the potential for deterioration of a foundation material. The following chemical tests were conducted on samples from the

BBNPP site: resistivity; chloride ion content; and sulphate ion content . The results of the tests are provided in Table 2.5-37.

2.5.4.2.3.2 LABORATORY PERFORMANCE TEST

2.5.4.2.3.2.1 UNCONFINED COMPRESSION

Unconfined Compression tests were conducted on representative rock core samples to determine their compressive strength, in accordance ASTM D7012-04 (ASTM, 2004a). Table 2.5-38 presents a summary of the Unconfined Compression test results. The core samples of the Mahantango formation are typically a medium to dark gray shale rock with a recovery ratio of 90 percent and a RQD of 70 percent or higher. Therefore, most of the samples did not present problems during the specimen preparation. Section 2.5.4.2.4 provides the recommended geotechnical performance parameters which in part are based on the results of the unconfined compressive strength. The unconfined compressive strength of the specimens from the Mahantango formation is medium high to high with an average slightly above 9000 psi (62 MPa).

2.5.4.2.3.2.2 ROCK SAMPLE URCS ENGINEERING CLASSIFICATION

The Mahantango Formation was the main target of the investigation and the specimens showed: minimum to no weathering (Grade A); unconfined compressive strength between 8000 and 13000 psi (55 to 90 MPa) (Grade B); no discontinuities (Grade A); and a unit weight around 170 pcf (27 kN/m³) (Grade A). The URCS classification of the Mahantango formation is ABAA.

2.5.4.2.3.2.3 HYDRAULIC CONDUCTIVITY

Laboratory tests were performed to determine the hydraulic conductivity of undisturbed samples, according to ASTM D5084 (ASTM, 2003). Results of the tests are presented in Table 2.5-39. The tests were performed on undisturbed samples recovered from the overburden glacial soils. Section 2.4 presents detailed information related to the hydrogeological field investigation and additional information regarding permeability and hydraulic conductivity.

2.5.4.2.3.2.4 RESONANT COLUMN TORSIONAL SHEAR

Resonant Column Torsional Shear (RCTS) tests were conducted according to the procedure developed by the University of Texas at Austin (UTA) entitled, PBRCTS-1, Rev. 4, Technical Procedures for RCTS Tests, (UT, 2004a). The tests targeted the Glacial Overburden soils and two remolded samples recovered from borrow area sites. The on-site samples were obtained using thin-walled samplers. One attempt of RCTS test was made on a solid rock core (B-304, R2). The specimen cracked right after subcoring to an approximate diameter of 0.6 in (1.5 cm). The RCTS testing program included a total of five tests, of which one was the cracked rock core. The samples used for testing are listed by Table 2.5-40. It was anticipated that the RCTS tests on Glacial Overburden would reflect the behavior of the finer particle matrix rather than that of the gravelly fragments. For the case of the fill samples, laboratory staff had to scalp the specimens so that the largest particles had a diameter less than 1/6th of the specimen diameter. The focus of the RCTS testing program was to evaluate the material that will likely form the foundation fills for the plant facilities. These materials will originate from either excavation soils or from borrow areas and will be screened and compacted according to specifications. The RCTS on borrow area material was performed on remolded samples.

The RCTS test is performed in a series of steps that incorporate different confining pressures and loading frequencies. The Torsional Shear portion of the test is able to capture physical properties at large strains under lower frequency loading that best resembles the seismic demand. The details of the testing methodology are documented by the procedure, PBRCTS-1, Revision 4, Technical Procedures for RCTS Tests, (UT, 2004a).

Resonant Column (RC) and/or Resonant Column Torsional Shear (RCTS) testing are performed to measure two critical parameters in laboratory soil (and sometimes rock) specimens:

1. Shear modulus, which is directly related to shear wave velocity of the soil (Equation 2.5.4-1)

$$G = \rho V_s^2 \quad \text{Eq. 2.5.4-1}$$

2. Damping, which allows for the dissipation of the energy released during an earthquake or any given vibratory process.

Both the shear modulus and damping depend on:

- The amount of strain (or unit deformation),
- The confining pressure,
- The frequency of the motion, in this context, the frequency of the cyclic load applied during testing.

Table 2.5-41 presents the results for shear modulus and damping at low strains. The table highlights the medium range confining pressure applied during testing. The values of the shear stress in the samples range between the 590 to 5800 ksf and damping ranged between 0.4 and 2.80 percent. The remolded and compacted samples had higher values of shear modulus. A discussion of the recommended values for engineering purposes is included in Section 2.5.4.2.4. The recommended properties take into account the effect that confining pressure has on the low strain shear modulus. The strain dependency variation of the shear modulus and damping is shown in the form of normalized plots by Figure 2.5-131, Figure 2.5-132, Figure 2.5-133, respectively for each of the samples tested. A discussion for recommended values is presented in Section 2.5.4.2.4 and Section 2.5.4.7.

2.5.4.2.3.2.5 UNCONFINED RESONANT COLUMN "FREE-FREE" TESTING

The Free-Free Resonant Column Tests (FF) was conducted according to the procedure, also developed by UTA, entitled, URC-1, Revision 4, Technical Procedures for URC Tests (UTA, 2004b). The Free-Free resonant column device allows for a simpler approach compared to the RCTS that can measure small-strain shear modulus (G_{max}) and small-strain material damping (D_{min}). The term "Free-Free" is used to differentiate from the "Fixed-Free" condition of the typical RC test, meaning that one end of the sample is fixed while the other is free to rotate or displace. No confining pressure is used in this test. A total of eight "Free-Free" tests were performed on special care rock samples retrieved from various boring locations. Table 2.5-42 lists the samples and presents the results. A discussion of how the "Free-Free" testing results are used for the analysis is presented in Section 2.5.4.2.4 and Section 2.5.4.7.

2.5.4.2.4 ENGINEERED SOILS

Category 1 Granular Structural Fills and Backfills will be created from screened granular soils from either the excavated in-situ soils or borrow areas in the proximity of the project. Cohesive fill (permeability lowered to less than $1.0E-08$ m/s) will be required for the construction of the ESWEMS Retention Pond. A distinction is made between fill and backfill as follows: the term "Category 1 Structural Fill" or "fill" is used for engineered soil that will be placed beneath the foundation of Safety Related Facilities; the term "Category 1 Structural Backfill" or "backfill" is used for material that will be placed around and above the foundation level of Safety Related Facilities.

2.5.4.2.4.1 CATEGORY 1 GRANULAR STRUCTURAL FILL

Bowers Construction (Bowers) of Berwick, PA provided excavation of test pits to collect subsurface soil and perform screening of soil samples for the purpose of composite soil sampling soil collection for geotechnical analysis. The borrow site is approximately 4,200 ft (1,280 meters) southwest of the site at the intersection of Rockaway Street and Salem Boulevard (Route 11), Berwick, PA.

Soil samples were collected from two identified test pits (Test Pit # 5 and Test Pit Face). Upon collection of soil, Bowers utilized a Fine Tec 540 screening machine and CAT 960 front end loader along with a 325 track hoe in order to prepare the composite soil sample. After the stockpile was split over the 2 in (5 cm) sieve, Bowers used a Cat 325 track hoe to turn over the stockpile and create a 15 ft x 8 ft x 3 ft (4.5 m x 2.4 m x 0.9 m) pile for each test pit. Rizzo personnel dug 4 holes at the top of the pile at diagonal corners to a depth of 1.5 ft (0.5 m) in depth. Six representative buckets were filled from the 4 holes and shipped the soil buckets to the representative laboratories. The description of the collected soil consisted of well graded Sand with Gravel (sw) - about 70 percent sand fine to coarse, sub rounded to rounded, 25 percent gravel fine to coarse, hard, sub round to rounded, 5 percent silt, no plasticity, no dilatancy no toughness, low strength with slight odor.

A Laboratory Testing Program has been implemented to fully characterize the properties of the proposed material. The tests included:

- Modified Proctor tests,
- Grain size,
- Resonant Column Torsional Shear,
- Chemical Tests

The Modified Proctor Test results, showing optimum moisture content and maximum unit weight are provided by Table 2.5-43. The optimum water content is about 6 percent and the material proved to be quite dense with maximum moist unit weights above 144 pcf (22.4 kN/m^3). The grain size analysis results are compared against the required specification. Table 2.5-43 provides the recommended properties for structural fill. Structural fill should be compacted to 95 percent of the optimum dry unit weight Modified Proctor. The fill moist, saturated, and dry unit weights exceed the U.S. EPR specified values of 128 pcf (20.1 kN/m^3), 134 pcf (21.1 kN/m^3), and 110 pcf (17.3 kN/m^3), respectively. The unit weight for the structural fills at the BBNPP site will be exceeded.

2.5.4.2.4.2 CATEGORY 1 GRANULAR STRUCTURAL BACKFILL

Category 1 Granular Structural Backfill will have the same specifications as the structural fill, but compacted to 90 percent Modified Proctor optimum dry unit weight. Table 2.5-45 provides the specifications for Structural Backfill. The backfill moist, saturated, and dry unit weights exceed the U.S. EPR specified values of 128 pcf (20.1 kN/m³), 134 pcf (21.1 kN/m³), and 110 pcf (17.3 kN/m³) respectively. The unit weight for the structural backfills at the BBNPP site will be exceeded.

2.5.4.2.5 RECOMMENDED SOIL, FILL, AND ROCK PROPERTIES

The following sections provide recommendations of soil properties for engineering analysis and design purposes. The properties are based on a combination of field measurements, laboratory testing, engineering analysis, engineering judgment, and available reference material. For a cohesionless structural fills at the site, the soil below and adjacent to the safety-related foundation basemat will have a friction angle in excess of 35 degrees. This strength meets the requirements of the US EPR. The requirement is also met and exceeded by the high strength parameters of the foundation bedrock. Details are provided in the following subsections.

The properties are given for each of the geologic units found during the investigation as described by Section 2.5.4.2.1 and presented by Figure 2.5-106. Those units are listed below:

- Soils - Glacial overburden
- Bedrock - Mahantango Formation

In addition to the existing soils, it is necessary to provide properties for engineered fills that will likely be placed as foundation media for safety related structures . The Nuclear Reactor Building and its adjacent facilities will be placed directly on top of the Mahantango Formation. This will not be the case for the south ESWS Cooling Towers or the south Emergency Power Generating Buildings. Therefore, soil properties are also given for:

- Category I Granular Structural Fill
- Category I Granular Structural Backfill

This Section is divided in:

- Classification and Index Properties,
- Strength Properties,
- Performance Properties,
- Static Elastic Properties,
- Dynamic Elastic Properties, and
- Chemical Properties.

The overburden soils consist of one soil layer: Glacial Overburden (sand and gravel with cobbles and boulders). The existing soil matter is not suitable for the support of large or safety-related structures due to the potential for liquefaction and will be removed in order for the foundation mats to bear directly on either of the Mahantango Formation, concrete fill, or engineered fill. The existing soil matter is not suitable for the support of large or safety-related structures. Additional

discussion related to this matter is presented in Section 2.5.4.8. The thickness of the overburden soils varies from about 12.5 to 62 ft (3.8 to 19 m), with an average thickness of 39 ft (12 m). The depth from surface boring elevation to the Mahantango Formation is shown by Figure 2.5-113. The thickness of the soil layers is based on estimating the termination elevations encountered for the layer at the boring locations from the boring logs included with the COLA.

2.5.4.2.5.1 INDEX PROPERTIES

Index properties are:

- USCS Classification (or URCS Classification for Rocks),
- Water Content,
- Unit Weight,
- Specific Gravity,
- Grain Size (or Fines Content),

Index properties determined for rocks are:

- Classification
- Unit Weight,
- Specific Gravity.

Selected samples were submitted for laboratory index tests and testing for determination of engineering properties. Section 2.5.4.3 presents the detail of the laboratory testing program. Table 2.5-45 provides the recommended index properties.

Of the index properties, only the dry, moist, and saturated unit weights are discussed in the U. S. EPR Tier 2 FSAR documentation. The site specific unit weights found at the BBNPP site exceed the U. S. EPR FSAR values of:

- Saturated soil = 134 lb/ft³.

- Moist soil = 128 lb/ft³.

- Dry soil = 110 lb/ft³.

At BBNPP:

- Saturated soil = 144 lb/ft³.

- Moist soil = 141 lb/ft³.

- Dry soil = 133 lb/ft³.

This is not necessarily a geotechnical problem. The U. S. EPR FSAR values were established according to one previous site specific experience.

2.5.4.2.5.2 STRENGTH PROPERTIES

Strength properties are obtained directly from laboratory tests or from field measurements and supplemental calculations. Triaxial testing on overburden soils was not considered useful due to the heterogeneity of the formation and the presence of large boulders. Undisturbed samples were collected only near the surface. At boring B-331, it was possible to collect an undisturbed sample at a depth of 17 ft (5 m). This sample was used for RCTS testing. The strength of the overburden soils is estimated with the use of soil classification and standard penetration data. The overburden soils will be removed and replaced by engineered fills due to the potential for liquefaction. Strength properties include the Mohr-Coulomb parameters commonly used for many geotechnical analysis issues such as bearing capacity, slope stability, retaining walls, and foundation design.

An equivalent friction and cohesion was estimated for the rock mass of the Mahantango Formation. The parameters were determined according to the classification system proposed by Bieniawski (Bieniawski, 1989). The Mahantango Formation is classified as a "Very Good" Rock Mass with a rating of 82, an equivalent cohesion of 7.3 ksf (350 MPa), and an equivalent friction angle of 40 degrees. Table 2.5-46 provides the detail of the Bienawski classification.

The following recommended strength properties for soil and rock at the site are provided by Table 2.5-46. For each property, the basis for the recommendation is explicitly mentioned in the observations column of the Table 2.5-46.

- Penetration Resistance (SPT)
- Cohesion
- Friction Angle
- Unconfined Compression.

Strength properties were determined by either correlation with SPT blow counts or by statistical averaging of the laboratory tests. Strength properties of the foundation formation (Mahantango Formation) exceed the requirements established in the U.S. EPR FSAR.

The position of the water table is close to the surface at a depth of about 8 ft (2.4 m) at the center line of the reactor footprint, at Elevation 659 ft (201 m) msl. The foundation grade of the BBNPP Nuclear Island (NI) and its adjacent facilities will be placed at Elevation 674 ft (205.4 m) msl, considerably higher due to the elevation of the Probable Maximum Flood level of 671 ft (204.5 m) msl.

2.5.4.2.5.3 PERFORMANCE PROPERTIES

Two performance properties are discussed: (1) hydraulic conductivity, and (2) consolidation.

Permeability

Section 2.4 presents detailed information related to the hydrogeological field investigation, and additional information regarding permeability and hydraulic conductivity is available. The Laboratory Testing Program of Section 2.5 focused on specific values at the site and tests were performed on samples extracted from the geotechnical boring program. As expected, the Glacial Overburden presents relatively high hydraulic conductivity. Table 2.5-48 provides the

recommended values for hydraulic conductivity. The recommendation is based on the results from field tests performed on the wells installed as part of the Hydrogeologic investigation.

Consolidation

The soils encountered at the site are granular in nature and long term settlement due to consolidation would not occur if these were used as foundation support.

2.5.4.2.5.4 STATIC ELASTIC PROPERTIES

The static elastic properties of interest are the elastic modulus, the shear modulus, and the Poisson's ratio. The shear modulus is derived directly from the elastic modulus and the Poisson's ratio.

Elastic Modulus

The static elastic modulus of soils and rocks is determined from data retrieved during the field investigation and laboratory testing. Several criteria are used, depending on the soil or fill analyzed:

1. American Society of Civil Engineering (ASCE) Typical recommended values,
2. ASCE N Correlation,
3. American Association of State Highway and Transportation Officials (AASHTO),
4. Rock Mass Rating.
5. American Concrete Institute (ACI).

Each of the criteria is applied and an average or a conservative approach is used for the recommended parameter. Table 2.5-49 presents the values according to each criterion and the recommended elastic modulus value. It is anticipated that static loading in excess of the current in-situ overburden pressure will not occur below the Mahantango Formation, and, therefore, the static elastic modulus is not a critical parameter.

Poissons Ratio

The most representative value of the Poissons ratio is obtained directly from the shear wave and compressional wave velocity measurements. Equation 2.5.4-2 is used to establish the Poissons ratio.

$$\frac{V_p}{V_s} = \sqrt{\frac{2-2\nu}{1-2\nu}} \quad \text{Eq. 2.5.4-2}$$

Static Shear Modulus

The static shear modulus is directly determined from the Elastic Modulus and the Poissons Ratio with the use of Eq. 2.5.4-3.

$$G = \frac{E}{2(1 + \nu)} \quad \text{Eq. 2.5.4-3}$$

where G is the static shear modulus, E is the Elastic Modulus and ν is Poissons Ratio.

Table 2.5-50 provides the recommendation for the static elastic properties.

2.5.4.2.5.5 DYNAMIC ELASTIC PROPERTIES

A comprehensive field geophysical investigation program and laboratory testing program were undertaken to establish the dynamic properties for the BBNPP. The properties are required for site amplification analysis, Soil Structure Interaction (SSI) analysis, and foundation design. The dynamic properties established are:

- Shear Wave Velocity (V_s),
- Compressional Wave Velocity (V_p),
- Density (ρ),
- Poisson's Ratio (ν),
- Maximum Dynamic Shear Modulus (G_{max}),
- Maximum Dynamic Elastic Modulus (E_{max}),
- Damping at small strain or initial damping (DS_o),
- Strain dependant shear modulus and damping (for Overburden and borrow area soils).

The shear wave velocity profile was determined by means of a data interpretation analysis that incorporated the results from downhole, and P-S Suspension Logging tests. The details of the analysis are described in Section 2.5.4.4. The recommended values for dynamic properties are presented in Table 2.5-51. More descriptions of the procedures followed to provide the recommendation are included in Section 2.5.4.7. The recommended shear wave velocity profile under the Nuclear Island is plotted by Figure 2.5-135.

For the case of the overburden soils, dynamic properties will vary depending on the level of strain present in the soil. The two strain dependant properties of interest are Shear Modulus and Damping. Figure 2.5-135 presents the recommended curves for the engineered fill and/or backfill. The recommended curve for the overburden soils is the generic curve that best adapts to the Torsional Shear experimental data. For Shear Modulus, this curve is generic curve

(Vucetic, 1991) that corresponds to a Plastic Index of 30 or 40. For Damping, the curve with a Plastic Index of 50 is recommended (Vucetic, 1991).

2.5.4.2.5.6 CHEMICAL PROPERTIES OF SOILS

The chemical properties of the soils are given by Table 2.5-37.}

2.5.4.3 Foundation Interfaces

The U.S. EPR FSAR includes the following COL Item in Section 2.5.4.3:

Foundation interfaces with underlying materials are site specific and will be addressed by the COL applicant. The COL applicant will confirm that the site soils have (1) sliding coefficient of friction equal to at least 0.7, (2) adequate shear strength to provide adequate static and dynamic bearing capacity, (3) adequate elastic and consolidation properties to satisfy the limits on settlement described in Section 2.5.4.10.2, and (4) adequate dynamic properties (i.e., shear wave velocity and strain-dependent modulus-reduction and hysteretic damping properties) to support the Seismic Category 1 structures of the U.S. EPR under earthquake loading.

This COL Item is addressed as follows:

{This section discusses the interfaces between the planned structures and other components and the subsurface characteristics. A plot plan showing the location of the borings, seismic lines, and downhole surveys is provided by Figure 2.5-106. Based on the information obtained during the subsurface investigation and laboratory testing program for the BBNPP, it was determined that exploratory trenches were not necessary in order to characterize the soils at the BBNPP. Cross sections showing the main geologic units are presented by Figure 2.5-108 through Figure 2.5-111. Contour plans of geologic unit elevations are given by Figure 2.5-113 through Figure 2.5-116.

2.5.4.3.1 U.S. EPR FSAR

The U.S. EPR FSAR provides criteria related to various sitting issues, which must be satisfied by the particular features of the BBNPP site. The U.S. EPR FSAR identifies the type of information that should be developed to demonstrate that the site is in compliance with the design. Generic soil profiles are listed by the U.S. EPR FSAR and these represent a broad range of foundation media characterized by shear wave velocities ranging from 700 ft/sec (213 m/sec) to those typical of hard rock conditions. It is expected that this range captures the static and dynamic response of plant SSCs which will, in general, envelop the actual response at sites exhibiting foundation soils with shear wave velocity at foundation level greater than 1,000 ft/sec (305 m/sec). At BBNPP, the shear wave velocity of foundation media (Mahantango Formation) for the Nuclear Island (NI), Emergency Power Generation Buildings, and Essential Service Water Cooling Towers facilities is approximately 7000 fps (2135 m/s). The NI basemat is a monolith that includes the Reactor Building (UJA), Safeguards Buildings (UJH- mechanical and UJK- electrical) and Fuel Building. Table 2.5-53 provides the soil conditions that were evaluated by the U.S. EPR FSAR. No departures or deviations were identified.

The seismic ground motion utilized in the design of NI structures is defined as a hypothetical free-field outcrop motion at approximately 36 ft (11 m) below grade, representing the bottom elevation of the containment base mat. On the other hand, the design of adjacent safety related

structures founded near the ground surface (Plant Grade) use the free-field soil surface ground motion for design. Section 2.5.2 presents foundation input response spectra (FIRS) for the NI at the base mat elevation. The FIRS are compared with the respective Certified Design Response Spectra (CDRS) presented by the U.S. EPR FSAR. Both the Foundation Input Response Spectra as well as the seismic response of the soil structure system depends on the subsurface soil stratigraphy including the soil layering, layer thickness, layer shear wave velocities and damping and impedance mismatch.

The foundation interface analysis relates to how the foundation medium and its variability affect the bearing pressure distribution and the settlement of the NI Basemat, and other safety related structures (Emergency Power Generation Buildings and Essential Service Water Cooling Towers) in the vicinity, particularly for soil sites. The foundation interface analysis also determines how these same items affect the seismic response of the structures and the foundation medium. The structural design of the NI Basemat is governed by the bearing pressure and its distribution due to dead and live load and seismic forces, as well as the foundation settlements. On the other hand, the seismic loads on the plant structures and foundations are determined by the vertical and the coupled horizontal and rocking response analysis as estimated with Soil-Structure Interaction (SSI) analysis or Rock-Structure Interaction (RSI) analysis, as the case may be.

Dynamic aspects of the foundation interface are discussed in BBNPP FSAR Sections 3.7 and 3.8. Static aspects such as bearing capacities, settlement and horizontal variability of stiffness and subgrade reaction under the base mats are discussed in Section 2.5.4.10. The subsurface soils beneath the NI base mat should have the capacity to support the bearing pressures with a factor of safety of 3.0 under static conditions and 2.0 under Safe Shutdown Earthquake conditions.

2.5.4.3.2 SITE CLASSIFICATION

Based on the review of the subsurface conditions at existing nuclear power plant sites, the potential sites for the U.S. EPR can be broadly categorized into four primary groups:

- Rock sites,
- Thin soil sites,
- Shallow soil sites, and
- Deep soil sites.

This categorization provides a framework for reporting site-specific conditions in a COLA referencing the U.S. EPR FSAR relative to the Plant Parameter Envelope (PPE) considered in the U.S. EPR design. Based on several combinations of site groups and their respective parameters, as specified by Table 2.5-54, the BBNPP site is classified as a Thin Soil Site over Hard or Firm Rock. As such, the Ground Motion Response Spectra (GMRS) is provided at the top of bedrock or top of Mahantango Formation. For the NI, this level corresponds to the top of rock or top of Mahantango Formation. The static and dynamic bearing capacity is verified without the need of time dependant settlement computations. Details related to shear wave velocity are included in Sections 2.5.4.2.5.5 and 2.5.4.2.2.1.3.

2.5.4.3.3 HORIZONTAL LAYERING

Most geotechnical analyses, including SSI analysis, settlement analysis and bearing capacity analysis, assume that the soil layers are horizontal and effects of non-horizontal layering are practically ignored. This assumption will hold if there is no significant inclination in the soil profiles such as the top of rock horizon.

Figure 2.5-115 shows the inclination of the top surface of the Mahantango Formation. In the direction of maximum gradient (approximately 30 degrees with respect to the North), the top of rock surface drops about 40 ft (12 m) in a distance of 300 ft (91 m), which corresponds to a 7.6 degree sloping angle. It is still applicable to assume a horizontal layered model for both Site Amplification and Soil Structure Interaction Analyses. The following justifications for this assumption apply:

- "The Foundation Interface Document Report on U.S. EPR Design reads: "Depending on the extent of the dip, the physical properties of the foundation medium may or may not vary systematically across a horizontal plane. If the dip is less than approximately 20 degrees, the site layering is defined as horizontal and no further substantiating analysis is required."
- The concrete between the Mahantango formation and the basemat will have a matching shear wave velocity and therefore the sloping effects will be mitigated.

2.5.4.3.4 UNIFORM SITE CONDITIONS

The variation of the dynamic properties between distant points of the NI facilities may be represented by a Lower Bound, Best Estimate and Upper Bound for the Vs value at the center point of the facility. The geotechnical and geophysical exploration programs show conclusive evidence that the subsurface conditions are uniform across the site.

The thickness of the Mahantango Formation was not determined since the BBNPP geotechnical investigation did not reach the bottom of the formation. The maximum exploration depth was 400 ft (122 m), and the average depth to reach the top of this formation is 39 ft (12 m) with respect to the ground level. Based on contour maps, the Mahantango Formation is present across the entire footprint of the power block. As such, the site may be considered as uniform.

2.5.4.3.5 INTERFACE FIGURES

The Interface Figures present cross sections of the site subsurface conditions with the location of the main components of the Project. Safety-related structures are shown at their planned foundation elevation and on top of the corresponding foundation material. Table 2.5-55 provides the depth, elevation, and foundation footprint of the BBNPP safety-related structures. Figure 2.5-136 provides a plan view of an excavation and fill plan with the location of a cross section. Two excavation profiles are shown in Figure 2.5-137 and Figure 2.5-138. A North-South direction cross section is shown in Figure 2.5-139. The Nuclear Island (NI) will sit on top of a concrete fill between its mat and the top of bedrock. The Emergency Power Generation Building and ESWS Cooling Towers will have an engineered soil fill in the south side of the power block. At the north side, these structures will bear directly on top of the Mahantango formation or on top of a concrete fill.

Section 2.5.4.5 provides the excavation details and Section 2.5.4.10 presents bearing capacities and estimated settlements.}

2.5.4.4 Geophysical Surveys

The U.S. EPR FSAR includes the following COL Item in Section 2.5.4.4:

Geophysical surveys are site specific and will be addressed by the COL applicant.

This COL Item is addressed as follows:

Section 2.5.4.2.2.3 presents the results of the geophysical investigation surveys . Section 2.5.4.2.5.5 provides the recommended dynamic soil properties, based on the results from the field investigation and on the post-processing analysis of the retrieved data.}

2.5.4.5 Excavation and Backfill

The U.S. EPR FSAR includes the following COL Item in Section 2.5.4.5:

Excavations and backfill are site specific and will be addressed by the COL applicant.

This COL Item is addressed as follows:

{Sections 2.5.4.5.1 through 2.5.4.5.5 are added as a supplement to the U.S. EPR FSAR.

BBNPP will utilize a combination of excavation slopes and temporary retaining structures to facilitate construction of below grade portions of the nuclear facility. The planned finish grade is at an elevation of approximately 674 ft (205.4 m).

The materials excavated as part of the site grading are primarily the overburden soils belonging to the sand and gravel units. Due to the presence of loose sand pockets that are prone to liquefaction, these soils are inadequate for foundation purposes and will be removed from the footprint of all the facilities. However, in-situ soils from the excavation may be used for fills and backfills if adequate screening and compaction techniques are implemented. These soils are predominantly of low plasticity or non plastic and their composition consists of sand and gravels with cobbler and boulders. No rebound (heave) in the ground due to the removal of the soils is expected at the Mahantango Formation.

The U.S. EPR minimum shear wave velocity is 1000 fps.

- The Nuclear Island, ESWEMS Pumphouse, North Emergency Power Generation Buildings (1UBP, 2UBP), and North ESWS Cooling Towers (1URB, 2URB) will bear on top of concrete or the Mahantango formation, which have shear wave velocities higher than 1000 fps.

- The South Emergency Power Generation Buildings (3UBP, 4UBP), and South ESWS Cooling Towers (1URB, 2URB) will bear on top of engineered fill, which will be constructed to achieve a shear wave velocity of 1000 fps.

- Category II SSE structures, such as the Fire Protection Building will bear on top of either bedrock, concrete or engineered fill, which will be constructed to achieve a shear wave velocity of 1000 fps.

2.5.4.5.1 Source and Quantity of Backfill and Borrow

As previously mentioned in Section 2.5.4.2.4.1, Bowers Construction (Bowers) of Berwick, PA provided excavation of test pits to collect subsurface soil and perform screening of soil samples for the purpose of composite soil sampling soil collection for geotechnical analysis. The borrow site is approximately 4,200 ft (1,280 m) southwest of the site at the intersection of Rockaway Street and Salem Boulevard (Route 11), Berwick, PA and has sufficient material to support site construction needs. Earthwork operations will be performed to achieve the planned site grades. Excavations for foundations of the proposed Category I structures within the Power Block area, including the ESWS pump house and the ESW Emergency Makeup Structure, will result in removing the overburden soils in their entirety, and will extend to top of the Mahantango Formation. The maximum depth of cut in the overburden soils is estimated to be about 62 ft (19 m). The estimated upper bound of the excavation and backfill volume is 600 thousand cubic yards (460 thousand cubic meters).

2.5.4.5.2 EXTENT OF EXCAVATIONS

Permanent excavation and fill slopes, created due to site grading, are addressed in Section 2.5.5. Temporary excavation slopes, such as those for foundation excavation, would be graded on an inclination of at least 1.5:1 horizontal to vertical (H:V) or flatter. The ESWEMS Retention Pond will be constructed as a dug reservoir in the natural soils. The bottom of the pond is planned at an elevation of 652 ft (199 m), and side slopes of 3:1 H: V. For the power block area, an excavation plan is provided by Figure 2.5-136. The approach for excavation, confirmed by the slope stability analysis (Section 2.5.5), will implement 1.5:1 H:V slopes, offset by 6 ft (1.8 m) at the base of excavation. A bench (8 ft (2.4 m) wide) should be located at the midpoint of the slope. At BBNPP, engineered fill or concrete will be required beneath the near-ground founded safety related structures. Figure 2.5-136 through Figure 2.5-138 show a excavation scheme for the NI structures (e.g., UJA, UJH, UJK, UKA, UKE and UKS), the Emergency Power Generating Buildings (UBP), the Essential Service Water (UQB and URB) structures, and the Turbine Building (UMA). A cut shown under the Reactor Building is to accommodate the tendon gallery.

2.5.4.5.3 Compaction Specifications

Structural fill sources were identified, as discussed in Section 2.5.4.5.1. Several samples of the materials were obtained and tested for indices and engineering properties, including moisture-density relationships. For foundation support, fill beneath mats is compacted to 95 percent Modified Proctor optimum dry density, and backfill against walls is compacted to 90 percent , as determined based on the Modified Proctor compaction test procedure . The fill is compacted to within 3 percent of its optimum moisture content, which is about 6 percent. Fill placement and compaction control procedures are addressed in a technical specification prepared during the detailed design stage of the project. It includes requirements for suitable fill, sufficient testing to address potential material variations, and in-place density and moisture content testing frequency, e.g., a minimum of one test per 10,000 ft² (900 m²) of fill placed. The technical specification also includes requirements for an on-site testing laboratory for quality control, especially material gradation and plasticity characteristics, the achievement of specified moisture-density criteria, fill placement/compaction, and other requirements to ensure that the fill operations conform to the earthwork specification for BBNPP. The soil testing company is required to be independent of the earthwork contractor and to have an approved quality program. A sufficient number of laboratory tests are required to be performed to ensure that variations in the fill material are accounted for. A trial fill program is normally conducted for the purposes of determining an optimum number of compactor coverages (passes), the maximum loose lift

thickness, and other relevant data for optimum achievement of the specified moisture-density (compaction) criteria.

2.5.4.5.4 DEWATERING AND EXCAVATION METHODS

Temporary groundwater control will be required during construction. Measurement of the groundwater conditions at the site indicate that the lower portions of the site excavations will be below the groundwater level. Thus site grading and excavation plans will implement measures to divert these groundwater flows away from excavations, such as, runoff prevention measures or trenches. Seismic Category I foundations are planned within the upper water-bearing Mahantango Formation. Groundwater conditions and dewatering are discussed in detail in Section 2.4.12 and 2.5.4.16.

On dewatered conditions, excavations are expected to be performed using conventional earth-moving equipment. Excavations will not present any major difficulties. Excavations in the top of the Mahantango Formation will not require greater excavating effort, such as ripping tools and explosives. However, excavation into the Mahantango Formation will extend up to about 10 ft (3 m) under the Nuclear Island Facilities. Such excavation will require ripping or minor amounts of explosives. Upon reaching the final excavation levels, all excavations will be cleaned of any loose materials, by either removal or compaction in place. All final subgrades will be inspected and approved prior to being covered by backfill or concrete. The inspection and approval procedure(s) will be addressed in the foundation and earthwork specifications that will be developed during the detailed design stage of the project. These specifications will include measures, such as proof-rolling, excavation and replacement of unsuitable soils, and protection of surfaces from deterioration.

2.5.4.5.5 Monitoring and Quality Control

Monitoring program specifications will be developed during the detailed design stage of the project. The specification document will address issues, such as the installation of a sufficient quantity of instruments in the excavation zone, monitoring and recording frequency, and evaluation of the magnitude of settlement during excavations and foundation construction.

2.5.4.6 Ground Water Conditions

The U.S. EPR FSAR includes the following COL Item in Section 2.5.4.6:

The COL applicant will address site-specific ground water conditions.

This COL Item is addressed as follows:

{The ground water data collection and monitoring program is still in progress subsequent to the final monitoring of wells at the BBNPP site. Details of available ground water conditions at the site are given in Section 2.4.12. At the site, the Glacial Overburden is the aquifer that has a direct influence on the foundation of the proposed facilities. The Glacial Overburden aquifer unit includes all of the glacial outwash, kame, kame terrace, till, colluvium, alluvium, and other unconsolidated surficial deposits that overlie the bedrock, are saturated, and transmit groundwater.

Based on available information through June 2008, the shallow (surficial) groundwater level ranges from approximately elevation 655.7 ft (199.9 m) to elevation 659.3 ft (201.0 m), with an

average elevation of 657.7 ft (200.5 m). The adopted design ground water elevation in the geotechnical calculations is 659.0 ft (200.9 m). This value is bounded by the U.S. EPR FSAR value, since plant grade is placed at elevation 674.0 ft (205.5 m). The shallow groundwater levels have been accounted for in the analyses of the stability of foundations. During construction, dewatering along with site grading and excavation plans will divert flows away from excavations.

Sections 2.5.4.6.1 through 2.5.4.6.4 are added as a supplement to U.S. EPR FSAR.

2.5.4.6.1 DEWATERING DURING CONSTRUCTION

An active construction dewatering system will be implemented prior to construction to maintain the site conditions dry. The system will continue to operate until the subgrade portions for the structures are completed and the excavation is backfilled. The dewatering system will be decommissioned as the structures are completed and the backfill is placed to establish the final grade. Detailed descriptions of the hydrogeologic conditions are presented in Section 2.4.12.

Prior to initiating dewatering activities, preparations must be made to receive the water discharged from the excavation. Effluent from the dewatering system will be routed through a storm water pond which will be used during plant operation as the detention pond for the plant storm runoff. Thus, it would be beneficial to construct this pond prior to excavation activities in order to use it as a collection area for the dewatering system.

The power block excavation is expected to fully penetrate the glacial soils and the upper weathered bedrock to expose the bearing surface. The depth of excavation in the vicinity of the NI will exceed depths of 60 ft (18.3 m) (from existing grades) through saturated granular deposits. Figure 2.5-137 and Figure 2.5-138 depict cross sections of the excavations in the NI area.

For the ESWEMS pump house and the ESWEMS Retention Pond, the excavation will extend from the current ground surface (about 680 ft (207 m) to at least elevation 640 ft (195 m)) and will terminate at the top of bedrock or well graded gravels, cobbles or shale depending upon the location. This excavation will extend through soils that are generally water bearing granular glacial deposits.

To facilitate quality construction methods in the NI and ESWEMS areas, the excavations should be performed in a dry condition with conventional construction equipment. Given the layout of these areas, a common dewatering system consisting of deep wells surrounding the excavations is designed to facilitate both excavation areas. These excavations can proceed as the dewatering takes place provided the dewatering system maintains the groundwater level below that of the excavations. As the excavation advances, a series of groundwater monitoring wells will be observed to verify the effectiveness of the dewatering system in reducing the groundwater level.

The dewatering system will consist of deep wells penetrating the glacial overburden soils down to the top of the bedrock. The radius of influence of dewatering wells for the NI and the ESWEMS could extend out more than 3,000 ft (915 m) with anticipated drawdown of 20 ft (6.1 m) to 30 ft (9.1 m) being experienced some distance away from the wells if no flow barrier is utilized. This would incur a large impact on the nearby wetlands, flow in Walker Run, and potentially affect (and possibly dry up) any nearby domestic or commercial water wells within the radius of influence of the dewatering activity. Some of the nearby wetlands would most likely dry up as

well. To avoid these negative impacts, a flow barrier, such as a soil-bentonite slurry wall, will be implemented around the NI and ESWEMS excavation. This will reduce the drawdown effect of the dewatering wells, since the wells would be located within the limits of the flow barrier. The flow barrier would be installed by keying it into the underlying bedrock. The minimum design permeability of the flow barrier is 1×10^{-7} cm/s (3×10^{-10} ft/s) with an approximate thickness of 3 ft (0.9 m).

Approximately 30 deep wells will be required to maintain a dry condition at the bottom of the excavation. If a build-up of groundwater occurs on the north side of the NI excavation or extreme levels of seepage are encountered, additional pumping wells can be integrated into the system.

There is potential for some water seepage through the bedrock in the bottom of the excavation. Trenches and ditches will be required in the bottom of the excavation to direct any up flow through the rock away from the center of the excavation to the perimeter ditches. Sumps and pumps will be utilized to remove this water from the excavation.

The water removed from the excavation is likely suitable for reuse as dust control, soil compaction, and concrete mixing based on the available water quality information. Chemical testing of the water will be required if it is to be used for concrete mixing. The existing monitoring wells within the NI and ESWEMS excavation limits should be utilized to monitor the effectiveness of the flow barrier. Additional monitoring wells will be installed to provide adequate monitoring on all four sides of the excavation. The monitoring program should include recording water levels on both the inside and outside of the flow barrier.

2.5.4.6.2 ANALYSIS AND INTERPRETATION OF SEEPAGE

Analysis of the groundwater conditions at the site is described in Section 2.4.12. A groundwater model, based on information currently available, has been prepared for the overall groundwater conditions at the site and is addressed in detail in Section 2.4.12.

2.5.4.6.3 PERMEABILITY TESTING

Evaluation of permeability of the site soils was performed with lab testing of Shelby-tube samples obtained in shallow soils above the Glacial Overburden aquifer. Slug and pumping tests were performed on screened monitoring wells. A detailed description of the tests and results are provided in Section 2.4.12.

2.5.4.6.4 HISTORY OF GROUNDWATER FLUCTUATIONS

A detailed discussion of the groundwater conditions is provided in Section 2.4.12.}

2.5.4.7 Response of Soil and Rock to Dynamic Loading

The U.S. EPR FSAR includes the following COL Item in Section 2.5.4.7:

The COL applicant will address site-specific response of soil and rock to dynamic loading, including the determination of strain-dependent modulus-reduction and hysteretic damping properties.

This COL Item is addressed as follows:

{The Safe Shutdown Earthquake (SSE) spectra and its specific location at a free ground surface reflect the seismic hazard in terms of Probabilistic Seismic Hazard Analysis (PSHA) and geologic characteristics of the site and represent the site-specific ground motion response spectrum. These spectra would be expected to be modified as appropriate to develop ground motion for design considerations. Detailed descriptions on response of site soils and rocks to dynamic loading are addressed in Section 2.5.2.

Sections 2.5.4.7.1 through 2.5.4.7.6 are added as a supplement to the U.S. EPR FSAR.

2.5.4.7.1 SEISMIC HISTORY

The seismic history of the area and the site, including any prior history of seismicity, evidence of liquefaction or boils, is addressed in Sections 2.5.1.1 and 2.5.1.2.

2.5.4.7.2 FIELD DYNAMIC MEASUREMENTS

The following techniques were used to measure field dynamic properties:

- P-S suspension logging surveys in 4 borings ranging in depth from about 200 to 400 ft (60 to 120 m) below ground surface, including overburden soil and rock.
- Downhole seismic velocity surveys in 4 borings ranging in depth from about 200 to 400 ft (60 to 120 m) below ground surface, including overburden soil and rock.
- Seismic refraction surveys were performed along 6 profile lines.
- Geophysical testing borehole locations are shown on Figure 2.5-106. The results for each of the tests are shown in Figure 2.5-121 through Figure 2.5-124.

Data obtained from borehole survey techniques were integrated for development of the site velocity profiles. Each borehole velocity profile was evaluated and compared against the stratigraphic logging and laboratory test data of borehole samples to correlate velocities with soil and rock types by elevation and corresponding depth below ground surface. After each individual borehole velocity data set was evaluated, borehole profiles were grouped based on site-specific location and were compiled using a common reference point (elevation or depth below ground surface).

2.5.4.7.3 DYNAMIC LABORATORY TESTING

Dynamic testing, consisting of RCTS and FF tests, to obtain data on shear modulus and damping characteristics of rocks, is described by Section 2.5.4.2.3.2.4.

2.5.4.7.4 RECOMMENDED SOIL PROFILE

The Uniform Hazard Spectra (UHS) described in Section 2.5.2 are defined on hard rock, which is located 300 to 350 ft (91 to 107 m) below the ground surface at the BBNPP site. This location was confirmed with shear wave velocity measurements above the 9200 ft/sec (2800 m/sec) threshold. To determine the dynamic motion at the ground surface, it was necessary to adjust the UHS for amplification or de-amplification as the vibratory ground motion propagated through the rock and soil media. The adjustment was made by conducting Site Response Analyses following Approach 2B described in NUREG-6728 (NRC, 2001). These analyses consist of defining the shear wave velocity and material damping characteristics in the soil and rock profile

between the ground surface and the depth of hard rock, and then conducting site response studies using a one-dimensional, equivalent linear computer code: SHAKE (Schnabel, 1972).

The NI foundation material is the Mahantango Formation which has a shear-wave velocity of approximately 6,800 ft/sec (2070 m/sec). Consequently, the site amplification to define the GMRS for the BBNPP Site is computed at the top of the Mahantango Formation layer. For the NI, the GMRS corresponds to its FIRS.

The Subsurface Investigation at the BBNPP site included extensive Boring and Geophysical Exploration Programs. The field data available are divided into three sets:

1. Shear-wave velocities,
2. Compressional wave velocities, and
3. Layer thickness.

Six seismic refraction lines were concentrated near the center of the NI Reactor Building. The spatial variability of geotechnical properties along the site was investigated through the boring program, the point geophysical measurements (P-S Suspension and Downhole), and the surface measurements (Refraction). The stratigraphy, layer notation and layer thickness are taken from the geotechnical boring logs. The results from the geophysical investigations are provided in Section 2.5.4.2.2.2.3.

The following steps have been used to develop the best estimate of the compression and shear-wave velocity profiles for the BBNPP site:

- The P-S Suspension Logging Data from B-301 is more reliable since the borehole remained uncased and this is the preferred configuration for the methodology, thus suspension logging data from G-301 is discarded at any depth where data from B-301 is available;
- Downhole data is more representative of the elastic properties under the frequency range imposed by seismic ground motion. A higher weight (at least 60 to 65 percent) is given to the downhole data in the measurements closer to the surface;
- As readings get deeper, the P-S Suspension data becomes more reliable since it does not depend on interpretation as much as the downhole data does. Since P-S Suspension data is consistently higher, the shear wave velocity is taken as the average of both methods;
- Closer to the surface, the only P-S Suspension Data available is from borehole G-301. At B-301, there was metal casing left at the hole to support the overburden soils and downhole readings with metal casing are not reliable. The most reliable data within the overburden soils is the one from the downhole and P-S Suspension Tests at G-301;
- Lower bound and upper bound estimates are determined by analyzing the spread in the data through a standard deviation. The standard deviation is obtained by grouping readings from similar formations;

- The best estimate is built using the results from the field tests along with engineering judgment and general knowledge gathered from the field conditions and the borehole conditions.
- Damping is established based on lower bound of rock dynamic testing results.
- Due to liquefaction concerns, overburden soils will be replaced by either engineered soil fills or concrete fills.
- A 7 percent to 17 percent Coefficient of Variation is used to provide an estimate of the upper and lower bound. The actual lower and upper bound used for the Soil Structure Interaction Analysis will be a product of the randomization process of the Site Amplification Analysis. The COV is determined by analyzing the spread in data from the mean and the standard deviation.

Dynamic Parameters of Concrete Fill

A concrete fill is placed between the foundation mat of the NI and the top of rock. The dynamic properties of the fill are determined as follows:

- Match the shear modulus of the concrete to the best estimate of the underlying rock;
- Back calculate the shear modulus and elastic modulus with the use of equations from elasticity;
- Back calculate the compressive strength of concrete (f'_c , ACI-318 (ACI, 1992))

The shear wave velocity assigned to the concrete fill is 7240 fps (2200 m/s), the unit weight is 150 pcf (23.6 kN/m³), and the Poisson Ratio is 0.2. These parameters are indicated by Table 2.5-51.

Fill and Backfill Dynamic Parameters

Table 2.5-51 provides the dynamic properties assigned to the fill and backfill materials. These properties are not used for the calculation of the GMRS for the NI. When the GMRS are determined as free-field outcrop motions on the uppermost in-situ competent material, only the effects of the materials below this elevation are included in the site response analysis. Therefore, the engineered fill around the structure is not accounted for.

Compliant base

Regulatory Guide 1.208 (NRC, 2007b) defines "Hard Rock" as materials with a shear-wave velocity of 9,200 ft/sec (2,800 m/sec) or higher. Site amplification models need to include the soil and soft rock materials down to a rock formation with a minimum shear-wave velocity of 9,200 ft/sec (2,800 m/sec). The BBNPP Subsurface Exploration Program (Figure 2.5-106) included deep borings with depths of 400 ft (122 m). At depths of about 300 ft (91 m), the geophysical measurements consistently provided measurements in the excess of 9200 ft/sec (2800 m/sec). For the NI amplification model, the base of the foundation is placed 36 ft (11 ft) below grade. The grade elevation is raised 8 ft (2.4 m) due to flooding levels and the compliant base is placed at a distance of 240 ft (73 m) below the position of the foundation mat.

Strain Dependant and Linear Properties

Resonant Column, Torsional Shear, Combined Resonant Column Torsional Shear, and Unconfined Resonant Column ("Free-Free") Laboratory Tests were performed on soil and rock samples. The complete set of results from these tests is reported in Section 2.5.4.2. To account for variations in shear-wave velocity across the site, 60 artificial profiles were generated. The procedures and methodologies to incorporate uncertainties of strain dependant properties are described in Section 2.5.2.5.1.3.

2.5.4.7.5 AMPLIFICATION FUNCTIONS

A site amplification analysis was performed to obtain the ground motion response parameters. Section 2.5.2.5.1 provides the amplification functions. Different amplification values are obtained at different elevations and at different locations throughout the power block footprint. The variation in elevation (depth) is due to the soil amplification phenomena related to the travel of vertically propagated seismic shear waves. The variation of the amplification values in location across the site is due to the variation of the depth to bedrock. This variation implies the existence of a different soil column that depends on the specific location of a given facility. Several cases were analyzed as part of a Foundation Input Response Spectra (FIRS) study. The resulting Peak Ground Acceleration (PGA) for these cases is provided by Table 2.5-52. The selection of earthquake coefficients for the analysis of lateral earth pressures, slope stability, and other small building facilities may be obtained from the FIRS analysis (Table 2.5-52).

2.5.4.7.6 ACCELERATION TIME HISTORY FOR SOIL-STRUCTURE INTERACTION ANALYSIS

A spectrum-compatible acceleration-time history was developed for use with the velocity profile described in Section 2.5.4.7.4. This acceleration-time history was chosen based on the probabilistic seismic hazard de-aggregation information described in Section 2.5.2.

The development of the single horizontal component spectrum-compatible time history is based on the mean 10⁻⁴ uniform hazard target spectrum described in Section 2.5.2. The spectrum compatible time history was developed for the frequency range of 100 Hz to 0.5 Hz.

Using the site-specific soil column extended to the ground surface including the amplification factor, and the performance-based hazard methodology utilized to develop the SSE (refer to Sections 2.5.2.5 and 2.5.2.6), a Ground Motion Response Spectra (GMRS) peak ground acceleration of 0.21g at the top of the Mahantango Formation was computed. These parameters apply to analysis of interaction of soils with structures. For reconciliation of site specific design parameters affecting the SSE analysis results, refer to Sections 3.7.1 and 3.7.2.}

2.5.4.8 Liquefaction Potential

The U.S. EPR FSAR includes the following COL Item in Section 2.5.4.8:

The COL applicant will address site-specific liquefaction potential. As stated in Section 2.5.2, the evaluation of liquefaction is performed for the seismic level of the site specific SSE.

This COL Item is addressed as follows:

{The potential for soil liquefaction at the Bell Bend Nuclear Power Plant site was evaluated following NRC Regulatory Guide 1.198 (NRC, 2003c). The soil properties and profiles utilized are those described in Section 2.5.4.2.

Section 2.5.4.8.1 and 2.5.4.8.2 are added as a supplement to the U.S. EPR FSAR.

2.5.4.8.1 REGULATORY GUIDE 1.198

Regulatory Guide 1.198, Procedures and Criteria for Assessing Seismic Soil Liquefaction at Nuclear Power Plant Sites, (NRC, 2003c) was used for the evaluation of the potential for soil liquefaction at the BBNPP site.

Under "Screening Techniques for Evaluation of Liquefaction Potential," NRC Regulatory Guide 1.198 (NRC, 2003c) lists the most commonly observed liquefiable soils as fluvial-alluvial deposits, eolian sands and silts, beach sands, reclaimed land, and uncompacted hydraulic fills. The liquefaction evaluation included all soils at the BBNPP site. NRC Regulatory Guide 1.198 (NRC, 2003c) indicates that clay to silt, silty clay to clayey sand, or silty gravel to clayey gravel soils can be considered potentially liquefiable. The geology at the BBNPP site includes glacial overburden soils that consist of wind deposited and glacial transported sands and boulders. These soils will not be used for foundation purposes and are classified as liquefiable due to the presence of loose sand pockets that returned extremely low blow counts. NRC Regulatory Guide 1.198 (NRC, 2003c) indicates that if the geologic site evaluation indicates the presence of potentially liquefiable soils, the resistance of these soils to liquefaction or significant strength loss to cyclic pore pressure generation should be evaluated. The liquefaction evaluation (Section 2.5.4.8.2) indicates that some zones at the BBNPP site are susceptible to liquefaction. Residual shear strength is not evaluated since these soils will be removed from the site and will not be used for the foundation of the facilities.

2.5.4.8.2 LIQUEFACTION ANALYSIS

The in-situ, overburden soils will not be directly used for the foundation of Safety Related Facilities. Even though recorded shear wave velocities were in the excess of 1000 fps (305 m/s), the liquefaction potential evaluation identified "pockets" or zones of loose sand with extremely low blow counts. These zones appear in the south side of the power block area, where the depth to rock is the largest.

Assessments of liquefaction for the BBNPP site were based on observations and conclusions from the filed investigation. The NI structures will be built on top of the Mahantango formation. Shallow foundations for other Category I and non-Category I Power Block structures are to be founded on concrete or structural fill.

Based on the information obtained during the investigations of the underlying soil encountered at the BBNPP site, an evaluation of the soil liquefaction potential was performed using the screening techniques proposed in the Regulatory Guide 1.198 (NRC, 2003c).

More than 500 samples of the 48 borings at different depths, from 7 ft to 405 ft (2 m to 123 m), were used in the evaluation.

The guidelines proposed by Youd (Youd, 2001) were followed in the evaluation. The factor of safety against liquefaction is determined by Equation 2.5.4-9

$$FS = \left(\frac{CRR_{7.5}}{CSR} \right) MSF \cdot K_{\sigma} \cdot K_{\alpha} \quad \text{Eq. 2.5.4-9}$$

- $CRR_{7.5}$ → Cyclic Resistance Ratio for a 7.5 Magnitude Earthquake,
 CSR → Cyclic Stress Ratio,
 MSF → Magnitude Scaling Factor for a different magnitude earthquake,
 K_{σ} → Confining Stress Correction Factor,
 K_{α} → Sloping Ground Correction Factor,

The CSR is provided by Equation 2.5.4-10

$$CSR = 0.65(a_{\max}) \left(\frac{\sigma_{vo}}{\sigma'_{vo}} \right) r_d \quad \text{Eq. 2.5.4-10}$$

- a_{\max} → Peak horizontal ground acceleration (0.25 g at BBNPP)
 σ_{vo} → Total vertical stress
 σ'_{vo} → Effective vertical stress
 r_d → Stress reduction coefficient (flexibility of soil profile)

The estimation of the Peak Ground Acceleration (PGA) should correspond to the maximum amplified acceleration at the point of the liquefaction assessment. For the purpose of the liquefaction evaluation, a PGA equal to 0.25 g is used. This value is obtained from the maximum amplified Ground Motion Response Spectra (GMRS). The GMRS PGA of 0.21 g (top of rock condition) and the maximum amplified value, obtained during the Foundation Input Response analysis of the south facilities (i.e., EWS Cooling Towers (3URB and 4URB) and Emergency Power Generating Building (34UBP) located south of the reactor building) is 0.24g. Refer to Section 2.5.2 for GMRS parameters.

Two criteria are applicable to evaluate the Cyclic Resistance Ratio (CRR):

1. Shear Wave Velocity Criterion
2. Standard Penetration Resistance

2.5.4.8.2.1 Shear Wave Velocity Criterion for Liquefaction Analysis

The Shear Wave Velocity criterion uses the shear wave velocity of the soils to provide a reasonable estimate of the CRR. Disadvantages of the shear wave velocity method are that no samples are extracted and that thin liquefiable layers may be undetected. Another disadvantage is that there is usually limited number of measurements at a site and a specific location with liquefaction potential might be left undetected.

The CRR is determined from Equation 2.5.4-11

$$\text{CRR} = a \left(\frac{V_{s1}}{100} \right)^2 + b \left(\frac{1}{V_{s1}^* - V_{s1}} - \frac{1}{V_{s1}^*} \right); V_{s1} = V_s \left(\frac{P_a}{\sigma'_{vo}} \right)^{0.25}; V_{s1} \leq V_{s1}^* \quad \text{Eq. 2.5.4-11}$$

- CRR → Cyclic Resistance Ratio,
a → Curve fitting parameter (0.022),
b → Curve fitting parameter (2.8),
 V_{s1} → Shear wave velocity with correction for overburden stress,
 V_{s1}^* → Limiting shear wave velocity,
 P_a → Atmospheric Pressure,
 σ'_{vo} → Effective vertical stress.

The limiting shear wave velocity varies between 656 fps (200 m/s) for soils with 35 percent fine content and 705 fps (215 m/s) for soils with fines content of 5 percent or less. A value of 690 fps (210 m/s) was used for the evaluation. The potential for liquefaction is analyzed by plotting the CRR against the corrected shear wave velocity and comparing against a curve that represents the onset of liquefaction (Youd, 2001). The plot is provided by Figure 2.5-140. The BBNPP data points are clearly away from the liquefaction zone. The minimum Factor of Safety against liquefaction is 1.7 and it is possible to conclude that, according to the shear wave velocity method, there is no potential for liquefaction at the site. However, as previously stated, one of the disadvantages of this methodology is the limited number of measurements and this is the case at the BBNPP site. Therefore, an SPT analysis approach is required.

2.5.4.8.2.2 SPT Criteria for Liquefaction Analysis

The SPT data was used to estimate liquefaction potential. The abundant amount of gravels and boulders encountered during the investigation may reduce the effectiveness of the SPT method. However, it is the best means to detect liquefiable sand pockets. With this method, the CRR is calculated as follows:

$$\text{CRR}_{7.5} = \frac{1}{32 - (N_1)_{60}} + \frac{(N_1)_{60}}{135} + \frac{50}{(10 \cdot (N_1)_{60} + 45)^2} - \frac{1}{200}; (N_1)_{60} < 30 \quad \text{Eq. 2.5.4-12}$$

where $(N_1)_{60}$ is the drill rod energy ratio divided by 60.

If $(N_1)_{60}$ is greater than 30, the soil is considered to be non-liquefiable. $(N_1)_{60}$ is calculated by dividing the drill rod energy ratio by 60. The lowest energy ratio recorded at the field from hammer calibration was 78 percent. This value is used to determine $(N_1)_{60}$ from the raw blow counts.

Figure 2.5-141 provides the results of the SPT liquefaction analysis. Each sample data point is categorized as liquefied, non-liquefied, or in the fringe of liquefaction. It is worth noting that some

instances registered zero blow counts, meaning that the weight of the hammer and the drilling rod was enough to penetrate the soil. These zones correspond to areas of wind deposited sands placed during the coldest period of the glacial event. Figure 2.5-141 provides a diagram of the location of the liquefiable zones. The depth of these zones is variable, ranging in depth from 10 ft (3 m) to 45 ft (14 m). The location of the loose sand pockets is shown in section view by Figure 2.5-108 through Figure 2.5-111.

Based on the SPT analysis, it is concluded that the "In-Situ" overburden soils at the BBNPP site are prone to liquefaction. Since the overburden soil was determined to be liquefiable using SPT data, the lack of CPT data is not an issue.

2.5.4.8.2.3 Liquefaction Analysis - Conclusion

Regardless of the high shear wave velocity of the Glacial Overburden, these soils will be removed from the site and will not be used in their natural condition for foundation or lateral support. The soils from this formation are candidates for engineered fill or backfill through enforcement of appropriate screening and compaction techniques.

Section 2.5.4.5 describes material specifications and compaction for structural fill and backfill. For foundation backfill, compaction will be done to 90 percent of Modified Proctor optimum dry density. For structural fill, a 95 percent Modified Proctor level will be set. The fill will be compacted to within 3 percent of its optimum moisture content.

Liquefaction in engineered fill is not an issue if the recommended compaction practices are followed. Liquefaction occurs in loose sands and/or silts with poor gradation. An engineered fill is a compacted and well graded soil structure. Compaction practices need to be monitored during construction.

Liquefaction of granular engineered fills will be prevented by assuring that the fill and backfill specifications are met during the implementation stages. Particular attention will be placed on the grain size and compaction requirements to ensure the specifications are fully met. Section 2.5.4.2.3 provides information related to the specifications for engineered soils. It is emphasized that the specification will include requirements for an on-site testing laboratory for quality control, especially material gradation and plasticity characteristics, the achievement of specified moisture-density criteria, fill placement/compaction, and other requirements to ensure that the fill operations conform to the earthwork specification for BBNPP.

2.5.4.9 Earthquake Site Characteristics

The U.S. EPR FSAR includes the following COL Item in Section 2.5.4.9:

Site-specific earthquake site characteristics will be described by the COL applicant.

This COL Item is addressed as follows:

{Section 2.5.2.6 describes the development of the Safe Shutdown Earthquake ground motion for the BBNPP site. The selected ground motion is based on the risk-consistent/performance-based approach of NRC Regulatory Guide 1.208, "A Performance-Based Approach to Define the Site-Specific Earthquake Ground Motion" (NRC, 2007b) with reference to NUREG/CR-6728 (NRC, 2001) and ASCE/SEI 43-05 (ASCE, 2005). Any deviation from the guidance provided in Regulatory Guide 1.208 is discussed in Section 2.5.2. Horizontal ground motion amplification

factors are developed in Section 2.5.2.5 using site-specific data and estimates of near-surface soil and rock properties presented in Sections 2.5.4.2, 2.5.4.4 and 2.5.4.7. These amplification factors are then used to scale the hard rock spectra, presented in Section 2.5.4.2, to develop Uniform Hazard Spectra (UHS), accounting for site-specific conditions using Approach 2B of NUREG/CR-6769 (NRC, 2002). Horizontal SSE spectra are developed from these soil UHS, using the performance-based approach of ASCE/SEI 43-05, accepted by Regulatory Guide 1.208. The Ground Motion Response Spectra (GMRS) is defined at the free ground surface of a hypothetical outcrop at the base of the foundation. Section 2.5.2.6 also describes vertical ground motion, which was developed by scaling the horizontal spectrum by a frequency-dependent vertical-to-horizontal (V:H) factor.}

2.5.4.10 Static Stability

{The area of planned BBNPP is graded to establish the final site elevation, which is to be at elevation 674 ft msl (205 m msl) at the center of the reactor building. The Reactor, Safeguard, and Fuel Buildings are seismic Category I structures and are supported on a common basemat. The common basemat has an irregular shape, estimated to be approximately 80,170 ft², (7450 m²) in plan. All Category I structures' size and depth ranges are summarized in Table 2.5-55.

Structure locations and designations are shown in Figure 2.5-106. Other major structures in the power block area are the Nuclear Auxiliary Building, RadWaste Building, and the Turbine Building, which are non-Category I structures.

Construction of the Nuclear Island basemat requires an excavation of about 39 ft (12 m) from the existing elevation of approximate elevation 667 ft (203 m) msl. No rebound (heave) in the ground due to the removal of the soils is expected at the Mahantango Formation. The Mahantango rock is extremely dense and was heavily consolidated by marine deposition. The removal of overburden soils will have no effect since the elastic modulus of the rock is very high.}

2.5.4.10.1 Bearing Capacity

The U.S. EPR FSAR includes the following COL Item in Section 2.5.4.10.1:

A COL applicant that references the U.S. EPR design certification will verify that site-specific foundation soils beneath the foundation basemats of Seismic Category I structures have the capacity to support the bearing pressure with a factor of safety of 3.0 under static conditions.

This COL Item is addressed as follows:

{The bearing capacity of the subsurface materials depends (1) on the properties of the foundation soils or rocks, including dimensions of bearing strata and geotechnical strength parameters, (2) on the geometry of the building foundations, (3) on the foundation depth, and (4) on the position of the water table, in case drained conditions are assumed for the calculations. Geotechnical properties and soil profiles are detailed in Section 2.5.4.2. The foundation depth and building geometry are provided in Section 2.5.4.3, and particularly in Table 2.5-55. The bearing capacity estimates for the Mahantango Formation are determined with the use of a rock mass equivalent cohesion and friction. The upper bound of the ultimate bearing capacity of structures placed on top of concrete is set at the compressive strength of concrete. If the bearing capacity of rock is higher than this threshold, then the concrete compressive strength is used as the recommended value. The bearing capacities from either concrete or bedrock are very high

and they conservatively exceed the minimum requirements established by the U.S. EPR FSAR. Section 2.5.4.10 details the methodologies used to obtain bearing capacity and settlement according to the reference documents. Table 5.0-1 of the U.S. EPR FSAR identifies the soil bearing capacity as a required parameter to be enveloped. It is defined as “Minimum bearing capacity (static) 22 ksf in localized areas at the bottom of the Nuclear Island basemat and 15 ksf on average across the total area of the bottom of the Nuclear Island basemat.” Accordingly, the Seismic Category I NI foundation is sized and reinforced to accommodate these bearing pressure values. Other facilities are placed directly on top of engineered backfill. In this case, the bearing capacity estimate is determined using drained conditions with a high water level at the elevation of the Probable Maximum Flood of 671 ft (205 m) msl.

The bearing capacity for the NI is estimated assuming that the foundation stratum is a homogenous layer with the properties of the Mahantango Formation. The backfill unit weight of 140 pcf (22.0 kN/m³) is used to calculate the embedment contribution to a depth of 36.0 ft (12 m). Other facilities have their foundation base resting on engineered backfill. A friction angle of 35° is assumed with no cohesion.

The ultimate (gross) bearing capacity is estimated by the Terzaghi theory (ASCE, 1994a) using the Vesic capacity factors (Vesic, 1975).

$$q_{ult} = cN_c s_c + \gamma' D_f N_q s_q + \frac{1}{2} \gamma B N_\gamma s_\gamma \quad \text{Eq. 2.5.4-13}$$

- c → Cohesion,
- γ' → Effective unit weight of soil,
- D_f → Depth to calculate effective overburden pressure at base of foundation,
- B → Width of foundation,
- N_c, N_q, N_γ → Bearing capacity factors (defined in Vesic, 1975),
- s_c, s_q, s_γ → Shape factors (defined in Vesic, 1975).

The subsurface conditions and material properties were described in Section 2.5.4.2. Material properties, conservatively designated for the various strata, were used for foundation evaluation, as shown by the recommended strength parameters shown on Table 2.5-46. A summary of the estimated allowable bearing pressures are presented in Table 2.5-57. A factor of safety of 3.0 was applied to obtain the allowable values.

Design values of foundation pressures for the other Category I structures were estimated based on project knowledge. For the BBNPP site-specific conditions, the calculated allowable bearing pressures for the NI meet the minimum 22 ksf and the average 15 ksf identified in the U.S. EPR FSAR. The site-specific foundation soils beneath the NI basemat and other safety class facilities have been verified to have the capacity to support the required bearing pressures with a Factor of Safety of 3.0 under static conditions and a Factor of Safety of 2.0 under dynamic conditions.}

2.5.4.10.2 Settlement

The U.S. EPR FSAR includes the following COL Item in Section 2.5.4.10.2:

A COL applicant that references the U.S. EPR design certification will verify that the differential settlement value of ½ inch per 50 ft in any direction across the foundation basemat of a Seismic Category I structure is not exceeded. Settlement values larger than this may be demonstrated acceptable by performing additional site specific evaluations.

This COL Item is addressed in the following section and in Section 3.8.5.

{The safety-related Category I facilities at the BBNPP site will bear either on top of the Mahantango Formation or on top of concrete or engineered soil fill, which in turn bears directly on top of the bedrock. The overburden deposits will not be used for foundation purposes as these have an inherent risk for liquefaction. Elastic short term settlements will occur in either the Mahantango formation or the concrete or engineered fill.

SETTLEMENT ESTIMATION BY SIMPLIFIED METHODS

Three of the ASCE (ASCE, 1994b) recommended methods of analysis were used to estimate settlements:

1. Improved Janbu Approximation - Provides an average estimate of the settlement beneath the foundation. Settlement is estimated using Eq. 2.5.4-14.

$$\rho_i = \mu_o \cdot \mu_1 \cdot \frac{q \cdot B}{E_s^*} \quad \text{Eq. 2.5.4-14}$$

ρ_i	→	Settlement,
μ_o	→	Embedment adjustment coefficient,
μ_1	→	Shape Adjustment Coefficient,
q	→	Service pressure load,
B	→	Foundation width,
E_s^*	→	Equivalent Young's Modulus.

2. Perloff Approximation - Provides settlement at both center and edge of the foundation. This methodology is useful to analyze differential displacements. Settlement is estimated using Eq. 2.5.4-15.

$$\rho_i = I \cdot q \cdot B \left(\frac{1 - \nu^2}{E_s} \right) \quad \text{Eq. 2.5.4-15}$$

ρ_i	→	Settlement,
I	→	Stress influence factor at either depth or edge of foundation
q	→	Service pressure load,
B	→	Foundation width,
ν	→	Poisson Ratio,
E_s	→	Young's Modulus.

3. Kay and Cavagnaro Approach - This approach can adapt to layers of variable elastic properties, and provides settlements at both center and edge of the foundation. It is based on these same principles, as reflected in Eq. 2.5.4-15.

Settlement estimates utilizing the three simplified methods above have been calculated for each of the facilities listed in Table 2.5-58. The adopted elastic modulus is the lesser of that recommended for the Mahantango Formation or the one recommended for the engineered fill. This recommendation is provided by Table 2.5-49. Table 2.5-58 provides the settlement estimates at the site, obtained from the three noted methodologies. Overall, the results indicate very limited to no settlement for the NI and the safety related structures. The load used for the calculation is a U.S. EPR FSAR recommended service pressure of 14 ksf (670 kPa). A more detailed analysis methodology was performed to estimate settlements. The procedure and results are provided by the following section.

SETTLEMENT ESTIMATES FOR THE NI FROM DETAILED ANALYSIS

A detailed analysis was used to evaluate the foundation mat displacements and rotations for the NI Buildings due to potential elastic settlements of the subgrade soils. The loads assigned are different for each area of the NI, according to the [specifications described in the U.S. EPR FSAR. Section 2.5.4.10 details the methodologies used to obtain bearing capacity and settlement according to the reference documents. The calculations are performed assuming a 10 ft (3 m) concrete layer over a 200 ft (61 m) compressible layer with the properties of the Mahantango Formation. The methodology utilized here quantifies the settlements, foundation mat displacements and rotation associated with the proposed site specific subsurface profile.

The first part of the evaluation estimates elastic settlements due to the total construction loads of the Nuclear Island Buildings: Reactor (UJA), Fuel Building (UFA) and four Safeguard Buildings (UJH).

The settlement analysis performs the calculations for two cases: (1) assuming a rigid foundation and (2) a flexible foundation (i.e., the foundation mat which imposes the loads to the foundation medium has no stiffness). The first assumption is more representative of the real conditions. Settlements that are reported correspond to the top of the firm incompressible layer beneath the rock formation (interface between the foundation mat and the sub-laying soft rock) for the rigid

foundation case. In the second part of the evaluation, the surface settlements are used to compute equivalent Winkler springs representing the deformation characteristics of the subsurface.

The Winkler springs are incorporated into a three-dimensional structural finite element analysis which assumes a rigid foundation mat for each of the buildings included in the analysis. This analysis uses applied loads on the foundation and calculates the foundation mat deformations. Because the settlements estimated in the first step and, consequently, the equivalent springs vary over the foundation area (soft springs at locations of large settlements and stiff springs at locations of small settlements), the structural analysis redistributes the applied loads on the foundation mat consistent with the stiffness of the mat relative to the subsurface. For example, the elastic settlements are larger near the centers of the loaded disks. Consequently, the soil springs near the center are softer than those at locations closer to the outer edge of the mat, assuming that the mat carries uniformly distributed load. Consistent with this distribution, the structural analysis redistributes the applied loads away from the center of the disks.

In an iterative procedure, the bearing pressures resulting from the structural analysis are used to recalculate the elastic settlements and the corresponding soil springs, and the structural analysis is repeated until a satisfactory agreement is obtained for average settlements.

Surface loads are applied as uniformly loaded flexible disks and the resulting stresses in the soil medium are calculated using an axisymmetric analysis. At-depth stresses are calculated for each of the profile points where settlement is desired due to each of the loaded disks, consistent with the locations of the profile points relative to the center of the disks. The stresses from each of the disks are then superimposed to compute the stresses due to the entire loaded foundation. The at-depth stresses are updated each time the cumulative load is specified.

The analysis uses a three dimensional finite element model representing the soil-structure system. The model considers a rigid plate element for the Nuclear Island base mat. The foundation medium is represented by supports with stiffness of the Winkler Soil Springs. Calculations are performed using computer codes specifically designed to calculate soil settlements (Dapset), and structural response (SAP). Dapset and SAP have been subjected to the verification and validation procedures stipulated in Rizzo's Quality Assurance Manual. Computer software control for Dapset and SAP has been done according to Rizzo's Quality Assurance Manual. The loads used in the analysis are shown in Figure 2.5-142.

Immediate elastic settlements resulting from the applied loads at different locations across the Nuclear Island are presented in Figure 2.5-143. The differential settlement value of 0.5 in (1.3 cm) in 50 ft (15.2 m) in any direction across the basemat of a Seismic Category I structure is not exceeded.

As a result of a different load distribution among the buildings of the Nuclear Island (the Fuel Building has a bigger load than the Safeguard Buildings 2 and 3) the north-south direction of the [foundation mat presents a slight differential settlement that can be considered as negligible for practical purposes. No considerable differential settlement was observed on the east-west direction since the applied loads are practically symmetrical. As shown in Table 2.5-59, the maximum differential settlement in 50 ft (15.2 m) in any direction across the basemat is less than 0.1 in (0.3 cm).

SETTLEMENT ANALYSIS CONCLUSIONS

Displacements will be immediate during and after construction of civil works. Differential settlements estimated using simplified methodologies, as opposed to the detailed analyses described in the previous section, are less than 0.1 in (0.3 cm) in 50 ft (15.2 m) in any direction across the basemat.

Settlements will take place concurrent with construction and these will have taken place prior to placing the equipment, piping, and the final finishes. Hence, post-construction total and differential settlements are expected to be lower than the values noted herein, particularly after accounting for foundation mat rigidity.

The detailed analysis yields lower settlement values since it considers a more realistic distribution load and accounts for the true stress distribution through the subsurface. The results from the detailed analysis are reported in Table 2.5-59. This table provides the best estimate for settlement at the NI.

Settlements are within tolerable thresholds and all foundations will be able to safely tolerate the anticipated total and differential settlements. Additionally, engineering measures are incorporated into design for control of differential movements between adjacent structures, piping, and appurtenances sensitive to movement, consistent with settlement estimates. This includes the development and implementation of a monitoring plan that supplies and requires evaluation of information throughout construction and post-construction on ground heave, settlement, pore water pressure, foundation pressure, building tilt, and other necessary data. This information provides a basis for comparison with design conditions and for projections of future performance.

Analysis indicates favorable conditions for total and differential settling. In order to monitor and verify settling, the BBNPP major structure foundations will be monitored for any settling movement during and after construction.

2.5.4.10.2.1 EARTH PRESSURES

Static and seismic lateral earth pressures are addressed for plant below-ground walls. Seismic earth pressure diagrams are structure-specific and are, therefore, only addressed generically herein. Specific earth pressure diagrams are developed for specific structures based upon each structure's final configuration. Passive earth pressures are not addressed; they are ignored for conservatism for general purpose applications. Fill and backfill will be granular, compacted soils formed by sand/gravel mixtures. Typical values of the friction angle for these types of fills are in excess of 38 degrees (Carter, 1991). A friction angle is conservatively selected. Structural backfill material is verified to meet the design requirements prior to use during construction. }

2.5.4.10.2.1.1 STATIC LATERAL EARTH PRESSURES

]

The static active earth pressure, p_{AS} , is estimated using the following expression:

$$p = K \cdot \gamma \cdot z \quad \text{Eq. 2.5.4-16}$$

- p → Active (p_a), Passive (p_p), or At Rest (p_o) Pressure,
 K → Active (K_a), Passive (K_p), or At Rest (K_o) Pressure Coefficient as defined by Section 2.5.4.5.6.
 γ → Unit weight of backfill (140 pcf),
 z → Depth below ground surface.

2.5.4.10.2.1.2 DYNAMIC EARTH PRESSURES

The following symbols apply:

- P_{ae} → Dynamic active earth force,
- P_{pe} → Dynamic passive earth force,
- K_{ae} → Dynamic active earth pressure coefficient,
- K_{pe} → Dynamic passive earth pressure coefficient,
- k_h → Horizontal earthquake acceleration (0.25 g based on FIRS analysis, Section 2.5.4.7.5; the 0.25 g is selected as the best estimate of the range between the 0.21 g value at the top of rock and the 0.30 g value at the ground surface)
- k_v → Vertical earthquake acceleration (0.18 g based on FIRS analysis, Section 2.5.4.7.5; the 0.25 g is selected as the best estimate of the range between the 0.18 g value at the top of rock and the 0.33 g value at the ground surface)
- γ_{sat} → Saturated Unit Weight,
- γ' → Effective Unit Weight,
- F_r → Resultant force associated with dynamic soil pressure distribution,
- M_r → Resultant overturning moment about base of retaining structure,
- H → Embedment Height,
- α_h → Horizontal earthquake acceleration (g),
- ν → Poisson's ratio,
- C_v, D_v → Empirical Coefficients as a function of Poisson's ratio.

The active/passive earth force on a wall (cohesionless and dry backfill) is estimated as follows:

$$P_{ae} = \frac{1}{2} \gamma K_{ae} H^2 (1 - k_v) \quad ; \quad P_{pe} = \frac{1}{2} \gamma K_{pe} H^2 (1 - k_v) \quad \text{Eq. 2.5.4-17}$$

The total active/passive thrust, P_{ae} , can be divided into a static component, P_a , and a dynamic component, ΔP_{ae} :

$$P_{ae} = P_a + \Delta P_{ae} \quad ; \quad P_{pe} = P_a + \Delta P_{pe} \quad \text{Eq. 2.5-18}$$

The static component is known to act at $H/3$ above the base of the wall. Seed and Whitman (Seed, 1970) recommended that the dynamic component be taken to act at approximately $0.6H$. On this basis, the total active thrust will act at a height given by:

$$h = \frac{P_a H / 3 + \Delta P_{ae} (0.6H)}{P_{ae}} \quad \text{Eq. 2.5.4-19}$$

When there is no significant structure-structure interaction, a conservative estimate of dynamic soil pressures may be obtained from a parabolic distribution with a maximum value at a height of 60 to 70 percent of the total fill height (ASCE, 1998). The corresponding resultant force and overturning moment may be obtained by Eq. 2.5.4-20.

$$\begin{aligned} F_r &= \alpha_h C_v \gamma H^2 \\ M_r &= \alpha_h D_v \gamma H^3 \end{aligned} \quad \text{Eq. 2.5.4-20}$$

2.5.4.10.2.1.3 SAMPLE EARTH PRESSURE DIAGRAMS

Using the relationship outlined above and assumed backfill properties, sample earth pressures were estimated. Sample earth pressure diagrams are provided in Figure 2.5-145 for a wall height of 40 ft (12.2 m), level ground surface, and, for conservative purposes, with groundwater level at 3.3 ft (1 m) below the surface. The backfill is a granular soil, with an angle of friction of 35 degrees and a unit weight of 140 pcf (22.4 kN/m³). The horizontal ground acceleration is taken as 0.25g, which is the PGA at elevation 666 ft (203 m). The validity of assumptions regarding surcharge loads, backfill properties, and structural configurations is confirmed during the detailed design stage. Actual earth pressure evaluations are performed at that time for the design of below-grade walls, based on actual project conditions. The results of these earth pressure evaluations shall be included in an update to this FSAR at that time.

2.5.4.10.2.1.4 SELECTED DESIGN PARAMETERS

The field and laboratory test results are discussed in Section 2.5.4.2. The parameters employed for the bearing capacity, settlement, and earth pressure evaluations are based on the material characterization addressed in Section 2.5.4.2. Normal Groundwater Elevation is approximately 15 ft (4.6 m) below grade. A value of 3.0 is commonly used as the factor of safety when determining the bearing capacity of soils. An angle of shearing resistance of 35 degrees was used for characterization of a structural backfill for earth pressure evaluations, which is considered conservative for granular fill compacted to 90 percent Modified Proctor compaction.

2.5.4.10.2.1.5 EARTH PRESSURE COEFFICIENTS

Active, passive, and at-rest lateral earth pressure coefficients, K_A , K_P , and K_O , respectively, were estimated assuming frictionless vertical walls and horizontal backfill by the following relationships:

Active Earth Pressure Coefficient:

$$K_a = \tan^2 \left(45 - \frac{\phi'}{2} \right) \quad \text{Eq. 2.5.4-4}$$

Passive Earth Pressure Coefficient:

$$K_p = \tan^2 \left(45 + \frac{\phi'}{2} \right) \quad \text{Eq. 2.5.4-5}$$

At-Rest Earth Pressure Coefficient:

The At-Rest Earth pressure coefficient depends mainly on the deposition process of the formation, and its subsequent stress history. Its value is between the active and passive earth pressure coefficients and there are documented relationships to estimate its value, for example:

$$\text{General Application (Bowles, 1996), } K_o = 1 - \sin \phi$$

Eq. 2.5.4-6

In order to account for compaction effects on engineered fills, the Passive Earth Pressure Coefficient is modified with Equation 2.5.4-10 (Bowles, 1996).

$$K_{oc} = K_o (5.8\sin(\phi') - 2.1)$$

Eq. 2.5.4-7

Dynamic Active and Passive Earth Pressure Coefficient:

The Dynamic Active and Passive Earth Pressure Coefficients are determined with the use of the Mononobe-Okabe theory. For a vertical wall and a horizontal grade the theory provides Equations 2.5.4-8(a) through 2.5.4-8(c) .

$$K_{ae} = \frac{\cos^2(\phi - \theta)}{\cos\theta\cos(\delta + \theta)\left(1 + \sqrt{\frac{\sin(\phi + \delta)\sin(\phi - \theta)}{\cos(\delta + \theta)}}\right)^2} \quad \text{Eq. 2.5.4-8 (a)}$$

$$K_{pe} = \frac{\cos^2(\phi - \theta)}{\cos\theta\cos(\delta + \theta)\left(1 - \sqrt{\frac{\sin(\phi + \delta)\sin(\phi - \theta)}{\cos(\delta + \theta)}}\right)^2} \quad \text{Eq. 2.5.4-8 (b)}$$

$$\theta = a \tan\left(\frac{F_h}{F_v}\right) = \frac{k_h}{1 \pm k_v} \quad \text{Eq. 2.5.4-8 (c)}$$

Where:

- K_{ae} → Dynamic active earth pressure coefficient,
- K_{pe} → Dynamic passive earth pressure coefficient,
- θ → Angle of resultant of seismic load,
- ϕ → Friction angle (Drained conditions),
- δ → Friction between wall and soil ($\delta = 2\phi/3$ (Das, 1993)),
- F_h → Horizontal earthquake force,
- F_v → Vertical earthquake force,
- k_h → Horizontal earthquake acceleration (0.25 g)
- k_v → Vertical earthquake acceleration (0.25 g),

Based on the previous equations, Table 2.5-56 provides the recommended earth pressure coefficients .}

2.5.4.10.3 Uniformity and Variability of Foundation Support Media

The U.S. EPR FSAR includes the following COL Item in Section 2.5.4.10.3:

A COL applicant that references the U.S. EPR design certification will investigate and determine the uniformity of the underlying layers of site specific soil conditions beneath the foundation basemats. The classification of uniformity or non-uniformity will be established by a geotechnical engineer.

These COL Item is addressed as follows:

{Three criteria are identified in the U.S. EPR FSAR for establishing uniformity in foundation support media, namely, 1) presence of soil and rock, 2) dip angle of soil layers, and 3) shear wave velocity. Each is addressed below:

1. Foundations of all Seismic Category I structures at the BBNPP site are supported on either compacted structural fill or concrete fill which is in turn supported on bedrock. Bedrock at the site is at a depth of 12.5 ft (3.8 m) to 62.0 ft (18.9 m) below ground surface. Regardless of the variable depth to bedrock, as depicted by Figure 2.5-115, non-uniform foundation conditions resulting from combined soil-rock support are not applicable to foundations at the BBNPP site. Each of the Seismic Category 1 structures will be founded either on top of rock, on top of concrete fill, or on top of engineered fill.

2. Detailed subsurface information is presented in Section 2.5.4.2. Stratigraphic profiles (presented in Figure 2.5-108 through Figure 2.5-111 of the referenced section) indicate that there is only one stratigraphic line and it corresponds to the boundary between the overburden and the Mahantango formation. In the direction of maximum gradient (approximately 30 degrees with respect to the North), this boundary presents a dipping angle of approximately seven to eight degrees. Figure 2.5-115 shows the inclination of the top surface of the Mahantango Formation. It is still applicable to assume a horizontal layered model for both Site Amplification and Soil Structure Interaction Analyses, and therefore uniform conditions are considered. Section 2.5.4.10.3, of the U.S. EPR Final Safety Analysis Report reads: "If the dip is less than or equal to 20 degrees, the layer is defined as horizontal and analyses using horizontal layers are applicable." In addition, the concrete above the Mahantango formation will have a matching shear wave velocity and therefore the sloping effects will be mitigated. On this basis, the soil layers at the BBNPP site are considered horizontal.

3. Classification of uniformity (or non-uniformity) in foundation support media resides with the geotechnical engineer, per the U.S. EPR FSAR. Shear wave velocity (V_s) measurements are used for this determination because they are a) in-situ measurements reflecting the natural ground conditions and b) important input to the safety evaluation of structures such as in soil-structure interaction and seismic analyses.

The V_s values were evaluated to a depth of approximately 350 ft (107 m) below the Nuclear Island (NI) foundation basemat, corresponding to El. 280 ft msl (85 m msl). The 350 ft (107 m) value was selected based on the three U.S. EPR FSAR criteria of: 1) 1.5 times an equivalent radius of foundation basemat, 2) 1.0 times the maximum foundation basemat dimension, or 3) no less than 200 ft below the bottom of the foundation basemat; with criterion (2) selected as the governing condition for the BBNPP NI basemat for its greater dimension. It is noted that minor appendages and protrusions in the irregularly-shaped U.S. EPR NI foundation were ignored in selecting this depth.

Detailed V_s data are presented in Section 2.5.4.2.2, along an evaluation of the shear wave velocity conditions. Figure 2.5-121 through Figure 2.5-124 present the plots for compressional and shear wave velocities. The plots provide the results from the two different surveys performed: downhole test, and PS-Suspension Logging. Overburden soils will not be used for foundation purposes and therefore an analysis of the variation of the shear wave velocity is only applicable for the Mahantango formation.

The recommended shear wave velocity profile under the Nuclear Island is plotted by Figure 2.5-135. The shear wave velocity shows an increasing trend, directly related to depth or confining pressure. Therefore, as shown by the figure, the Mahantango formation was subdivided in sub-layers to depict the vertical variation of the shear wave velocity. The minimum value of 6800 fps (2075 m/s) was presented at the uppermost zone in the boundary with the overburden. In a distance of about 350 ft (107 m) the shear wave velocity increases up to 9600 fps (2930 m/s). At each sub-layer the Coefficient of Variation (COV) originated from different readings at different locations and with different methodologies is close to 10% and not exceeding 15%. This relatively low COV is mainly due to the homogeneity of the Mahantango formation. Variation only exists in the vertical direction and this was accounted for in the site amplification analysis by the layer subdivision of this formation. Therefore, they have been accounted for in developing the site-specific horizontal and vertical ground motion response spectra (GMRS) shown in Figure 2.5-65. The GMRS are defined at the foundation level for the U.S. EPR Nuclear Island (NI). Therefore, the GMRS coincide with the FIRS for the NI. There are no significant variations of the shear wave velocity in the horizontal directions.}

2.5.4.10.4 Site Investigation for Uniform Sites

No departures or supplements.

2.5.4.10.5 Site Investigation for Non-uniform Sites

No departures or supplements.

2.5.4.11 Design Criteria

No departures or supplements.

2.5.4.12 Techniques to Improve Subsurface Conditions

The U.S. EPR FSAR includes the following COL Items in Section 2.5.4.12:

Techniques used for improving subsurface conditions are site specific and will be addressed by the COL applicant.

This COL Item is addressed as follows:

{Major structures will derive support from the Mahantango Formation or concrete or engineered structural fills. Ground improvement will be limited to excavation of unsuitable soils, such as liquefiable sands. No in-situ soils in their natural state will be used for foundation or lateral support purposes. Foundation soils will include proof-rolling of foundation subgrade for the purpose of identifying any unsuitable soils for further excavation and replacement, which further densifies the upper portions of the subgrade. In absence of subsurface conditions at the site that

require ground improvement, ground control, that is, maintaining the integrity of existing dense or stiff foundation soils, will be the primary focus of earthworks during foundation preparation. These measures will include such steps as groundwater control, use of appropriate measures and equipment for excavation and compaction, subgrade protection, and other similar measures.

2.5.4.13 References

This section is added as a supplement to the U.S. EPR FSAR.

AASHTO, 1998. Load and Resistance Factor Design (LRFD) Bridge Design Specifications, Second Edition, American Association of State Highway and Transportation Officials, 1998.

ACI, 1992. Manual of Concrete Practices, ACI-318, American Concrete Institute, 1992.

ASCE, 1998. Seismic Analysis of Safety-Related Nuclear Structures, ASCE 4-98, American Society of Civil Engineers, 1998.

ASCE, 1994a. Bearing Capacity of Soils, Technical Engineering and Design Guide, American Society of Civil Engineers, 1994.

ASCE, 1994b. Settlement Analysis, Technical Engineering and Design Guide, American Society of Civil Engineers, 1994.

ASCE, 2005. Seismic Design Criteria for Structures, Systems, and Components in Nuclear Facilities, ASCE/SEI 43-05, American Society for Civil Engineers/Structural Engineering Institute, 2005.

ASTM, 1999. Standard Test Method for Penetration Test and Split-Barrel Sampling of Soils, ASTM D1586-99, American Society for Testing and Materials, 1999.

ASTM, 2000a. Standard Practices for Preserving and Transporting Soil Samples, ASTM D4220-95(2000), American Society for Testing and Materials, 2000.

ASTM, 2000b. Standard Practice for Thin-Walled Tube Sampling of Soils for Geotechnical Purposes, ASTM D1587-00, American Society for Testing and Materials, 2000.

ASTM, 2000c. Standard Test Method Prebored Pressuremeter Testing in Soils, ASTM D4719-00, American Society for Testing and Materials, 2000.

ASTM, 2002a. Standard Test Method for Particle Size Analysis of Soils, ASTM D422-63 (reapproved 2002), American Society for Testing and Materials, 2002.

ASTM, 2003. Standard Test Methods for Measurement of Hydraulic Conductivity of Saturated Porous Materials Using a Flexible Wall Permeameter, ASTM D5084-03, American Society for Testing and Materials, 2003.

ASTM, 2004a. Standard Test Method for Compressive Strength and Elastic Moduli of Intact Rock Core Specimens under Varying States of Stress and Temperatures, ASTM D7012-04, American Society for Testing and Materials, 2004.

ASTM, 2004b. Standard Practice for Determining the Normalized Penetration Resistance of Sands for Evaluation of Liquefaction Potential, ASTM D6066-96(2004), American Society for Testing and Materials, 2004.

ASTM, 2005a. Standard Test Method for Energy Measurement for Dynamic Penetrometers, ASTM D4633-05, American Society for Testing and Materials, 2005.

ASTM, 2005b. Standard Test Method for Specific Gravity and Absorption of Rock for Erosion Control, ASTM D6473-99(2005), American Society for Testing and Materials, 2005.

ASTM, 2005c. Standard Test Method for Laboratory Determination of Water (Moisture) Content of Soil and Rock by Mass, ASTM D2216-05, American Society for Testing and Materials, 2005.

ASTM, 2005d. Standard Test Method for Standard Guide for Using Rock Mass Classification Systems for Engineering Purposes, ASTM D5878-05, American Society for Testing and Materials, 2005.

ASTM, 2006a. Standard Test Method for Classification of Soils for Engineering Purposes (Unified Soil Classification System), ASTM D2487-06, American Society for Testing and Materials, 2006.

ASTM, 2006b. Test Method for Specific Gravity of Soil Solids by Water Pycnometer, ASTM D854-06, American Society for Testing and Materials, 2006.

ASTM, 2006c. Standard Practice for Description and Identification of Soils (Visual-Manual Procedure), ASTM D2488-06, American Society for Testing and Materials, 2006.

ASTM, 2006d. Standard Test Methods for Amount of Material in Soils Finer than No. 200 (75- μ m) Sieve, ASTM D1140-00(2006), American Society for Testing and Materials, 2006.

ASTM, 2006e. Standard Practice for Rock Core Drilling and Sampling of Rock for Site Investigation, ASTM D2113-06, American Society for Testing and Materials, 2006.

ASTM, 2006f. Standard Practices for Preserving and Transporting Rock Core Samples, ASTM D5079-02(2006), American Society for Testing and Materials, 2006.

Bieniawski, 1989. Engineering Rock Mass Classifications, Wiley Interscience, Z.T. Bieniawski, 1989.

Carter, 1991. Correlations of Soil Properties, Pentech Press Limited, M. Carter and S.P Bentley, 1991.

Bowles, 1996. Foundation Analysis and Design, 5th Edition, McGraw-Hill Book Company, J. Bowles, 1966.

Dobrin, 1976, Introduction to Geophysical Prospecting, McGraw Hill, Inc., M.B. Dobrin, 1976.

NRC, 2001. Technical Basis for Revision of Regulatory Guidance on Design Ground Motion: Hazard- and Risk- Consistent Ground Motion Spectra Guidelines, NUREG/CR 6728, Nuclear Regulatory Commission, 2001.

NRC, 2002. Technical Basis for Revision of Regulatory Guidance on Design Ground Motion: Development of Hazard- and Risk- Consistent Seismic Spectra for Two Sites, NUREG/CR 6769, Nuclear Regulatory Commission, 2002.

NRC, 2003a. Site Investigations for Foundations of Nuclear Power Plants, Regulatory Guide 1.132, Nuclear Regulatory Commission, 2003

NRC, 2003b. Laboratory Investigations of Soils for Engineering Analysis and Design of Nuclear Power Plants, Regulatory Guide 1.138, Revision 2, Nuclear Regulatory Commission, 2003.

NRC, 2003c. Procedures and Criteria for Assessing Seismic Soil Liquefaction at Nuclear Power Plant Sites, Regulatory Guide 1.198, Nuclear Regulatory Commission, 2003.

NRC, 2007a. Combined License Applications for Nuclear Power Plants (LWR Edition), Regulatory Guide 1.206, Nuclear Regulatory Commission, 2006.

NRC, 2007b. A performance-Based Approach to Define the Site-Specific Earthquake Ground Motion, Regulatory Guide 1.208, Nuclear Regulatory Commission, 2007.

Peck, 1967. Soil Mechanics in Engineering Practice, 2nd edition, Wiley & Sons, R.B. Peck & K. Terzaghi, 1967.

Peck, 1974. Foundation Engineering, 2nd edition, Wiley & Sons, R. B. Peck, 1974.

PPL, 2004. Susquehanna Steam Electric Station, Units 1 and 2, Final Safety Analysis Report, Pennsylvania Power & Light Company, 2004.

Schnabel, 1972. SHAKE, A Computer Program for Earthquake Response Analysis Of Horizontally Layered Site, B. Schnabel, J. Lysmer and H.B. Seed, 1972.

Seed, 1970. Design of Earth Retaining Structures for Dynamic Loads, ASCE Specialty Conference on Lateral Stresses and Earth Retaining Structures, H.B. Seed and R.V. Whitman, June 1970.

Terzaghi, 1996. Soil Mechanics in Engineering Practice, 3rd Edition, John Wiley and Sons Inc., Terzaghi, 1996

UT, 2004a. PBRCTS-1, Revision 4, Technical Procedures for Resonant Column and Torsional Shear (RCTS) Testing of Soil and Rock Samples, Department of Civil Engineering, University of Texas, Austin, Texas, August 2004.

UT, 2004b. URC-1, Revision 4, Technical Procedures for URC Tests, Department of Civil Engineering, University of Texas, Austin, Texas, August 2004.

Vesic, 1975. Foundation Engineering Handbook, Winterkorn and Fang, A.S. Vesic, 1975.

Vucetic, 1991. Effect of Soils Plasticity on Cyclic Response, Journal of Geotechnical Engineering, ASCE 117 (1), M. Vucetic and R. Dobry, 1991.

Weston, 2008. Final Report on Seismic Refraction Survey, Seismic Refraction Surveys For the Bell Bend Site Characterization, Weston Geophysical Corporation, 2008.

Youd, 2001. Liquefaction Resistance of Soils: Summary Report from the 1996 NCEER and 1998 NCEER/NSF Workshops on Evaluation of Liquefaction Resistance of Soils, Journal of Geotechnical and Geoenvironmental Engineering, T.L. Youd, M. Idriss, R.D. Andrus, I. Arango, G. Castro, J.T. Christian, R. Dobry, W.D. Finn, L.F. Harder Jr., M.E. Hynes, K. Ishihara, J.P. Koester, S.S. Liao, W.F. Marcuson III, G.R. Martin, J.K. Mitchell, Y. Moriwaki, M.S. Power, P.K. Robertson, R.B. See, and K.H. Stokoe II, October 2001.

2.5.5 STABILITY OF SLOPES

The U.S. EPR FSAR includes the following COL Item for Section 2.5.5:

A COL applicant that references the U.S. EPR design certification will evaluate site-specific information concerning the stability of earth and rock slopes, both natural and manmade (e.g., cuts, fill, embankments, dams, etc.), of which failure could adversely affect the safety of the plant.

This COL Item is addressed as follows:

This section addresses the stability of constructed and natural slopes. It was prepared based on the guidance in relevant Section of NRC Regulatory Guide 1.206, "Combined License Applications for Nuclear Power Plants (LWR Edition)," (NRC, 2007). Constructed slopes evolve as part of the overall site development.

{The site of the Bell Bend Nuclear Power Plant (BBNPP) is comprised of generally flat topography in the vicinity of the primary structures and components. The site is planned to be graded in order to establish the final grade for the project, resulting in minor cuts and fills, as well as slopes. The stability of these slopes and their potential impact on safety-related structures are evaluated herein. In the vicinity of the primary structures and components there are no significant natural slopes at the site or any steep slopes, undergoing continuous erosion. There is a nine degree slope on the North side of the power block, which is analyzed for stability and the results are reported in this section.

2.5.5.1 Slope Characteristics

The characteristics of constructed and natural slopes are described below.

2.5.5.1.1 Characteristics of Constructed Slopes

Site grading areas for the BBNPP will include the structures in the power block, switchyard, cooling towers, and Essential Service Water Emergency Makeup System (ESWEMS) Pumphouse Building and Retention Pond. The power block includes the Reactor Building, Fuel Building, Safeguards Building, Emergency Power Generation Building, Nuclear Auxiliary Building, Access Building, Radioactive Waste Building, and Turbine Building. The centerline of the BBNPP power block is planned to be graded to approximately elevation 674 ft (205.4 m) msl. The finished grade in the area of each major structure will be approximately:

- Power block: Elevation 674 ft (205.4 m) msl
- Switchyard: Elevation 680 ft (207.3 m) msl
- Cooling Tower: Elevation 753 ft (229.5 m) msl
- ESWEMS: Elevation 674 ft (205.4 m) msl

Locations of these structures are shown in Figure 2.5-145.

2.5.5.1.1.1 Temporary Slopes

The site grading will require the excavation of the natural overburden soils, with a current estimated maximum depth of 61 ft (18.6 m) and an average of 40 ft (12.2 m). The natural

overburden soils are inadequate for the foundation of large safety related facilities. These will be replaced by granular backfill formed with screen glacial and alluvial soils from either on-site or off-site sources. As discussed in Section 2.5.4, Category 1 Granular Structural Fills and Backfills will be provided by Bowers Construction (Bowers) from Berwick, PA. The proposed borrow site is located approximately 4,200 ft (1,280 m) southwest of the site at the intersection of Rockaway Street and Salem Boulevard (Route 11), Berwick, PA. Oversight of Bowers' operations was performed while collecting soil samples from two identified test pits (Test Pit # 5 and Test Pit Face). The soil samples were transported to laboratory testing facilities for grain size, compaction, and dynamic resonant column torsional shear testing. The results of these tests are discussed in Section 2.5.4. The cut/fill operations will not result in permanent slopes in and around the power block area.

Temporary construction slopes will be constructed in cuts with a minimum 1.5:1 (horizontal to vertical) slope. The maximum possible height will be limited to approximately 40 ft (12.2 m), from the surface to the position of horizontal benches or to the top of the Manhantago Formation. The overburden soil classifications are discussed in Section 2.5.4 and a representation depicting the classifications is shown in Figure 2.5-106.

2.5.5.1.1.2 Permanent Slopes

The only permanent slopes will be the slopes of the ESWEMS Retention Pond. The design of the retention pond is addressed in Section 2.4 and Section 9.2.5 of the BBNPP FSAR. Based on the findings of the drilling program, the ground surface elevations near the retention pond center are 691.6 ft (210.8 m) near the north slope and 671.2 ft (204.6 m) near the south slope. The proposed finished grade is 674.0 ft (205.4 m). The excavation line and resulting pond side surface will have a 3:1 (horizontal to vertical) slope. The depth of the excavation is 22.0 ft (6.7 m) down to elevation 652.0 ft (198.7 m). The ESWEMS Pumphouse will be supported on concrete fill on top of the Mahantango bedrock. The stability of the ESWEMS Pumphouse Building is not affected by the adjacent slopes and its presence does not affect the stability of adjacent slopes.

2.5.5.1.2 Characteristics of Natural Slopes

The finish grade elevation along the center line of the Power Block is 674 ft (205.4m) msl. Within the area of the Power Block area the natural grade changes elevation by less than 3 ft (1 m) over distances of approximately 1000 ft (305 m). The same variation extends to the ESWEMS Retention Pond. Overall, the natural grade has variation of one percent. There are no natural slope instability concerns in the plant vicinity. A very mild elevation increase exists on the North side of the Power Block area. This increase forms a slope with an angle of approximately nine degrees. Figure 2.5-146 presents the shape and extent of this slope and the subsurface materials beneath it. Section 2.5.5.2 provides the slope stability analysis results.

2.5.5.1.3 Exploration Program and Geotechnical Conditions

The geotechnical exploration program, groundwater conditions, sampling, materials and properties, liquefaction potential, and other geotechnical parameters are addressed in Section 2.5.4. A summary relevant to the slope stability evaluation is presented below.

A geotechnical subsurface investigation was performed to characterize the upper 400 ft (122 m) of soil and rock materials. The site geology is comprised of glacial soil deposits underlain by the Mahantango formation (bedrock), which is, on average 38.9 ft (11.9 m) below the ground surface and was present down to the bottom of the deepest boring.

As explained in Section 2.5.4, the subsurface is divided into the following stratigraphic units:

Overburden Soil: - Glacial Till

Bedrock: - Mahantango Formation

Figure 2.5-106 provides a general geologic column profile. Overall, the subsurface conditions encountered throughout the site are uniform, in both depth and area extension. The thickness of the glacial till varies from 12.5 to 63.5 ft (3.8 to 19.4 m). In general, the till consists of consolidated brown silty sand or sand containing gravel and large rounded cobbles and boulders. The presence of the boulders increases with depth.

The overburden soil is not an adequate foundation strata for safety related structures or facilities that will impose high contact pressures. In the South side of the Power Block area, beneath borings B-313, B-314, B-315, B-316, B-317, B-320, B-321, B-322, and B-323, the glacial till has pockets of loose saturated sands that are susceptible to liquefaction. Figure 2.5-106 provides the locations of these borings.

The overburden soils will be removed in the power block area. No permanent slopes will be implemented except for the slopes of the ESWEMS Retention Pond. At the ESWEMS Pond, the lack of cohesion of the in-situ soils will result in sloughing failures of the ESWEMS Pond slopes with a high probability of erosion. These soils will be replaced with a cohesive fill. The slopes of the ESWEMS will be protected from erosion to avoid soil debris falling into the pond and diminishing the design retention capacity.

The depth of the groundwater table at the site varies from 0 ft (0 m) to 10 ft (3 m) depending on location. On average, the groundwater depth is 4 ft (1.2) to 6 ft (1.8 m) below the ground surface. Since the plant grade is placed at elevation 674.0 ft (205.4 m) msl, the slope stability analysis of the ESWEMS Retention Pond slopes is governed by the forces imposed by the pond water level.

Temporary slopes will be developed under dry conditions within a dewatered zone.

2.5.5.2 Design Criteria and Analysis

The stability of constructed slopes was assessed using limit equilibrium methods, which generally consider moment or force equilibrium of a potential sliding mass by discretizing the mass into vertical slices. This approach results in a Factor of Safety (FOS) that can be defined as (Duncan, 2005) :

$$\text{FOS} = \frac{\text{Shear Strength of Soil}}{\text{Shear Stress Required for Equilibrium}} \quad (\text{Eq. 2.5.5-1})$$

Factor of Safety is defined as the ratio of the available strength of the cross section versus the forces placed upon it, such as water or seismic force. A Factor of Safety greater than one indicates that the available strength is greater than the stresses being placed upon the cross section and implies that under these particular circumstances there should be no measureable damage or permanent displacements of the cross section.

Various limit equilibrium methods are available for slope stability evaluation, including the Ordinary method (Fellenius, 1936), Bishop's simplified method (Bishop, 1955), Janbu's simplified

method (Janbu, 1968), and the Morgenstern-Price method (Morgenstern, 1965), among others. These methods were selected for evaluation of slopes for they are routinely used, and their limitations, and advantages, are well documented. The main differences are:

1. Equations of statics that are included and satisfied.
2. Interslice forces that are included in the analysis.
3. Assumed relationship between the interslice shear and normal forces.

The Ordinary (Fellenius, 1936) method is one of the earliest methods developed. It ignores all interslice forces and satisfies only moment equilibrium. Both Bishop's (Bishop, 1955) simplified method and Janbu's (Janbu, 1968) simplified method include the interslice normal force, E , but ignore the interslice shear force. Bishop's (Bishop, 1955) and Janbu's (Janbu, 1968) simplified methods satisfy only moment equilibrium and horizontal force equilibrium, respectively.

The slope stability analysis is performed using the latest version of Computer Program GSTABL7 with STEDwin (Gregory 2003). This program was originally developed by Purdue University for the Indiana State Highway Commission in 1986 and later revised and marketed by Geotechnical Engineering Software Company. The program calculates the factor of safety against slope failure utilizing a two-dimensional limit equilibrium method. The calculation of the factor of safety against slope instability is performed using the Simplified Bishop method of slices, which is applicable to circular shaped failure surfaces, or the Simplified Janbu method of slices, which is applicable to failure surfaces of a general shape. GSTABL7 may incorporate up to 20 soil options with nonlinear undrained shear strength parameters, isotropic or anisotropic soils, and fiber reinforcement. Stabilizing structures such as piles, tiebacks, or nails may also be considered. None of these stabilizing options are required at the BBNPP site and isotropic soils are used in the analysis.

Dynamic analysis of the slopes can be performed using a pseudo-static approach, which represents the effects of seismic shaking by accelerations that create inertial forces. These forces act in the horizontal and vertical directions at the centroid of each slice, and are defined as:

$$F_h = (a_h / g)W = k_h W \quad (\text{Eq. 2.5.5-2})$$

$$F_v = (a_v / g)W = k_v W \quad (\text{Eq. 2.5.5-3})$$

Where a_h and a_v are horizontal and vertical ground accelerations, respectively, W is the slice weight, and g is the gravitational acceleration constant. The inertial effect is specified by k_h and k_v coefficients, based on site seismic considerations.

Typical minimum acceptable values of FOS are 1.5 for normal long-term loading conditions and 1.0 to 1.2 for infrequent loading conditions (Duncan, 2005), e.g., during earthquakes.

2.5.5.2.1 Stability of Constructed Slopes

The ESWEMS Retention Pond at the BBNPP will be constructed primarily via excavation of overburden soils and replacement of soils with cohesive fill material. The cohesive fill material will compose the entirety of the earthen embankment sides of the ESWEMS Retention Pond.

The excavation will cut in part through the overburden soil layer. The soil profile was verified with seven borings placed directly within the area near and surrounding the ESWEMS Retention Pond. The location of the borings (B-331, B-332, B-333, B-334, B-341, B-342, and B-343) is shown in Figure 2.5-106. Four separate sections are analyzed to represent the various design differences of slopes for the ESWEMS Retention Pond. These sections are shown in Figure 2.5-147. These sections represent the elevations on each side of the rectangular ESWEMS Pond. The overall design and elevations are similar. They will be composed primarily of cohesive fill in place of the overburden present on-site. The embankment sides will be built up to the ESWEMS Pumphouse Building grade at elevation 674.5 ft (205.6 m).

The ESWEMS Retention Pond is constructed by excavation from grade, therefore there is no downstream slope of significance to require a stability analysis. The upstream sections govern the analysis.

The analyses are performed for steady state loading conditions as well as earthquake loading conditions. The total stress strength parameters of the soils provided in Section 2.5.4 are utilized in the analyses.

Both circular and wedge analyses are performed on the cross sections. The circular failure analysis uses the Simplified Bishop Method. Wedge analysis utilizes the Simplified Janbu method.

For the ESWEMS Retention Pond, the phreatic surface is defined as the boundary between the saturated and unsaturated zones in the cross sectional profile. Normally, Casagrande's solution for seepage through an earthen dam can be used to calculate the expected phreatic surface (Das, 2002). Under the conditions presented for the ESWEMS Retention Pond there is no significant downstream slope thereby making Casagrande's equation and approach to determining the phreatic surface non-applicable to this situation. Instead engineering judgment was substituted to visually approximate a conservative phreatic surface for the cross section. The phreatic surface is conservative for a gradual drop in water surface from elevation 670 ft (204.2 m) (the normal water level) as it passes through the slope. The phreatic surface is shown in Figure 2.5-147, noted as the normal pool water level on the cross sections.

The Safe Shutdown Earthquake (SSE) load consists of horizontal and vertical seismic loads applied pseudo-statically to the model. Using data derived from a Foundation Input Response Spectra (FIRS), a peak horizontal seismic acceleration was found to be $a_h = 0.28g$ and a peak vertical ground acceleration $a_v = 0.30g$. The higher of the two, $a_v = 0.30g$, is used in the analysis. Total stress parameters for the soil properties are used for the earthquake loading analysis. The seismic coefficients are considered to be half of the peak ground acceleration according to the Hynes-Griffin and Franklin model (Abramson, 2001) resulting in $k_h = 0.14g$ and $k_v = 0.15g$. The method of analysis and data are presented in Section 2.5.2.

In order to find the worst case slope failure, the program GSTABL7 allows the calculation of numerous iterations and provides the corresponding location and Factor of Safety of the worst case scenario. The worst case is the location exhibiting the lowest Factor of Safety.

The slope stability analyses results are summarized in Table 2.5-60 and the critical failure surfaces are shown in Figure 2.5-147. The static case analysis indicate that the BBNPP ESWEMS Retention Pond side slopes have Factor of Safety values ranging from 4.4 to 9.2 depending upon the slope configuration and analysis method. The Factor of Safety under dynamic conditions is between 2.0 and 4.1. Therefore it can be stated that the current design is safe.

The North Side Slope critical failure surfaces are shown by Figure 2.5-146. The Factors of Safety provided by Table 2.5-60 (1.6 dynamic and 5.7 static) indicate that this slope does not represent a threat to the integrity of the facilities in the power block area.

At the BBNPP site, there are no dams or embankments, for which adverse conditions such as high water levels attributable to the Probable Maximum Flood (PMF), sudden drawdown, or steady seepage at various levels may occur.

The slope stability analysis at the ESWEMS site was done with the phreatic surface at elevation 670 ft (204.2 m), compared to the PMF level of 671 ft (204.5 m). Earthquake loading was incorporated without modifying the water level of 670 ft (204.2 m). As such, the unlikely event of simultaneous flooding and an earthquake is considered to be adequately addressed in the analysis.

2.5.5.2.2 Stability of Temporary Fill Slopes

Temporary cut and fill slopes will exist in dry conditions during construction. The slope stability analyses are performed for the sections shown by Figure 2.5-148. Results are summarized in Table 2.5-60 and the critical failure surfaces are shown in the sections of Figure 2.5-148. Analysis for temporary construction slopes is performed for the static condition. The Factor of Safety is 1.3 for minor, close to the surface planes.

2.5.5.2.3 Concluding Remarks

Based on analyses provided in this Section, it is concluded that the constructed and natural slopes at the site are sufficiently stable and present no failure potential that would adversely affect the safety of the proposed BBNPP.

2.5.5.3 Logs of Borings

Logs of borings, and associated references, are provided in Part 11 of the COLA.

2.5.5.4 Compacted Fill

Compacted fill, and associated references, are addressed in Section 2.5.4.5.

2.5.5.5 References

Abramson, 2001. Slope Stability and Stabilization Methods, Second Edition, Wiley and Sons, L.W. Abramson, et al., 2001.

Bishop, 1955, The Use of Slip Surface Circle in Stability Analysis of Slopes, Geotechnique Volume 5, Number 1, pp. 7-17, A.W. Bishop, 1955.

Das, 2002. Principles of Geotechnical Engineering, Fifth Edition, Brooks/Cole, B. Das, 2002.

Duncan, 2005. Soil Strength and Slope Stability, Wiley and Sons, J.M. Duncan and S.G. Wright, 2005.

Fellenius, 1936, Calculation of the Stability of Earth Dams, Proceedings of the Second Congress of Large Dams, Volume 4, pp. 445-463, 1936.

Gregory, 2003. GSTABL7 with STEDwin: Slope Stability Analysis System Program Manual, G.H. Gregory, 2003.

Janbu, 1968. Slope Stability Computations, Soil Mechanics and Foundation Engineering, The Technical University of Norway, N. Janbu, 1968.

Morgenstern, 1965. The Analysis of the Stability of General Slip Surfaces, Geotechnique, Volume 15, pp. 79-93, N.R. Morgenstern and V.E. Price, 1965.

NRC, 2007. Combined License Applications For Nuclear Power Plants (LWR Edition), Regulatory Guide 1.206, U.S. Nuclear Regulatory Commission, 2007.}

2.5.6 REFERENCES

No departures or supplements.

Table 2.5-1 {USGS Earthquake Catalog for the CEUS with $m_b \geq 3.0$ }

(Page 1 of 65)

m_b	Longitude (degree)	Latitude (degree)	Depth (km)	Year	Month	Day	Hour	Minute	Second	Catalog Reference
6.3	-70.1	47.7	0	1534	1	1	0	0	0	DNAG
6.5	-71.8	44.4	0	1638	6	11	19	0	0	Ebel
7	-70.1	47.6	0	1663	2	5	22	30	0	Ebel
3.5	-71.5	42.5	0	1668	12	19	0	0	0	Ebel
3.5	-70.8	42.8	0	1685	2	18	21	0	0	Ebel
3	-70.8	42	0	1697	2	20	11	15	0	Ebel
3.3	-73.5	41.4	0	1702	1	1	0	0	0	NCEER
3.3	-71.1	42.4	0	1705	6	27	0	0	0	NCEER
5.1	-70.6	42.8	0	1727	11	10	3	40	0	NCEER
3.3	-70.6	42.8	0	1728	5	16	0	0	0	NCEER
3.3	-70.6	42.8	0	1728	7	30	15	0	0	NCEER
3.5	-70.6	42.8	0	1729	2	10	14	0	0	NCEER
3.3	-70.6	42.8	0	1729	3	30	19	0	0	NCEER
3.3	-73.5	41.4	0	1729	8	6	0	0	0	NCEER
3.3	-70.6	42.8	0	1729	9	19	20	30	0	NCEER
3.3	-70.6	42.8	0	1729	10	10	21	30	0	NCEER
3.3	-70.6	42.8	0	1729	11	25	13	0	0	NCEER
3.3	-70.6	42.8	0	1730	2	20	1	0	0	NCEER
3.3	-70.6	42.8	0	1730	4	24	1	0	0	NCEER
3.3	-70.6	42.8	0	1730	12	7	1	20	0	NCEER
3.3	-70.6	42.8	0	1731	1	13	0	0	0	NCEER
3.3	-70.6	42.8	0	1731	7	16	10	0	0	NCEER
3.3	-70.6	42.8	0	1731	10	13	4	0	0	NCEER
3.3	-70.6	42.8	0	1732	2	19	0	0	0	NCEER
5.8	-73.6	45.5	0	1732	9	16	16	0	0	NCEER
3.3	-70.6	42.8	0	1734	11	23	5	0	0	NCEER
3.3	-70.6	42.8	0	1736	2	13	22	45	0	NCEER
3.3	-70.6	42.8	0	1736	10	12	6	30	0	NCEER
3.3	-70.6	42.8	0	1736	11	23	7	0	0	NCEER
3.3	-71	42.4	0	1737	2	17	21	30	0	NCEER
3.3	-70.6	42.8	0	1737	9	20	15	20	0	NCEER
5.2	-74	40.8	0	1737	12	19	3	45	0	NCEER
3.3	-70.6	42.8	0	1739	8	13	7	30	0	NCEER
3.3	-70.6	42.8	0	1741	2	5	20	50	0	NCEER
3.3	-71.2	46.8	0	1744	5	27	0	0	0	NCEER
4.6	-70.9	42.5	0	1744	6	14	15	15	0	NCEER
3.6	-76.3	40	0	1752	12	17	23	30	0	SRA
5.8	-70.3	42.7	0	1755	11	18	9	12	0	NCEER
3.3	-71.1	42.3	0	1757	7	8	19	15	0	NCEER
3.5	-76.5	38.9	0	1758	4	25	2	30	0	NCEER
3.3	-71	42.35	0	1759	2	2	7	0	0	NCEER
4.3	-71	42.5	0	1761	3	12	7	15	0	NCEER
3.3	-71.5	43.1	0	1761	11	2	1	0	0	NCEER
3.5	-66	45.3	0	1764	9	30	0	0	0	NCEER
3.3	-70.3	43.7	0	1766	1	23	10	0	0	NCEER

Table 2.5-1 {USGS Earthquake Catalog for the CEUS with $m_b \geq 3.0$ }

(Page 2 of 65)

m_b	Longitude (degree)	Latitude (degree)	Depth (km)	Year	Month	Day	Hour	Minute	Second	Catalog Reference
3.3	-70.77	43.07	0	1766	3	2	8	0	0	NCEER
3.3	-70.8	43.1	0	1766	12	17	11	48	0	NCEER
3.3	-70.3	43.7	0	1769	10	19	0	0	0	NCEER
4.6	-77.4	37.2	0	1774	2	21	19	0	0	NCEER
3.3	-78.8	37.7	0	1775	3	16	19	15	0	NCEER
4	-82	39.9	0	1776	1	1	0	0	0	NCEER
3.3	-83	35.2	0	1776	11	5	0	0	0	NCEER
3.3	-84	36	0	1777	11	16	7	0	0	NCEER
3.8	-87.2	30.4	0	1780	2	6	0	0	0	NCEER
3.3	-70.9	42.5	0	1780	11	29	0	0	0	NCEER
4.9	-74.5	41	0	1783	11	30	3	50	0	NCEER
3.3	-71.2	46.8	0	1784	1	2	10	0	0	NCEER
3.3	-78.8	37.7	0	1791	1	13	9	0	0	NCEER
3.3	-77.5	37.5	0	1791	1	15	10	0	0	NCEER
4.5	-72.4	41.5	0	1791	5	16	13	22	0	NCEER
6	-70.5	47.4	0	1791	12	6	20	0	0	NCEER
3.3	-72.5	41.5	0	1792	8	29	3	0	0	NCEER
3.3	-72.5	41.5	0	1794	3	6	19	0	0	NCEER
3.4	-89.9	39	0	1795	1	8	9	0	0	NCEER
4	-79	42.9	0	1796	12	26	11	0	0	NCEER
4.4	-80	32.9	0	1799	4	11	8	20	0	NCEER
3.9	-76.39	40.12	0	1800	11	20	5	0	0	NCEER
3.3	-72.3	43.7	0	1800	12	20	0	0	0	NCEER
3.3	-71.1	41.9	0	1800	12	25	0	0	0	NCEER
3.3	-70.8	43.1	0	1801	3	1	20	30	0	NCEER
3.5	-79.1	37.4	0	1802	8	23	10	0	0	NCEER
3.3	-70.9	42.5	0	1803	1	18	14	50	0	NCEER
4.4	-87.8	42	0	1804	8	20	20	10	0	USHIS
4.2	-89	42	0	1804	8	24	20	10	0	NCEER
3.3	-70.9	42.5	0	1805	4	25	0	0	0	NCEER
3.3	-69	44.5	0	1805	6	12	12	30	0	NCEER
3.3	-72.5	41.5	0	1805	12	30	11	0	0	NCEER
3.3	-71.1	43	0	1807	1	14	4	0	0	NCEER
3.5	-79.1	37.4	0	1807	5	1	9	0	0	NCEER
3.3	-70.5	43.5	0	1807	5	6	18	0	0	NCEER
3.5	-69	44.4	0	1808	6	26	2	50	0	NCEER
3.9	-70.9	43	0	1810	11	10	2	15	0	NCEER
3.3	-80.2	36.1	0	1811	11	27	8	0	0	NCEER
3.3	-77.4	37.6	0	1812	2	2	9	30	0	NCEER
7.4	-89.6	36.5	0	1812	2	7	9	45	0	NCEER ¹
3.3	-77.5	37.5	0	1812	4	22	4	0	0	NCEER
4	-70.3	43.7	0	1814	11	29	0	14	0	NCEER
3	-89.5	36.6	0	1816	7	25	15	0	0	NCEER
5.2	-73.6	45.5	0	1816	9	9	0	0	0	NCEER
5	-80	32.9	0	1817	1	8	9	0	0	USHIS

Table 2.5-1 {USGS Earthquake Catalog for the CEUS with $m_b \geq 3.0$ }

(Page 3 of 65)

m_b	Longitude (degree)	Latitude (degree)	Depth (km)	Year	Month	Day	Hour	Minute	Second	Catalog Reference
4.7	-67.2	45	0	1817	5	22	20	0	0	NCEER
4.2	-71.2	42.5	0	1817	10	5	16	45	0	NCEER
3.1	-84.5	38.5	0	1817	12	11	0	0	0	NCEER
3	-90.2	38.6	0	1818	4	11	20	0	0	NCEER
3.3	-71.2	46.9	0	1818	10	11	0	0	0	NCEER
3.3	-76.5	44	0	1818	12	7	0	0	0	NCEER
3.4	-89.7	37.7	0	1819	9	2	8	0	0	NCEER
3.1	-89.8	38.1	0	1819	9	17	4	0	0	NCEER
3	-89.5	36.6	0	1820	1	1	0	0	0	NCEER
3.3	-79.3	33.4	0	1820	9	3	8	30	0	NCEER
3.4	-89.5	37.3	0	1820	11	9	22	0	0	NCEER
3.8	-68.8	44.8	0	1821	5	5	12	30	0	NCEER
3.3	-70	43.9	0	1823	3	7	15	0	0	NCEER
3.5	-68.8	44.8	0	1823	6	10	17	0	0	NCEER
3.8	-70.6	42.9	0	1823	7	23	11	55	0	NCEER
3.5	-66.5	46.5	0	1824	7	9	0	0	0	NCEER
4.1	-80.5	39.7	0	1824	7	15	16	20	0	NCEER
3.3	-81.56	30.08	0	1826	2	26	14	0	0	NCEER
3.3	-81.2	36.1	0	1827	5	11	0	0	0	NCEER
4.8	-87.5	38	0	1827	7	5	11	30	0	NCEER
4.8	-88	38	0	1827	8	7	4	30	0	NCEER
4	-85.8	38.3	0	1827	8	7	7	0	0	NCEER
3.3	-72.1	41.4	0	1827	8	23	0	0	0	NCEER
4.8	-80	37	0	1828	3	9	0	0	0	NCEER
3.3	-70	43.9	0	1828	7	25	11	0	0	NCEER
3.3	-69.8	44.2	0	1829	8	27	21	45	0	NCEER
5.2	-70.5	47.3	0	1831	5	8	0	0	0	NCEER
5	-70.1	47.6	0	1831	7	14	0	0	0	NCEER
4	-85.6	42.3	0	1833	2	4	0	0	0	NCEER
3.3	-70.17	47.65	0	1833	3	1	0	0	0	NCEER
3.3	-70.2	47.7	0	1833	4	1	0	0	0	NCEER
4.6	-78	37.7	0	1833	8	27	11	0	0	NCEER
3.8	-76.14	39.85	0	1834	2	5	22	30	0	NCEER
3.4	-86	38	0	1834	11	20	19	40	0	NCEER
3.1	-81.7	41.5	0	1836	7	9	2	15	0	NCEER
3.3	-70.9	42.5	0	1837	1	15	7	0	0	NCEER
3.5	-72.7	41.7	0	1837	4	12	0	0	0	NCEER
5	-88	38.5	0	1838	6	9	14	45	0	NCEER
3.1	-83.8	38.6	0	1839	9	5	0	0	0	NCEER
3.7	-75	43	0	1840	1	16	20	0	0	NCEER
3.7	-72.9	41.5	0	1840	8	9	20	30	0	NCEER
4	-79.85	43.2	0	1840	9	10	0	0	0	NCEER
3.3	-74.25	40.79	0	1841	1	25	5	30	0	NCEER
4.2	-89.2	36.6	0	1841	12	28	5	50	0	NCEER
3.1	-89.2	36.6	0	1842	5	28	5	0	0	NCEER

Table 2.5-1 {USGS Earthquake Catalog for the CEUS with $m_b \geq 3.0$ }

(Page 4 of 65)

m_b	Longitude (degree)	Latitude (degree)	Depth (km)	Year	Month	Day	Hour	Minute	Second	Catalog Reference
3.4	-89.2	36.6	0	1842	11	4	6	30	0	NCEER
3.8	-73.2	46	0	1842	11	9	0	0	0	NCEER
5.4	-89.6	35.5	0	1843	1	5	2	45	0	NCEER
3.1	-90.3	38.8	0	1843	2	16	0	0	0	NCEER
4.4	-90.5	35.5	0	1843	2	17	5	0	0	NCEER
3.3	-72.5	44.4	0	1843	3	14	0	0	0	NCEER
4.1	-87.1	35.6	0	1843	8	9	0	0	0	NCEER
3.3	-71.2	41.1	0	1843	10	24	0	0	0	NCEER
3.5	-78.33	43.05	0	1844	10	22	7	0	0	NCEER
3.3	-73.6	45.5	0	1844	11	1	0	0	0	NCEER
3.6	-83.27	35.79	0	1844	11	28	8	0	0	NCEER
3.8	-73.67	41.22	0	1845	10	26	23	15	0	NCEER
3.3	-70.3	42.7	0	1846	5	30	18	30	0	NCEER
4.1	-70.8	42.5	0	1846	8	25	9	45	0	NCEER
3.3	-69.1	44.2	0	1847	2	2	0	0	0	NCEER
4.2	-70.1	41.7	0	1847	8	8	15	0	0	NCEER
3.7	-82.53	39.65	0	1848	4	6	0	0	0	NCEER
4.4	-73.85	41.11	0	1848	9	9	0	0	0	NCEER
3.4	-89.2	36.6	0	1849	1	24	0	0	0	NCEER
4.3	-88	37	0	1850	4	5	2	5	0	NCEER
3.1	-81.7	41.5	0	1850	10	1	10	25	0	NCEER
3.3	-78.4	37.3	0	1850	10	17	0	0	0	NCEER
3.3	-69.6	44.6	0	1851	1	4	4	30	0	NCEER
3.3	-71.4	41.2	0	1852	1	10	11	40	0	NCEER
4.9	-81.6	36.6	0	1852	4	29	18	0	0	NCEER
3.3	-82	33.48	0	1852	8	25	2	40	0	NCEER
4.4	-78.6	37.6	0	1852	11	2	23	35	0	NCEER
3.7	-70.9	43	0	1852	11	28	4	45	0	NCEER
4.5	-75.5	43.7	0	1853	3	12	7	0	0	NCEER
3.3	-79.4	43.1	0	1853	3	13	10	0	0	NCEER
4.4	-79.5	38.5	0	1853	5	2	14	20	0	NCEER
4	-81.96	33.49	0	1853	5	20	5	10	0	NCEER
3.3	-70.2	43.5	0	1853	7	17	10	30	0	NCEER
3.3	-71.9	43	0	1853	11	28	0	0	0	NCEER
4.1	-89.2	36.6	0	1853	12	12	0	0	0	NCEER
3	-83.8	37.2	0	1854	2	12	0	0	0	NCEER
3.6	-84	37.6	0	1854	2	28	0	0	0	NCEER
3.1	-85.2	38.2	0	1854	3	8	0	0	0	NCEER
3.3	-83.62	32.82	0	1854	3	20	6	15	0	NCEER
3.3	-72.3	42.9	0	1854	10	24	0	0	0	NCEER
3.4	-70.8	43	0	1854	12	11	5	30	0	NCEER
4	-71	44	0	1855	1	16	23	0	0	NCEER
3.9	-78.6	37	0	1855	2	2	8	0	0	NCEER
3.3	-69.6	44.6	0	1855	2	19	0	0	0	NCEER
3.1	-89.2	37	0	1855	5	3	3	33	0	NCEER

Table 2.5-1 {USGS Earthquake Catalog for the CEUS with $m_b \geq 3.0$ }

(Page 5 of 65)

m_b	Longitude (degree)	Latitude (degree)	Depth (km)	Year	Month	Day	Hour	Minute	Second	Catalog Reference
3.3	-71.6	44.7	0	1855	5	29	10	0	0	NCEER
3.3	-65.5	44.7	0	1855	6	1	0	0	0	NCEER
3.3	-73.7	43.3	0	1855	12	17	19	0	0	NCEER
3.3	-78.2	39.2	0	1856	1	16	8	0	0	NCEER
3.3	-72.6	41.4	0	1856	3	13	3	0	0	NCEER
4.1	-89.5	36.6	0	1856	11	9	10	0	0	NCEER
3.1	-74.75	40.08	0	1857	2	10	23	30	0	NCEER
3.9	-81.05	42.22	0	1857	2	27	20	30	0	NCEER
3.3	-80.6	41.8	0	1857	3	1	1	40	0	NCEER
3.4	-83.18	33	0	1857	3	1	22	45	0	NCEER
5.1	-89.2	38.7	0	1857	10	8	10	0	0	NCEER
4	-78.97	42.74	0	1857	10	23	20	15	0	NCEER
3.3	-68	46.7	0	1857	12	8	20	0	0	NCEER
4.1	-80.73	32.78	0	1857	12	19	8	50	0	NCEER
3.9	-70.2	44.1	0	1857	12	23	18	30	0	NCEER
3.3	-78.5	42.9	0	1858	1	1	7	0	0	NCEER
3.1	-81.3	41.7	0	1858	4	10	11	30	0	NCEER
3.3	-72.1	45.5	0	1858	5	17	20	0	0	NCEER
3.3	-73	41.3	0	1858	7	1	3	45	0	NCEER
4	-89.2	36.5	0	1858	9	21	0	0	0	NCEER
3.1	-81.5	37.1	0	1859	3	22	0	0	0	NCEER
4.5	-94.8	46	0	1860	1	1	0	0	0	NCEER
4.3	-80.57	33.68	0	1860	1	19	18	0	0	NCEER
3.3	-70.5	42.2	0	1860	3	17	2	30	0	NCEER
4	-83.64	35.08	0	1860	4	24	20	0	0	NCEER
4.3	-87.5	37.5	0	1860	8	7	15	30	0	NCEER
6	-70.1	47.5	0	1860	10	17	11	15	0	NCEER
3.2	-82.64	34.13	0	1860	10	22	5	0	0	NCEER
4.3	-83.36	35.09	0	1861	1	3	16	30	0	NCEER
5	-75.4	45.4	0	1861	7	12	0	0	0	NCEER
5.2	-82.3	36.18	0	1861	8	31	5	0	0	NCEER
3.5	-73.7	45.6	0	1861	10	1	0	0	0	NCEER
3.3	-72.5	41.5	0	1862	2	3	1	0	0	NCEER
3.3	-73	44.5	0	1863	6	9	21	30	0	NCEER
3.8	-71.2	46.9	0	1864	4	20	18	15	0	NCEER
3.3	-73.6	45.5	0	1864	10	21	9	10	0	NCEER
4.6	-89.5	36.5	0	1865	8	17	15	0	0	NCEER
3.3	-71.2	46.8	0	1866	11	9	16	10	0	NCEER
5.2	-96.3	39.2	0	1867	4	24	20	22	0	NCEER
3.1	-95.8	40.7	0	1867	4	28	0	0	0	NCEER
4.7	-75.15	44.65	0	1867	12	18	8	0	0	NCEER
3.3	-80	32.9	0	1869	1	1	0	0	0	NCEER
3.4	-84.5	38.1	0	1869	2	20	0	0	0	NCEER
5.1	-67.2	45	0	1869	10	22	11	0	0	NCEER
4	-70.5	47.5	0	1869	12	1	0	0	0	NCEER

Table 2.5-1 {USGS Earthquake Catalog for the CEUS with $m_b \geq 3.0$ }

(Page 6 of 65)

m_b	Longitude (degree)	Latitude (degree)	Depth (km)	Year	Month	Day	Hour	Minute	Second	Catalog Reference
3.3	-69.8	44.1	0	1870	2	8	0	0	0	NCEER
3.3	-66.5	45.5	0	1870	3	17	11	0	0	NCEER
6.5	-70.5	47.4	0	1870	10	20	16	30	0	NCEER
3	-89.2	36.6	0	1870	12	14	0	0	0	NCEER
3.5	-74.6	45.6	0	1871	1	3	0	0	0	NCEER
3.3	-71.2	46.8	0	1871	5	20	7	0	0	NCEER
3.3	-71.5	43.2	0	1871	7	20	0	0	0	NCEER
3.4	-90	38.5	0	1871	7	25	6	40	0	NCEER
3.8	-75.5	39.7	0	1871	10	9	14	40	0	NCEER
3.4	-83.8	43.5	0	1872	2	6	14	0	0	NCEER
3	-89.2	37	0	1872	2	8	11	0	0	NCEER
3.7	-78	37.7	0	1872	6	5	3	0	0	NCEER
3	-83.22	33.06	0	1872	6	17	14	30	0	NCEER
3.1	-93.5	39.8	0	1872	7	9	2	30	0	NCEER
3	-73.8	40.9	0	1872	7	11	10	25	0	NCEER
3.6	-97	42.7	0	1872	10	9	16	0	0	NCEER
3.4	-71.6	43.2	0	1872	11	18	19	0	0	NCEER
3	-84.2	39.7	0	1873	4	23	4	14	0	NCEER
3.5	-74.2	44.8	0	1873	4	25	19	0	0	NCEER
3.1	-79.9	43.3	0	1873	4	30	0	0	0	NCEER
3.3	-74.7	45	0	1873	4	30	0	0	0	NCEER
3	-97.7	30.2	0	1873	5	1	4	30	0	NCEER
3.7	-89.6	36	0	1873	5	3	21	0	0	NCEER
4	-78.94	42.69	0	1873	7	6	0	0	0	NCEER
3.3	-73.2	45.5	0	1873	9	30	11	50	0	NCEER
3.3	-76	46.5	0	1873	9	30	11	50	0	NCEER
3.6	-78.2	37.2	0	1873	10	3	12	45	0	NCEER
3.2	-83.9	33	0	1873	10	4	0	0	0	NCEER
3.3	-71.2	43.6	0	1874	1	6	0	0	0	NCEER
3.3	-71.4	42.6	0	1874	1	25	17	0	0	NCEER
3.3	-71.5	43	0	1874	1	26	7	0	0	NCEER
3.3	-82.1	35.7	0	1874	2	22	0	0	0	NCEER
3.7	-67.28	45.18	0	1874	2	28	3	40	0	NCEER
3.3	-82.1	35.7	0	1874	3	17	0	0	0	NCEER
3.3	-82.1	35.7	0	1874	4	14	0	0	0	NCEER
3	-89.2	37	0	1874	7	9	22	0	0	NCEER
3.3	-69.1	48.6	0	1874	7	31	9	0	0	NCEER
3	-70.9	42.7	0	1874	11	24	0	0	0	NCEER
3.4	-73.8	40.9	0	1874	12	11	3	25	0	NCEER
3.4	-82.51	35.29	0	1875	4	10	0	0	0	NCEER
4.7	-84	40.2	0	1875	6	18	13	43	0	NCEER
3.4	-73	41.9	0	1875	7	28	9	10	0	NCEER
4.1	-89.6	36.1	0	1875	10	7	0	0	0	NCEER
3.1	-90	35.1	0	1875	10	28	3	0	0	NCEER
4.8	-82.9	33.49	0	1875	11	1	22	30	0	NCEER

Table 2.5-1 {USGS Earthquake Catalog for the CEUS with $m_b \geq 3.0$ }

(Page 7 of 65)

m_b	Longitude (degree)	Latitude (degree)	Depth (km)	Year	Month	Day	Hour	Minute	Second	Catalog Reference
3.8	-95.7	39	0	1875	11	8	10	40	0	NCEER
3.6	-84	36	0	1875	11	12	7	0	0	NCEER
3.3	-72.3	42.9	0	1875	12	1	9	0	0	NCEER
4.8	-78.5	37.6	0	1875	12	23	4	45	0	NCEER
3.4	-84.2	40.4	0	1876	6	1	0	0	0	NCEER
3.1	-99.6	44.1	0	1876	8	17	5	25	0	NCEER
3.6	-71.3	41.5	0	1876	9	22	4	30	0	NCEER
4.7	-87	38.5	0	1876	9	25	6	15	0	NCEER
3.3	-80	32.9	0	1876	12	12	0	0	0	NCEER
3.3	-77.5	37.4	0	1876	12	23	4	45	0	NCEER
3.4	-83.5	38.8	0	1877	1	23	21	0	0	NCEER
3.6	-84	36	0	1877	5	25	0	0	0	NCEER
3	-87.9	38.2	0	1877	5	26	21	0	0	NCEER
4.2	-89.7	36.8	0	1877	7	15	0	40	0	NCEER
3.1	-83.3	42.3	0	1877	8	17	16	50	0	NCEER
3.3	-74.9	40.3	0	1877	9	10	14	59	0	NCEER
4.7	-73.9	45.2	0	1877	11	4	0	0	0	NCEER
5	-97	41	0	1877	11	15	17	45	0	NCEER
3.7	-84	35.5	0	1877	11	16	7	38	0	NCEER
3	-89.2	37	0	1877	11	19	11	10	0	NCEER
3.5	-76.85	45.7	0	1877	12	18	10	0	0	NCEER
3	-89.2	37	0	1878	1	9	4	30	0	NCEER
3.9	-89.1	36.8	0	1878	3	12	10	0	0	NCEER
3.4	-74	41.5	0	1878	10	4	7	30	0	NCEER
5.2	-90.7	35.5	0	1878	11	19	5	52	0	NCEER
3.3	-99.1	39.6	0	1879	3	1	0	0	0	NCEER
3.3	-75.5	39.2	0	1879	3	26	0	30	0	NCEER
3.3	-73.6	45.6	0	1879	6	11	0	0	0	NCEER
3.3	-79.2	43.2	0	1879	8	21	8	0	0	NCEER
3.7	-90.3	35.3	0	1879	9	26	3	10	0	NCEER
3.3	-71.5	43	0	1879	10	26	2	30	0	NCEER
3.1	-81.08	34.37	0	1879	10	26	20	0	0	NCEER
3.6	-97.3	42.9	0	1879	12	29	6	30	0	NCEER
3.4	-71	42.7	0	1880	5	12	12	45	0	NCEER
3.3	-75.3	45.2	0	1880	5	31	0	0	0	NCEER
3.7	-90.3	35.3	0	1880	7	14	2	30	0	NCEER
3.3	-71.5	43	0	1880	7	20	0	0	0	NCEER
3.3	-73.8	45.2	0	1880	9	6	5	30	0	NCEER
3.3	-70.5	47.45	0	1880	11	28	13	30	0	NCEER
3	-97.2	49	0	1880	12	28	7	15	0	NCEER
3.3	-70	44	0	1881	1	21	2	40	0	NCEER
3.1	-85.8	41.6	0	1881	4	20	0	0	0	NCEER
4	-89.1	41.3	0	1881	5	27	0	0	0	NCEER
3.3	-70.2	47.6	0	1881	10	1	6	40	0	NCEER
3.3	-71.6	43.2	0	1881	10	6	5	3	0	NCEER

Table 2.5-1 {USGS Earthquake Catalog for the CEUS with $m_b \geq 3.0$ }

(Page 8 of 65)

m_b	Longitude (degree)	Latitude (degree)	Depth (km)	Year	Month	Day	Hour	Minute	Second	Catalog Reference
3.1	-90	35.1	0	1881	10	7	16	52	0	NCEER
3.1	-84.2	40.4	0	1882	2	9	20	0	0	NCEER
3.3	-71.7	43.2	0	1882	4	17	0	0	0	NCEER
3.4	-89.2	36.9	0	1882	7	20	10	0	0	NCEER
3.9	-90.6	37.6	0	1882	7	28	0	0	0	NCEER
3.3	-67.4	49.3	0	1882	8	15	15	30	0	NCEER
4.4	-89.5	38.7	0	1882	9	27	10	20	0	NCEER
4.8	-95.6	33.6	0	1882	10	22	22	15	0	NCEER
6.2	-105.5	40.5	0	1882	11	8	1	30	0	USHIS
3.1	-79.25	43	0	1882	11	27	23	30	0	NCEER
3.6	-71.4	43.2	0	1882	12	19	22	24	0	NCEER
3.5	-67	45	0	1883	1	1	2	55	0	NCEER
3.3	-67.7	44.6	0	1883	1	1	7	58	0	NCEER
4.7	-88.5	37	0	1883	1	11	7	12	0	NCEER
4.7	-85.6	42.3	0	1883	2	4	11	0	0	NCEER
3.3	-71.2	43.6	0	1883	2	4	20	5	0	NCEER
3.6	-71.3	41.5	0	1883	2	28	3	30	0	NCEER
3.1	-76.4	39.5	0	1883	3	11	23	57	0	NCEER
3.3	-74.5	45.1	0	1883	3	12	0	0	0	NCEER
4.5	-89.2	37	0	1883	4	12	8	30	0	NCEER
3.1	-82.6	38.4	0	1883	5	23	4	30	0	NCEER
4	-90	35.1	0	1883	6	11	18	16	0	NCEER
3.7	-89.1	37	0	1883	7	14	7	30	0	NCEER
3.1	-90.2	38.7	0	1883	11	15	3	14	0	NCEER
4	-91.2	35.7	0	1883	12	5	15	20	0	NCEER
3.3	-71.7	43.2	0	1884	1	18	7	0	0	NCEER
3.7	-77.59	34.59	0	1884	1	18	8	0	0	NCEER
3.1	-100.7	41.1	0	1884	3	17	20	0	0	NCEER
3.6	-83.05	32.8	0	1884	3	21	4	30	0	NCEER
5.2	-74	40.6	0	1884	8	10	19	7	0	NCEER
3.3	-83.83	36.07	0	1884	8	24	19	45	0	NCEER
4.8	-84.1	40.7	0	1884	9	19	20	14	0	NCEER
3.7	-71.7	43.2	0	1884	11	23	5	30	0	NCEER
3.5	-89.7	35.5	0	1884	11	30	5	0	0	NCEER
3.3	-71.5	43.7	0	1884	12	17	7	0	0	NCEER
3.9	-77.5	39.2	0	1885	1	3	2	12	0	NCEER
3.4	-73.9	41.3	0	1885	1	4	11	6	0	NCEER
3.5	-81.6	41.16	0	1885	1	18	10	30	0	NCEER
3.3	-81.1	36.9	0	1885	2	2	12	10	0	NCEER
3.3	-66.1	45.1	0	1885	6	1	0	0	0	NCEER
3.4	-81.83	36.12	0	1885	8	6	9	0	0	NCEER
4.4	-78.8	37.7	0	1885	10	10	4	35	0	NCEER
3.6	-82.71	33.17	0	1885	10	17	18	20	0	NCEER
3.3	-71.5	42.9	0	1886	1	6	0	10	0	NCEER
3.3	-73.8	41.6	0	1886	1	25	0	4	0	NCEER

Table 2.5-1 {USGS Earthquake Catalog for the CEUS with $m_b \geq 3.0$ }

(Page 9 of 65)

m_b	Longitude (degree)	Latitude (degree)	Depth (km)	Year	Month	Day	Hour	Minute	Second	Catalog Reference
3.5	-88	32.8	0	1886	2	5	1	0	0	NCEER
3.3	-81.52	35.93	0	1886	2	5	2	0	0	NCEER
3	-85.5	39	0	1886	3	1	16	0	0	NCEER
4.2	-89.2	37	0	1886	3	18	5	59	0	NCEER
3.8	-82.24	39.36	0	1886	5	3	3	0	0	NCEER
3.3	-67.4	49.3	0	1886	5	18	19	30	0	NCEER
3.3	-74	46	0	1886	8	12	0	0	0	NCEER
3	-86.1	39.7	0	1886	8	14	0	0	0	NCEER
3.8	-80.14	33.38	0	1886	8	27	8	30	0	NCEER
3.3	-81.7	30.4	0	1886	9	1	0	0	0	NCEER
6.8	-80	32.9	0	1886	9	1	2	51	0	NCEER
4.4	-81.94	33.93	0	1886	9	1	8	55	0	NCEER
4.2	-82.86	34.3	0	1886	9	1	9	45	0	NCEER
4.3	-81.56	33.41	0	1886	9	1	23	50	0	NCEER
3.6	-81.23	34.72	0	1886	9	2	23	0	0	NCEER
3.3	-72.5	41.5	0	1886	9	5	0	0	0	NCEER
4.1	-80.97	33.05	0	1886	9	7	11	42	0	NCEER
4.3	-80.68	32.7	0	1886	9	7	17	0	0	NCEER
3.7	-80.96	32.23	0	1886	9	19	0	0	0	NCEER
3.2	-80.05	36.7	0	1886	9	25	2	0	0	NCEER
3.4	-81.62	34.7	0	1886	9	27	22	0	0	NCEER
4.1	-81.66	34.71	0	1886	10	22	0	0	0	NCEER
5.2	-81.01	33.87	0	1886	10	22	14	45	0	NCEER
3.9	-80.39	33.9	0	1886	10	31	14	20	0	NCEER
5.3	-80.42	33.4	0	1886	11	5	12	25	0	NCEER
3.8	-81.06	33.04	0	1886	12	2	2	20	0	NCEER
3.6	-82.06	34.18	0	1886	12	11	16	0	0	NCEER
3.6	-97.06	30.15	0	1887	1	5	17	57	0	SRA
3.1	-82.42	34.35	0	1887	1	12	6	0	0	NCEER
4.5	-88.5	39	0	1887	2	6	22	15	0	NCEER
3.1	-80	45.35	0	1887	2	19	0	0	0	NCEER
3.3	-67.4	49.3	0	1887	2	22	22	59	0	NCEER
3.3	-70.5	47.5	0	1887	3	11	0	0	0	NCEER
3.7	-80.37	33.9	0	1887	5	22	20	45	0	NCEER
4	-70.5	47.45	0	1887	5	27	6	15	0	NCEER
3.6	-81	34	0	1887	6	3	8	45	0	NCEER
3.3	-71.5	43.2	0	1887	6	30	22	0	0	NCEER
3.7	-80.77	33.74	0	1887	7	10	13	5	0	NCEER
3.8	-78.83	34.41	0	1887	8	2	1	0	0	NCEER
4.6	-88.5	37.2	0	1887	8	2	18	36	0	NCEER
3.9	-79.95	33.83	0	1887	8	10	7	1	0	NCEER
4.2	-80.62	32.49	0	1887	8	26	23	45	0	NCEER
4	-81.22	33.52	0	1887	8	27	4	56	0	NCEER
3.9	-80.86	33.66	0	1887	8	28	22	57	0	NCEER
3.3	-77.1	45.8	0	1888	1	11	9	0	0	NCEER

Table 2.5-1 {USGS Earthquake Catalog for the CEUS with $m_b \geq 3.0$ }

(Page 10 of 65)

m_b	Longitude (degree)	Latitude (degree)	Depth (km)	Year	Month	Day	Hour	Minute	Second	Catalog Reference
4.4	-80.17	34.18	0	1888	1	12	9	55	0	NCEER
3.3	-70.1	44.65	0	1888	2	1	0	0	0	NCEER
3	-82.5	36.4	0	1888	3	17	0	0	0	NCEER
3.3	-70.5	47.45	0	1888	4	19	5	30	0	NCEER
3.3	-70	44.3	0	1888	8	15	1	15	0	NCEER
3.1	-81.08	34.37	0	1888	8	15	18	30	0	NCEER
3.5	-83.35	33.42	0	1888	9	17	21	30	0	NCEER
3.1	-90.4	35.4	0	1888	11	3	0	0	0	NCEER
3.3	-68.7	48.5	0	1888	12	7	14	25	0	NCEER
3.9	-79.2	33.16	0	1889	2	5	19	40	0	NCEER
3.3	-71.6	43.5	0	1889	3	8	0	0	0	NCEER
4.1	-76	40	0	1889	3	8	23	40	0	NCEER
3.7	-88.1	35.9	0	1889	6	6	16	25	0	NCEER
4.4	-80.33	32.4	0	1889	7	11	21	47	0	NCEER
4	-90	35.2	0	1889	7	20	1	32	0	NCEER
3.3	-73.7	43.4	0	1889	8	10	0	0	0	NCEER
3.5	-84.87	35.03	0	1889	9	29	0	0	0	NCEER
3.1	-82.6	34.72	0	1889	10	24	10	0	0	NCEER
3.8	-95.2	31.7	0	1891	1	8	6	0	0	NCEER
3	-90	35.1	0	1891	1	14	0	0	0	NCEER
3.7	-71.6	43.2	0	1891	5	2	0	10	0	NCEER
4.2	-87.5	37.9	0	1891	7	27	2	28	0	NCEER
5.5	-88.5	38.3	0	1891	9	27	4	55	0	NCEER
3.3	-80	32.9	0	1891	10	13	5	55	0	NCEER
3.3	-71.7	44.3	0	1892	12	11	16	30	0	NCEER
3.3	-74	40.6	0	1893	3	9	5	30	0	NCEER
3.3	-72.7	42.3	0	1893	3	14	0	0	0	NCEER
3.3	-81.7	30.4	0	1893	6	21	7	7	0	NCEER
3.3	-80	32.9	0	1893	7	5	8	10	0	NCEER
3.3	-80	32.9	0	1893	9	19	7	5	0	NCEER
3.3	-80	32.9	0	1893	11	8	4	40	0	NCEER
5.2	-73.3	45.5	0	1893	11	27	16	50	0	NCEER
3.3	-80	32.9	0	1893	12	27	6	51	0	NCEER
3.3	-66.8	49.7	0	1894	1	11	9	0	0	NCEER
3.3	-80	32.9	0	1894	1	30	4	5	0	NCEER
3.3	-72.5	41.6	0	1894	4	10	0	0	0	NCEER
3.3	-80	32.9	0	1894	6	16	2	16	0	NCEER
4.3	-106.3	42.9	0	1894	6	25	0	0	0	NCEER
3.3	-80	32.9	0	1894	12	11	5	27	0	NCEER
3.3	-73.8	42.5	0	1894	12	17	0	0	0	NCEER
3.3	-80	32.9	0	1895	1	8	5	40	0	NCEER
3.3	-80	32.9	0	1895	4	27	7	40	0	NCEER
3.3	-80	32.9	0	1895	7	25	4	1	0	NCEER
3	-88.2	35.2	0	1895	7	27	0	0	0	NCEER
4.3	-74.3	40.46	0	1895	9	1	11	9	0	NCEER

Table 2.5-1 {USGS Earthquake Catalog for the CEUS with $m_b \geq 3.0$ }

(Page 11 of 65)

m_b	Longitude (degree)	Latitude (degree)	Depth (km)	Year	Month	Day	Hour	Minute	Second	Catalog Reference
3.3	-80	32.9	0	1895	10	6	6	25	0	NCEER
3.5	-77.5	35.9	0	1895	10	7	4	30	0	NCEER
3.5	-103.3	43.9	0	1895	10	11	23	55	0	NCEER
5.4	-89.4	37	0	1895	10	31	11	8	0	NCEER
3.3	-80	32.9	0	1895	11	12	23	33	0	NCEER
3.3	-78.6	36.3	0	1896	2	11	1	45	0	NCEER
3.1	-84.2	40.3	0	1896	3	15	7	0	0	NCEER
3.3	-80	32.9	0	1896	3	19	8	22	0	NCEER
3.8	-67.2	45.2	0	1896	3	23	0	56	0	NCEER
3.3	-66.6	45.9	0	1896	5	16	4	0	0	NCEER
3.3	-80	32.9	0	1896	8	11	5	58	0	NCEER
3.3	-71.8	44.3	0	1896	10	22	10	30	0	NCEER
3.3	-80	32.9	0	1896	11	14	8	15	0	NCEER
3.3	-66.8	44.5	0	1897	1	28	0	0	0	NCEER
3.1	-79.2	43.1	0	1897	3	7	0	0	0	NCEER
5	-73.6	45.5	0	1897	3	23	23	7	0	NCEER
3.7	-89.6	35.8	0	1897	4	26	4	0	0	NCEER
3.3	-89	37	0	1897	5	1	4	0	0	NCEER
4.5	-73.5	44.5	0	1897	5	28	3	16	0	NCEER
5	-80.7	37.3	0	1897	5	31	18	58	0	NCEER
3.3	-71.6	43.7	0	1897	7	1	9	20	0	NCEER
3.3	-72.5	41.5	0	1897	9	5	0	0	0	NCEER
4.1	-68.7	44.7	0	1897	9	25	18	5	0	NCEER
4.1	-81.1	36.9	0	1897	10	22	3	20	0	NCEER
4.5	-106.3	42.9	0	1897	11	14	0	0	0	NCEER
3.3	-77.5	37.7	0	1897	11	27	20	56	0	NCEER
4	-97.7	37.7	0	1897	12	2	7	10	0	NCEER
4.6	-77.5	37.7	0	1897	12	18	23	45	0	NCEER
3.3	-74.3	45.1	0	1898	1	7	6	0	0	NCEER
3.3	-66.8	44.7	0	1898	1	11	9	0	0	NCEER
3.1	-90.6	34.6	0	1898	1	27	1	35	0	NCEER
4.3	-81	37	0	1898	2	5	20	0	0	NCEER
3.3	-72.6	42.8	0	1898	6	11	6	45	0	NCEER
4	-88.7	36.5	0	1898	6	14	15	6	0	NCEER
3.1	-97.3	42.6	0	1898	9	16	9	59	0	NCEER
4.3	-81	37	0	1898	11	25	20	0	0	NCEER
4.4	-81	37	0	1899	2	13	9	30	0	NCEER
3.3	-76.3	36.9	0	1899	3	3	0	0	0	NCEER
3.3	-80	32.9	0	1899	3	10	5	45	0	NCEER
4.6	-87.4	38.5	0	1899	4	30	2	5	0	NCEER
3.6	-72.6	41.6	0	1899	5	17	1	15	0	NCEER
3.3	-69.5	44	0	1899	10	5	11	30	0	NCEER
3.2	-86.5	42.1	0	1899	10	11	4	0	0	NCEER
3.1	-83	39.3	0	1899	11	12	14	0	0	NCEER
3.1	-94.4	36.8	0	1899	12	1	18	50	0	NCEER

Table 2.5-1 {USGS Earthquake Catalog for the CEUS with $m_b \geq 3.0$ }

(Page 12 of 65)

m_b	Longitude (degree)	Latitude (degree)	Depth (km)	Year	Month	Day	Hour	Minute	Second	Catalog Reference
3.3	-80	32.9	0	1899	12	4	12	48	0	NCEER
3.5	-99	44.5	0	1899	12	6	12	0	0	NCEER
3	-89.5	45.5	0	1900	3	14	3	0	0	NCEER
4	-81.8	41.4	0	1900	4	9	13	0	0	NCEER
3.5	-81.7	30.4	0	1900	10	31	16	15	0	NCEER
3.1	-96.8	36	0	1900	12	1	0	0	0	NCEER
3.5	-94	37.8	0	1901	1	4	3	12	0	NCEER
3.8	-90	36	0	1901	2	15	0	15	0	NCEER
4.3	-82.66	38.95	0	1901	5	17	7	0	0	NCEER
3.3	-80	32.9	0	1901	12	2	0	26	0	NCEER
4.3	-89	42.3	0	1902	1	24	10	18	0	NCEER
3	-85.2	39.9	0	1902	3	10	6	0	0	NCEER
3.4	-80.6	37.3	0	1902	5	18	4	0	0	NCEER
4.2	-85.3	35.1	0	1902	5	29	7	30	0	NCEER
3.3	-81.4	40.3	0	1902	6	14	7	0	0	NCEER
4.2	-97.5	42.5	0	1902	7	28	18	0	0	NCEER
3.6	-97.6	30.1	0	1902	10	9	19	0	0	SRA
3.2	-85.3	35	0	1902	10	18	22	0	0	NCEER
4.1	-80	32.9	0	1903	1	24	1	0	0	NCEER
4.8	-89.3	37.8	0	1903	2	9	0	21	0	NCEER
3	-89.5	39.1	0	1903	3	17	11	50	0	NCEER
3	-71	42.7	0	1903	4	24	12	30	0	NCEER
3.1	-86.3	39.4	0	1903	9	20	0	0	0	NCEER
3.1	-88.1	38.7	0	1903	9	21	0	0	0	NCEER
3.7	-90.2	38.3	0	1903	10	5	2	56	0	NCEER
3	-89.3	37.8	0	1903	11	3	18	0	0	NCEER
4.9	-89.8	36.5	0	1903	11	4	19	14	0	NCEER
3.9	-89.5	37	0	1903	11	27	7	0	0	NCEER
3.5	-75.5	44.7	0	1903	12	25	12	30	0	NCEER
3.4	-83.5	35.7	0	1904	3	5	0	30	0	NCEER
5	-67.2	45	0	1904	3	21	6	4	0	NCEER
3.5	-100.2	37.5	0	1904	10	28	4	30	0	NCEER
3.4	-91.1	30.5	0	1905	2	3	0	0	0	NCEER
3.4	-87.7	45.1	0	1905	3	13	16	30	0	NCEER
3.6	-91.6	40.4	0	1905	4	13	16	30	0	NCEER
4.4	-70	44.2	0	1905	7	15	10	10	0	NCEER
4.5	-88.4	47.3	0	1905	7	27	0	20	0	NCEER
5.2	-89.3	37.2	0	1905	8	22	5	8	0	NCEER
3.4	-70.7	43.1	0	1905	8	30	22	40	0	NCEER
3.3	-72.2	44.9	0	1905	10	22	0	0	0	NCEER
3.3	-71.3	41.5	0	1905	11	26	0	30	0	NCEER
4.9	-96.5	39.2	0	1906	1	8	0	15	0	NCEER
3.1	-91.4	39.7	0	1906	3	6	0	0	0	NCEER
3.4	-83.6	40.7	0	1906	4	23	7	12	0	NCEER
3.6	-85.8	39.5	0	1906	5	8	6	58	0	NCEER

Table 2.5-1 {USGS Earthquake Catalog for the CEUS with $m_b \geq 3.0$ }

(Page 13 of 65)

m_b	Longitude (degree)	Latitude (degree)	Depth (km)	Year	Month	Day	Hour	Minute	Second	Catalog Reference
3.3	-72.5	41.5	0	1906	5	8	13	30	0	NCEER
3	-75.7	38.7	0	1906	5	8	17	41	0	NCEER
3.1	-85.9	39.2	0	1906	5	9	6	38	0	NCEER
4.2	-101.3	43	0	1906	5	10	0	27	0	NCEER
3.3	-87.2	38.5	0	1906	5	11	6	15	0	NCEER
3.4	-88.4	38.7	0	1906	5	21	19	0	0	NCEER
3.3	-88.4	47.3	0	1906	5	26	14	42	0	NCEER
3.2	-81.6	40.4	0	1906	6	27	21	10	0	NCEER
3.7	-88.4	47.3	0	1906	8	8	0	0	0	NCEER
3.1	-86.8	39.7	0	1906	8	13	13	19	0	NCEER
3.8	-87.7	38.2	0	1906	9	7	16	33	0	NCEER
4	-70.5	43.5	0	1906	10	20	16	0	0	NCEER
3.3	-75.41	45.61	0	1906	11	17	14	0	0	NCEER
3.3	-77.1	41.2	0	1907	1	10	9	45	0	NCEER
3.1	-97	37.1	0	1907	1	11	7	45	0	NCEER
3.4	-86.6	39.5	0	1907	1	30	5	30	0	NCEER
3.6	-89.5	38.9	0	1907	1	31	5	30	0	SRA
4	-78.3	37.7	0	1907	2	11	13	22	0	NCEER
3.9	-80	32.9	0	1907	4	19	8	30	0	NCEER
3.3	-70.5	43.5	0	1907	6	29	0	0	0	NCEER
3.2	-90.4	37.8	0	1907	7	4	9	0	0	NCEER
3.3	-70.16	47.65	0	1907	8	5	12	43	0	NCEER
3.5	-71	42.8	0	1907	10	16	0	10	0	NCEER
3.3	-76.68	45.47	0	1907	11	14	5	0	0	NCEER
3.1	-89.8	42.3	0	1907	11	28	16	30	0	NCEER
3.1	-90.2	38.6	0	1907	12	11	4	32	0	NCEER
3.3	-70.5	47.45	0	1908	3	10	0	0	0	NCEER
3.1	-75.5	40.6	0	1908	5	31	17	42	0	NCEER
3.5	-74.8	45.1	0	1908	6	16	20	41	0	NCEER
3.3	-76.35	45.43	0	1908	7	17	7	10	0	NCEER
3.5	-67.6	46.3	0	1908	8	8	12	0	0	NCEER
3.5	-77.9	37.5	0	1908	8	23	9	30	0	NCEER
3.5	-89.6	36.6	0	1908	9	28	19	34	0	NCEER
3.6	-89.2	37	0	1908	10	28	0	27	0	NCEER
3.8	-93.2	38.7	0	1908	11	12	12	0	0	SRA
3.3	-71.7	43.5	0	1908	11	23	13	0	0	NCEER
3.7	-88	37.5	0	1908	12	27	21	15	0	NCEER
3.4	-88.6	47.2	0	1909	1	23	3	15	0	NCEER
3.3	-97.8	42.3	0	1909	1	26	20	15	0	NCEER
3.3	-73.57	45.51	0	1909	2	1	8	20	0	NCEER
3.5	-78	39.4	0	1909	4	2	7	25	0	NCEER
3.3	-74.3	46.1	0	1909	5	10	1	20	0	NCEER
5.5	-104	49	0	1909	5	16	4	15	0	NCEER
5	-88.1	41.6	0	1909	5	26	14	42	0	USHIS
3.3	-74.28	46.05	0	1909	6	8	8	25	0	NCEER

Table 2.5-1 {USGS Earthquake Catalog for the CEUS with $m_b \geq 3.0$ }

(Page 14 of 65)

m_b	Longitude (degree)	Latitude (degree)	Depth (km)	Year	Month	Day	Hour	Minute	Second	Catalog Reference
4.3	-90.7	40.3	0	1909	7	19	4	34	0	NCEER
3.8	-90.1	38.3	0	1909	8	16	22	45	0	NCEER
3.7	-86.5	38.7	0	1909	9	22	0	0	0	NCEER
4.8	-87.4	39.5	0	1909	9	27	9	45	0	NCEER
3.3	-85	34.9	0	1909	10	8	10	0	0	NCEER
3.1	-90.6	37.6	0	1909	10	22	22	0	0	NCEER
3.3	-89.7	41.8	0	1909	10	22	22	30	0	NCEER
4.3	-89.5	37	0	1909	10	23	7	10	0	NCEER
3.9	-87.8	39	0	1909	10	23	9	47	0	NCEER
3.3	-75.6	45.4	0	1909	12	10	6	24	10	NCEER
3.8	-70	48	0	1910	2	1	0	0	0	NCEER
3.2	-78.7	38.8	0	1910	2	8	14	0	0	NCEER
3.1	-79.8	43.2	0	1910	2	25	0	0	0	NCEER
3.8	-97.4	41.4	0	1910	2	26	8	0	0	NCEER
3.5	-78.4	37.7	0	1910	5	8	21	10	0	NCEER
3.2	-96	30.1	0	1910	5	12	0	0	0	NCEER
4.3	-109.3	41.5	0	1910	7	26	1	30	0	DNAG
3.3	-71.1	42.7	0	1910	8	21	18	45	0	NCEER
3.3	-72.1	43.4	0	1910	8	30	14	30	0	NCEER
3.3	-68.8	44.3	0	1910	10	20	21	50	0	NCEER
4	-69.8	47.6	0	1910	10	25	9	30	0	NCEER
3.3	-79.4	36.6	0	1911	2	10	10	22	0	NCEER
3.1	-90.3	38.7	0	1911	2	28	9	0	0	NCEER
3.3	-71.5	43.2	0	1911	3	2	21	30	0	NCEER
4.6	-91.8	34	0	1911	3	31	16	57	0	NCEER
3.5	-92.2	33.8	0	1911	3	31	18	10	0	NCEER
3.3	-75.5	38.3	0	1911	4	8	1	0	0	NCEER
3.5	-82.7	35.1	0	1911	4	20	22	0	0	NCEER
4.2	-98.2	44.2	0	1911	6	2	22	34	0	NCEER
3.3	-87.6	41.8	0	1911	7	29	0	0	0	NCEER
4.7	-89	42.3	0	1912	1	2	16	21	0	NCEER
3.4	-79.7	43.2	0	1912	5	27	12	52	0	NCEER
4.9	-80	32.9	0	1912	6	12	10	30	0	NCEER
3.5	-81	32	0	1912	6	20	0	0	0	NCEER
3.3	-78.4	37.7	0	1912	8	8	1	0	0	NCEER
3	-89.1	42.3	0	1912	9	25	0	0	0	NCEER
3.3	-68	49.5	0	1912	10	23	0	0	0	NCEER
3.3	-83.5	32.7	0	1912	10	23	1	15	0	NCEER
3.3	-80	32.9	0	1912	11	17	12	30	0	NCEER
3.3	-81.7	34.7	0	1912	12	7	19	10	0	NCEER
5	-81.7	34.7	0	1913	1	1	18	28	0	NCEER
3.3	-85	34.5	0	1913	3	13	5	0	0	NCEER
4	-83.7	36.2	0	1913	3	28	21	50	0	NCEER
3.7	-84.2	35.3	0	1913	4	17	16	30	0	NCEER
4.4	-75.33	44.87	0	1913	4	29	0	28	57	NCEER

Table 2.5-1 {USGS Earthquake Catalog for the CEUS with $m_b \geq 3.0$ }

(Page 15 of 65)

m_b	Longitude (degree)	Latitude (degree)	Depth (km)	Year	Month	Day	Hour	Minute	Second	Catalog Reference
3.3	-74.4	45.68	0	1913	6	8	6	30	0	NCEER
3.7	-88.9	35.8	0	1913	6	9	15	30	0	NCEER
3.8	-84	36	0	1913	8	3	16	45	0	NCEER
3.4	-74	44	0	1913	8	10	5	15	0	NCEER
3.7	-89.7	41.8	0	1913	10	17	2	15	0	NCEER
3.3	-71.5	41.5	0	1913	11	3	14	30	0	NCEER
3.1	-85.8	38.2	0	1913	11	11	14	0	0	NCEER
3.3	-67.2	45.1	0	1914	1	13	8	0	0	NCEER
3.5	-84.5	35.6	0	1914	1	24	3	24	0	NCEER
5.5	-75	46	0	1914	2	10	18	31	0	NCEER
3.5	-73.6	46.4	0	1914	2	14	9	34	0	NCEER
3.8	-70.5	45	0	1914	2	22	19	15	0	NCEER
4.6	-83.5	33.5	0	1914	3	5	20	5	0	NCEER
3.3	-79.8	34.2	0	1914	3	7	1	20	0	NCEER
3.3	-67.61	49.31	0	1914	4	12	0	0	0	NCEER
3.3	-80	32.9	0	1914	7	14	1	53	0	NCEER
4.3	-80	32.9	0	1914	9	22	7	4	0	NCEER
3.1	-89.4	43.1	0	1914	10	7	21	0	0	NCEER
3.5	-95.9	30.5	0	1914	12	30	1	0	0	NCEER
3.6	-82.2	36.6	0	1915	1	14	9	20	0	NCEER
3.1	-88.6	37.7	0	1915	2	5	6	55	0	NCEER
3.1	-89.2	37.1	0	1915	2	19	4	35	0	NCEER
3.5	-71.4	42.7	0	1915	2	21	1	20	0	NCEER
3.3	-73.4	44.7	0	1915	2	21	23	41	0	NCEER
3	-88.4	47.3	0	1915	3	3	7	45	0	NCEER
3.7	-88.1	38.7	0	1915	4	15	13	20	0	NCEER
3.1	-89.5	36.5	0	1915	4	28	23	40	0	NCEER
3.1	-103.6	48.1	0	1915	8	8	15	15	0	NCEER
3	-99.3	42.8	0	1915	9	16	19	0	0	NCEER
3.3	-88.4	47.3	0	1915	10	4	14	2	0	NCEER
3.7	-95.3	35.7	0	1915	10	8	16	50	0	NCEER
3.8	-101.5	43.8	0	1915	10	23	6	5	0	NCEER
3.4	-88.6	36.7	0	1915	10	26	7	40	0	NCEER
4.4	-90	36	0	1915	12	7	18	40	0	NCEER
4	-73.7	43.7	0	1916	1	5	13	56	0	NCEER
3.7	-87	39.1	0	1916	1	7	19	45	0	NCEER
3.8	-74	43	0	1916	2	3	4	26	0	NCEER
5.2	-83.55	35.62	0	1916	2	21	22	39	0	Chapman
3.3	-70.9	46.8	0	1916	2	29	5	15	0	NCEER
3.3	-82.7	34.5	0	1916	3	2	5	2	0	NCEER
4	-77	47	0	1916	4	24	16	7	45	NCEER
3.6	-89.5	36.6	0	1916	5	21	18	24	0	NCEER
3.3	-73.8	41	0	1916	6	8	21	15	0	NCEER
3.5	-89.2	37	0	1916	8	24	9	0	0	NCEER
3.6	-81	36	0	1916	8	26	19	36	0	NCEER

Table 2.5-1 {USGS Earthquake Catalog for the CEUS with $m_b \geq 3.0$ }

(Page 16 of 65)

m_b	Longitude (degree)	Latitude (degree)	Depth (km)	Year	Month	Day	Hour	Minute	Second	Catalog Reference
5.2	-86.2	33.5	0	1916	10	18	22	3	40	NCEER
3.5	-73.7	43.3	0	1916	11	2	2	32	0	NCEER
3.7	-89.2	36.6	0	1916	12	19	5	42	0	NCEER
3.4	-83.5	36.1	0	1917	1	25	21	15	0	NCEER
3.5	-74.5	46.8	0	1917	1	26	19	35	0	NCEER
3.1	-95	47.9	0	1917	2	6	17	26	0	NCEER
3.3	-72.5	41.5	0	1917	2	16	9	0	0	NCEER
3.4	-84	36	0	1917	3	5	2	7	0	NCEER
3.6	-83.5	36.1	0	1917	3	25	19	15	0	NCEER
3.8	-101.3	35.3	0	1917	3	27	19	56	0	NCEER
4.9	-90	37	0	1917	4	9	20	52	0	NCEER
3.1	-90.2	38.1	0	1917	4	9	23	38	0	NCEER
3.9	-90.4	36.8	0	1917	5	9	9	0	0	SRA
3.9	-75.6	45.1	0	1917	5	22	9	0	26	NCEER
3.8	-89.4	36.8	0	1917	6	9	13	14	0	NCEER
4	-68	49	0	1917	6	12	2	0	0	NCEER
3.8	-83	36	0	1917	6	21	0	0	0	NCEER
3.4	-87.5	32.7	0	1917	6	30	1	23	0	NCEER
4.2	-94.8	46.3	0	1917	9	3	21	30	0	NCEER
3	-97.7	35.5	0	1918	1	1	0	0	0	NCEER
3.3	-83.9	35.9	0	1918	1	16	15	45	0	NCEER
3.7	-89.2	37	0	1918	2	17	8	10	0	NCEER
3.1	-84.2	42.8	0	1918	2	22	0	0	0	NCEER
4.7	-78.4	38.7	0	1918	4	10	2	9	0	NCEER
3.5	-84.1	36.1	0	1918	6	22	1	0	0	NCEER
3.1	-91.4	39.7	0	1918	7	1	19	2	0	NCEER
3.3	-71.35	46.85	0	1918	7	23	12	0	0	NCEER
4.2	-70.5	44.2	0	1918	8	21	4	11	54	USHIS
3.6	-98	35.5	0	1918	9	10	16	30	0	NCEER
4	-91.1	35	0	1918	10	4	9	21	0	NCEER
3.5	-91	36.1	0	1918	10	13	9	30	0	NCEER
4.2	-90	36	0	1918	10	16	2	15	0	NCEER
3.5	-87.5	37.8	0	1919	2	11	3	37	0	NCEER
3	-91.3	36.2	0	1919	4	8	12	30	0	NCEER
3.7	-89.2	36.6	0	1919	5	23	12	30	0	NCEER
3.8	-87.5	38.3	0	1919	5	25	9	45	0	NCEER
3.7	-97.3	37.7	0	1919	5	27	4	0	0	NCEER
3.7	-89.5	36.4	0	1919	5	28	13	45	0	NCEER
3.3	-70	43.9	0	1919	7	11	1	40	0	NCEER
3.3	-70.3	43.7	0	1919	7	23	11	50	0	NCEER
3.6	-97.3	37.7	0	1919	7	26	13	55	0	NCEER
3.8	-78.2	38.8	0	1919	9	6	2	46	0	NCEER
3.3	-70	47.6	0	1919	10	26	10	28	0	NCEER
3.6	-91	36.3	0	1919	11	3	20	40	0	NCEER
3.3	-69.71	48.15	0	1920	2	6	0	0	0	NCEER

Table 2.5-1 {USGS Earthquake Catalog for the CEUS with $m_b \geq 3.0$ }

(Page 17 of 65)

m_b	Longitude (degree)	Latitude (degree)	Depth (km)	Year	Month	Day	Hour	Minute	Second	Catalog Reference
3.9	-93.3	37.2	0	1920	2	29	3	5	0	NCEER
3.7	-88.2	36.3	0	1920	4	7	20	45	0	NCEER
3.5	-89.1	38.6	0	1920	4	30	15	12	0	NCEER
3.9	-89.6	38	0	1920	5	1	15	15	0	NCEER
3.3	-71.5	43.1	0	1920	5	23	8	0	0	NCEER
3.3	-70.5	43.5	0	1920	6	7	8	0	0	NCEER
3.5	-103.2	43.2	0	1920	7	14	23	0	0	NCEER
3.3	-78.4	38.7	0	1920	7	24	0	0	0	NCEER
3.7	-94.3	38.6	0	1920	10	3	14	15	0	NCEER
3.4	-73.43	46.01	0	1920	11	8	0	0	0	NCEER
3.3	-67.1	45	0	1920	11	9	0	40	0	NCEER
3.4	-85	36	0	1920	12	24	7	30	0	NCEER
3.3	-89.5	36.4	0	1921	1	9	21	54	0	NCEER
3.2	-74.91	40.01	0	1921	1	26	23	40	0	NCEER
3.7	-89.2	37	0	1921	2	27	22	16	0	NCEER
4	-88	40	0	1921	3	14	12	15	0	NCEER
3	-96.7	43.5	0	1921	3	16	23	45	0	NCEER
3.1	-87.8	37.9	0	1921	3	31	20	3	0	NCEER
3.3	-70.4	42.5	0	1921	7	29	21	14	0	NCEER
3.8	-78.4	37.8	0	1921	8	7	6	30	0	NCEER
3.4	-76	47	0	1921	8	27	8	12	16	NCEER
3.5	-90.1	38.3	0	1921	9	9	3	0	0	NCEER
3.1	-98.7	43.7	0	1921	9	24	0	30	0	NCEER
3.5	-88.6	37.7	0	1921	10	1	9	0	0	NCEER
3.7	-90.1	38.3	0	1921	10	9	7	50	0	NCEER
3.3	-67	44.8	0	1921	10	10	13	0	0	NCEER
3.4	-84.6	35.8	0	1921	12	15	13	20	0	NCEER
4	-99.3	43.8	0	1922	1	2	14	50	0	NCEER
3.7	-87.8	37.9	0	1922	1	11	3	42	0	NCEER
4.6	-88.4	37.9	0	1922	3	22	22	30	0	NCEER
4.6	-89.4	37.4	0	1922	3	23	2	22	0	USHIS
3.8	-88.9	37	0	1922	3	23	21	45	0	NCEER
3.8	-90.4	36.7	0	1922	3	28	16	42	0	NCEER
3.1	-86.7	35.5	0	1922	3	30	1	20	0	NCEER
3.3	-82.3	36.8	0	1922	3	30	3	21	0	NCEER
3.9	-89.6	36.1	0	1922	3	30	16	53	0	NCEER
3.3	-82.2	36.5	0	1922	3	30	22	20	0	NCEER
3.3	-71.4	43.4	0	1922	5	7	22	40	0	NCEER
3.5	-66.6	46.5	0	1922	7	2	22	25	35	NCEER
3.4	-88.5	43.8	0	1922	7	7	0	0	0	NCEER
4.6	-88.2	37.4	0	1922	11	27	3	31	0	NCEER
3.5	-75.1	44.4	0	1922	12	8	21	24	0	NCEER
3.9	-89.4	38.9	0	1923	3	9	2	45	0	SRA
3.7	-89.7	34.6	0	1923	3	27	8	0	0	NCEER
3.7	-89.2	37	0	1923	5	6	7	50	0	NCEER

Table 2.5-1 {USGS Earthquake Catalog for the CEUS with $m_b \geq 3.0$ }

(Page 18 of 65)

m_b	Longitude (degree)	Latitude (degree)	Depth (km)	Year	Month	Day	Hour	Minute	Second	Catalog Reference
3	-96.2	41.7	0	1923	9	10	6	30	0	NCEER
4.1	-90	35.3	0	1923	10	28	17	10	0	NCEER
3.3	-89.9	40	0	1923	11	10	4	0	0	NCEER
3.6	-90.4	35.5	0	1923	11	26	23	25	0	NCEER
3.1	-89.2	37	0	1923	11	29	23	20	0	NCEER
3.3	-82.5	34.8	0	1923	12	31	20	6	0	NCEER
4.3	-90	36	0	1924	1	1	3	5	0	NCEER
3.3	-78.1	39.1	0	1924	1	5	0	0	0	NCEER
3.5	-70.2	47.8	0	1924	3	4	19	15	0	NCEER
4	-88.8	37	0	1924	4	2	11	15	0	NCEER
3.7	-89.8	36.5	0	1924	6	7	5	42	0	NCEER
3.7	-76.5	45.7	0	1924	7	15	0	10	0	NCEER
3.4	-104.5	36	0	1924	8	13	4	23	0	NCEER
3.1	-100.1	40.9	0	1924	9	24	11	0	0	NCEER
4.4	-82.6	35	0	1924	10	20	8	30	0	NCEER
4	-82.2	36.6	0	1924	11	13	10	30	0	NCEER
3.3	-76.3	45.5	0	1924	11	14	1	32	0	NCEER
3.5	-79.9	37.3	0	1924	12	26	4	30	0	NCEER
3.6	-103.5	43.5	0	1924	12	30	22	10	0	NCEER
3.9	-70.6	42.6	0	1925	1	7	13	7	0	NCEER
3.6	-91.7	36.2	0	1925	1	27	22	42	0	NCEER
6.6	-69.84	47.76	9	1925	3	1	2	19	14.7	NCEER
3.3	-71.5	42.9	0	1925	3	9	0	0	0	NCEER
3.4	-83.9	39.5	0	1925	3	27	4	6	0	NCEER
3.6	-70.8	41.7	0	1925	4	24	7	56	0	NCEER
4.9	-88.2	38	0	1925	4	27	4	5	0	NCEER
3.3	-70.9	42.5	0	1925	5	4	17	51	0	NCEER
3.6	-88.6	36.7	0	1925	5	13	12	0	0	NCEER
3.5	-77.5	37.3	0	1925	5	16	1	30	0	NCEER
3.5	-93.2	36.2	0	1925	7	8	16	0	0	NCEER
3.8	-90	38.8	0	1925	7	13	0	0	0	NCEER
3.3	-77.5	37.6	0	1925	7	14	21	20	0	NCEER
3.1	-101.2	34.5	0	1925	7	29	11	30	0	NCEER
3.4	-100.3	34.5	0	1925	7	30	8	0	0	NCEER
4.8	-101.3	35.4	0	1925	7	30	12	17	0	NCEER
3.1	-97.4	42.8	0	1925	8	25	6	27	0	NCEER
4.5	-87.2	37.9	0	1925	9	2	11	55	0	NCEER
3.3	-71.22	46.82	0	1925	10	9	5	0	0	NCEER
4	-71.1	43.7	0	1925	10	9	13	55	0	NCEER
3.3	-70.2	44.1	0	1925	10	18	21	30	0	NCEER
3.5	-73	47	0	1925	10	19	12	5	17	NCEER
3.4	-72.4	41.7	0	1925	11	14	13	4	0	NCEER
3.3	-72.7	41.8	0	1925	11	16	6	20	0	NCEER
4.3	-107	44.6	0	1925	11	18	1	50	0	NCEER
3.3	-71.8	41.6	0	1926	1	4	0	0	0	NCEER

Table 2.5-1 {USGS Earthquake Catalog for the CEUS with $m_b \geq 3.0$ }

(Page 19 of 65)

m_b	Longitude (degree)	Latitude (degree)	Depth (km)	Year	Month	Day	Hour	Minute	Second	Catalog Reference
4	-94.9	35.6	0	1926	1	20	0	0	0	NCEER
3.5	-75	40	0	1926	1	26	23	40	0	NCEER
3.3	-74.1	44.3	0	1926	1	27	0	0	0	NCEER
3.3	-71	47.7	0	1926	2	19	20	20	0	NCEER
3.5	-71.8	42.8	0	1926	3	18	21	9	0	NCEER
3.5	-88.6	37.8	0	1926	3	22	14	30	0	NCEER
3.9	-89	36.2	0	1926	4	28	2	16	0	SRA
3	-73.9	40.9	0	1926	5	12	3	30	0	NCEER
4	-94.9	35.6	0	1926	6	20	14	20	0	NCEER
3.5	-82.1	35.9	0	1926	7	8	9	50	0	NCEER
3.3	-71.5	47	0	1926	7	18	6	0	0	NCEER
3.3	-77.1	45.8	0	1926	8	23	16	40	0	NCEER
3.4	-70	44.7	0	1926	8	28	21	0	0	NCEER
3.5	-90.4	36.7	0	1926	10	27	16	22	0	NCEER
3.4	-83.6	41.7	0	1926	10	28	8	42	0	NCEER
3.8	-82.1	39.1	0	1926	11	5	16	53	0	USHIS
3.3	-67.5	45	0	1926	11	24	19	30	0	NCEER
3.7	-89.4	36.7	0	1926	12	13	23	3	0	NCEER
3.5	-89.5	36.4	0	1926	12	17	0	0	0	NCEER
3.6	-97.7	38.3	0	1927	1	7	9	30	0	NCEER
3.9	-89.7	37.4	0	1927	2	2	1	30	0	SRA
3.8	-90.4	36.7	0	1927	2	3	8	0	0	SRA
3.1	-82.5	40.7	0	1927	2	17	5	30	0	NCEER
3.4	-71.4	43.3	0	1927	3	9	4	8	0	NCEER
3.3	-75.2	44.6	0	1927	3	12	22	12	0	NCEER
3.9	-95.3	39.9	0	1927	3	18	17	25	0	NCEER
3.3	-72.8	41.7	0	1927	3	30	0	0	0	NCEER
3.5	-89.5	36.3	0	1927	4	18	10	30	0	NCEER
4.7	-90.2	36	0	1927	5	7	8	28	0	NCEER
3.9	-74	40.3	0	1927	6	1	12	23	0	NCEER
3.6	-79	38	0	1927	6	10	7	16	0	NCEER
3.6	-86	34.7	0	1927	6	16	12	0	0	NCEER
4	-71	47.3	0	1927	7	25	0	56	0	NCEER
4.1	-89.5	36.4	0	1927	8	13	16	10	0	NCEER
3.3	-85.3	35.1	0	1927	10	8	4	30	0	NCEER
3.1	-98.9	41.6	0	1927	10	14	16	10	0	NCEER
3.3	-73.8	44.7	0	1927	10	24	11	0	0	NCEER
3.3	-76.2	36.3	0	1927	10	27	0	0	0	NCEER
3.4	-81.2	40.9	0	1927	10	29	0	0	0	NCEER
3.1	-79.06	43.1	0	1927	11	13	0	50	0	NCEER
3.4	-90.2	32.3	0	1927	11	13	16	21	0	NCEER
3.3	-78	33.9	0	1927	11	23	0	50	0	NCEER
3.5	-89.4	28.9	0	1927	12	15	4	30	0	NCEER
3.3	-71.6	41.2	0	1928	1	13	19	50	0	NCEER
3.1	-90	42	0	1928	1	23	9	19	0	NCEER

Table 2.5-1 {USGS Earthquake Catalog for the CEUS with $m_b \geq 3.0$ }

(Page 20 of 65)

m_b	Longitude (degree)	Latitude (degree)	Depth (km)	Year	Month	Day	Hour	Minute	Second	Catalog Reference
3.3	-70.2	48	0	1928	1	27	0	0	0	NCEER
3.5	-69	45.3	0	1928	2	8	0	0	0	NCEER
3.5	-87	35.6	0	1928	3	7	2	45	0	NCEER
3.3	-90.2	38.6	0	1928	3	17	21	15	0	NCEER
4	-74.3	44.5	0	1928	3	18	15	25	0	NCEER
3.3	-69	45.3	0	1928	3	22	13	30	0	NCEER
3.1	-89.5	36.6	0	1928	4	15	11	0	0	NCEER
3.1	-89.5	37.3	0	1928	4	15	15	5	0	NCEER
3.1	-89.2	36.5	0	1928	4	23	11	0	0	NCEER
3.8	-71.2	44.5	0	1928	4	25	23	38	0	NCEER
3.1	-89.5	36.6	0	1928	5	31	22	40	0	NCEER
3	-84.1	40.4	0	1928	10	27	0	0	0	NCEER
3.4	-77.5	37.5	0	1928	10	30	11	45	0	NCEER
4.6	-82.83	36.11	0	1928	11	3	4	2	49.8	NCEER
3.1	-89.1	39.5	0	1928	11	8	14	15	0	NCEER
3.1	-91.1	36.1	0	1928	11	10	6	20	0	NCEER
3.5	-103.7	44.1	0	1928	11	16	13	45	0	NCEER
3.2	-67.2	45	0	1928	11	20	2	30	0	NCEER
3.7	-82.3	35.8	0	1928	11	20	3	45	0	NCEER
4	-81.5	50	0	1928	12	1	0	0	0	NCEER
3.3	-80.3	35.3	0	1928	12	23	2	30	0	NCEER
3.1	-93.9	47.6	0	1928	12	23	6	10	0	NCEER
3.1	-91.1	36.1	0	1928	12	26	3	25	0	NCEER
3.3	-80.3	33.9	0	1929	1	3	12	5	0	NCEER
3.3	-70.3	44	0	1929	2	5	19	9	0	NCEER
3.2	-87.6	38.3	0	1929	2	14	20	12	0	NCEER
3.1	-90.6	37.6	0	1929	2	26	8	15	0	NCEER
3.7	-84.2	40.4	0	1929	3	8	9	6	0	NCEER
3.3	-71.9	45.4	0	1929	5	11	9	30	0	NCEER
3.5	-89.5	36.4	0	1929	5	13	3	50	0	NCEER
3.4	-89.4	28.9	0	1929	7	28	17	0	0	NCEER
5.2	-78.4	42.91	9	1929	8	12	11	24	48.7	NCEER
3.9	-96.6	39	0	1929	9	23	11	0	0	NCEER
3.4	-97.4	42.8	0	1929	10	6	12	30	0	NCEER
3.3	-82.4	34.3	0	1929	10	28	2	15	0	NCEER
3.1	-99.8	37.2	0	1929	11	26	16	20	0	NCEER
3.4	-96.6	39.2	0	1929	12	7	8	2	0	NCEER
3.6	-78.5	38.1	0	1929	12	26	2	56	0	NCEER
4	-97.9	35.5	0	1929	12	28	0	30	0	NCEER
4.6	-65.83	46.73	0	1930	1	4	14	30	38	NCEER
3.1	-91.1	36.1	0	1930	1	26	21	0	0	NCEER
3	-90.2	37	0	1930	2	25	12	45	0	NCEER
3.3	-71.6	43.3	0	1930	3	19	0	15	0	NCEER
3.5	-90	35.1	0	1930	3	26	8	56	0	SRA
3.1	-89.7	36.1	0	1930	4	2	9	39	0	NCEER

Table 2.5-1 {USGS Earthquake Catalog for the CEUS with $m_b \geq 3.0$ }

(Page 21 of 65)

m_b	Longitude (degree)	Latitude (degree)	Depth (km)	Year	Month	Day	Hour	Minute	Second	Catalog Reference
3.6	-71.22	45.73	0	1930	6	19	12	6	56	NCEER
3.2	-84	40.5	0	1930	6	26	21	45	0	NCEER
3.1	-83.2	40.6	0	1930	7	11	0	15	0	NCEER
3.1	-69.83	47.5	0	1930	7	13	4	52	39.3	NCEER
3.1	-70.8	41.5	0	1930	8	1	2	0	0	NCEER
3.1	-91.4	39.7	0	1930	8	8	18	31	0	NCEER
3.5	-89.1	37	0	1930	8	29	6	26	54	NCEER
3.5	-84.4	35.9	0	1930	8	30	9	28	0	NCEER
3.7	-89.4	36.6	0	1930	9	1	20	27	24	NCEER
3.5	-84.3	40.3	0	1930	9	30	20	40	0	NCEER
3.9	-68.7	48.93	0	1930	10	8	1	8	41	NCEER
3.6	-83.9	36	0	1930	10	16	21	50	0	NCEER
4.2	-91	30.1	0	1930	10	19	12	12	0	NCEER
3.3	-76.5	39.1	0	1930	11	1	1	34	0	NCEER
3.3	-92.8	34.3	0	1930	11	16	12	30	0	NCEER
3.5	-70.17	47.65	0	1930	12	13	23	18	23.7	NCEER
3.2	-90.7	38.5	0	1930	12	23	14	44	0	NCEER
3.1	-80.3	34.5	0	1930	12	26	3	0	0	NCEER
3.5	-87	39	0	1931	1	6	2	51	0	SRA
5.4	-70.4	47.3	0	1931	1	8	0	13	0.3	NCEER
3.1	-98.7	43.7	0	1931	1	17	18	45	0	NCEER
3	-84.2	40.4	0	1931	3	21	15	48	0	NCEER
3.5	-88.3	36.9	0	1931	4	1	23	20	9	NCEER
3.1	-89	36.8	0	1931	4	6	15	37	3	NCEER
4.8	-73.78	43.47	5	1931	4	20	19	54	30.6	NCEER
3.1	-78.9	42.9	0	1931	4	22	0	0	0	NCEER
4.2	-86.6	33.7	0	1931	5	5	12	18	0	NCEER
3	-73.4	41.6	0	1931	7	1	2	45	0	NCEER
3.3	-89.5	36.6	0	1931	7	18	14	52	0	NCEER
3.3	-65.77	44.62	0	1931	8	7	0	0	0	NCEER
3.8	-94.7	39.1	0	1931	8	9	6	18	37	NCEER
4.7	-84.27	40.43	5	1931	9	20	23	4	54	NCEER
4.5	-76.07	47	0	1931	9	23	22	47	37	NCEER
3.4	-70.17	47.33	0	1931	11	14	14	2	29.5	NCEER
3.3	-89.9	35.9	0	1931	12	10	8	11	36	NCEER
4.7	-89.8	34.1	0	1931	12	17	3	36	0	NCEER
3.1	-78.4	37.6	0	1932	1	5	4	5	0	NCEER
3.1	-81.6	41.1	0	1932	1	21	0	0	0	NCEER
3.8	-99.6	39	0	1932	1	29	0	15	0	NCEER
3.8	-74.67	46.47	0	1932	3	9	5	23	38.8	NCEER
3.6	-96.4	31.7	0	1932	4	9	10	15	0	NCEER
3.4	-90.2	36	0	1932	11	22	7	56	42	NCEER
3.2	-74.1	44.4	0	1932	12	7	3	15	0	NCEER
3.2	-70.5	47.45	0	1933	1	11	23	32	0	NCEER
3.8	-74.65	45.3	0	1933	1	21	16	4	39.5	NCEER

Table 2.5-1 {USGS Earthquake Catalog for the CEUS with $m_b \geq 3.0$ }

(Page 22 of 65)

m_b	Longitude (degree)	Latitude (degree)	Depth (km)	Year	Month	Day	Hour	Minute	Second	Catalog Reference
3.3	-74.7	40.2	0	1933	1	25	2	0	0	NCEER
3.8	-99.9	39.8	0	1933	2	20	17	0	0	NCEER
3.3	-84.2	40.3	0	1933	2	23	3	20	0	NCEER
3.4	-69.93	47.43	0	1933	2	25	9	43	2.7	NCEER
3.1	-90.4	36.7	0	1933	3	11	12	48	0	NCEER
3.4	-83.7	38.6	0	1933	5	28	15	10	0	NCEER
3.3	-83.5	33.3	0	1933	6	9	11	30	0	NCEER
3	-73.8	41	0	1933	6	26	14	10	0	NCEER
3.3	-89.9	37.9	0	1933	7	13	14	42	39	NCEER
3.9	-75.7	45.42	0	1933	7	14	4	48	40	NCEER
3.1	-89.9	37.9	0	1933	8	4	4	34	15	NCEER
3.3	-103.7	41.9	0	1933	8	8	0	0	0	NCEER
3.4	-98	35.5	0	1933	8	19	19	30	0	NCEER
3.1	-73.7	43	0	1933	10	29	0	0	0	NCEER
3.3	-90.6	38.6	0	1933	11	16	9	29	1	NCEER
3.1	-89.2	42.9	0	1933	12	7	5	55	0	NCEER
4	-90.2	35.8	0	1933	12	9	8	50	0	NCEER
3.5	-80	32.9	0	1933	12	23	9	40	0	NCEER
3.1	-97.7	45.9	0	1934	1	29	12	30	0	NCEER
3.3	-72.6	41.8	0	1934	1	30	10	30	0	NCEER
3.6	-72.7	44	0	1934	4	11	3	0	0	NCEER
3.9	-95.5	33.9	0	1934	4	12	1	40	0	SRA
3.9	-73.8	44.7	0	1934	4	15	2	58	0	NCEER
3.3	-74.3	44.8	0	1934	4	15	18	5	0	NCEER
3.2	-98.7	41.5	0	1934	5	11	10	40	0	NCEER
3	-89.9	37.9	0	1934	5	15	14	28	0	NCEER
3.1	-90	35.2	0	1934	7	3	3	10	41	NCEER
4.3	-103	42.7	0	1934	7	30	7	20	0	NCEER
3.2	-70.3	43.7	0	1934	8	2	14	59	0	NCEER
4.3	-89.2	36.9	0	1934	8	20	0	47	0	NCEER
3	-67	44.9	0	1934	8	26	11	36	0	NCEER
3.1	-99.1	43.4	0	1934	8	30	3	50	0	NCEER
3.2	-80.2	42	0	1934	10	29	20	7	0	NCEER
3.3	-88.5	37.5	0	1934	10	30	2	25	47	NCEER
3.4	-100.2	42.6	0	1934	11	8	4	45	0	NCEER
3.9	-90.5	41.5	0	1934	11	12	14	45	0	NCEER
3.3	-80	32.9	0	1934	12	9	9	0	0	NCEER
3.4	-83.6	35.1	0	1935	1	1	8	15	0	NCEER
3	-90.6	41.5	0	1935	1	5	18	40	0	NCEER
3.3	-77.4	37.2	0	1935	2	10	23	45	0	NCEER
4.8	-96.2	40.3	0	1935	3	1	10	59	44	NCEER
3.3	-70.2	42.2	0	1935	4	24	1	24	0	NCEER
3.1	-89.5	36.4	0	1935	7	24	1	38	0	NCEER
6.2	-79.07	46.78	0	1935	11	1	6	3	40	NCEER
3.3	-78.9	38.9	0	1935	11	1	8	30	0	NCEER

Table 2.5-1 {USGS Earthquake Catalog for the CEUS with $m_b \geq 3.0$ }

(Page 23 of 65)

m_b	Longitude (degree)	Latitude (degree)	Depth (km)	Year	Month	Day	Hour	Minute	Second	Catalog Reference
4.9	-78.17	47.23	0	1935	11	2	14	31	58	NCEER
3.3	-81.7	29.6	0	1935	11	14	3	30	0	NCEER
3.1	-83.2	41.2	0	1936	1	31	19	30	0	NCEER
3.1	-89.7	36.2	0	1936	2	17	5	5	8	NCEER
3.4	-95.2	34	0	1936	3	14	17	20	0	NCEER
4	-70.25	47.33	0	1936	3	29	0	49	23.4	NCEER
3.4	-71.5	43.5	0	1936	6	14	5	40	0	NCEER
4.4	-100.77	35.31	5	1936	6	20	3	24	3.5	NCEER
3.3	-74.2	44.7	0	1936	6	21	4	20	0	NCEER
3	-102.9	36.9	0	1936	7	12	0	23	0	NCEER
3.9	-89	36.7	0	1936	8	2	22	16	25	NCEER
3.3	-84.4	39.3	0	1936	10	8	16	30	0	NCEER
3.1	-103.5	43.5	0	1936	10	30	10	30	0	NCEER
3.3	-71.4	43.6	0	1936	11	10	2	46	0	NCEER
3.2	-71.7	44.7	0	1936	11	10	4	2	0	NCEER
3.3	-89.7	36.2	2	1937	1	30	8	57	9	NCEER
3.6	-78.7	37.7	0	1937	2	3	1	26	0	NCEER
4.9	-84.27	40.49	2	1937	3	2	14	47	33.3	NCEER
3.3	-75.2	44.6	0	1937	3	10	5	29	0	NCEER
4	-90.6	36.1	0	1937	5	17	0	49	46	NCEER
3.2	-96.9	35.3	0	1937	6	8	14	26	0	NCEER
3.5	-73.71	40.72	0	1937	7	19	3	51	0	NCEER
4.5	-65.43	47.8	5	1937	9	30	7	58	3.4	NCEER
4	-75.82	46.78	24	1937	11	6	14	31	20.6	NCEER
3.7	-74.47	46.1	1	1937	11	12	16	57	31.3	NCEER
4	-89.1	38.6	0	1937	11	17	17	4	0	NCEER
3.5	-98.2	44.5	0	1938	1	2	17	5	0	NCEER
3.2	-75.18	44.9	0	1938	1	6	13	28	42.2	NCEER
3	-76.27	45.57	0	1938	1	24	5	29	2	NCEER
3.8	-87	41.6	0	1938	2	12	6	27	0	NCEER
3.2	-75.4	46.38	0	1938	2	23	17	56	35.7	NCEER
3.1	-83.2	42.4	0	1938	3	13	16	10	0	NCEER
3.3	-103.4	42.7	0	1938	3	24	13	11	0	NCEER
3.6	-83.5	35.6	0	1938	3	31	10	10	0	NCEER
3.2	-79.08	46.72	0	1938	4	12	18	55	47	NCEER
3.1	-93.5	34.2	0	1938	4	26	5	42	0	NCEER
3	-74.5	45.37	0	1938	5	5	0	33	0.3	NCEER
3.9	-68	49	0	1938	5	17	18	32	0	NCEER
3	-66.8	46.5	0	1938	6	15	5	7	43	NCEER
3.2	-78.43	40.68	1	1938	7	15	22	46	12	NCEER
3.1	-73.7	41.08	0	1938	8	2	9	2	30	NCEER
3.8	-68.79	44.89	5	1938	8	22	12	48	9.4	NCEER
3.8	-74.36	40.05	21	1938	8	23	5	4	53.4	NCEER
3	-74.9	45.87	0	1938	9	7	23	18	18.9	NCEER
4.8	-90.254	35.413	1	1938	9	17	3	34	28.3	USHIS

Table 2.5-1 {USGS Earthquake Catalog for the CEUS with $m_b \geq 3.0$ }

(Page 24 of 65)

m_b	Longitude (degree)	Latitude (degree)	Depth (km)	Year	Month	Day	Hour	Minute	Second	Catalog Reference
3.2	-72.2	41.5	0	1938	9	20	0	0	0	NCEER
4.1	-69.58	48.78	0	1938	9	28	4	33	16	NCEER
3.8	-99.3	43.8	0	1938	10	1	22	15	0	NCEER
3.8	-96.7	43.5	0	1938	10	11	9	37	0	NCEER
3.3	-98.9	43.2	0	1938	11	4	22	10	0	NCEER
3.5	-75.25	44.75	0	1938	11	18	22	19	6	NCEER
4.2	-76.2	47.03	0	1938	11	26	7	47	57.5	NCEER
3.9	-75.4	47.6	0	1938	12	25	7	46	0	NCEER
3.3	-79.85	43.25	0	1939	1	14	8	10	16	NCEER
3.6	-95.8	46.8	0	1939	1	28	17	55	0	NCEER
3	-78.3	42.9	0	1939	2	24	0	20	0	NCEER
3.6	-77.5	46.4	0	1939	3	16	20	21	0	NCEER
3.3	-84	40.4	0	1939	3	18	14	3	0	NCEER
3.2	-89.4	36.8	0	1939	4	15	17	25	0	NCEER
3.3	-85.8	33.7	0	1939	5	5	2	45	0	NCEER
3.9	-96.4	35	0	1939	6	1	7	30	0	NCEER
3.1	-98.9	43	0	1939	6	10	18	30	0	NCEER
3.1	-84	40.3	0	1939	6	18	3	20	0	NCEER
4.1	-92.6	34.1	0	1939	6	19	21	43	12	NCEER
3.4	-86.6	34.7	0	1939	6	24	10	27	0	NCEER
4.5	-69.98	47.59	14	1939	6	24	17	20	18.3	NCEER
5.6	-69.8	47.8	15	1939	10	19	11	53	58	NCEER
4.1	-70.5	47.8	0	1939	11	7	2	40	32	NCEER
3.8	-75.05	39.58	3	1939	11	15	2	53	48.7	NCEER
4.9	-90.14	38.18	0	1939	11	23	15	14	52	NCEER
3.5	-76.6	39.5	0	1939	11	26	5	20	0	NCEER
3.6	-71.4	47.97	0	1939	12	8	1	17	47	NCEER
3	-79.08	46.72	0	1940	1	5	0	34	14	NCEER
3.4	-70.8	41.6	0	1940	1	28	23	12	0	NCEER
4	-76.83	46.5	0	1940	2	10	20	57	17.3	NCEER
3.5	-78.5	38.8	0	1940	3	26	0	1	0	NCEER
3.8	-70.73	47.73	0	1940	4	13	8	13	34	NCEER
3.6	-73.2	45.8	0	1940	5	16	14	0	17.1	NCEER
3.4	-88.6	37.1	0	1940	5	31	19	3	0	NCEER
3.1	-82.3	40.9	0	1940	6	16	4	30	0	NCEER
3.1	-74.78	46.25	0	1940	8	4	16	20	52	NCEER
3	-74.83	45.77	0	1940	8	7	23	57	35.3	NCEER
3.5	-71.13	47	0	1940	9	11	1	6	55.4	NCEER
4.7	-69.8	47.8	0	1940	10	13	19	50	51	NCEER
3.3	-85.1	34.7	0	1940	10	19	5	54	0	NCEER
5	-90.1	38.2	0	1940	11	23	21	15	0	NCEER
3.1	-94	33	0	1940	12	2	16	16	0	NCEER
5.5	-71.37	43.87	10	1940	12	20	7	27	26.2	NCEER
3.2	-82.9	35.9	0	1940	12	25	6	5	0	NCEER
3.6	-87.3	37.9	0	1940	12	29	2	30	0	SRA

Table 2.5-1 {USGS Earthquake Catalog for the CEUS with $m_b \geq 3.0$ }

(Page 25 of 65)

m_b	Longitude (degree)	Latitude (degree)	Depth (km)	Year	Month	Day	Hour	Minute	Second	Catalog Reference
3.4	-83.9	36	0	1941	3	4	6	15	0	NCEER
3	-75.5	46.27	0	1941	3	5	7	29	23.2	NCEER
3.3	-73.92	44.73	0	1941	4	4	8	10	43.7	NCEER
3.3	-82.6	35.6	0	1941	5	10	11	12	0	NCEER
3.7	-103.5	43.5	0	1941	5	25	6	25	0	NCEER
3	-70.34	47.39	0	1941	6	22	9	59	31	NCEER
4.1	-76.83	47.4	0	1941	6	26	4	5	44.9	NCEER
3	-90.8	32.3	0	1941	6	28	18	30	0	NCEER
3.7	-67.9	46.1	0	1941	8	30	10	21	0	NCEER
3	-85.3	35	0	1941	9	8	9	45	0	NCEER
4	-70.73	47.63	0	1941	10	6	16	34	27.6	NCEER
3.3	-89.7	36.2	0	1941	10	8	7	51	0	NCEER
3	-72.3	42.3	0	1941	10	11	8	15	0	NCEER
3.2	-99	35.4	0	1941	10	18	7	48	0	NCEER
3.3	-74.8	44.77	0	1941	10	21	6	10	41	NCEER
3.3	-89.1	37	0	1941	10	21	16	53	0	NCEER
3.6	-74.3	45.7	0	1941	10	24	14	13	59.3	NCEER
3.1	-90	35.1	0	1941	11	15	3	7	0	NCEER
4.2	-89.7	35.5	0	1941	11	17	3	8	0	NCEER
3.3	-90.3	38.4	0	1942	1	14	18	5	0	NCEER
3.3	-81	26.5	0	1942	1	19	0	0	0	NCEER
3.1	-74.77	46.83	0	1942	2	18	7	55	12	NCEER
3.6	-89.7	41.2	0	1942	3	1	14	43	10	NCEER
3.2	-70.4	44.2	0	1942	3	8	23	37	0	NCEER
3	-103.5	44.4	0	1942	3	11	16	55	0	NCEER
3	-88.6	37.7	0	1942	3	29	12	43	0	NCEER
4.4	-74.67	45.77	0	1942	5	20	12	19	22.8	NCEER
3.9	-73.8	44.7	0	1942	5	24	11	33	0	NCEER
3.5	-97.9	36.4	0	1942	6	12	4	50	0	NCEER
3.7	-77.5	46.8	0	1942	8	26	17	54	0	NCEER
3.1	-89.2	37	0	1942	8	31	9	28	0	NCEER
3.1	-71.5	46.97	0	1942	9	5	14	30	24.1	NCEER
3.4	-99.3	38.8	0	1942	9	10	9	0	0	NCEER
3.7	-67.4	49.22	0	1942	9	11	11	5	13	NCEER
3.3	-76	46.78	0	1942	9	15	22	32	46	NCEER
3	-73.8	42.57	0	1942	10	2	22	29	50.5	NCEER
3.3	-78.4	37.6	0	1942	10	7	2	15	0	NCEER
3.4	-75.25	40.97	0	1942	10	24	17	27	3.6	NCEER
3.6	-75.05	46.42	0	1942	11	16	0	13	29.4	NCEER
3	-90.2	38.6	0	1942	11	17	18	18	0	NCEER
4.2	-76.07	46.97	0	1942	12	5	21	10	51.2	NCEER
4.4	-69.33	45.16	0	1943	1	14	21	32	38	NCEER
3.7	-75.77	46.5	0	1943	2	28	16	40	1.2	NCEER
4.4	-81.31	41.63	7	1943	3	9	3	25	24.9	NCEER
3.9	-71.6	43.7	0	1943	3	14	14	2	0	NCEER

Table 2.5-1 {USGS Earthquake Catalog for the CEUS with $m_b \geq 3.0$ }

(Page 26 of 65)

m_b	Longitude (degree)	Latitude (degree)	Depth (km)	Year	Month	Day	Hour	Minute	Second	Catalog Reference
3.1	-85.8	38.3	0	1943	4	13	17	0	0	NCEER
3.2	-73.83	44.77	0	1943	5	9	11	3	12.5	NCEER
3.1	-103.5	43.5	0	1943	5	16	19	40	0	NCEER
3	-90.4	38.6	0	1943	6	8	19	50	0	NCEER
4	-105	48.5	0	1943	6	25	4	25	0	NCEER
3.8	-73.03	44.84	22	1943	7	6	22	10	16	NCEER
3.3	-70.65	47.55	0	1943	9	25	5	52	36.1	NCEER
3.8	-70.4	47.27	0	1943	9	28	16	30	25.2	NCEER
3.9	-70.08	47.38	0	1943	11	6	0	6	40.5	NCEER
3.2	-74.87	47.68	0	1943	12	6	7	19	40	NCEER
3	-69.6	44.6	0	1943	12	19	9	0	44	NCEER
3.3	-80.2	33	0	1943	12	28	10	25	0	NCEER
3.2	-89.7	37.5	0	1944	1	7	5	18	0	NCEER
4.2	-75.5	39.8	0	1944	1	8	0	0	0	DNAG
4.3	-76.78	45.83	0	1944	1	22	21	55	9.1	NCEER
3.3	-80	32.9	0	1944	1	28	17	30	0	NCEER
4	-70.5	47.4	0	1944	2	5	12	37	52.5	NCEER
3.7	-76.2	40.8	0	1944	2	5	16	22	0	NCEER
4.1	-78.9	46.7	0	1944	3	8	12	49	0	NCEER
4.9	-67.4	49.9	0	1944	4	9	12	44	0	NCEER
3.7	-70.28	47.3	0	1944	6	9	15	19	8.7	NCEER
5.1	-67.75	49.42	0	1944	6	23	6	37	53	NCEER
3.7	-74.25	46	0	1944	6	24	23	48	38.5	NCEER
5.8	-74.72	44.96	12	1944	9	5	4	38	45.7	NCEER
5	-107.5	39	0	1944	9	9	4	12	20	DNAG
3.9	-90	37.9	0	1944	9	25	11	37	23	NCEER
4.2	-67	48.5	0	1944	10	14	13	26	17	NCEER
4.4	-80.8	48.7	0	1944	11	5	19	7	0	NCEER
4.1	-84.4	40.4	0	1944	11	13	11	52	0	NCEER
3.1	-87.1	45.7	0	1944	12	10	11	0	0	NCEER
3.6	-72.8	41.6	0	1944	12	14	3	15	0	NCEER
3.1	-89.7	36.2	0	1944	12	23	7	23	0	NCEER
3.2	-90.2	37.8	0	1945	1	16	2	0	0	NCEER
3.3	-80	32.9	0	1945	1	30	20	20	0	NCEER
3.7	-90.2	38.6	0	1945	3	28	1	45	58	NCEER
3.1	-76.4	43	0	1945	4	15	13	15	0	NCEER
3.3	-89.7	36.5	0	1945	5	2	11	22	0	NCEER
3.1	-90.2	38.6	0	1945	5	21	7	51	0	NCEER
4.3	-75.4	47.08	0	1945	6	12	7	58	15.1	NCEER
3.6	-84.5	35	0	1945	6	14	3	25	0	NCEER
4.7	-71.09	47.34	5	1945	6	18	15	20	4.7	NCEER
3.9	-76.8	48.47	0	1945	7	2	13	29	52.1	NCEER
3.3	-67	44.9	0	1945	7	15	10	44	0	NCEER
4	-81.38	33.75	5	1945	7	26	10	32	16.4	NCEER
3.1	-89.8	37	0	1945	9	23	6	22	0	NCEER

Table 2.5-1 {USGS Earthquake Catalog for the CEUS with $m_b \geq 3.0$ }

(Page 27 of 65)

m_b	Longitude (degree)	Latitude (degree)	Depth (km)	Year	Month	Day	Hour	Minute	Second	Catalog Reference
4.7	-69.81	47.99	5	1945	10	9	13	18	42	NCEER
3.3	-78.5	37.5	0	1945	10	12	19	0	0	NCEER
3.1	-97.9	43	0	1945	11	10	8	0	0	NCEER
3.7	-89.2	37	0	1945	11	13	8	21	0	NCEER
3	-74.9	45	0	1945	12	2	15	22	32	SRA
4.3	-68.7	49.4	0	1946	1	17	8	4	52	NCEER
3.3	-89.1	38.6	0	1946	2	25	0	52	0	NCEER
3.8	-84.9	35.2	0	1946	4	7	5	0	0	NCEER
3.6	-73.43	45.73	0	1946	4	21	5	5	55.5	NCEER
4	-90.8	36.6	0	1946	5	15	6	10	0	NCEER
3	-74.53	44.65	0	1946	6	27	21	6	22	NCEER
4	-98.6	44.1	0	1946	7	23	6	45	0	NCEER
3.3	-71.47	47.33	0	1946	9	1	4	39	41	NCEER
3	-74.88	44.9	0	1946	9	4	19	30	0	NCEER
3.2	-75	47.72	0	1946	9	19	0	53	28.8	NCEER
3.4	-72.15	46.43	0	1946	9	26	21	19	8.2	NCEER
4	-90.6	37.5	0	1946	10	8	1	12	2	NCEER
3.1	-103.6	48.1	0	1946	10	26	20	37	0	NCEER
3.6	-76.6	41.5	0	1946	10	28	20	36	0	NCEER
3.1	-77.45	42.87	0	1946	11	10	11	41	23.1	NCEER
3	-74.9	45	0	1946	11	11	10	20	47	SRA
3.1	-74.68	45.17	0	1946	11	24	10	20	47.2	NCEER
3	-74.9	44.9	0	1946	12	25	4	48	3	NCEER
3.3	-73.6	41	0	1947	1	4	18	51	0	NCEER
3.9	-76.7	46.8	0	1947	1	19	0	45	1.7	NCEER
4.2	-70.53	47.67	0	1947	2	2	16	50	32.3	NCEER
3.1	-88.3	42.1	0	1947	3	16	15	30	0	NCEER
4	-88.4	37	0	1947	3	26	0	0	0	NCEER
4	-70.23	47.37	0	1947	3	29	12	28	52.4	NCEER
3.5	-87.9	43	0	1947	5	6	21	27	0	NCEER
3.1	-100.9	46	0	1947	5	14	5	2	0	NCEER
3	-100.3	44.4	0	1947	5	16	5	45	0	NCEER
3.4	-84	36	0	1947	6	6	12	55	0	NCEER
4.2	-90.2	38.4	0	1947	6	30	4	23	53	NCEER
4.4	-81.1	46.5	0	1947	8	8	5	39	0	NCEER
4.5	-85	41.93	2	1947	8	10	2	46	41.3	NCEER
3.1	-98.9	43.1	0	1947	8	25	14	0	0	NCEER
4.3	-81.3	47	0	1947	9	14	19	29	0	NCEER
3.3	-92.6	31.9	0	1947	9	20	21	30	0	NCEER
3.8	-70.72	47.55	0	1947	10	22	9	36	38.3	NCEER
3.3	-80	32.9	0	1947	11	2	4	30	0	NCEER
4.5	-81.2	45.7	0	1947	11	3	19	51	0	NCEER
3.7	-90.6	36.7	0	1947	12	1	7	47	33	NCEER
4	-90.1	35.6	0	1947	12	16	3	27	0	SRA
3.2	-85.3	35	0	1947	12	27	19	0	0	NCEER

Table 2.5-1 {USGS Earthquake Catalog for the CEUS with $m_b \geq 3.0$ }

(Page 28 of 65)

m_b	Longitude (degree)	Latitude (degree)	Depth (km)	Year	Month	Day	Hour	Minute	Second	Catalog Reference
3.8	-69.2	45.2	0	1947	12	28	19	58	0	NCEER
4.5	-70.4	47.3	0	1948	1	1	18	33	45.3	NCEER
3.3	-78.3	37.7	0	1948	1	5	2	45	0	NCEER
3.5	-78.5	37.5	0	1948	1	5	3	20	0	NCEER
3.1	-89.1	38.6	0	1948	1	6	1	34	0	NCEER
3.1	-89.7	43.1	0	1948	1	15	17	40	0	NCEER
3.7	-69	50	0	1948	1	16	6	2	56	NCEER
3.4	-84.1	36.4	0	1948	2	10	0	4	0	NCEER
4.6	-102.48	36.22	5	1948	3	12	4	29	6.3	NCEER
3.1	-97.3	37.7	0	1948	4	3	3	0	0	NCEER
3.1	-91.8	41.7	0	1948	4	20	14	17	0	NCEER
3.2	-71.8	41.4	0	1948	5	4	2	23	0	NCEER
4	-73.69	45.86	3	1948	5	7	12	2	27.3	NCEER
3.7	-73.87	45.23	0	1948	6	9	3	4	12.2	NCEER
3.3	-82.2	26.5	0	1948	11	8	17	44	0	NCEER
3.5	-70.3	46.7	0	1948	11	13	16	49	56.6	NCEER
3	-69.2	45.2	0	1948	11	29	4	56	0	NCEER
3.5	-89.7	36.4	0	1949	1	14	3	49	0	NCEER
3.3	-80	32.9	0	1949	2	2	10	52	0	NCEER
3.6	-77.6	37.6	0	1949	5	8	11	1	0	NCEER
3.3	-99	42.5	0	1949	5	13	4	15	0	NCEER
3.1	-100	45	0	1949	6	3	0	0	0	NCEER
3.3	-80	32.9	0	1949	6	27	6	53	0	NCEER
3.2	-83	36.7	0	1949	9	17	9	30	0	NCEER
4.7	-70.58	44.84	20	1949	10	5	2	33	47.8	NCEER
4.2	-74.9	45.49	14	1949	10	16	23	33	45.4	NCEER
3.4	-72.12	46.47	0	1949	10	30	20	51	13.7	NCEER
5	-109.5	35.7	0	1950	1	17	0	51	0	DNAG
5.3	-110.5	40.5	0	1950	1	18	1	55	51	USHIS
3.7	-92.7	37.7	0	1950	2	8	10	37	0	NCEER
3.3	-95.2	46.1	0	1950	2	15	10	5	0	NCEER
4	-74.5	46	0	1950	3	6	16	14	11.8	NCEER
3.1	-97.1	33.5	0	1950	3	20	13	24	0	NCEER
3.3	-75.8	41.5	0	1950	3	20	22	55	11.5	NCEER
4.9	-75.5	47.83	0	1950	4	14	18	20	48.5	NCEER
3.1	-84.2	39.8	0	1950	4	20	0	0	0	NCEER
3.5	-84	35.8	0	1950	6	19	4	19	0	NCEER
4.3	-68.1	49.9	0	1950	6	29	9	13	33	NCEER
3.2	-70.25	47.33	0	1950	8	4	6	45	21	NCEER
4	-74.72	45.2	0	1950	8	4	14	29	28.7	NCEER
3	-89.9	35.7	0	1950	9	17	5	48	0	NCEER
3	-77.12	45.82	0	1950	10	29	5	59	26	NCEER
3.3	-78.3	37.7	0	1950	11	26	7	45	0	NCEER
3.2	-72.5	41.5	0	1951	1	26	3	27	0	NCEER
3.3	-80	32.9	0	1951	3	4	2	55	0	NCEER

Table 2.5-1 {USGS Earthquake Catalog for the CEUS with $m_b \geq 3.0$ }

(Page 29 of 65)

m_b	Longitude (degree)	Latitude (degree)	Depth (km)	Year	Month	Day	Hour	Minute	Second	Catalog Reference
3.5	-77.6	37.6	0	1951	3	9	7	0	0	NCEER
3.7	-71.53	41.52	5	1951	6	10	17	20	37.7	NCEER
4.3	-103.04	35.22	1	1951	6	20	18	37	11.1	NCEER
4.2	-67.5	50	0	1951	6	28	1	3	57	NCEER
3.3	-71.37	47.2	0	1951	7	25	0	22	51.5	NCEER
3.3	-74.67	45.93	0	1951	8	8	9	36	24.1	NCEER
3.6	-73.86	41.35	18	1951	9	3	21	26	24.8	NCEER
4.3	-66.25	49.3	0	1951	9	19	8	19	38	NCEER
3.3	-89.9	38.7	0	1951	9	20	2	38	0	NCEER
3.7	-75.37	46.22	0	1951	9	25	15	45	0	NCEER
3.8	-74.73	45.27	0	1951	10	25	7	7	52.8	NCEER
3.9	-73.55	44.92	31	1951	11	6	17	54	45.9	NCEER
3.3	-75.5	40.6	0	1951	11	23	6	45	0	NCEER
3.3	-80	32.9	0	1951	12	30	7	55	0	NCEER
3.1	-73.2	44.5	0	1952	1	30	4	0	0	NCEER
3.3	-69.38	46.33	0	1952	2	18	20	56	7	NCEER
3.9	-89.5	36.4	0	1952	2	20	22	34	39	NCEER
3.7	-70.2	46.8	0	1952	2	26	0	56	0	NCEER
3.8	-76.17	47.1	0	1952	3	17	4	14	41	NCEER
4.1	-69.88	47.83	0	1952	3	30	13	11	7	NCEER
5.1	-97.85	35.52	10	1952	4	9	16	29	28.4	NCEER
3.8	-70.58	47.47	0	1952	4	19	2	50	52.8	NCEER
3.7	-78.5	47	0	1952	4	26	4	59	0	NCEER
3.3	-89.7	36.6	0	1952	5	28	9	54	14	NCEER
3.3	-82.3	36.3	0	1952	6	11	20	20	0	NCEER
3.9	-82.02	39.64	9	1952	6	20	9	38	8.6	NCEER
4	-89.6	36.2	0	1952	7	16	23	48	10	NCEER
4.3	-75.84	46.87	1	1952	7	19	1	16	17.2	NCEER
3.2	-74.5	43	0	1952	8	25	0	7	0	NCEER
3.1	-96.5	35.1	0	1952	10	8	4	15	0	NCEER
4.3	-74	41.7	0	1952	10	8	21	40	0	DNAG
4.9	-69.8	47.8	0	1952	10	14	22	3	44.8	NCEER
3.1	-89.6	36.2	0	1952	10	17	4	16	18	NCEER
3.1	-93.7	30.1	0	1952	10	17	15	48	0	NCEER
3.1	-103.5	44.1	0	1952	11	15	0	0	0	NCEER
3.3	-84.6	30.6	0	1952	11	18	20	12	0	NCEER
3.1	-80	32.9	0	1952	11	19	0	0	0	NCEER
3.1	-81	43.8	0	1952	12	25	0	0	0	NCEER
3.6	-89.8	35.9	0	1952	12	25	4	23	24	NCEER
4.6	-66	49.07	0	1953	1	24	9	58	37	NCEER
3.1	-89.5	36	0	1953	1	26	23	18	0	NCEER
3.3	-78.1	37.7	0	1953	2	7	7	5	0	NCEER
3.3	-89.5	36.5	0	1953	2	11	10	50	54	NCEER
3.1	-89.8	36.1	0	1953	2	17	11	45	0	NCEER
3.5	-74.43	48.07	0	1953	2	28	6	24	2.5	NCEER

Table 2.5-1 {USGS Earthquake Catalog for the CEUS with $m_b \geq 3.0$ }

(Page 30 of 65)

m_b	Longitude (degree)	Latitude (degree)	Depth (km)	Year	Month	Day	Hour	Minute	Second	Catalog Reference
4.2	-98	35.6	0	1953	3	17	14	25	0	NCEER
3.3	-81.4	28.6	0	1953	3	26	0	0	0	NCEER
3	-73.5	41.1	0	1953	3	27	8	50	0	NCEER
3.6	-73	43.7	0	1953	3	31	2	50	0	NCEER
3	-73.5	44.7	0	1953	4	26	1	17	0	NCEER
3.1	-90.3	35.6	0	1953	5	12	18	50	0	NCEER
3.1	-96.7	34.7	0	1953	6	6	17	40	0	NCEER
3.5	-83.6	41.7	0	1953	6	12	0	0	0	NCEER
4.3	-110.163	38.997	0	1953	7	30	5	45	0	DNAG
3.1	-74	41	0	1953	8	17	4	22	50	NCEER
3.9	-90.1	38.8	0	1953	9	11	18	26	28	NCEER
4.4	-65.2	49.1	0	1953	9	14	22	52	57	NCEER
3.3	-83.9	36	0	1953	10	11	4	0	0	NCEER
3	-102.9	45.2	0	1953	12	21	22	43	0	NCEER
3.3	-89.1	38.6	0	1953	12	30	22	0	0	NCEER
3.1	-99.3	43.1	0	1953	12	31	20	30	0	NCEER
3.8	-83.2	37.3	0	1954	1	1	2	30	0	NCEER
4.4	-83.7	36.6	0	1954	1	2	3	25	0	NCEER
3.2	-76	40.3	0	1954	1	7	7	25	0	NCEER
3.1	-68.23	49.17	0	1954	1	10	21	4	30	NCEER
3.1	-89.4	36	0	1954	1	17	7	15	0	NCEER
3.4	-105.5	41.5	0	1954	1	20	20	50	1	NCEER
3.1	-84.4	35.3	0	1954	1	23	1	0	0	NCEER
3.1	-77.3	42.9	0	1954	1	31	12	30	0	NCEER
3.3	-76.65	43.03	0	1954	2	1	0	37	50	NCEER
4.3	-90.3	36.7	0	1954	2	2	16	53	0	NCEER
3.8	-70.25	47.6	0	1954	2	7	20	24	16	NCEER
3.5	-70.62	47.67	0	1954	2	21	9	0	37	NCEER
3.1	-96.4	35	0	1954	4	11	0	0	0	NCEER
4.3	-76.12	47	6	1954	4	12	21	22	0.1	NCEER
3.1	-73.5	44.7	0	1954	4	21	15	45	0	NCEER
4.1	-79.2	43.1	0	1954	4	27	2	14	8	NCEER
3.9	-90	35.1	0	1954	4	27	4	9	0	NCEER
3	-74.2	45	0	1954	5	20	22	0	0	NCEER
3.7	-70.12	47	0	1954	6	30	7	41	7	NCEER
3.5	-70.7	42.81	1	1954	7	29	19	56	56	NCEER
3.1	-87.3	38.5	0	1954	8	9	0	0	0	NCEER
3.3	-76	40.3	0	1954	8	11	3	40	0	NCEER
3.6	-68.37	49.03	0	1954	9	8	1	29	53	NCEER
4.6	-75.66	47.18	28	1954	9	11	18	55	55.6	NCEER
3	-74.6	44.6	0	1954	12	13	3	53	0	NCEER
3.1	-88.4	47.3	0	1955	1	5	20	0	0	NCEER
3.1	-82.2	36.6	0	1955	1	6	20	30	0	NCEER
3.4	-88.6	47.1	0	1955	1	7	5	0	0	NCEER
3.3	-78.4	37.3	0	1955	1	17	12	37	0	NCEER

Table 2.5-1 {USGS Earthquake Catalog for the CEUS with $m_b \geq 3.0$ }

(Page 31 of 65)

m_b	Longitude (degree)	Latitude (degree)	Depth (km)	Year	Month	Day	Hour	Minute	Second	Catalog Reference
4	-73.8	43	0	1955	1	21	8	40	0	DNAG
4.3	-89.83	36.07	8	1955	1	25	7	24	39.1	NCEER
3.1	-83.9	36	0	1955	1	25	19	34	0	NCEER
4	-70.5	47.67	0	1955	2	1	12	40	27	NCEER
4.1	-89.1	30.4	0	1955	2	1	14	45	0	NCEER
4.3	-107	40.5	0	1955	2	10	17	30	0	NCEER
3.3	-98.6	41.3	0	1955	2	25	1	45	0	NCEER
4.3	-89.78	38.23	11	1955	4	9	13	1	23.3	NCEER
3.2	-81.4	41.3	0	1955	5	26	18	9	0	NCEER
3.1	-81.4	41.3	0	1955	6	29	1	16	33	NCEER
3	-79.63	43.77	0	1955	6	29	1	17	40	NCEER
3.5	-78.3	42.9	0	1955	8	16	7	35	0	NCEER
3.4	-89.5	36	0	1955	9	6	1	45	0	NCEER
3.1	-89.5	36.4	0	1955	9	24	18	45	0	NCEER
3.5	-81.3	36.6	0	1955	9	28	7	1	41.5	NCEER
3.5	-73.9	45.22	0	1955	10	7	18	9	52	NCEER
3.4	-70.2	48.93	0	1955	10	20	21	31	6	NCEER
3.5	-75.87	46.5	0	1955	11	1	7	45	52	NCEER
3.4	-89.5	36	0	1955	12	13	7	43	0	NCEER
3.3	-82.4	34.3	0	1956	1	5	8	0	0	NCEER
4	-98.35	37.58	29	1956	1	6	11	58	7.4	NCEER
3.8	-94.8	29.3	0	1956	1	7	23	30	0	SRA
3.3	-75.47	45.67	0	1956	1	10	12	8	18	NCEER
3.7	-84	40.5	0	1956	1	27	11	3	27	NCEER
3.9	-89.8	35.76	16	1956	1	29	4	44	15.5	NCEER
3.7	-71.17	47.05	0	1956	1	30	9	43	13	NCEER
3.1	-74.82	45.45	0	1956	2	2	19	24	16	NCEER
3.9	-97.3	35.4	0	1956	2	16	23	30	0	NCEER
3.1	-75.38	44.85	0	1956	3	6	23	38	10	NCEER
3.7	-90.4	40.5	0	1956	3	13	15	5	0	SRA
3.5	-95.6	34.2	0	1956	4	2	16	3	18	NCEER
3.3	-82.4	34.3	0	1956	5	19	19	0	0	NCEER
3.9	-76.43	47.1	0	1956	6	15	0	53	37	NCEER
3.1	-87.7	43.6	0	1956	7	18	21	30	0	NCEER
3.4	-73.78	44.7	0	1956	7	27	1	34	44	NCEER
3.6	-66.17	49.42	0	1956	8	3	12	52	9	NCEER
4	-83.79	36.44	5	1956	9	7	13	35	50.8	NCEER
4.2	-84	35.5	0	1956	9	7	13	49	29	NCEER
3.2	-86.7	35.8	0	1956	9	9	22	45	0	SRA
3.8	-88.4	31.9	0	1956	9	27	14	15	0	NCEER
3.1	-87.9	42.9	0	1956	10	13	0	0	0	NCEER
3.4	-69	48.25	0	1956	10	27	14	40	6	NCEER
3.4	-89.7	36.1	0	1956	10	29	9	23	44	NCEER
4	-95.8	36.2	0	1956	10	30	10	36	21	USHIS
4	-75.42	45.96	1	1956	11	4	11	53	29.2	NCEER

Table 2.5-1 {USGS Earthquake Catalog for the CEUS with $m_b \geq 3.0$ }

(Page 32 of 65)

m_b	Longitude (degree)	Latitude (degree)	Depth (km)	Year	Month	Day	Hour	Minute	Second	Catalog Reference
4.3	-90.39	36.91	1	1956	11	26	4	12	43.3	NCEER
3	-88.8	43.5	0	1957	1	8	16	0	0	NCEER
4	-83.7	36.6	0	1957	1	25	18	15	0	NCEER
3.5	-69.93	48.4	0	1957	2	19	5	18	33	NCEER
3.3	-74.9	44.9	0	1957	2	20	15	45	0	NCEER
4	-94.7	32.6	0	1957	3	19	16	37	38	NCEER
3.5	-74.8	40.6	0	1957	3	23	19	2	0	NCEER
3.1	-88.4	37	0	1957	3	26	8	27	6	NCEER
4.3	-86.72	33.77	5	1957	4	23	9	23	39	NCEER
3.3	-72	44.42	0	1957	4	24	0	41	59	NCEER
4.4	-70.25	43.53	5	1957	4	26	11	40	8.6	NCEER
4.1	-82.14	35.8	5	1957	5	13	14	24	51.1	NCEER
3.3	-84.1	35.95	5	1957	6	23	6	34	16	NCEER
3.1	-81.3	42.9	0	1957	6	29	11	25	9	NCEER
3.9	-82.7	35.6	0	1957	7	2	9	33	1	NCEER
3.7	-67.08	46.58	0	1957	8	4	12	40	58	NCEER
4	-70.42	47.48	0	1957	8	6	23	50	38	NCEER
3.3	-70.12	46.73	0	1957	8	17	1	30	7	NCEER
3.1	-89.5	36.2	0	1957	8	17	23	0	0	NCEER
3	-76.17	44.8	0	1957	8	21	2	40	33	NCEER
3.1	-69.9	48.42	0	1957	10	9	14	16	58	NCEER
3.2	-78.75	46.38	0	1957	10	27	8	48	27	NCEER
3.3	-84	36	0	1957	11	7	17	15	0	NCEER
3.5	-69.55	48.67	0	1957	11	13	20	49	19	NCEER
3.9	-83.5	35	0	1957	11	24	20	6	17	NCEER
3.1	-98.2	43.8	0	1957	12	3	7	30	0	NCEER
4.5	-87.9	38.4	0	1958	1	8	2	41	43	DNAG
3.3	-74.9	44.9	0	1958	1	11	16	36	0	NCEER
3.5	-81.3	45	0	1958	1	24	17	10	0	NCEER
3.8	-89.7	36.1	0	1958	1	26	16	55	37	NCEER
3.9	-89.2	37.1	0	1958	1	28	5	56	40	NCEER
3.9	-76.03	46.9	0	1958	3	1	17	41	49	NCEER
3.4	-77.8	34.2	0	1958	3	5	11	53	43	NCEER
3.1	-77.13	46	0	1958	3	19	6	39	25	NCEER
3.4	-67.12	45.55	0	1958	3	23	22	4	17	NCEER
3.4	-89.2	36.3	0	1958	4	8	22	25	33	NCEER
3.2	-89.5	36.4	0	1958	4	26	7	30	0	NCEER
3.1	-81.8	41.5	0	1958	5	1	22	46	31	NCEER
3.7	-70.32	48.57	0	1958	5	6	16	2	49	NCEER
5	-76.82	47.09	1	1958	5	14	17	41	16.7	NCEER
3.3	-82.6	35.6	0	1958	5	16	22	30	0	NCEER
3.1	-90.4	35.5	0	1958	5	20	1	25	0	NCEER
3.2	-71.4	46.7	0	1958	7	18	23	56	27	NCEER
4.4	-79.5	43	0	1958	7	22	1	46	40	NCEER
3.8	-75.8	46.57	0	1958	7	25	3	45	11	NCEER

Table 2.5-1 {USGS Earthquake Catalog for the CEUS with $m_b \geq 3.0$ }

(Page 33 of 65)

m_b	Longitude (degree)	Latitude (degree)	Depth (km)	Year	Month	Day	Hour	Minute	Second	Catalog Reference
3	-70.3	47.32	0	1958	7	27	8	58	0	NCEER
3.8	-80	43.13	0	1958	8	4	20	25	58	NCEER
3.1	-106	41.1	0	1958	8	7	0	46	43	NCEER
3.6	-70.38	47.93	0	1958	8	8	22	15	3	NCEER
3.9	-69.38	48.6	0	1958	8	12	3	22	12	NCEER
3.6	-79	43	0	1958	8	22	14	25	5	NCEER
3	-70.2	43.6	0	1958	9	19	17	45	0	NCEER
3.3	-69.27	48.38	0	1958	9	29	10	45	29	NCEER
3.7	-73.73	45.18	0	1958	9	30	0	13	58	NCEER
3.5	-82.7	34.5	0	1958	10	20	6	16	0	NCEER
4.1	-68	49.6	0	1958	10	21	9	32	51	NCEER
3	-81.9	37.2	5	1958	10	23	2	29	44.3	NCEER
3.1	-90.1	29.9	0	1958	11	6	23	8	0	NCEER
4.4	-88.01	38.44	5	1958	11	8	2	41	12.6	NCEER
3.3	-91.2	30.5	0	1958	11	19	18	15	0	NCEER
3.3	-71.7	44	0	1958	11	21	23	30	0	NCEER
3.7	-69.82	46.98	0	1958	12	23	23	14	16	NCEER
3.1	-98.1	44.9	0	1959	1	12	13	0	0	NCEER
3.1	-89.5	36.3	0	1959	1	21	15	35	0	NCEER
3.1	-81	43	0	1959	2	9	0	0	0	NCEER
4.2	-100.9	35.5	0	1959	2	10	20	5	0	NCEER
3.2	-89.5	36.1	0	1959	2	13	8	37	0	NCEER
3.4	-73.27	41.92	0	1959	4	13	21	20	19	NCEER
3.5	-70.33	47.12	0	1959	4	16	16	36	25	NCEER
3.7	-80.68	37.39	1	1959	4	23	20	58	39.5	NCEER
3.9	-76.45	46.55	0	1959	5	21	9	38	51	NCEER
3.5	-79.2	48.8	0	1959	5	24	10	52	0	NCEER
3.6	-84.3	35.4	0	1959	6	13	1	0	0	SRA
3.7	-96.7	34.7	0	1959	6	15	12	45	0	NCEER
4.1	-98.06	34.64	5	1959	6	17	10	27	10.6	NCEER
3.1	-80.7	37.3	0	1959	7	7	23	17	0	NCEER
4.1	-68.32	48.42	0	1959	8	1	13	52	49	NCEER
3.9	-86.56	34.79	5	1959	8	12	18	6	1.4	NCEER
3.2	-80.7	37.3	0	1959	8	21	17	20	0	NCEER
3.2	-70.78	46.95	0	1959	8	22	3	52	30	NCEER
3.4	-93.1	29.8	0	1959	10	15	15	45	0	NCEER
4	-80.2	34.5	0	1959	10	27	2	7	28	NCEER
3.4	-89.34	36.03	5	1959	12	21	16	23	39.6	NCEER
4.3	-106.2	41.1	0	1959	12	25	9	50	0	NCEER
3.7	-75.67	46.97	0	1960	1	20	20	7	40	NCEER
3.4	-75.5	41.5	0	1960	1	22	20	53	22	SRA
3.2	-89.5	36	0	1960	1	28	21	38	0	NCEER
3.3	-70.38	47.8	0	1960	2	6	0	44	2	NCEER
4.2	-80.12	33.07	9	1960	3	12	12	47	44	NCEER
3.5	-84	35.8	0	1960	4	15	10	10	10	NCEER

Table 2.5-1 {USGS Earthquake Catalog for the CEUS with $m_b \geq 3.0$ }

(Page 34 of 65)

m_b	Longitude (degree)	Latitude (degree)	Depth (km)	Year	Month	Day	Hour	Minute	Second	Catalog Reference
3.4	-89.5	36	0	1960	4	21	10	45	0	NCEER
4	-70.34	47.88	5	1960	4	23	11	47	47.1	NCEER
3.1	-92	34.2	0	1960	5	4	16	31	32	NCEER
3.7	-80	32.9	0	1960	7	24	3	37	30	NCEER
3.3	-79.3	37.4	0	1960	9	4	18	40	0	NCEER
5.5	-107.6	38.3	49	1960	10	11	8	5	30.5	USHIS
3.6	-95.5	34.9	0	1961	1	11	1	40	0	NCEER
3.8	-66.93	46.38	0	1961	1	29	0	49	39	NCEER
3.7	-83.3	41.2	0	1961	2	22	9	45	3	NCEER
3.2	-75.28	45.17	0	1961	3	13	10	55	45	NCEER
3.6	-99.77	39.98	1	1961	4	13	21	14	55.2	NCEER
3.2	-74.8	45	0	1961	4	20	13	13	0	NCEER
3.6	-95	34.6	0	1961	4	26	7	5	0	NCEER
3.8	-95.3	34.9	0	1961	4	27	7	30	0	NCEER
3.4	-70.5	47.33	0	1961	8	22	18	55	51	NCEER
3.8	-90.19	35.96	5	1961	9	9	22	42	55	NCEER
4.3	-75.5	40.8	0	1961	9	15	2	16	56	DNAG
3.1	-74.9	44.9	0	1961	9	29	6	30	0	NCEER
3.8	-76.58	48.67	0	1961	10	7	22	36	51	NCEER
3.9	-94.24	39.32	9	1961	12	25	12	58	16.8	NCEER
3.3	-74.8	40.5	0	1961	12	27	17	6	0	NCEER
4	-100.72	44.25	23	1961	12	31	16	36	5.8	NCEER
3.8	-74.85	45.92	0	1962	1	27	12	11	17	NCEER
3.5	-67.13	47.5	0	1962	1	31	14	32	38	NCEER
4.3	-89.51	36.37	4	1962	2	2	6	43	30	NCEER
3	-88.7	37	0	1962	2	16	0	0	0	NCEER
3.3	-69.47	47.18	0	1962	3	23	2	2	21	NCEER
4	-66.02	47.57	0	1962	3	25	5	15	5	NCEER
3	-79.3	43	0	1962	3	27	6	35	0	NCEER
4.3	-72.97	44.11	5	1962	4	10	14	30	45.2	NCEER
3.3	-98.6	35.3	0	1962	4	28	6	9	11	NCEER
3	-89.5	36.5	0	1962	5	24	0	0	0	NCEER
3.2	-90.39	35.38	1	1962	6	1	11	23	38.6	NCEER
3.2	-72.64	45.44	1	1962	6	21	2	6	47	NCEER
5.4	-88.64	37.9	0	1962	6	27	1	28	59.3	NCEER
3.2	-89.82	36.56	1	1962	7	14	2	23	44	NCEER
3.6	-89.4	36.04	8	1962	7	23	6	5	15.7	NCEER
3.9	-70.67	47.25	0	1962	7	27	17	56	57	NCEER
3.2	-97.4	34.8	0	1962	8	10	20	47	19	SRA
3.6	-70.05	47.53	0	1962	8	11	3	5	16	NCEER
3.3	-77.7	39.5	0	1962	9	4	23	40	0	NCEER
3.3	-78.2	39.7	0	1962	9	7	14	0	0	NCEER
3.1	-110.89	39.2	7	1962	9	7	16	50	23.8	SRA
3.2	-98.4	34.7	0	1962	9	7	22	53	44	SRA
3.3	-74.3	44.8	0	1962	10	2	23	45	0	NCEER

Table 2.5-1 {USGS Earthquake Catalog for the CEUS with $m_b \geq 3.0$ }

(Page 35 of 65)

m_b	Longitude (degree)	Latitude (degree)	Depth (km)	Year	Month	Day	Hour	Minute	Second	Catalog Reference
3	-69.13	45.57	0	1962	12	1	21	29	23	NCEER
3.4	-110.42	39.36	7	1962	12	11	10	28	13.5	SRA
3	-71.7	42.8	0	1962	12	29	6	19	0	NCEER
3.3	-80.1	37.3	0	1963	1	17	14	26	50.8	NCEER
3	-75.9	44	0	1963	1	30	14	50	0	NCEER
3.4	-92.1	34.4	0	1963	2	7	21	18	36	NCEER
4.3	-109.2	42.6	33	1963	2	25	18	45	16.5	SRA
3	-79.57	43.2	0	1963	2	27	6	0	0	NCEER
3.4	-75.73	41.51	0	1963	3	2	20	24	32	NCEER
4.8	-90.05	36.64	15	1963	3	3	17	30	10.6	NCEER
3.1	-95.9	34.6	0	1963	3	13	9	33	34	NCEER
3.9	-109.8	45.1	33	1963	4	3	9	55	12.6	SRA
3.1	-89.58	36.46	6	1963	4	6	8	12	22.7	NCEER
3.1	-89.54	36.67	10	1963	5	2	1	9	21.4	NCEER
3.3	-80.19	32.97	5	1963	5	4	21	1	50.3	NCEER
3	-96.4	34.3	0	1963	5	7	20	3	29	SRA
3.5	-75.2	43.5	0	1963	5	19	19	14	0	NCEER
4.4	-104	39.3	0	1963	6	5	0	13	50.6	NCEER
4	-104.4	36.6	0	1963	6	6	8	5	33	SNMX
3.3	-73.75	42.37	0	1963	7	1	19	59	12	NCEER
3.1	-90.47	36.97	0	1963	7	8	23	51	42.1	NCEER
3	-66.5	46.8	0	1963	8	1	6	34	16	NCEER
4.4	-88.77	36.98	7	1963	8	3	0	37	49.1	NCEER
3.5	-73.95	45.18	0	1963	8	26	16	29	35	NCEER
4.3	-111.22	38.1	7	1963	9	30	9	17	39.3	SRA
3.2	-82.5	33.9	0	1963	10	8	6	1	43.4	SRA
3.6	-78.197	39.655	0	1963	10	10	14	59	52.3	SRA
4.5	-108.3	42.2	30	1963	10	14	8	31	23	SRA
4.2	-77.47	46.37	8	1963	10	15	13	59	50.8	NCEER
3.8	-70.42	42.4	14	1963	10	16	15	30	59.7	NCEER
3.7	-81	36.7	0	1963	10	28	22	38	0.3	NCEER
3.4	-70.8	42.7	0	1963	10	30	22	36	57.9	NCEER
3.2	-71.6	43.6	9	1963	12	4	21	32	34.8	NCEER
3.2	-86.97	37.15	1	1963	12	5	6	51	0.5	NCEER
3.4	-104.133	35.133	0	1963	12	19	16	47	28	SNMX
3.9	-77.53	46.23	0	1964	1	8	10	3	26	NCEER
3.3	-89.46	36.84	0	1964	1	16	5	9	58	NCEER
3.1	-70.7	46.92	27	1964	1	20	18	57	45.3	NCEER
3	-89.5	36.5	0	1964	1	25	19	54	10	NCEER
3.4	-99.7	35.1	0	1964	2	2	8	23	0	NCEER
3.3	-77.96	40.38	1	1964	2	13	19	46	40.8	NCEER
3.3	-85.4	34.7	0	1964	2	17	22	47	0	SRA
3.3	-82.39	33.72	5	1964	3	7	18	2	58.6	NCEER
3.9	-83.31	33.19	1	1964	3	13	1	20	17.5	NCEER
3.5	-89.6	36.2	0	1964	3	17	2	16	6	NCEER

Table 2.5-1 {USGS Earthquake Catalog for the CEUS with $m_b \geq 3.0$ }

(Page 36 of 65)

m_b	Longitude (degree)	Latitude (degree)	Depth (km)	Year	Month	Day	Hour	Minute	Second	Catalog Reference
3.5	-103.5	43.5	0	1964	3	24	6	12	0	NCEER
3.4	-104.1	42.7	0	1964	3	28	3	0	0	NCEER
4.5	-101.8	43	30	1964	3	28	10	8	46.5	NCEER
4.3	-74.9	44.9	0	1964	3	29	9	16	0	NCEER
3.1	-71.5	43.6	0	1964	4	1	11	21	34	NCEER
3.8	-81.1	46.4	0	1964	4	5	13	21	0	NCEER
3.7	-81.1	33.84	3	1964	4	20	19	4	44.1	NCEER
3.6	-93.81	31.42	5	1964	4	24	7	33	51.9	NCEER
3.2	-76.41	40.3	1	1964	5	12	6	45	10.7	NCEER
3.9	-90.02	36.58	3	1964	5	23	11	25	34.5	NCEER
4.2	-94	31.3	0	1964	6	2	23	0	0	SRA
3	-94	31	0	1964	6	3	9	37	0	NCEER
3.3	-74.3	40.9	0	1964	6	16	0	0	0	NCEER
3.8	-71.68	43.4	1	1964	6	26	11	4	49	NCEER
3.7	-79.2	47.8	0	1964	6	27	19	17	0	NCEER
3.8	-67.42	49.43	0	1964	7	1	21	41	30	NCEER
3.4	-71.41	46.72	0	1964	7	12	0	0	41	NCEER
3.3	-76.25	46.65	0	1964	7	24	10	34	11	NCEER
3	-83.9	36	0	1964	7	28	0	0	0	NCEER
4	-106	39.7	0	1964	8	4	11	13	25.2	NCEER
3	-110.92	38.95	7	1964	8	5	15	17	56.2	SRA
3	-93.8	31.4	0	1964	8	16	11	35	31	NCEER
4.5	-104.7	42.9	0	1964	8	22	3	28	11	NCEER
3	-102.25	43.77	20	1964	8	26	16	58	55.1	NCEER
3.1	-73.87	48.4	0	1964	9	9	6	16	26	NCEER
4.1	-107.8	41.9	33	1964	9	10	6	19	50.7	SRA
4	-109.7	50	33	1964	9	19	20	51	5	DNAG
3	-91.1	37.1	0	1964	9	24	8	9	34	NCEER
3.4	-96.4	44	0	1964	9	28	15	41	0	NCEER
3	-89.8	47.4	0	1964	10	10	8	30	0	NCEER
3	-90.3	47.3	0	1964	10	10	11	30	0	NCEER
3.2	-83.9	36	0	1964	10	13	16	30	0	NCEER
3.9	-67.25	47.67	0	1964	10	17	14	13	7	NCEER
3.1	-73.7	41.2	0	1964	11	17	17	8	0	NCEER
3.6	-81.698	37.394	6	1964	11	25	2	50	6.4	SRA
3.1	-110.916	38.923	7	1964	12	16	21	39	25.2	DNAG
3	-72	43.5	0	1965	1	3	17	5	1	NCEER
3.5	-78.5	48	0	1965	1	8	12	29	45	NCEER
3.3	-110.35	39.44	7	1965	1	14	12	30	10.8	SRA
3.4	-103.8	35.1	0	1965	2	3	11	32	34	SNMX
3	-103	31.9	0	1965	2	3	19	59	32	SRA
3.3	-89.59	36.52	3	1965	2	11	3	40	24.8	NCEER
3	-93.3	36.9	0	1965	2	14	20	3	20	NCEER
3.1	-71.25	47.5	0	1965	3	1	2	22	8	NCEER
3.2	-78.83	47.72	0	1965	3	5	12	11	1	NCEER

Table 2.5-1 {USGS Earthquake Catalog for the CEUS with $m_b \geq 3.0$ }

(Page 37 of 65)

m_b	Longitude (degree)	Latitude (degree)	Depth (km)	Year	Month	Day	Hour	Minute	Second	Catalog Reference
4	-91.03	37.4	7	1965	3	6	21	8	50.3	NCEER
3.1	-83	45	0	1965	3	6	21	13	0	NCEER
3.1	-67.53	49.77	0	1965	3	18	12	9	5	NCEER
3.7	-89.52	36.46	3	1965	3	25	12	59	27.7	NCEER
3.4	-80.5	46	0	1965	4	1	6	30	20	NCEER
3.5	-81.6	37.32	5	1965	4	26	15	26	19.7	NCEER
3.3	-89.9	36.1	0	1965	5	25	7	15	43	NCEER
4.3	-106.3	39.4	33	1965	5	30	17	31	4.1	SRA
3	-89.5	36.5	0	1965	6	1	7	24	57	NCEER
4.7	-106.5	43.6	33	1965	6	3	19	30	25.8	SRA
3.3	-89.5	36.5	0	1965	7	8	7	3	50	NCEER
3	-78.08	43.04	18	1965	7	16	11	6	57	NCEER
3.1	-109.9	39.5	33	1965	7	18	3	55	51.4	SRA
3.9	-109.8	44.7	33	1965	8	6	15	39	49.2	SRA
3.8	-89.31	37.23	1	1965	8	14	13	13	56.9	NCEER
3.3	-110.6	42.3	33	1965	8	22	17	54	33.3	SRA
3.1	-78.1	43	0	1965	8	28	1	55	0	SRA
3.5	-102.3	32.1	0	1965	8	30	5	17	38	NCEER
3.2	-65.28	46	0	1965	8	31	8	38	44	NCEER
3.2	-81.2	34.7	0	1965	9	9	14	42	20	NCEER
3.8	-79.05	46.72	0	1965	9	15	17	56	28	NCEER
3.3	-74.4	41.4	0	1965	9	29	20	57	0	NCEER
3.9	-67.66	49.78	0	1965	10	5	14	36	55	NCEER
3.3	-79.75	40.08	0	1965	10	8	2	17	27	NCEER
3.1	-97.7	36.1	0	1965	10	10	23	51	33	NCEER
4.9	-90.94	37.48	5	1965	10	21	2	4	39.1	NCEER
3	-70.1	41.3	0	1965	10	24	17	45	0	NCEER
3.4	-90.92	37.03	4	1965	11	4	7	43	37.9	NCEER
4.2	-76.36	47.25	10	1965	11	7	20	57	41.8	NCEER
3.3	-83.2	33.2	0	1965	11	8	12	58	1	SRA
3.7	-76.28	46.93	0	1965	11	24	21	28	1	NCEER
3.2	-71.4	41.7	0	1965	12	8	3	2	0	NCEER
4.1	-70.6	47.83	0	1965	12	16	13	53	19	NCEER
3.8	-89.76	36.03	1	1965	12	19	22	19	12	NCEER
3.9	-78.25	42.84	2	1966	1	1	13	23	39	NCEER
3.9	-67.47	48.9	0	1966	1	14	15	29	25	NCEER
3.6	-89.87	35.95	1	1966	2	12	4	32	12.8	NCEER
3.5	-87	33.6	0	1966	2	13	6	29	43	SRA
3.6	-90.9	37.04	6	1966	2	13	23	19	37.8	NCEER
3	-90	36.2	0	1966	3	13	14	24	42	NCEER
3.2	-76.16	46.5	0	1966	3	20	23	45	33	NCEER
3.4	-103.333	35.283	0	1966	4	21	14	14	19	SNMX
3.3	-71.9	44.1	0	1966	4	28	12	2	0	NCEER
4.3	-78.13	37.66	2	1966	5	31	6	18	59.5	NCEER
3.1	-88.2	38.6	0	1966	6	22	11	27	53	NCEER

Table 2.5-1 {USGS Earthquake Catalog for the CEUS with $m_b \geq 3.0$ }

(Page 38 of 65)

m_b	Longitude (degree)	Latitude (degree)	Depth (km)	Year	Month	Day	Hour	Minute	Second	Catalog Reference
3.4	-73.83	45.16	0	1966	6	25	0	5	51	NCEER
3.1	-103.43	44.3	2	1966	6	26	11	59	43.1	NCEER
3.3	-66	49.5	0	1966	7	12	1	6	38	NCEER
3.7	-101.33	35.64	3	1966	7	20	9	4	58.8	NCEER
3.2	-70	47.75	0	1966	7	20	20	8	29	NCEER
3	-67.6	44.5	0	1966	7	24	1	59	0	NCEER
3.7	-68.55	49.63	0	1966	7	24	22	19	46	NCEER
3.1	-110.36	39.44	7	1966	7	30	3	25	31	SRA
4.3	-102.339	32.115	3	1966	8	14	15	25	53.7	USHIS
3	-84	35.8	0	1966	8	24	6	0	0	NCEER
4.2	-107.6	38.3	33	1966	9	4	9	52	34.5	SRA
3.1	-98.81	41.3	27	1966	9	9	9	50	34.2	NCEER
3.1	-80.3	39.3	0	1966	9	28	0	0	0	NCEER
3.2	-65.25	46.92	0	1966	9	28	20	11	35	NCEER
3	-70.33	47.66	0	1966	10	1	17	23	55	NCEER
4.5	-104.1	37.4	0	1966	10	3	2	26	2.3	NCEER
3	-104.6	39.3	0	1966	10	13	0	33	0	SRA
3.2	-71.8	43	0	1966	10	23	23	5	0	NCEER
3.9	-106.9	40.2	33	1966	11	1	7	40	28	SRA
3.6	-76.3	47	0	1966	11	13	15	43	0	NCEER
3	-92.8	38.9	0	1966	12	6	8	0	47	NCEER
3.4	-68.17	49	0	1966	12	12	21	4	12	NCEER
3.7	-107.017	36.983	0	1966	12	16	2	0	40	SNMX
3.3	-106.5	39	5	1966	12	19	20	52	33.3	SRA
4.4	-107.51	38.98	33	1967	1	12	3	52	6.2	SRA
4.1	-107.86	37.67	33	1967	1	16	9	22	45.9	SRA
3.8	-107.05	40.05	33	1967	1	18	6	12	0.6	SRA
3.6	-109.77	44.74	33	1967	1	21	0	18	16	SRA
3.1	-84.6	42.7	0	1967	2	2	6	30	0	NCEER
3.3	-71.4	41.4	0	1967	2	2	13	40	9	NCEER
3	-110.1	39.55	33	1967	2	5	10	7	16.6	SRA
3.1	-90	36	0	1967	2	12	0	0	0	SRA
3.4	-110.37	39.27	5	1967	2	15	15	2	16.5	SRA
3.1	-110.28	42.05	7	1967	3	10	2	20	33.2	SRA
3.6	-109.9	45.16	33	1967	3	28	20	31	35.4	SRA
3	-107.75	38.32	33	1967	4	4	22	53	39.5	SRA
3.7	-82.53	39.65	1	1967	4	8	5	40	30.5	NCEER
3	-89.7	36.1	0	1967	4	11	23	44	45	NCEER
4.7	-108.77	43.41	5	1967	4	26	10	17	59.4	SRA
4.8	-105.9	43.66	0	1967	5	11	21	15	6.6	NCEER
3.2	-69.9	42.3	0	1967	5	15	22	47	12	NCEER
4.3	-90.84	33.55	6	1967	6	4	16	14	12.6	NCEER
3.7	-75.03	46.58	0	1967	6	11	1	49	39	NCEER
3.9	-78.23	42.84	1	1967	6	13	19	8	55.5	NCEER
3.8	-69.9	44.4	0	1967	7	1	16	11	18.9	SRA

Table 2.5-1 {USGS Earthquake Catalog for the CEUS with $m_b \geq 3.0$ }

(Page 39 of 65)

m_b	Longitude (degree)	Latitude (degree)	Depth (km)	Year	Month	Day	Hour	Minute	Second	Catalog Reference
3.4	-90.4	35.8	0	1967	7	6	16	43	51	NCEER
4.6	-90.44	37.44	15	1967	7	21	9	14	48.8	NCEER
3.1	-91.1	37.1	0	1967	8	25	19	15	18	NCEER
3.4	-70.7	46.93	0	1967	9	23	16	27	55	NCEER
4.7	-65.63	49.44	15	1967	9	30	22	39	48	NCEER
3	-89.5	36.5	0	1967	10	18	5	8	36	NCEER
3.4	-80.22	32.8	19	1967	10	23	9	4	2.5	NCEER
3.2	-73.8	41.2	0	1967	11	22	22	10	0	NCEER
3.5	-99.6	43.56	1	1967	11	23	6	23	42.1	NCEER
3.5	-81.6	37.36	2	1967	12	16	12	23	33.4	NCEER
3.1	-95.55	34.85	0	1968	1	4	22	30	0	NCEER
3.8	-106.8	42.7	33	1968	1	9	2	16	39.3	SRA
3.3	-89.8	36.2	0	1968	1	23	16	16	0	NCEER
3.8	-89.86	36.52	7	1968	2	10	1	34	30.6	NCEER
3.2	-110.61	41.72	7	1968	2	20	6	34	26.4	SRA
3.4	-80.77	37.28	8	1968	3	8	5	38	15.7	NCEER
3.1	-70.49	47.94	18	1968	3	30	15	28	59	NCEER
4.5	-89.85	38.02	1	1968	3	31	17	58	9.6	NCEER
3.5	-70.4	47.6	0	1968	4	11	9	18	0	NCEER
3.8	-102.1	37.8	0	1968	4	21	7	8	7	NCEER
3.3	-66.66	46.9	18	1968	5	27	19	21	56	NCEER
3.5	-89.5	36.5	0	1968	5	30	1	59	33	NCEER
3.3	-110.45	39.21	7	1968	6	2	18	59	23.2	SRA
3	-110.47	41.93	7	1968	6	14	21	11	15.3	SRA
3.8	-107.41	39.31	33	1968	6	23	20	16	13	SRA
3.7	-100.74	46.59	27	1968	7	8	16	50	14.7	NCEER
3.1	-89.5	36.5	0	1968	7	14	4	21	25	SRA
3	-90.8	35.7	0	1968	7	15	4	21	25	NCEER
3.1	-71.3	47.01	18	1968	7	24	23	16	37	NCEER
3	-84.2	40.4	0	1968	7	26	15	2	53.7	SRA
3.1	-81.48	34.11	1	1968	9	22	21	41	18.2	NCEER
3.3	-69.45	45.17	18	1968	9	23	15	38	50	NCEER
3.4	-81.66	45.8	18	1968	10	10	20	10	41	NCEER
3.5	-96.8	34	0	1968	10	14	14	42	54	NCEER
3.2	-74.1	45.3	0	1968	10	19	10	37	0	NCEER
3.6	-70.6	47.5	0	1968	10	20	2	36	0	NCEER
3.7	-83	43	0	1968	10	31	0	0	0	NCEER
3.3	-72.5	41.4	0	1968	11	3	8	33	0	NCEER
3.1	-76.3	46.17	18	1968	11	3	20	50	49	NCEER
5.5	-88.37	37.91	21	1968	11	9	17	1	40.5	NCEER
3.3	-77.9	34.1	0	1968	11	25	20	0	0	NCEER
3.2	-74.6	39.7	0	1968	12	10	9	12	0	NCEER
3.4	-87.6	37.8	0	1968	12	11	15	0	0	NCEER
3	-85.8	38.3	0	1968	12	11	16	0	0	NCEER
4.4	-92.69	34.99	7	1969	1	1	23	35	38.7	NCEER

Table 2.5-1 {USGS Earthquake Catalog for the CEUS with $m_b \geq 3.0$ }

(Page 40 of 65)

m_b	Longitude (degree)	Latitude (degree)	Depth (km)	Year	Month	Day	Hour	Minute	Second	Catalog Reference
3.4	-90.4	37.8	0	1969	1	20	19	25	0	NCEER
3.5	-96.3	34.2	0	1969	4	13	6	27	51	NCEER
3.3	-96.31	35.29	8	1969	5	2	11	33	21.7	NCEER
3.6	-70.65	47.47	18	1969	5	10	18	43	29	NCEER
3.5	-82.58	33.95	0	1969	5	18	0	0	0	NCEER
3.1	-78.245	39.61	0	1969	5	22	14	59	51.6	SRA
3.5	-104.4	40.4	0	1969	5	26	1	30	8.6	NCEER
3	-97.8	34.8	0	1969	5	30	14	8	5	NCEER
3.1	-81.45	49.67	18	1969	6	4	9	36	2	NCEER
3	-97	37.4	0	1969	7	1	3	36	58	NCEER
4.1	-83.69	36.12	1	1969	7	13	21	51	9.8	NCEER
3.8	-70.09	47.83	18	1969	7	14	3	6	59	NCEER
3.1	-89.5	36.5	0	1969	7	27	0	0	0	SRA
3.5	-71.4	43.8	0	1969	8	6	16	2	0.5	NCEER
3.2	-70.07	47.49	18	1969	8	31	7	20	27	NCEER
3.3	-74.6	41.1	0	1969	10	6	0	0	0	NCEER
3.1	-106.58	48.29	18	1969	10	6	20	24	53	NCEER
4.5	-75.06	46.31	2	1969	10	10	0	7	4.9	NCEER
4.6	-80.93	37.45	5	1969	11	20	1	0	9.3	NCEER
3.6	-77.67	37.84	1	1969	12	11	23	44	37.4	NCEER
3.7	-82.85	35.04	6	1969	12	13	10	19	29.7	NCEER
3.1	-89.9	35.2	0	1970	1	7	17	45	0	NCEER
3.8	-103.417	35.9	0	1970	1	12	11	21	15	SNMX
3.1	-97	31	0	1970	2	3	0	0	0	NCEER
4	-108.31	37.92	33	1970	2	3	5	59	35.6	SRA
3.4	-90.6	37.9	0	1970	2	6	4	53	2	NCEER
3.1	-77.78	48.24	18	1970	2	27	8	8	36	NCEER
3.3	-89.54	36.6	5	1970	3	27	3	44	29.2	NCEER
3.1	-81.22	49.7	18	1970	4	25	0	46	27	NCEER
3.2	-78.275	39.619	0	1970	5	27	17	59	41.4	SRA
3.7	-82.206	36.99	12	1970	7	30	15	15	16.9	SRA
3.5	-83.4	37.7	0	1970	7	31	0	31	0	SRA
3.3	-66.12	45.8	18	1970	8	8	0	10	30	NCEER
3.2	-82.05	38.23	10	1970	8	11	6	14	25.5	NCEER
3.2	-70.3	47.92	18	1970	9	7	21	39	27	NCEER
3.1	-81.42	36.02	1	1970	9	10	1	41	5.2	NCEER
3	-71.03	48.72	18	1970	10	9	16	35	1	NCEER
3.3	-76.25	47.07	18	1970	10	15	18	56	11	NCEER
3	-90	36	0	1970	11	5	10	25	35	NCEER
4.4	-89.95	35.86	16	1970	11	17	2	13	54.1	NCEER
3	-89.5	36.3	0	1970	11	30	4	46	53	NCEER
3	-89	36	0	1970	12	8	23	16	0	NCEER
4.9	-107.55	43.96	15	1970	12	12	15	57	19.1	SRA
3.4	-89.55	36.71	15	1970	12	24	10	17	56.8	NCEER
3	-75.96	47.17	18	1971	1	6	6	22	8	NCEER

Table 2.5-1 {USGS Earthquake Catalog for the CEUS with $m_b \geq 3.0$ }

(Page 41 of 65)

m_b	Longitude (degree)	Latitude (degree)	Depth (km)	Year	Month	Day	Hour	Minute	Second	Catalog Reference
3.8	-107.31	39.49	33	1971	1	7	20	39	52.1	SRA
3.1	-75.18	46.92	18	1971	1	19	13	44	25	NCEER
3.1	-87.85	38.5	15	1971	2	12	12	44	27.5	NCEER
3	-83.2	37.1	0	1971	2	19	23	11	42	NCEER
3.6	-87.84	33.18	12	1971	3	14	17	27	54.6	NCEER
3.7	-88.3	32.8	0	1971	3	16	2	37	28	NCEER
4.4	-106.97	40.7	10	1971	3	18	9	8	59.9	SRA
3	-81.6	37.4	0	1971	4	1	5	5	11	NCEER
3	-90.1	35.8	0	1971	4	13	14	0	51	NCEER
3.2	-73.37	45.1	18	1971	5	14	6	20	9	NCEER
3.7	-80.66	33.36	1	1971	5	19	12	54	3.6	NCEER
4.1	-74.48	43.9	2	1971	5	23	6	24	27.9	NCEER
3	-76.28	46.55	18	1971	7	6	17	47	49	NCEER
3.1	-81.2	46.74	18	1971	7	9	5	5	26	NCEER
3.7	-109.6	40.24	7	1971	7	10	17	22	36.8	SRA
3.4	-84	36	0	1971	7	13	2	3	0	SRA
3.4	-84.3	36	0	1971	7	13	3	3	0	NCEER
3.6	-83	34.8	0	1971	7	13	11	42	26	NCEER
3.3	-75.6	39.7	0	1971	7	14	0	0	0	NCEER
3.6	-103.17	31.64	5	1971	7	30	1	45	51.4	NCEER
3.8	-80.63	33.34	4	1971	7	31	20	16	55	NCEER
3.6	-77.59	38.15	5	1971	9	12	0	6	27.6	NCEER
3.2	-70.24	47.56	18	1971	9	12	8	31	43	NCEER
3	-103.2	31.6	0	1971	9	24	1	1	54	SRA
3.2	-75.17	45.71	18	1971	9	27	8	47	23	NCEER
4.1	-90.49	35.77	9	1971	10	1	18	49	38.5	NCEER
3.7	-83.37	35.8	8	1971	10	9	16	43	32.7	NCEER
3	-89.6	36.7	0	1971	10	18	6	39	31	NCEER
3.7	-101.26	43.69	17	1971	10	19	21	7	37.4	NCEER
3.4	-71.2	42.7	0	1971	10	21	0	54	0	NCEER
3.3	-83	36	0	1971	10	22	21	55	0	SRA
3	-67.13	49.23	18	1971	10	27	7	13	24	NCEER
4	-108.68	38.91	5	1971	11	12	9	30	44.6	SRA
3	-73.87	45.06	18	1971	11	15	10	38	55	NCEER
3	-76.28	47.24	18	1971	11	22	5	29	7	NCEER
3	-76.62	45.83	18	1971	11	23	16	32	30	NCEER
4.1	-110.34	42.49	7	1971	12	3	7	44	59.2	SRA
4	-74.67	46.01	13	1971	12	18	15	36	24.5	NCEER
3.3	-75.6	39.7	0	1971	12	29	0	0	0	NCEER
3.7	-81.6	37.4	0	1972	1	9	23	24	29	NCEER
3.7	-90.85	36.37	3	1972	2	1	5	42	9.5	NCEER
4.5	-80.58	33.31	2	1972	2	3	23	11	9.7	NCEER
3.3	-75.6	39.7	0	1972	2	11	0	16	0.3	NCEER
4.3	-105.12	44.29	0	1972	2	18	11	43	38.1	NCEER
3.7	-89.74	36.12	7	1972	3	29	20	38	31.7	NCEER

Table 2.5-1 {USGS Earthquake Catalog for the CEUS with $m_b \geq 3.0$ }

(Page 42 of 65)

m_b	Longitude (degree)	Latitude (degree)	Depth (km)	Year	Month	Day	Hour	Minute	Second	Catalog Reference
3.3	-75.99	46.67	18	1972	4	25	3	24	25	NCEER
3.4	-89.97	35.93	1	1972	5	7	2	12	8.7	NCEER
3.9	-82.2	37	0	1972	5	20	19	39	6	NCEER
3.1	-90.37	37.62	12	1972	6	9	19	15	18.9	NCEER
4.5	-89.08	37	13	1972	6	19	16	15	18.8	NCEER
3	-77.86	47.9	18	1972	7	17	1	58	46	NCEER
4.3	-104.93	49.35	5	1972	7	26	3	58	19	NCEER
3.1	-104.033	32.65	0	1972	7	26	4	35	40	SNMX
3.3	-75.6	39.7	0	1972	8	14	1	9	0	NCEER
3	-81.4	33.2	0	1972	8	14	15	5	19	NCEER
3.9	-66.47	49.54	18	1972	8	22	19	17	48	NCEER
3.4	-77.7	37.6	0	1972	9	5	16	0	0	NCEER
3.2	-77.56	46.18	18	1972	9	12	9	15	38	NCEER
4.4	-89.37	41.64	10	1972	9	15	5	22	15.9	NCEER
3.7	-99.6	42.3	0	1972	10	16	5	47	33	NCEER
3	-74.56	44.76	0	1972	11	2	5	15	8.8	SRA
3.3	-112.74	49.12	18	1972	11	21	6	8	46	DNAG
3.5	-76.24	40.14	2	1972	12	8	3	0	33.3	NCEER
4.1	-108.39	43.65	20	1972	12	8	18	47	39.4	SRA
3.9	-75.1	45.64	10	1972	12	16	19	1	37.2	NCEER
3.2	-87.22	37.4	14	1973	1	7	22	56	6.2	NCEER
3.5	-90.6	33.8	0	1973	1	8	9	11	37	NCEER
3.2	-90.48	37.89	17	1973	1	12	11	56	56.2	NCEER
3.1	-70	47.98	10	1973	1	28	13	7	50	NCEER
3.2	-110.425	36.43	5	1973	2	9	17	38	37	SRA
3	-70	44.5	0	1973	2	26	13	42	0	SRA
3.8	-75.43	39.69	12	1973	2	28	8	21	33.2	NCEER
3.4	-77.7	37.3	0	1973	4	9	23	11	0	NCEER
4.8	-107.85	42.64	33	1973	4	22	6	7	12.4	SRA
3.4	-90.8	33.9	0	1973	5	25	14	40	14	NCEER
3.1	-66.5	49.48	18	1973	6	14	15	9	55	NCEER
4.8	-71.12	45.31	12	1973	6	15	1	9	5.1	NCEER
3.3	-75.7	39.7	0	1973	7	10	4	38	0.2	NCEER
3.5	-74.47	43.87	2	1973	7	15	8	20	30.7	NCEER
3.1	-66.96	49.56	18	1973	7	20	17	6	39	NCEER
4.2	-104.57	37.15	5	1973	9	23	3	58	54.9	NCEER
3.4	-90.05	35.87	6	1973	10	3	3	50	19.8	NCEER
3.8	-89.62	36.49	3	1973	10	9	20	15	26.5	NCEER
3.5	-80.65	28.48	5	1973	10	27	6	21	2	NCEER
3.5	-84.12	35.76	1	1973	10	30	22	58	39	NCEER
3.1	-69.01	49.6	18	1973	11	15	17	31	35	NCEER
3.1	-70.29	47.55	10	1973	11	16	1	36	34	NCEER
3.1	-94.7	35	0	1973	11	18	10	3	53	NCEER
4.6	-83.99	35.89	12	1973	11	30	7	48	40.5	NCEER
3	-80.27	32.97	6	1973	12	19	10	16	8.7	NCEER

Table 2.5-1 {USGS Earthquake Catalog for the CEUS with $m_b \geq 3.0$ }

(Page 43 of 65)

m_b	Longitude (degree)	Latitude (degree)	Depth (km)	Year	Month	Day	Hour	Minute	Second	Catalog Reference
3.1	-89.69	36.14	10	1973	12	20	10	45	0.9	NCEER
3.1	-98.3	29	0	1973	12	25	2	46	0	NCEER
3.9	-89.47	36.18	7	1974	1	8	1	12	38.1	NCEER
4.5	-100.69	36.4	0	1974	2	15	13	33	49.2	NCEER
3.8	-93.04	34.03	10	1974	2	15	22	49	4.4	NCEER
3	-67.09	49.54	18	1974	2	17	12	57	28	NCEER
3	-90.41	35.69	5	1974	3	4	14	24	28.1	NCEER
3.2	-89.8	35.64	5	1974	3	12	12	30	29.2	SRA
3.5	-107.05	40.7	5	1974	3	31	11	58	47.1	SRA
4.7	-88.07	38.55	15	1974	4	3	23	5	2.8	NCEER
3	-98	29	0	1974	4	20	23	46	10	SRA
3.2	-75.907	40.974	0	1974	4	27	14	45	39.9	SRA
3.3	-75.6	39.8	0	1974	4	28	14	19	0	NCEER
3.8	-89.36	36.74	4	1974	5	13	6	52	18.7	NCEER
3.6	-80.54	37.46	5	1974	5	30	21	28	35.3	NCEER
3.2	-84.75	38.48	10	1974	6	5	0	16	40.2	NCEER
3.2	-89.91	38.65	12	1974	6	5	8	6	10.7	NCEER
3.4	-98	29	0	1974	6	24	18	3	10	SRA
3.4	-67.22	49.58	10	1974	7	2	4	46	51	NCEER
3	-98	29	0	1974	8	1	13	33	10	SRA
4.1	-82.53	33.91	4	1974	8	2	8	52	11.1	NCEER
3.2	-76.08	45.93	18	1974	8	8	11	55	33	NCEER
3.2	-91.16	36.93	6	1974	8	11	14	29	45.4	NCEER
4.4	-107.38	44.11	10	1974	9	19	15	36	11.4	SRA
3	-83.49	41.21	1	1974	9	29	2	26	19.1	NCEER
3.1	-82.4	33.9	0	1974	10	8	23	22	28	NCEER
3.8	-81.61	39.06	4	1974	10	20	15	13	55.6	NCEER
3.2	-75.48	46.08	10	1974	10	23	22	52	57	NCEER
3	-81.92	33.79	0	1974	10	28	11	33	0	NCEER
3.2	-75.03	46.07	10	1974	11	2	13	47	56	NCEER
3.7	-82.22	33.73	0	1974	11	5	3	0	0	NCEER
4.3	-80.16	32.92	6	1974	11	22	5	25	56.7	NCEER
3.3	-79.11	43.33	0	1974	11	27	10	28	51.7	SRA
4	-104.017	32.633	0	1974	11	28	3	35	20	SNMX
3.5	-75.5	46.25	10	1974	12	2	10	58	5	NCEER
3.6	-82.5	33.95	0	1974	12	3	8	25	0	NCEER
3.2	-87.46	31.23	18	1974	12	10	6	1	35	NCEER
3.1	-91.86	34.49	3	1974	12	13	5	3	55.5	NCEER
3	-69.8	42.37	0	1974	12	22	20	46	48.7	SRA
3.5	-67.44	49.14	18	1974	12	27	0	50	12	NCEER
3.7	-103.11	30.92	5	1974	12	30	8	5	27.1	NCEER
3	-90.9	34.9	0	1975	1	2	9	19	0	NCEER
3.1	-74.6	44.9	0	1975	1	15	19	16	0	NCEER
4.1	-108.65	39.27	5	1975	1	30	14	48	40.3	SRA
3	-103.1	35.067	0	1975	2	2	20	39	23	SNMX

Table 2.5-1 {USGS Earthquake Catalog for the CEUS with $m_b \geq 3.0$ }

(Page 44 of 65)

m_b	Longitude (degree)	Latitude (degree)	Depth (km)	Year	Month	Day	Hour	Minute	Second	Catalog Reference
3.3	-83.2	41.3	0	1975	2	3	10	31	0	NCEER
3.4	-89.59	36.55	3	1975	2	13	19	43	58	NCEER
3	-82.35	38.88	4	1975	2	16	23	21	34.4	NCEER
3.5	-87.98	33.55	18	1975	3	1	11	50	0.2	NCEER
3	-80.48	37.32	5	1975	3	7	12	45	13.5	NCEER
4.8	-108.1	42.67	10	1975	3	25	14	59	58	SRA
3.1	-74.24	45.73	5	1975	4	3	19	3	17	NCEER
3	-80.22	33	10	1975	4	28	5	46	52.6	NCEER
3.3	-98.5	42.07	1	1975	5	13	7	53	40	NCEER
3.1	-103.7	43.2	0	1975	5	16	5	57	1	NCEER
3.2	-75.19	47.23	18	1975	5	29	21	19	16	NCEER
3.7	-108.8	41.91	5	1975	6	7	4	36	21.7	SRA
3.5	-73.65	44.87	11	1975	6	9	18	39	22.7	NCEER
3.9	-89.68	36.54	9	1975	6	13	22	40	27.5	NCEER
3.5	-89.44	36.21	7	1975	6	20	7	29	6.6	DNAG
3.7	-87.84	33.7	4	1975	6	24	11	11	36.6	NCEER
3	-79.77	43.4	10	1975	6	30	20	15	23	NCEER
4.6	-96.1	45.5	8	1975	7	9	14	54	21.3	NCEER
4.2	-76.31	46.54	17	1975	7	12	12	37	13.8	NCEER
3.1	-66.81	49.16	18	1975	7	18	4	21	6	NCEER
3.1	-70.18	47.44	5	1975	8	21	4	29	37	NCEER
3.6	-78.118	48.123	1	1975	8	21	21	42	51.1	PDE
3	-89.84	36.05	11	1975	8	25	7	11	8	NCEER
3	-65.34	46.8	18	1975	8	27	22	28	22	NCEER
4.4	-86.59	33.66	4	1975	8	29	4	22	52.1	NCEER
3.3	-69.74	48.29	2	1975	9	2	6	21	17	NCEER
3.8	-104.38	48.37	0	1975	9	5	20	47	40.7	NCEER
3	-89.3	30.7	0	1975	9	9	11	52	44	NCEER
3.2	-97.22	34.13	5	1975	9	13	1	25	5.6	NCEER
3.2	-97.7	35.5	5	1975	10	12	2	58	11.5	NCEER
3.1	-65.89	45.11	18	1975	10	15	3	26	17	NCEER
3.3	-83	34.9	0	1975	10	18	4	31	0	NCEER
3.1	-68.13	49.13	18	1975	10	21	20	50	2	NCEER
4.1	-68.62	49.83	2	1975	10	23	21	17	48.7	NCEER
4	-74.65	43.91	5	1975	11	3	20	54	55.3	NCEER
3.5	-87.33	33.31	4	1975	11	7	23	39	31.7	NCEER
3.2	-80.89	37.22	1	1975	11	11	8	10	37.6	NCEER
3.2	-82.9	34.93	10	1975	11	25	15	17	34.8	NCEER
3.5	-97.42	34.68	14	1975	11	29	14	29	44.9	NCEER
3.3	-94.62	38.24	0	1975	12	4	18	59	59.9	SRA
3.6	-78.89	47.01	0	1975	12	19	15	25	0.1	NCEER
3.5	-107.65	42.85	0	1975	12	19	23	26	19.5	SRA
4.6	-108.212	35.817	0	1976	1	5	6	23	33.9	SNMX
3.4	-92.16	35.9	7	1976	1	16	19	42	56.9	NCEER
3.3	-103.1	31.9	0	1976	1	19	4	3	30	NCEER

Table 2.5-1 {USGS Earthquake Catalog for the CEUS with $m_b \geq 3.0$ }

(Page 45 of 65)

m_b	Longitude (degree)	Latitude (degree)	Depth (km)	Year	Month	Day	Hour	Minute	Second	Catalog Reference
3.8	-83.86	36.87	1	1976	1	19	6	20	39.6	NCEER
3.3	-100.087	31.9	4	1976	1	25	4	48	28.5	SRA
3.4	-83.73	41.88	5	1976	2	2	21	14	2.3	NCEER
3.6	-84.7	34.97	14	1976	2	4	19	53	53	NCEER
3.5	-71.21	41.56	0	1976	3	11	8	29	32.2	NCEER
3.1	-69.97	41.66	0	1976	3	14	23	12	24.6	NCEER
3.1	-95.6	35.43	5	1976	3	16	7	39	45.3	NCEER
3.5	-104.27	49.39	5	1976	3	25	0	12	16	NCEER
4.9	-90.48	35.58	17	1976	3	25	0	41	20.8	NCEER
3.3	-67.86	49.34	18	1976	3	29	21	23	27	NCEER
3	-86.7	39.3	0	1976	4	8	7	38	53	NCEER
3.2	-74.03	40.8	0	1976	4	13	15	39	12.9	NCEER
3.3	-87.31	37.38	4	1976	4	15	7	3	34.4	NCEER
3.5	-99.79	36.04	8	1976	4	19	4	42	46.9	NCEER
3.5	-109.1	35.39	5	1976	4	19	23	35	45.5	SRA
3	-103.14	32.27	0	1976	5	1	11	13	40.8	SRA
3.1	-73.9	49.56	18	1976	5	5	3	1	4	NCEER
3.1	-79.9	39.6	0	1976	5	6	18	46	8.1	NCEER
3.3	-68.62	49.84	3	1976	5	15	21	6	52	NCEER
3.2	-89.83	36.03	9	1976	5	22	7	40	46.1	NCEER
3	-104.02	37.41	5	1976	5	30	1	43	37.3	SRA
3.3	-81.6	37.34	1	1976	6	19	5	54	13.4	NCEER
3	-103.283	35.617	0	1976	6	24	15	27	32	SNMX
3.1	-74.1	45.18	9	1976	7	13	3	51	14	NCEER
3.1	-110.3	40.75	7	1976	7	30	22	19	0.2	SRA
3	-103.02	31.57	0	1976	8	5	18	53	9	SRA
3.1	-74.98	49.77	18	1976	8	7	7	50	11	NCEER
3.4	-106.57	45.03	5	1976	8	10	13	54	57.5	SRA
4.5	-106.15	44.04	10	1976	9	3	4	18	16.2	SRA
4.3	-80.77	36.62	9	1976	9	13	18	54	38	NCEER
3	-103.1	32.21	0	1976	9	17	2	47	45.4	SRA
3.1	-102.5	31.4	0	1976	9	17	3	56	29	DNAG
3.4	-67.1	49.36	18	1976	9	18	0	40	32	NCEER
3.5	-90.47	35.58	8	1976	9	25	14	6	55.8	NCEER
3.5	-106.57	45.03	0	1976	10	8	13	54	0	SRA
3	-97.06	35.38	5	1976	10	22	17	15	50.5	NCEER
3	-78.05	48.16	18	1976	10	22	18	50	56	NCEER
3.1	-88.98	32	10	1976	10	23	0	40	59.2	NCEER
4.2	-69.78	47.82	18	1976	10	23	20	58	18	NCEER
3	-75.96	47.11	18	1976	11	6	6	9	29	NCEER
4.2	-91.04	38.1	0	1976	12	11	7	5	1.1	NCEER
3.5	-90.26	37.81	9	1976	12	13	8	35	55.1	NCEER
3.7	-82.5	32.06	14	1976	12	27	6	57	15.2	NCEER
3.6	-89.71	37.58	5	1977	1	3	22	56	48.5	NCEER
3	-80.17	33.06	1	1977	1	18	18	29	14.1	NCEER

Table 2.5-1 {USGS Earthquake Catalog for the CEUS with $m_b \geq 3.0$ }

(Page 46 of 65)

m_b	Longitude (degree)	Latitude (degree)	Depth (km)	Year	Month	Day	Hour	Minute	Second	Catalog Reference
4.5	-66.73	46.88	18	1977	2	6	9	1	19	DNAG
3.1	-70.42	47.54	8	1977	2	14	0	35	4.1	NCEER
3.4	-78.63	37.9	0	1977	2	27	20	5	34.6	NCEER
3.1	-109.903	44.608	1	1977	3	2	18	7	24.2	DNAG
3.8	-107.15	41.24	5	1977	3	3	17	50	28	SRA
4.2	-108.222	35.748	0	1977	3	5	3	0	55.8	SNMX
3.7	-107	44.6	0	1977	3	24	8	55	0	DNAG
3.3	-103.1	31.9	0	1977	4	26	9	3	7	NCEER
3.3	-88.44	31.96	0	1977	5	4	2	0	24.3	NCEER
3.6	-94.17	34.56	10	1977	6	2	23	29	10.6	NCEER
3.2	-84.71	40.71	1	1977	6	17	15	39	46.9	NCEER
3.1	-70.16	47.77	8	1977	6	20	5	5	54.7	NCEER
3.4	-74.38	46.04	4	1977	7	14	7	39	29.8	NCEER
3	-102.7	31.8	0	1977	7	22	4	1	10	DNAG
3.5	-84.41	35.42	5	1977	7	27	22	3	20.8	NCEER
3.1	-80.7	33.37	9	1977	8	4	4	20	7.7	NCEER
3.9	-67.05	49.77	18	1977	8	8	23	8	40	NCEER
3.1	-80.69	33.39	0	1977	8	25	4	20	7	NCEER
3.5	-107.31	39.31	5	1977	9	24	11	16	48.4	SRA
4.8	-110.47	40.47	6	1977	9	30	10	19	20.4	USHIS
3	-73.82	46.52	1	1977	10	16	21	29	19.1	NCEER
3	-67.05	47	18	1977	10	24	18	9	12	NCEER
3.4	-89.173	33.928	16	1977	11	4	11	21	10.2	SRA
3	-75.15	46.27	5	1977	11	7	20	48	52.7	NCEER
3	-75.86	46.69	1	1977	11	25	18	47	24.4	NCEER
3.1	-92.91	34.39	10	1977	11	26	4	18	18.1	NCEER
3	-80.18	32.88	9	1977	12	15	19	16	43.1	NCEER
3.1	-70.68	41.79	0	1977	12	20	17	44	23.8	NCEER
3.5	-76.91	46.84	11	1977	12	22	14	57	1.3	NCEER
3.2	-71.64	43.2	0	1977	12	25	15	35	53.5	NCEER
3.2	-70.55	44.07	9	1978	1	4	19	28	10.8	NCEER
3.1	-88.21	32.7	1	1978	1	8	11	34	23.4	NCEER
3.8	-81.6	28.1	0	1978	1	12	21	10	0	DNAG
3	-105.31	42.43	5	1978	1	16	3	50	3.1	SRA
3	-88.01	38.244	5	1978	1	28	16	40	58.8	DNAG
3.3	-109.7	42.5	30	1978	2	7	5	3	10.4	SRA
4.1	-74.11	46.35	7	1978	2	18	14	48	25	NCEER
3.5	-102.5	31.55	1	1978	3	2	10	4	53	NCEER
3.1	-90	36.63	9	1978	4	3	12	24	21.5	NCEER
3	-69.89	47.751	22	1978	4	8	8	21	45	PDE
3.1	-78.24	39.7	15	1978	4	26	19	30	23.3	SRA
3.6	-101.95	42.26	38	1978	5	7	16	6	23	NCEER
3.2	-69.99	47.72	3	1978	5	26	2	31	0.4	NCEER
3	-107.32	39.28	5	1978	5	29	16	45	18	SRA
3.2	-88.46	38.41	20	1978	6	2	2	7	28.9	NCEER

Table 2.5-1 {USGS Earthquake Catalog for the CEUS with $m_b \geq 3.0$ }

(Page 47 of 65)

m_b	Longitude (degree)	Latitude (degree)	Depth (km)	Year	Month	Day	Hour	Minute	Second	Catalog Reference
3.8	-107.83	43.63	5	1978	6	6	21	23	34.7	SRA
3.3	-88.595	32.042	2	1978	6	9	23	15	19.6	SRA
3.4	-101.94	31.05	0	1978	6	29	20	58	45.1	DNAG
3.2	-68.39	48.75	18	1978	6	30	0	17	0	NCEER
3.1	-76.22	39.9	0	1978	7	16	6	39	29.7	NCEER
3.1	-105.04	34.68	0	1978	7	21	5	2	36.2	SNMX
3.4	-65.61	49.3	18	1978	7	29	13	56	43	NCEER
3.6	-74.44	45.68	7	1978	7	30	10	54	44	NCEER
3	-70.22	47.669	18	1978	8	14	22	55	58	PDE
3.1	-74.51	44.52	0	1978	8	21	8	47	0	NCEER
3	-76.43	47.17	5	1978	8	26	3	54	34.1	NCEER
3.5	-111.48	48.49	5	1978	8	30	16	33	21.2	SRA
3.5	-89.44	36.09	1	1978	8	31	0	31	0.6	NCEER
3	-90.28	38.58	1	1978	9	20	12	24	8.9	NCEER
3.1	-91.92	33.96	33	1978	9	23	7	34	3.7	NCEER
3	-76.15	40.08	0	1978	10	6	19	25	47.4	NCEER
3.8	-82.65	30.2	0	1978	11	6	23	0	0	DNAG
3.3	-67.62	48.96	18	1978	12	2	8	36	44	NCEER
3.5	-88.37	38.56	23	1978	12	5	1	48	2	NCEER
3.5	-88.47	31.91	3	1978	12	11	2	6	50.1	NCEER
3.3	-107.86	40.82	5	1979	1	20	6	59	8.4	SRA
3	-74.26	40.32	0	1979	1	30	16	30	52	NCEER
3.2	-90.1	35.84	10	1979	2	5	5	31	9.4	NCEER
3.3	-113.299	49.233	5	1979	2	24	15	49	15.5	PDE
3.4	-91.2	35.96	10	1979	2	27	22	54	54.8	NCEER
3.2	-74.5	40.72	0	1979	3	10	4	49	39.6	NCEER
3	-76.46	45.84	18	1979	3	18	16	31	12	NCEER
3.1	-108.9	40.18	2	1979	3	19	14	59	29.7	SRA
3.2	-70.1	47.69	10	1979	3	23	22	53	5	NCEER
3.2	-112.41	48.59	5	1979	4	14	9	39	6.4	SRA
3.1	-95.54	46.7	20	1979	4	16	6	40	16.7	SRA
4	-69.79	43.97	17	1979	4	18	2	34	15.3	NCEER
3.2	-66.03	45.24	18	1979	4	20	10	32	49.2	NCEER
3.1	-71.24	43.04	0	1979	4	23	0	5	45.7	NCEER
3.8	-111.02	37.88	7	1979	4	30	2	7	10.3	SRA
3.3	-75.68	46.18	1	1979	5	26	21	58	32.8	NCEER
3	-74.99	45	2	1979	5	29	20	48	49.1	NCEER
3.3	-67.54	49.37	18	1979	6	5	8	58	20	NCEER
3	-99.76	35.22	2	1979	6	7	7	39	36.3	NCEER
3.1	-73.86	44.43	0	1979	6	7	13	45	53.3	NCEER
3.8	-89.64	36.15	15	1979	6	11	4	12	17.1	NCEER
3	-110.904	37.861	7	1979	6	16	1	8	44.7	DNAG
3	-74.38	41.35	0	1979	6	20	19	20	17.8	SRA
3	-90.45	35.56	7	1979	6	25	17	11	13.8	NCEER
3	-97.29	39.92	7	1979	6	30	20	46	42.3	NCEER

Table 2.5-1 {USGS Earthquake Catalog for the CEUS with $m_b \geq 3.0$ }

(Page 48 of 65)

m_b	Longitude (degree)	Latitude (degree)	Depth (km)	Year	Month	Day	Hour	Minute	Second	Catalog Reference
3.8	-76.6	46.87	18	1979	7	8	1	29	18	NCEER
3.1	-89.31	36.91	2	1979	7	8	12	35	15.5	NCEER
3.7	-74.65	46.54	18	1979	7	9	8	16	26	NCEER
3.2	-100.32	40.18	4	1979	7	16	0	3	48.4	NCEER
3.1	-110.591	37.592	7	1979	7	25	23	56	11.7	DNAG
3.5	-70.44	43.29	11	1979	7	28	23	29	12	NCEER
3	-81.358	34.333	3	1979	8	7	19	32	17.2	SRA
3.8	-111.47	48.49	5	1979	8	9	17	12	55.4	SRA
3.7	-84.36	35.21	10	1979	8	13	5	18	56.8	NCEER
4.6	-69.9	47.67	10	1979	8	19	22	49	30.4	NCEER
3.7	-82.956	34.916	1	1979	8	26	1	31	45	USHIS
3.8	-91.5	36.3	0	1979	8	26	11	28	0	DNAG
3.2	-83.24	35.3	10	1979	9	6	20	38	16.3	NCEER
3.2	-83.91	35.58	12	1979	9	12	6	24	4	NCEER
3.4	-99.47	35.19	1	1979	9	13	0	49	21.5	NCEER
3.6	-82.08	36.44	5	1979	10	8	8	53	52.8	SRA
3.5	-110.93	37.89	7	1979	10	23	4	17	19.9	SRA
3.2	-91.04	36.46	6	1979	11	5	16	35	25.9	NCEER
3.6	-82.81	38.49	1	1979	11	9	21	29	59.8	NCEER
3.3	-98.41	35.63	5	1979	11	27	9	10	36.7	NCEER
3.8	-66.72	49.43	18	1979	12	19	18	58	10	NCEER
3.5	-91.22	49.62	18	1980	2	27	6	13	41	NCEER
3.1	-74.2	42.58	12	1980	2	29	5	53	56.1	SRA
3.7	-71.87	46.79	18	1980	3	11	4	15	55	NCEER
3.3	-75.09	40.15	0	1980	3	11	6	0	26.9	NCEER
3	-88.44	37.89	20	1980	3	13	2	23	13	NCEER
3.3	-86.76	37.6	9	1980	3	23	21	38	16.2	NCEER
4	-67.95	48.77	18	1980	4	3	16	57	24	NCEER
3.2	-68.36	44.71	0	1980	4	10	15	36	43.8	NCEER
4.1	-81.64	49.64	18	1980	4	13	22	40	23	NCEER
3.6	-112.34	48.79	5	1980	4	14	3	27	33.8	SRA
3	-81.324	34.329	3	1980	4	24	6	16	57.2	SRA
3	-75	40.3	0	1980	5	2	19	2	0	NCEER
3	-75.25	45.26	19	1980	5	19	23	40	50	DNAG
3.4	-74.55	44.89	0	1980	5	23	8	39	44	NCEER
3.5	-75.23	43.56	1	1980	6	6	13	15	51.9	NCEER
3.4	-101.01	35.48	1	1980	6	9	22	37	12.3	NCEER
3	-82.81	35.46	1	1980	6	10	23	47	32.2	NCEER
3.3	-84.03	35.73	1	1980	6	25	18	2	1.6	NCEER
3.4	-70.75	47.56	10	1980	7	1	3	6	38	NCEER
3.1	-70.33	47.3	10	1980	7	2	7	50	33	NCEER
3.5	-89.6	36.56	4	1980	7	5	8	54	40.1	NCEER
3.2	-99.7	35.18	5	1980	7	18	14	29	46.8	NCEER
3.1	-74.17	45.14	5	1980	7	25	6	22	34	NCEER
3.1	-87.44	33.94	0	1980	7	25	15	30	12.5	SRA

Table 2.5-1 {USGS Earthquake Catalog for the CEUS with $m_b \geq 3.0$ }

(Page 49 of 65)

m_b	Longitude (degree)	Latitude (degree)	Depth (km)	Year	Month	Day	Hour	Minute	Second	Catalog Reference
5.2	-83.89	38.19	16	1980	7	27	18	52	21.4	NCEER
3.2	-81.364	34.351	1	1980	7	29	1	10	22.7	SRA
3	-82.04	49.9	18	1980	7	31	10	10	4	NCEER
3.1	-74.15	40.43	8	1980	8	2	17	20	59.7	SRA
3.3	-75.16	43.54	0	1980	8	11	14	54	46.1	NCEER
3.2	-82.99	41.99	1	1980	8	20	9	34	53.4	NCEER
3.1	-84.87	37.98	1	1980	8	23	3	49	3.7	NCEER
3	-74.9	39.8	0	1980	8	30	9	19	0	NCEER
3.2	-73.78	41.11	13	1980	9	4	4	30	55.8	SRA
3.2	-69	44.67	8	1980	9	8	5	59	55.2	NCEER
3.2	-105.12	41.18	0	1980	9	12	22	33	55.4	SRA
3.2	-74.02	43.63	0	1980	9	21	20	52	45.1	DNAG
3	-69.9	47.67	6	1980	9	30	18	26	1	NCEER
3.4	-80.57	43.15	5	1980	10	14	0	58	56.4	NCEER
3.1	-72.9	41.3	0	1980	10	24	17	27	38.2	NCEER
3	-97.76	35.46	1	1980	11	2	10	0	48.9	NCEER
3	-79.9	38.18	4	1980	11	5	21	48	14.7	NCEER
3.8	-89.43	36.17	5	1980	12	2	8	59	29.7	NCEER
3.4	-78.44	37.72	6	1981	2	11	13	44	16.4	NCEER
3.8	-91.8	30	0	1981	2	13	2	15	0	DNAG
3.3	-74.93	45.96	18	1981	2	19	7	7	10	NCEER
4.3	-104.96	39.91	8	1981	4	2	16	10	6.4	NCEER
3.5	-89.38	38.87	1	1981	4	8	1	53	13	SRA
3.3	-82.05	35.51	0	1981	4	9	7	10	31.2	NCEER
3.7	-65.7	45.93	18	1981	4	13	17	31	38	NCEER
3.5	-82.42	35.33	10	1981	5	5	21	21	56.7	NCEER
3	-91.63	36.76	1	1981	5	25	22	50	18.2	SRA
3	-110.37	36.83	1	1981	5	29	3	9	2.2	SRA
3	-81.67	36.18	1	1981	6	3	20	54	22.4	SRA
3.2	-94.32	31.99	5	1981	6	9	1	46	32.7	NCEER
3.4	-89.03	37.82	19	1981	6	9	14	15	47.8	NCEER
3.8	-89.9	43.9	0	1981	6	12	15	30	0	DNAG
3.7	-70	47.47	8	1981	6	16	17	55	4	NCEER
3.5	-90.07	35.85	9	1981	6	26	8	33	27	NCEER
3.1	-71.55	43.57	0	1981	6	28	22	42	35	NCEER
3.7	-74.62	45.14	13	1981	7	4	23	16	32	NCEER
3.5	-97.73	34.85	5	1981	7	11	21	9	21.8	NCEER
3.7	-66.8	49.82	18	1981	7	13	4	48	4	NCEER
3	-110.31	36.82	0	1981	7	14	19	29	51	SRA
4	-89.18	36.03	11	1981	8	7	11	53	44	NCEER
3	-73.54	44.07	1	1981	8	10	23	6	59.3	DNAG
3.3	-72.24	48.66	5	1981	8	23	23	17	20	NCEER
3.3	-80.59	43.15	1	1981	8	28	10	51	33	NCEER
3	-85.17	34.63	3	1981	9	4	17	21	44.5	NCEER
3.1	-81.41	42.8	9	1981	9	5	5	49	21	NCEER

Table 2.5-1 {USGS Earthquake Catalog for the CEUS with $m_b \geq 3.0$ }

(Page 50 of 65)

m_b	Longitude (degree)	Latitude (degree)	Depth (km)	Year	Month	Day	Hour	Minute	Second	Catalog Reference
3.1	-100.52	42.89	5	1981	9	7	0	38	9.1	SRA
3.1	-110.56	37.5	2	1981	9	10	7	55	9	SRA
3.4	-101.85	43.04	5	1981	9	13	22	16	29.7	NCEER
3.1	-66.11	49.53	18	1981	9	18	2	24	11	NCEER
3.5	-75.02	46.11	0	1981	9	18	7	16	7	NCEER
3.5	-75.56	46.37	0	1981	9	30	23	41	39	NCEER
3.3	-98.54	41.17	5	1981	10	9	21	54	27.8	NCEER
3	-112.92	49.29	18	1981	10	20	3	47	36	DNAG
3.7	-72.57	41.14	5	1981	10	21	16	49	6.9	NCEER
3.9	-65.25	49.83	18	1981	10	28	19	56	14	NCEER
3.2	-95.26	32.02	5	1981	11	6	12	36	40.5	NCEER
3	-89.39	36.09	12	1981	11	8	17	11	19	NCEER
3.4	-77.04	46.98	18	1981	11	12	18	40	14	NCEER
3.7	-66.61	47.03	5	1981	11	28	5	12	3	NCEER
3.3	-72.64	45.38	3	1981	12	6	16	11	27	NCEER
3.1	-86.43	35.18	13	1982	1	2	2	0	26.2	NCEER
3.9	-102.49	31.18	5	1982	1	4	16	56	8.1	NCEER
5.7	-66.6	47	5	1982	1	9	12	53	52	NCEER
4.7	-71.62	43.51	7	1982	1	19	0	14	42.6	NCEER
4.3	-92.22	35.22	0	1982	1	24	3	22	44.4	NCEER
3.3	-70.38	47.45	6	1982	1	27	1	35	56	NCEER
3	-70.94	41.87	0	1982	1	27	18	50	4.6	NCEER
3.4	-81.39	32.98	7	1982	1	28	4	52	51.9	SRA
3	-67.48	49.18	18	1982	1	30	15	44	35	DNAG
3.1	-90.06	35.92	10	1982	2	2	9	26	46.3	NCEER
3.3	-104.03	48.51	18	1982	3	9	13	10	50.1	NCEER
3	-82.48	46.65	1	1982	3	13	4	34	32	NCEER
3.1	-103.27	35.36	5	1982	3	16	11	3	2.7	NCEER
3	-79.88	46.3	18	1982	3	19	16	48	13	NCEER
3.4	-113.25	49.07	18	1982	3	21	21	43	21	DNAG
3	-98.46	29.85	5	1982	3	28	23	24	32.9	NCEER
3	-82.04	36.51	3	1982	4	13	13	4	13.3	NCEER
3	-111.3	38.22	9	1982	4	17	6	0	12.5	SRA
3.5	-92.24	35.18	0	1982	4	21	21	17	55	NCEER
3.1	-96.47	33.99	5	1982	5	3	7	54	48.6	NCEER
3.4	-109.7	44.64	11	1982	5	9	21	7	36.5	SRA
3	-77.96	40.41	0	1982	5	12	18	29	33	SRA
3.5	-92.23	35.2	2	1982	5	31	18	21	19.7	NCEER
3.5	-76.95	47.38	18	1982	6	23	0	22	0	NCEER
3.5	-92.21	35.22	6	1982	7	5	4	13	52	NCEER
3.6	-96.72	44.01	5	1982	7	11	19	42	28.4	NCEER
3.8	-74.55	46.09	17	1982	7	13	2	18	49	NCEER
3	-69.02	46.08	6	1982	7	15	7	27	55.4	SRA
3.1	-81.55	34.32	2	1982	7	16	14	16	2.9	SRA
3.7	-75.46	45.89	19	1982	8	6	6	29	10	NCEER

Table 2.5-1 {USGS Earthquake Catalog for the CEUS with $m_b \geq 3.0$ }

(Page 51 of 65)

m_b	Longitude (degree)	Latitude (degree)	Depth (km)	Year	Month	Day	Hour	Minute	Second	Catalog Reference
3.2	-92.24	35.19	4	1982	8	9	11	12	31.6	SRA
3.1	-88.73	37.25	5	1982	8	11	10	32	38.8	NCEER
3.7	-78.61	46.67	18	1982	8	13	1	6	42	NCEER
4.3	-105.38	49.06	18	1982	8	17	4	49	25	NCEER
3.4	-70.38	47.37	20	1982	8	29	2	7	11	NCEER
3	-74.19	43.2	5	1982	8	31	10	16	28.4	NCEER
3.2	-108.85	42.72	5	1982	8	31	22	2	18.5	SRA
3	-82.9	34.96	3	1982	9	2	21	52	45.5	SRA
3.7	-76.61	45.67	12	1982	9	3	23	14	3	NCEER
3.2	-84.51	35.19	13	1982	9	5	10	11	9.4	NCEER
3.4	-84.25	35.68	8	1982	9	24	22	19	16.9	NCEER
3.5	-92.23	35.21	5	1982	9	25	23	17	5.5	SRA
3	-73.057	43.125	8	1982	9	28	22	24	12.5	DNAG
3.9	-102.57	36.1	5	1982	10	14	12	52	46.3	NCEER
3.3	-65.3	49.82	18	1982	10	29	21	50	57	NCEER
3.1	-84.89	32.64	0	1982	10	31	3	12	12.2	NCEER
3.3	-108.695	35.305	0	1982	11	3	17	54	1.9	SNMX
3.1	-100.2	35.2	0	1982	11	7	0	4	19	SRA
4.3	-97.85	43.01	5	1982	11	15	2	58	22.9	NCEER
3.5	-92.08	35.25	0	1982	11	21	16	35	31	NCEER
3	-73.43	45.34	5	1982	11	24	7	34	39	PDE
3	-71.52	43.62	6	1982	12	1	22	52	22.9	SRA
3.9	-70.22	47.54	16	1982	12	4	16	8	32	NCEER
3	-83.53	32.85	0	1982	12	11	0	25	0	NCEER
3.3	-78.83	46.82	18	1983	1	10	21	31	27	NCEER
4.1	-67.06	49.11	18	1983	1	17	19	35	52	NCEER
3.9	-92.16	35.28	0	1983	1	19	2	30	42	NCEER
3.1	-83.45	48.72	18	1983	1	20	9	16	45	NCEER
3.1	-67.86	47.46	15	1983	1	20	14	17	21	NCEER
3.3	-81.02	41.75	10	1983	1	22	7	46	58	NCEER
3.5	-83.56	32.85	0	1983	1	26	14	7	44.7	NCEER
3.1	-83.63	36.06	13	1983	1	27	22	9	35.1	NCEER
3.3	-110.674	37.778	7	1983	1	27	23	37	11.8	SRA
3.2	-88.31	34.73	0	1983	2	5	13	8	19	NCEER
3.5	-68.33	48.98	18	1983	2	11	15	46	56	NCEER
4	-105.729	42.232	5	1983	2	13	13	44	44	SRA
3.5	-112.373	48.539	14	1983	2	16	6	22	9.3	SRA
3.6	-89.6	36.19	1	1983	2	23	8	51	27	NCEER
3	-73.66	41.55	7	1983	2	26	19	59	35.4	NCEER
4.4	-99.41	44.21	5	1983	3	4	6	32	18.6	NCEER
3.4	-71.72	42.96	1	1983	3	24	14	27	20.4	NCEER
3.3	-82.46	35.33	12	1983	3	25	2	47	11.1	NCEER
3.2	-92.15	35.2	0	1983	3	30	4	15	26	NCEER
3.4	-102.38	35.32	5	1983	4	3	4	55	24.2	NCEER
3	-66.98	49.34	18	1983	4	13	16	6	53	DNAG

Table 2.5-1 {USGS Earthquake Catalog for the CEUS with $m_b \geq 3.0$ }

(Page 52 of 65)

m_b	Longitude (degree)	Latitude (degree)	Depth (km)	Year	Month	Day	Hour	Minute	Second	Catalog Reference
3	-110.633	38.305	2	1983	5	3	12	43	37.7	SRA
3.3	-102.198	42.955	5	1983	5	6	6	14	46.9	SRA
3.9	-66.6	47	5	1983	5	13	23	40	57	NCEER
4.3	-89.57	38.77	0	1983	5	15	5	16	22	NCEER
3.8	-69.89	47.7	11	1983	5	16	2	1	57	NCEER
3	-92.36	38.48	0	1983	5	16	14	3	4	NCEER
3.7	-69.46	45.54	10	1983	5	27	23	4	35.2	NCEER
4.4	-70.4	44.49	3	1983	5	29	5	45	49.9	NCEER
3.4	-70.22	47.45	10	1983	6	2	6	30	23	NCEER
3	-69.65	47.46	10	1983	6	4	5	0	23	NCEER
3.5	-66.68	47.04	5	1983	6	28	8	5	49	NCEER
3	-90.94	37.1	0	1983	7	8	9	41	40	NCEER
3.4	-84.15	35.55	10	1983	7	8	19	29	5.9	NCEER
3	-74.91	46.06	18	1983	7	17	22	47	45	NCEER
3	-70.95	46.53	10	1983	7	23	3	25	38	NCEER
3.4	-98.131	28.743	5	1983	7	23	15	24	38.2	SRA
3.7	-67.68	44.97	12	1983	8	12	14	8	47.6	NCEER
3.5	-82.77	38.47	10	1983	8	17	14	3	15	NCEER
3.4	-104.314	37.469	5	1983	8	17	15	3	27.6	SRA
3.1	-83.82	36.68	18	1983	8	28	22	45	7.4	NCEER
3.1	-104.43	34.922	0	1983	9	15	23	25	37.5	SNMX
4.1	-108.837	40.789	5	1983	9	24	16	57	45.7	SRA
3.1	-79.79	43.44	2	1983	10	4	17	18	40	NCEER
5.2	-74.31	44.03	7	1983	10	7	10	18	47	NCEER
4.2	-75.77	45.21	15	1983	10	11	4	10	55	NCEER
3.1	-75.05	45.62	11	1983	10	16	3	0	47	NCEER
3.8	-93.39	30.24	5	1983	10	16	19	40	50.8	NCEER
3.2	-66.31	47.21	5	1983	10	17	22	58	56	NCEER
3.1	-77.97	48.14	1	1983	10	24	1	0	6	NCEER
3.5	-73.9	45.68	18	1983	11	1	10	16	52	NCEER
3.3	-80.16	32.94	10	1983	11	6	9	2	19.8	NCEER
3	-105.955	43.016	5	1983	11	15	12	33	12.1	SRA
3.8	-66.6	47	5	1983	11	17	15	32	18	NCEER
3.3	-69.16	45.19	2	1983	12	4	10	48	33.6	NCEER
3	-67.17	45.11	7	1983	12	8	12	23	5	NCEER
3	-92.704	33.183	5	1983	12	9	20	52	10.5	SRA
3.2	-76.29	46.69	18	1983	12	14	1	52	3	NCEER
3.1	-73.97	45.24	18	1983	12	21	15	4	44	NCEER
3.4	-76.33	47.01	18	1983	12	28	12	24	21	NCEER
3	-89.75	37.59	2	1984	1	12	2	48	15.7	SRA
3.5	-67.16	44.88	18	1984	1	14	9	9	32	NCEER
3	-83.43	41.65	0	1984	1	14	20	14	31	NCEER
3.3	-110.845	47.149	5	1984	1	16	19	50	25.2	SRA
3.1	-75.12	45.56	19	1984	1	17	19	4	46	NCEER
3.2	-89.92	36.61	1	1984	1	28	21	29	22.1	SRA

Table 2.5-1 {USGS Earthquake Catalog for the CEUS with $m_b \geq 3.0$ }

(Page 53 of 65)

m_b	Longitude (degree)	Latitude (degree)	Depth (km)	Year	Month	Day	Hour	Minute	Second	Catalog Reference
3.2	-97.36	34.67	5	1984	2	3	4	38	28	NCEER
3.6	-83.74	36.13	10	1984	2	14	20	54	30.9	NCEER
3.6	-89	37.21	0	1984	2	14	22	56	10	NCEER
3.7	-66.6	47	5	1984	2	24	3	17	14	PDE
3.2	-108.638	41.539	2	1984	3	1	18	13	0.9	SRA
3.8	-98.461	28.852	5	1984	3	3	1	3	26.5	SRA
3	-84.05	35.83	7	1984	3	17	23	26	11.4	NCEER
3	-66.49	46.91	5	1984	3	27	22	56	24	DNAG
3.2	-66.46	49.61	18	1984	3	29	22	52	50	DNAG
3.4	-102.4	35.32	0	1984	4	3	4	55	24	SRA
3.8	-67.52	49.3	18	1984	4	11	19	7	42	DNAG
3.1	-66.6	47	5	1984	4	13	15	35	51	DNAG
3.4	-88.44	38.38	0	1984	4	17	4	44	44	NCEER
3.1	-107.19	39.281	5	1984	4	22	17	30	56.7	SRA
4.1	-76.37	39.95	4	1984	4	23	1	36	0	NCEER
3.2	-107.228	39.322	5	1984	5	14	10	14	17.2	SRA
3.4	-102.4	35.4	0	1984	5	21	13	30	14	SRA
3.1	-102.228	35.067	5	1984	5	21	13	31	13.5	SRA
3.6	-102.155	39.22	5	1984	5	27	23	30	19.3	SRA
3.2	-66.33	49.6	18	1984	5	28	21	4	52	DNAG
3.5	-80.78	46.63	1	1984	6	20	16	10	22	PDE
3.2	-89.39	36.1	12	1984	6	26	15	15	19.9	NCEER
3.1	-75.68	46.23	0	1984	6	28	3	8	49	DNAG
3.8	-88.47	37.7	2	1984	6	29	7	58	29.3	NCEER
3	-66.6	47	5	1984	7	2	5	24	54	DNAG
4.1	-81.17	46.53	1	1984	7	6	17	24	52	PDE
3	-89.53	36.5	7	1984	7	16	3	50	53.5	NCEER
4	-87.07	39.22	10	1984	7	28	23	39	27.4	NCEER
3	-90.92	37.82	7	1984	7	30	7	33	46.5	NCEER
3	-67.05	45.32	18	1984	8	3	13	41	11	DNAG
3	-98.362	29.133	5	1984	8	8	1	31	27.3	SRA
3.2	-86.3	34.62	8	1984	8	9	2	42	35.8	NCEER
4.2	-78.324	37.868	8	1984	8	17	18	5	46.9	SRA
3.2	-73.48	44.875	11	1984	8	20	10	58	17	SRA
3.1	-87.45	39.11	10	1984	8	29	6	50	59.5	NCEER
3.1	-84.34	35.57	13	1984	8	30	16	26	28.4	NCEER
5	-106.11	44.138	15	1984	9	8	0	59	31.1	USHIS
3.2	-100.697	31.991	5	1984	9	11	14	47	33.5	SRA
3.2	-108.582	41.61	2	1984	9	14	19	4	26.3	SRA
3.4	-92.21	35.25	5	1984	9	27	13	3	6	NCEER
3	-91.7	35.72	5	1984	9	27	13	16	22.9	NCEER
4.2	-85.2	34.75	12	1984	10	9	11	54	26.9	NCEER
3	-66.59	47.08	5	1984	10	13	1	45	15	DNAG
3.3	-65.66	44.72	18	1984	10	13	12	53	45	DNAG
5.4	-105.735	42.317	22	1984	10	18	15	30	22	USHIS

Table 2.5-1 {USGS Earthquake Catalog for the CEUS with $m_b \geq 3.0$ }

(Page 54 of 65)

m_b	Longitude (degree)	Latitude (degree)	Depth (km)	Year	Month	Day	Hour	Minute	Second	Catalog Reference
3.2	-81.68	36.36	11	1984	10	22	18	58	41.7	NCEER
3.5	-73.93	43.59	0	1984	10	23	6	26	21.9	NCEER
4.7	-108.919	42.534	5	1984	11	3	9	30	8.4	USHIS
3.1	-97.41	34.71	5	1984	11	20	10	57	31.9	NCEER
3.2	-75.05	45.19	14	1984	11	26	9	3	49	PDE
3.7	-66.58	46.98	14	1984	11	30	5	54	22	PDE
3	-89.7	36.16	11	1984	12	3	11	55	44.6	NCEER
3.6	-66.04	47.52	1	1984	12	9	18	12	21	DNAG
3.5	-82.6	46.5	0	1984	12	17	9	38	36	PDE
3	-70.25	47.4	19	1984	12	22	12	46	30	DNAG
3	-89.91	35.93	9	1985	1	30	9	35	12.4	SRA
3.1	-89.51	36.29	7	1985	2	7	23	44	35.3	NCEER
3	-87.5	38.42	3	1985	2	13	10	22	24	SRA
3.3	-89.34	37.23	6	1985	2	15	15	56	9.9	NCEER
3.2	-70.48	47.39	14	1985	3	3	12	15	17	PDE
3.2	-105.85	38.558	5	1985	3	16	21	55	2.4	SRA
3.1	-69.96	47.52	12	1985	4	10	5	52	57	DNAG
3.1	-70.704	45.364	2	1985	4	12	5	27	30.5	SRA
3.2	-80.4	41.59	18	1985	4	14	11	39	54	DNAG
3.4	-108.92	35.26	0	1985	4	14	21	48	2.9	SNMX
3.1	-90.77	36.27	9	1985	5	4	7	7	12.5	SRA
3.2	-75.9	46.83	18	1985	5	16	13	39	7	DNAG
3.2	-80.485	37.248	11	1985	6	10	12	22	38.3	SRA
3.6	-82.038	37.222	1	1985	6	19	22	28	8.9	SRA
3	-85.156	35.198	3	1985	7	12	18	20	28.4	SRA
3.3	-92.202	35.219	5	1985	8	3	4	23	11	DNAG
3.5	-108.649	41.817	5	1985	8	13	20	57	0.8	SRA
4.3	-108.06	42.813	10	1985	8	16	6	5	22.6	SRA
3.1	-67.67	49.3	0	1985	8	16	22	48	37	DNAG
3	-110.232	46.109	5	1985	8	22	2	12	5	SRA
3.1	-76.64	45.67	18	1985	8	24	6	4	2	PDE
3.6	-93.118	35.809	10	1985	9	6	22	17	2.8	SRA
3	-88.014	41.848	5	1985	9	9	22	6	31	SRA
3.3	-97.051	33.548	5	1985	9	18	15	54	4.6	SRA
4	-66.6	47	5	1985	10	5	5	34	14	PDE
3	-109.498	40.407	21	1985	10	7	20	33	40.1	SRA
3.1	-71.471	42.528	13	1985	10	15	20	0	38.4	SRA
3.9	-73.829	40.983	6	1985	10	19	10	7	40.3	USHIS
3.3	-73.45	45.29	5	1985	11	1	23	33	39	PDE
3.3	-92.188	35.223	4	1985	11	8	19	56	48.5	SRA
3.2	-113.36	49.18	18	1985	12	4	8	38	14	DNAG
3.8	-89.99	35.88	5	1985	12	5	22	59	41.2	SRA
3	-104.665	35.437	0	1985	12	15	7	14	52.6	SNMX
3.1	-66.6	47	5	1985	12	21	6	3	11	DNAG
3.3	-83.72	35.701	13	1985	12	22	0	56	5	SRA

Table 2.5-1 {USGS Earthquake Catalog for the CEUS with $m_b \geq 3.0$ }

(Page 55 of 65)

m_b	Longitude (degree)	Latitude (degree)	Depth (km)	Year	Month	Day	Hour	Minute	Second	Catalog Reference
3.5	-88.965	38.552	5	1985	12	29	8	56	56.3	SRA
3.2	-84.762	35.609	22	1986	1	7	1	26	43.3	SRA
3.3	-77.32	45.8	18	1986	1	10	9	59	48	PDE
4	-70.18	47.7	18	1986	1	11	13	30	28	PDE
3.3	-100.693	32.066	5	1986	1	30	22	26	37	SRA
4.9	-81.162	41.65	2	1986	1	31	16	46	42.3	USHIS
3.5	-82.907	34.793	5	1986	2	13	11	35	45.3	SRA
3.1	-102.514	35.308	5	1986	3	3	11	45	17.4	SRA
3.5	-66.6	47	5	1986	3	6	8	34	51	PDE
3	-85.51	35.187	27	1986	4	19	7	40	53	SRA
4.4	-87.347	33.335	1	1986	5	7	2	27	0.4	SRA
3.3	-66.14	46.54	18	1986	5	9	9	4	33	PDE
3.2	-110.319	37.294	8	1986	5	14	15	2	55.7	SRA
3	-92.217	35.178	5	1986	5	24	8	16	1.5	SRA
3.4	-89.88	36.58	10	1986	5	24	12	48	13.5	SRA
3.4	-98.289	43.937	5	1986	5	25	7	13	22.1	SRA
3.4	-66.6	47	5	1986	6	1	14	53	14	PDE
3	-99.781	39.344	5	1986	6	2	4	4	5.2	SRA
3.3	-75.09	46.34	8	1986	6	5	12	13	22	PDE
3	-105.694	42.397	20	1986	6	12	15	14	34	SRA
3.8	-84.987	34.937	13	1986	7	11	14	26	14.8	USHIS
4.5	-84.371	40.537	10	1986	7	12	8	19	37.9	USHIS
3.4	-68.198	46.17	9	1986	7	12	20	32	48.4	SRA
3.5	-75.22	46.37	18	1986	8	6	11	19	36	PDE
3.3	-74.246	45.131	24	1986	8	13	4	55	18.4	PDE
4	-110.574	37.42	5	1986	8	22	13	26	33.3	SRA
3.7	-89.79	38.32	5	1986	8	26	16	41	24.8	SRA
3.1	-105.17	35.12	0	1986	8	27	18	6	58	SNMX
3.5	-107.09	38.912	5	1986	9	3	6	20	50.9	SRA
4.2	-70.32	47.3	22	1986	9	19	15	53	1	PDE
4.1	-66.6	47	5	1986	10	17	14	47	59	PDE
3	-101.372	37.918	5	1986	10	20	4	32	49	SRA
3.9	-71.59	43.399	5	1986	10	25	17	16	38.4	SRA
3.3	-108.896	41.922	5	1986	11	3	0	23	45	SRA
3	-110.297	37.43	1	1986	11	7	1	31	53.7	SRA
3	-82.88	34.898	9	1986	12	11	14	7	11.5	SRA
3.5	-89.58	36.42	14	1986	12	30	7	15	19.1	SRA
3.5	-103.482	42.788	5	1987	1	1	8	2	24	PDE
3	-89.978	35.893	5	1987	1	16	3	25	35.7	PDE
3.1	-98.097	35.828	5	1987	1	24	16	8	17	PDE
3.8	-110.616	40.442	1	1987	3	5	3	2	50.4	PDE
4.2	-84.229	35.567	19	1987	3	27	7	29	30.4	USHIS
5.2	-87.954	38.713	10	1987	6	10	23	48	54.8	USHIS
4.1	-89.686	36.605	5	1987	6	13	21	17	12.8	PDE
3.6	-89.173	36.839	5	1987	7	7	19	19	5.7	PDE

Table 2.5-1 {USGS Earthquake Catalog for the CEUS with $m_b \geq 3.0$ }

(Page 56 of 65)

m_b	Longitude (degree)	Latitude (degree)	Depth (km)	Year	Month	Day	Hour	Minute	Second	Catalog Reference
3	-98.292	44.332	10	1987	7	9	22	6	45.4	PDE
3.4	-83.817	36.103	25	1987	7	11	0	4	29.4	PDE
3.8	-80.767	41.896	5	1987	7	13	5	49	17.4	PDE
3.4	-79.472	43.491	6	1987	7	23	9	32	28.5	PDE
3.1	-89.688	38.308	5	1987	8	31	17	12	35.5	PDE
3.3	-84.311	35.623	19	1987	9	22	17	23	50.1	PDE
3.7	-74.517	44.375	10	1987	9	26	17	44	6.9	PDE
4.5	-89.21	36.84	5	1987	9	29	0	4	57.2	USHIS
3.6	-107.381	45.771	5	1987	10	5	18	54	49.3	PDE
3.8	-88.793	37.049	5	1987	10	14	15	49	39.5	PDE
3	-98.599	44.472	5	1987	10	15	10	54	33.8	PDE
3.5	-83.099	36.848	14	1987	11	27	18	58	29.5	PDE
3.7	-98.024	36.055	5	1987	12	8	1	42	40.3	PDE
3	-82.628	34.244	5	1987	12	12	3	53	28.7	PDE
3.3	-84.201	35.275	12	1988	1	9	1	7	40.7	PDE
3.6	-89.621	46.559	5	1988	1	14	17	23	36.5	PDE
3.3	-80.157	32.935	7	1988	1	23	1	57	16.3	PDE
4.9	-65.58	48	18	1988	1	28	8	38	28	PDE
3.5	-90.465	35.681	10	1988	1	31	0	12	43.4	PDE
3.3	-108.532	40.626	5	1988	2	14	18	32	40.5	PDE
3.2	-82.304	36.561	5	1988	2	16	15	26	54.5	PDE
3.5	-83.853	35.366	5	1988	2	18	0	37	45.9	PDE
3.3	-66.6	47	5	1988	3	6	18	13	18.1	PDE
3.9	-75.716	46.341	18	1988	3	10	14	42	55.2	PDE
3.4	-99.155	39.093	5	1988	4	14	9	39	31.4	PDE
4.1	-81.987	37.238	0	1988	4	14	23	37	31.1	PDE
3.4	-66.6	47	5	1988	5	9	1	23	3.6	PDE
3.5	-75.58	45.17	7	1988	5	15	6	10	5.6	PDE
3.3	-92.77	37.288	5	1988	5	20	23	6	22.6	PDE
3.3	-110.448	36.374	5	1988	7	15	0	38	9.5	PDE
3.5	-74.955	44.995	10	1988	8	9	13	57	26.9	PDE
5.4	-110.869	39.128	10	1988	8	14	20	3	3.9	USHIS
3.8	-66.59	46.99	5	1988	8	26	5	59	10.2	PDE
4.6	-83.878	38.143	10	1988	9	7	2	28	9.5	USHIS
3.5	-87.931	38.69	5	1988	10	5	0	38	52.2	PDE
3.9	-71.158	44.539	5	1988	10	20	13	9	50.1	USHIS
3.8	-70.386	44.424	5	1988	11	14	6	15	43.1	PDE
5.8	-71.183	48.117	28	1988	11	25	23	46	4.5	PDE
3.3	-92.702	34.189	13	1988	12	25	15	57	57.7	PDE
3.5	-69.342	44.514	10	1988	12	28	6	28	44.4	PDE
3.5	-89.428	36.185	5	1988	12	31	14	24	20.5	PDE
3.8	-67.357	49.264	18	1989	1	1	17	55	53.6	PDE
3.1	-112.862	49.056	5	1989	1	4	18	50	9.7	PDE
3.4	-104.103	35.183	0	1989	1	29	5	7	15.6	SNMX
3.8	-101.898	42.685	5	1989	2	9	5	15	45.8	PDE

Table 2.5-1 {USGS Earthquake Catalog for the CEUS with $m_b \geq 3.0$ }

(Page 57 of 65)

m_b	Longitude (degree)	Latitude (degree)	Depth (km)	Year	Month	Day	Hour	Minute	Second	Catalog Reference
3.5	-87.092	33.643	0	1989	2	28	17	31	50.8	PDE
4.4	-69.9	47.7	18	1989	3	11	8	31	52.1	PDE
3.5	-71.144	44.511	5	1989	4	6	2	35	51.3	PDE
3.7	-105.602	47.716	5	1989	4	7	8	26	48.9	PDE
3	-89.711	36.557	5	1989	4	15	16	39	51.1	PDE
4.4	-89.768	36.006	10	1989	4	27	16	47	49.8	USHIS
3.7	-89.71	36.74	2	1989	5	14	0	16	9.5	PDE
3.9	-99.477	39.165	5	1989	6	8	18	18	43.3	PDE
3.1	-83.569	38.607	10	1989	7	15	0	8	2.6	PDE
3.1	-98.876	36.434	5	1989	7	20	6	7	50.4	PDE
3.3	-79.53	43.21	18	1989	8	5	21	7	59.1	PDE
3.5	-65.82	46.65	18	1989	8	10	21	17	43.5	PDE
3.4	-87.086	33.632	0	1989	8	13	20	16	2.9	PDE
3.9	-87.645	34.736	10	1989	8	20	0	3	17.8	USHIS
3	-70.899	41.614	5	1989	8	24	15	56	59.3	PDE
3	-108.948	47.547	5	1989	8	31	4	2	38.3	PDE
3.4	-89.62	36.545	11	1989	9	14	17	31	28	PDE
3	-107.027	41.207	5	1989	11	2	6	23	56.2	PDE
4	-76.59	46.57	18	1989	11	16	9	24	52	PDE
3	-107.767	38.055	5	1989	11	19	3	21	13.6	PDE
3.3	-99.908	45.317	5	1989	11	26	1	6	14.6	PDE
3.2	-90.744	35.245	5	1989	12	25	8	29	26.9	PDE
3.9	-86.434	38.133	5	1990	1	24	18	20	24.4	PDE
4	-102.504	43.313	5	1990	1	28	4	59	59.1	PDE
3.6	-89.219	38.868	10	1990	3	2	7	1	47.7	PDE
3	-91.49	36.72	5	1990	3	18	16	22	33	PDE
3.5	-68.23	47.28	18	1990	3	30	1	54	9	PDE
3.1	-112.37	48.717	6	1990	4	4	21	42	33.6	PDE
3.5	-109.519	40.082	3	1990	4	7	15	37	54.8	PDE
3	-84.852	40.46	5	1990	4	17	10	27	34.7	PDE
3	-88.23	39.556	10	1990	4	24	9	41	24.3	PDE
3	-110.828	38.952	11	1990	6	25	17	15	33.5	PDE
3	-98.954	41.507	5	1990	7	18	2	47	3.9	PDE
3	-89.24	36.85	6	1990	8	7	5	5	56.4	PDE
3.8	-83.34	36.794	10	1990	8	17	21	1	17.9	PDE
3.5	-89.66	35.83	13	1990	8	29	19	34	59.9	PDE
3.3	-83.731	38.061	5	1990	9	8	0	3	57.4	PDE
3	-106.206	39.701	5	1990	9	12	21	38	57.6	PDE
4.9	-89.577	37.165	12	1990	9	26	13	18	51.3	PDE
3	-101.505	41.815	5	1990	9	30	0	6	24	PDE
3.9	-75.19	46.32	17	1990	10	7	8	47	30.5	PDE
4.9	-75.59	46.47	13	1990	10	19	7	1	57.4	PDE
3	-75.506	39.512	10	1990	10	23	1	34	48.2	PDE
3.3	-88.99	38.31	5	1990	10	24	8	20	4.3	PDE
3.9	-98.472	43.794	5	1990	10	25	6	25	25.5	PDE

Table 2.5-1 {USGS Earthquake Catalog for the CEUS with $m_b \geq 3.0$ }

(Page 58 of 65)

m_b	Longitude (degree)	Latitude (degree)	Depth (km)	Year	Month	Day	Hour	Minute	Second	Catalog Reference
3.5	-89.62	36.54	8	1990	11	9	3	39	15.9	PDE
3.2	-80.136	32.947	3	1990	11	13	15	22	13	PDE
3.8	-97.59	34.76	5	1990	11	15	11	44	41.4	PDE
4.1	-76.219	47.128	18	1990	11	15	13	47	15.7	PDE
3.5	-66.6	47	5	1990	12	12	5	15	7.1	PDE
3.2	-87.044	40.068	10	1990	12	17	5	24	59.1	PDE
3.6	-86.671	39.57	10	1990	12	20	14	4	17.1	PDE
4.3	-72.556	47.579	18	1990	12	31	3	53	58.3	PDE
3	-88.86	37.946	5	1991	1	23	9	25	23.5	PDE
3	-97.3	36.378	5	1991	1	24	5	0	26.9	PDE
3.3	-81.453	41.536	5	1991	1	26	3	21	22.6	PDE
3.4	-111.429	37.681	9	1991	1	26	21	49	38	PDE
3	-89.95	35.98	14	1991	2	11	0	0	6.1	PDE
3.3	-109.483	40.091	1	1991	3	2	8	41	37.4	PDE
3.9	-76.874	46.282	18	1991	3	6	5	26	53.6	PDE
3.8	-77.916	37.746	17	1991	3	15	6	54	8.2	PDE
3.9	-66.594	49.698	18	1991	3	21	4	10	59.3	PDE
3	-106.857	42.031	5	1991	4	13	19	8	5.1	PDE
3.5	-80.207	37.941	14	1991	4	22	1	1	20.2	PDE
3.6	-66.6	47	5	1991	4	23	3	19	19	PDE
4.7	-89.823	36.564	5	1991	5	4	1	18	54.9	PDE
3.6	-74.4	45.5	18	1991	5	17	18	8	47	PDE
3.5	-99.4	39.2	5	1991	5	30	22	7	44	PDE
3.6	-112.007	48.374	5	1991	6	5	9	24	7.6	PDE
4.3	-76.7	47	18	1991	6	16	16	46	53	PDE
4	-74.678	42.63	5	1991	6	17	8	53	16.7	PDE
3	-110.358	37.209	1	1991	6	25	21	2	13.6	PDE
3.2	-81.668	38.276	5	1991	6	28	18	34	51.9	PDE
3.3	-91.71	37.49	5	1991	7	2	3	49	1.7	PDE
3.8	-73.896	45.232	18	1991	7	5	1	47	36.7	PDE
3.9	-91.643	36.658	5	1991	7	7	21	24	2.6	PDE
3	-89.44	36.14	12	1991	7	8	23	49	7.4	PDE
3.5	-98.042	28.908	10	1991	7	20	23	38	19.2	PDE
3.5	-108.861	43.502	5	1991	8	7	12	49	16.6	PDE
3	-77.657	40.786	1	1991	8	15	7	16	7.1	PDE
3.4	-100.533	42.162	5	1991	8	26	11	49	15.4	PDE
3.1	-84.095	35.711	5	1991	9	24	7	21	6.4	PDE
3.1	-89.432	36.841	5	1991	10	3	11	46	4.8	PDE
3	-73.578	41.07	10	1991	10	28	20	58	26.1	PDE
3.8	-87.894	38.713	10	1991	11	11	9	20	47.4	PDE
3	-90.27	35.72	9	1991	11	13	9	43	15.9	PDE
3	-108.895	47.952	10	1991	12	5	10	10	0.7	PDE
4	-69.8	47.7	18	1991	12	8	3	0	30	PDE
3.1	-106.917	41.936	5	1991	12	18	21	36	47.9	PDE
3.4	-106.715	45.82	5	1991	12	23	20	32	27.2	PDE

Table 2.5-1 {USGS Earthquake Catalog for the CEUS with $m_b \geq 3.0$ }

(Page 59 of 65)

m_b	Longitude (degree)	Latitude (degree)	Depth (km)	Year	Month	Day	Hour	Minute	Second	Catalog Reference
5	-103.187	32.302	0	1992	1	2	11	45	35.3	SNMX
3.2	-82.465	33.946	5	1992	1	3	4	21	22.2	PDE
3	-74.341	40.363	7	1992	1	9	8	50	45.2	PDE
3.5	-81.245	41.911	5	1992	3	15	6	13	55.2	PDE
3.3	-89.479	35.828	12	1992	4	3	3	6	3.9	PDE
3.2	-104.773	37.335	5	1992	4	15	22	46	5	PDE
3.1	-90.41	36.92	5	1992	4	30	0	1	30.9	PDE
3.2	-70.407	47.446	2	1992	5	1	0	37	51.4	PDE
3.1	-104.778	37.378	5	1992	5	2	10	19	29.8	PDE
3.7	-74.964	46.444	18	1992	5	19	5	59	41	PDE
3.3	-99.549	38.76	5	1992	7	15	2	56	40.7	PDE
4.2	-80.116	33.05	10	1992	8	21	16	31	55.1	PDE
3	-102.708	32.173	5	1992	8	26	3	24	52.6	PDE
3.3	-89.68	37.63	5	1992	8	26	5	41	38.4	PDE
3.6	-107.041	43.825	5	1992	8	31	1	40	14.2	PDE
3.4	-71.578	43.324	5	1992	10	6	15	38	4	PDE
4	-108.242	42.819	5	1992	10	10	15	40	56.2	PDE
3	-104.389	42.74	5	1992	11	2	6	54	10.3	PDE
3.3	-112.611	49.001	5	1992	11	17	3	37	22.9	PDE
4.2	-74.862	45.764	18	1992	11	17	3	58	0.9	PDE
3.5	-97.581	34.744	5	1992	12	17	7	18	4.2	PDE
3.2	-89.63	37.5	5	1992	12	27	10	12	58.9	PDE
3	-82.09	35.877	3	1993	1	1	5	8	5.3	PDE
3.3	-112.19	48.897	5	1993	1	1	15	57	41.9	PDE
3.5	-90.03	35.83	21	1993	1	8	13	1	18.8	PDE
3.1	-98.275	36.595	5	1993	1	14	17	6	10.4	PDE
3.1	-84.974	35.075	1	1993	1	15	2	2	51.8	PDE
3	-89.617	36.222	13	1993	1	21	19	46	19.3	PDE
3.4	-112.403	49.212	5	1993	1	22	6	2	32.7	PDE
3.2	-89.04	39.038	5	1993	1	29	13	56	23.2	PDE
3.5	-89.73	36.66	7	1993	2	6	2	9	45.5	PDE
3.5	-101.461	42.83	5	1993	2	20	13	8	10.1	PDE
3.7	-106.062	44.932	5	1993	2	25	3	44	15.5	PDE
3.1	-89.49	36.67	8	1993	3	2	0	29	11.8	PDE
3.2	-106.617	43.399	5	1993	3	10	3	54	31.1	PDE
3.2	-90.55	35.67	10	1993	3	16	7	38	10.2	PDE
3	-104.438	35.15	0	1993	3	24	2	32	5.9	SNMX
3.3	-89.42	36.79	5	1993	3	31	20	23	21.2	PDE
4.2	-98.124	28.811	5	1993	4	9	12	29	19.1	PDE
3.6	-89.44	36.19	7	1993	4	28	22	40	1.9	PDE
3.5	-75.5	46.3	18	1993	5	6	1	23	25.9	PDE
3.8	-107.575	42.304	5	1993	6	1	21	33	22.9	PDE
4.1	-96.293	45.674	10	1993	6	5	1	24	53	PDE
3	-105.373	42.985	5	1993	6	30	6	50	57.8	PDE
3.1	-106.715	39.227	5	1993	7	8	4	3	52.2	PDE

Table 2.5-1 {USGS Earthquake Catalog for the CEUS with $m_b \geq 3.0$ }

(Page 60 of 65)

m_b	Longitude (degree)	Latitude (degree)	Depth (km)	Year	Month	Day	Hour	Minute	Second	Catalog Reference
3.7	-88.341	31.747	5	1993	7	16	10	54	32.8	PDE
3.7	-105.703	42.478	5	1993	7	23	6	30	23.8	PDE
3.9	-74.12	45.26	8	1993	7	30	22	30	54	PDE
3	-89.88	36	11	1993	8	5	7	21	37.4	PDE
3.2	-81.595	33.633	5	1993	8	8	9	24	31.1	PDE
3	-109.921	43.576	5	1993	8	23	5	29	47.6	PDE
3	-106.837	42.033	5	1993	8	23	13	12	13.8	PDE
3.3	-90.36	38.09	16	1993	8	27	0	8	34	PDE
3.5	-75.05	46.457	15	1993	8	30	5	15	28.5	PDE
3.7	-74.605	46.065	18	1993	9	23	6	45	28.4	PDE
3	-103.56	35.568	0	1993	9	29	2	1	28.5	SNMX
3.7	-105.868	42.421	5	1993	10	10	4	17	46.7	PDE
3.5	-81.012	41.698	5	1993	10	16	6	30	5.3	PDE
3.5	-107.384	43.884	5	1993	11	16	7	26	4	PDE
4.2	-73.495	45.182	17	1993	11	16	9	31	44.2	PDE
3.3	-103.157	35.808	0	1993	11	30	3	7	36.3	SNMX
3.5	-70.06	47.53	8	1993	12	1	12	47	15	PDE
3.5	-105.499	42.333	5	1993	12	13	14	51	3	PDE
4.3	-75.606	46.506	18	1993	12	25	16	44	22.3	PDE
4.7	-110.132	43.483	8	1993	12	28	21	2	28.7	PDE
3.8	-70.367	47.453	7	1993	12	30	23	1	47.5	PDE
4.6	-76.037	40.33	5	1994	1	16	1	49	16.2	PDE
3.3	-100.141	42.627	5	1994	1	25	2	44	39.8	PDE
4.2	-89.18	37.37	16	1994	2	5	14	55	37.7	PDE
3.1	-95	45	5	1994	2	9	8	45	35.5	PDE
3.2	-82	36.8	5	1994	2	12	2	40	24.5	PDE
3.5	-77.876	42.782	1	1994	3	12	10	43	15.7	PDE
3.6	-65.74	48.99	18	1994	3	28	16	28	23	PDE
3.2	-85.493	34.961	5	1994	4	5	22	21	59	PDE
3.1	-89.27	38.123	10	1994	4	6	17	38	55.8	PDE
3	-87.174	34.198	5	1994	5	4	9	12	2.7	PDE
3.2	-92.671	33.013	5	1994	6	10	23	34	2.9	PDE
4	-66.6	47	5	1994	7	14	12	41	52	PDE
3.7	-76.751	35.067	5	1994	8	6	19	54	9.9	PDE
4.1	-111.333	48.489	5	1994	8	16	11	3	41.7	PDE
3.5	-91.058	36.136	5	1994	8	20	10	45	44.6	PDE
3.5	-84.604	42.798	5	1994	9	2	21	23	6.5	PDE
3	-69.232	43.861	5	1994	9	5	14	13	52.2	PDE
4.5	-107.976	38.151	10	1994	9	13	6	1	23	PDE
3.6	-68.223	45.306	5	1994	9	16	4	22	42.5	PDE
4.2	-69.96	47.77	17	1994	9	25	0	53	28	PDE
3.6	-88.935	36.929	5	1994	9	26	14	23	22	PDE
3.6	-72.277	42.347	10	1994	10	2	11	27	22.5	PDE
3.4	-108.269	40.04	5	1994	11	3	11	40	10.1	PDE
4	-104.811	39.29	10	1994	12	25	19	6	7.5	PDE

Table 2.5-1 {USGS Earthquake Catalog for the CEUS with $m_b \geq 3.0$ }

(Page 61 of 65)

m_b	Longitude (degree)	Latitude (degree)	Depth (km)	Year	Month	Day	Hour	Minute	Second	Catalog Reference
4.1	-97.596	34.774	5	1995	1	18	15	51	39.4	PDE
5.2	-109.64	41.529	1	1995	2	3	15	26	10.6	PDE
3.1	-94.952	40.505	5	1995	2	11	5	54	10.1	PDE
3.5	-75.04	45.9	18	1995	2	15	15	53	57	PDE
3.6	-83.47	39.12	10	1995	2	19	12	57	6	PDE
3	-74.426	44.233	4	1995	3	2	5	33	51.4	PDE
3.3	-112.35	48.65	10	1995	3	5	12	17	11.5	PDE
3.3	-84.922	35.425	17	1995	3	18	22	6	21	PDE
3.3	-104.212	35	5	1995	3	19	18	36	43.9	PDE
4.1	-108.925	40.179	5	1995	3	20	12	46	16.3	PDE
3.9	-80.068	32.947	10	1995	4	17	13	45	57.8	PDE
3.3	-67.73	49.15	15	1995	4	20	4	37	5	PDE
3.9	-66.6	47	5	1995	5	6	7	51	35	PDE
3.5	-89.43	36.17	6	1995	5	27	19	51	10.4	PDE
3.4	-87.827	33.191	1	1995	5	28	15	28	36.9	PDE
3	-96.732	34.287	5	1995	6	1	4	49	29.3	PDE
3.6	-76.29	47.02	18	1995	6	3	22	44	32	PDE
3.8	-71.915	44.286	5	1995	6	16	12	13	11.4	PDE
3.5	-81.452	36.747	5	1995	6	26	0	36	17	PDE
3.8	-104.814	36.246	5	1995	7	4	3	59	4.5	PDE
3.7	-84.212	35.366	10	1995	7	5	14	16	44.4	PDE
3	-81.873	36.515	11	1995	7	7	21	1	2.8	PDE
3.3	-87.665	33.478	1	1995	7	15	1	3	28.3	PDE
3	-89.632	36.528	5	1995	7	20	2	10	34.4	PDE
3	-74.953	46.168	20	1995	7	28	5	47	37.1	PDE
3.1	-89.409	36.102	5	1995	8	17	23	18	50.8	PDE
3	-73.28	45.41	18	1995	8	20	16	15	26	PDE
3.7	-74.43	45.61	18	1995	9	12	3	59	5	PDE
3.9	-98.69	36.87	5	1995	9	15	0	31	33.2	PDE
3.1	-74.21	45.08	18	1995	9	21	23	3	27	PDE
3.3	-78.77	46.42	18	1995	10	10	7	19	20	PDE
3.7	-96.864	45.788	5	1995	10	20	15	57	18.7	PDE
3.6	-104.917	38.732	5	1995	12	23	6	51	48.8	PDE
4.2	-110.878	39.12	0	1996	1	6	12	55	58.6	PDE
3.6	-97.542	42.513	5	1996	2	6	15	10	28.2	PDE
3.7	-103.729	43.981	5	1996	2	6	16	8	36.7	PDE
4.3	-74.43	45.99	18	1996	3	14	10	42	26	PDE
3.1	-71.242	41.69	11	1996	3	22	20	22	12.5	PDE
3.3	-102.601	35.61	5	1996	3	25	6	43	46.8	PDE
3.3	-88.671	32.131	5	1996	3	25	14	15	50.5	PDE
3.7	-104.102	43.069	5	1996	4	9	2	48	8.1	PDE
3.3	-91.162	34.969	5	1996	4	11	21	54	57.6	PDE
4	-81.95	37.187	1	1996	6	29	19	30	42.6	PDE
3.8	-104.247	37.398	5	1996	8	1	5	44	22.7	PDE
3.4	-90.874	33.577	10	1996	8	11	18	17	49.8	PDE

Table 2.5-1 {USGS Earthquake Catalog for the CEUS with $m_b \geq 3.0$ }

(Page 62 of 65)

m_b	Longitude (degree)	Latitude (degree)	Depth (km)	Year	Month	Day	Hour	Minute	Second	Catalog Reference
3.5	-112.405	49.076	5	1996	8	15	20	7	29.9	PDE
3.6	-82.92	49.21	18	1996	8	16	4	56	46	PDE
3.7	-71.352	44.184	10	1996	8	21	7	54	14	PDE
4.2	-106.056	43.09	5	1996	10	19	13	27	57.9	PDE
3.7	-109.27	42.549	5	1996	10	21	13	51	39.5	PDE
3.2	-104.232	37.349	5	1996	11	1	3	9	28.3	PDE
3	-100.504	35.04	5	1996	11	23	10	54	18.5	PDE
4.2	-89.927	35.919	20	1996	11	29	5	41	33.6	PDE
3.6	-89.37	36.29	5	1996	11	29	10	47	9	PDE
3.4	-107.693	42.369	5	1996	12	11	3	55	44	PDE
3.1	-87.4	39.5	5	1996	12	16	1	58	31.3	PDE
3	-100.89	34.947	5	1997	2	12	23	53	10.7	PDE
3.2	-100.569	34.973	5	1997	2	15	9	8	55.4	PDE
3.4	-93.435	34.209	5	1997	3	16	19	7	27.9	PDE
3.8	-98.054	27.717	5	1997	3	24	22	31	34.5	PDE
3.5	-72.33	45.98	5	1997	4	3	4	44	12	PDE
3.1	-108.732	42.683	5	1997	4	25	10	39	6.7	PDE
3.7	-112.65	49.13	5	1997	5	1	21	38	36	PDE
3.1	-87.4	31	5	1997	5	4	3	39	12.9	PDE
4.1	-74.421	45.978	10	1997	5	24	18	52	6.3	PDE
3.4	-95.966	33.182	5	1997	5	31	3	26	41.3	PDE
3.5	-84.808	35.056	10	1997	7	19	17	6	34.3	PDE
3.8	-83.509	36.436	5	1997	7	30	12	29	23.3	PDE
3.2	-75.37	43.624	5	1997	7	31	7	15	29.7	PDE
3.4	-97.185	41.795	5	1997	8	9	17	46	3.9	PDE
3.7	-70.29	47.53	18	1997	8	20	9	12	4	PDE
4.3	-96.435	34.66	5	1997	9	6	23	38	0.9	PDE
3.8	-90.457	35.619	5	1997	9	17	18	16	31.6	PDE
3.1	-90.924	37.179	5	1997	9	20	5	55	50.4	PDE
3.2	-89.817	36.545	5	1997	9	24	4	20	24.8	PDE
3	-89.484	36.201	5	1997	9	27	12	14	9.3	PDE
3	-74.968	44.36	4	1997	10	13	23	6	40.2	PDE
4.9	-87.339	31.118	10	1997	10	24	8	35	17.8	PDE
4.7	-69.91	47.67	11	1997	10	28	11	44	18	PDE
4.9	-71.41	46.8	22	1997	11	6	2	34	33	PDE
3	-76.252	40.146	5	1997	11	14	3	44	11	PDE
4	-87.306	33.466	1	1997	12	12	8	42	20.2	PDE
3.4	-103.408	37.828	5	1998	1	2	15	47	16.4	PDE
3	-89.712	36.123	10	1998	2	12	9	37	49.5	PDE
3	-107.513	44.333	5	1998	2	13	2	28	4	PDE
3.6	-76.36	46.07	18	1998	2	26	14	20	31	PDE
3.9	-81.07	46.49	1	1998	3	9	5	5	58	PDE
3.1	-111.35	38.25	3	1998	3	29	12	12	42	PDE
3.2	-89.02	36.94	13	1998	4	8	18	16	49	PDE
3.8	-80.466	34.61	5	1998	4	13	9	56	11.3	PDE

Table 2.5-1 {USGS Earthquake Catalog for the CEUS with $m_b \geq 3.0$ }

(Page 63 of 65)

m_b	Longitude (degree)	Latitude (degree)	Depth (km)	Year	Month	Day	Hour	Minute	Second	Catalog Reference
3.9	-74.99	45.57	18	1998	4	18	16	22	52	PDE
3.2	-102.383	35.453	5	1998	4	27	15	22	46.2	PDE
4.2	-98.416	34.782	5	1998	4	28	14	13	1.6	PDE
3.7	-81.174	46.457	1	1998	5	25	15	47	2	PDE
3.2	-80.821	35.479	5	1998	6	5	2	31	1.9	PDE
3.4	-73.72	44.75	4	1998	6	9	8	53	51	PDE
3.6	-84.405	35.926	10	1998	6	17	8	0	23.4	PDE
3.4	-103.003	42.622	5	1998	6	18	16	26	38.3	PDE
3.4	-87.954	32.501	5	1998	6	24	15	20	1.3	PDE
3.2	-97.589	34.719	5	1998	7	7	18	44	44.4	PDE
3.1	-101.111	43.554	5	1998	7	12	16	28	49.6	PDE
3.1	-89.52	36.69	13	1998	7	15	4	24	51	PDE
4	-66.61	47.02	5	1998	7	15	7	8	4	PDE
3.6	-104.706	48.37	5	1998	7	29	3	31	58.9	PDE
4.1	-74.73	46.16	10	1998	7	30	8	57	22	PDE
3.6	-107.19	41.953	10	1998	8	6	18	22	7.1	PDE
4.9	-80.388	41.495	5	1998	9	25	19	52	52	PDE
3.4	-111.091	36.033	5	1998	10	18	7	13	10.6	PDE
3.5	-78.367	37.381	13	1998	10	21	5	56	47.2	PDE
4.1	-66.88	49.34	18	1998	10	22	9	43	35	PDE
3.5	-97.6	36.8	5	1998	10	30	17	41	22.2	PDE
3.3	-104.032	48.548	5	1998	11	11	11	59	37.6	PDE
3.3	-77.93	43.83	18	1998	12	25	13	30	26	PDE
3	-99.378	38.674	5	1999	1	7	5	16	26.9	PDE
3	-70.98	42.84	2	1999	1	10	10	52	16.1	PDE
3	-83.691	36.854	5	1999	1	17	18	38	4.7	PDE
4.3	-87.255	33.405	1	1999	1	18	7	0	53.4	PDE
3.4	-80.939	49.267	18	1999	2	1	22	22	5.6	PDE
3.8	-69.52	44.48	3	1999	2	26	3	38	43	PDE
4	-104.63	32.591	1	1999	3	14	22	43	17.9	PDE
4.8	-66.32	49.61	18	1999	3	16	12	50	48	PDE
4.3	-107.741	41.451	10	1999	4	6	0	41	9.5	PDE
3	-94.7	39.1	5	1999	5	13	14	18	22.7	PDE
3.9	-104.664	32.575	10	1999	5	30	19	4	25.6	PDE
3.1	-108.459	42.559	5	1999	7	21	2	36	6.9	PDE
3.1	-89.503	36.264	9	1999	8	23	12	12	41.1	PDE
3.5	-89.433	41.721	5	1999	9	2	16	17	29.7	PDE
3.8	-91.02	36.49	19	1999	10	21	8	18	0	PDE
3	-99.659	36.846	26	1999	10	25	23	19	58.3	PDE
3.9	-74.32	45.85	18	1999	10	31	20	14	10	PDE
3.5	-105.467	45.512	10	1999	11	3	13	28	52	PDE
3.1	-107.477	43.479	5	1999	11	9	8	17	41.1	PDE
3.6	-78.997	43.71	12	1999	11	26	22	33	1.4	PDE
3.8	-87.253	33.416	1	1999	11	28	11	0	9.3	PDE
3	-69.37	44.94	5	1999	12	25	0	21	41	PDE

Table 2.5-1 {USGS Earthquake Catalog for the CEUS with $m_b \geq 3.0$ }

(Page 64 of 65)

m_b	Longitude (degree)	Latitude (degree)	Depth (km)	Year	Month	Day	Hour	Minute	Second	Catalog Reference
5	-78.93	46.888	18	2000	1	1	11	22	57	PDE
3.5	-70.17	44.31	9	2000	1	3	21	5	50	PDE
3	-110.34	42.1	12	2000	1	8	22	43	37	PDE
3.5	-70.44	44.57	16	2000	1	17	8	16	20	PDE
3.5	-83.214	32.993	5	2000	1	18	22	19	31.9	PDE
3	-71.18	43	1	2000	1	27	14	49	40	PDE
4.4	-109.679	41.464	1	2000	1	30	14	46	51.3	PDE
3	-106.732	42.24	5	2000	2	1	22	15	45.3	PDE
3	-106.666	40.601	5	2000	2	7	17	24	54.3	PDE
3.3	-105.813	42.409	5	2000	4	13	18	17	31.7	PDE
3.6	-86.75	39.76	5	2000	4	14	3	54	20	PDE
3.9	-74.257	43.949	5	2000	4	20	8	46	55.4	PDE
3.1	-79.099	43.806	18	2000	5	24	10	22	46.2	PDE
4	-107.57	42.196	5	2000	5	26	21	58	46.6	PDE
3	-87.82	33.809	5	2000	5	28	11	32	7	PDE
3.7	-69.81	47.67	10	2000	6	15	9	25	54	PDE
3.3	-72.82	42.1	9	2000	6	16	4	2	53	PDE
3	-109.31	40.69	1	2000	6	20	17	55	46	PDE
3.8	-92.75	35.8	0	2000	6	27	1	28	45	PDE
3	-88.87	37.13	4	2000	6	27	6	2	57	PDE
4.2	-71.1	47.52	10	2000	7	12	15	1	49	PDE
4.1	-74.97	46.19	18	2000	8	6	8	52	24	PDE
3.9	-101.814	35.39	5	2000	8	17	1	8	5.4	PDE
3.2	-108.26	42.554	5	2000	8	19	2	55	43.7	PDE
3.9	-91.106	36.492	8	2000	8	22	20	12	14	PDE
3.2	-69.382	44.355	5	2000	9	7	10	7	40.7	PDE
3.8	-74.02	45.13	18	2000	10	6	13	59	4	PDE
3	-107.693	43.437	5	2000	11	8	2	16	49.9	PDE
3.7	-109.23	40.28	5	2000	11	11	21	17	53	PDE
3.9	-87.66	37.973	5	2000	12	7	14	8	49.4	PDE
3.9	-101.8	35.4	5	2000	12	16	22	8	54	PDE
4.3	-80.802	41.942	5	2001	1	26	3	3	20	PDE
3.2	-77.394	42.345	0	2001	2	3	20	15	15	PDE
3	-92.66	33.19	5	2001	3	3	10	46	13	PDE
3.2	-84.81	35.51	6	2001	3	7	17	12	25	PDE
3.9	-76.28	47.05	18	2001	3	19	10	40	17	PDE
3.2	-85.439	34.857	3	2001	3	21	23	35	35	PDE
3.1	-93.327	37.933	5	2001	3	30	17	13	55.6	PDE
3	-83.34	36.53	0	2001	4	13	16	36	20.7	PDE
4.5	-92.194	35.205	10	2001	5	4	6	42	12.6	PDE
3.3	-103.141	32.334	5	2001	6	2	1	55	53.7	PDE
3.2	-80.767	41.905	5	2001	6	3	22	36	46.4	PDE
3	-89.396	36.279	14	2001	7	7	20	45	42.7	PDE
3.1	-105.129	39.022	5	2001	7	22	19	22	45.5	PDE
3	-97	37.7	5	2001	7	24	14	2	35	PDE

Table 2.5-1 {USGS Earthquake Catalog for the CEUS with $m_b \geq 3.0$ }

(Page 65 of 65)

m_b	Longitude (degree)	Latitude (degree)	Depth (km)	Year	Month	Day	Hour	Minute	Second	Catalog Reference
3.2	-83.575	35.932	5	2001	7	26	5	26	44.7	PDE
3.1	-93.213	34.292	5	2001	8	4	1	13	25.3	PDE
4	-107.378	39.66	5	2001	8	9	22	38	54.5	PDE
4.5	-104.618	37.143	5	2001	9	5	10	52	7.8	PDE-W
4.3	-110.051	43.459	5	2001	9	27	22	5	21.7	PDE-W
3.2	-68.67	45.2	9	2001	10	25	0	24	29.8	PDE-W
3.4	-107.384	38.851	1	2001	11	5	8	34	23	PDE-W
3.3	-100.208	39.996	5	2001	11	13	1	56	13.1	PDE-W
3.1	-102.631	31.786	5	2001	11	22	0	7	8	PDE-W
3.1	-107.374	38.813	1	2001	12	4	18	20	9.1	PDE-W
3.9	-86.245	34.735	5	2001	12	8	1	8	21.5	PDE-W
3.3	-104.797	36.859	5	2001	12	15	7	58	31.3	PDE-W
3.8	-76.49	46.87	18	2001	12	24	16	58	21	PDE-W
3.8	-75.11	40.61	3	2003	8	26	18	24	18	PDE
3.1	-74.12	42.6	15	2007	7	24	1	56	49	PDE

1. The New Madrid events occurred in a cluster of three events. The event shown in the catalog is determined by USGS as the New Madrid event for the 1811-1812 cluster set. Two other events are considered as the foreshock/aftershock events and are filtered out from the catalog by USGS. The event shown in the catalog is not considered in the general are source hazard integration since its magnitude is above the maximum magnitude limit considered. This New Madrid event is accounted for in the PSHA in the New Madrid Characteristic Cluster events. The following events are the New Madrid set considered for the characteristic earthquake analysis:

Longitude (degree)	Latitude (degree)	m_b	Year	Month	Day	Hour	minute	Event Group
-90	36	7.2	1811	12	16	8	15	1
-90	36	7.0	1811	12	16	14	15	
-89.6	36.3	7.1	1812	1	23	15	0	2
-89.6	36.5	7.4	1812	2	7	9	45	3

Table 2.5-2 {Conversion Between Body-Wave (m_b) and Moment (M) Magnitude}

Conversion Model	m_b to M	M to m_b	Weight
Atkinson and Boore 1987	$M = 2.715 - 0.277m_b + 0.127 m_b^2$	$m_b = -4.249 + 3.3935M^2 + 0.0168M^3$	0.333
EPRI 1993	$M = 0.3281 + 1.9437m_b - 0.43m_b^2 + 0.0419m_b^3$	$m_b = -10.23 + 6.105M - 0.7632M^2 + 0.03436M^3$	0.334
Johnston 1996	$M = 1.14 + 0.24m_b + 0.0933m_b^2$	$m_b = -0.919 + 1.7864M - 0.1351M^2 + 0.0052M^3$	0.333

Notes:

m_b indicates body wave magnitude

M indicates moment magnitude

Table 2.5-3 {Summary of Bechtel Group Seismic Sources}

Code	Name	b value	b weight	M _{max} (m _b)	M _{max} weight
3	Charlevoix	0.707	0.33	6.4	0.10
		0.498	0.34	6.7	0.40
		0.808	0.33	7.0	0.40
				6.6	0.10
11	Clarendon - Linden	0.497	0.33	5.4	0.10
		0.498	0.34	5.7	0.40
		0.808	0.33	6.0	0.40
				6.6	0.10
13	Mesozoic Basins	0.991	0.33	5.4	0.10
		0.985	0.34	5.7	0.40
		1.037	0.33	6.0	0.10
				6.6	0.10
24	Bristol Block	0.844	0.33	5.7	0.10
		0.836	0.34	6.0	0.40
		0.979	0.33	6.3	0.40
				6.6	0.10
25	NY-AL Lineament	1.057	0.33	5.4	0.10
		1.055	0.34	5.7	0.40
		1.043	0.33	6.0	0.40
				6.6	0.10
D	Niagara	0.952	0.33	5.4	0.10
		0.953	0.34	5.7	0.40
		0.998	0.33	6.0	0.40
				6.6	0.10
BZ5 Background	Southern Appalachian	0.912	0.33	5.7	0.10
		0.920	0.34	6.0	0.40
		0.937	0.33	6.3	0.40
				6.6	0.10
BZ6 Background	Southern Eastern Craton	1.074	0.33	5.4	0.10
		1.073	0.34	5.7	0.40
		1.084	0.33	6.0	0.40
				6.6	0.10
BZ7 Background	Northern Eastern Craton	1.066	0.33	6.0	0.10
		1.075	0.34	6.3	0.40
		1.087	0.33	6.6	0.50

Table 2.5-4 {Summary of Dames & Moore Seismic Sources}

Code	Name	b value	b weight	M _{max} (m _b)	M _{max} weight
3	Adirondacks	1.043	0.75	6.3	0.80
		1.047	0.25	7.2	0.20
4	Paleozoic Fold Belts	1.042	0.75	6.0	0.80
		1.047	0.25	7.2	0.20
8	Eastern Marginal Basin	1.042	0.75	5.6	0.80
		1.052	0.25	7.2	0.20
9	Clarendon - Linden	1.035	0.37	6.5	0.75
		1.011	0.12		
		1.031	0.38	7.2	0.25
		1.004	0.13		
41	Southern Cratonic	1.035	0.75	6.1	0.80
		1.028	0.25	7.2	0.20
42	Newark-Gettysburg Basin	1.015	0.75	6.3	0.75
		0.947	0.25	7.2	0.25
53	Southern Appalachian Mobile Belt	1.043	0.75	5.6	0.80
		1.053	0.25	7.2	0.20
59	Charlevoix	0.70*	1.00	7.2	1.00

* Updated using USGS 2001 catalog and Dames and Moore Source geometry for the source zone.

Table 2.5-5 {Summary of Law Engineering Seismic Sources}

Code	Name	b value	b weight	M _{max} (m _b)	M _{max} weight
8-17	East Coast Mesozoic Basements	1.057	1.00	6.8	1.00
12	Charlevoix	0.756	1.00	6.4	0.20
				7.4	0.80
17	Eastern Basements	0.992	1.00	5.7	0.20
				6.8	0.80
22	Eastern Seaboard Normal Faults	1.054	1.00	6.8	1.00

Table 2.5-6 {Summary of Rondout Associates Seismic Sources}

Code	Name	b value	b weight	M _{max} (m _b)	M _{max} weight
30	Shenandoah	1.010	1.00	5.2	0.30
				6.3	0.55
				6.5	0.15
31	Quakers	0.960	1.00	5.8	0.15
				6.5	0.60
				6.8	0.25
33	Niagara	1.000	1.00	5.2	0.30
				6.3	0.55
				6.5	0.15
34	Nessmuk	0.920	1.00	5.2	0.30
				6.3	0.35
				6.5	0.15
37	Charlevoix	0.700	1.00	7.1	0.10
				7.3	0.80
				7.4	0.10
41	Vermont	1.100	1.00	5.2	0.30
				6.3	0.55
				6.5	0.15
50-2	Greenville - Background	1.010	1.00	4.8	0.20
				5.5	0.60
				5.8	0.20

Table 2.5-7 {Summary of Weston Geophysical Seismic Sources}

Code	Name	b value	b weight	M_{max} (m_b)	M_{max} weight
1	Charlevoix	0.79	1.00	7.2	1.00
6	Adirondack Mountains	0.933	0.50	5.4	0.38
		0.936	0.50	6.0	0.46
				6.6	0.16
8	Clarendon - Linden	0.846	1.00	5.4	0.26
				6.0	0.50
				6.6	0.24
21	New York Nexus	0.934	1.00	5.4	0.62
				6.0	0.29
				6.6	0.09
28 B	Zone of Mesozoic Basin	0.854	1.00	5.4	0.65
				6.0	0.25
				6.6	0.10
28 E	Zone of Mesozoic Basin	0.918	1.00	5.4	0.65
				6.0	0.25
				6.6	0.10
102 Background	Appalachian Plateau	1.007	0.20	5.4	0.62
		1.007	0.80	6.0	0.29
				6.6	0.09
103 Background	Southern Appalachian	0.993	0.20	5.4	0.26
		0.996	0.80	6.0	0.58
				6.6	0.16
104 Background	Southern Coastal Plain	0.997	0.20	5.4	0.24
		0.997	0.80	6.0	0.61
				6.6	0.15

Table 2.5-8 {Summary of Woodward-Clyde Consultants Seismic Sources}

Code	Name	b value	b weight	M _{max} (m _b)	M _{max} weight
12	Charlevoix	0.70*	1.00	6.5	0.33
				7.0	0.34
				7.5	0.33
18	Adirondack Uplift	1.006	0.25	5.4	0.33
		1.001	0.25	6.3	0.34
		0.930	0.25	6.9	0.33
		0.861	0.25		
20 A	Mohawk River Trend	1.010	0.33	5.5	0.33
		0.922	0.34	6.0	0.34
		0.836	0.33	7.0	0.33
21	NJ Gravity Saddle	0.781	0.25	5.3	0.33
		0.950	0.25	6.5	0.34
		0.873	0.25	6.9	0.33
		0.798	0.25		
25	Hudson River Trend	1.201	0.25	5.5	0.33
		1.056	0.25	6.3	0.34
		0.989	0.25	6.8	0.33
		0.926	0.25		
33	W. NY- S Ontario Seismic Zone	0.951	0.25	5.5	0.33
		0.977	0.25	6.5	0.34
		0.924	0.25	7.0	0.33
		0.873	0.25		
34	Attica, NY Intersection	0.780	0.33	5.6	0.33
		0.725	0.34	6.3	0.34
		0.672	0.33	7.4	0.33
61	Tyrone- Mt. Union Lineament	1.030	0.33	5.4	0.33
		0.939	0.34	6.5	0.34
		0.850	0.33	7.1	0.33
63	Pittsburgh- Washington Lineament	0.997	0.33	5.4	0.33
		0.904	0.34	6.3	0.34
		0.811	0.33	7.1	0.33
B16	Susquehanna Background	0.924	0.25	4.9	0.17
		0.993	0.25	5.4	0.28
		0.903	0.25	5.8	0.27
		0.814	0.25	6.5	0.28

Table 2.5-9 {Alternative New Madrid Fault Locations}

Fault arm	New Madrid South		Reelfoot		New Madrid North		Combined Weight
	Distance to Site (km)	Weight	Distance to Site (km)	Weight	Distance to Site (km)	Weight	
1	1268	0.6	1259	0.7	1213	0.7	0.294
2					1185	0.3	0.126
3			1259	0.3	1213	0.7	0.126
4					1185	0.3	0.054
5	1280	0.4	1259	0.7	1213	0.7	0.196
6					1185	0.3	0.084
7			1259	0.3	1213	0.7	0.084
8					1185	0.3	0.036

Table 2.5-9—{Alternative New Madrid Fault Locations}

Fault arm	New Madrid South		Reelfoot		New Madrid North		Combined Weight
	Distance to Site (mile)	Weight	Distance to Site (mile)	Weight	Distance to Site (mile)	Weight	
1	788	0.6	782	0.7	754	0.7	0.294
2					736	0.3	0.126
3			782	0.3	754	0.7	0.126
4					736	0.3	0.054
5	796	0.4	782	0.7	754	0.7	0.196
6					736	0.3	0.084
7			782	0.3	754	0.7	0.084
8					736	0.3	0.036

Table 2.5-10 {Earthquake Frequencies for Repeating New Madrid Earthquake Sequences}

Rupture Set	Weight	Magnitude, M			Weight	Rupture Model	Weight	Combined Weight
		NMS	RF	NMN				
1	0.1667	7.8	7.7	7.5	1	A	0.667	0.1112
		7.8	7.7	7.5	0.333	B	0.333	0.0185
		7.3	7.7	7.5	0.333			0.0185
		7.8	7.7	7.0	0.333			0.0185
2	0.1667	7.9	7.8	7.6	1	A	0.667	0.1112
		7.9	7.8	7.6	0.333	B	0.333	0.0185
		7.4	7.8	7.6	0.333			0.0185
		7.9	7.8	7.1	0.333			0.0185
3	0.2500	7.6	7.8	7.5	1	A	0.667	0.1668
		7.6	7.8	7.5	0.333	B	0.333	0.0277
		7.1	7.8	7.5	0.333			0.0277
		7.6	7.8	7.0	0.333			0.0277
4	0.0833	7.2	7.4	7.2	1	A	0.667	0.0556
		7.2	7.4	7.2	0.333	B	0.333	0.0092
		7.0	7.4	7.2	0.333			0.0092
		7.2	7.4	7.2	0.333			0.0092
5	0.1667	7.2	7.4	7.0	1	A	0.667	0.1112
		7.2	7.4	7.0	0.333	B	0.333	0.0185
		7.0	7.4	7.0	0.333			0.0185
		7.2	7.4	7.0	0.333			0.0185
6	0.1667	7.3	7.5	7.0	1	A	0.667	0.1112
		7.3	7.5	7.0	0.333	B	0.333	0.0185
		7.0	7.5	7.0	0.333			0.0185
		7.3	7.5	7.0	0.333			0.0185

Notes:

- 1) Adapted from the Seismic Hazards Report for the EGC ESP Site
See Table 4.1-2 of Appendix B (EGC, 2006)
- 2) NMS indicates New Madrid South Arm
- 3) RF indicates New Madrid Reelfoot Arm
- 4) NMN indicates New Madrid North Arm

Table 2.5-11 {Controlling Earthquakes for BBNPP}

Hazard	Reference Earthquake (RE)		De-aggregation Earthquakes (DE)			
	Mag. (M)	Dist. (km)	Event	Mag. (M)	Dist. (km)	Weight
Mean 10 ⁻⁴ 1 and 2.5Hz	7.19	286.25	DEL	5.55	16.84	0.203
			DEM	6.45	112.09	0.249
			DEH	7.36	339.47	0.547
Mean 10 ⁻⁴ 5 and 10 Hz	5.83	43.65	DEL	5.40	17.62	0.551
			DEM	6.18	107.41	0.357
			DEH	7.09	307.72	0.091
Mean 10 ⁻⁵ 1 and 2.5Hz	7.30	287.56	DEL	5.79	13.67	0.387
			DEM	6.86	105.56	0.211
			DEH	7.38	340.39	0.402
Mean 10 ⁻⁵ 5 and 10 Hz	5.71	15.90	DEL	5.54	11.62	0.862
			DEM	6.77	100.70	0.122
			DEH	7.11	291.43	0.015

Note: Distance range of each event

DEL: 0 to 50 km

DEM: 50 to 200 km

DEH: > 200 km

Table 2.5-11—{Controlling Earthquakes for BBNPP}

Hazard	Reference Earthquake (RE)		De-aggregation Earthquakes (DE)			
	Mag. (M)	Dist. (mile)	Event	Mag. (M)	Dist. (mile)	Weight
Mean 10 ⁻⁴ 1 and 2.5Hz	7.19	171.40	DEL	5.55	10.46	0.203
			DEM	6.45	69.66	0.249
			DEH	7.36	210.98	0.547
Mean 10 ⁻⁴ 5 and 10 Hz	5.83	26.14	DEL	5.40	10.95	0.551
			DEM	6.18	66.76	0.357
			DEH	7.09	191.25	0.091
Mean 10 ⁻⁵ 1 and 2.5Hz	7.30	172.19	DEL	5.79	8.49	0.387
			DEM	6.86	65.61	0.211
			DEH	7.38	211.55	0.402
Mean 10 ⁻⁵ 5 and 10 Hz	5.71	9.52	DEL	5.54	7.22	0.862
			DEM	6.77	62.59	0.122
			DEH	7.11	181.13	0.015

Note: Distance range of each event

DEL: 0 to 31 mile

DEM: 31 to 125 mile

DEH: > 125 mile

Table 2.5-12 {Recommended Horizontal and Vertical SSE Amplitudes and common V/H Ratio}

Freq (Hz)	Horizontal SSE (g)	Vertical SSE (g)	V/H
0.1000	0.0056	0.0032	0.5818
0.1269	0.0084	0.0049	0.5818
0.1610	0.0123	0.0071	0.5818
0.2043	0.0174	0.0101	0.5818
0.2593	0.0242	0.0141	0.5818
0.3290	0.0327	0.0190	0.5818
0.4175	0.0433	0.0252	0.5818
0.5000	0.0529	0.0308	0.5818
0.6723	0.0598	0.0348	0.5818
0.8532	0.0616	0.0358	0.5818
1.0000	0.0588	0.0342	0.5818
1.3738	0.0757	0.0449	0.5932
1.7500	0.0896	0.0539	0.6020
2.2122	0.1035	0.0633	0.6114
2.5000	0.1101	0.0679	0.6169
3.5622	0.1488	0.0942	0.6330
4.5204	0.1830	0.1200	0.6558
5.0000	0.2091	0.1402	0.6705
7.5000	0.2870	0.2078	0.7240
10.0000	0.3630	0.2718	0.7487
11.7210	0.4152	0.3221	0.7757
14.8735	0.4743	0.3823	0.8060
18.8739	0.5089	0.4192	0.8238
25.0000	0.5471	0.4904	0.8963
30.3920	0.5265	0.4911	0.9328
38.5662	0.4987	0.4999	1.0025
48.9390	0.4420	0.4620	1.0452
62.1017	0.3515	0.3738	1.0635
78.8046	0.2509	0.2527	1.0071
100.0000	0.2090	0.1851	0.8857

Table 2.5-13 {Amplification Factors for 10⁻⁴ and 10⁻⁵ Input Motions and HF and LF Rock Spectra}

Page 1 of 2

Freq(Hz)	10 ⁻⁴ LF				10 ⁻⁴ HF			
	DEL	DEM	DEH	Ave.	DEL	DEM	DEH	Ave.
	0.0133	0.0387	0.9481		0.0535	0.0880	0.8585	
0.1000	1.0468	1.0040	1.0014	1.0113	1.1959	1.0478	1.0000	1.1251
0.1269	1.0817	1.0003	1.0001	1.0168	1.0980	1.0117	1.0004	1.0583
0.1610	1.0211	0.9989	1.0002	1.0042	1.0414	1.0056	1.0001	1.0248
0.2043	1.0036	1.0002	1.0001	1.0008	1.0307	1.0050	1.0003	1.0188
0.2593	0.9989	1.0000	1.0002	0.9999	1.0167	1.0006	1.0006	1.0095
0.3290	0.9984	1.0013	1.0001	1.0000	1.0027	0.9999	1.0001	1.0015
0.4175	0.9988	1.0005	1.0006	1.0002	1.0053	1.0012	1.0002	1.0033
0.5000	1.0021	1.0015	1.0006	1.0011	1.0048	1.0010	1.0006	1.0031
0.6723	1.0016	1.0011	1.0010	1.0012	1.0020	1.0014	1.0012	1.0017
0.8532	1.0025	1.0024	1.0019	1.0021	1.0038	1.0030	1.0021	1.0034
1.0000	1.0052	1.0022	1.0034	1.0035	1.0057	1.0037	1.0025	1.0047
1.3738	1.0085	1.0057	1.0044	1.0056	1.0079	1.0074	1.0049	1.0075
1.7500	1.0100	1.0123	1.0077	1.0093	1.0099	1.0109	1.0073	1.0100
2.2122	1.0155	1.0133	1.0142	1.0142	1.0142	1.0147	1.0122	1.0142
2.5000	1.0191	1.0172	1.0145	1.0161	1.0234	1.0173	1.0168	1.0206
3.5622	1.0373	1.0357	1.0329	1.0345	1.0365	1.0373	1.0323	1.0364
4.5204	1.0551	1.0608	1.0540	1.0559	1.0594	1.0609	1.0543	1.0595
5.0000	1.0575	1.0642	1.0646	1.0631	1.0642	1.0692	1.0621	1.0658
7.5000	1.1091	1.1297	1.1284	1.1248	1.1330	1.1113	1.1244	1.1245
10.0000	1.1981	1.1916	1.1823	1.1878	1.2029	1.1867	1.1969	1.1966
11.7210	1.2085	1.2067	1.2211	1.2150	1.2254	1.2141	1.2105	1.2200
14.8735	1.2176	1.2033	1.2228	1.2169	1.2184	1.2216	1.2189	1.2196
18.8739	1.1757	1.1840	1.1933	1.1874	1.1883	1.1775	1.1927	1.1848
25.0000	1.1946	1.1653	1.1615	1.1692	1.1788	1.1599	1.1667	1.1710
30.3920	1.1641	1.1681	1.1643	1.1652	1.1627	1.1509	1.1583	1.1581
38.5662	1.1361	1.1507	1.1696	1.1581	1.1541	1.1598	1.1560	1.1563
48.9390	1.1440	1.1631	1.1148	1.1328	1.1599	1.1471	1.1384	1.1533
62.1017	1.1506	1.1433	1.1171	1.1304	1.1563	1.1489	1.1193	1.1503
78.8046	1.1368	1.1661	1.1585	1.1560	1.1760	1.1572	1.1760	1.1693
100.0000	1.2615	1.2905	1.3655	1.3256	1.2993	1.3190	1.3514	1.3111
Note:Distance range of each event DEL: 0 to 50 km (0 to 31 mile) DEM: 50 to 200 km (31 to 125 mile) DEH: > 200 km (> 125 mile)								

Table 2.5-13—{Amplification Factors for 10-4 and 10-5 Input Motions and HF and LF Rock Spectra}

Freq(Hz)	10 ⁻⁵ LF				10 ⁻⁵ HF			
	DEL	DEM	DEH	Ave.	DEL	DEM	DEH	Ave.
	0.0332	0.0370	0.9297		0.1532	0.0811	0.7657	
0.1000	1.0389	0.9990	1.0005	1.0150	1.0421	0.9978	1.0014	1.0360
0.1269	1.0107	1.0009	1.0000	1.0043	1.0662	0.9997	1.0000	1.0570
0.1610	0.9975	1.0008	1.0001	0.9992	1.0123	1.0014	1.0002	1.0107
0.2043	0.9989	1.0006	1.0000	0.9997	1.0097	0.9998	1.0004	1.0083
0.2593	1.0024	1.0004	1.0003	1.0011	1.0065	1.0011	1.0008	1.0058
0.3290	1.0009	1.0002	1.0002	1.0005	1.0023	1.0007	1.0006	1.0021
0.4175	0.9997	1.0004	1.0003	1.0001	1.0012	1.0003	1.0002	1.0010
0.5000	1.0010	1.0005	1.0008	1.0008	1.0013	1.0009	1.0003	1.0012
0.6723	1.0017	1.0011	1.0009	1.0012	1.0012	1.0015	1.0009	1.0012
0.8532	1.0020	1.0018	1.0018	1.0019	1.0042	1.0013	1.0025	1.0038
1.0000	1.0031	1.0031	1.0034	1.0032	1.0038	1.0030	1.0030	1.0036
1.3738	1.0048	1.0048	1.0045	1.0047	1.0062	1.0055	1.0046	1.0061
1.7500	1.0095	1.0078	1.0066	1.0080	1.0056	1.0106	1.0078	1.0062
2.2122	1.0131	1.0111	1.0137	1.0129	1.0121	1.0122	1.0121	1.0121
2.5000	1.0178	1.0158	1.0149	1.0162	1.0197	1.0185	1.0167	1.0195
3.5622	1.0419	1.0329	1.0334	1.0366	1.0435	1.0366	1.0321	1.0425
4.5204	1.0571	1.0530	1.0565	1.0560	1.0580	1.0587	1.0550	1.0580
5.0000	1.0683	1.0616	1.0674	1.0666	1.0798	1.0635	1.0623	1.0775
7.5000	1.1315	1.1294	1.1270	1.1292	1.1416	1.1336	1.1237	1.1403
10.0000	1.2165	1.1996	1.1868	1.2010	1.1953	1.1968	1.1923	1.1955
11.7210	1.2160	1.2149	1.2288	1.2209	1.2212	1.2044	1.2167	1.2191
14.8735	1.2122	1.2271	1.2197	1.2184	1.2143	1.2027	1.2168	1.2130
18.8739	1.1868	1.1851	1.1783	1.1830	1.1702	1.1808	1.1907	1.1718
25.0000	1.1708	1.1654	1.1568	1.1640	1.1740	1.1614	1.1635	1.1723
30.3920	1.1603	1.1644	1.1609	1.1614	1.1552	1.1577	1.1505	1.1554
38.5662	1.1500	1.1633	1.1645	1.1586	1.1547	1.1631	1.1645	1.1558
48.9390	1.1457	1.1284	1.1177	1.1308	1.1438	1.1573	1.1357	1.1453
62.1017	1.1395	1.1318	1.1297	1.1339	1.1424	1.1273	1.1439	1.1406
78.8046	1.1927	1.1437	1.1551	1.1672	1.1340	1.1439	1.1682	1.1357
100.0000	1.3012	1.3143	1.2837	1.2969	1.2311	1.2979	1.3019	1.2404
Note: Distance range of each event DEL: 0 to 50 km (0 to 31 mile) DEM: 50 to 200 km (31 to 125 mile) DEH: > 200 km (> 125 mile)								

Table 2.5-14 {Uniform Hazard Response Spectra (Hard Rock Conditions)}

Frequency (Hz)	10 ⁻⁴ SA, g		10 ⁻⁵ SA, g		10 ⁻⁶ SA, g	
	Mean	Median	Mean	Median	Mean	Median
0.5	0.0357	0.0219	0.1103	0.0560	0.2437	0.1321
1.0	0.0454	0.0320	0.1183	0.0757	0.2606	0.1741
2.5	0.0807	0.0653	0.2202	0.1914	0.5565	0.5330
5.0	0.1307	0.1238	0.4068	0.3990	1.1081	1.0739
10.0	0.1888	0.1850	0.6474	0.6366	1.8252	1.7707
25.0	0.2802	0.2648	1.0043	0.9680	3.1000	2.8950
100.0	0.0973	0.0945	0.3611	0.3516	1.0914	1.0350

Table 2.5-15 {Earthquake Frequencies for Repeating New Madrid Earthquake Sequences}

Model	Weight of model	Mean repeat time (years)	Equivalent annual frequency, $\lambda_{\text{rate of cluster}}$	Weight of $\lambda_{\text{rate of cluster}}$	Combined weight, w_c	$\lambda_{\text{rate of cluster times } w_c}$
Poisson	0.5	161	6.20E-03	0.10108	0.05054	0.00031
		262	3.82E-03	0.24429	0.12215	0.00047
		410	2.44E-03	0.30926	0.15463	0.00038
		694	1.44E-03	0.24429	0.12215	0.00018
		1563	6.40E-04	0.10108	0.05054	0.00003
Renewal $\alpha = 0.3$	0.5x0.2 = 0.1	333	3.39E-03	0.10108	0.01011	0.00003
		410	1.07E-03	0.24429	0.02443	0.00003
		485	3.02E-04	0.30926	0.03093	0.00001
		574	5.95E-05	0.24429	0.02443	0.00000
		709	4.30E-06	0.10108	0.01011	0.00000
Renewal $\alpha = 0.5$	0.5x0.5 = 0.25	316	4.85E-03	0.10108	0.02527	0.00012
		440	2.18E-03	0.24429	0.06107	0.00013
		573	8.89E-04	0.30926	0.07732	0.00007
		746	2.58E-04	0.24429	0.06107	0.00002
		1032	2.97E-05	0.10108	0.02527	0.00000
Renewal $\alpha = 0.7$	0.5x0.3 0.15	325	4.45E-03	0.10108	0.01516	0.00007
		506	2.25E-03	0.24429	0.03664	0.00008
		719	1.02E-03	0.30926	0.04639	0.00005
		1011	3.37E-04	0.24429	0.03664	0.00001
		1521	4.49E-05	0.10108	0.01516	0.00000
sums	1.00				1.00	0.00199
Average return period =					503	years

Note:

Adapted from the Seismic Hazards Report for the Clinton ESP Site
See Figure 4.1-1 and Table 4.1-3 (EGC 2006)

Table 2.5-16 {USGS 2008 Seismicity Smoothing Models}

Model	Incompleteness Year	Minimum Magnitude, m_b	Correlation Distance		Weight	
			km	mile	Main Source	Background
1	1924	3.0	50	31	0.50	0.40
2	1860	4.0	75	47	0.25	0.20
3	1700	5.0	75	47	0.25	0.20
4	Uniformly distributed		-	-	-	0.20

Table 2.5-17 {Selected Controlling Rock Motion Time Histories}
Page 1 of 4

Hazard	Controlling Event			Earthquake Acceleration Time History				
	Mag. (M)	Dist. (km)	Dist. (mi)	Event	Station	Mag. (M)	Dist. (km)	Dist. (mi)
10 ⁻⁴ Near field event, DEL	5.55	16.84	10.47	Livermore	San Roamon - eastman Kodak	5.4	17.6	10.9
						5.4	17.6	10.9
						5.8	12.2	7.6
10 ⁻⁴ Middle field event, DEM	6.45	112.09	69.66	San Fernando	Maricopa Array #3	5.8	12.2	7.6
						6.6	113.0	70.2
						6.6	113.0	70.2
10 ⁻⁴ Far field event, DEH	7.36	339.47	210.98	Northridge	Riverside Airport	6.7	101.3	63.0
						6.7	101.3	63.0
						7.3	141.6	88.0
10 ⁻⁴ Far field event, DEH	7.36	339.47	210.98	Landers	San Gabriel - E Gran Ave	7.3	141.6	88.0
						7.3	141.6	88.0
						7.3	162.6	101.1
				Landers	Sun Valley - Sunland	7.3	162.6	101.1

Table 2.5-17—{Selected Controlling Rock Motion Time Histories}
Page 2 of 4

Hazard	Controlling Event			Earthquake Acceleration Time History				
	Mag. (M)	Dist. (km)	Dist. (mi)	Event	Station	Mag. (M)	Dist. (km)	Dist. (mi)
10 ⁻⁴ Near field event, DEL	5.40	17.62	10.95	Livermore	San Roamon - eastman Kodak	5.4	17.6	10.9
						5.4	17.6	10.9
				Coalinga	Palmer Ave.	5.8	12.2	7.6
10 ⁻⁴ Middle field event, DEM	6.18	107.41	6.76	Borrego Mtn	San Onofre - So Cal Edison	5.8	12.2	7.6
				San Fernando	San Onofre - So Cal Edison	6.8	124.7	77.5
						6.8	124.7	77.5
10 ⁻⁴ Far field event, DEH	7.09	307.72	191.25	Landers	San Gabriel - E Gran Ave	6.6	122.0	75.8
						6.6	122.0	75.8
				Tabas, Iran	Kashmar	7.3	141.6	88.0
						7.3	141.6	88.0
						7.4	199.1	123.7
7.4	199.1	123.7						

Table 2.5-17—{Selected Controlling Rock Motion Time Histories}
Page 3 of 4

Hazard	Controlling Event			Earthquake Acceleration Time History				
	Mag. (M)	Dist. (km)	Dist. (mi)	Event	Station	Mag. (M)	Dist. (km)	Dist. (mi)
10 ⁻⁵ Near field event, DEL	5.79	13.67	8.50	Morgan Hill	Gilroy - Gavilian Coll.	6.2	16.2	10.1
						6.2	16.2	10.1
				Morgan Hill	Gilroy Array #6	6.2	11.8	7.3
10 ⁻⁵ Middle field event, DEM	6.86	105.56	65.61	Landers	Duarte - Mel Canyon Rd	7.3	126.4	78.6
				Landers	Villa Park - Serrano Ave	7.3	126.4	78.6
				Landers	Villa Park - Serrano Ave	7.3	131.4	81.7
10 ⁻⁵ Far field event, DEH	7.38	340.39	211.55	Landers	Villa Park - Serrano Ave	7.3	194.1	120.6
				Landers	Villa Park - Serrano Ave	7.3	194.1	120.6
				Landers	Sun Valley - Sunland	7.3	162.6	101.1
						7.3	162.6	101.1

Table 2.5-17—{Selected Controlling Rock Motion Time Histories}
Page 4 of 4

Hazard	Controlling Event			Earthquake Acceleration Time History				
	Mag. (M)	Dist. (km)	Dist. (mi)	Event	Station	Mag. (M)	Dist. (km)	Dist. (mi)
10 ⁻⁵ Near field event, DEL	5.54	11.62	7.22	Whittier Narrows	Garvey Res. - Control Bldg.	6	12.1	7.5
						6	12.1	7.5
				Fruili, Italy	San Rocco	5.5	17.9	11.1
10 ⁻⁵ Middle field event, DEM	6.77	100.70	62.59	San Fernando	Maricopa Array #3	5.5	17.9	11.1
				Northridge	Riverside Airport	6.6	113.0	70.2
						6.6	113.0	70.2
10 ⁻⁵ Far field event, DEH	7.11	291.43	181.12	Landers	San Gabriel - E Gran Ave	6.7	101.3	101.3
				Tabas, Iran	Kashmar	6.7	101.3	101.3
						7.3	141.6	88.0
						7.3	141.6	88.0
						7.4	199.1	123.7
						7.4	199.1	123.7

Table 2.5-18 Comparison of Post-EPRI NP-6395-D 1989 Magnitude Estimates for the 1886 Charleston Earthquake

Study	Magnitude Estimation Method	Reported Magnitude Estimate	Assigned Weights	Mean Magnitude (M)
EPRI (1994)	worldwide survey of passive-margin, extended-crust earthquakes	M 7.56 ± 0.35	--	7.56
Martin (1994)	geotechnical assessment of 1886 liquefaction data	M 7 - 7.5	--	7.25
Johnston (1996)	isoseismal area regression, accounting for eastern North America anelastic attenuation	M 7.3 ± 0.26	--	7.3
Chapman (2002) (South Carolina Department of Transportation)	consideration of available magnitude estimates	M 7.1 M 7.3 M 7.5	0.2 0.6 0.2	7.3
Frankel et al. (2002) (USGS National seismic hazard mapping project)	consideration of available magnitude estimates	M 6.8 M 7.1 M 7.3 M 7.5	0.20 0.20 0.45 0.15	7.2
Bakun (2004)	isoseismal area regression, including empirical site corrections	M _I 6.4 - 7.2	--	6.9
Adopted from the Seismic Hazard Report for CCNPP Unit 3 FSAR 2007				

Table 2.5-19 {Mean and Fractile Rock Hazard Curves for PGA}

Ground motion level (g)	Annual Exceedance Frequency					
	Mean	5% Fractile	15% Fractile	50% Fractile	85% Fractile	95% Fractile
0.010	3.785E-03	2.404E-03	2.809E-03	3.664E-03	4.779E-03	5.584E-03
0.025	1.035E-03	5.204E-04	6.539E-04	9.649E-04	1.424E-03	1.789E-03
0.050	3.238E-04	1.620E-04	2.038E-04	3.016E-04	4.463E-04	5.616E-04
0.075	1.583E-04	8.525E-05	1.049E-04	1.494E-04	2.128E-04	2.618E-04
0.100	9.521E-05	5.413E-05	6.550E-05	9.067E-05	1.255E-04	1.519E-04
0.200	2.846E-05	1.744E-05	2.061E-05	2.741E-05	3.644E-05	4.308E-05
0.300	1.399E-05	8.279E-06	9.894E-06	1.340E-05	1.816E-05	2.170E-05
0.400	8.306E-06	4.607E-06	5.617E-06	7.878E-06	1.105E-05	1.347E-05
0.500	5.443E-06	2.817E-06	3.509E-06	5.102E-06	7.418E-06	9.240E-06
0.600	3.792E-06	1.836E-06	2.333E-06	3.511E-06	5.283E-06	6.713E-06
0.700	2.755E-06	1.252E-06	1.621E-06	2.519E-06	3.913E-06	5.067E-06
0.800	2.065E-06	8.845E-07	1.165E-06	1.864E-06	2.983E-06	3.930E-06
0.900	1.585E-06	6.422E-07	8.598E-07	1.414E-06	2.325E-06	3.112E-06
1.000	1.240E-06	4.771E-07	6.482E-07	1.093E-06	1.843E-06	2.505E-06
1.250	7.162E-07	2.451E-07	3.441E-07	6.136E-07	1.094E-06	1.536E-06
1.500	4.425E-07	1.370E-07	1.976E-07	3.693E-07	6.901E-07	9.959E-07
2.000	1.935E-07	5.082E-08	7.661E-08	1.543E-07	3.106E-07	4.682E-07
2.750	6.950E-08	1.519E-08	2.401E-08	5.243E-08	1.145E-07	1.810E-07
3.500	2.944E-08	5.606E-09	9.174E-09	2.125E-08	4.921E-08	8.054E-08
5.000	7.153E-09	1.113E-09	1.914E-09	4.821E-09	1.214E-08	2.088E-08

Table 2.5-20 {Mean and Fractile Rock Hazard Curves for 25 Hz}

Ground motion level (g)	Annual Exceedance Frequency					
	Mean	5% Fractile	15% Fractile	50% Fractile	85% Fractile	95% Fractile
0.010	8.506E-03	6.105E-03	6.856E-03	8.354E-03	1.018E-02	1.143E-02
0.025	3.601E-03	2.214E-03	2.614E-03	3.470E-03	4.606E-03	5.439E-03
0.050	1.566E-03	8.127E-04	1.011E-03	1.468E-03	2.132E-03	2.653E-03
0.075	8.854E-04	4.200E-04	5.370E-04	8.164E-04	1.241E-03	1.587E-03
0.100	5.707E-04	2.572E-04	3.338E-04	5.208E-04	8.125E-04	1.055E-03
0.200	1.806E-04	7.682E-05	1.014E-04	1.628E-04	2.615E-04	3.452E-04
0.300	8.872E-05	3.888E-05	5.088E-05	8.050E-05	1.273E-04	1.666E-04
0.400	5.315E-05	2.444E-05	3.153E-05	4.870E-05	7.522E-05	9.706E-05
0.500	3.562E-05	1.711E-05	2.179E-05	3.293E-05	4.975E-05	6.337E-05
0.600	2.565E-05	1.272E-05	1.605E-05	2.385E-05	3.546E-05	4.473E-05
0.700	1.940E-05	9.814E-06	1.231E-05	1.811E-05	2.665E-05	3.342E-05
0.800	1.521E-05	7.762E-06	9.709E-06	1.422E-05	2.083E-05	2.606E-05
0.900	1.225E-05	6.251E-06	7.819E-06	1.145E-05	1.678E-05	2.099E-05
1.000	1.008E-05	5.106E-06	6.401E-06	9.411E-06	1.384E-05	1.735E-05
1.250	6.622E-06	3.230E-06	4.095E-06	6.139E-06	9.203E-06	1.167E-05
1.500	4.655E-06	2.154E-06	2.775E-06	4.271E-06	6.576E-06	8.469E-06
2.000	2.609E-06	1.075E-06	1.432E-06	2.336E-06	3.810E-06	5.077E-06
2.750	1.318E-06	4.601E-07	6.423E-07	1.134E-06	2.004E-06	2.797E-06
3.500	7.563E-07	2.290E-07	3.324E-07	6.275E-07	1.185E-06	1.720E-06
5.000	3.095E-07	7.477E-08	1.152E-07	2.407E-07	5.031E-07	7.752E-07

Table 2.5-21 {Mean and Fractile Rock Hazard Curves for 10 Hz}

Ground motion level (g)	Annual Exceedance Frequency					
	Mean	5% Fractile	15% Fractile	50% Fractile	85% Fractile	95% Fractile
0.010	8.106E-03	5.951E-03	6.633E-03	7.979E-03	9.598E-03	1.070E-02
0.025	2.799E-03	1.770E-03	2.072E-03	2.708E-03	3.539E-03	4.141E-03
0.050	1.014E-03	5.615E-04	6.851E-04	9.619E-04	1.350E-03	1.648E-03
0.075	5.191E-04	2.812E-04	3.454E-04	4.904E-04	6.963E-04	8.553E-04
0.100	3.146E-04	1.750E-04	2.132E-04	2.985E-04	4.181E-04	5.094E-04
0.200	9.009E-05	5.639E-05	6.620E-05	8.703E-05	1.144E-04	1.343E-04
0.300	4.289E-05	2.801E-05	3.244E-05	4.166E-05	5.350E-05	6.196E-05
0.400	2.517E-05	1.653E-05	1.911E-05	2.447E-05	3.133E-05	3.622E-05
0.500	1.653E-05	1.073E-05	1.245E-05	1.604E-05	2.067E-05	2.399E-05
0.600	1.162E-05	7.400E-06	8.641E-06	1.126E-05	1.466E-05	1.712E-05
0.700	8.570E-06	5.329E-06	6.269E-06	8.271E-06	1.091E-05	1.284E-05
0.800	6.536E-06	3.966E-06	4.702E-06	6.286E-06	8.404E-06	9.964E-06
0.900	5.115E-06	3.028E-06	3.618E-06	4.902E-06	6.641E-06	7.936E-06
1.000	4.086E-06	2.361E-06	2.843E-06	3.901E-06	5.355E-06	6.447E-06
1.250	2.492E-06	1.359E-06	1.666E-06	2.357E-06	3.336E-06	4.089E-06
1.500	1.629E-06	8.418E-07	1.049E-06	1.526E-06	2.221E-06	2.767E-06
2.000	7.966E-07	3.744E-07	4.800E-07	7.332E-07	1.120E-06	1.436E-06
2.750	3.365E-07	1.400E-07	1.860E-07	3.019E-07	4.900E-07	6.510E-07
3.500	1.660E-07	6.221E-08	8.516E-08	1.454E-07	2.484E-07	3.400E-07
5.000	5.326E-08	1.672E-08	2.403E-08	4.462E-08	8.285E-08	1.191E-07

Table 2.5-22 {Mean and Fractile Rock Hazard Curves for 5 Hz}

Ground motion level (g)	Annual Exceedance Frequency					
	Mean	5% Fractile	15% Fractile	50% Fractile	85% Fractile	95% Fractile
0.010	6.489E-03	4.510E-03	5.119E-03	6.351E-03	7.880E-03	8.943E-03
0.025	1.854E-03	1.034E-03	1.259E-03	1.760E-03	2.461E-03	2.996E-03
0.050	5.974E-04	2.475E-04	3.292E-04	5.355E-04	8.710E-04	1.159E-03
0.075	2.900E-04	1.086E-04	1.487E-04	2.540E-04	4.339E-04	5.941E-04
0.100	1.693E-04	6.507E-05	8.844E-05	1.492E-04	2.517E-04	3.421E-04
0.200	4.336E-05	2.238E-05	2.790E-05	4.062E-05	5.915E-05	7.373E-05
0.300	1.895E-05	1.110E-05	1.331E-05	1.813E-05	2.470E-05	2.961E-05
0.400	1.037E-05	6.187E-06	7.375E-06	9.949E-06	1.342E-05	1.600E-05
0.500	6.414E-06	3.753E-06	4.501E-06	6.136E-06	8.364E-06	1.003E-05
0.600	4.285E-06	2.430E-06	2.943E-06	4.079E-06	5.654E-06	6.848E-06
0.700	3.020E-06	1.654E-06	2.025E-06	2.859E-06	4.036E-06	4.941E-06
0.800	2.214E-06	1.170E-06	1.448E-06	2.083E-06	2.996E-06	3.708E-06
0.900	1.673E-06	8.529E-07	1.067E-06	1.564E-06	2.291E-06	2.866E-06
1.000	1.295E-06	6.378E-07	8.063E-07	1.202E-06	1.793E-06	2.267E-06
1.250	7.387E-07	3.356E-07	4.346E-07	6.753E-07	1.049E-06	1.359E-06
1.500	4.578E-07	1.930E-07	2.554E-07	4.119E-07	6.642E-07	8.791E-07
2.000	2.065E-07	7.623E-08	1.048E-07	1.802E-07	3.100E-07	4.261E-07
2.750	8.009E-08	2.498E-08	3.597E-08	6.699E-08	1.247E-07	1.796E-07
3.500	3.715E-08	1.004E-08	1.503E-08	2.987E-08	5.937E-08	8.884E-08
5.000	1.090E-08	2.328E-09	3.702E-09	8.164E-09	1.800E-08	2.863E-08

Table 2.5-23 {Mean and Fractile Rock Hazard Curves for 2.5 Hz}

Ground motion level (g)	Annual Exceedance Frequency					
	Mean	5% Fractile	15% Fractile	50% Fractile	85% Fractile	95% Fractile
0.010	3.765E-03	2.187E-03	2.629E-03	3.598E-03	4.924E-03	5.918E-03
0.025	9.133E-04	3.131E-04	4.393E-04	7.828E-04	1.395E-03	1.957E-03
0.050	2.621E-04	4.515E-05	7.574E-05	1.829E-04	4.419E-04	7.413E-04
0.075	1.169E-04	1.470E-05	2.658E-05	7.297E-05	2.003E-04	3.621E-04
0.100	6.322E-05	7.472E-06	1.371E-05	3.855E-05	1.085E-04	1.989E-04
0.200	1.266E-05	2.401E-06	3.933E-06	9.125E-06	2.117E-05	3.468E-05
0.300	4.697E-06	1.457E-06	2.101E-06	3.923E-06	7.322E-06	1.056E-05
0.400	2.299E-06	9.031E-07	1.220E-06	2.036E-06	3.400E-06	4.592E-06
0.500	1.313E-06	5.464E-07	7.259E-07	1.178E-06	1.912E-06	2.540E-06
0.600	8.257E-07	3.369E-07	4.502E-07	7.377E-07	1.209E-06	1.615E-06
0.700	5.545E-07	2.161E-07	2.926E-07	4.902E-07	8.215E-07	1.112E-06
0.800	3.905E-07	1.444E-07	1.984E-07	3.410E-07	5.860E-07	8.051E-07
0.900	2.851E-07	1.000E-07	1.395E-07	2.458E-07	4.331E-07	6.038E-07
1.000	2.141E-07	7.142E-08	1.010E-07	1.822E-07	3.289E-07	4.650E-07
1.250	1.147E-07	3.407E-08	4.971E-08	9.465E-08	1.802E-07	2.629E-07
1.500	6.740E-08	1.809E-08	2.711E-08	5.407E-08	1.078E-07	1.617E-07
2.000	2.786E-08	6.277E-09	9.846E-09	2.121E-08	4.571E-08	7.170E-08
2.750	9.717E-09	1.768E-09	2.926E-09	6.908E-09	1.631E-08	2.700E-08
3.500	4.126E-09	6.286E-10	1.086E-09	2.760E-09	7.014E-09	1.212E-08
5.000	1.048E-09	1.199E-10	2.217E-10	6.316E-10	1.800E-09	3.326E-09

Table 2.5-24 {Mean and Fractile Rock Hazard Curves for 1 Hz}

Ground motion level (g)	Annual Exceedance Frequency					
	Mean	5% Fractile	15% Fractile	50% Fractile	85% Fractile	95% Fractile
0.010	1.435E-03	4.617E-04	6.593E-04	1.210E-03	2.221E-03	3.172E-03
0.025	3.220E-04	3.477E-05	6.510E-05	1.897E-04	5.529E-04	1.035E-03
0.050	8.283E-05	3.159E-06	7.386E-06	3.142E-05	1.337E-04	3.126E-04
0.075	3.311E-05	8.230E-07	2.093E-06	1.027E-05	5.043E-05	1.282E-04
0.100	1.611E-05	3.393E-07	8.904E-07	4.612E-06	2.389E-05	6.269E-05
0.200	2.256E-06	5.317E-08	1.366E-07	6.822E-07	3.407E-06	8.752E-06
0.300	6.488E-07	2.453E-08	5.744E-08	2.451E-07	1.046E-06	2.450E-06
0.400	2.665E-07	1.711E-08	3.592E-08	1.272E-07	4.507E-07	9.464E-07
0.500	1.346E-07	1.337E-08	2.552E-08	7.680E-08	2.312E-07	4.412E-07
0.600	7.744E-08	1.003E-08	1.801E-08	4.885E-08	1.326E-07	2.381E-07
0.700	4.858E-08	6.978E-09	1.223E-08	3.182E-08	8.282E-08	1.451E-07
0.800	3.240E-08	4.657E-09	8.160E-09	2.123E-08	5.524E-08	9.678E-08
0.900	2.261E-08	3.092E-09	5.482E-09	1.455E-08	3.863E-08	6.848E-08
1.000	1.634E-08	2.084E-09	3.755E-09	1.025E-08	2.798E-08	5.042E-08
1.250	8.088E-09	8.560E-10	1.610E-09	4.729E-09	1.389E-08	2.613E-08
1.500	4.466E-09	3.994E-10	7.804E-10	2.444E-09	7.657E-09	1.496E-08
2.000	1.673E-09	1.138E-10	2.360E-10	8.184E-10	2.838E-09	5.886E-09
2.750	5.237E-10	2.625E-11	5.805E-11	2.246E-10	8.692E-10	1.922E-09
3.500	2.050E-10	8.162E-12	1.892E-11	7.932E-11	3.325E-10	7.708E-10
5.000	4.632E-11	1.317E-12	3.263E-12	1.532E-11	7.198E-11	1.783E-10

Table 2.5-25 {Mean and Fractile Rock Hazard Curves for 0.5 Hz}

Ground motion level (g)	Annual Exceedance Frequency					
	Mean	5% Fractile	15% Fractile	50% Fractile	85% Fractile	95% Fractile
0.010	7.646E-04	1.285E-04	2.168E-04	5.292E-04	1.291E-03	2.180E-03
0.025	1.851E-04	8.350E-06	1.887E-05	7.577E-05	3.042E-04	6.875E-04
0.050	5.573E-05	8.105E-07	2.278E-06	1.327E-05	7.727E-05	2.172E-04
0.075	2.506E-05	2.383E-07	7.229E-07	4.793E-06	3.178E-05	9.638E-05
0.100	1.311E-05	1.027E-07	3.221E-07	2.263E-06	1.590E-05	4.987E-05
0.200	1.936E-06	1.215E-08	3.961E-08	2.968E-07	2.225E-06	7.250E-06
0.300	4.986E-07	3.141E-09	1.023E-08	7.659E-08	5.734E-07	1.867E-06
0.400	1.731E-07	1.181E-09	3.794E-09	2.776E-08	2.031E-07	6.524E-07
0.500	7.306E-08	5.662E-10	1.780E-09	1.254E-08	8.837E-08	2.778E-07
0.600	3.543E-08	3.227E-10	9.862E-10	6.624E-09	4.449E-08	1.360E-07
0.700	1.910E-08	2.096E-10	6.198E-10	3.936E-09	2.499E-08	7.390E-08
0.800	1.118E-08	1.499E-10	4.276E-10	2.553E-09	1.525E-08	4.349E-08
0.900	6.983E-09	1.147E-10	3.154E-10	1.768E-09	9.911E-09	2.724E-08
1.000	4.597E-09	9.164E-11	2.430E-10	1.281E-09	6.754E-09	1.791E-08
1.250	1.920E-09	5.513E-11	1.363E-10	6.382E-10	2.988E-09	7.389E-09
1.500	9.521E-10	3.139E-11	7.555E-11	3.377E-10	1.510E-09	3.633E-09
2.000	3.165E-10	9.298E-12	2.289E-11	1.063E-10	4.941E-10	1.216E-09
2.750	9.195E-11	2.030E-12	5.280E-12	2.694E-11	1.374E-10	3.575E-10
3.500	3.418E-11	6.008E-13	1.631E-12	8.951E-12	4.912E-11	1.333E-10
5.000	7.492E-12	1.035E-13	2.937E-13	1.738E-12	1.028E-11	2.918E-11

Table 2.5-26 {Summary Of Thicknesses And Termination Elevations For Various Strata}

English Units

	Thickness (feet)			Top (feet msl)		
	Minimum	Maximum	Average	Minimum	Maximum	Average
Glacial Overburden	12.5	62.0	38.7	656.6	801.3	678.7
Mahantango Formation	*	*	*	594.3	774.2	639.3

Note: * This layer was not fully penetrated

Table 2.5-26—{Summary Of Thicknesses And Termination Elevations For Various Strata}

SI Units

	Thickness (m)			Top (m msl)		
	Minimum	Maximum	Average	Minimum	Maximum	Average
Glacial Overburden	3.8	18.9	11.8	200.2	244.3	206.9
Mahantango Formation	*	*	*	181.2	236.0	194.9

Note: * This layer was not fully penetrated

Table 2.5-27 {Summary Of Geotechnical Field Tests}

Test	Specification	Quantity
Soil and Rock Borings	ASTM D1586/1587	48
Seismic Refraction Survey	NA	6
P-S Suspension Logging Surveys (boreholes)	NA	4
Downhole Velocity Measurements	NA	4
Pressuremeter Test (PMT)	ASTM D4719-00	8
SPT Hammer Energy Measurements	ASTM D4633	2

Table 2.5-28 {Boring Locations And Surface Elevations}

Structural (Foundation)	Boring	Horizontal Coordinates		El. (ft)	Boring Depth (ft)			Type of Test
		Plant N	Plant E		Soil	Rock	Total	
ESWEMS	B-331	339,872.65	2,406,407.01	683.70	41.0	29.0	70.0	SPT/Coring
	B-332	339,907.33	2,406,874.31	691.55	49.0	21.0	70.0	SPT/Coring
	B-333	339,667.26	2,406,421.42	678.29	34.0	36.3	70.3	SPT/Coring
	B-334	339,700.60	2,406,888.49	671.21	45.5	25.0	70.5	SPT/Coring
Cooling Towers	B-335	340,767.34	2,405,475.56	793.71	19.0	51.0	70.0	SPT/Coring
	B-336	340,492.18	2,405,516.32	801.32	30.0	40.0	70.0	SPT/Coring
	B-337	340,239.46	2,405,528.14	790.57	19.0	80.5	99.5	SPT/Coring
	B-338	340,738.30	2,406,234.46	720.08	22.8	48.7	71.5	SPT/Coring
	B-339	340,479.98	2,406,149.45	710.66	18.0	52.0	70.0	SPT/Coring
	B-340	340,298.18	2,406,433.93	702.37	12.5	67.5	80.0	SPT/Coring
UHS Pumphouse and Supply Line)	B-341	339,825.65	2,406,458.83	680.71	49.4	50.6	100.0	SPT/Coring
	B-342	339,721.50	2,406,467.46	678.15	38.0	62.0	100.0	SPT/Coring
	B-343	339,772.49	2,406,467.46	681.17	48.4	51.6	100.0	SPT/Coring
	B-344	339,761.98	2,406,301.53	683.12	42.0	58.0	100.0	SPT/Coring
	B-345	339,746.44	2,406,203.70	688.02	25.0	75.0	100.0	SPT/Coring
Auxiliary Geophysics	G-301	339,151.79	2,405,430.68	666.81	40.0	365.0	405.0	SPT/Coring
	G-302	339,297.55	2,405,219.00	668.25	21.0	183.0	204.0	SPT/Coring
	G-303	338,698.96	2,405,865.49	659.18	42.5	162.5	205.0	SPT/Coring

Table 2.5-29 {Summary of Hammer-Rod Energy Measurements}

Drill Rig	Measurement in Boring No.	ETR Range (%)	Average ETR (%)	EnergyAdjustment (ETR%/60%)
CME - 55 340665	B-336	75-87	84	1.40
CME 55 300 Carrier	B-327	60-80	78	1.30

Note: ETR = Percentage of theoretical hammer energy measured in the field

Table 2.5-30 {Summary Of Field-Measured Standard Penetration Test (Spt) N-Values}

Stratum	SPT N-values (blows / feet)		
	Minimum	Maximum	Average
Glacial Overburden	0	131	35

Table 2.5-31 {Summary Of Adjusted Spt N-Values Based On Energy Measurements}

Stratum	Adjusted Minimum N-Value (blows/feet)	Adjusted Maximum N-Value (blows/feet)	Adjusted Average N-Value (blows/feet)	Recommended N-Value for Engineering Purposes (blows/ft)
Glacial Overburden	0	97	27	20

Table 2.5-32 {Summary Of Borehole Pressuremeter Test Results}

English Units

Boring	Depth (ft)	E _p (ksf)	p _{creep} (ksf)	p _{limit} (ksf)
B-301	45	12932	*	*
B-301	55	29098	*	*
B-322	64	104006	*	*
B-322	74	9124	*	*
B-325	22	22908	*	*
B-325	31.5	25932	*	*
B-327	25	9986	*	*
B-327	35	11122	*	*

Table 2.5-32—{Summary Of Borehole Pressuremeter Test Results}

SI Units

Boring	Depth (m)	E _p (kPa)	p _l (kPa)	E _s (kPa)
B-301	13.9	619200	*	*
B-301	17.0	1393200	*	*
B-322	19.8	4979800	*	*
B-322	22.9	436900	*	*
B-325	6.8	1096800	*	*
B-325	9.8	1241600	*	*
B-327	7.7	478100	*	*
B-327	10.8	532500	*	*

Note:

* Tests terminated before creep and limit pressures could be established

p_l - Pressuremeter limit pressure

E_p - Pressuremeter Modulus

Table 2.5-33 {Summary Of Laboratory Tests}

Test	Specification	Quantity
Engineering Classification	ASTM D2487-06 / ASTM D5878-05	114
Moisture Content	ASTM D2216-05	35
Unit Weight	From weight-volume relationship	19
Specific Gravity	ASTM D854-06 / ASTM D6473-99(2005)	13
Grain Size Analysis	ASTM D422-63 (2002)	114
Hydraulic Conductivity	ASTM D5084-03	3
Compaction Tests	ASTM D1557-07 Method C	2
Unconfined Compression	ASTM D7012-04	19
Resonant Column Torsional Shear	Technical Procedures for RCTS Tests ⁽¹⁾	5
Free-Free Test	Technical Procedures for URC Tests ⁽²⁾	8
Sonic Pulse Test	ASTM D 2845-05	3
Organic Content	ASTM D2974-07	2
pH	ASTM D4792	38
Resistivity	ASTM G187-05	38
Chloride ion content	AASHTO T291	38
Sulphate ion content	AASHTO T290	38

⁽¹⁾ PBRCTS-1 Rev. 4, October 2004, University of Texas at Austin, Performed at FUGRO

⁽²⁾ URC-1 Rev. 1, August 2004, University of Texas at Austin, Performed at FUGRO

Table 2.5-34 {Summary Of Moisture Content}

(Page 1 of 2)

Formation	Boring	Depth		Moisture Content (%)
		(ft)	(m)	
Glacial Overburden	B-301	5.8	1.8	3.8
	B-301	8.8	2.7	2.6
	B-302	0.8	0.2	16.7
	B-302	2.0	0.6	13.2
	B-302	8.8	2.7	3.3
	B-303	6.3	1.9	7.0
	B-303	9.3	2.8	13.6
	B-303	12.3	3.7	5.2
	B-303	2.5	0.8	9.9
	B-305	2.3	0.7	4.6
	B-305	3.8	1.1	8.6
	B-305	6.8	2.1	14.1
	B-308	5.8	1.8	10.2
	B-308	13.3	4.0	11.2
	B-309	5.3	1.6	20.9
	B-309	8.3	2.5	20.6
	B-309	11.3	3.4	18.9
	B-311	0.8	0.2	9.0
	B-311	5.3	1.6	4.7
	B-311	6.8	2.1	4.7
	B-317	0.8	0.2	21.2
	B-317	3.8	1.1	19.9
	B-317	14.3	4.3	25.6
	B-318	0.8	0.2	13.5
	B-318	3.8	1.1	13.2
	B-319	4.0	1.2	12.8
	B-324	2.3	0.7	6.3
	B-324	5.3	1.6	3.4
	B-324	8.3	2.5	3.2
	B-326	2.3	0.7	4.4
	B-326	6.8	2.1	10.8
	B-327	3.0	0.9	10.4
	B-333	5.8	1.8	12.2
B-333	13.3	4.0	5.7	
B-303 U2	2.5	0.8	9.9	
B-319 U2	4.0	1.2	12.8	
B-327 ST2	3.0	0.9	10.4	

10.8

Table 2.5-34 {Summary Of Moisture Content}

(Page 2 of 2)

Formation	Boring	Depth		Moisture Content (%)
		(ft)	(m)	
Mahantango Formation	B-301	197.8	60.3	NR
	B-301	152.4	46.4	NR
	B-302	318.1	97.0	0.3
	B-302	52.3	15.9	0.4
	B-302	214.1	65.3	0.4
	B-302	110.6	33.7	0.5
	B-303	142.7	43.5	0.0
	B-304	109.8	33.5	0.3
	B-304	170.8	52.1	0.3
	B-304	273.5	83.4	0.3
	B-309	54.7	16.7	0.6
	B-310	57.2	17.4	0.6
	B-318	93.5	28.5	0.0
	B-319	41.1	12.5	NR
	B-324	27.6	8.4	0.6
	B-326	41.1	12.5	1.2
	B-327	34.0	10.4	1.1
	B-331	67.5	20.6	0.9
B-334	64.6	19.7	NR	

Table 2.5-35 {Summary Of Unit Weight Tests Special Care Rock Samples And Undisturbed Samples}

Formation	Boring	Depth (ft)	Dry Unit Weight (pcf)	Moist Unit Weight (pcf)
Glacial Overburden	B-303 U2	2.5	99	109
	B-319 U2	4.0	118	133
	B-327 ST2	3.0	86	95
	B-331 ST2	17.0	105	126
	B-310 U3	6.0	100	124
			102	121
Mahantango Formation	B-301, R20	197.8	NR	170
	B-301, R15	152.4	NR	171
	B-302, R32	318.1	172	173
	B-302, R3	52.3	171	172
	B-302, R21	214.1	172	173
	B-302, R11	110.6	172	173
	B-303, R24	142.7	172	172
	B-304, R8	109.8	172	173
	B-304, R-14	170.8	172	173
	B-304, R26	273.5	171	172
	B-309, R7	54.7	NR	ND
	B-310, R2	57.2	170	171
	B-318, R14	93.5	172	172
	B-319, R4	41.1	NR	172
	B-324, R2	27.6	171	172
	B-326, R1	41.1	166	168
	B-327, R3	34.0	164	166
	B-331, R7	67.5	170	172
B-334, R9	64.6	NR	172	
			171	171

NR - Not Recorded

ND - Not Detected

**Table 2.5-35—{Summary Of Unit Weight Tests Special Care Rock Samples
And Undisturbed Samples}**

Formation	Boring	Depth (m)	Dry Unit Weight (N/m ³)	Moist Unit Weight (N/m ³)
Glacial Overburden	B-303 U2	0.8	15550	17090
	B-303 U2	1.2	18470	20840
	B-319 U2	0.9	13510	14910
	B-331 ST2	5.2	16500	19810
	B-310 U3	1.8	15730	19540
			17010	18965
Mahantango Formation	B-301, R20	60.3	NR	26770
	B-301, R15	46.4	NR	26890
	B-302, R32	97.0	27030	27110
	B-302, R3	15.9	26930	27030
	B-302, R21	65.3	27010	27110
	B-302, R11	33.7	27090	27220
	B-303, R24	43.5	27080	27080
	B-304, R8	33.5	27030	27110
	B-304, R-14	52.1	27020	27100
	B-304, R26	83.4	26920	27000
	B-309, R7	16.7	NR	ND
	B-310, R2	17.4	26700	26860
	B-318, R14	28.5	27030	27030
	B-319, R4	12.5	NR	26990
	B-324, R2	8.4	26900	27070
	B-326, R1	12.5	26080	26390
	B-327, R3	10.4	25730	26010
	B-331, R7	20.6	26730	26970
B-334, R9	19.7	NR	26990	
			27027	27047

NR - Not Recorded

ND - Not Detected

Table 2.5-36 {Summary Of Specific Gravity Tests Special Care Rock Samples And Undisturbed Samples}

English Units

Formation	Boring	Depth (ft)	Depth (m)	SG
Glacial Overburden	B-303 U2	2.5	0.8	2.69
	B-319 U2	4.0	1.2	2.72
	B-327 ST2	3.0	0.9	2.69
Mahantango Formation	B-301 R20	197.8	60.3	2.77
	B-302 R3	152.4	46.4	2.76
	B-302 R11	318.1	97.0	2.76
	B-304 R8	52.3	15.9	2.76
	B-310 R2	214.1	65.3	2.77
	B-318 R14	110.6	33.7	2.76
	B-319 R4	142.7	43.5	2.83
	B-324 R2	109.8	33.5	2.76
	B-326 R1	170.8	52.1	2.67
	B-334 R9	273.5	83.4	2.77

Table 2.5-37 {Chemical Test Results Of Soil And Rock Samples}

Location		Depth		Formation	pH	Resistivity (Ω-cm)		Sulfates* (ppm)	Chlorides* (ppm)
Boring	ID	(ft)	(m)			As Received	100% Saturated		
B-301	S-12	18.5	5.6	Glacial Overburden	7.7	18130	12432	94	20
B-301	R-1	41.0	12.5	Mahantango Formation	8.6	>3.11e6	566000	62	<10
B-302	S-10	17.0	5.2	Glacial Overburden	7.1	59570	41440	70	<10
B-302	R-1	28.5	8.7	Mahantango Formation	8.8	>2.13e6	776000	29	<10
B-303	S-3	7.0	2.1	Glacial Overburden	7.0	62160	41440	73	<10
B-303	S-5	10.0	3.0	Glacial Overburden	7.1	18907	17353	43	<10
B-303	R-1	30.0	9.1	Mahantango Formation	8.0	>5.90e6	4.34E+06	20	<10
B-308	S-2	3.5	1.1	Glacial Overburden	6.4	59570	38850	24	<10
B-310	S-5	12.0	3.7	Glacial Overburden	7.0	20202	18389	81	<10
B-310	S-27	45.0	13.7	Glacial Overburden	4.3	11396	7511	1443	13
B-311	R-2	50.8	15.5	Mahantango Formation	8.7	>3.2e6	1.89E+06	21	<10
B-312	S-5	6.0	1.8	Glacial Overburden	8.5	699300	108780	20	13
B-312	S-6	7.5	2.3	Glacial Overburden	7.3	284900	62160	26	<10
B-312	S-7	9.0	2.7	Glacial Overburden	7.1	602100	73590	23	13
B-312	S-8	10.5	3.2	Glacial Overburden	7.8	21238	20720	33	13
B-314	S-11	15.0	4.6	Glacial Overburden	8.0	22523	16725	21	13
B-314	S-12	16.5	5.0	Glacial Overburden	7.8	16056	9812	45	<10
B-314	S-13	18.0	5.5	Glacial Overburden	6.0	14272	12934	77	<10
B-314	S-14	19.5	5.9	Glacial Overburden	8.3	7136	5798	127	13
B-314	S-15	21.0	6.4	Glacial Overburden	7.7	21631	12934	111	13
B-315	S-10	22.5	6.9	Glacial Overburden	6.9	33670	28490	64	<10
B-315	S-11	25.0	7.6	Glacial Overburden	6.8	12950	10878	150	<10
B-315	S-12	27.5	8.4	Glacial Overburden	7.7	8697	8028	91	<10
B-317	S-2	1.5	0.5	Glacial Overburden	6.3	31080	25123	42	13
B-317	S-9	12.0	3.7	Glacial Overburden	7.5	13468	10360	74	13
B-317	S-36	52.5	16.0	Glacial Overburden	8.5	7770	5957	366	13
B-318	R-1	28.0	8.5	Mahantango Formation	8.1	>6.29e6	1.54E+06	133	<10
B-320	S-1	0.0	0.0	Glacial Overburden	6.7	2676	2453	19	20
B-320	S-2	1.5	0.5	Glacial Overburden	6.2	38850	20979	46	<10
B-322	S-16	22.5	6.9	Glacial Overburden	7.7	31080	25900	90	<10
B-322	S-17	24.0	7.3	Glacial Overburden	6.5	13209	12691	148	<10
B-322	S-18	25.5	7.8	Glacial Overburden	7.2	33670	28490	89	<10

Table 2.5-37 {Chemical Test Results Of Soil And Rock Samples}

Location		Depth		Formation	pH	Resistivity (Ω-cm)		Sulfates* (ppm)	Chlorides* (ppm)
Boring	ID	(ft)	(m)			As Received	100% Saturated		
B-324	S-6	9.0	2.7	Glacial Overburden	6.9	468300	26760	71	40
B-324	R-2	22.0	6.7	Glacial Overburden	8.8	>3.73e6	780000	36	<10
B-327	S-5	15.0	4.6	Glacial Overburden	7.8	37910	33450	32	20
B-327	R-1	20.5	6.3	Mahantango Formation	6.5	>6.04e6	2.25E+06	530	<10
Test Pit Face ⁽¹⁾		NA	NA	Borrow area material	6.2	96690	82040	16	<10
Test Pit #5 ⁽¹⁾		NA	NA	Borrow area material	5.8	73250	52740	13	10

^(*) Water Soluble Ion Content

¹ Borrow area fill Material

Table 2.5-38 {Summary Of Unconfined Compressive Strength Tests Special Care Rock Samples}

English Units

Page 1 of 2

Formation	Boring	Depth (ft)	UCS (psi)		UCS (psf)	
Mahantango Formation	B-301, R20	197.8	3687	9250	530900	1331350
	B-301, R15	152.4	9929		1429800	
	B-302, R32	318.1	13833		1992000	
	B-302, R3	52.3	8495		1223300	
	B-302, R21	214.1	9042		1302000	
	B-302, R11	110.6	8666		1247900	
	B-303, R24	142.7	9207		1325800	
	B-304, R8	109.8	12070		1738100	
	B-304, R-14	170.8	8381		1206900	
	B-304, R26	273.5	9924		1429100	
	B-309, R7	54.7	(*)		(*)	
	B-310, R2	57.2	12580		1811500	
	B-318, R14	93.5	7556		1088100	
	B-319, R4	41.1	6770		974900	
	B-324, R2	27.6	(*)		(*)	
	B-326, R1	41.1	(*)		(*)	
	B-327, R3	34.0	9006		1296900	
	B-331, R7	67.5	9535		1373000	
B-334, R9	64.6	(*)	(*)			

(*) Specimen broke during preparation

**Table 2.5-38—{Summary Of Unconfined Compressive Strength Tests
Special Care Rock Samples}**

SI Units
Page 2 of 2

Formation	Boring	Depth (m)	UCS (MPa)
Mahantango Formation	B-301	60.3	25
	B-301	46.4	68
	B-302	97.0	95
	B-302	15.9	59
	B-302	65.3	62
	B-302	33.7	60
	B-303	43.5	63
	B-304	33.5	83
	B-304	52.1	58
	B-304	83.4	68
	B-309	16.7	(*)
	B-310	17.4	87
	B-318	28.5	52
	B-319	12.5	47
	B-324	8.4	(*)
	B-326	12.5	(*)
	B-327	10.4	62
B-331	20.6	66	
B-334	19.7	(*)	

(*) Specimen broke during preparation

Table 2.5-39 {Hydraulic Conductivity Test Results}

English Units
Page 1 Of 2

Soil Type	Boring	Depth (ft)	Eff. Confining Pressure (psf)	Hydraulic Conductivity (fps)
Glacial Overburden	B-303	2.5	500	6.89E-06
Glacial Overburden	B-319	4.0	500	9.84E-07
Glacial Overburden	B-327	3.0	500	2.89E-06

Table 2.5-39—{Hydraulic Conductivity Test Results}

SI Units
Page 2 Of 2

Soil Type	Boring	Depth (m)	Eff. Confining Pressure (kPA)	Hydraulic Conductivity (cm/s)
Glacial Overburden	B-303	0.8	24	2.10E-04
Glacial Overburden	B-319	1.2	24	3.00E-05
Glacial Overburden	B-327	0.9	24	8.80E-05

Table 2.5-40 {Dynamic Testing Program Samples}

Location		Depth		Formation	Test
Boring	ID	(ft)	(m)		
B-331	ST2	17.0	5.2	Glacial Overburden	RCTS
B-310	U3	6.0	1.8	Glacial Overburden	RCTS
B-304	R2	41.0	12.5	Mahantango Formation	RCTS
Test Pit Face				Fill and Backfill Borrow Material	RCTS
Test Pit #5				Fill and Backfill Borrow Material	RCTS
B-301	R-1	48.3	14.7	Mahantango Formation	URC
B-301	R-10	108.4	33.0	Mahantango Formation	URC
B-309	R-34	189.6	57.8	Mahantango Formation	URC
B-301	R-25	242.2	73.8	Mahantango Formation	URC
B-302	R-27	272.1	82.9	Mahantango Formation	URC
B-304	R-30	305.8	93.2	Mahantango Formation	URC
B-302	R-35	344.1	104.9	Mahantango Formation	URC
B-301	R-42	395.0	120.4	Mahantango Formation	URC
B-303	R-4	44.3	13.5	Mahantango Formation	SP
B-309	R-25	147.0	44.8	Mahantango Formation	SP
B-313	R-11	95.9	29.2	Mahantango Formation	SP

RCTS: Resonant Column Torsional Shear

URC: Unconfined Resonant Column, Free-Free Test

SP: Sonic Pulse Test

Table 2.5-41 {Resonant Column Low Strain Properties}

English Units
Page 1 of 2

Sample	Location		Depth (ft)	Formation	Confining Pressures (psf)			γ (psf)	G_{max} (ksf)	V_s (fps)	D (%)
	Boring	ID			σ_o (min)	σ_o (site)	σ_o (max)				
B-331-ST2	B-331	B-331	17	Glacial Overburden	σ_o (min)	288		126	472	347	1.32
					σ_o (site)	1008		126	980	500	1.12
					σ_o (max)	3888		126	2191	748	0.96
B-310-U3	U3	U3	6	Glacial Overburden	σ_o (min)	288		124	575	386	1.06
					σ_o (site)	1152		124	1091	531	0.84
					σ_o (max)	4752		124	2268	766	0.55
Test Pit Face				Borrow Area Fill	σ_o (min)	576		133	1093	515	2.07
					σ_o (site)	2448		133	2564	788	1.75
					σ_o (max)	9936		133	5735	1179	1.68
Test Pit #5				Borrow Area Fill	σ_o (min)	576		136	1307	556	1.64
					σ_o (site)	2448		136	2839	820	1.47
					σ_o (max)	9936		136	5877	1180	1.34

Table 2.5-41—{Resonant Column Low Strain Properties}

SI Units
Page 2 of 2

Sample	Location		Depth (m)	Formation	Confining Pressures (kPa)			γ (kN/m ³)	G_{max} (MPa)	V_s (m/s)	D (%)
	Boring	ID			σ_o (min)	σ_o (site)	σ_o (max)				
B-331-ST2	B-331	B-331	5.18	Glacial Overburden	σ_o (min)	14		20	23	106	1.32
					σ_o (site)	48		20	47	153	1.12
					σ_o (max)	186		20	105	228	0.96
B-310-U3	U3	U3	1.83	Glacial Overburden	σ_o (min)	14		20	28	118	1.06
					σ_o (site)	55		20	52	162	0.84
					σ_o (max)	228		20	109	234	0.55
Test Pit Face				Borrow Area Fill	σ_o (min)	28		21	52	157	2.07
					σ_o (site)	117		21	123	240	1.75
					σ_o (max)	476		21	275	359	1.68
Test Pit #5				Borrow Area Fill	σ_o (min)	28		21	63	170	1.64
					σ_o (site)	117		21	136	250	1.47
					σ_o (max)	476		21	281	360	1.34

Table 2.5-42 {"Free-Free" Test Results}

English Units

Location		Depth (ft)	γ (pcf)	V_s (fps)	D_s (%)	V_c (fps)	D_c (%)	V_p (fps)
Boring	ID							
B-301	R-1	48.3	169.9	7680	2.51	12020	1.58	12940
B-301	R-10	108.4	171.0	9030	0.98	13590	1.26	13810
B-309	R-34	189.6	171.5	9360	0.75	14260	1.26	14690
B-301	R-25	242.2	170.9	9670	1.14	15030	1.37	15980
B-302	R-27	272.1	171.6	9290	0.86	14100	1.68	14490
B-304	R-30	305.8	170.8	9460	0.79	14390	1.46	14850
B-302	R-35	344.1	169.5	9600	0.7	14690	1.38	15120
B-301	R-42	395.0	171.1	9670	0.79	14870	1.16	15320

γ - Unit Weight
 V_s - Shear Wave Velocity
 D_s - Shear Wave Damping
 V_c - Compression Wave Velocity (Unconstrained Test)
 D_c - Compression Wave Damping
 V_p - Compression Wave Velocity (Constrained Test)

Table 2.5-42—{"Free-Free" Test Results}

English Units

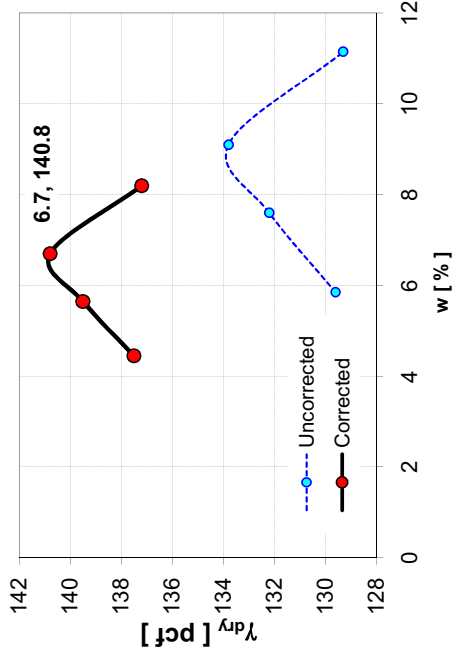
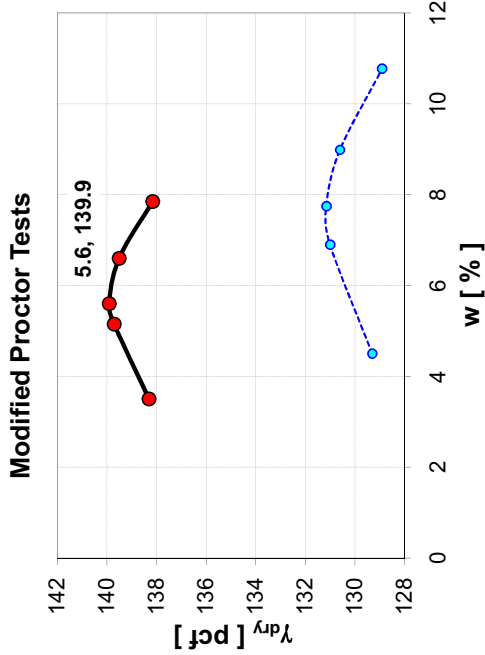
Location		Depth (m)	γ (kN/m ³)	V_s (m/s)	D_s (%)	V_c (m/s)	D_c (%)	V_p (m/s)
Boring	ID							
B-301	R-1	14.7	26.7	2341	2.51	3665	1.58	3945
B-301	R-10	33.0	26.9	2753	0.98	4143	1.26	4210
B-309	R-34	57.8	26.9	2854	0.75	4348	1.26	4479
B-301	R-25	73.8	26.8	2948	1.14	4582	1.37	4872
B-302	R-27	82.9	27.0	2832	0.86	4299	1.68	4418
B-304	R-30	93.2	26.8	2884	0.79	4387	1.46	4527
B-302	R-35	104.9	26.6	2927	0.7	4479	1.38	4610
B-301	R-42	120.4	26.9	2948	0.79	4534	1.16	4671

γ - Unit Weight
 V_s - Shear Wave Velocity
 D_s - Shear Wave Damping
 V_c - Compression Wave Velocity (Unconstrained Test)
 D_c - Compression Wave Damping
 V_p - Compression Wave Velocity (Constrained Test)

Table 2.5-43 {Category 1 Structural Fill and Backfill Properties}

English Units

Parameter	Category 1		Category 1 Backfill ²
	Structural Fill ¹	Backfill ²	
Grain Size Analysis	[%]	57.0	57.0
% Gravel	[%]	37.7	37.7
% Sands	[%]	7.6	7.6
% Fines	[%]	133	126
Solids	[lbm]	8	8
Mass (in 1 ft ³)	[lbm]	141	134
Water	[lbm]	6.1	6.1
Total	[lbm]	88.3	73.2
Moisture Content	[%]	2.6	2.6
Moisture Content	[%]	133	126
Saturation	[%]	141	134
Saturation	[%]	144	140
Specific Gravity	[]		
Specific Gravity	[]		
Dry	[pcf]		
Dry	[pcf]		
Moist	[pcf]		
Moist	[pcf]		
Saturated	[pcf]		
Saturated	[pcf]		



¹ 95% Modified Proctor ² 90% Modified Proctor

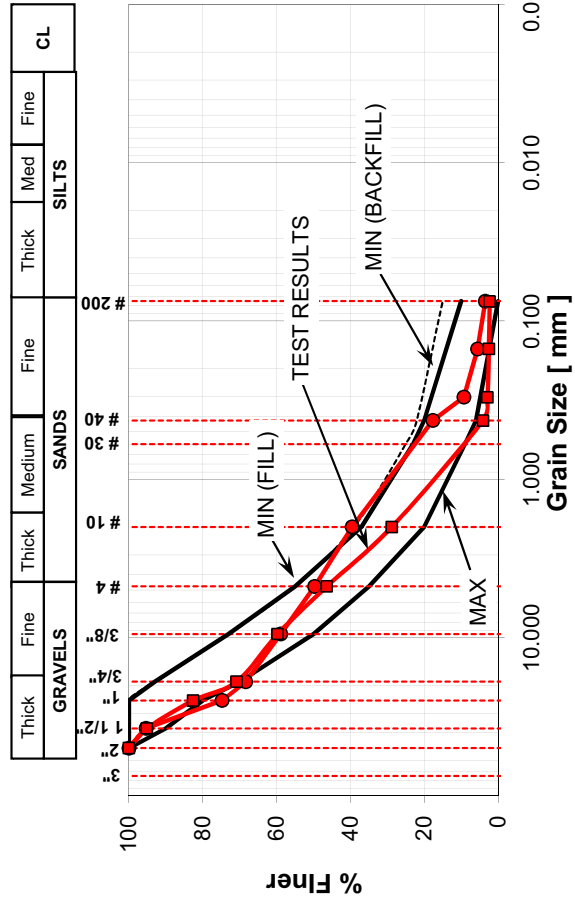
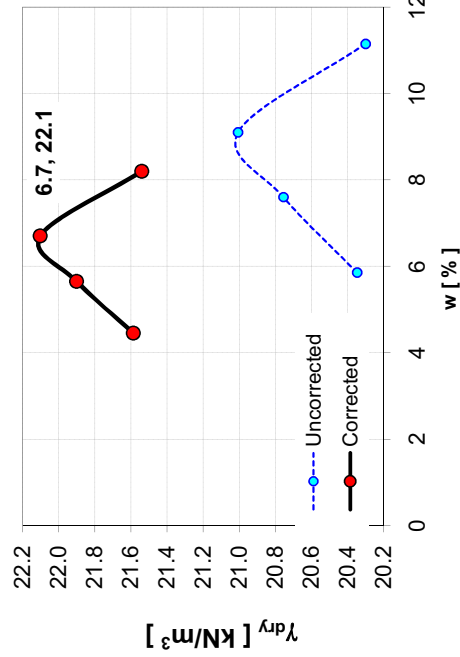
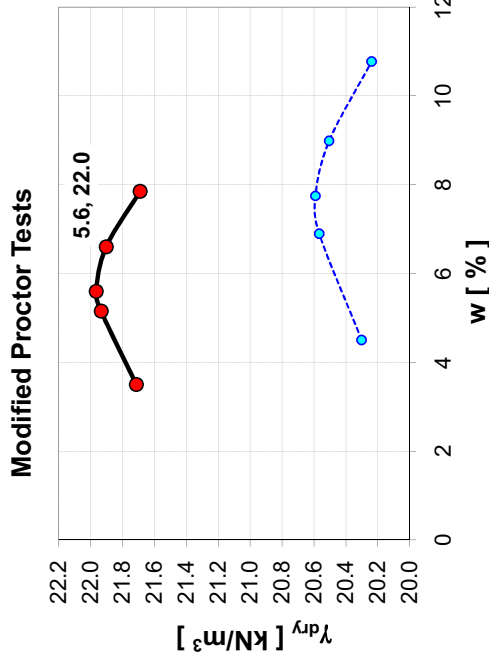


Table 2.5-44 {Category 1 Structural Fill and Backfill Properties}

SI Units

Parameter	Category 1		Category 1 Backfill ²	
	Structural Fill ¹	Backfill ²		
Grain Size Analysis	% Gravel	[%]	57.0	57.0
	% Sands	[%]	37.7	37.7
	% Fines	[%]	7.6	7.6
Mass (in 1 m ³)	Solids	[kg]	198	188
	Water	[kg]	12	11
	Total	[kg]	210	199
Moisture Content	w	[%]	6.1	6.1
	S	[%]	88.3	73.2
Specific Gravity	SG	[]	2.6	2.6
	γ_{dry}	[N/m ³]	20.9	19.8
Unit Weight	γ_{moist}	[N/m ³]	22.2	21.0
	γ_{sat}	[N/m ³]	22.7	22.0



¹ 95% Modified Proctor ² 90% Modified Proctor

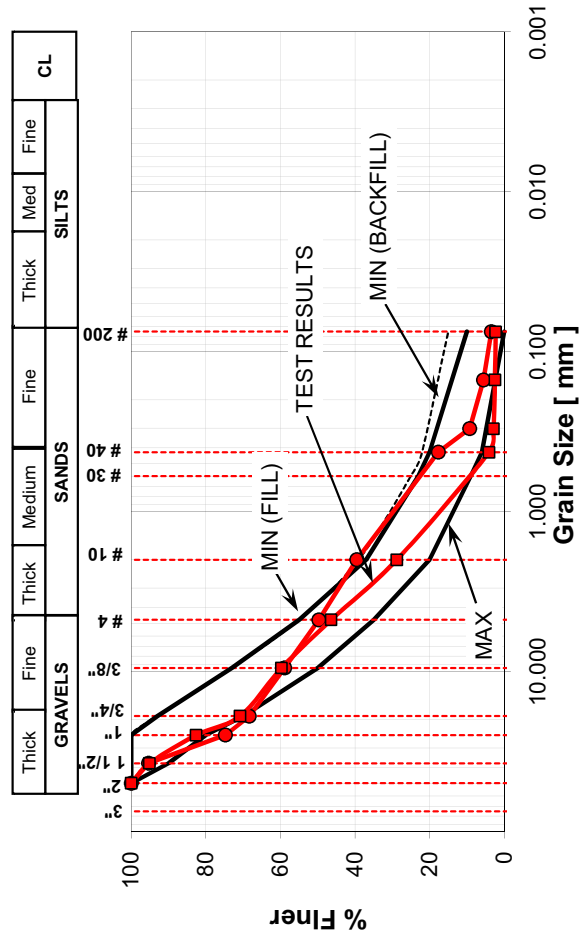


Table 2.5-45 {Recommended Values Of Index Properties}

English Units

Unit	USCS or URCS	Water Content (%)	Unit Weight (pcf)			Observations
			Dry	Moist	Sat	
Glacial Overburden	SW	11.0	109	121	144	-URCS Classification: (Weathering, Strength, Discontinuity, Weight) NA: Not Applicable
Mahantango Formation	ABAA	0.5	169	170	170	
Category 1 Granular Fill	SW	6.1	133	141	144	
Category 1 Granular Backfill	SW	6.1	126	134	140	
Concrete Fill	NA	NA	NA	150	NA	

Table 2.5-45—{Recommended Values Of Index Properties}

SI Units

Unit	USCS or URCS	Water Content (%)	Unit Weight (kN/m ³)			Observations
			Dry	Moist	Sat	
Glacial Overburden	SW	11.0	17.1	19.0	22.7	-URCS Classification: (Weathering, Strength, Discontinuity, Weight) NA: Not Applicable
Mahantango Formation	ABAA	0.5	26.6	26.7	26.7	
Category 1 Granular Fill	SW	6.1	20.9	22.2	22.7	
Category 1 Granular Backfill	SW	6.1	19.8	21.1	22.2	
Concrete Fill	NA	NA	NA	23.6	NA	

Table 2.5-46 {Rock Mass Rating For Mahantango Formation}

English Units

Item	Value	Rating
Unconfined Compressive Strength (ksf)	1040	12
Rock Quality Designation (%)	83	17
Spacing of Discontinuities (m)	>0.61	20
Condition of Discontinuities	Slightly Rough Weathered Walls	25
Groundwater Conditions	Damp, less than 0.35 cf/min	10
Adjustment for Orientation	Favorable	-2
Total Rating		82
Type of Rock	Very Good Rock	I
Equivalent Cohesion (ksf)	7.3	
Equivalent Friction (°)	40.0	

Table 2.5-46—{Rock Mass Rating For Mahantango Formation}

SI Units

Item	Value	Rating
Unconfined Compressive Strength (ksf)	50	12
Rock Quality Designation (%)	83	17
Spacing of Discontinuities (m)	>2	20
Condition of Discontinuities	Slightly Rough Weathered Walls	25
Groundwater Conditions	Damp, less than 10 l/min	10
Adjustment for Orientation	Favorable	-2
Total Rating		82
Type of Rock	Very Good Rock	I
Equivalent Cohesion (kPa)	7.3	
Equivalent Friction (°)	40.0	

Table 2.5-47 {Recommended Values For Strength Properties}

English Units

Formation	SPT	c [ksf]	ϕ [°]	q_u [ksf]	Observations
Glacial Overburden	20	0	32.0	NA	<ul style="list-style-type: none"> • Friction obtained from SPT Correlation for Dense Sands and Gravels (Peck, 1974) • q_u determined from Unconfined Compressive Test • For the Mahantango Formation equivalent cohesion and friction based on Rock Mass Rating (Bieniawski, 1989)- Concrete strength consistent with $V_s = 6800$ fps • Friction for granular fill based on common practice and conservatism • NM: Not Measured • NA: Not Applicable
Mahantango Formation	NA	7.3	40.0	1050	
Category 1 Granular Fill	NM	0.0	35.0	NA	
Category 1 Granular Backfill	NM	0.0	35.0	NA	
Concrete Fill	f'c = 5000				

Table 2.5-47—{Recommended Values For Strength Properties}

SI Units

Formation	SPT	c [kPa]	ϕ [°]	q_u [kPa]	Observations
Glacial Overburden	20	0	32.0	NA	<ul style="list-style-type: none"> • Friction obtained from SPT Correlation for Dense Sands and Gravels (Peck, 1974) • q_u determined from Unconfined Compressive Test • For the Mahantango Formation equivalent cohesion and friction based on Rock Mass Rating (Bieniawski, 1989)- Concrete strength consistent with $V_s = 6800$ fps • Friction for granular fill based on common practice and conservatism • NM: Not Measured • NA: Not Applicable
Mahantango Formation	NA	350	40.0	50270	
Category 1 Granular Fill	NM	0.0	35.0	NA	
Category 1 Granular Backfill	NM	0.0	35.0	NA	
Concrete Fill	f'c = 34450				

Table 2.5-48 {Recommended Values For Hydraulic Conductivity}

English Units

Formation	K (Laboratory) (fps)	K (Field) (fps)	K (Recommended) (fps)	Observations
Glacial Overburden	3.6E-06	1.2E-03	1.2E-03	NM: Not Measured Fill and Compacted Fill recommendation based on typical values for clean sands and gravels (Terzaghi, Peck 1967, 1996)
Mahantango Formation	NM	2.0E-05	2.0E-05	
Category 1 Granular Fill	NM	NM	3.3E-03	
Category 1 Granular Backfill	NM	NM	3.3E-03	
Concrete Fill	NM	NM	3.3E-12	

Table 2.5-48—{Recommended Values For Hydraulic Conductivity}

SI Units

Formation	K (Laboratory) (cm/s)	K (Field) (cm/s)	K (Recommended) (cm/s)	Observations
Glacial Overburden	3.6E-06	1.2E-03	1.2E-03	NM: Not Measured Fill and Compacted Fill recommendation based on typical values for clean sands and gravels (Terzaghi, Peck 1967, 1996)
Mahantango Formation	NM	2.0E-05	2.0E-05	
Category 1 Granular Fill	NM	NM	3.3E-03	
Category 1 Granular Backfill	NM	NM	3.3E-03	
Concrete Fill	NM	NM	3.3E-12	

Table 2.5-49 {Recommended Values For Elastic Modulus}

English Units

Formation	E (ksf)						Observations
	Method 1	Method 2	Method 3	Method 4	Method 5	Recomm	
Glacial Overburden	2000	3600	2000	-	-	2000	Method 1: ASCE Typical Method 2: ASCE N Correlation Method 3: AASHTO Typical Method 4: Rock Mass Rating Method 5: Concrete strength ACI318
Mahantango Formation	-	-	523000	376000	-	376000	
Category 1 Granular Fill	-	-	2000	-	-	2000	
Category 1 Granular Backfill	-	-	2000	-	-	2000	
Concrete Fill	-	-	-	-	500000	500000	

Table 2.5-49—{Recommended Values For Elastic Modulus}

SI Units

Formation	E (MPa)						Observations
	Method 1	Method 2	Method 3	Method 4	Method 5	Recomm	
Glacial Overburden	96	172	96	-	-	96	Method 1: ASCE Typical Method 2: ASCE N Correlation Method 3: AASHTO Typical Method 4: Rock Mass Rating Method 5: Concrete strength ACI318
Mahantango Formation	-	-	25000	18000	-	18000	
Category 1 Granular Fill	-	-	96	-	-	96	
Category 1 Granular Backfill	-	-	96	-	-	96	
Concrete Fill	-	-	-	-	23900	23900	

Table 2.5-50 {Recommended Values For Static Elastic Properties}

English Units

Formation	E (ksf)	ν	G (ksf)	Observations
Glacial Overburden	2000	0.40	710	Elastic Properties obtained from field measurements and published values References:- Peck, 1974 - AASHTO, 1998
Mahantango Formation	3.76E+05	0.30	144620	
Category 1 Granular Fill	2000	0.35	740	
Category 1 Granular Backfill	2000	0.35	740	
Concrete Fill	500000	0.20	208300	

Table 2.5-50—{Recommended Values For Static Elastic Properties}

SI Units

Formation	E (MPa)	ν	G (MPa)	Observations
Glacial Overburden	100	0.40	36	Elastic Properties obtained from field measurements and published values References:- Peck, 1974- AASHTO, 1998
Mahantango Formation	18000	0.30	6923	
Category 1 Granular Fill	100	0.35	40	
Category 1 Granular Backfill	100	0.35	37	
Concrete Fill	23940	0.20	9975	

Table 2.5-51 {Recommended Values For Low Strain Dynamic Elastic Properties At Center Of Nuclear Island Footprint}
English Units

Unit	Depth (ft) (')	V _s (fps)	V _p (fps)	P (p _m cf)	v	G _{max} (ksf)	E _{max} (ksf)	DS _o (%)	Observations
SOILS	Glacial Overburden 1	1150	2550	126	0.37	5180	14220	1.00	$G_{max} = \rho V_s^2$ $E_{max} = 2(1 + \nu)G_s$ - Velocities determined fro, best estimate soil profile - Poisson's Ratio determined from velocity ratio squared - Initial Shear Damping (DS _o): determined from "Free-Free" Testing for Rocks, and RCTS Testing for Overburden
	Glacial Overburden 2	2300	7000	126	0.44	20700	59590	1.00	
ROCK FORMATIONS	Mahantango Formation Layer 1	6800	12900	170	0.31	244120	638430	0.80	
	Mahantango Formation Layer 2	7150	15300	170	0.36	269900	734290	0.80	
	Mahantango Formation Layer 3	7600	16100	170	0.36	304940	827390	0.70	
	Mahantango Formation Layer 4	8500	16100	170	0.31	381440	996910	0.70	
	Mahantango Formation Layer 5	8950	16750	170	0.30	422900	1099710	0.70	
	Mahantango Formation Layer 6	9600	16850	170	0.26	486560	1225840	0.70	
FILLS	Category 1 Granular Fill/Backfill	0.0	1250	140	0.35	1570	4240	1.00	NA: Not Applicable
		10.0	1670	140	0.35	2780	7510	1.00	
	> 20.0	1000	2100	140	0.35	4350	11770	1.00	
	Concrete	7240	11820	150	0.20	244180	585920	0.80	

Table 2.5-51—{Recommended Values For Low Strain Dynamic Elastic Properties At Center Of Nuclear Island Footprint}

SI Units

Unit	Depth (m) (')	V _s (m/s)	V _p (m/s)	ρ (kg/m ³)	ν	G _{max} (MPa)	E _{max} (MPa)	DS _o (%)	Observations
SOILS	Galcial Overburden 1	351	777	2020	0.37	250	690	1.00	$G_{max} = \rho V_s^2$ $E_{max} = 2(1 + \nu)G_s$ - Velocities determined fro. best estimate soil profile - Poisson's Ration determined from velocity ratio squared - Initial Shear Damping (DSo): determined from "Free-Free" Testing for Rocks, and RCTS Testing for Overburden
	Glacial Overburden 2	701	2134	2020	0.44	990	2850	1.00	
ROCK FORMATIONS	Mahantango Formation Layer 1	2073	3933	2720	0.31	11690	30570	0.80	
	Mahantango Formation Layer 2	2180	4665	2720	0.36	12930	35180	0.80	
	Mahantango Formation Layer 3	2317	4909	2720	0.36	14600	39610	0.70	
	Mahantango Formation Layer 4	2729	5107	2720	0.30	20250	52660	0.70	
	Mahantango Formation Layer 5	2927	5137	2720	0.26	23300	58700	0.70	
	Mahantango Formation Layer 6	2927	5137	2720	0.26	23300	58700	0.70	
FILLS	Category 1 Granular Fill/Backfill	183	381	2240	0.35	70	190	1.00	
		244	509	2240	0.35	130	350	1.00	
	Concrete	305	640	2240	0.35	210	570	1.00	NA: Not Applicable
	NA	2207	3604	2400	0.20	11690	28050	0.80	

Table 2.5-52 {Peak Ground Acceleration from FIRS Study}

English Units

Structure		Foundation		Base to Rock (ft) ⁽²⁾	Base to OGS (ft) ⁽³⁾	Eng Fill ⁴ (ft)	Contact Soil ⁵	Hor PGA (g)	Ver PGA (g)
		Depth (ft)	El. ¹ (ft msl)						
Nuclear Island ⁽⁶⁾	NI	36.0	638.0	12.6	-28.0	12.6	C-M	0.21	0.18
ESWES Cooling Towers (URB)	URB1	22.0	652.0	3.0	-23.0	3.0	C	0.21	0.18
	URB2	22.0	652.0	4.5	-17.0	4.5	C	0.21	0.18
	URB3	22.0	652.0	58.5	-5.5	58.5	EF	0.21	0.21
	URB4	22.0	652.0	41.0	-5.5	41.0	EF	0.24	0.25
Emergency Power Building (UBP)	UBP12 ⁽⁷⁾	5.0	669.0	27.0	-3.0	27.0	C	0.21	0.19
	UBP12	5.0	669.0	27.0	-3.0	27.0	EF	0.30	0.33
	UBP34	5.0	669.0	67.0	12.0	67.0	EF	0.21	0.22
ESWEMS Pumphouse		33.0	641.0	7.0	-40.0	7.0	C	0.21	0.18

¹ Plant Grade El. (ft msl) 674

² Distance between rock and base of foundation

³ Distance between foundation base original ground surface

⁴ Engineered fill (Concrete for NI and soil for other facilities)

⁵ Concrete (C), Mahantango Formation (M), Glacial Overburden (GO), Engineered Fill (EF)

⁶ Depth given for containment building, other NI facilities have 41.3 ft

⁷ Concrete fill is the preferred configuration for this facility

Table 2.5-52—{Peak Ground Acceleration from FIRS Study}

SI Units

Structure		Foundation		Base to Rock (m) ⁽²⁾	Base to OGS (m) ⁽³⁾	Eng Fill ⁴ (m)	Contact Soil ⁵	Hor PGA (g)	Ver PGA (g)
		Depth (m)	El. ¹ (m msl)						
Nuclear Island ⁽⁶⁾	NI	11.0	194.5	3.8	-8.5	3.8	C-M	0.21	0.18
ESWES Cooling Towers (URB)	URB1	6.7	198.8	0.9	-7.0	0.9	C	0.21	0.18
	URB2	6.7	198.8	1.4	-5.2	1.4	C	0.21	0.18
	URB3	6.7	198.8	17.8	-1.7	17.8	EF	0.21	0.21
	URB4	6.7	198.8	12.5	-1.7	12.5	EF	0.24	0.25
Emergency Power Building (UBP)	UBP12 ⁽⁷⁾	1.5	204.0	8.2	-0.9	8.2	C	0.21	0.19
	UBP12	1.5	204.0	8.2	-0.9	8.2	S	0.30	0.33
	UBP34	1.5	204.0	20.4	3.7	20.4	EF	0.21	0.22
ESWEMS Pumphouse		10.1	195.4	2.1	-12.2	2.1	C	0.21	0.18

¹ Plant Grade El. (m msl) 205

² Distance between rock and base of foundation

³ Distance between foundation base original ground surface

⁴ Engineered fill (Concrete for NI and soil for other facilities)

⁵ Concrete (C), Mahantango Formation (M), Glacial Overburden (GO), Engineered Fill (EF)

⁶ Depth given for containment building, other NI facilities have 12.6 m

⁷ Concrete fill is the preferred configuration for this facility

Table 2.5-53 {Soil Conditions For The U.S. EPR Standard Plant}

English Units

Soil Case No.	Seismic Control Motion Applied	Soil Profile (Half Space or Layered)	Shear-wave Velocity of Soil ⁽¹⁾ (fps)
1u	EUR Soft	Half-space	700
2u (A and B)	EUR Soft and Medium	Half-space	1,640
3u	EUR Medium	Half-space	2,625
4u (A and B)	EUR Medium and Hard	Half-space	3,937
5u	EUR Hard	Half-space	5,249
5a	EUR Hard	Half-space	13,123
1n2u	EUR Soft	Linear gradient within a 100 ft layer over a half-space	820 to 1,640
2sn4u	EUR Medium	49 ft uniform layer over a half- space	1,640/3,937
2n3u	EUR Medium	Linear gradient within a 200 ft layer over a half-space	1,640 to 2,625
3r3u	EUR Medium	20 ft uniform layer over 46 ft stiffer layer followed by soil half-space	2,625/5,249/2,625

⁽¹⁾ Shear wave velocities of generic soil profiles are taken as strain-compatible properties

Table 2.5-53—{Soil Conditions For The U.S. EPR Standard Plant}

SI Units

Soil Case No.	Seismic Control Motion Applied	Soil Profile (Half Space or Layered)	Shear-wave Velocity of Soil ⁽¹⁾ (m/s)
1u	EUR Soft	Half-space	215
2u (A and B)	EUR Soft and Medium	Half-space	500
3u	EUR Medium	Half-space	800
4u (A and B)	EUR Medium and Hard	Half-space	1,200
5u	EUR Hard	Half-space	1,600
5a	EUR Hard	Half-space	4,000
1n2u	EUR Soft	Linear gradient within a 30 m layer over a half-space	250 to 500
2sn4u	EUR Medium	15 m uniform layer over a half- space	500/1,200
2n3u	EUR Medium	Linear gradient within a 60 m layer over a half-space	500 to 800
3r3u	EUR Medium	6 m uniform layer over 14 m stiffer layer followed by soil half-space	800/1,600/800

⁽¹⁾ Shear wave velocities of generic soil profiles are taken as strain-compatible properties

Table 2.5-54 {Soil Conditions For The U.S. EPR Standard Plant}

English Units

Site Class		Shear Wave Velocity (mean) (fps)	Location of GMRS	Geotechnical Analysis Requirements
Rock Site (Rock is at the ground surface at the site)	Hard and Firm Rock Site	$V_s > 3,500$	At top of Rock	Static and dynamic bearing capacity to be verified; no time-dependent settlement analysis required.
	Soft Rock Site	$2,400 < V_s < 3,500$	At top of Rock	Static and dynamic bearing capacity to be verified; no time-dependent settlement analysis required.
Thin Soil Site (Rock is generally within 40 to 60 feet of the ground surface and the EPR Nuclear Island is founded on rock)	Thin Soil Site over Hard or Firm Rock	At depth below Nuclear Island Basemat, $V_s > 3,500$	At Top of Outcropping Rock	Static and dynamic bearing capacity to be verified; no time-dependent settlement analysis required.
	Thin Soil Site over Soft Rock	At depth below Nuclear Island Basemat, $V_s < 3,500$	At Grade Elevation	Static and dynamic bearing capacity to be verified; no time-dependent settlement analysis required.
Soil Sites (Foundation underlain by < 200? of soil for Shallow and > 200? feet for Deep)	Shallow Soil and Deep Soil Sites	$1,000 < V_s < 3,500$ with soil below Nuclear Island Basemat of unlimited thickness	At free-field soil surface	Static and dynamic bearing capacity analysis required; requires verification that time-dependent settlement falls within EPR envelope.

Table 2.5-54—{Soil Conditions For The U.S. EPR Standard Plant}

SI Units

Site Class		Shear Wave Velocity (mean) (m/s)	Location of GMRS	Geotechnical Analysis Requirements
Rock Site (Rock is at the ground surface at the site)	Hard and Firm Rock Site	$V_s > 1,070$	At top of Rock	Static and dynamic bearing capacity to be verified; no time-dependent settlement analysis required.
	Soft Rock Site	$730 < V_s < 1,070$	At top of Rock	Static and dynamic bearing capacity to be verified; no time-dependent settlement analysis required.
Thin Soil Site (Rock is generally within 40 to 60 feet of the ground surface and the EPR Nuclear Island is founded on rock)	Thin Soil Site over Hard or Firm Rock	At depth below Nuclear Island Basemat, $V_s > 3,500$	At Top of Outcropping Rock	Static and dynamic bearing capacity to be verified; no time-dependent settlement analysis required.
	Thin Soil Site over Soft Rock	At depth below Nuclear Island Basemat, $V_s < 1,070$	At Grade Elevation	Static and dynamic bearing capacity to be verified; no time-dependent settlement analysis required.
Soil Sites (Foundation underlain by < 200? of soil for Shallow and > 200? feet for Deep)	Shallow Soil and Deep Soil Sites	$305 < V_s < 1,070$ with soil below Nuclear Island Basemat of unlimited thickness	At free-field soil surface	Static and dynamic bearing capacity analysis required; requires verification that time-dependent settlement falls within EPR envelope.

Table 2.5-55 {Foundation Elevations}
 English Units
 (Page 1 of 2)

Structure	Foundation		Shape	Base to Rock (ft) ²	Base to OGS (ft) ³	Fill Thickness		Contact Soil ⁵	Area (ft ²)	Contact Pressure (ksf) ⁶		
	Depth (ft)	EI. ¹ (ft msl)				In-Situ	Eng ⁴			Average Static	Maximum Static	Dynamic
Nuclear Island ⁽⁷⁾	36.0	638.0		12.6	-28.0	0.0	12.6	C-M	80,170	14.7	22.0	25.0
Nuclear Auxiliary Building	41.5	632.5		19.5	-27.5	0.0	19.5	EF	12,510	9.8	22.0	25.0
Rad Waste Building	36.0	638.0		41.0	-19.5	0.0	41.0	EF	16,880	4.3	22.0	25.0
EWSW Cooling Towers	22.0	652.0		3.0	-23.0	0.0	3.0	C	22,120	5.4	22.0	25.0
	22.0	652.0		4.5	-17.0	0.0	4.5	C	22,120	5.4	22.0	25.0
	22.0	652.0		58.5	-5.5	0.0	58.5	EF	22,120	5.4	22.0	25.0
	22.0	652.0		41.0	-5.5	0.0	41.0	EF	22,120	5.4	22.0	25.0
Emergency Power Building (UBP)	5.0	669.0		27.0	-3.0	0.0	27.0	C	12,650	3.2	22.0	25.0
	5.0	669.0		67.0	12.0	0.0	67.0	EF	12,650	3.2	22.0	25.0

Table 2.5-55 {Foundation Elevations}

English Units
(Page 2 of 2)

Structure	Foundation		Shape	Base to Rock (ft) ²	Base to OGS (ft) ³	Fill Thickness		Contact Soil ⁵	Area (ft ²)	Contact Pressure (ksf) ⁶		
	Depth (ft)	EI. ¹ (ft msl)				In-Situ	Eng ⁴			Average Static	Maximum Static	Dynamic
Turbine Building	UMA	33.0	641.0		33.0	-27.0	0.0	33.0	100,000	4.2	10.0	12.0

¹ Plant Grade El. [ft msl] 674

² Distance between rock and base of foundation

³ Distance between foundation base original ground surface

⁴ Engineered fill (Concrete for NI and soil for other facilities)

⁵ Concrete (C), Mahantango Formation (M), Glacial Overburden (GO), Engineered Fill (EF)

⁶ As prescribed by the U.S. EPR FSAR and Foundation Interface Document

⁷ Depth given for containment building, other NI facilities have 41.3 ft

Table 2.5-55—{Foundation Elevations}

SI Units
(Page 1 of 2)

Structure	Foundation		Shape	Base to Rock (m) ²	Base to OGS (m) ³	Fill Thickness		Contact Soil ⁵	Area (m ²)	Contact Pressure (kPa) ⁶		
	Depth (m)	EI. ¹ (m msl)				In-Situ	Eng ⁴			Average Static	Maximum Static	Dynamic
Nuclear Island	11.0	194.5		3.8	-8.5	0.0	3.8	C-M	7,452	700	1,050	1,200
Nuclear Auxiliary Building	12.7	192.8		5.9	-8.4	0.0	5.9	EF	1,163	470	1,050	1,200
Rad Waste Building	11.0	194.5		12.5	-5.9	0.0	12.5	EF	1,569	210	1,050	1,200
ESWS Cooling Towers	6.7	198.8		0.9	-7.0	0.0	0.9	C	2,056	260	1,050	1,200
	6.7	198.8		1.4	-5.2	0.0	1.4	C	2,056	260	1,050	1,200
	6.7	198.8		17.8	-1.7	0.0	17.8	EF	2,056	260	1,050	1,200
	6.7	198.8		12.5	-1.7	0.0	12.5	EF	2,056	260	1,050	1,200
Emergency Power Building (UBP)	1.5	204.0		8.2	-0.9	0.0	8.2	C	1,176	150	1,050	1,200
	1.5	204.0		20.4	3.7	0.0	20.4	EF	1,176	150	1,050	1,200

Table 2.5-55—{Foundation Elevations}

SI Units
(Page 2 of 2)

Structure	Foundation		Shape	Base to Rock (m) ²	Base to OGS (m) ³	Fill Thickness		Contact Soil ⁵	Area (m ²)	Contact Pressure (kPa) ⁶		
	Depth (m)	EI. ¹ (m msl)				In-Situ	Eng ⁴			Average Static	Maximum Static	Dynamic
Turbine Building	UMA	10.1	195.4		10.1	-8.2	0.0	10.1	9,295	200	480	570

¹ Plant Grade EI. [m msl] 205.5

² Distance between rock and base of foundation

³ Distance between foundation base original ground surface

⁴ Engineered fill (Concrete for NI and soil for other facilities)

⁵ Concrete (C), Mahantango Formation (M), Glacial Overburden (GO), Engineered Fill (EF)

⁶ As prescribed by the U.S. EPR FSAR and Foundation Interface Document

Table 2.5-56 {Earth Pressure Coefficients}

Formation	ϕ (°)	k_a	k_p	k_o	k_{AE}	k_{PE}	Observations
Glacial Overburden	35	0.27	3.69	0.43	0.58	8.12	NA - Not Applicable ka - Active Earth Pressure Coefficient kp - Passive Earth Pressure Coefficient ko - At Rest Earth Pressure Coefficient
Mahantango Formation	NA	NA	NA	NA	NA	NA	
Granular Fill/Backfill	35	0.27	3.69	0.43	0.58	8.12	
Concrete Fill	NA	NA	NA	NA	NA	NA	

Table 2.5-57 {Bearing Capacity (Failure Controlled)}
English Units

Structure		Foundation		Footprint Shape	Simplified		Contact Surface ²	Bearing Capacity (ksf)	
		Depth (ft)	El. ¹ (ft msl)		B (ft)	L (ft)		Ultimate	Allowable FS=3.0
Nuclear Island	NI	36.0	638.0		284	284	C-M	720.0	240.0
Nuclear Auxiliary Building	UKA	41.5	632.5		105	120	C	239.6	79.9
Radioactive Waste Building	UKS	36.0	638.0		130	130	C	245.3	81.8
ESWS Cooling Towers	URB1	22.0	652.0		124	180	C	720.0	240.0
	URB2	22.0	652.0		124	180	C	720.0	240.0
	URB3	22.0	652.0		124	180	EF	222.8	74.3
	URB4	22.0	652.0		124	180	EF	222.8	74.3
Emergency Power Generation Building	UBP1	5.0	669.0		90	140	C	720.0	240.0
	UBP2	5.0	669.0		90	140	EF	139.1	46.4
Turbine Building	UMA	33.0	641.0		300	330	EF	436.6	145.5
10 x 10' Footing on Fill (3' Deep)		3.0	671.0		10	10	EF	22.9	7.6

¹ Plant Grade El. (ft msl) 674

² Concrete (C), Mahantango Formation (M), Glacial Overburden (GO), Engineered Fill (EF)

Table 2.5-57—{Bearing Capacity (Failure Controlled)}

SI Units

Structure		Foundation		Footprint Shape	Simplified		Contact Surface ²	Bearing Capacity (kPa)	
		Depth (m)	El. ¹ (m msl)		B (m)	L (m)		Ultimate	Allowable FS=3.0
Nuclear Island	NI	11.0	194.5		87	87	C-M	34,470	11,490
Nuclear Auxiliary Building	UKA	12.7	192.8		32	37	C	11,470	3,820
Radioactive Waste Building	UKS	11.0	194.5		40	40	C	11,750	3,920
ESWS Cooling Towers	URB1	6.7	198.8		38	55	C	34,470	11,490
	URB2	6.7	198.8		38	55	C	34,470	11,490
	URB3	6.7	198.8		38	55	EF	10,670	3,560
	URB4	6.7	198.8		38	55	EF	10,670	3,560
Emergency Power Generation Building	UBP1	1.5	204.0		27	43	C	34,470	11,490
	UBP2	1.5	204.0		27	43	EF	6,660	2,220
Turbine Building	UMA	10.1	195.4		91	101	EF	20,900	6,970
10 x 10' Footing on Fill (3' Deep)		0.9	204.6		3	3	EF	1,100	370

¹ Plant Grade El. [m msl] 205

² Concrete (C), Mahantango Formation (M), Glacial Overburden (GO), Engineered Fill (EF)

Table 2.5-58 {Elastic Settlement Analysis By Simplified Approximations}

English Units

Structure		Foundation		Contact Surface ²	Service Load (ksf)	Settlement Approximation (in)					
		Depth (ft)	El. ¹ (ft msl)			Janbu		Perloff		Kay & Cav.	
						Center	Edge	Center	Edge	Center	Edge
Nuclear Island	NI	36.0	638.0	C-M	14.7	0.0	-	0.0	0.0	0.0	0.0
Nuclear Auxiliary Building	UKA	41.5	632.5	C	9.8	0.3	-	1.1	0.4	0.4	0.2
Radioactive Waste Building	UKS	36.0	638.0	C	4.3	0.3	-	0.9	0.4	0.4	0.2
ESWS Cooling Towers	URB1	22.0	652.0	C	5.4	0.0	-	0.0	0.0	0.0	0.0
	URB2	22.0	652.0	C	5.4	0.0	-	0.0	0.0	0.0	0.0
	URB3	22.0	652.0	EF	5.4	0.6	-	1.8	0.7	0.9	0.4
	URB4	22.0	652.0	EF	5.4	0.4	-	1.1	0.4	0.6	0.3
Emergency Power Generation	UBP1	5.0	669.0	C	3.2	0.0	-	0.0	0.0	0.0	0.0
	UBP2	5.0	669.0	EF	3.2	0.4	-	0.9	0.4	0.7	0.3
Turbine Building	UMA	33.0	641.0	EF	4.2	0.4	-	0.7	0.3	0.3	0.1
10 x 10' Footing on Fill (3' Deep)		3.0	671.0	EF	2.0	0.0	-	0.1	0.0	0.1	0.0

¹ Plant Grade El. (ft msl) 674.0

² Concrete (C), Mahantango Formation (M), Glacial Overburden (GO), Engineered Fill (EF)

Table 2.5-58—{Elastic Settlement Analysis By Simplified Approximations}

SI Units

Structure		Foundation		Contact Surface ²	Service Load (kPa)	Settlement Approximation (in)					
		Depth (m)	El. ¹ (m msl)			Janbu		Perloff		Kay & Cav.	
						Center	Edge	Center	Edge	Center	Edge
Nuclear Island	NI	11.0	194.5	C-M	700	0.0	-	0.1	0.0	0.1	0.0
Nuclear Auxiliary Building	UKA	12.7	192.8	C	470	0.7	-	2.9	1.1	1.1	0.5
Radioactive Waste Building	UKS	11.0	194.5	C	210	0.8	-	2.3	0.9	1.1	0.5
ESWS Cooling Towers	URB1	6.7	198.8	C	260	0.0	-	0.0	0.0	0.0	0.0
	URB2	6.7	198.8	C	260	0.0	-	0.0	0.0	0.0	0.0
	URB3	6.7	198.8	EF	260	1.5	-	4.6	1.9	2.4	1.0
	URB4	6.7	198.8	EF	260	1.0	-	2.8	1.1	1.4	0.6
Emergency Power Generation	UBP1	1.5	204.0	C	150	0.0	-	0.0	0.0	0.0	0.0
	UBP2	1.5	204.0	EF	150	1.1	-	2.4	1.1	1.8	0.7
Turbine Building	UMA	10.1	195.4	EF	200	1.0	-	1.7	0.7	0.7	0.4
10 x 10' Footing on Fill (3' Deep)		0.9	204.6	EF	100	0.1	-	0.2	0.1	0.2	0.1

¹ Plant Grade El. (m msl) 205.5

² Concrete (C), Mahantango Formation (M), Glacial Overburden (GO), Engineered Fill (EF)

Table 2.5-59 {Detailed Elastic Settlement Analysis}

English Units

Structure		Depth (ft)	El. ¹ (ft msl)	Contact Surface	Service Load (ksf)	Settlement	
						Total (in)	Differential (in/50ft)
Nuclear Island ³	NI	36.0	638.0	C-M	14.7	< .5	<.1

1 Plant Grade El. (ft msl) 674.0

2 Concrete (C), Mahantango Formation (M), Glacial Overburden (GO), Engineered Fill (EF)

3 Depth shown for UJA (Containment Building). Depth is 41.5 feet around containment

Table 2.5-59—{Detailed Elastic Settlement Analysis}

SI Units

Structure		Depth (m)	El. ¹ (m msl)	Contact Surface	Service Load (kPa)	Settlement	
						Total (cm)	Differential (cm/100 m)
Nuclear Island ³	NI	11.0	194.5	C-M	700.0	<0.2	<2

1 Plant Grade El. (m msl) 205.5

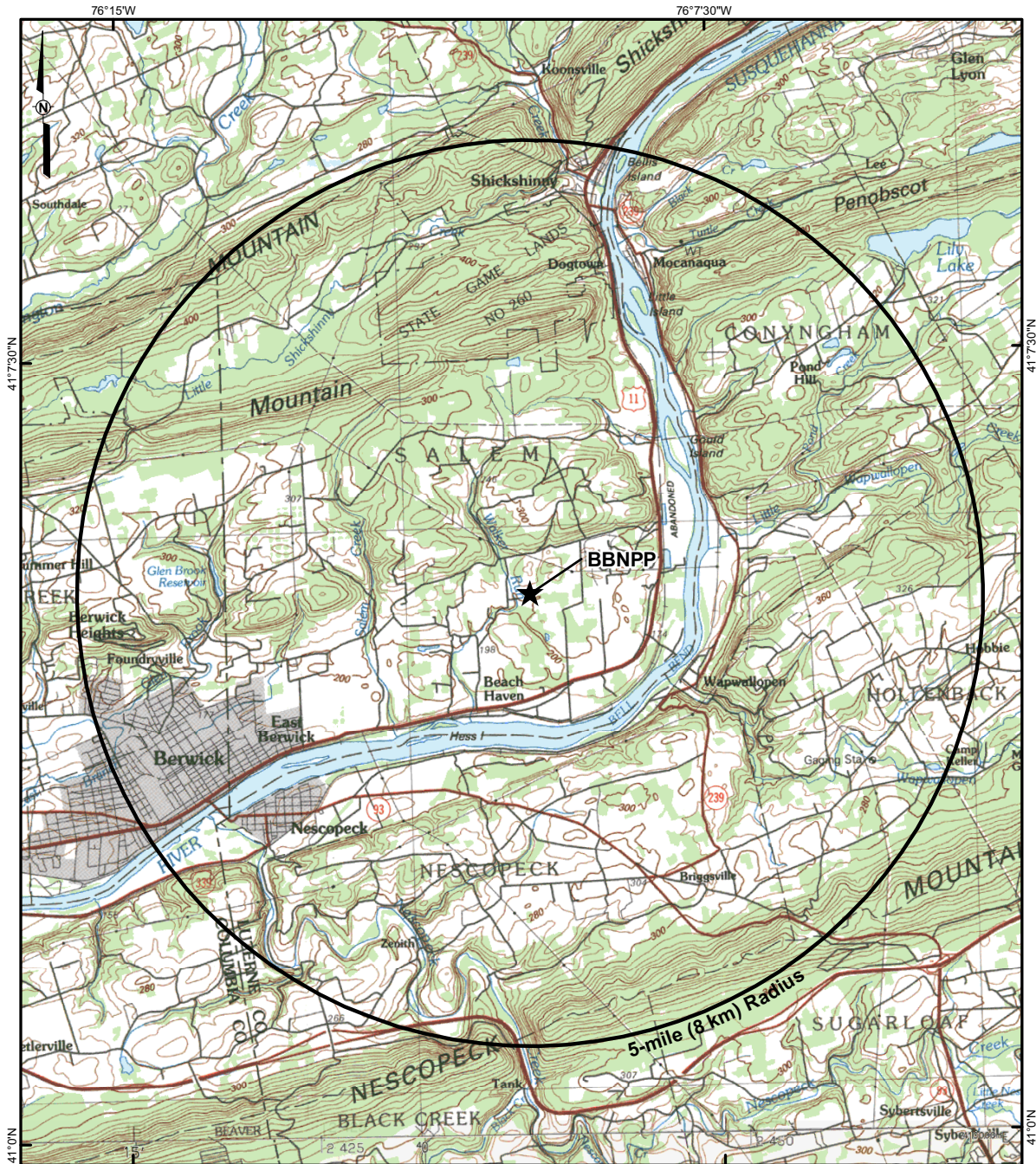
2 Concrete (C), Mahantango Formation (M), Glacial Overburden (GO), Engineered Fill (EF)

3 Depth shown for UJA (Containment Building). Depth is 12.7 m around containment

Table 2.5-60 {Factor Of Safety Against Sliding}

		Circular Failure		Wedge Failure		Observations
		Static	Dynamain	Static	Dynamic	
Permanent Slopes (ESWEMS Retention Pond)	Section 1	5.6	2.9	7.9	3.3	
	Section 2	6.9	2.4	9.2	4.1	
	Section 3	4.4	2.0	5.9	2.2	
	Section 4	5.7	2.1	7.0	2.9	
Temporary Slopes	Section 1	1.3			1.4	Dynamic case not applicable for temporary slopes.
	Section 2	2.5		2.5		
North Slope	Section 1			5.7	1.6	North slope analyzed to examine risk of landslide on-site. Only wedge failure is applicable.

Figure 2.5-1 {Site Region Topographic Map 200-mile (322 km) Radius}



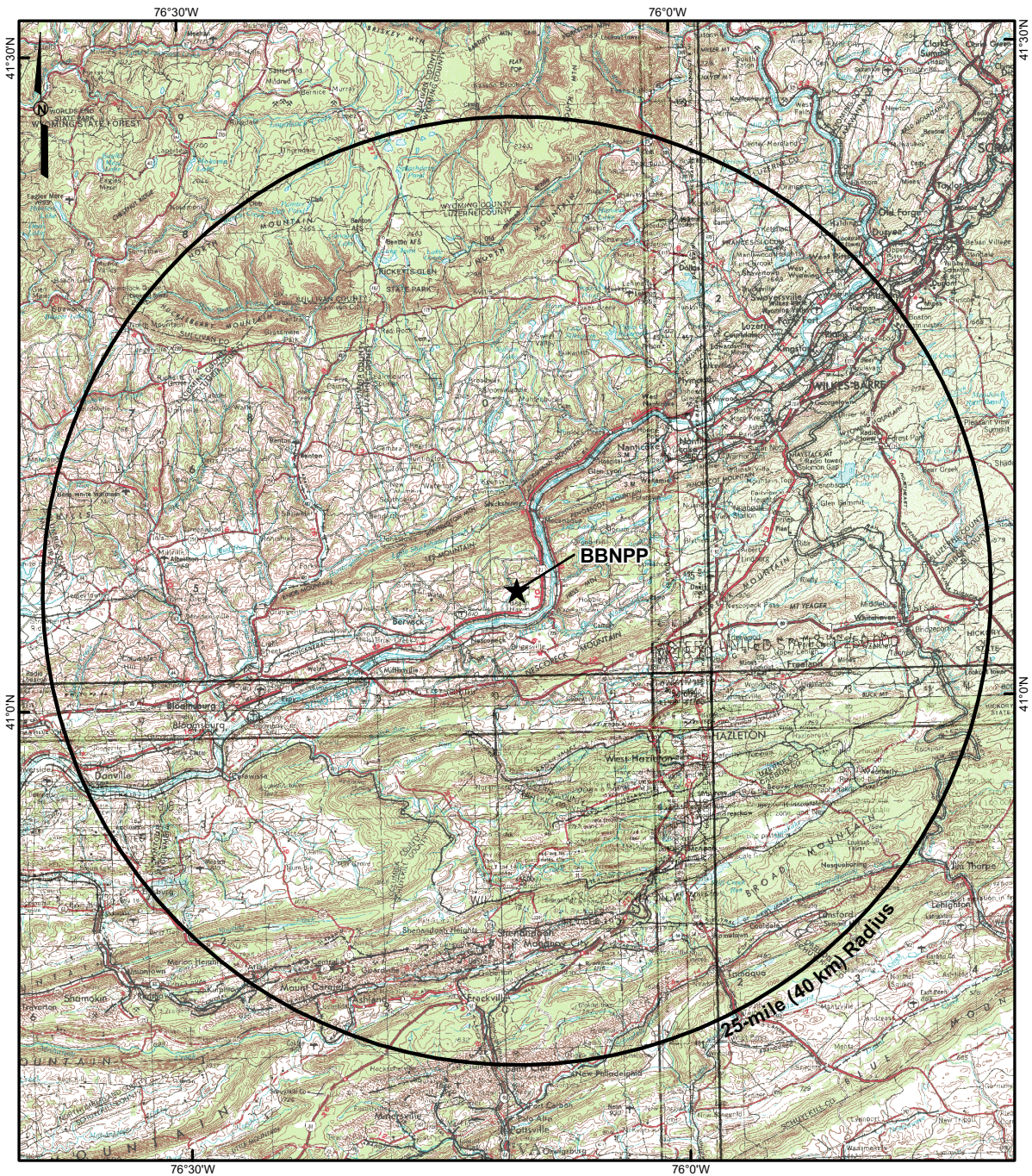
LEGEND

- ★ Center Point of Proposed Bell Bend NPP (BBNPP)
- NPP Reactor 5-mile (8 km) Radius



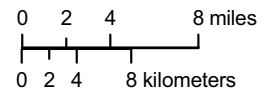
REFERENCE:
• USGS, 1984.

Figure 2.5-2 {Site Vicinity Topographic Map 25-mile (40 km) Radius}



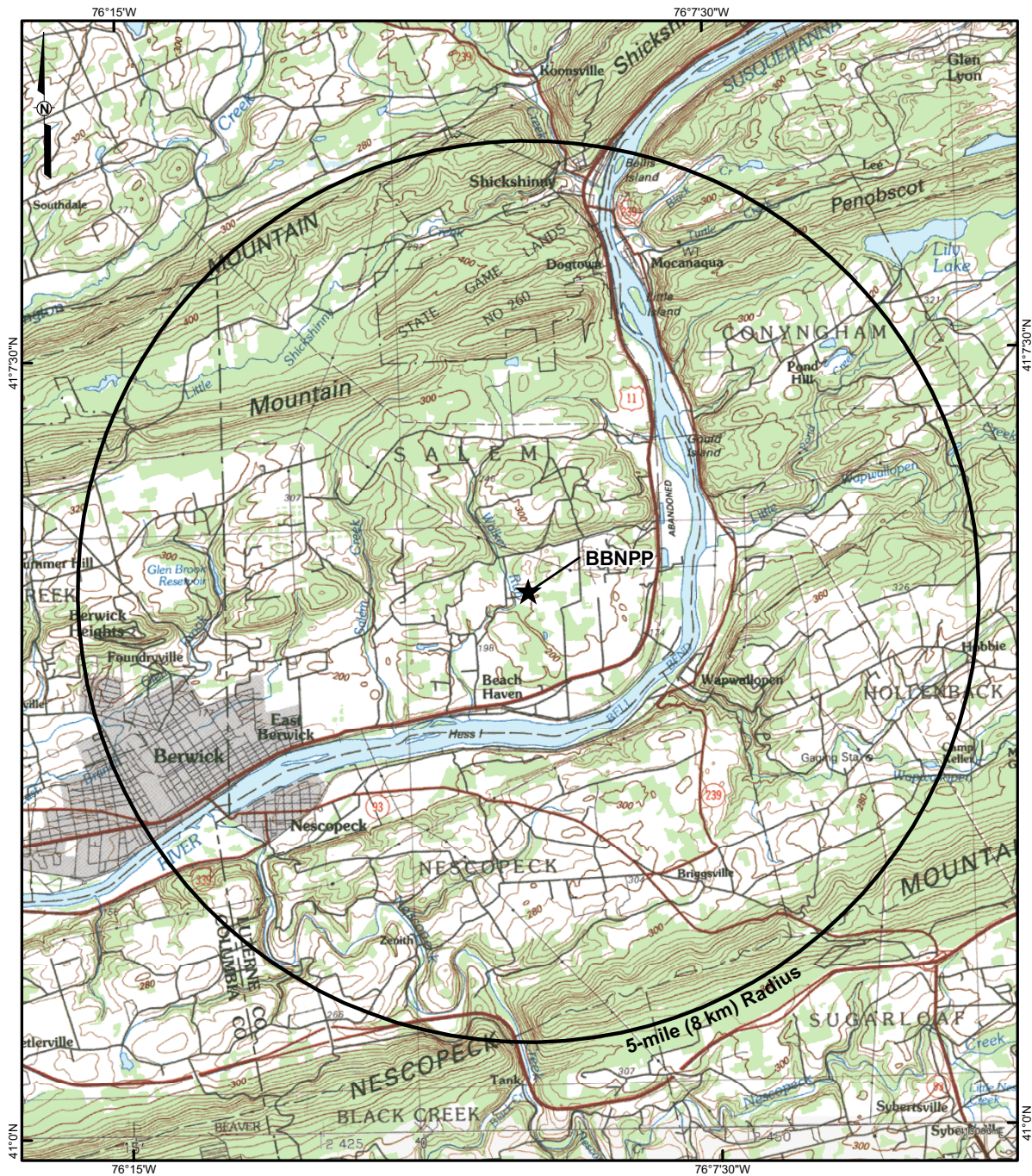
LEGEND

- ★ Center Point of Proposed Bell Bend NPP (BBNPP)
- NPP Reactor 25-mile (40 km) Radius



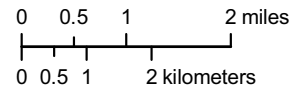
REFERENCE:
 • USGS, 1969; 1974; and 1976.

Figure 2.5-3 {Site Topographic Map 5-Mile (8 km) Radius}



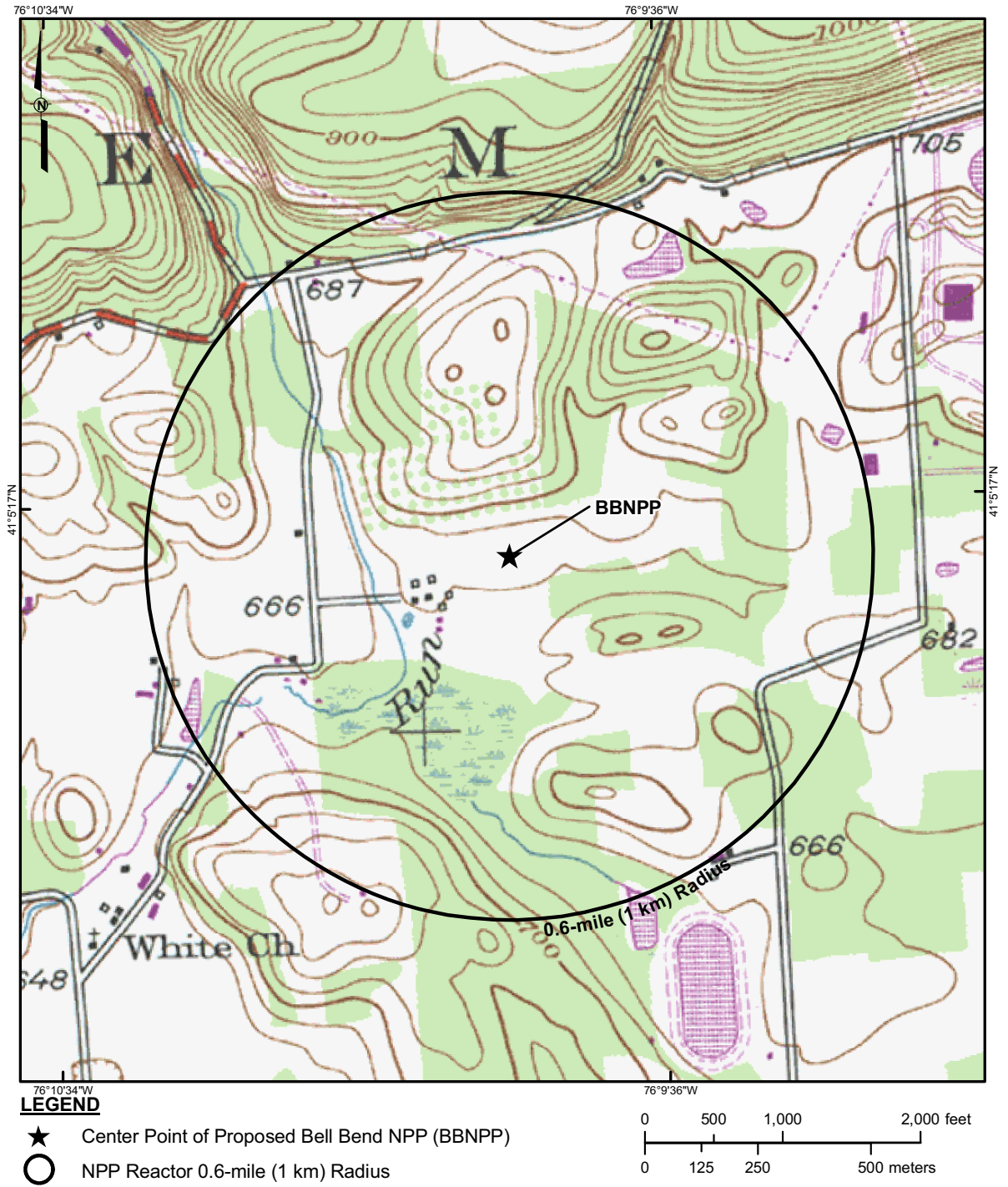
LEGEND

- ★ Center Point of Proposed Bell Bend NPP (BNPP)
- NPP Reactor 5-mile (8 km) Radius



REFERENCE:
• USGS, 1984.

Figure 2.5-4 {Site Topographic Map 0.6-mile (1 km) Radius}



REFERENCE:
• USGS, 1989.

Figure 2.5-5 {Regional Geology Map 200-Mile (322 km) Radius}

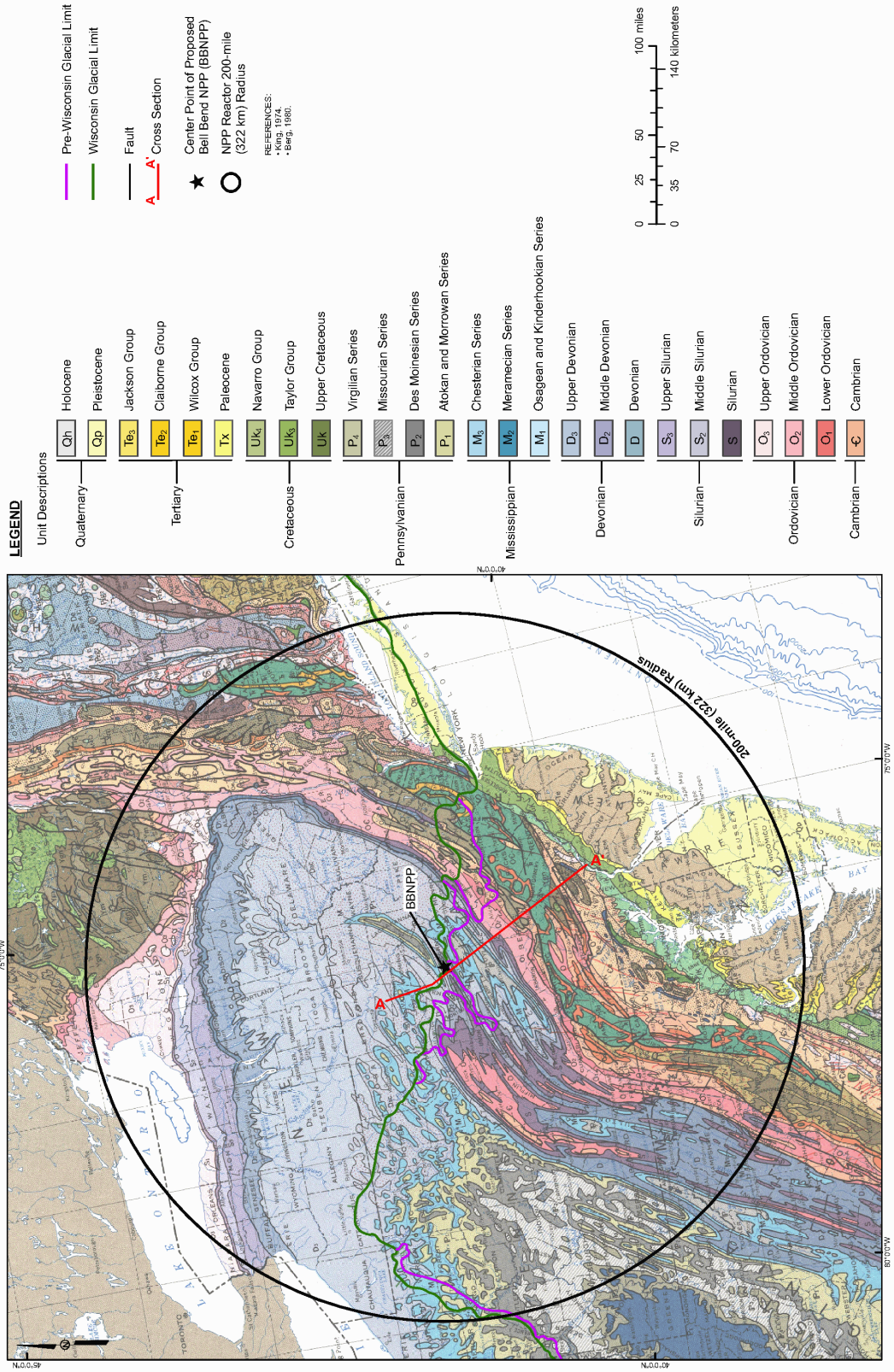


Figure 2.5-6 {Physiographic Provinces of Pennsylvania (Geologic Map of Pennsylvania) 25-mile (40 km) and 5-mile (8 km) Radii}

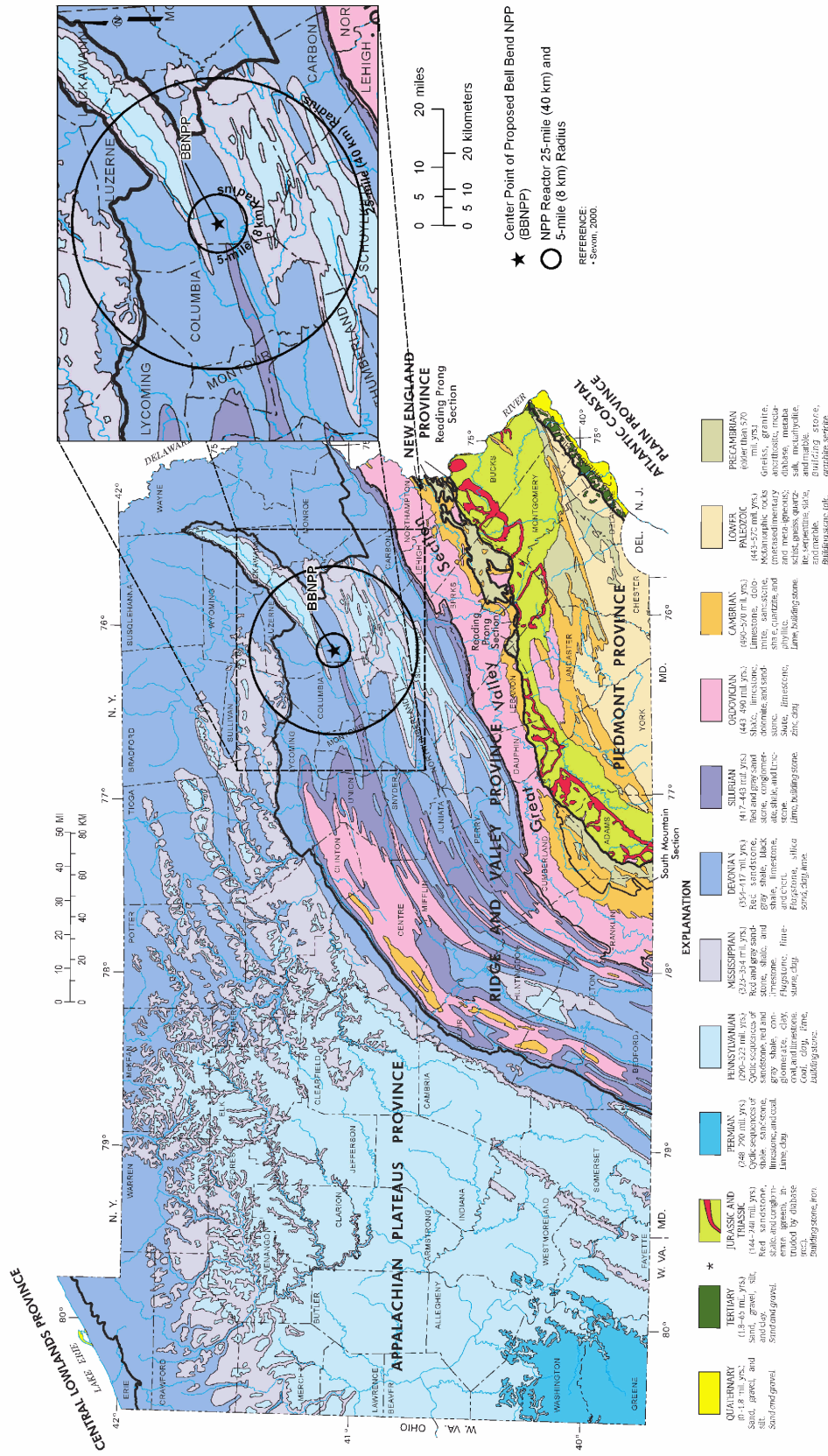
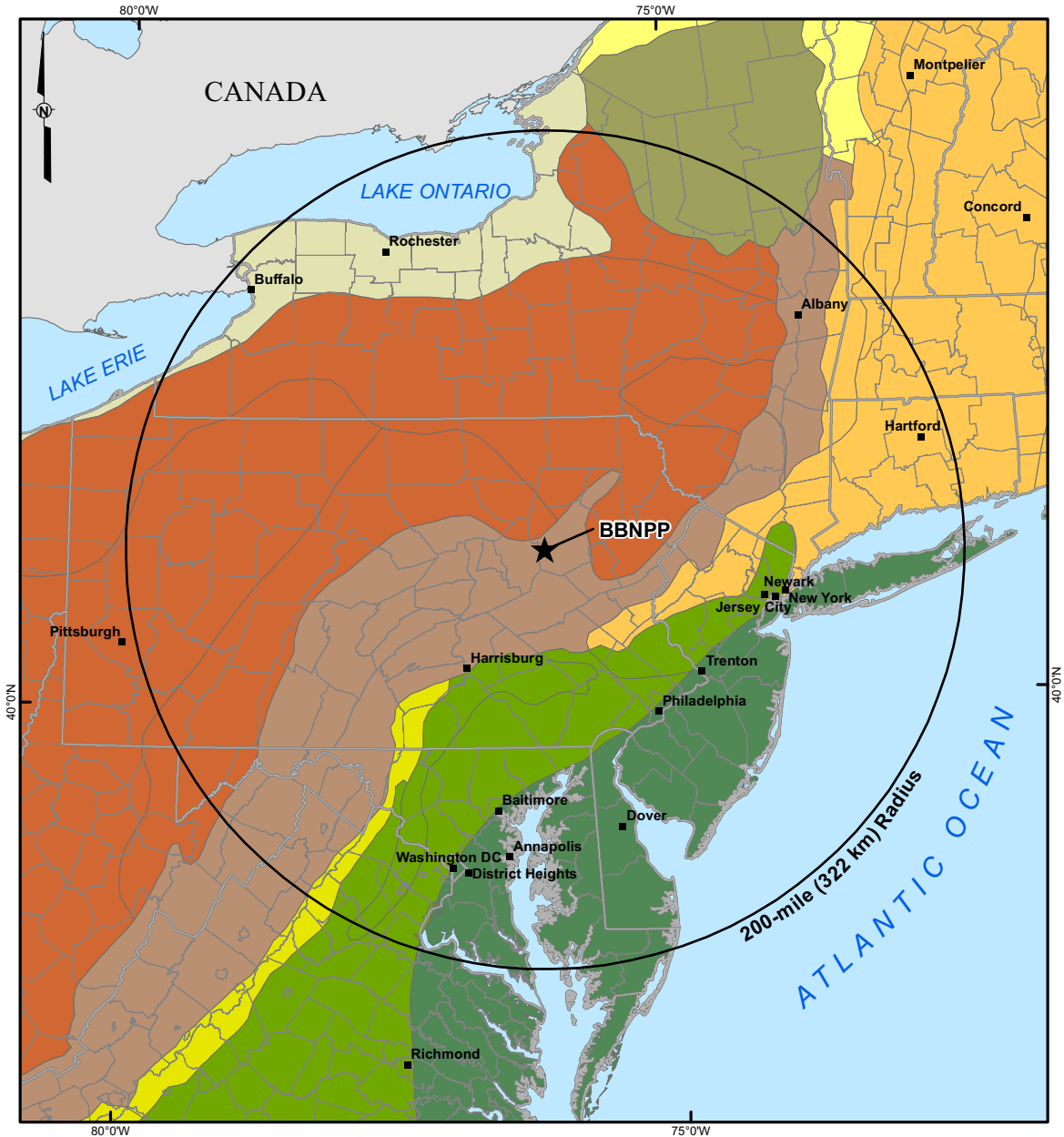


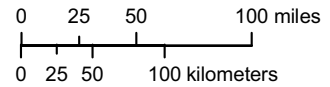
Figure 2.5-7 {Physiographic Provinces (National) 200-mile (322 km) Radius}



LEGEND

- ★ Center Point of Proposed Bell Bend NPP (BBNPP)
- NPP Reactor 200-mile (322 km) Radius

- Adirondack
- Appalachian Plateaus
- Blue Ridge
- Central Lowlands
- Atlantic Coastal Plain
- New England
- Piedmont
- St. Lawrence Valley
- Ridge and Valley



REFERENCES:
• USGS, 2002.

Figure 2.5-9 {Glacial Deposits of Pennsylvania 25-Mile (40 km) and 5-Mile (8 km) Radii}

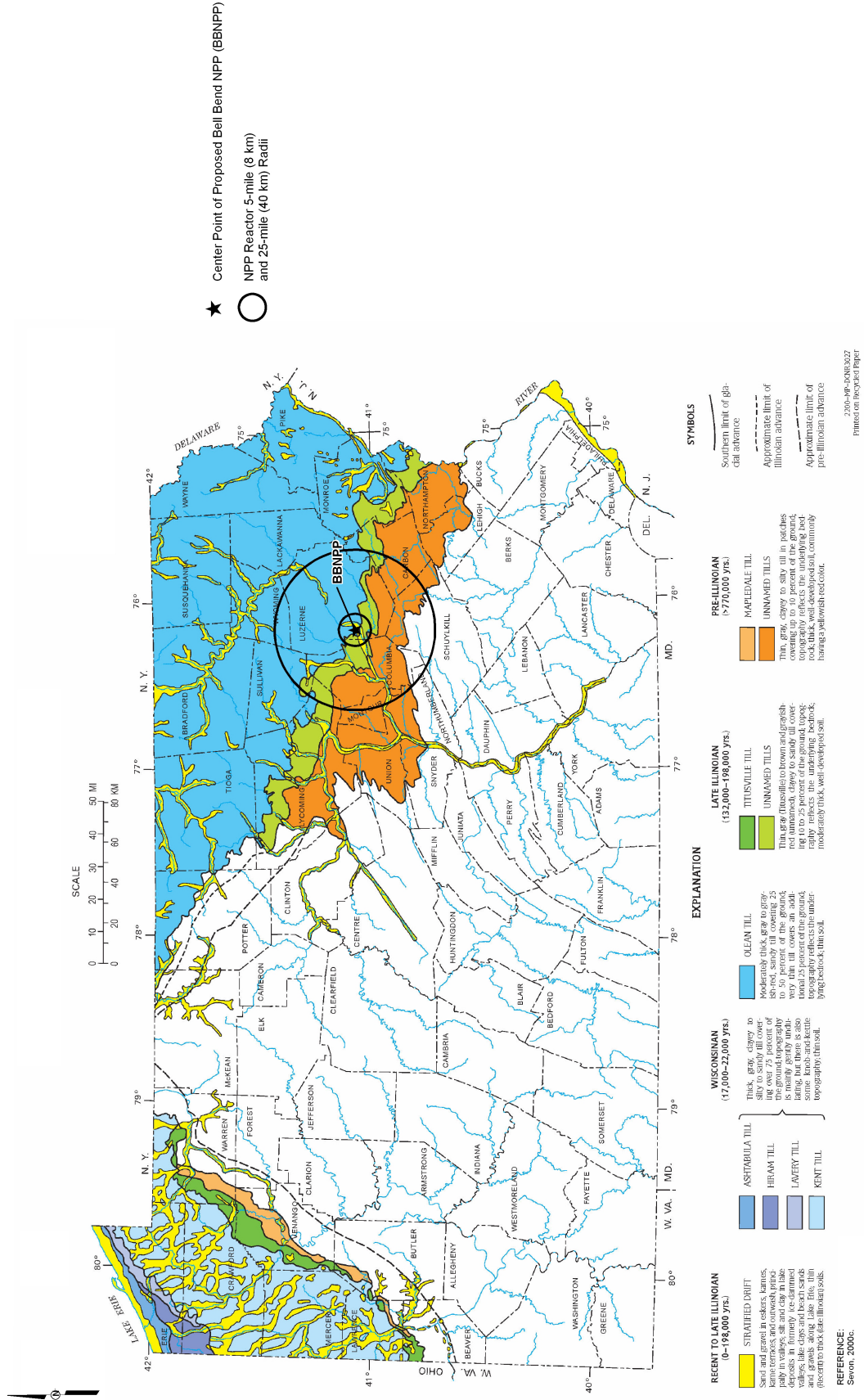
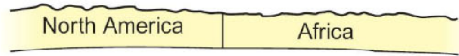
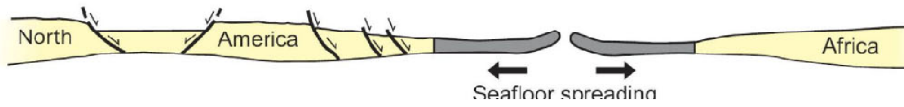


Figure 2.5-10 {Evolution of the Appalachian Orogen}

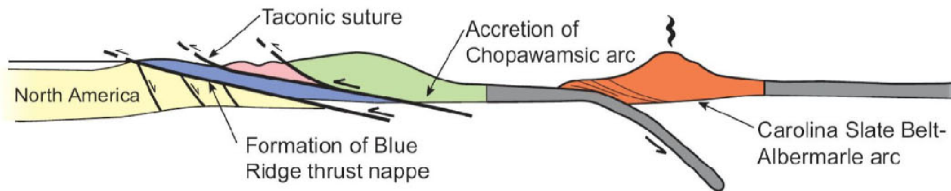
Close of Grenville Orogeny (~1 Ga)



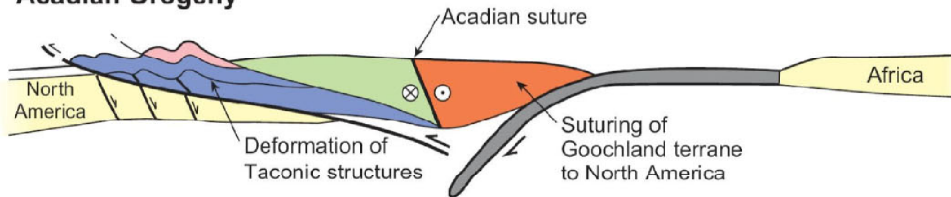
Late Precambrian rifting; opening of Iapetus Ocean



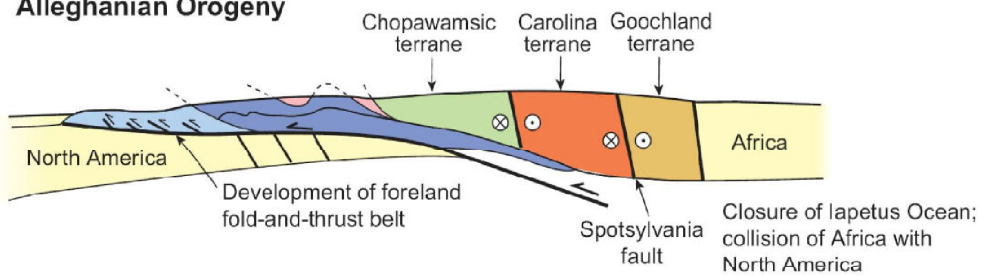
Taconic Orogeny



Acadian Orogeny



Alleghanian Orogeny



Triassic Rifting

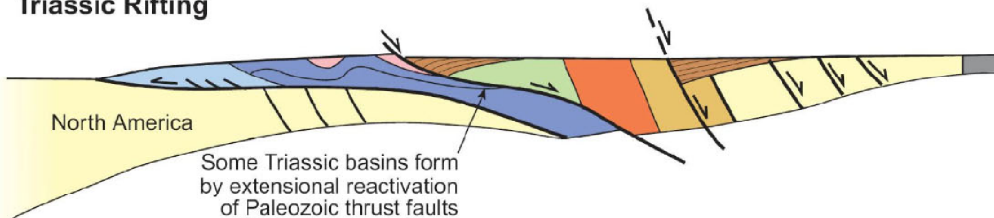
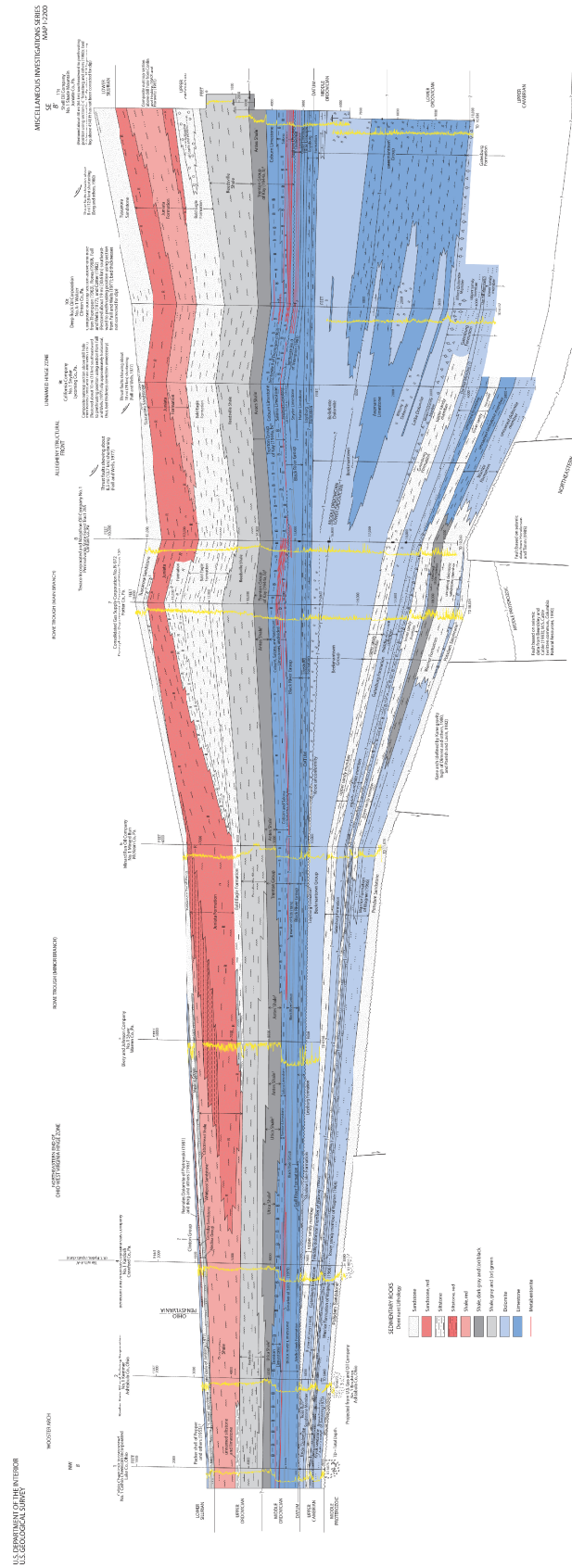


Figure 2.5-11 {Cross Section Showing the Cambrian and Ordovician Rocks of the Appalachian Basin}



NOTE:
 Refer to Figure 2.5-11b for Location Map.
 Refer to Figure 2.5-11c for Rock Correlation Chart.
 REFERENCE:
 • Crangle, Jr., 2002.

Figure 2.5-12 {Map Showing the Location of the Appalachian Basin Cross Section}

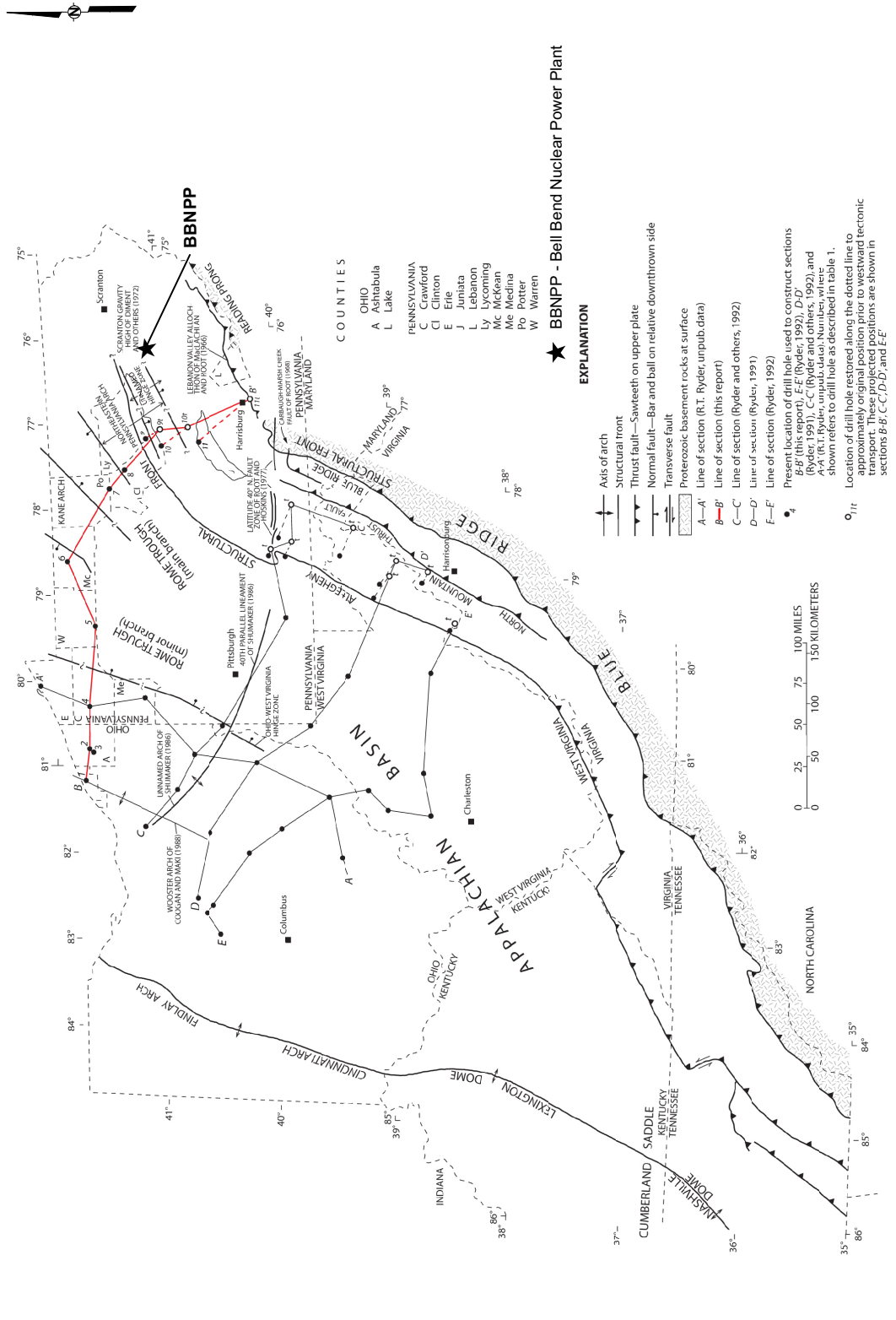
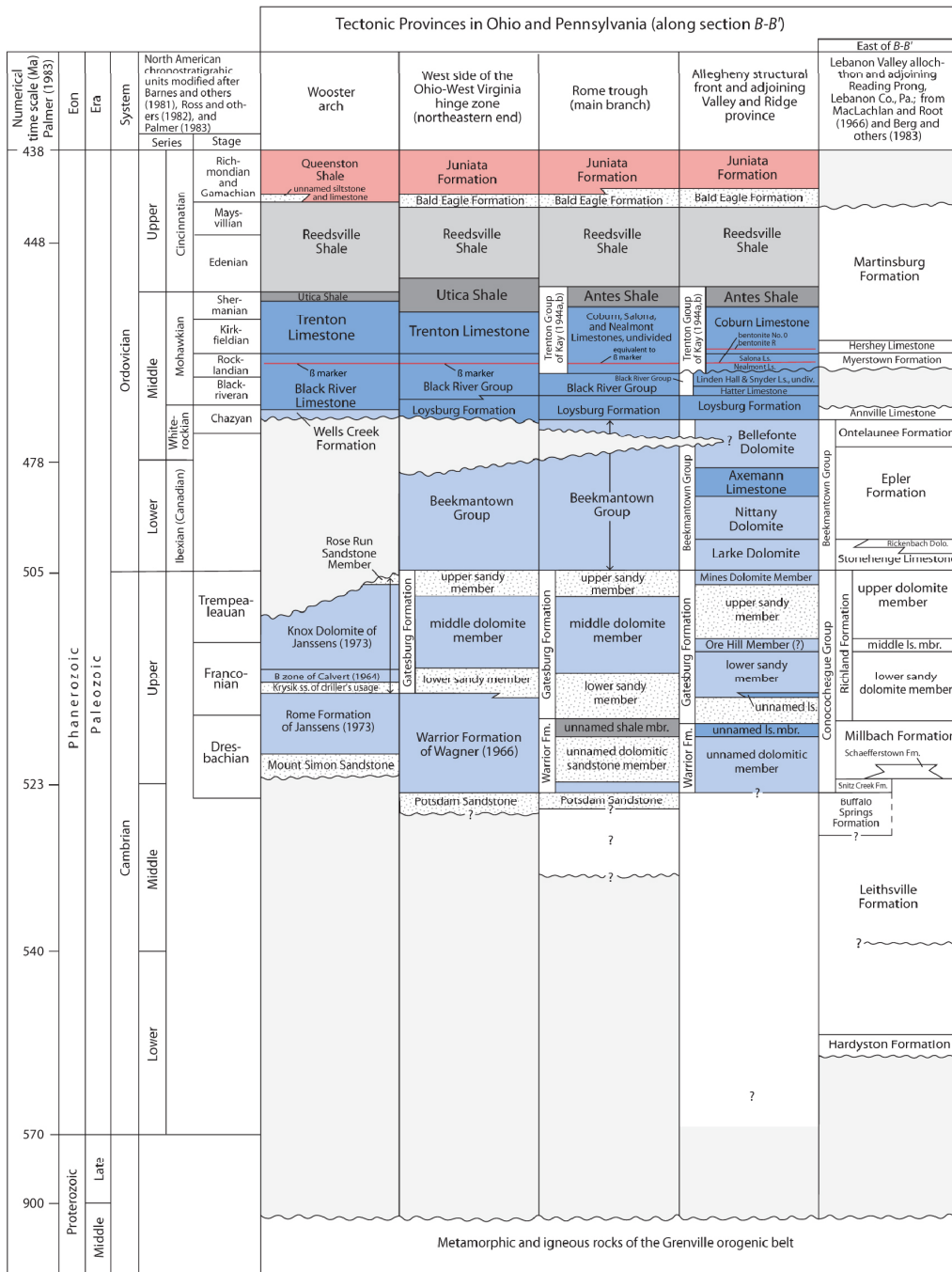


Figure 2.5-13 {Correlation Chart of Appalachian Basin}



EXPLANATION

- Metabentonite
- ~ Hiatus

Figure 2.5-14 {Precambrian Basement Map of Appalachian Basin 25 mile (40 km) and 5 mile (8 km) Radii}

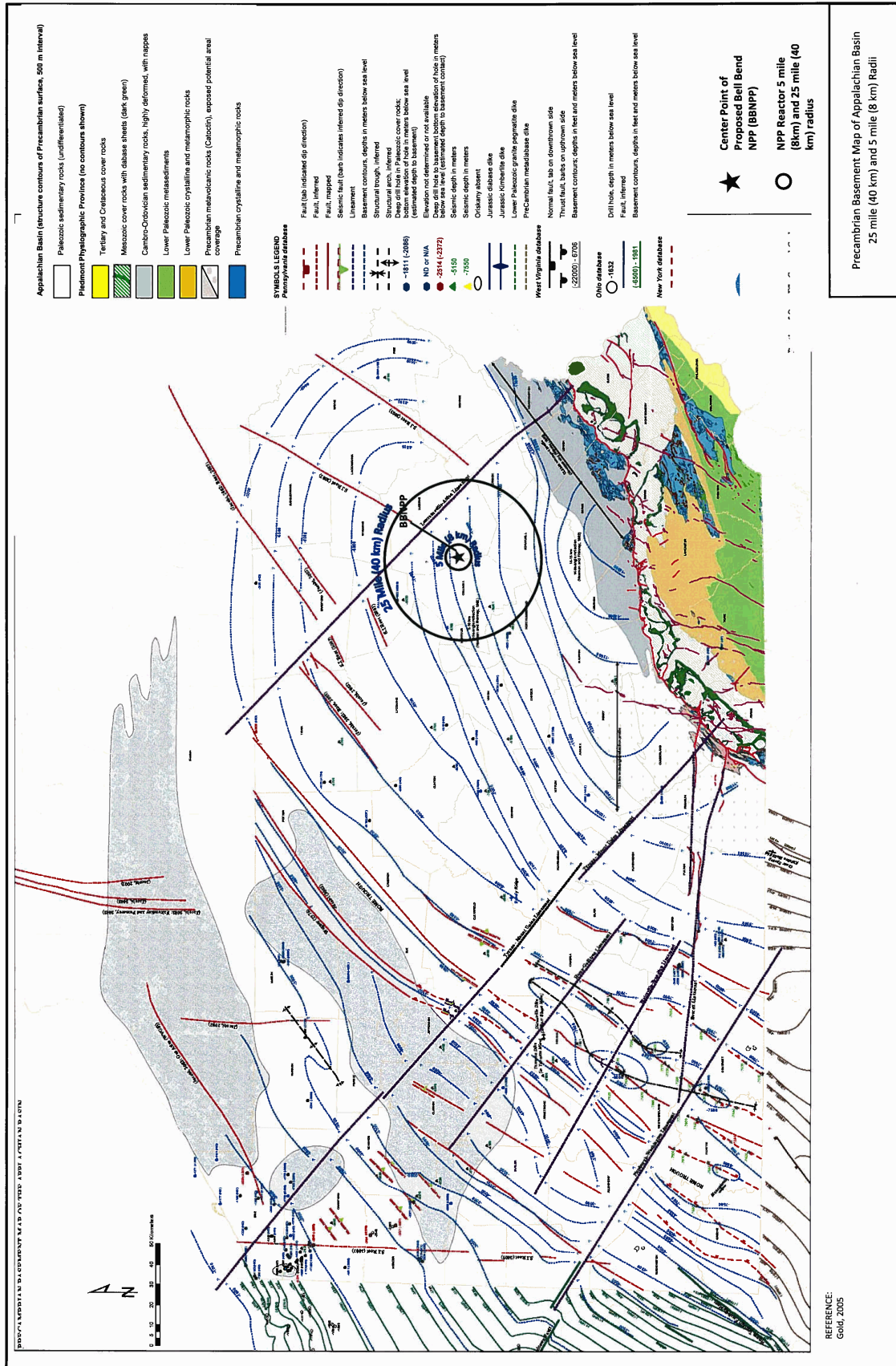
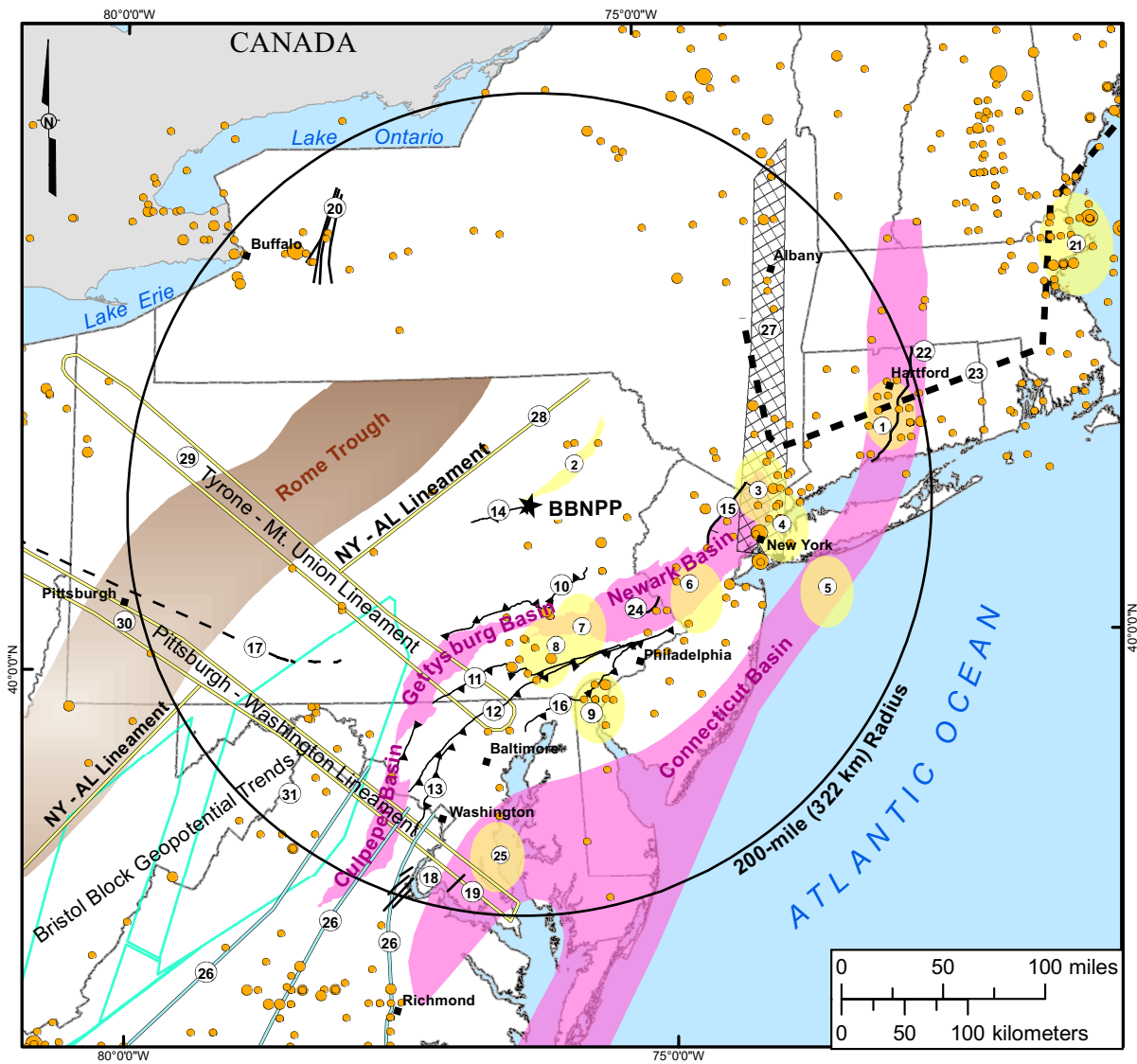


Figure 2.5-15 {Site Region Tectonic Features}



LEGEND

- ★ Center Point of Proposed Bell Bend NPP (BBNPP)
- City
- NPP Reactor 200-mile (322 km) Radius
- Basin
- State Boundary
- Earthquakes by Magnitude, mb (USGS 2001 Catalog)
 - 3.0 - 3.9
 - 4.0 - 4.9
 - 5.0 - 5.9
 - 6.0 - 6.9
 - 7.0 - 7.9

Tectonic Features

- | | | |
|---|-----------------------------------|-------------------------------------|
| ① Moodus Seismic Zone | ⑭ Light Street Fault | ⑳ Hudson River Valley Trend |
| ② Anthracite Zone | ⑮ Ramapo Fault | ㉑ New York-Alabama Lineament |
| ③ Dobbs Ferry Fault Zone | ⑯ Rosemont Shear Zone | ㉒ Tyrone-Mt. Union Lineament |
| ④ Mosholu Fault | ⑰ Transylvania Fault System | ㉓ Pittsburgh-Washington Lineament |
| ⑤ New York Bright Fault | ⑱ Stafford Fault System | ㉔ Bristol Block Geopotential Trends |
| ⑥ Kingston Fault | ⑲ Brandywine Fault | |
| ⑦ Cacoosing Valley Earthquake | ㉔ Clarendon-Lindin Fault Zone | |
| ⑧ Lancaster Seismic Zone | ㉕ Clinton-Newbury Liquefaction | |
| ⑨ New Castle County Faults | ㉖ East Border Fault | |
| ⑩ Yellow Breeches Fault | ㉗ Offset Glaciated Surfaces | |
| ⑪ Martic Fault | ㉘ Furlong-Flemington Fault System | |
| ⑫ Pleasant Valley - Huntingdon Valley Fault | ㉙ Upper Marlboro Faults | |
| ⑬ Plummers Island Fault | ㉚ Fall Lines | |

REFERENCES:

- ESRI, 2007.
- USGS, 2001.
- Hibbard, 2006.
- King, 1978.
- Weems, 1998.
- Wheeler, 2006.
- National Atlas, 2008.

Figure 2.5-16 {Seismic Zones and Seismicity in CEUS}

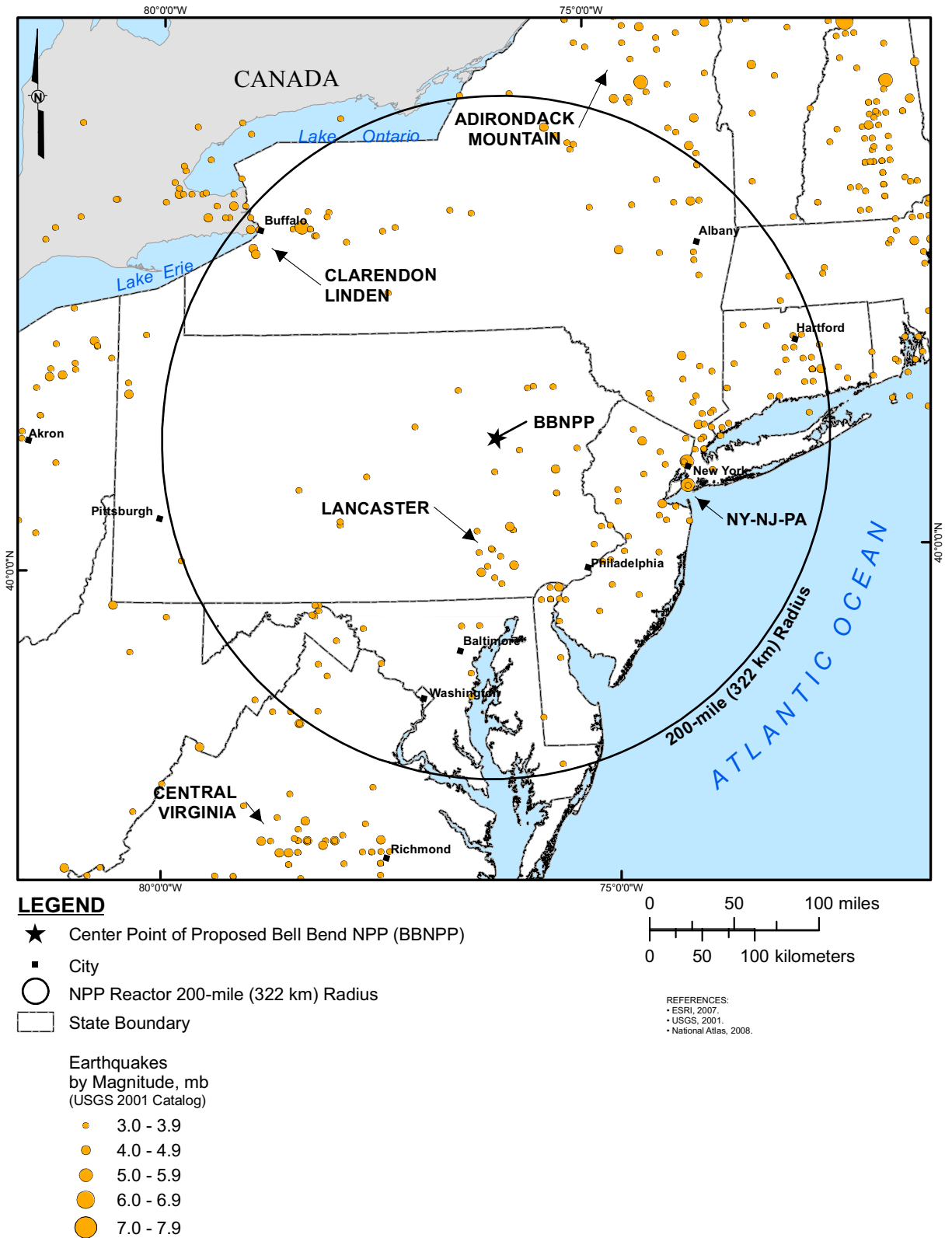
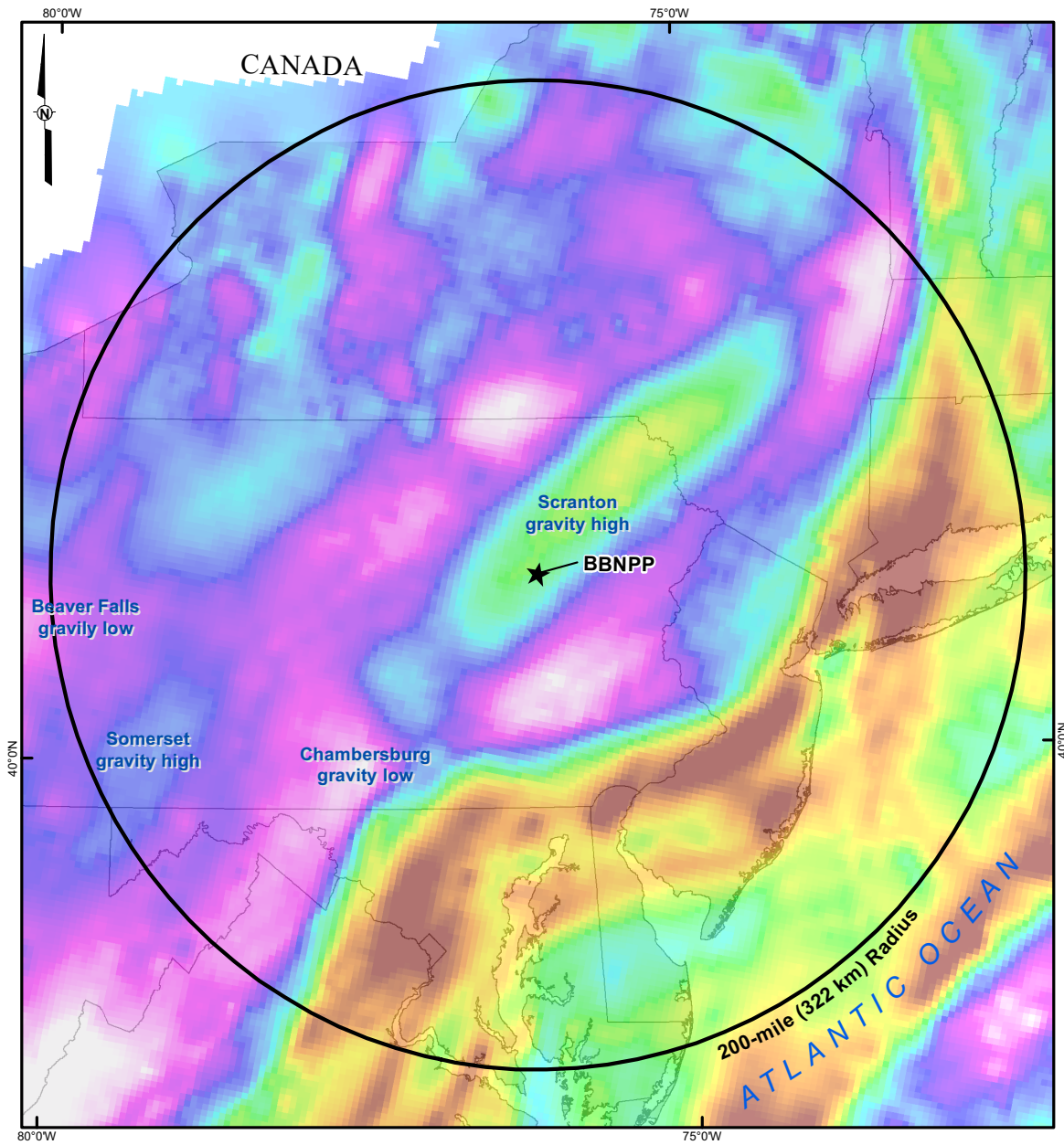


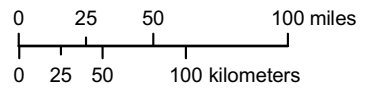
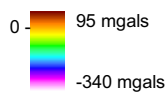
Figure 2.5-17 {Regional Bouguer Gravity anomaly Map}



LEGEND

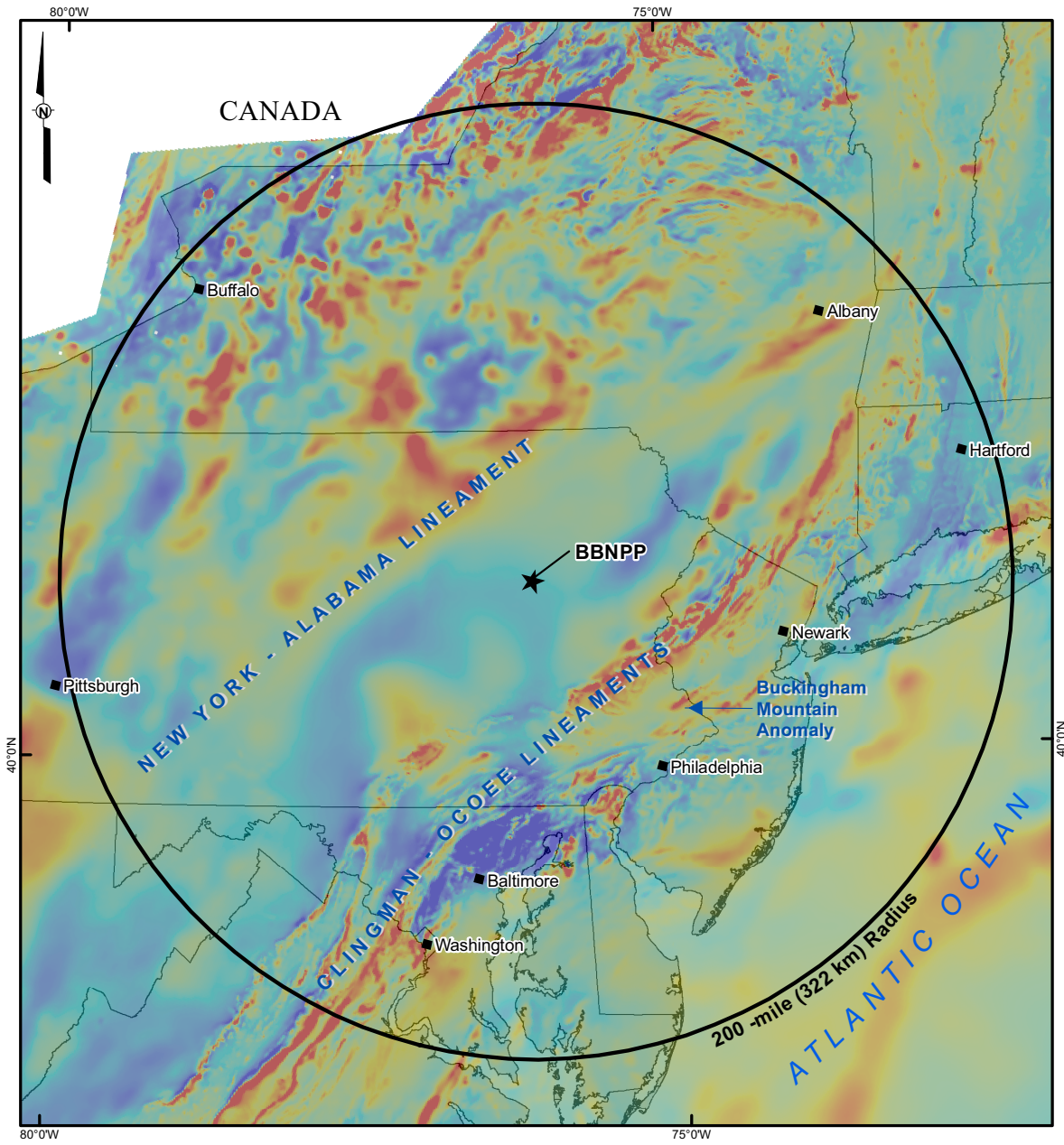
- ★ Center Point of Proposed Bell Bend NPP (BBNPP)
- NPP Reactor 200-mile (322 km) Radius

Gravity Anomaly



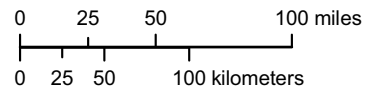
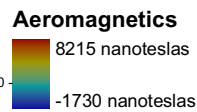
REFERENCE:
• Kucks, 1999.

Figure 2.5-18 {Regional Magnetic Anomaly Map}



LEGEND

- ★ Center Point of Proposed Bell Bend NPP (BBNPP)
- NPP Reactor 200-mile (322 km) Radius



REFERENCE:
• Bankey, 2002.

Figure 2.5-19 {Regional Cross Section}

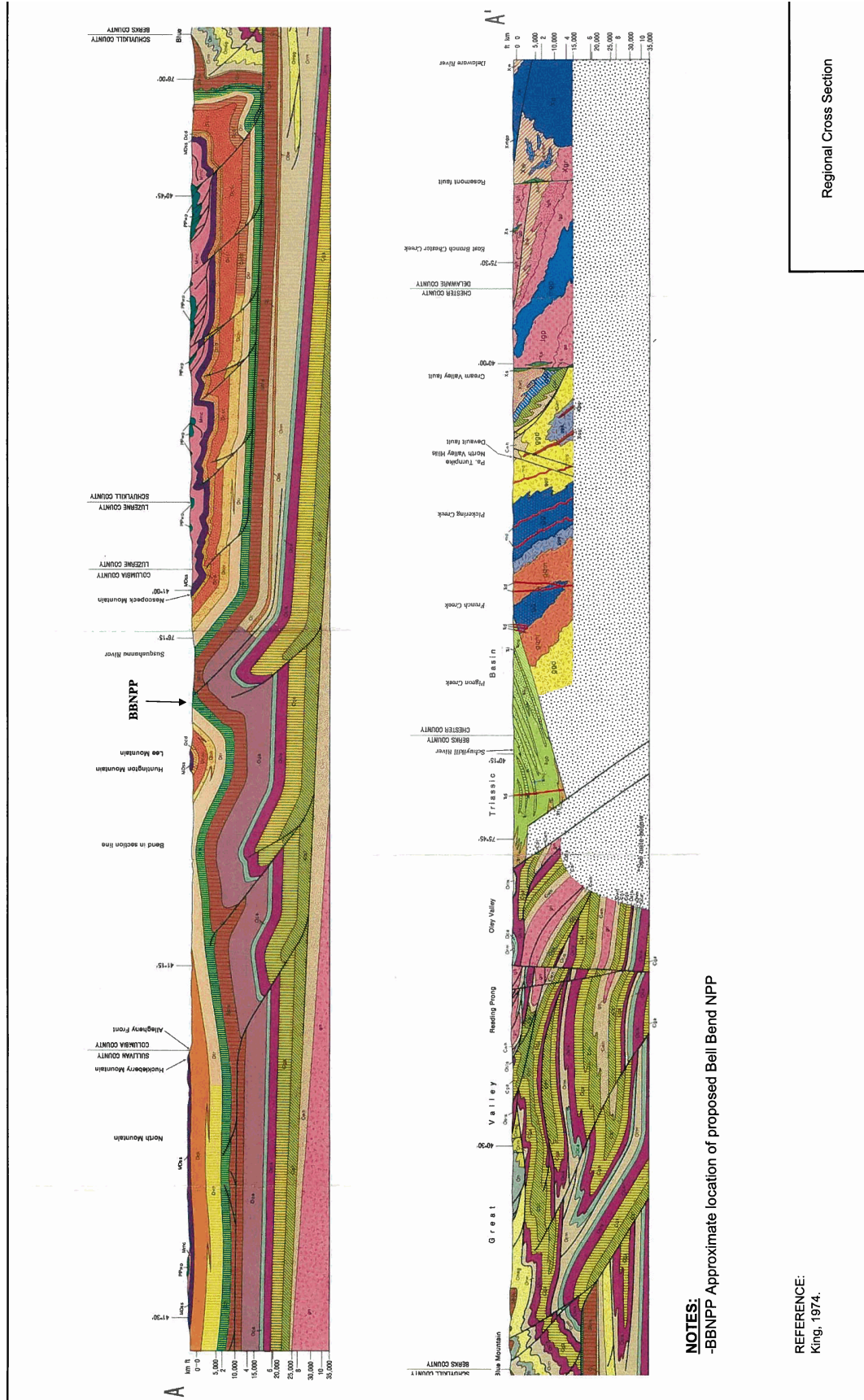
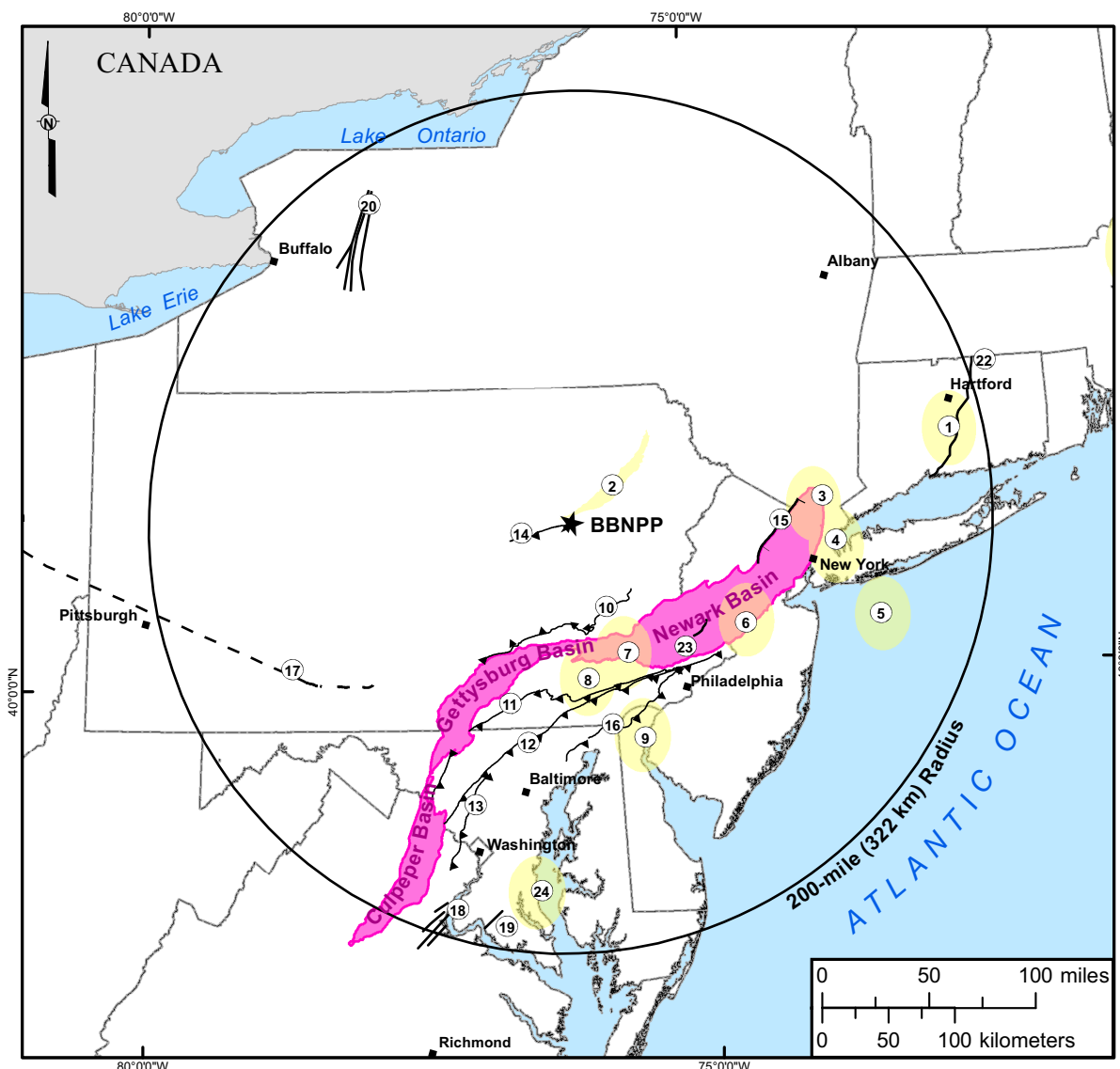


Figure 2.5-21 {Site Specific Stratigraphic Column}

Era	Period	Epoch	Age (Ma)	Unit	Thickness (ft)
Cenozoic	Quaternary	Holocene	0.01	Stratified Drift	38.5
		Pleistocene	1.8		
Paleozoic	Devonian	Middle	370	Mahantango Formation	1,500
				Marcellus Formation	350
				Onondaga Formation	175
		Lower	391	Old Port Formation	100-150
	Silurian	Upper	417	Keyser Formation	125
				Tonoloway Formation	100
				Wills Creek Formation	750
				Bloomsburg Formation	464
		Lower	423	Mifflintown Formation	336
				Keefer Formation	670-1,070
				Rose Hill Formation	
				Tuscarora Formation	400-700
	Ordovician	Upper	443	Juniata Formation	600-1,125
				Bald Eagle Formation	700-1,313
				Reedsville Formation	600-1,800
		Middle	458	Trenton Group Antes Shale Coburn Limestone Salona Limestone	842
				Black River Group	632
				Loysburg Formation	263-475
		Lower	470	Beekmantown Group Bellefonte Dolomite Axemann Limestone Nittany Dolomite Stonehenge Formation	3,159-4,200
		Cambrian	Upper	490	Gatesburg Formation
Middle			510	Warrior Formation	400-1,340
				Pleasant Hill Formation	NOT REPORTED
Lower	520	Waynesboro Formation	1,000+		
Neo-Proterozoic	Ediacaran		543	Metamorphic/Igneous	

REFERENCES:
 •Crangle, 2002
 •Gold, 2003
 •Inners, 1978
 •Kauffman, 1999
 •Laughrey, 1999
 •McElroy, 2007
 •Thompson, 1999

Figure 2.5-22 {Mesozoic Basins with Faults}



LEGEND

- ★ Center Point of Proposed Bell Bend NPP (BBNPP)
- Fault
- |— Normal Fault
- ▲— Thrust Fault
- - - Inferred Fault
- Mesozoic Basin
- City
- NPP Reactor 200-mile (322 km) Radius
- State Boundary

Tectonic Features

- ① Moodus Seismic Zone
- ② Anthracite Zone
- ③ Dobbs Ferry Fault Zone
- ④ Mosholu Fault
- ⑤ New York Bright Fault
- ⑥ Kingston Fault
- ⑦ Cacoosing Valley Earthquake
- ⑧ Lancaster Seismic Zone
- ⑨ New Castle County Faults
- ⑩ Yellow Breeches Fault
- ⑪ Martic Fault
- ⑫ Pleasant Valley - Huntingdon Valley Fault
- ⑬ Plummers Island Fault
- ⑭ Light Street Fault
- ⑮ Ramapo Fault
- ⑯ Rosemont Shear Zone
- ⑰ Transylvania Fault System
- ⑱ Stafford Fault System
- ⑲ Brandywine Fault
- ⑳ Clarendon-Lindin Fault Zone
- ㉑ Clinton-Newbury Liquefaction
- ㉒ East Border Fault

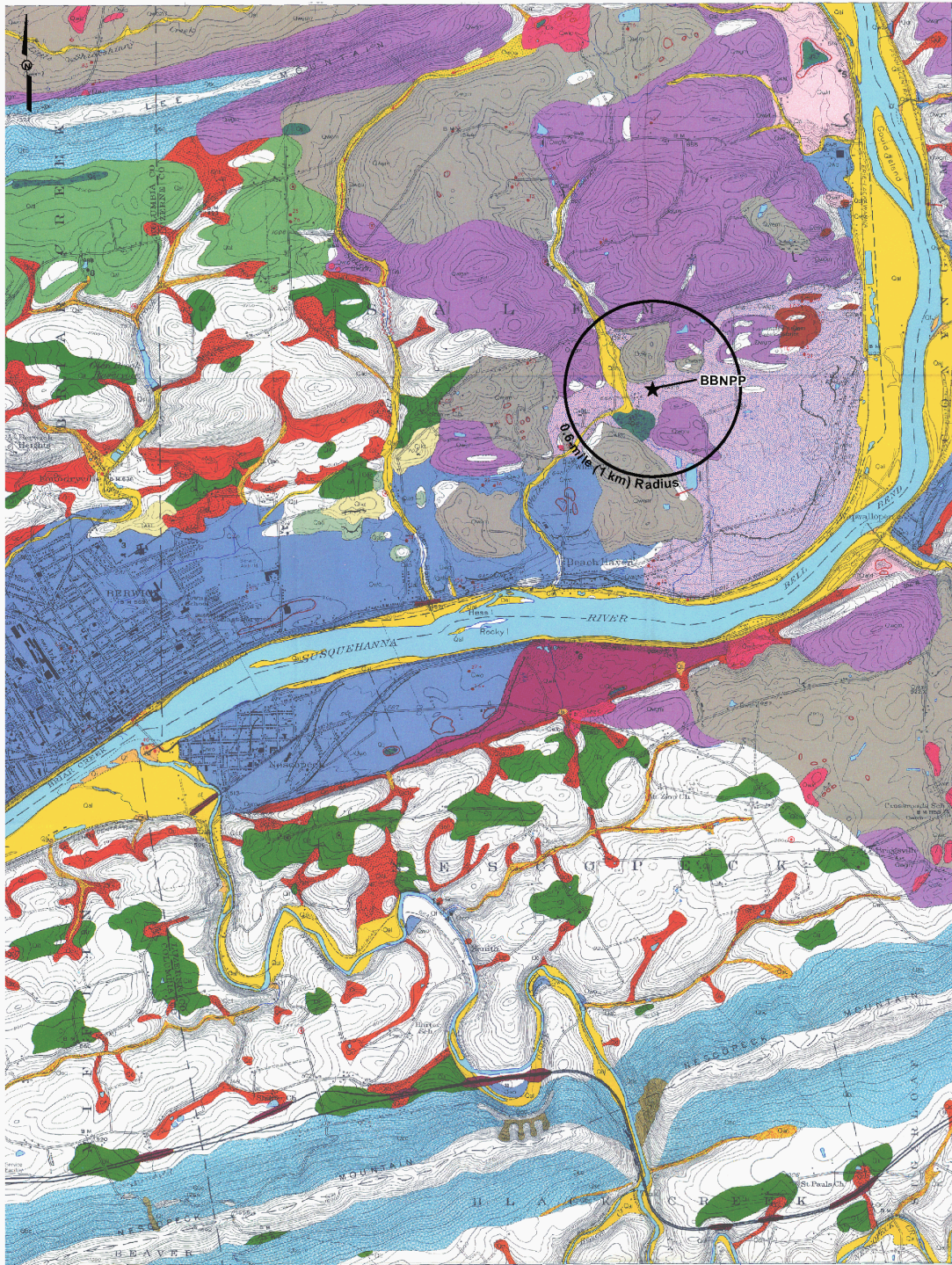
- ㉓ Furlong-Flemington Fault System
- ㉔ Upper Marlboro Faults

REFERENCES:
 • ESRI, 2007.
 • Hibbard, 2006.
 • King, 1978.
 • Wheeler, 2006.
 • National Atlas, 2008.

Figure 2.5-23 {Bedrock Geologic Map Pennsylvania}



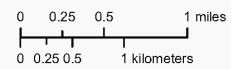
Figure 2.5-24 {Surficial Geologic Map of Berwick Quadrangle}



LEGEND:

★ Proposed Center Point of Bell Bend NPP (BBNPP)

○ NPP Reactor 0.6-mile (1 km) Radius



NOTE:

Refer to Figure 2.5.1-21b for Legend.